UNIVERSITEIT VAN PRETORIA
UNIVERSITY OF PRETORIA
YUNIBESITHI YA PRETORIA

PARTICLE SIZE SEGREGATION AND EXCESS PORE WATER PRESSURE WITH RESPECT TO RATE OF RISE OF TAILINGS DAMS

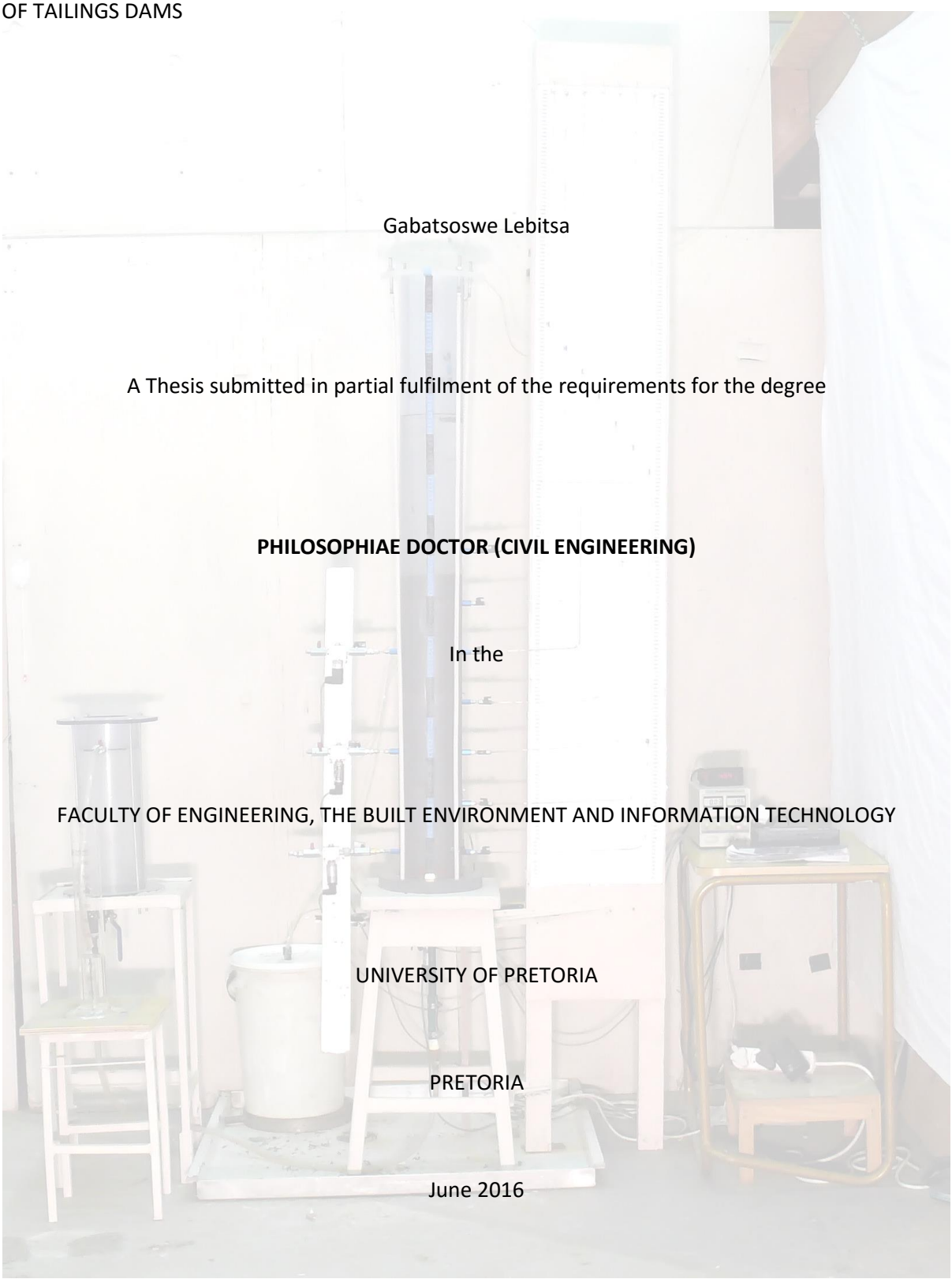

Gabatsoswe Lebitsa

A Thesis submitted in partial fulfilment of the requirements for the degree

PHILOSOPHIAE DOCTOR (CIVIL ENGINEERING)

In the

FACULTY OF ENGINEERING, THE BUILT ENVIRONMENT AND INFORMATION TECHNOLOGY

UNIVERSITY OF PRETORIA

PRETORIA

June 2016

THESIS SUMMARY

PARTICLE SIZE SEGREGATION AND EXCESS PORE WATER PRESSURE WITH RESPECT TO RATE OF RISE OF TAILINGS DAMS

G.L. LEBITSA

Supervisor: Professor G. Heymann (University of Pretoria)
Co-Supervisor: Professor E. Rust (University of Pretoria)
Department: Civil Engineering
Degree: Philosophiae Doctor (Civil Engineering)

Gold tailings were deposited in thick lifts at full depth where tailings slurry was deposited to fill up the settling column in one lift within the shortest time possible (2 minutes) and thin lifts (660mm to 580mm) under simulated rates of rise of 20m/yr and 10m/yr in the laboratory using instrumented settling column apparatus. Rate of rise (RoR) was taken as the vertical increase in height of settled tailings over a given period of time expressed in metres per year.

The deposited tailings segregated along the height of settling columns depicting a height profile ranging from fine grained to coarse grained particles from the top to the bottom of the settling columns. Tailings permeability values of the segregated tailings profiles increased with decreasing settling column height. Scanning electron microscope micrographs based fabric, particle size gradations, saturated vertical permeability and excess pore water pressures correlated well with segregated tailings profiles.

Low magnitude excess pore water pressures in the range of 6kPa maximum were recorded. Full depth deposition yielded the highest values of excess pore water pressures followed by the excess pore water pressures for 20m/yr RoR at 50% of the full depth deposition magnitudes, with the least excess pore water pressures generated for the 10m/yr RoR which were 30% of the full depth deposition excess pore water pressure magnitudes. 90% of the excess pore water pressures dissipated during the sedimentation phase and coincided with the occurrence of the bulk of the tailings settlement. The remaining 10% of excess pore water pressures took a disproportionately longer period of time to dissipate and were resurgent with any disturbances.

Keys words: Particle size segregation, rate of rise (RoR), excess pore water pressure, gold tailings.

Acknowledgement

I would like to acknowledge the guidance and leadership of my study supervisors: Professor Gerhard Heymann and Professor Eben Rust. I have learnt immensely and grown as an academic during the course of this research work. I am also indebted to Professor C.R.I. Clayton and Professor SW Jacobsz for their assistance.

I am grateful for the financial support I received from both my employer, the University of Botswana and the University of Pretoria for the funds that procured the apparatus for this study as well as being the research host.

The following University of Pretoria Civil Engineering Laboratory members of staff helped me in various ways during the course of the study: Jaap Peens, Derek Mostert, Jenny Callanan, Johan Scholtz, Rikus Kock, Vanessa Doman, Jurie van Stadan, Samuel Nkadimeng, Daniel Sithole, Daniel Motloung and Paulos Maluleke. Special mention is well deserved of the following people: Mr. Rikus Kock who identified a suitable location for the sensitive experiment after numerous unsuccessful attempts. Many thanks also to Rikus for his help with the electronics and computers. Messrs. Nkadimeng, Sithole and Silipius Mbawalla (a fellow PhD student) who formed my slurry deposition team. Mr. Neels Smith of the Mechanical Engineering Department who together with Mr Paulos Maluleke helped with building of the three sacrificial settling column apparatus. Mr. Jurie van Stadan who assisted in the geotechnical laboratory, Mrs Callanan who helped administratively as well as Ms Doman who carried out the Mastersizer Laser diffraction gradation tests and the Helium gas displacement specific gravity tests.

The Piezocone team comprising Oom Piet, Warren Vorster and the crew are thanked for their assistance in various ways. The facilitation of the above assistance by Prof Rust is highly appreciated.

Fraser Alexander (Pty) Ltd. is thanked for allowing us to take samples at both Mooifontein tailings dam and at Chemwes Dam 5.

The Scanning Electron Microscope team of the University of Pretoria comprising Mr Andre Botha, Mr Alan Hall and Ms Antoinette Buys who facilitated viewing of samples under the microscope are greatly acknowledged.

Ms Wiebke Grote and Ms Jeannette E Dykstra at the XRD and XRF Facility of the Geology Department of the University of Pretoria who carried out the X ray diffraction mineral analysis

and the X ray fluorescence spectrometer chemical analysis on the samples are also acknowledged.

Many students at the University of Pretoria who researched on topics related to this research are also acknowledged as their findings helped shape this study into what it has finally turned out to be. Specific mention is in order for Ms Ina Mari de Villers who also provided one of the samples used in this research as well as Mr Fritz Hagan, Mr Drain Roos, Mr Rikus de Beer and Mr Wessel Wagner.

My family is thanked for their support, sacrifice and encouragement during the study period.

Table of Contents

List of Figures

List of Tables

List of Symbols

$(u_e)_{Dis}$	Dissipated excess pore water pressure at time t
$(u_e)_{Rem}$	Remaining excess pore water pressure at time t
$(u_e)_i$	Excess pore water pressure at time t=0
$(u_e)_t$	Excess pore water pressure at time t
D_r	Relative density
G_s	Specific gravity of solid particles
G_{slurry}	Specific gravity of slurry
M_{slurry}	Mass of slurry
S_c	Consolidation settlement
S_r	Degree of saturation
S_t	Settlement at time t
T_v=T	Non dimensional time factor
V_s	Volume of solids
V_{slurry}	Volume of slurry
V_v	Volume of voids
V_w	Volume of water
W_s	Weight of solids
W_w	Weight of water
c_v	Coefficient of consolidation
d_n	Depth of the n^{th} layer
e_∞	Final void ratio
e_{max}	Maximum void ratio
e_{min}	Minimum void ratio
e_o	Initial void ratio
k_n	Permeability of the n^{th} layer
m_v	Coefficient of volume compressibility
q_∞	Steady state rate of flow
u_e	Excess pore water pressure
v	Particle settling velocity
v_s	Fall of particle under Stokes' law conditions

v_s'	Velocity of spherical particle in a dispersion of grains
ΔH	Head difference across a sample
Δz	Change in depth/depth
a and b	Constants for a given beach and tailings
A	Cross sectional area of sample
a	Standpipe cross sectional area
c	Concentration of solid particles
c'	Effective cohesion
C_c	Compression Index
C_u	Coefficient of uniformity = D_{60}/D_{10}
c_v	Coefficient of consolidation
C_z	Coefficient of curvature = $(D_{30})^2/(D_{10}D_{60})$
D	Stokes' diameter of particle
D_{10}	Particle diameter for 10% passing
D_{30}	Particle diameter for 30% passing
D_{60}	Particle diameter for 60% passing
D_{90}	Particle diameter for 90% passing
e	Void ratio
e_{sed}	Void ratio at the end of sedimentation and start of consolidation
g	Gravitational acceleration
H	Head at time t =t
H_o	Head at time t =0
i	Hydraulic gradient
k	Saturated permeability
L	Length of sample
LL	Liquid limit as a percentage
w	Moisture content
n0	Dimensionless constant dependent on tailings characteristics
P	Pulp density or percentage solids
Q	Total discharge
t	Time
U	Degree of consolidation
u	Pore water pressure

u_z	Excess pore water pressure at depth z and time t
$\bar{U}$	Average degree of consolidation
V	Total volume
x	Distance from tailings discharge point
X	Length of beach from discharge point to edge of pond
Y	Elevation between point of deposition and the pool liquid level
z	Depth/Height of layer
Z	Non dimensional drainage path ratio
y	Reduced or material coordinate
W	Total weight
n	Exponent between 2.32 & 2.65 depending upon grain Reynolds's number
γ_b	Bulk unit weight
γ_d	Dry unit weight
γ_{dmax}	Maximum dry unit weight
γ_{dmin}	Minimum dry unit weight
γ_s	Unit weight of solids
γ_t	Total unit weight
γ_w	Unit weight of water
ρ_f	Fluid density
ρ_s	Particle density
ρ_{slurry}	Density of slurry
σ'	Effective stress
σ_1'	Effective stress at time t
σ_o'	Initial effective stress
n	Exponent between 2.32 & 2.65 depending upon grain Reynolds's number
α	Tailings material constant
β	Tailings beach constant
$\beta(e)$	Interaction coefficient which is a function of void ratio
η	dynamic fluid viscosity
ξ	Spatial coordinate in vertical direction
σ	Total stress
ϕ'	Friction angle

Chapter 1

INTRODUCTION

1.1 Background

Mining dates back many years and it has always resulted in unwanted man-made waste materials in the form of rock fragments and small sized particles. Gold tailings in particular have been produced in South Africa since the beginning of the 19th century. There are numerous gold tailings dams in South Africa with the majority of the tailings dams located within the Witwatersrand basin where samples for this research were obtained.

The practice of soil mechanics has its genesis on naturally occurring soils which have evolved over very long geological periods spanning millions of years. Mine tailings on the contrary are young deposits in age. Geotechnical engineers and the related professionals have studied tailings using existing soil mechanics theories to great success, however, many challenges remain concerning mine tailings and the massive structures built from tailings.

Mine tailings structures in the form of tailings dams have become a big challenge for society in many different ways. To mining companies, tailings reduce the profitability of mining operations. To the geotechnical engineer and allied professionals it is a challenge in terms of using tailings as a material for dam wall construction as well as containing tailings as a spoil material within dams or in finding alternative uses for tailings. Tailings dams also pose a danger when the impoundment walls fail. Tailings are an environmental hazard in terms of the dust they emit and the chemical toxins tailings usually contain. Tailing dams disturb visual aesthetics of our landscape and their volumes which have been growing significantly over time have created the problem of dwindling storage space for mine tailings.

Many studies have been carried out in different parts of the world on several aspects of tailings dams including some of the challenges cited in the preceding paragraph. With regards to gold tailings in South Africa many studies have been carried out resulting with literature and data availed for various uses. Such works include works by Vermeulen (2001), Papageogiou (2004) and Chang (2009) amongst others. The construction aspects of gold tailings dams has also

received a lot of attention including from national research studies carried out in the late 1950s (NBRI, 1959 and Donaldson, 1960).

However even with the numerous studies that have been undertaken to date issues such as the allowable rate of rise of tailings dams, the magnitudes of excess pore water pressures generated when tailings are deposited and their effect on rate of rise, laboratory determination of the permeability of tailings in an undisturbed state as well as the extent of tailings segregation still remain contentious amongst the professionals involved with the management of mine tailings.

This study was initiated to address some of the problematic areas of tailings dams in South Africa particularly those aspects with relevance to the rate of rise of tailings dams namely:-the magnitudes of excess pore water pressures generated during tailings deposition under different rate of rise scenarios, sedimentation and consolidation phases of settled tailings, the segregation of different particle sizes as well as the resulting fabric and the saturated permeability of the tailings in an undisturbed state. Currently rate of rise is limited to 2m/yr to 3m/yr (Chamber of Mines of South Africa, 1996). Whilst rate of rise is dependent on various factors, limitation of rate of rise by excess pore water pressure is often advanced as one of the reasons for the limitation. This study focusses on excess pore water pressure as a limiting factor on rate of rise. Because rate of rise is dependent upon several other factors (listed later in the Literature Review Chapter), the practical significance of the findings of this study has to take cognisance of the other factors whose effects might require further research before the full benefits of the findings from this study could be realised.

1.2 Objectives

The purpose and main aim of the study is to experimentally investigate whether excess pore water pressures limit rate of rise in tailings dams. Of secondary importance observations of particle size segregation, determination of the permeability of tailings as well as fabric and mineralogy of the tailings and other pertinent properties were to be made.

The objectives of the research were:

(a) to simulate and characterise tailings deposition in settling columns with respect to rate of rise of tailings dams

(b) to assess excess pore water pressures generated in settling column experiments

(c) to gain a better understanding of sedimentation and the associated particle size segregation

(d) to quantify saturated permeability in settling columns

(e) to evaluate saturated density of sediments

(f) and to determine fabric and related parameters of mine tailings in settling columns.

It was hypothesised that mine tailings segregated into graded particle size fractions with high excess pore water pressures developed on fine tailings fractions while low excess pore water pressures developed on the coarse grained fraction. It was believed that the generated excess pore water pressures did not limit rate of rise. It was postulated that segregated tailings resulted in fabric that varied with the depth profile which in turn governed the saturated permeability of the tailings in a settling column. The horizontal variation of tailings properties as one traversed from dam walls, through tailings beaches towards the pond sections of the tailings dams was believed to follow similar patterns as the vertical profile variations along the depths of settled tailings in settling column experiments.

1.3 Scope

The subject of mine tailings by its nature is very broad. The study envisaged in the objectives listed in the preceding section of this chapter needed to be limited in scope to yield focused experiments from which meaningful data could be obtained. In this regard the following limitations were imposed.

Only gold tailings samples from Chemwes Tailings Complex's Dam 5 and Mooifontein tailings dam of the Crown Mines Complex were considered under this study. The main experiments reported in this thesis focus on the Chemwes Tailings Dam 5. Gold tailings are known to vary from one tailings dam to another due to many factors.

The limited samples collected from the vicinity of one hydrocyclone was assumed to be representative of samples collected from any other hydrocyclone and thus believed to be representative of the whole tailings dam.

Only saturated conditions were considered during this research except where settling columns were deliberately dried to obtain samples for standard laboratory tests and for viewing under the microscope as well as subjecting to other tests requiring dry samples.

Distilled water was used as the fluid in the tailings suspensions instead of tailings water whose chemistry differs markedly from that of distilled water and is known and reported to affect tailings properties (Vermeulen, 2001; Chang, 2009; and Villar et al., 2009).

Only one tailings suspension (slurry) relative density of 1.3 was used in all the experiments. Different suspension concentrations are known to influence experimental results and slurry tailings properties (Richardson et al., 2002).

Worst case scenarios of the tailings pond and dam wall portions of a tailings impoundment were modelled respectively by using saturated fine tailings and coarse tailings samples with distilled water in the settling column experiments.

1.4 Methodology

The research for this study was carried out by means of laboratory experiments. In order to achieve the objectives of the study, gold tailings samples were characterised to determine their basic physical properties, following which slurries were made with gold tailings and distilled water and subjected to sedimentation, consolidation and permeability testing in instrumented settling column apparatus.

The data collected using settling column apparatus comprised pore water pressure measurements, soil water interface variation over time, piezometric heights, water level and amounts of water that seeped through settling columns over time.

The tailings settling columns in the tubes were allowed to dry under atmospheric conditions after which the recovered samples were observed under the scanning electron microscope and the samples subjected to particle size distribution tests.

The raw data collected was analysed using methods discussed in the literature review chapter yielding processed information that was used to draw conclusions and to make recommendations for further research.

1.5 Organisation of the thesis

This thesis is divided into six chapters. A background of the research is given in the first chapter together with the hypothesis guiding the study. The confines within which the work was carried out is also provided. The first chapter concludes with a summary of the experimental procedures carried out to achieve the objectives of the study.

Chapter 2 contains a summary of the literature studied relating to the research questions posed in the study. The chapter presents the basis of the analysis of raw data and the analytical tools used to process the data.

The methodology used in the six main settling column experiments is described under chapter 3. The experimental procedures, the design and fabrication of the apparatus used as well as the relevant standards are contained in the chapter.

Chapter 4 presents the data obtained from the six experiments.

Chapter 5 covers the analysis of the results of the experiments that were presented in chapter 4. Chapter 5 discusses the results using the analytical tools, methods and knowledge obtained from the literature study of the research.

The in-depth analysis of chapter 5 leads to conclusions and recommendations for further research which are contained in chapter 6.

The remaining parts of the thesis lists the references used in the study and the appendices which augment and supplement information contained in the various chapters of the thesis.

Chapter 2

LITERATURE REVIEW

2.1 Introduction

This chapter presents a synthesis and a critical summary of literature on tailings dams in general and gold tailings in particular as the tailings material studied for this thesis. The literature review focuses on rate of rise of tailings dams and the attendant aspects of particle size segregation and development of excess pore pressures which arise when tailings dams are constructed.

The chapter starts with a brief examination of the geology and the extraction of gold from source rock, the creation of tailings and outlines tailings disposal methods. Rate of rise (RoR) of tailings dams and its significance is then considered together with the processes involved in the formation of tailings from hydraulically deposited slurries. The formation processes entail sedimentation and consolidation as well as the related particle size segregation and excess pore water pressures which are the emphasis of this study. Geotechnical engineering properties of gold tailings gleaned from literature are also presented. Settling column experiments which are used to achieve the objectives of the study are described and evaluated in the context of their use by previous workers and their intended use under this research. The use of the scanning electron microscope (SEM) and the determination of mineralogy of tailings using both x-ray diffraction (XRD) and x-ray fluorescence spectroscopy (XRF) techniques are also discussed. The literature review ends with a summary highlighting the role played by the review within this research.

2.2 The Geology and Extraction of Gold Tailings from Ore

2.2.1 Introduction

The gold tailings samples investigated during this study were obtained from the Stilfontein Chemwes tailings dam No. 5 and the Mooifontein tailings dam of the Crown Mines Tailings Dam Complex. Both these tailings dams stored the wastes from the mineral extraction and processing of gold valuables from the ore sourced within the Witwatersrand Basin in South

Africa. This section presents a brief geology of the Witwatersrand Basin followed by the production of tailings as a by-product of the extraction of gold from ore as well as when tailings dams are re-mined to recover residual gold, uranium and to produce sulphuric acid.

2.2.2 Geology of the Witwatersrand Basin

The Witwatersrand Basin shown in Figure 2.1 comprise an oval area of approximately 42,000 square kilometres across the Gauteng, North West and Freestate provinces of South Africa (Vermeulen, 2001). The ore bearing rocks within the Witwatersrand Basin are conglomerates commonly referred to as "banket" or "reefs" within which both gold and uranium deposits are present (Adamson, 1973; Stanley,1987). The reefs have an average thickness of 30 centimetres and occur as tilted and faulted strata which reflect their geological history since deposition in horizontal layers under water approximately 3 billion years ago (Vermeulen, 2001).

Figure 2.2 shows the geological map of the Witwatersrand Basin in which the younger rock deposits which later overlaid ore-bearing conglomerates have been removed. Approximate locations of the tailings dams from which samples used in the study are shown in the figure. The gold bearing conglomerates comprise mostly pebbles of quartz cemented with a fine grained mosaic of quartz phyllosilicates and sulphides. Gold within the conglomerates is reported to have formed from ditrital particles that underwent low grade metamorphism which led to re-crystallisation (Vermeulen, 2001). The conglomerates vary from fresh to highly weathered and oxidised state (Stanley, 1987). Both the mineralogy and state of weathering of the ore bearing rocks determine the properties of the resulting tailings materials. Table 2.1 summarises the mineral composition of typical gold and uranium bearing conglomerates.

2.2.3 Production of Tailings

Tailings are produced when ore-bearing rocks, conglomerates in the case of gold tailings, are ground to a rock flour which is the required particle size in order to efficiently liberate the mineral valuables from the ore which are extracted using metallurgical processes. The metallurgical processes and ore-dressing techniques entail the use of various chemicals to enhance the processes but as a result some of the chemicals form part of the residue rendering tailings into a finely ground and chemically treated rock flour (Vermeulen, 2001). The tailings fluid or liquor is a combination of various chemicals.

Table 2.1: Mineral composition of a typical Witwatersrand gold reef (Stanley, 1987)

Mineral	Abundance
Quartz (SiO_2), primary and secondary	70-90%
Muscovite and other phyllosilicates	10-30%
Pyrites	3-4%
Other Sulphides	1-2%
Grains of primary minerals	1-2%
Uraniferous Kerogen	1%
Gold	~45 ppm in the Vaal Reef & Ventersdorp Contact Reef

The tailings considered in this thesis consisted of waste products extracted from ore-bearing rocks as well as "second generation" tailings resulting from the re-mining of existing tailings dams. Figure 2.3 depicts the tailings generation process from ore while Figure 2.4 outlines the re-mining of tailings dams to produce new mine tailings.

The production of tailings from source rock comprise three main stages which are the ore-winning processes (drilling, blasting and separation), the ore-dressing stage (crushing, grinding, milling and particle size or particle density classification) and the metallurgical extraction stage where cyanidation has replaced amalgamation.

The waste rock as seen in Figure 2.3 resulting from deposits overlaying the bearing rocks and barren rocks are deposited as waste rock dumps and these fall outside the scope of this research. The ore-dressing stage is the most important stage that determines tailings properties. The multi-stage crushing encompassing the preliminary, the primary, the secondary and the tertiary crushing stages begins the determination of particle size properties in the tailings material. The grinding and milling that follows together with the separation of particles by size and by density facilitated with the use of screens and hydro-cyclones initiates sorting and segregation of tailings materials. It is also at the ore-dressing stage that chemicals are introduced into the

tailings in the form of flocculants the most common of which is lime and other organic compounds.

Overall the nature of the ore body and the tailings generation process greatly influence the properties of the resulting tailings. The mineralogy and weathering state of the source rocks mostly determine tailings mineralogy. The tailings produced from weathered rocks will differ from tailings arising from fresh rock in terms of the minerals each tailings type contains whereby weathered rock tailings would comprise of more secondary minerals as well. The ore-dressing stage plays a major role in determining the particle size characteristics of the tailings. By the time the metallurgical processes stage is reached, the key tailings properties have largely been formed and this stage has an insignificant effect on tailings properties.

The re-mining of tailings dams as shown in Figure 2.4 commences with dissolution of tailings from an existing disposal facility into a slurry using high pressure water jets (25-30 Bars) emitted from monitor guns. The slurry is transported by means of pumping through pipelines and is screened for foreign matter prior to being thickened for the process plant stage where the mineral valuables are concentrated and extracted leaving behind tailings which are hydraulically deposited (Robinson, 2008).

It is noticeable from Figure 2.4 that the re-mining of tailings dams to recover residual valuables from existing tailings dams as an ore body does not alter the gradation and mineralogical content of the original tailings. It is evident however that more water is added to the tailings as well as additional chemicals in the process plant stage especially when other valuables in addition to gold extraction such as uranium recovery and the production of sulphuric acid is targeted.

Once again the result of mining and mineral processing which is a mixture of ground rock flour particles and mine liquor in the form of slurry is ready for disposal.

2.3 Tailings Disposal Methods

2.3.1 Introduction

The tailings resulting from the mineral reduction processes are in a slurry form and can be disposed of either in the "wet" or "dry" state. Dry state in the context of this study means tailings with a negligible moisture content which will not allow for the tailings to be pumped. Disposing of tailings in the dry state require removal of the bulk of the water from the slurry prior to disposal which would entail expenses in dewatering and drying processes as well as the transportation of dry tailings. The wet disposal of tailings on the other hand is the preferred option owing to the relatively cheap option of pumping milled tailings slurry or paste through pipelines to a disposal site. This section describes tailings disposal methods based on the historical development of tailings dams proposed by Cincilla et al. (1997), followed by classification of tailings disposal methods using type of topography, wall development system and deposition system as classification criteria. The section concludes with the importance of using the classification approach as adopted under this study for tailings disposal methods.

2.3.2 Historical Development of Tailings Disposal Methods

Cincilla et al. (1997) have traced the historical development of "wet" disposal of tailings which they categorised into four generations of tailings management practice. Using the four broad historical categories of tailings disposal methods advocated by Cincilla et al (1997) together with the elaborations on the four generations of wet tailings disposal methods advanced by Robinson (2008), the evolution of disposal methods can be summarised as shown in Figure 2.5.

The first generation disposal methods entailed uncontrolled or free discharge of tailings. The second generation facilities deposited tailings into preformed impoundment walls built with imported materials other than using tailings. The third generation methods applied engineering principles to tailings as a construction material with the main objective of designing a structure out of the tailings material itself. The fourth generation methods emphasised the reduction of water in the tailings slurry as a material first before the deposition of the tailings (Cincilla et al., 1997 and Robinson, 2008).

The main emphasis of this study is on third and fourth generation tailings disposal methods but excluding the use of paste tailings technology. It is for these methods where the disposal of tailings into embankments built mainly of tailings materials that rate of rise of tailings dams become more important together with the associated effects of particle size segregation and the generation of excess pore water pressures.

2.3.3 Tailings Dams Classification

The classification of tailings disposal methods using the historical development approach as the only criterion is limited and lacks details on tailings disposal methods as we know them today.

Several workers (Legge et al., (1982); Vick, (1983); Fell et al., (1992); Chamber of Mines of South Africa (1996) and Blight (2010)) have published articles and tailings dams' guideline manuals detailing descriptions and classification of tailings dams which have presented tailings disposal methods under various subheadings and classes. The various publications have used different classification terms such as tailings deposition methods, tailings construction methods, tailings operational systems, methods of tailings discharge, tailings embankment dam types etc. in their descriptions. It has been observed that the various terminologies used actually refer to the same aspects of tailings dam disposal methods. The use of many different terms has not only clouded and masked the interrelationships of concepts used in tailings disposal methods but has also led to the use of inconsistent terminology in the industry. A need to harmonise the use of tailings disposal methods terminology is discernible from the comparative study of tailings literature as presented in the main published literary works of mine tailings and tailings dams aspects by the above cited works as well as in other works which use the above listed publications as original sources.

Robinson (2008) has presented an orderly and unified approach which utilises various criteria or "definers" of tailings dams to classify tailings disposal methods. The approach is adopted for this study because of its clarity of presentation which brings different descriptive aspects of tailings dam disposal methods together. Figure 2.6 depicts the approach. The three criteria used to bring together and classify different aspects of tailings disposal methods are the

topography based dam classification, the wall development and deposition system based criteria.

Using the topography of the site as a first criterion, tailings dams are divided into valley dams, side hill dams and ring dyke dams. It is noted that the ring dyke dam wall is the appropriate dam type for flat topographies which differ from both valley and hill landscapes. The second criterion of wall development system will be more pronounced for dams constructed on flat topographies. The wall development pattern alternatives include downstream, upstream and centreline as well as hybrids and combinations of the wall development patterns comprising downstream, upstream and centreline patterns. Figure 2.7 shows the three wall development systems whose main distinguishing feature is the direction of the movement of the dam crest during the deposition history of the dam walls. Combinations of the three wall development systems (hybrids) are common which take advantage of the strengths of one system and at the same time mitigate the disadvantages of the other wall development system used within the hybrid method (Vick, 1983; Robinson, 2008; Blight, 2010). Examples of hybrid systems comprising upstream and downstream wall development systems are given in Legge et al., (1982), Fell et al. (1992) and Blight (2010). Fell et al. (1992) compared and contrasted the essential features of each wall development system relative to the other with the upstream system flagged as the most risky. Table 2.2 adapted from Vick (1983) summarises the comparisons of the three wall development systems.

In dry and semi-arid environments where there is sunlight induced evaporation which exceeds precipitation (Blight, 2010), special case wall development systems have evolved over the past hundred years with the South African gold mining industry pioneering the developments (NBRI report, 1959; Mrost,1974 and Robinson, 2008). Two main wall development systems under this category are the paddock dams previously known as daywall and nightwall dams and the hybrid dam system which evolved from the earlier day and night wall development systems.

The paddock dams are described in detail in NBRI report (1959), Mrost (1974), Wates (1983), McPhail and Wagner (1989) and Robinson (2008). The typical paddock dam wall development system is shown in Figure 2.8. The paddock dams comprise depositions of thin 150mm to 200mm thick layers of tailings slurry deposited successively onto 12m to 30m wide enclosures

around the tailings dam exterior during the daytime when adequate site supervision was available to observe and monitor tailings behaviour.

Table 2.2: Comparisons of wall development systems (after Vick (1983)

Wall Development System	Mine Tailings Requirements	Water Storage Suitability	Seismic Resistance	Rate of Rise Restrictions	Relative Embank-ment Cost
Upstream	High Sand content segregating tailings	Not suitable	Poor	5-9m/yr desirable. >15m/yr hazardous	Low
Downstream	All tailings	Good	Good	None	High
Centreline	Sands or low plasticity slimes	Temporary storage possible	Acceptable	May apply to individual raises	Moderate

The deposited layers of tailings slurry is allowed to settle, and water is decanted because of the tailings dam slope towards the pool area and allowed to gain strength through sun drying before subsequent layers are deposited. Some of the settled and dried tailings were then used to form the paddock walls. The deposition of slurry on the daywall is carried out progressively around the perimeter of the dam with a rest period of two to three weeks between successive depositions at a given location. During the night time when there is not sufficient site supervision, the tailings slurry is deposited into an inner wall of about 45m width constructed in-between the daywall and the pool area of the tailings dam. This latter deposition comprised the nightwall. Figure 2.9 shows this wall development system. The paddock wall development system utilised the open ended discharge slurry deposition outlet system (Robinson, 2008). The hybrid paddock system which is widely used today entails the use of spigotted tailings slurry as well as the omission of a nightwall whereby all deposition beyond the daywall is placed into the interior of the dam or the nightpan. Under the hybrid systems the night time deposition of tailings is placed anywhere beyond the daywall in the absence of a nightwall (Robinson, 2008).

The daywall-nightpan paddock system is described in many works including McPhail and Wagner (1989), Priscu (1999) and Blight (2010).

The third and final definer of tailings dams as shown in Figure 2.6 is the deposition system criterion. The deposition of tailings could be carried out under water (subaqueous deposition) or in air (subaerial deposition). Each deposition system would result in tailings with different engineering properties arising from the respective deposition systems. In general the sub-aerial deposition result in stronger more stable tailings structure while the subaqueous deposition result in loose saturated low strength tailings material (Blight, 2010).

While the subaqueous and subaerial deposition systems classification approach considered the medium within which the tailings slurry were deposited as a classification criterion, the deposition system as a definer of tailings dams can also be considered from the point of view of the type of outlet that discharged the tailings when it was deposited. From this point of view, tailings dams can be categorised as open end discharged tailings, spigotted tailings and on-wall cycloned tailings. In the open-ended discharged tailings a pipe outlet is used to discharge either slurry, cycloned tailings fractions (overflow and underflow) or their combination or even thickened tailings. The different materials discharged from the pipe lead to tailings dams with varying engineering behaviours arising from the differing materials deposited. Spigotting involves the discharge of tailings through more than one exit point as opposed to the single discharge under open-ended deposited tailings. Spigotting is effected through the use of either multiple pipe discharge points or through the use of spray bars. Spigotting leads to more segregation of the deposited tailings causing the coarse material to be deposited close to the daywall and the fine material further down the beach.

The use of hydrocyclones located on the tailings dam walls falls under a third deposition system which is effected when the relatively coarse tailings fraction is deposited on the dam wall while the fine tailings fraction is deposited on the tailings dam beach area. The cyclone separates the whole tailings into a coarse and a fine fraction through the use of centrifugal force (Vick, 1983; Stanley, 1987; Fell et al., 1992; Blight, 2010). Figure 2.10 adopted from Blight (2010) demonstrate the on-wall cyclone deposition system as used on tailings dams.

It is to be noted in Figure 2.10 that the feed whole tailings material that enters the hydrocyclone tangentially under pressure is split into two size fractions. The coarse particles with very little

water content are thrown to the outside of the cyclone where it spirals downwards and exits at the apex or spigot as "underflow". The fine particles with most of the water moves towards the centre of the cyclone and upwards where it escapes into the finder and is then deposited as "overflow". Figure 2.10 also indicates a typical split of whole tailings in terms of mass of solids and mass of water. The proportions are reported to be influenced by pressure of slurry feed, length and angle of the cone, length of vortex finder and diameter of the spigot (Steenkamp et al., 2008 and Blight, 2010). The cyclone deposition can be applied to upstream, downstream and centreline wall development systems and their various combinations (Blight, 2010 and Legge et al., 1982).

It is worth noting that cycloning does not work very well for uniformly graded materials such as gold tailings. Steenkamp et al. (2008) stated that based on their experience, materials that can be efficiently cycloned for wall building purposes should have about 20% of their particles coarser than 75μm.

2.3.4 Nomenclature of Tailings Disposal Methods

Robinson (2008) cautions tailings dam practitioners against the use of abbreviated names for tailings dams which obscures and omit important descriptive components of the dam building process. He noted that the use of terms such as valley dams, spigotted dams, impoundment dams, cycloned dams and paddock dams as is common practice is not satisfactory since by not using a full and more useful description like a multiple discharge hand packed upstream ring dyke impoundment with a fixed penstock; or describing as a cycloned dam an upstream cycloned valley dam with a floating decant, the abbreviated shortened name discards the other descriptive parts of a dam's make up. The value of the use of full descriptive names especially in technical reports cannot be overemphasised.

A consideration of both Figures 2.5 and 2.6 highlights the shortcomings of the abbreviated nomenclature for tailings dams which highlights only one aspect of a tailings dam building process to the exclusion of the other equally important factors such as the generation of the tailings method, the topography, the wall development system, the deposition system as well as the manner of decanting the supernatant water from the pool area. All the above listed

aspects of the tailings dam are important for understanding tailings dams which is critical for their management and upkeep.

From the point of view of tailings disposal methods, this study will amongst others focus on third and fourth generation tailings dams as indicated in Figure 2.5. The study will consider ring dyke or raised embankments, upstream and centreline wall development systems and their combinations including special case dam methods. All the deposition systems entailing open-ended discharged tailings, spigotted tailings and on-wall cycloned tailings will also be of interest to the research.

Figures 2.5 and 2.6 taken with Table 2.2 delineate aspects of tailings dams that are relevant to rate of rise of tailings dams and its bearing on the development of excess pore water pressures. The next sections of the literature review consider rate of rise of tailings dams and consolidation of tailings materials.

2.4 Rate of rise of tailings dams

2.4.1 Introduction

Rate of rise of tailings dams in the context of this study refers to the vertical increase in the height of a tailings dam over a period of time measured in meters per year (m/yr). Rate of rise in its most common use for tailings dams entails the rate of building a tailings dam component which could be the building up of dam walls or dam beaches. For this study the emphasis is on building dam walls with settled, consolidated and sun-dried tailings solid particles which could be fully saturated, partially saturated or dry. Rate of rise is thus viewed as a specific parameter of tailings dams. This section summarises literature on rate of rise of tailings dams with specific reference to the aim and objectives of the research work which relates rate of rise to both tailings segregation and generation of excess pore water pressures within tailings materials. It commences by defining rate of rise, followed by the application of rate of rise to tailings dams and concludes by exploring any limiting factors on rate of rise with specific emphasis on the generated excess pore water pressures when tailings are deposited at varying rates of rise.

2.4.2 Rate of Rise (RoR)

In the published literature rate of rise of tailings dams has been referred to as the raising rate of tailings dams (Vick, 1983) , the dam heightening rate (Priscu, 1999) and the rate of dam construction (Jones and Wagener, 1996) amongst other terms used. Wates (1983) defined maximum rate of rise as the deposition rate that allows a low enough cycle time on the dam's day paddocks to facilitate drying out of the tailings. McPhail and Wagner (1989) expressed the view that rate of rise is a term that is applied to describe and quantify the controlling influence of drainage and consolidation on a tailings dam. More specific definitions of rate of rise of tailings dams are given in Vermeulen (2001) and Robinson (2008) in which the emphasis is on the more prevalent and reasonable view of rate of rise as the change in dam height over time. Robinson (2008) differentiated between three types of rate of rise of tailings dams which were listed as average rate of rise, cumulative rate of rise and current/annual rate of rise. Robinson (2008) further discussed the concepts of an allowable, a restricted and a limiting rate of rise.

An examination of the various definitions of rate of rise has revealed the use of different terms to describe the same concept by several workers. The definitions also reveal different approaches used for specifying rate of rise. On the one hand the physical phenomena which make up rate of rise is used as the object of the definition such as the use of dam height over time. On the other hand, other workers emphasize the mechanics that contribute to rate of rise as the basis for defining rate of rise. The use of cycle time and deposition rate in defining rate of rise is instances of this practise. Of more importance some of the definitions of rate of rise demonstrate a failure to differentiate rate of rise from deposition rates and slurry discharge rates. It is believed that for rate of rise to remain a significant parameter that describes the critical aspect of height increase of tailings dams over time, rate of rise ought to be separated from slurry deposition rates and tailings discharge rates. Both slurry deposition rates and tailings discharge rates take place when tailings solids form initially under sedimentation and the early stages of consolidation. Both processes though related to dam height differ significantly from dam height increase over time which is rate of rise. Rate of rise also must be distinguished from the general rate of discharge of tailings materials from processing plants into tailings dams because it is only after such materials have undergone sedimentation, consolidation and desiccation that rate of rise becomes a key parameter that captures the specific height increase over time of a tailings dam.

2.4.3 Application of Rate of Rise in Tailings Dams

The construction of tailings dams started over a hundred years ago and is still largely based on experience (NBRI report, 1959; Donaldson, 1973; Robinson, 2008). Donaldson (1973) reported that the first engineering study on the construction of tailings dams was carried out in 1953 following a then past history of fifty years of dam construction using only previous experience. It has emerged from the 1953 - 1959 study that rate of rise was not a specific concern at the time of that investigation. However in addressing the need to understand the processes through which tailings dam wall stability was achieved, the 1959 study recommended that on the basis of experience a 50mm thick layer of settled tailings solids be deposited fortnightly to guarantee sufficient strength gain through sun-drying of mostly gold tailings. This recommendation translated into a rate of rise of 1.32m/yr and an approximate slurry deposition layer thickness of about 100mm.

The South African Chamber of Mines (1996) stated that in order to allow adequate sun-drying of tailings required for the stability of tailings dams, a rate of rise of a tailings dam has to be limited to 2-3 m/yr. Robinson (2008) cites rules of thumb maximum rates of rise applied by the mining industry of the order of 1.0m/yr to 2.0m/yr for tailings slurries and up to 6m/yr for cycloned coarse tailings. A stipulated rate of rise limit of 2-3m/yr corresponds to a deposition of gold tailings slurry of thickness of between 150mm to 200mm (or even up to 300mm thickness) every two weeks which approximates a solids slimes (materials smaller than 63µm in size) settled layer of about 100mm thickness. It is apparent that the stipulated rate of rise limits quoted in literature cannot be traced to any specific rational scientific derivation.

Vick (1983) has specified desirable rates of rise for upstream tailings dams of between 4.6m/yr and 9.1m/yr but warns against rates of rise exceeding 15m/yr. Vick (1983) maintained that rate of rise is not limited in any way for both downstream and centreline dam construction systems in general.

Wates (1983) defined rate of rise in terms of relative density (specific gravity of tailings slurry) and cycle time for slurry desiccation through sun-drying. He reiterated the South African Chamber of Mines (1996) Guideline's recommendation that for gold and uranium tailings dams in the Transvaal and Orange Free States gold fields, a maximum rate of rise of 2.5m/yr was to

be observed. Wates (1983) believed that cycle time rather than rate of rise was the controlling factor for tailings dam stability. He argued that it was the amount of water in the tailings or moisture content and therefore the tailings slurry specific gravity (relative density) that mattered most. He believed that it was the time it took to dry out the water within the tailings slurry (cycle time) that controlled tailings dam stability concerns and consequently rate of rise. The argument was further advanced that shortening the cycle time (required for the desiccation of tailings by the adjustment of paddock dimensions), cycloning of tailings, and deposition by spigotting and dewatering of slimes (which all varied the slurry specific gravity (relative density) and moisture content of tailings) all tended to allow a higher rate of rise.

On the basis of data obtained from experiments conducted at Jones and Wagener offices on Vaal Reefs slimes (Jones and Wagener reports, 1996), Wates (1983) derived a rate of rise and tailings slurry specific gravity design chart shown in Figure 2.11. The design chart captured the argument that desiccation of slimes consolidated the tailings thereby making the tailings trafficable for wall building purposes as well as reducing the permeability anisotropy ratio of tailings materials. The argument went further that the anisotropy ratio assisted to limit the recharging of the phreatic surface within the tailings dam walls.

Figure 2.11 shows the variation of rate of rise with the specific gravity of tailings slurry (relative density) which is related to cycle time of tailings desiccation for varying conditions and given parameters on the chart (dolomite foundations, normal operating conditions for tailings dams and optimal dam building procedures). Figure 2.11 serves as a tailings dam design guide as well as a tool for sizing of tailings dams (McPhail and Wagner, 1989).

Blight (1969) investigated the slope stability of gold tailings dams in relation to the rate of rise of dams. McPhail and Wagner (1989) list factors that influence slope stability of tailings dams as foundation soils [grading, Atterberg limits, permeability, consolidation characteristics, shear strength], properties of the tailings product (grading), rate of rise, position of the phreatic surface and slope geometry. Blight (1969) on the contrary derived design charts for tailings dams considering only foundation soils permeability, rate of rise and slope angle which are shown as Figures 2-12(a) and (b). According to Blight (1969) the rate of rise and slope stability design charts were based on the Bishop type of slip circle theory of slope stability analysis and specifically utilised the method of stability analysis of normally consolidated clay slope proposed by Gibson and Morgenstern (1962). The slope stability analysis was coupled with the

assumptions that the slope was a cutting in a normally consolidated soil with the water table at the surface, whereby failure took place through the slimes with the foundation soils not involved and with a factor of safety of 1.5 applied. It needs to be noted that the 1959 NBRI tailings investigation report recommended a slimes dam factor of safety of 1.5 as well.

Based on Figures 2.12 (a) and (b) tailings dams of specified heights could be constructed at different rates of rise for slope angles of up to 40°. McPhail and Wagner (1989) noted that the small change in slope angle of between 2° and 6° corresponded to very large increases in dam height and dam capacity respectively. In other words, on average the design charts yielded a height increase of between 8m and 14m for a small change in slope of only 4°.

Donaldson (1973) had observed that based on the rate of rise design charts of Figures 2.12(a) and (b) produced by Blight (1969) a tailings dam could be built at a slope angle of 30° at a rate of rise of 3m/yr for a height of up to 40m. He further made the statement that according to the same design charts where side slopes of 18° were adopted to enable the use of mechanised equipment to maintain tailings dam surfaces that dams built on impervious bases using the design charts could be constructed to unlimited heights at rapid rates of rise. The latter statement could however not be verified using the published charts which cover side slopes from 30° to 40°.

Whilst the rate of rise design charts generated by Blight (1969) are quite useful in tailings dam design, a shortcoming of the design charts is their lack of making a distinction between rate of rise of tailings dams and rate of deposition of slurries in a tailings dam. Rate of rise and deposition rates are quite different in their magnitudes as well as in terms of the processes that tailings materials undergo from the slurry phase. After tailings deposition and sedimentation, deposition rates result, while in contrast all the processes of tailings formation up to the sun-dried tailings should have taken place in order for the placement rate of tailings to characterise rate of rise of tailings dams.

Figure 2.13 illustrates typical differences between deposition rates and rate of rise in terms of differences in the respective void ratios of a tailings material following deposition and that of a tailings that was extracted from a dam wall that was built at given rates of rise. It is observable from Figure 2.13 that at a consolidation pressure of 25kPa equivalent deposition stage void ratio of 1.45 obtains while for sun-dried tailings state the corresponding void ratio would be

0.8. The height of tailings solids at void ratios of 1.45 and 0.8 differ considerably for a given time making the deposition rate in m/yr to be much greater than the rate of rise in m/yr for a given tailings product.

The South African Chamber of Mines guidelines (1996) noted that whilst from a practical point of view, a limited rate of rise of 2m/yr was imposed by the need for the tailings material to dry under the sun, higher rate of rise for the same tailings were feasible based on theoretical considerations of the coefficient of consolidation of the tailings. The Chamber of Mines (1996) guideline reported that by applying Gibson's (1958) theory of consolidation of a deposit that increases in height at a constant rate over time, a safe rate of rise could be determined. Blight (2010) and South African Chamber of Mines (1996) guideline published modified Gibson's (1958) theory based consolidation and rate of rise design chart which is shown in Figure 2.14. Figure 2.14 is based on consolidation theory and relates degree of consolidation at various depths of tailings dams for specified rates of rise. The design charts catered for tailings dams constructed on both impervious and pervious foundations.

It is to be noted that this later approach of the application of rate of rise to tailings dams which incorporates consolidation theories allows for the evaluation of excess pore water pressures within a tailings dam and their correlation with rate of rise which the earlier approaches lacked. However a major weakness of the approach as currently presented lies again in the approach not making a distinction between deposition rates (m) of tailings slurry and rate of rise (RoR) of tailings dams. The claim made in the South African Chamber of Mines guideline (1996) that the consolidation approach offered a higher rate of rise than the practical experience based sun-drying rate of rise could be attributed in part due to the fact that the consolidation approach yielded a deposition rate (m) while the experience based method resulted in a rate of rise (RoR). Deposition rate (m) and rate of rise (RoR) are two different values all together.

The rate of solids accumulation under Gibson's (1958) theory of a layer that accretes over time has been reflected differently by other authors who view it as a deposition rate rather than as rate of rise of tailings dams. Mittal and Morgenstern (1976) for instance refer to the solids accumulation as deposition rate or sedimentation rate which is the same term used by Gibson (1958) in his derivation. Tailings consolidation together with tailings formation processes and their relation to rate of rise will be discussed later in this review.

2.4.4 Rate of Rise and Excess Pore Water Pressures

It can be observed from the preceding sections of this chapter on rate of rise of tailings dams that rate of rise is affected by many factors. These factors include sedimentation rates and deposition rates, cycle time and specific gravity of tailings slurry (Wates, 1983), sun-drying desiccation, tailings dam foundation drainage conditions, tailings consolidation characteristics, tailings dam wall development systems (Vick, 1983), particle size and grading properties of tailings and the seepage regime of tailings dams. It is equally apparent that the above listed factors which affect rate of rise of tailings dams have a lot to do with the amount of water in the tailings material as noted by Wates (1983). One would expect therefore from a superficial theoretical standpoint that loading a tailings material filled with water should generate excess pore water pressures (Gibson et al., 1989) within the tailings. The dissipation of the excess pore water pressures from the tailings would be dependent on the consolidation and permeability properties of the tailings as well as on the prevailing boundary conditions governing drainage characteristics of the tailings system under consideration.

Priscu (1999) noted that as a tailings dam increased in height under normal conditions loading occurred slowly enough for load induced pore pressures to dissipate but cautioned that when dam heightening was fast, excess pore water pressures build up would occur which threatened dam stability. There is therefore an implicit linkage of rate of rise and excess pore water pressures with excess pore water pressures limiting the rate of rise beyond which dam construction would not be safe. Vermeulen (2001) also pointed out that rate of rise was a restraining factor of impoundment storage capacities but also added that should a tailings structure rise too quickly the development of pore pressures in excess of equilibrium levels can adversely affect stability of impoundments constructed from low permeability tailings products. Here again the reasoning is that a rate of rise exists at which equilibrium excess pore water pressures are generated which correspond to stable impoundment wall construction and that beyond the equilibrium levels, excess pore water pressures would be generated which would threaten dam stability and safety, consequently the rate of rise responsible for such high excess pore water pressures would have to be restrained. Stated differently it is implied that excess pore water pressures limit rate of rise. Papageogiou (2004) was more explicit when he noted that rate of rise is limited as the beach requires sufficient time to consolidate and for excess pore water pressures to dissipate to form a stable foundation for the overlying tailings.

Stauffer and Obermeyer (1988) as well as Martin (1998) also reported correlations between excess pore water pressures and rate of rise in tailings dams. The above scenario describes a traditional view that has been accepted as true without thorough investigation. This has led to a blanket belief that excess pore water pressures limit rate of rise of tailings dams.

2.5 Formation Processes of Tailings from Slurry

2.5.1 Introduction

Tailings solids stored within tailings impoundments were formed when slurries discharged from mineral processing plants delivered through pipelines were hydraulically deposited, then settled and consolidated which culminated with the desiccation of the tailings materials. The formation of tailings from slurries are quite complex in terms of the physical processes involved when a slurry flows into a tailings dam up to the point when tailings solids settle as well as from the point of view of the different stages and aspects of the settling processes and how they relate to each other.

From the point of view of the physical processes taking place on a tailings dam, the incoming slurry is subjected to gravity settling by size and density. The slurry is transported along the surface of the tailings dam where it undergoes deposition and settling through sedimentation both laterally and vertically as the slurry flows from the tailings dam walls where it is discharged through the dam beach towards the pool area. As the tailings slurry flows along the beach, the slurry could undergo flocculation, segregation or both, followed by sedimentation before the tailings sediment is subjected to self-weight consolidation. In most cases the tailings deposits are further subjected to desiccation through evaporation and sun-drying.

This section discusses the tailings formation processes. The section gives a summary of the processes taking place with a focus on sedimentation and consolidation which are relevant to the objectives of this study.

2.5.2 Settling Processes

In the context of this study settling processes include particle settling, flocculation, segregation, sedimentation, channelling and consolidation in that order all of which are interrelated with some of the processes occurring simultaneously (Jeeravipoolvarn, 2010).

Figure 2.15 adopted from Pedroni et al. (2006) who modified the work of Imai (1981) shows the interrelationships between the different components of the settling process. The settling processes in Figure 2.15 are summarised in the works Schiffman et al. (1988) and Imai (1980) among others. A summary of some of the works which was compiled as part of this research work can be found in Lebitsa et al. (2009).

It is noted that both the work of Imai (1981) and that of McRoberts and Nixon (1976) show that the settling plots for sandy materials and those for clay-water mixes differ. Figure 2.16 shows an idealised settling plot for sandy material which differs from Figure 2.15 for clayey mixes by the absence of the flocculation stage as well as the sandy material displaying linear settling rates as opposed to curved settling plots for clayey materials.

Based on the research on settling processes which goes beyond the past hundred and fifty years as reflected in Burger and Wendland (2001), a general classification of settling processes depicted in Figure 2.17 have been adopted for this study. In Figure 2.17 settling processes have been divided into free settling and hindered settling categories which are dictated by the concentration of the solids within the settling suspension. Table 2.3 adopted from Imai (1980) summarises the different settling types.

Published works by Ward and Kammermeyer (1940), Work and Kohler (1940), Michaels and Bolger (1962), McRoberts and Nixon (1976), Imai (1980) and Lui and Lohnes (1984) demonstrated a trend of settling plots from free settling to compression settling with increasing concentration of solids and that as the concentration of the dispersion gets higher the settling velocity of the interface was lowered.

It can be observed from Figure 2.17 and Table 2.3 that settling processes can be distinguished from each other by their solid concentration levels and their solids-liquid flow governing

mechanisms. Free unhindered settling takes place when discrete individual particles settle independently under very low solids concentration (discrete settling). Kenimer et al. (2005) have noted that when individual particles stick together into flocs under a relatively high solids concentration facilitated by chemical and biological reactions which enhance particle attachment flocculent settling occurs. Under hindered settling, the solids concentration is high enough for the particles to interfere with each other's movements as well as to inhibit water movement which is confined to flowing through the tortuous paths in between the solid particles or around the particles. Depending on the relative solids concentration amounts in the suspensions, hindered settling can be further subdivided into zone settling, channel settling and compression settling as shown in Figure 2.17.

Table 2.3: Summary of characteristics of different settling types

Settling Type	Description
Dispersed Free Settling	Particles do not flocculate but disperse and settle freely without interactions. Coarse particles settle faster than fine particles. Segregation takes place. Stokes's Law settling taking place.
Flocculated Free Settling	Flocs of different sizes formed and settle freely per their varying sizes. No sharp interface formed.
Zone Settling	Flocs are formed and settle with strong interaction among them. Sharp interface formed and settling rate constant. Hindered settling scenario.
Consolidation Settling	Visible flocs not formed. Mixture settles as a whole due to consolidation. Compression settling and channel settling scenarios.

Burger and Wendland (2001) and Kurt (2006) in their respective works gave a good description of zone settling. Burger and Wendland (2001) attributed the origin of the identification of the four different zones that comprise zone settling to the work of Coe and Clevenger (1916) who reported settling experiments on various materials. The authors stated that zone settling was associated with flocculent suspensions. Figure 2.18 shows the four components of zone settling

in typical batch settling experiments which are directly related to settling column tests. In Figure 2.18 Kurt (2006) summarised batch settling in a five stage settling process. Kurt (2006) captured zone setting as follows: "zone A, is a region of clear fluid. Zone B (the hindered settling zone) is a uniform concentration zone that has the same concentration and distribution as the initial concentration. Zone C (the transition zone) is the boundary between the hindered settling and compression zones. It is a region of non-uniform concentration. Zone D (the compression zone), consists of networked solids. Channels occur through the compression zone. The fluid that is entrapped during the settling process in zone D is forced out as it compresses."

In a segregating suspension the sediment zone of the settling process would comprise different segregated layers of the particles deposited during different times of the settling process.

Rhodes (2008) offers a unique view of settling processes and believes there are two main types of settling modes depending on the initial concentration of the suspension. Figure 2.19 gave the range of initial concentrations of a multiple particle suspension for each type of settling mode. In Figure 2.19, C_{B1} is the suspension concentration at the intersection point between projected line of tangency and particle flux plot (plot of particle superficial velocity versus particle concentration). This is the concentration below which Type 1 settling would take place. C_{B2} is the concentration at the point of tangency. The two types of settling are shown in Figures 2.20 and 2.21 which illustrate the two settling types in terms of the settling zones formed and the resulting settling plots. Figure 2.21 (settling type 2 plot) is in agreement with the presentation by Kurt (2006) shown in Figure 2.18. In both these figures four similar zones are identified with the variable zone labelled as zone C (Kurt, 2006) and as zone E (Rhodes, 2008).

At very large solids concentrations of suspensions the solid particles or their flocs are in contact with each other and therefore the solids within the suspension settle *enmasse*. During the process the particles settle by compressing and consolidating the mass below them (compression settling). Tory and Shannon (1965) in their study of compression settling using calcium carbonate slurries found that in compression settling the elimination of fluid from the compressed mass is a function of time (thinking permeability in geotechnical engineering terms) and not concentration dependent as in the free settling scenario. Channel settling occurs at solids concentrations intermediate between zone settling and compression settling solids concentration levels. In the case of channel settling the fluid escapes through the sediment

forming flow paths (channels) in the process. Zone, channel and compression settling as noted before can be differentiated by their settling plots as shown in Figure 2.22.

It is important for the current study whose emphasis is rate of rise of tailings dams together with both particle size segregation and excess pore water pressure development that both sedimentation and consolidation be reviewed in detail. The two processes are the main components of the settling process which is of interest to particle size segregation, excess pore water pressure development and rate of rise of tailings dams. The two processes of sedimentation and consolidation are thus considered further in the remaining parts of the literature review.

2.5.3 Sedimentation

Introduction

American Society of Civil Engineers (ASCE) manuals numbers 54 and 110 of Engineering practice on sedimentation engineering (Gottchalk, 2006 and MacArthur et al., 2008) define sedimentation in its broadest sense as embodying the processes of erosion, entrainment, transport, deposition and compaction of sediments through either water, wind, gravity or ice as sedimentation agents. Publications in sedimentology by Twenhofel (1961), Leeder (1982), Selley (1982) and Lewis (1984) also follow similar definitions. In geotechnical engineering publications, however, definitions of sedimentation range from sedimentation as the all-encompassing process of settling, sediment formation and consolidation (Imai, 1981) to the more refined definition of sedimentation as the settling of grains in a slurry or a suspension that behaves like a fluid in which there is no effective stress (Tan et al., 1990).

Rhodes (2008) defines sedimentation from a particle technology point of view as settling of particle suspensions. Under this study, sedimentation is taken as the settling of solid particles or groups of particles in a fluid under the influence of gravity. The definition is inclusive of the movement of a fluid relative to the solid particles as well. Sedimentation therefore is viewed in line with Figure 2.15 where sedimentation is the settling of solids immediately preceding or concurrent with flocculation but ending at the commencement or just overlapping with consolidation of the sediment. It is believed that flocculation precedes sedimentation only when the fine solids in the suspension are clayey in nature. In other words it is when the fine particles

include clay minerals that flocculation is significant. Where the solid particles in the suspension have a low plasticity, flocculation is not expected to be significant even when there is an abundance of fine particles in the suspension which are not of a clayey nature.

Richardson et al. (2002) drew a distinction between fine particle sedimentation, coarse particle sedimentation and two components mixture sedimentation. They hinted that a study of two component mixture sedimentation could be used to understand sedimentation of a complex mixture such a multi-sized particles suspension similar to that typical of mine tailings. As expected the authors noted that segregation was likely to result in sedimentation involving more than one type of solid particles. The authors noted that there was likely to be flocculation in a suspension of fine particles because of the very high specific surface of the particles but without qualifying the need for the fines to be clay minerals. As for coarse particles with lots of fine particles, Richardson et al. (2002) stated that coarse particles will settle faster through a suspension of fine particles which will settle later leading to segregation. The authors expressed the view that sedimentation is a function of the height of suspension, diameter of the vessel containing the suspension and the concentration of the suspension.

Sedimentation Theories

Sedimentation which forms part of the settling process (Figure 2.15) can be categorised as particulate or free sedimentation which occurs at a low particle concentration and hindered sedimentation which takes place under high particle concentration. This classification follows a similar pattern displayed in Figure 2.17 for the more general all-encompassing settling process discussed earlier in this review. Theories of sedimentation have also followed this trend of classification with Stokes's Law representing free sedimentation while Kynch's theory describes hindered sedimentation.

Stokes's law (1851) is shown as Equation 2.1 and represents particulate sedimentation. Kynch's theory (1952) described by Equation 2.2 caters for hindered sedimentation behaviour (Priscu, 1999; Kurt, 2006; Jeeravipoolvarn, 2010).

$$v_s = \frac{\rho_s - \rho_f}{18\eta} g D^2 \qquad 2.1$$

$$\frac{\partial c}{\partial t} + \frac{d}{dc}[c.v_s(c)]\frac{\partial c}{\partial \xi} = 0 \qquad 2.2$$

Where v_s =particle settling velocity

ρ_s =particle density

ρ_f =fluid density

D =Stokes' diameter of particle

η =absolute fluid viscosity

g =gravitational acceleration

c =concentration of solid particles

t =time

ξ =spatial coordinate in vertical direction

The conditions for the derivation of Stokes's law are that the particles are spherical and they fall through a fluid unhindered by their neighbours. The condition requires a low solids concentration and that different particles will fall at different rates dictated by their sizes, densities and shapes which would result in particle segregation mostly into size ranges. A shortcoming of Stokes's law with regards to mine tailings and natural soil deposits however is that the particles are not spherical in shape and that in nature particles tend to fall in groups rather than individually. The scenario in nature therefore is likely to be particles falling in the vicinity of other particles. In light of the above stated difficulty, Richardson and Zaki (1954) modified Stokes's law to cater for a particle falling in a suspension of particles of a given concentration (Leeder, 1982) which is shown as Equation 2.3.

$$v_s' = v_s(1-c)^n \qquad 2.3$$

Where v_s =fall of particle under Stokes' law conditions

v_s' =velocity of spherical particle in a dispersion of grains

c =volume concentration of grains in the falling suspension

D =Stokes' diameter of particle

n =exponent varying between 2.32 & 2.65 depending upon grain Reynolds's number

Kynch's (1952) theory of hindered sedimentation focussed on the continuity of the solid phase even though effective stress was ignored (Priscu, 1999). The theory for the first time produced a partial differential equation (Equation 2.2) whose solution explained the observed sedimentation behaviour (Burger and Wendland, 2001). In addition to other assumptions made to derive the theory, it was assumed that the velocity of particles depended on local concentration only and that all the particles were of the same size. It is reported that McRoberts and Nixon (1976) extended Kynch's theory to a soil with multi-particle sizes thereby relaxing the assumption on all particles being the same size (Tan et al., 1990). McRoberts and Nixon's (1976) work however retained the requirement that the modified Kynch's theory did not allow for particle segregation by adopting a minimum concentration such that segregation does not take place. Priscu (1999) has noted that as the concentration of solid particles in a suspension approached zero in Equation 2.2, the Kynch theory (1952) differential equation reduced to Stokes's law. The Kynch theory was thus a general sedimentation theory with the Stokes's law as one of its special cases.

A more in-depth study and detailed summary of the development of sedimentation theories over the years from the time of Stokes's law (1851) to the present time is provided by several workers including the works by Been (1980), Elder (1985), Burger and Wendland (2001), Bartholomeeusen, (2003) and Kurt (2006).

Particle Segregation

Segregation is a part of the sedimentation process and it refers to when solid particles within a suspension undergoing sedimentation settle separately on the basis of differences in size, density and shape. Particle size segregation is reported to be the most prevalent mode of segregation (Rhodes, 2008). A direct result of segregation is the deposition of sand, silt and clay sized particles at different locations on the basis of their size either laterally or vertically.

Kupper (1991) and Jeeravipoolvarn (2010) list factors responsible for particle segregation as grain size distribution of solids, void ratio, rheological properties of the fines water matrix, type of carrier fluid, type of solids, slurry concentration and flow conditions. Kupper (1991) further emphasised that it was the finer fraction of the solids within the slurry that had a greater effect on segregating properties of slurries. Kupper (1991) and Jeeravipoolvarn (2010) also presented slurry behaviour diagrams similar to Figure 2.23. It was noted that the usefulness of illustrative

diagrams such as Figure 2.23 was in the mix design of tailings products targeted for specific purposes. The diagrams were also of great use in the identification of various slurry property boundaries. Some of the behaviour at boundaries that could be delineated by these diagrams were the segregating and non-segregating boundary, the sedimentation and consolidation demarcation which remains an area of controversy to this day, the liquid phase and solid phase divides in a suspension undergoing sedimentation as well as the separation of saturated from unsaturated states in a tailings product's behaviour. It was encouraging that while the diagrams could be constructed based on routine laboratory test results such as solids content, fines content and the fines-slurry ratio, the diagrams are useful for the characterisation and classification of tailings. The construction of similar diagrams for any given tailings product being managed would be quite useful to industry practitioners.

Several workers (Vick, 1983; Fell et al., 1992; Priscu, 1999; Vermeulen, 2001; Blight, 2010) have documented particle segregation that occurs in tailings dams. In most of the studies it has been reported that there is a general decrease in particle sizes as one moves from discharge points on the dam walls where the coarse particles predominate through the tailings beach area where intermediate size particles are found ending with the fine particles concentrated at the dam pool area. Figure 2.24 adopted from Priscu (1999) summarised the segregation on a tailings dam embankment constructed by the upstream wall development system. Vick (1983) and Fell et al. (1992) also noted that particle segregation has been observed both horizontally along a tailings dam surface as well as vertically across the profiles of the layers of a tailings dam. Both Vick (1983) and Fell et al. (1992) listed Jerabek and Hartman, 1965; Kearly and Busch, 1971; Blight and Bentel, 1983; Blight et al., 1985; and Blight, 1987 and 1988 as some of the researchers who had used laboratory models and experiments to study particle segregation in tailings dams. Various beach profile equations have also been reported in literature with the original concept of a master beach profile credited to Melentev et al. (1973). Most of the beach profile equations are similar in form and there is a general consensus that the equations predict beach profiles, model tailings dams and beach profiles of actual tailings dams reasonably well (Fell et al., 1992; Blight, 2008). Figure 2.25 shows beach profiles for various tailings products based on the form of equation proposed by Blight (1987) shown as Equation 2.4 (Qiu, 2000). Figure 2.25 listed typical values of the dimensionless constant n0.

$$\frac{h_w}{Y} = \left(1 - \frac{H}{X}\right)^{n0} \qquad 2.4$$

Where h_w =pond water level elevation

Y =elevation between point of deposition and the pool liquid level

H =distance along beach from deposition point

X =length of beach from discharge point to edge of pond

n0 =dimensionless constant dependent on tailings characteristics

Segregation of particles from slurries and suspensions has also been observed in settling column tests. Been (1980) and Bowden (1988) have carried out particle size analysis tests on settled sediment extracted from different depths of settling columns and they have demonstrated the variations in particle size distribution at varying depths of the settling column. Both works by Been (1980) and Bowden (1988) depicted variations of gradations with depths from the bottom of the settled column where particles were coarser than the average gradation of the source slurry while gradation of samples from the top of the settled column were much finer than the average slurry particle size gradation curve.

Bowden (1988) emphasised that there should be sufficient height to allow differential settling in addition to other factors needed to cause segregation of slurries such as differences in density, size, shape, particle freedom and independence.

2.5.4 Consolidation

Introduction

Consolidation is the expulsion of pore water from a soil or a tailings material which is associated with the dissipation of excess pore water pressures as well as the resulting settlement that takes place due to the loss of water under imposed loading. Consolidation can take place due to the consolidating material's own self weight acting as a load or due to an externally imposed load.

For this study on tailings dams whose emphasis is on the development of excess pore water pressures under different rate of rise scenarios, the Terzaghi (1923) one dimensional consolidation theory, the Gibson (1958) equation for a clay layer that increases in depth over time and the Gibson et al. (1967 and 1981) finite strain consolidation theories expressed in

excess pore water pressure terms (with excess pore water pressure as the dependent variable) are of great interest. This section therefore addresses the above three consolidation theories. Consolidation is a broad subject that has been extensively researched over the years with more theoretical expressions than those considered for this study. Schiffman (1980), Elder (1985) and Priscu (1999) reviewed some of the different consolidation theories and highlighted interrelationships between the various theories. Research has also demonstrated the need for a link between sedimentation and consolidation theories (Been, 1980 and Pane and Schiffman, 1985).

Terzaghi's One Dimensional Consolidation Theory

In his book *Theoretical Soil Mechanics*, Karl Terzaghi (1943) described the one dimensional conventional consolidation theory he founded in 1923 which heralded the birth of modern soil mechanics (Schiffman et al., 1984; Qiu, 2000). The theory is expressed by Equations 2.5 and 2.6.

$$\frac{\partial u_e}{\partial t} = c_v \frac{\partial^2 u_e}{\partial z^2} \qquad 2.5$$

$$c_v = \frac{k}{m_v \gamma_w} \qquad 2.6$$

Where u_e =excess pore water pressure
t = time
c_v =coefficient of consolidation
z =layer thickness
K = saturated permeability
m_v =coefficient of volume compressibility
γ_w =unit weight of water

In deriving the theory Terzaghi made five main assumptions and three supplementary ones (Terzaghi, 1943). The assumptions included incompressible soil solids and water particles, a fully saturated homogeneous soil in which Darcy's Law is valid and flow was only in the vertical direction. Small strains, constant compressibility and permeability charateristics as well as a unique relationship between void ratio and effective stress which was independent of time were also assumed (Knappett and Craig, 2012). Analytical and graphical solutions of

Equation 2.5 under various boundary conditions are widely reported in literature (Taylor, 1948; Lambe and Whitman, 1969; Dunn et al., 1980; Holtz and Kovacs, 1981; Das, 1983 and Barnes, 2000). Equations 2.7 and 2.8 gave solutions of the classical consolidation theory for excess pore water pressure at a given depth and time (Equation 2.7) as well as the degree of consolidation at given depths and times (Equation 2.8). Figure 2.26 gave a graphical solution of Equation 2.8 depicting the change of degree of consolidation throughout a consolidating layer at given depths and times. In Figure 2.26, time factor, T_v is designated as T.

$$u_z = \sum_{m=0}^{m=\infty} \frac{2u_o}{M}\left(sin\frac{Mz}{H}\right)e^{-M^2T_v} \qquad 2.7$$

$$U_z = 1 - \sum_{m=0}^{m=\infty} \frac{2}{M}\left(sin\frac{Mz}{H}\right)e^{-M^2T_v} \qquad 2.8$$

$$T_v = \frac{c_v t}{H^2} \qquad 2.9$$

Where Z $=\frac{z}{H}$ is non dimensional drainage path ratio

T_v =non dimensional time factor

M $= \frac{\pi}{2}(2m+1)$

m = dummy variable representing the numbers 1, 2, 3,...

H = total depth of clay layer

u_o = initial excess pore water pressure at any depth

u_z = excess pore water pressure at depth z and time t

U_z = degree of consolidation at depth z and time t

Most writers have pointed to the limitations of the classical consolidation theory of Terzaghi (1923) which arise from some of its founding assumptions. These include the assumption of thin layers which limits the theory's use on thick layers, the theory's non consideration of self-weight effects on consolidation, the assumptions of small strains as well as the assertion that both compressibility and permeability of the consolidating material remain constant under a given load increment (Carrier III et al., 1983; Cargill, 1984; Priscu, 1999; Jeeravipoolvarn, 2010).

The above listed assumptions mean that the theory cannot be satisfactorily applied to the consolidation of hydraulically deposited soils, mine tailings and other soft soil deposits in which the loads are mainly the self-weight of the materials, wherein the materials usually comprise thick layers and consequently undergo large strains. Arising from the foregoing both permeability and compressibility of these materials also vary significantly over time.

The above notwithstanding, the classical consolidation theory of Terzaghi (1923) is still widely used in practice even for soft materials such as mine tailings (Blight, 2010). Closely associated with the one dimensional consolidation theory of Terzaghi (1923) is the degree of consolidation, U, defined as the measure of the amount of consolidation which is complete at a given time (Knapett and Craig, 2012). Equations 2.10 through Equation 2.13 illustrate degree of consolidation in excess pore water pressure, settlement, void ratio and effective stress terms. For practical use the term average degree of consolidation designated as $\overline{U}$ is used to represent degree of consolidation across the whole consolidating layer at a given time. Two concepts related to the degree of consolidation which are the remaining excess pore water pressure and remaining excess pore water pressure ratio ($(u_e)_{ratio}$) which are used in the current work are also defined as Equation 2.14.

$$U = \frac{(u_e)_{Dis}}{(u_e)_i} = 1 - \frac{(u_e)_t}{(u_e)_i} \qquad 2.10$$

$$U = \frac{S_t}{S_c} \qquad 2.11$$

$$U = \frac{e_o - e_t}{e_o - e_\infty} \qquad 2.12$$

$$U = \frac{\sigma' - \sigma'_o}{\sigma'_1 - \sigma'_o} \qquad 2.13$$

$$(u_e)_{ratio} = \frac{(u_e)_{Rem}}{(u_e)_i} = \frac{(u_e)_i - (u_e)_t}{(u_e)_i} \qquad 2.14$$

Where u_e =excess pore water pressure

U =degree of consolidation

$\overline{U}$ =average degree of consolidation

S_t	=settlement at time t
S_c	=consolidation settlement
e_o	=initial void ratio
e_t	=void ratio at time t
e_∞	= final void ratio
σ'	= final effective stress
σ_o'	= initial effective stress
σ_1'	= effective stress at time t
$(u_e)_i$	= excess pore water pressure at time t=0
$(u_e)_t$	=excess pore water pressure at time t
$(u_e)_{Rem}$	=remaining excess pore water pressure at time t
$(u_e)_{Dis}$	=dissipated excess pore water pressure at time t

Gibson (1958) Consolidation Theory of Accreting Clay Layer

Gibson (1958) presented a consolidation equation for a clay layer whose thickness increases with time. In the formulation of the theory assumptions similar to those applicable to the classical consolidation theory of Terzaghi (1923) were utilised (Fahey et al., 2010) except that in the new theory by Gibson (1958) the consolidating layer accreted over time. In particular the assumptions of small strains as well as constant permeability and compressibility characteristics were retained while the effects of self-weight of the consolidating layer were taken on board. Equation 2.15 is the Gibson (1958) consolidation theory of a layer that increases in depth over time. Equation 2.16 represents the applicable solution for constant deposition (h=mt) rate. The case where deposition rate is proportional to the square root of time is not applicable to this research and is not discussed. It is reported that the two cited cases for Equation 2.15 are the only ones with known solutions (Gibson, 1958). Equation 2.16 is shown graphically in Figures 2.27 and 2.28 for impermeable and permeable bases respectively.

$$c_v \frac{\partial^2 u_e}{\partial x^2} = \frac{\partial u_e}{\partial t} - \gamma' \frac{dh}{dt} \qquad 2.15$$

$$u = \gamma' mt - \gamma' (\pi c_v t)^{-1/2} \exp -\frac{x^2}{4c_v t} \int_0^\infty \xi \tanh \frac{m\xi}{2c_v} \cosh \frac{x\xi}{2c_v t} \exp -\frac{\xi^2}{4c_v t} d\xi \qquad 2.16$$

$$c_v = \frac{m^2 t}{T_G} \qquad 2.17$$

Where u_e =excess pore water pressure
c_v =coefficient of consolidation
t =time
γ' =buoyant unit weight
h =thickness of sediment
m =deposition rate
x = depth from impermeable base
ξ = spatial coordinate in vertical direction
T_G = non dimensional time factor (Gibson equation)

Gibson (1958) made a distinction between excess pore water pressures in a layer that was undergoing sedimentation over time to which Equation 2.16 was applicable for the constant deposition rate. In the same work Gibson (1958) further pointed out that once deposition had ceased the consolidation of the deposited layer would dissipate excess pore water pressures in accordance with the Terzaghi (1923) one dimensional consolidation theory.

In the later works by other writers, however, deposition rate (m) for Equations 2.16 in Gibson (1958) equations have been equated with terms such as rate of placing (Mittal and Morgenstern, 1976), rate of embankment increase (Vick, 1983) and rate of rise (South African Chamber of Mines Guideline, 1996; Blight, 2010). It is believed that the excess pore water pressure in a layer that is undergoing deposition and thus increasing in height over time differs from the excess pore water pressure regime in a layer in which deposition had been completed before a new layer was superimposed as added load. The rationale behind the belief arises from the differences in behaviour between an already deposited layer and a layer that is undergoing sedimentation to deposit and form a new layer.

With respect to excess pore water pressures in tailings dams which this research has set out to investigate, it needs to be noted that application of Gibson (1958) theory is limited in that the theory was formulated for small strains as well as assumptions made to the effect that both permeability and compressibility properties were constant. Fahey et al. (2010) have confirmed

that gold tailings undergo large strains when loaded and that their permeability and compressibility vary over time under a given load.

Robinson (2003) has noted that whilst Gibson's (1958) theory has been applied to tailings dam consolidation analysis there has not been any analytical substantiation of the use of the theory nor has there been any calibration of the use of the equation against practical experience. Robinson (2003) further observed that mine tailings are non-cohesive while Gibson's (1958) theory was derived for clays and that the phreatic surface on tailings dams was rarely at the surface of tailings dams contrary to one of the assumptions of the Gibson (1958) equation derivation which maintained the water table above the surface of the depositing layer. In addition, while the Gibson (1958) equation examined a homogeneous layer, tailings are always layered which further discounted the use of the Gibson (1958) consolidation theory to analyse consolidation in tailings dams.

Fahey et al. (2010) also allude to the limitation of the use of the Gibson (1958) equation when deposition is stopped (a rest) and later resumed. The authors further note the inapplicability of the theory when additives such as cement are introduced into mine tailings. The paddock deposition of gold tailings relies on rest periods between depositions and therefore it would be a great challenge to appropriately model such constructed tailings dams using the Gibson (1958) consolidation equation. In agreement with Fahey et al. (2010) it is believed that Gibson's (1958) equation could be used as an initial design tool but being cognisant of its many limitations.

Finite Strain Consolidation

The consolidation theories dealt with thus far though formulated in excess pore water pressures terms relevant for this research have all fallen short of adequately addressing the consolidation of tailings formed from slurry. The assumption of constant material properties and small strains formulations were among the shortcomings of the previously tabled theories which has led to their inability to adequately predict soft soil consolidation behaviour. Soft soils are reported to display nonlinear compressibility and permeability behaviours as well as to undergo large strains under self-weight loading conditions (Jeeravipoolvarn, 2010).

Gibson et al. (1967, 1981) formulated non-linear finite strain consolidation theories for both thin and thick homogeneous saturated clay layers to address some of the shortcomings of the earlier theories. The finite strain consolidation equations were derived using both the traditional Eulerian coordinate system and the Lagrangian as well as the convective coordinate systems to cater for large strains formulations. The equations could be derived with void ratio, porosity and excess pore water pressure as dependent variables. The excess pore water pressures derivation is the emphasis for this study and will be covered under this literature review. It is worth noting that Gibson et al. (1981) observed that the void ratio based finite strain consolidation equation was much easier to solve hence their choice of void ratio as the dependent variable. Pane and Schiffman (1995) have noted that finite strain consolidation equations expressed in Eulerian coordinates system with excess pore water pressure as the dependent variable resulted in the equation still having void ratio as a second dependent variable which made the equation very difficult to solve.

Equations 2.18 and 2.19 represent finite strain consolidation theories expressed in excess pore water pressures terms derived under Lagrangian and Eulerian coordinates system respectively (Priscu, 1999; Jeeravipoolvarn, 2010). Equation 2.18 is attributed to Koppula (1970) and Somogyi (1980). Equation 2.19 on the other hand was presented by Pane et al. (1990).

$$\frac{\partial}{\partial y}\left[\frac{k(e)}{\gamma_w(1+e)}\right]\frac{\partial u_e}{\partial y}+\frac{k(e)}{\gamma_w(1+e)}\frac{\partial^2 u_e}{\partial y^2}+\frac{de}{d\sigma'}\frac{\partial u_e}{\partial t}-\frac{de}{d\sigma'}\left[(G_s-1)\gamma_w\frac{d(\Delta y)}{d}\right]=0 \qquad 2.18$$

$$(1+e)\frac{\partial}{\partial y}\left[\frac{k(e)}{\gamma_w(1+e)}\frac{\partial u_e}{\partial y}+\frac{d(t)}{1+e}\right]=\frac{a_v}{1+e}\frac{\partial u_e}{\partial t} \qquad 2.19$$

Where k = permeability
e = void ratio
y =reduced or material coordinate
σ' = effective stress

The derivation of finite strain consolidation theory equations and the underlying assumptions are covered in Gibson et al. (1967, 1981), Schiffman et al. (1988), Priscu (1999) as well as in many other literature sources.

Been (1980) had shown that Kynch's (1952) hindered sedimentation theory was a special case of the finite strain consolidation theory when the effective stress was set to zero (Been, 1980; Jeeravipoolvarn, 2010). Bartholomeeusen (2003) reported that the same conclusion of Kynch equation being a special case of finite strain consolidation has also emerged from the works of Toorman (1999) and Merkelbach (2000). Been (1980) also demonstrated that there was a link between sedimentation and consolidation. An observation has been made that the boundary between the two processes was blurred with a transition zone in between where both sedimentation and consolidation overlapped each other (Michaels and Bolger, 1962; Tan et al., 1990; Been and Sills, 1981). In order to address this dilemma, an interaction coefficient, β(e), to account for the sedimentation-consolidation transition zone when effective stress partially exist was introduced by Pane and Schiffman (1985) to bridge the sedimentation-consolidation linkage (Tan et al., 1990; Priscu, 1999; Qiu, 2000; Jeeravipoolvarn, 2010). Equation 2.20 shows the modified effective stress equation incorporating the interaction coefficient, β(e). It is worthnoting that the interaction coefficient is a function of void ratio (e) hence its designation as β(e).

$$\sigma = \beta(e)\sigma' + u \qquad 0 \leq \beta(e) \geq 1 \qquad 2.20$$

Where σ =total stress

$\beta(e)$ =interaction coefficient which is a function of void ratio

σ' =effective stress

u = pore water pressure

Schiffman (1979) has demonstrated that Terzaghi's one dimensional consolidation theory is a special case of the finite strain consolidation theory and that most of the other consolidation theories reported in the literature were also special cases of the finite strain consolidation theory, thereby making the finite strain consolidation theory the most general consolidation theory. Whereas the finite strain consolidation theory seems well suited for soft soils, Gibson et al. (1981) cited limitations of the finite strain consolidation theory as assumptions that the finite strain coefficient of consolidation was constant and that both creep effects and soil heterogeneity were ignored. The finite strain consolidation theory's solutions are also quite complex and require the use of numerical methods for solution. The complexity of the forms of solutions have led to limited use of the theory and has resulted in the current state of affairs

where the less appropriate consolidation theories which are easy to implement and use are widely used such as the classical consolidation theory by Terzaghi (1923) and the Gibson (1958) equation. This is despite these theories' shortcomings some of which are said to be underestimation of excess pore water pressures at a given time and overestimation of the time of consolidation (Gibson et al., 1981; Schiffman et al., 1988). Qiu (2000) reported that on the basis of a comparison of a 15 meter thick clay layer it was observed that relative to a finite strain consolidation theory attributable to Schiffman et al. (1984), the conventional theory was found to over predict settlement times and that the rates of settlement were much faster than the rates of excess pore water pressure dissipation.

It however needs to be noted that Schiffman et al. (1988) also reported a comparison of pore pressures where both the small strain consolidation theory and the finite strain consolidation theory yielded similar results up to a depth of 30 meters contrary to expectations. This anomaly was also reported by Blight (2010). No sound explanation of the anomaly has been offered to date. The above notwithstanding, various efforts have been undertaken to apply finite strain consolidation to soft materials. Priscu (1999) listed some of the earlier efforts undertaken to apply finite strain consolidation theory which are summarised in Table 2.4.

It appears from the literature that finite strain consolidation formulations are the most appropriate theories for the prediction of excess pore water pressures in tailings dams at the current time. It has to be taken into consideration however that finite strain consolidation theories in their current format do not cater for consolidation of multi-layered materials as observed in tailings dams. The finite strain theories unlike the Gibson (1958) theory of a clay layer that accretes over time do not directly model rate of rise aspects and associated excess pore water pressure development. A finite strain consolidation theory with an in-built allowance for increase in height over time that also considers silts and not only clays would therefore best describe the consolidation of materials such as gold tailings when constructed at varying rates of rise in tailings dams.

Table 2.4: Summary of finite strain consolidation modelling through the years 1967-1998 (After Priscu, 1999).

Authors	Institution	Numerical Technique Used	Remarks
Gibson et al., 1967	Kings's college, UK	Nonlinear partial differential equations	Self-weight consolidation of clay layer
Koppula, 1970	University of Alberta		Pore pressure consolidation equation
Monte & Krizek, 1976	NorthWestern University	Finite differences	Used c_v with kaolinite clay
Somogyi, 1980	NorthWestern University	Finite differences	Pore pressure consolidation equation
Been & Sills, 1981	University of Oxford, UK	Finite differences	Linear k and constant c_v for mud
Gibson et al., 1981	UK and US	Finite differences	Void ratio consolidation equation on clay
Koppula & Morgenstern, 1982	Hardy Assoc. and University of Alberta	Finite differences	Pore pressure consolidation equation on deltaic deposits
Somogyi et al., 1984	NorthWestern University	Finite differences	Pore pressure consolidation equation, Quasi 2D on waste clay
Schiffman et al., 1988	University of Colorado, Boulder	Finite differences	Void ratio consolidation equation on copper marine sediments
Schiffman et al., 1988	University of Colorado, Boulder	Finite differences	Void ratio consolidation equation on copper, marine sediments& phosphate clays
Murphy & Williams, 1990	Australia	Finite differences	Pore pressure consolidation equation, seepage forces on gold tailings
Schiffman & Carrier III., 1990	University of Colorado/ Bromwell Carrier	Finite differences	Void ratio consolidation equation on copper tailings
Shodja & Feldkamp, 1993	NorthWestern University	Moving finite Element method	Void ratio consolidation equation on mud
Schiffman et al., 1994	University of Colorado/ University of Oxford	Finite differences	Void ratio consolidation equation on copper tailings and Florida phosphates
Seneviratne et al., 1996	University of Western Australia	Finite differences/ finite Element method	Pore pressure consolidation equation, evaporation on gold tailings
Gassner & Fourie, 1998	University of Witwatersrand, South Africa	Finite differences	Void ratio consolidation equation, rate of rise on metal tailings and coal

2.6 Geotechnical Engineering Properties of Gold Tailings

2.6.1 Introduction

The geotechnical engineering properties of mine tailings in general reflect their short geological history as man-made materials. The properties of the tailings are thus similar to those of the source rock from which they were extracted bearing the imprints of the extraction processes on the source materials, the formation processes from a hydraulically deposited slurry as well as the current state in which the tailings are in. A specific batch of gold tailings would thus have engineering properties that reflect the state of weathering of the source rock. The tailings solid particle shapes and sizes would have been influenced by the blasting, grinding and milling processes employed as well as the metallurgical treatments used to extract gold from the ore. The slurry properties and the manner of slurry deposition onto tailings dams would also come to bear on the resultant tailings properties.

This section discusses the geotechnical engineering properties of gold tailings. Basic soil parameters relevant to mine tailings are described together with presentation of index properties, particle size grading, permeability, consolidation and shear strength characteristics of gold tailings.

2.6.2 Soil Phase Relationships

The soil phase relationships for mine tailings are mainly derived from soil mechanics terminology. Isolated use of mineral processing and metallurgical terms (Fell et al., 1992; Robinson, 2008) and tailings industry practice terms is also common. The use of terminology originating from more than one discipline results in conflicting use of terms from the different disciplines. Mine tailings production processes produce tailings in slurry form which has resulted in the use of soil phase diagrams that represent tailings both in slurry and settled forms (Fell et al., 1992). This has made it necessary to define slurry parameters as well. Mine tailings just like soils comprise of solid, liquid and gas phases (unsaturated tailings) as well as a two phase system of ether fully saturated or dry tailings.

Figure 2.29 shows both a three phase and a two phase soil diagram. Figure 2.29(b) is the emphasis of this study which considers only fully saturated gold tailings.

Equations 2.21 through 2.33 show the parameters which are of importance to the current study.

$$w = \frac{W_w}{W_s} \quad 2.21$$

$$w = \frac{W_w}{(W_w + W_s)} \quad 2.22$$

$$G_s = \frac{W_s}{\gamma_s \gamma_w} \quad 2.23$$

$$e = \frac{V_v}{V_s} \quad 2.24$$

$$e = \frac{mG_s}{S_r} = \frac{G_s - G_{slurry}}{G_{slurry} - 1} = \frac{G_s \gamma_w}{\gamma_d} - 1 = \frac{(1+m) G_s \gamma_w}{\gamma_t} - 1 \quad 2.25$$

$$\gamma_b = \frac{W}{V} = \frac{G_s + S_r e}{1+e} \gamma_w = \frac{1+w}{1+e} G_s \gamma_w \quad 2.26$$

$$\gamma_d = \frac{W_s}{V} = \frac{G_s}{1+e} \gamma_w = \frac{\gamma_b}{1+m} = \frac{G_s \gamma_w}{1 + \left(\frac{w G_s}{S_r}\right)} = \frac{G_s \gamma_w}{1 + [(1-P)/P] G_s / S_r} \quad 2.27$$

$$S_r = \frac{V_w}{V_v} = \frac{\gamma_d w G_s}{G_s \gamma_w - \gamma_d} \quad 2.28$$

$$P = \frac{W_s}{W} = \frac{1}{1+w} = \frac{G_s}{G_s + e} \quad 2.29$$

$$\rho_{slurry} = \frac{M_{slurry}}{V_{slurry}} \quad 2.30$$

$$G_{slurry} = \frac{\rho_{slurry}}{\rho_w} = \frac{G_s + e}{1+e} \quad 2.31$$

$$G_{slurry} = \left(\frac{1+w}{\frac{1}{\rho_s} + \frac{w}{\rho_w}} \right) / 1000 \quad 2.32$$

$$D_r = \frac{\gamma_{dmax}}{\gamma_d} x \frac{\gamma_d - \gamma_{dmin}}{\gamma_{dmax} - \gamma_{dmin}} x 100\% = \frac{e_{max} - e}{e_{max} - e_{min}} x 100\% \quad 2.33$$

Where w =moisture content

W_w =weight of water

W_s = weight of solids

G_s = specific gravity of solid particles

γ_s = unit weight of solids

γ_w = unit weight of water

e = void ratio

V_v = volume of voids

V_s = volume of solids

S_r = degree of saturation

G_{slurry} =specific gravity of slurry

γ_d =dry unit weight

γ_t = total unit weight

γ_b =bulk unit weight

W = total weight

V = total volume

P = pulp density or percentage solids

V_w = volume of water

ρ_{slurry} = density of slurry

M_{slurry} = mass of slurry

V_{slurry} = volume of slurry

D_r =relative density

γ_{dmax} = maximum dry unit weight

γ_{dmin} = minimum dry unit weight

e_{max} =maximum void ratio

e_{min} = minimum void ratio

It should be noted that gravimetric moisture content used in civil engineering differs from moisture content used in metallurgical practice (Robinson, 2008). That the use of the term relative density (RD) to refer to the specific gravity of the slurry or how heavy the slurry is relative to water and its other use to refer to how the in situ density relates to the loosest and densest states of tailings (Equation 2.33) brings about a conflict in the use of terminology. It is

suggested that the current standard terminology described above in relation to the term relative density and specific gravity be adopted as the norm in mine tailings practice and move away from the old practice (TMH1, 1979) of equating relative density with specific gravity.

2.6.3 Index Properties of Gold Tailings

This subsection presents fundamental and index properties of gold tailings among which are the mineralogy of the tailings, particle shape, particle size, specific gravity, Atterberg limits, density and void ratio. South African gold tailings have been tested extensively over the years to determine their properties. Research by Vermeulen (2001) has shown the mineralogy of Witwatersrand gold reef to comprise 75% quartz, 10% muscovite, 5% pyrophillyte, 5% illite and small percentages of clinochlore, kaolinite and pyrite (Chang, 2009) which falls within the range established by earlier researchers such as Stanley (1987).

Table 2.5 adopted from Vermeulen's (2001) work summarises the basic properties of the main constituents in gold tailings which influences its fundamental properties. The specific gravity of the solid particles (G_s) is shown by its symbol in the table.

It can be observed from Table 2.5 that gold tailings particles would be expected to comprise angular grains (quartz) with some platy shaped particles (muscovite). The specific gravity of the solid tailings particles would be close to the specific gravity of quartz its main constituent at about 2.70. The Specific gravity of gold tailings solids obtained from various sources is shown in Table 2.6.

Robinson (2008) noted that specific gravity of solid particles influenced tailings solids settling and deposition characteristics. He further observed that particles with a high specific gravity behaved coarser than they were whilst particles with a low specific gravity behaved finer than they actually were. Robinson (2008) argued that two particles of the same size but with different specific gravity of the solids will settle differently. The particle with a high G_s value will settle faster than the particle with a low G_s value. In other words the high G_s particle behaves as if its size is bigger (coarser) than the other particle of the same size but with a low G_s value. Both Robinson (2008) and Blight (2010) cite instances where tailings were bimodal with the occurrence of more than one specific gravity of solids within a tailings sample. In

other words tailings do exhibit variable specific gravity of solid particles which would tend to promote segregation by density in addition to segregation by size.

Table 2.5 Properties of the Principal Minerals Present in Gold Tailings.

Mineral	Formula	G_s	Remarks
Quartz	SiO_2	2.63	Occurs as well-formed coarse and fine crystals, appear as angular Grains
Muscovite	$(Ba,K)Al_2(Si_3Al)O_{10}(OH)_2$	2.82	Platy in Shape
Pyrophyllite	$Al_2Si_4O_{10}(OH)_2$	2.84	
Illite	$(K,H_3O)Al_2Si_3AlO_{10}(OH)_2$	2.75	
Clinochlore	$(Mg,Fe)_6(Si,Al)_4O_{10}(OH)_8$	2.65	Crystalline in form
Kaolinite	$Al_2Si_2O_5(OH)_4$	2.30	
Pyrite	FeS_2	5.01	Has a crystalline structure, appears as cubic grains

Table 2.6 Specific Gravity of Gold Tailings Solids

Reference	**G_s**
Pettibone and Kearly (1971)	2.5-3.5
Hamel and Gunderson (1973)	3.1
Soderberg and Busch (1977)	2.6-2.7
East et al. (1988)	3.02
Vermeulen (2001)	2.75
Chang (2009) Pond Beach	2.75 2.70

Mine tailings solids can be classified as coarse or fine particles in terms of particle size. Usually either the 63µm or the 75µm sieve size is used as the dividing size. This thesis adopts the latter

definition where fine tailings particles are those particle sizes less than 75µm size (also known as slimes). Table 2.7 lists typical shapes of both coarse and fine tailings particles.

According to Pettibone and Kearly (1971), Van Zyl (1993) and Vermeulen (2001) gold tailings comprise 10% sand sized particles, 80% of silt sizes and 10% clay sizes. Based on the composition given, gold tailings are essentially a silt with very little plasticity (Hammel & Gunderson, 1973; Vermeulen, 2001 and Chang, 2009). Table 2-8 summarises the Atterberg limits of gold tailings based on work of previous researchers (Wagener et al., 1998; Vermeulen, 2001 and Chang, 2009).

Table 2.7: Typical shapes of coarse and fine gold tailings particles.

Tailings Fraction	Shape	References
Coarse Tailings (>75 µm) or Sand	Very angular to sub angular with sharp edges	Mittal & Morgenstern (1975); Lucio et al. 1981; Garga & Mckay 1984 and Mlynarek et al. 1995
	Bulk silt sized particles	Vermeulen, 2001; Chang, 2009
Fine Tailings (<75 µm) or Slime	Angular needle shaped with sharp edges	Hamel & Gunderson, 1973
	Rough surface textures	Papageorgiou et al, 1999
	Flat plate like particles	Vermeulen, 2001; Chang, 2009

Table 2.8: Atterberg Limits of Typical Gold Tailings

Sample	Liquid Limit (%)	Plastic Limit (%)	Plasticity Index(%)	References
Whole Tailings Coarse Tailings Fines	29 28 43-56	22 22 32-39	7 6 11-17	Vermeulen, 2001
General	23-43	22-35	1-8	Wagener et al., 1998
Pond Beach	51 25-30	39 NP	12 NP	Chang, 2009

Tailings properties discussed in the foregoing have been concerned with tailings solids only with the exception of Atterberg limits which reflected the behaviour of a portion of the solid particles passing the 425μm sieve size in the presence of water. The emphasis of the Atterberg limits, however, was on the fines with clay mineral properties. The fundamental properties that describe tailings slurry and settled tailings from a slurry include density in its various forms which include slurry specific gravity shown by Equation 2.31 which is often referred to as relative density (RD), pulp density (Equation 2.30), void ratio and relative density as given by Equation 2-33.

Slurry density and grading are the two most significant criteria that influence deposition of tailings (Robinson, 2008). The importance of slurry density is reflected through its direct measurement on site using a Marsi scale. However it is not the slurry density that is widely used in the tailings industry practice, but the ratio of how heavy the slurry is relative to the weight of water (Robinson, 2008) or the slurry specific gravity which is referred to as the slurry relative density or just relative density which as noted before conflicts with the use of the same term in conjunction with Equation 2.33. The specific gravity of slurry has a direct relationship with slurry segregation where low specific gravity slurry is prone to segregation while high specific gravity slurry would not segregate as the tailings solids are closely in contact with each other. Slurries deposited on South African gold tailings dams usually fall within a specific gravity of slurry range of 1.2 to 1.6 (Robinson, 2008).

Pulp density or the percentage of tailings solids in discharged slurry also controls particle size segregation (Soderberg and Busch, 1977; Vick, 1983) with lower pulp densities said to promote greater segregation.

It is worth noting that slurry density, pulp density, void ratio and specific gravity of the slurry continuously change as the deposited slurry undergoes a change of moisture content during the settling process cycle which entails sedimentation, consolidation, desiccation and rewetting. Vermeulen (2001) noted that depending on the specific gravity of the tailings solids, the sediment in the pond area of a tailings dam could settle to a dry density of about 1000kg/m^3 at a moisture content of 60% whilst on the beach a dry density of 1450kg/m^3 at a moisture content range of 20-50% was more common. Table 2.9 summarises values of density and void ratio of gold tailings (Vermeulen, 2001; Chang, 2009).

Carrier III et al. (1983) proposed that void ratio at the end of sedimentation and at the start of consolidation could be calculated using Equation 2.34.

$$e_{sed} = 7G_s\frac{LL}{100} \qquad 2.34$$

Where e_{sed} =void ratio at the end of sedimentation and start of consolidation
G_s = specific gravity of the solid particles
LL = Liquid limit as a percentage

2.6.4 Particle Size Grading

Particle size grading involves the separation of a tailings sample into its component parts on the basis of particle size. Size gradations are as a result used to evaluate segregation that takes place in tailings dams because of hydraulic sorting either due to size, shape or density differences. According to Robinson (2008) grading is the single most significant parameter affecting the behaviour and performance of a tailings facility to the extent that no testing work on a tailings dam is complete without a particle size grading test. Gold tailings particle size distribution has been described as uniformly graded with 80% within the silt size range, 10% within the sand category and 10% in the clay size range (Pettibone and Kealy 1971; Van Zyl,

1993). Vermeulen (2001) presented gold tailings particle size grading curves from various workers over the years 1965 through 1999 which are given in Figure 2-30 which also cites the research work under which the respective grading curves were undertaken. Particle size grading parameters computed from Vermeulen (2001) and Chang (2009) are summarised in Table 2.10. Blight (2010) noted however that particle size grading may be variable both within a single mine and from one mine to another as well as being variable on single tailings storage facility.

A well graded soil has a coefficient of curvature of between 1 and 3 (Knappet and Craig, 2012). A uniformity coefficient of one (1) would be a near vertical particle size grading curve and thus represent an almost single sized material which would be uniform. A coefficient of uniformity of 36 is the value of the "ideal" Fuller curve (Fuller and Thompson, 1907) where the densest packing of spherical particles is achieved by selecting particles sizes corresponding to the Fuller equation. In order to achieve the densest parking of particles the successive particle sizes are arranged such that a given small sized particles range fit into the voids left in between the particle size range immediately greater than the small sized spheres.

The same process is repeated for all the particle size ranges considered. Vermeulen (2001) noted that if the coefficient of uniformity, C_u, was greater than 36 such a soil would have voids between coarse particles which are not filled with fines leading to a density lower than the optimum density represented by the Fuller grading. The grading could thus be improved by the addition of fines to fill the voids. On the contrary when the coefficient of uniformity, C_u, was less than 36 it was noted that there would be an abundance of fines in between the coarse particles which keeps the coarse particles apart leading to a density less than maximum density. The gradation deficit in this case cannot be overcome by adding more fines as the material would be disrupted further away from the ideal Fuller curve conditions (Vermeulen, 2001). It is also worth noting that gold tailings fine particles are mainly platy whilst the Fuller curves were based on spherical particles.

Table 2.9: In situ Densities and Void Ratios of Gold Tailings (After Chang, 2009)

Reference	Description	Density (kg/m^3)	Void Ratio
Blight (1989)	After deposition After evaporation After sun drying		1.7 1.25 0.5
Blight and Steffen (1979)	General		1.1-1.2
Blight (1981)	In situ dry density	1835	
Vick (1983)	Tailings sand Low plasticity slimes High plasticity slimes		0.6-0.9 0.7-1.3 5-10
East et al. (1988)	In situ dry density Average dry density	1340-1740 1650	
Van Zyl (1993)	In situ dry density	1000-1450	
Vermeulen (2001)	Delivery pulp dry density In situ dry density (sands) In situ dry density (slimes) In situ void ratio (coarse) In situ void ratio (coarse)	300-750 1250-1650 1000	 0.77-0.87 1.39-1.49

Table 2.10: Summaries of Gradation Parameters (After Chang, 2009)

References	Description	D_{10} (μm)	D_{30} (μm)	D_{60} (μm)	D_{90} (μm)	C_u	C_z
Vermeulen (2001)	Whole tailings	2	10	55	125	27.5	0.91
	Coarse tailings	2-3	9-25	43-75	115-145	21.5-25	0.94-2.78
	Fine tailings	1.5-1.7	3.2-4.5	8.3-16	41-55	4.9-10.7	0.75-0.84
Chang (2009)	Pond Fines	2	4	6	12	2.6	1.6
	Beach tailings	6	31	95	190	11-24	1-2

Where C_u = coefficient of uniformity = D_{60}/D_{10}

C_z =coefficient of curvature = $(D_{30})^2/(D_{10}D_{60})$

D_{10} = Particle diameter for 10% passing

D_{30} =Particle diameter for 30% passing

D_{60} =Particle diameter for 60% passing

D_{90} =Particle diameter for 90% passing

2.6.5 Tailings Permeability

Permeability or the ease with which water flows through a material (Gulhati, 1978) in a given time under given pressure conditions (Robinson, 2008), depends on particle size, mineralogy, void ratio (dry density), methods of deposition and degree of saturation (Fell et al., 1992). Unlike other engineering properties of soil, permeability is difficult to generalise even for tailings and spans over several orders of magnitude (Vick, 1983; Robinson, 2008; Blight, 2010). Table 2.11 summarises typical permeability values for gold tailings.

Table 2.11: Typical Permeability Values for Gold Tailings (After Chang, 2009)

Reference	Description	Permeability (m/yr)
Blight (1980)	General (Range)	1-50
Blight (1981)	General	3
Vermeulen (2001)	Whole Tailings	10
	Coarse	2.5-15
	Fines	1.5-5

Studies by Kearly and Busch (1979) and Blight et al. (1985) have shown that tailings dam permeability values varied from high values at the dam wall, which comprise mostly sands where the slurry is discharged, and decrease in size through the tailings beach area where intermediate permeability values occurred ending with low permeability values in the pond area where slimes (particles sizes less than 75µm) dominate. Blight et al. (1985) and Chamber of Mines of South Africa (1996) provided Equation 2.35 for estimating permeability values across gold tailings dams for the part of the dam extending from the dam walls up to the pool area of the tailings dam.

$$k = \alpha e^{-\beta x} \qquad 2.35$$

Where k =permeability of tailings at a distance x from the discharge point down the beach

while =α and β are constants for the given beach and tailings.

Several workers have reported permeability anisotropy ratios for tailings dams which reflect the highly layered nature of tailings dams which arise from the settling processes from which tailings form. Table 2.12 gives a summary of the anisotropy ratios published in literature for gold tailings. Vick (1983) pointed out that a high anisotropy ratio of 100 and above was recorded at sands and slimes inter-layering where slurry discharge procedures were uncontrolled. McPhail and Wagner (1989) reported a ratio of 10, but noted that with desiccation cracks filled with coarse tailings the resulting permeability ratios dropped to the range 1.5 to 3. Rust et al. (1995) and Van der Berg (1995) gave anisotropy ratios ranging between 7 and 22.

The values reported were based on piezocone tests. The authors used the relationship between the slope of the phreatic surface and the slope of the pore pressure increase with depth to calculate the ratio of horizontal and vertical permeability. The results therefore accounted for the development of cracks and their subsequent in filling as well as the multi layering typical of tailings dams. They noted that the permeability values obtained from field tests were therefore expected to be higher than those obtained from laboratory tests.

Table 2.12: Anisotropy Ratio for Gold Tailings

Reference	Anisotropy Ratio ($\frac{k_h}{k_v}$)
Pettibone and Kearly, 1971	5-10
Kearly and Busch, 1979	10
Vick, 1983	2-10
Vick, 1983 (Uncontrolled discharge)	100 or more
Wagener et al., 1989	25
McPhail and Wagner, 1989	10
	1.5-3
Van der Berg, 1995 Rust et al., 1995	7-22

In Table 2.12, k_h is the equivalent permeability along bedding planes while k_v is the permeability across bedding planes. The equivalent permeabilities are represented by Equations 2.36 and 2.37 (Knappett and Craig, 2012) respectively.

$$k_h = \frac{1}{d}(k_1 d_1 + k_2 d_2 + \cdots + k_n d_n) \qquad 2.36$$

$$k_v = \frac{d}{\left(\frac{d_1}{k_1} + \frac{d_2}{k_2} + \cdots + \frac{d_n}{k_n}\right)} \qquad 2.37$$

Where d $= d_1 + d_2 + \ldots + d_n$ is the total layer thickness

k_n =permeability of the n^{th} layer

d_n =depth of the n^{th} layer

Grading which is dominated by particle size effects, more precisely the voids left by the smaller sized particles (Robinson, 2008), has also been noted to have a great influence on permeability. Hazen's (1892) equation which captures the effects of grading on permeability is used to estimate permeability of tailings. Vermeulen (2001) collated several equations used to estimate permeability including various forms of Hazen's equations which are listed in Table 2.13 as Equations 2.38 through to Equation 2.42. The equation numbers are given within square brackets [] in Table 2.13.

Based on the research findings by Day and Daniel (1985), Chen and Yamamoto (1987) and Pregl (1987), Blight (2010) summarised some of the key factors to be considered for the measurement of permeability. Blight (2010) listed the key factors as the need to test a large enough sample that is representative of the structure and features of the soil being tested, that the setting up of the permeability test be such that side wall leakage between the permeameter and the sample is prevented and lastly that the permeability test seepage or flow gradient be compatible with the seepage gradient expected under field conditions. It was observed that the coefficient of permeability was also sensitive to effective stress. It was noted that the level of effective stress for the test should be established since permeability of the same specimen under high effective stress would be lower than its permeability at a low effective stress.

Permeability can be measured using laboratory methods, field methods as well as estimated from basic soil test results using empirical relations (formulae) as shown by Equations 2.38 to 2.42 including Equation 2.35 in Table 2.13 collated from various literature sources by Vermeulen (2001).

For the current research where settling column experiments were used to study tailings properties, laboratory methods of measuring permeability offered the best method with regards to the evaluation of permeability of the settled materials inside settling tubes. An emphasis was placed on the laboratory permeability tests which avoided removal of the settled tailings from settling tubes and as a result minimised sample disturbance. The constant head or constant gradient test and the falling head or reducing gradient test (Blight, 2010) were therefore selected as the most appropriate permeability tests for the current study. The constant head test was more preferable because as a steady state test it enables determination of permeability under relatively constant conditions as opposed to the falling head test which is inherently

transient in nature and entails continually changing effective stresses which alter the permeability values meant to be measured by the test.

Table 2.13: Empirical Equations for Estimating Permeability

Reference	Equation	Remarks
Hazen, 1892	$k = cD_{10}^2$ (cm/s) [2.38]	c varies from 1.0 to 1.5
Mittal & Morgenstern (1975)	$k = D_{10}^2$ (cm/s) [2.39]	c=1 for tailings sands
Sherard et al. (1984, 1984a)	$k = 0.35D_{15}^2$ [2.40]	
Blight et al. (1985)	$k = \alpha e^{-\beta x}$ [2.35]	Beach Profile Equation
Carrier et al. (1983)	$k = \left(95.2G_s \frac{\text{PI}}{100}\right)^{-4.29} \frac{e^{4.29}}{1+e}$ [2.41]	k in m/s
Bates & Wayment (1967)	$\ln(K_{20}) = 11.02 + 2.912\ln(e.D_{10}) - 0.085\ln(e)\ln(CU) + 0.19e.CU - 56.5D_{10}D_{50}$ [2.42]	K_{20} = permeability at 20°C in inches/hr

Both of the laboratory permeability test methods are based on Darcy's Law which was expressed in measurable quantities to enable computations of permeability. Equations 2.43 and 2.44 (Knappett and Craig, 2012) give the constant head and falling head permeability tests equations respectively. Equation 2.45 represents Darcy' Law while Equation 2.46 shows permeability obtained using settling column depth, Δz, and total head change (ΔH) in a settling column.

$$k = \frac{q_\infty L}{A\Delta H} \quad 2.43$$

$$k = \frac{aL}{At} ln \frac{H_o}{H} \quad 2.44$$

$$Q = kiA \quad 2.45$$

$$k = \frac{\Delta z}{\Delta H} . \frac{Q}{A} \qquad 2.46$$

Where q_∞ = steady state rate of flow
A =cross sectional area of sample
L =length of sample
ΔH =Total head change
H_o =head at time t =0
H = head at time t =t
a = standpipe cross sectional area
Q =total discharge
Δz =change in depth
i =hydraulic gradient

2.6.6 Consolidation and Shear Strength Characteristics of Tailings

This section presents the consolidation and shear strength characteristics of gold tailings as published in the literature. Both consolidation and shear strength characteristics play a key role in the stability analysis of tailings dams and they are considered to be amongst the factors that determine allowable rate of rise of tailings dams (Vermeulen, 2001; Robinson, 2008).

Terzaghi's one dimensional consolidation theory is still the most widely used theory on tailings dams despite its many shortcomings cited earlier under this study. Because of the wide usage of Terzaghi consolidation theory, consolidation parameters of gold tailings in the published literature are related to the theory and its associated derivations. The consolidation parameters characterising gold tailings presented under this work are therefore the compression Index, C_c, which indicates the magnitude of settlement a tailings material is likely to undergo and the coefficient of consolidation, c_v, which reflects the rate of consolidation of a given tailings material. Tables 2.14 and 2.15 lists compression indices and coefficients of consolidation values quoted by various investigators as captured by both Vermeulen (2001) and Chang (2009). Table 2.16 presents shear strength parameters of gold tailings available from literature (Vermeulen, 2001; Chang, 2009).

Table 2.14: Compression Indices, C_c, of Gold Tailings

Reference	Compression Indices, C_c	
	Coarse	Fine
Blight and Steffen (1979)		0.35
Vick (1983)	0.05-0.1	0.2-0.3
Qiu and Sego (2001)		0.083-0.156

Table 2.15: Coefficient of consolidation, c_v, of Gold Tailings

Reference	Coefficient of consolidation, c_v, (m^2/yr)	
	Coarse	Fine
Blight and Steffen (1979)		198
Vick (1983)	1,600-600,000	0.3-30
Sully (1985)		55-112
Stone et al. (1994)		15-26
Vermeulen (2001)	800-6900	210-1200
Qiu and Sego (2001)		13.58-80.07

2.7 Settling Column Experiments

Settling column experiments have been used widely over many years to study settling phenomena in general. The main focus of the studies has been on particulate materials which included different soil types, tailings, wastes, sludge and various other chemicals. A partial list of some of the earlier settling tests which did not measure pore water pressures can be found in Elder (1985). Among those listed are settling column tests by Gaudin and Fuerstenan (1958), Michaels and Bolger (1962), Migniot (1968), Owen (1970), Keshian et al. (1977) and Long and Ryu (1979).

Settling column tests which have been carried out in the recent past have included the measurement of pore water pressures in addition to the other parameters such as density and interface settlement over time. The more advanced settling column tests gleaned from published literature include the works by Lecasse et al. (1977), Kusuda et al. (1980), Been (1980), Imai (1980, 1981), Been and Sills (1981), Sills and Thomas (1981), Elder (1985),

Table 2.16: Shear strength parameters of gold tailings

Reference	Material Tested	Type of test	c' (kPa)'	ϕ' (º)
Hamel & Gunderson (1973)	Loose air-dry	Direct shear	0	39
	Dense saturated		11	24
Mittal & Morgenstern (1975)	Peak, loose	Direct shear	0	34
Blight and Steffen (1979)	Slimes		0	28-41
Blight (1981)	General		0	35
Vick (1983)	General			30-37
Sully (1985)	Average	Direct shear	5	33
Van Zyl (1993)	Sand/slimes		0	35
Blight (1997)	Sand/slimes	Triaxial/ Direct shear	0	29-35
Vermeulen (2001)	Average	Triaxial	0	34
Chang (2009)	Upper Beach	Triaxial	0	31.1
	Middle Beach		0	33.6
	Pond		0	31.5

Bowden (1988), Toorman (1999), Merckelbach (2000), Batholomeusen (2003), Kurt (2006), Jeeravipoolvarn (2006 and 2010), Miller et al. (2011) etc. Pedroni (2012) provides a more comprehensive summary of settling column tests used by various workers. Lebitsa et al. (2013) listed some of the investigations that utilised the settling column apparatus.

The settling columns used by various researchers have mainly been made of transparent acrylic or PVC or Plexiglas ranging in size from 200mm diameter and 350mm high acrylic tube used by Yong and Elmonayeri (1984) to a 914mm diameter and 10,500mm high polyethylene settling column utilized by Jeeravipoolvarn (2006). Settling columns have been used mostly for research purposes. The equipment can be classified into three categories which are the small capacity (up to 1 Litre) measuring cylinder type, the short and tall settling column tests. Elder (1985) categorised column tests of height of one metre and above as tall column tests. The same classification is adopted for this study.

Whilst many different individuals and institutions have carried out research using settling columns, it is worth mentioning that the University of Oxford in the United Kingdom, the Deft University of Technology in the Netherlands and Ecole Polytechnique in Canada have undertaken sustained research utilising settling columns over the years in the process developing advanced equipment and measurement instrumentation associated with settling columns (Dearnaley, 2002; Pedroni et al.,2006). Figure 2.31 shows the Ecole Polytechnique apparatus and its component parts (Pedroni et al., 2006). The given figure shows the settling column and its support (1), pressure transducers and read out system (2), digital camera and signal treatment system (3) and density measurement system (4).

The settling column apparatus has been used to measure mostly the following:

1. Density using x-ray or gamma ray radiation (Been, 1980; Dromer et al., 2004; Pedroni et al., 2006)

2. Pore water pressure using standpipe piezometers and pore pressure transducers (Been, 1980; Don Scott et al., 1985; Pedroni et al., 2006; Samadi-Boroujeni et al., 2008).

3. Soil water interface time plots or soil surface settlements over time (Been, 1980; Pedroni et al., 2006, Samadi-Boroujeni et al., 2008).

4. Visual observations of settling processes including segregation and channelling (Been, 1980; Kurt, 2006).

5. Use of settled column within settling tubes for insitu testing using miniature cone tests (Elder, 1985).

6. Recovery of settled column samples for purposes of carrying out other laboratory tests such as grading, permeability, fabric studies etc. (Bowden, 1988).

Several investigators have acknowledged edge and wall effects as well as accuracy in measuring solids content of the material being subjected to column testing as the main sources of errors in settling column tests measurements. Jeeravipoolvarn (2010) noted that Been and Sills (1981) observed that mud of void ratio between 4 and 10 experienced negligible side wall friction whilst Elder (1985) made the observation that column diameters of 100mm or larger did not influence settling rates, an observation corroborated by other workers (Michaels and Bolger, 1962; Been, 1980; Sills, 1997; Merckelbach, 2000). Jeeravipoolvarn (2010) cited that Caughill (1992) had found that where the diameter to height ratio exceeded 2:1 wall effects were minimised even at small void ratios.

Merckelbach (2000) reported that Michaels and Bolger (1962) had found that for settling tubes of heights up to 1.2m with diameters ranging from 48mm to 65mm at initial concentrations of 5 to 130 g/L indicated a negligible diameter effect for flocculated kaolin suspensions. Richardson et al. (2002) also stated that wall effects were negligible where the ratio of the vessel diameter to particle diameter exceeded 100. Dimitrova (2011) investigated the sensitivity of sedimentation velocity ratio, $\frac{u_t}{u_\infty}$, to the particle - vessel diameter ratio, $\frac{d}{D}$, for a settling column using a tailings slurry of porosity 0.84. It was reported that a tenfold increase in container size from an initial particle to vessel diameter ratio, $\frac{d}{D}$, of 0.002 led to a 0.4% increase of the sedimentation velocity ratio which implied that wall effects had a very negligible influence on the settling velocity of tailings in the suspension.

Richardson et al. (2002) also reported that settling processes of suspensions in settling columns including sedimentation rate are affected by the height of suspension, the diameter of the containing vessel and the volumetric concentration of the suspension.

2.8 Microscopy and Mineral Determination Tests of Tailings Samples

This section covers the scanning electron microscope (SEM) viewing of samples, X-ray diffraction (XRD) tests, X-ray fluorescence spectroscopy (XRF) tests, gas displacement

specific gravity test and laser diffraction particle size analyser method used on tailings samples in the study.

2.8.1 Scanning Electron Microscope (SEM)

The Scanning Electron Microscope was used to view prepared specimen from the tailings samples. A brief summary of how the SEM works is given together with the basic principles of the technique and the background to SEM sample preparation and viewing. In the SEM an incident beam of electrons strikes a sample whereby the interactions of the incident electrons with the sample produce signals which when detected reproduce the sample's surface topography and composition amongst others (Reed, 1993). Of interest to the SEM viewing, the outcome of the electron beam striking the sample is reported to be mainly secondary electrons and back-scattered electrons. Specialised detectors are used to record the secondary electrons and back-scattered electrons from which an image of the viewed specimen is composed. Secondary electrons which originate near the surface of the specimen under observation produce good resolution imaging which display specimen topography. The back-scattered electrons which on the contrary originate from relatively great depths from within the viewed specimen show contrast due to variations in the chemical composition of the specimen. The resolution for SEM is reported to be between 1nm and 10nm coupled with a great depth of field as well as the viewed specimen features being in focus (Egerton, 2005).

The SEM column is required to be at a vacuum to enable proper functioning of the electron beam. Wet samples such as tailings from settling column tests were to be dehydrated so that the low atmospheric pressure of a vacuum did not cause water in the sample to evaporate quickly thereby destroying the sample. Specimen of insulating materials such as gold tailings do not provide paths to ground specimen current which is the static electricity charge that build up in insulators when exposed to the electron probe. Gold sputter coating of the surface of the specimen was used as a solution to charge build-up which is reported to result in image distortion and fluctuations in image intensity (Egerton, 2005).

Vermeulen (2001) and Chang (2009) detailed gold tailings samples preparation methods for viewing under the scanning electron microscope. Vermeulen (2001) recommended oven drying samples at 35^{o} C. Chang (2009) reported a technique of breaking samples into smaller fragments to reveal undisturbed surfaces and provided details about the equipment used which

included the JOEL JSM-840 Scanning Microscope, probe current $3x10^{11}$ A, working distance 12mm, acceleration voltage 5kV, vacuum chamber $1x10^{-5}$ torr, magnification x50, x200, x500, x1000 and x2000 to examine macro and micro fabric of gold tailings. Under this study fabric is considered as the gold tailings particles arrangement and pore spaces between the particles. Macro fabric would be inclusive of cracks and laminations while micro fabric would focus on particle aggregation and the small pores between them (Mitchell and Soga, 2005 and Chang, 2009).

2.8.2 X Ray Diffraction (XRD) Tests and X ray Fluorescence (XRF) Spectroscopy Tests

The XRD tests were used to determine the crystalline mineralogical make-up of the tailings whereas the XRF tests were used to determine the chemical composition of the gold tailings. The XRD and XRF tests complement each other. Loubser and Verryn (2008) carried out a study in which they showed that combining XRD with XRF analyses enhanced the identification and quantification of mineralogical content and chemical composition of materials.

X ray powder diffraction works by recording the diffraction pattern of scattered x-rays of crystals of the object beamed with x-rays for observation. The scattering angles and their respective intensities which comprise scattering patterns of specific and particular crystals of a given material are characteristic of the mineral (Cullity, 1978 and Cullity and Stock, 2001). The diffraction pattern is then compared to the diffraction patterns of standard materials in databases in order to identify the mineral that yielded that specific diffraction pattern. Hence the mineralogical make-up can be determined and inferred from crystals within the material being studied (Cullity and Stock, 2001).

X ray fluorescence spectroscopy (XRF) works by bombarding the material being investigated with high energy X rays or gamma rays. The bombardment causes fluorescence of the object in the form of emissions of characteristic fluorescent X-rays whose spectrum lines when analysed yield the chemical composition and the elements contained in the analysed material. The back loading preparation method which was reported to yield excellent results was used (Jenkins and Snyder, 1996). In addition, the Rietveld method in which a theoretical diffraction pattern was compared and brought close to the data observed from the sample subjected to XRD analysis by means of a least squares procedure was also used (Young, 1996).

2.8.3 Gas Displacement Specific Gravity Test

The test was used to measure solid particle density by obtaining the volume of a given mass of solid particles from the volume of helium gas that the sample displaces which it utilises together with the supplied mass of the sample in the calculation of particle density. The AccuPyc II 1340 gas pycnometer was used for this research. The gas pycnometer is usually connected to a computer which carries out the calculations. The method is a helium gas displacement method as opposed to the water displacement principle employed by the density bottle method routinely used in geotechnical laboratory tests.

The AccuPyc II 1340 test applies the ideal gas law to a system of two containers joined together by a valve. One calibrated container holds the sample whilst the second cell which is also calibrated facilitates attainment of equilibrium between the two cells when the valve is opened to which the ideal gas law equation is applied to obtain the volume of the sample.

Figure 2.32 illustrates the principle of the test. In the illustration in Figure 2.32, the sample cell is pressurised to a gauge pressure, P_{1g} and is allowed to equilibrate with the valve closed. The valve between the two cells is then opened and the system is allowed to reach equilibrium again with a gauge pressure P_{2g} attained. Equation 2.47 derived from the ideal gas law was used to calculate the volume of the sample, V_{SAMPLE} .

$$V_{SAMPLE} = V_{CELL} - \frac{V_{EXPANSION}}{\left[\frac{P_{1g}}{P_{2g}} - 1\right]} \qquad 2.47$$

2.8.4 Laser Diffraction Particle Size Analyser method

The laser diffraction particle size analyser method (Mastersizer system) is a rapid particle size analyser which uses a laser diffraction method. It comprises a sample dispersion cell, an optical unit and a computer with software to link all the three components together. The sample dispersion accessory contained the dispersant or the liquid medium in which the sample was placed and the sample whose particle size determination was desired. The optical unit provided the laser beam that was projected onto the sample as well as houses the detectors for the scattered, the refracted and the diffracted light. The computer system further enables

communication between all the components and the software carries out analysis encompassing data generation, storage, computation, plotting and presentation.

The Mastersizer system works on the basis that a size range of particles has a specific light scattering pattern. The optical unit thus records light scattering patterns of various particles sizes in the sample using its 52 detectors. Specific detectors focus on certain aspects of the light scattering to ensure a good coverage of the sizes concerned. The recorded data are then used to identify the particle size ranges by comparison with scattering patterns calculated using the Mie theory for known particle sizes.

It must be noted that the Mastersizer determines particle sizes on the basis that particles are spherical and it uses volume of the particles as the basis of the computations of the proportions of the particles. This obviously introduces errors since gold tailings particles are not spherical and because volumetric measurements are not directly proportional to the number of particles involved, let alone their respective masses, which are commonly used in particle size analysis methods in civil engineering. In addition the use of the Mastersizer and associated theories requires knowledge about particle properties such as the refractive index, absorption properties and details about the structure of the particles. The agglomeration of particles is dealt with through the application of ultrasonic waves which disperse the particles to ensure that they remained discrete for purposes of individual particle size grading. Chemical dispersants could be added as admixtures or alternatively the dispersants could be added to distilled water.

A comparison of Mastersizer test gradations with gradations from hydrometer sedimentation is likely to lead to differences in the particle size determination if the comparisons are not carried out with caution. The comparisons of the results of grading tests from the different particle size determination methods must pay attention to the details of how the respective particle sizes were determined. The comparisons ought to consider the following issues amongst others: the dispersants used and their amounts, the laser diffraction measurement method used and the details of the values entered into the software for the determinations of the sizes, the laser diffraction calculation procedure used (the Mie theory *versus* the Franhaufer approximation), the laser diffraction operation method used (manual *versus* standard operation procedure (SOP)), the sample preparation method used and the respective particle agglomeration techniques used in both the laser diffraction method and the Stokes's Law type sedimentation hydrometer analysis method.

2.9 Summary

The literature review has traced and described the origin and source of mine tailings. The mineralogy of the tailings has been outlined together with tailings disposal methods. Rate of rise of tailings dams has been explained within the context of tailings formation processes from slurry. Tailings segregation, generation of excess pore water pressures as well as the sedimentation and consolidation theories was reviewed. Geotechnical engineering properties of gold tailings have been listed and literature on settling column tests and their use summarised.

The review of literature has brought into focus the following: lack of consistency in the use of nomenclature of tailings disposal methods, the disparity between experience based rate of rise and consolidation theory based rate of rise, a prevalent but unsubstantiated belief that excess pore water pressures limit rate of rise, insufficient experimental evidence of segregation of tailings and its effects on excess pore water pressures and the absence of a laboratory based method of evaluating permeability of the segregated alternating multi tailings layers.

Under this study an experimental methodology is explored to investigate the relation between rate of rise of tailings dams and excess pore water pressures as well as to assess particle size segregation and its effects on the behaviour of tailings materials.

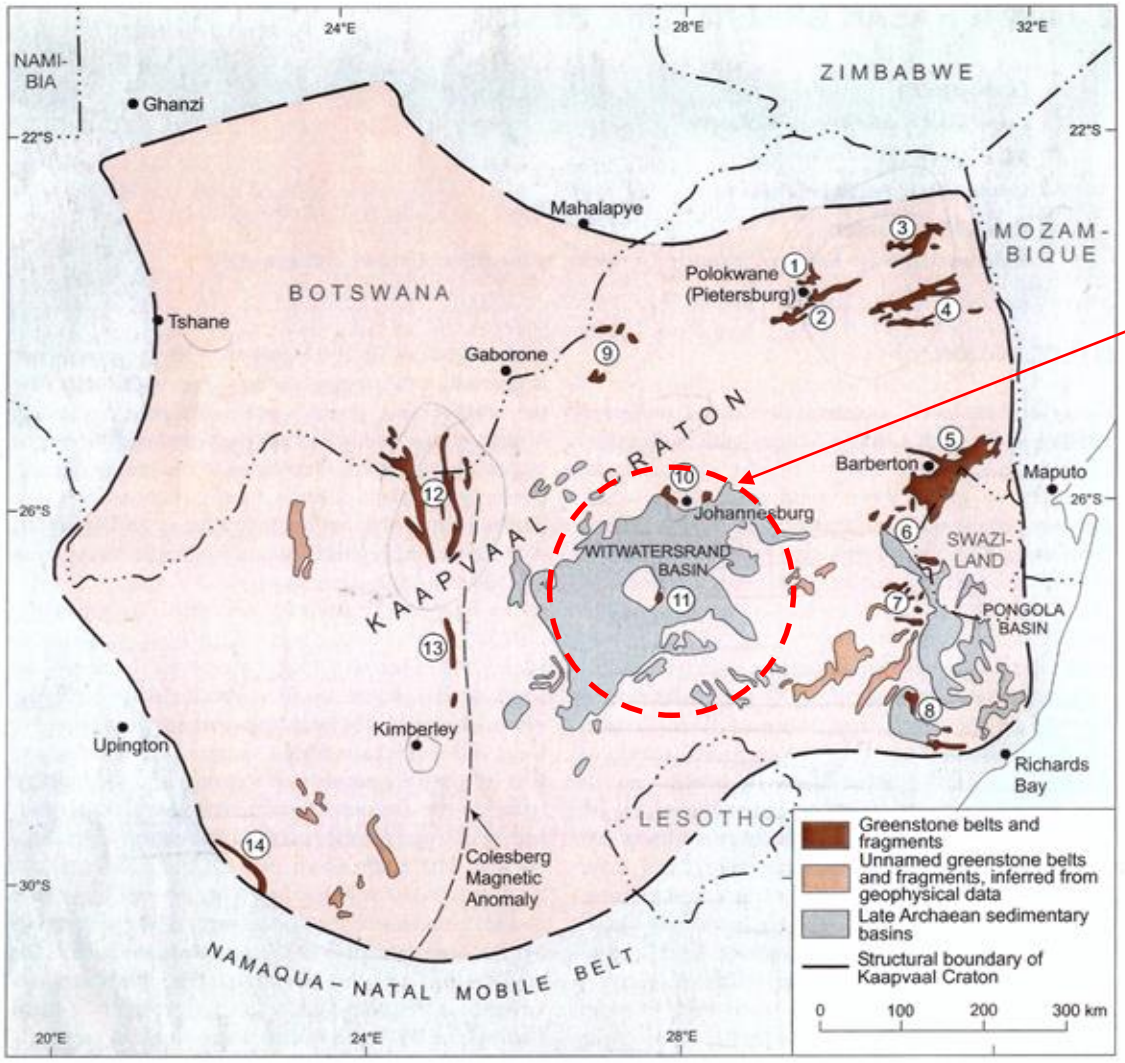

Figure 2.1: Location map of the Witwatersrand Basin (after Brandl et al., 2006)

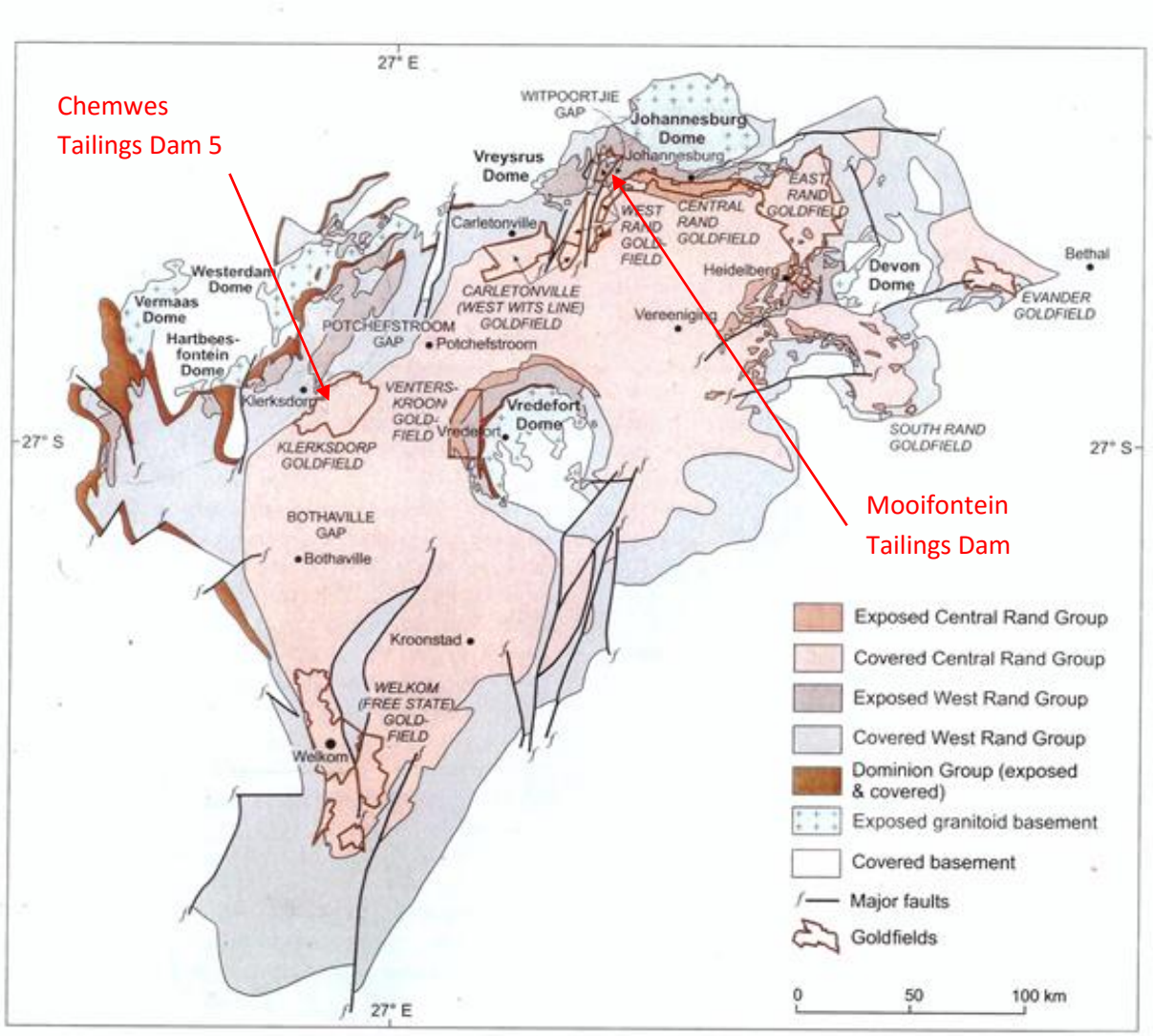

Figure 2.2: Geological map of the Witwatersrand Basin, with younger cover sequences removed (after Brandl et al., 2006)

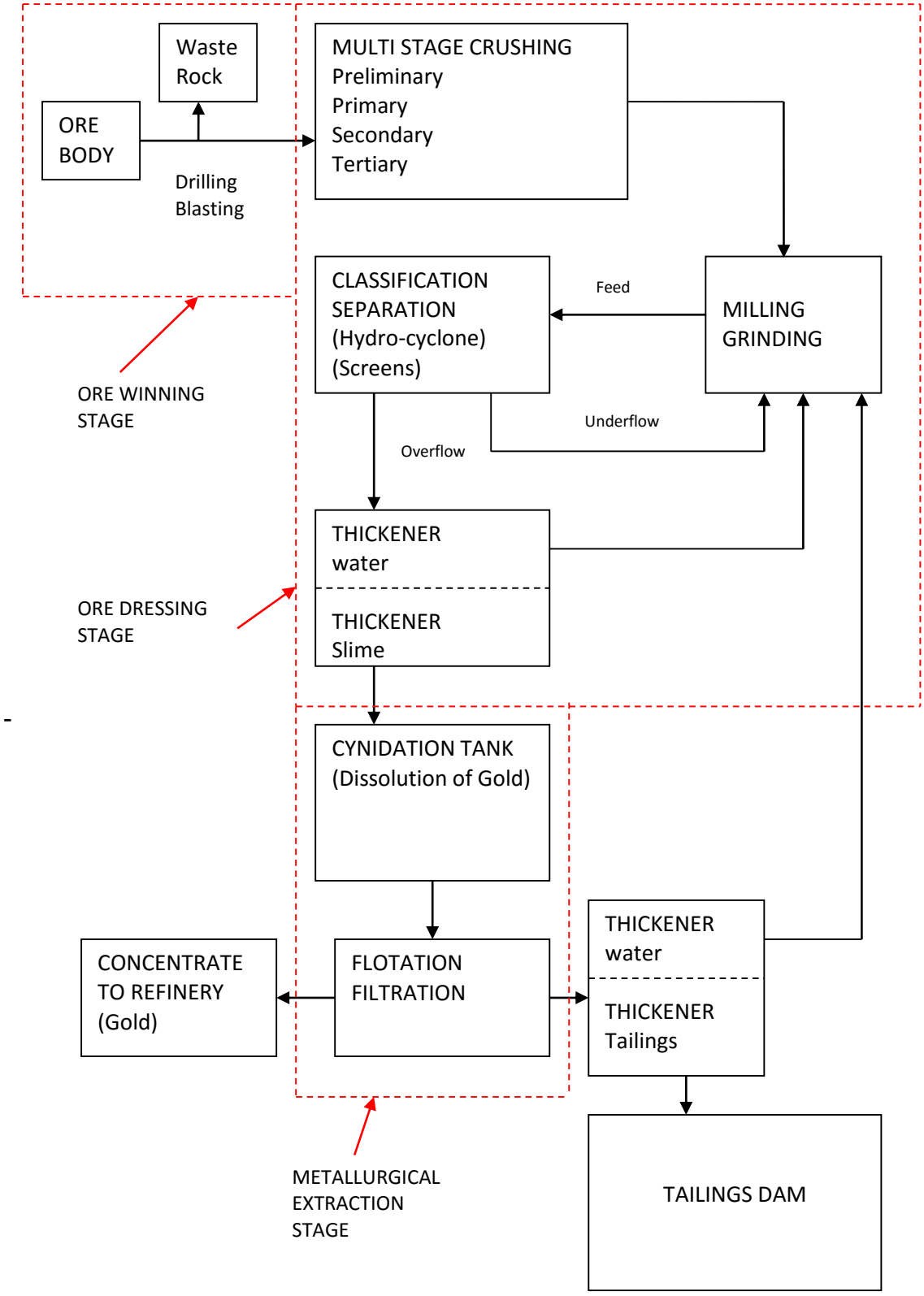

Figure 2.3: Tailings generation process (After Adamson, 1973 & Robinson, 2008).

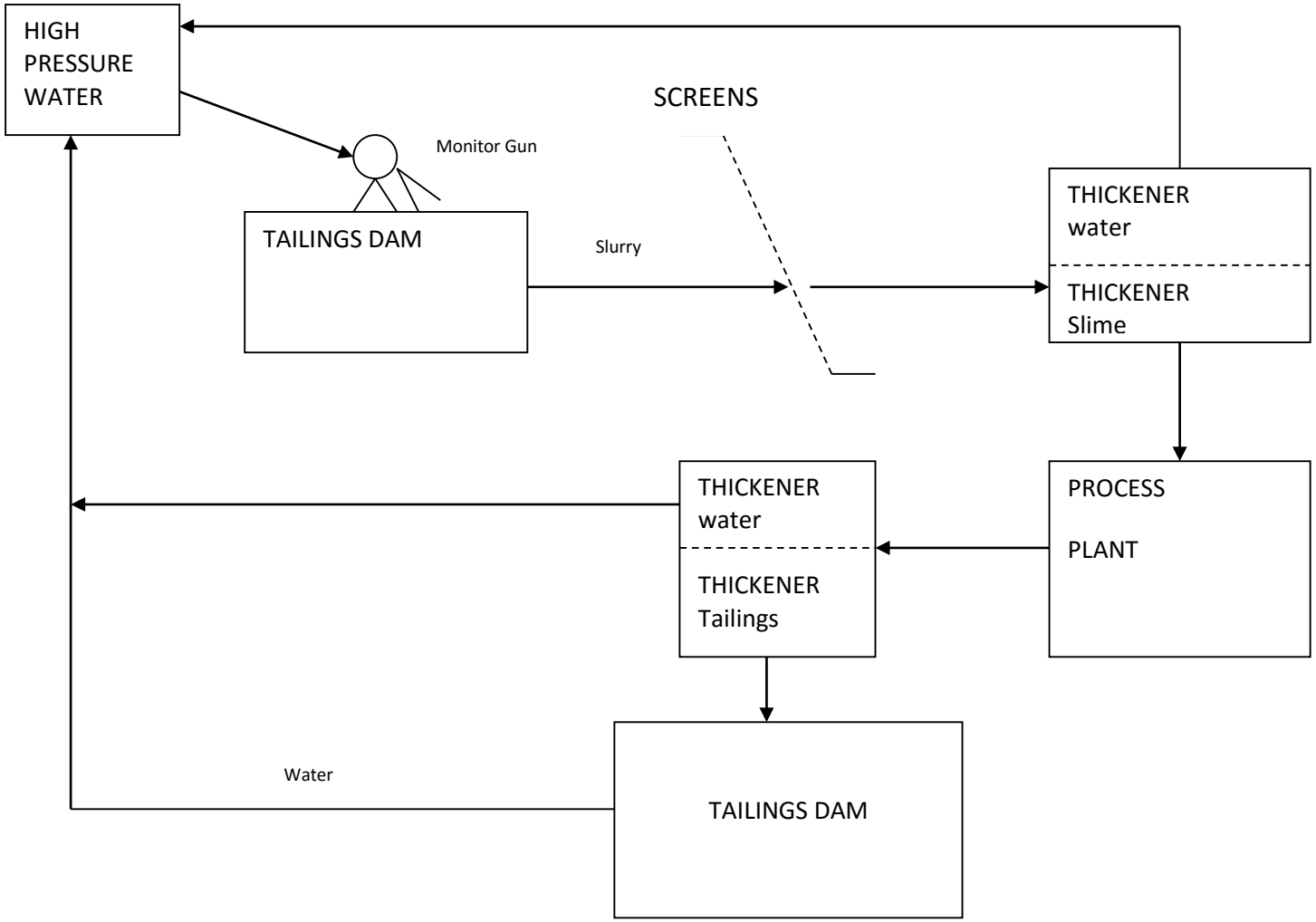

Figure 2.4: Hydraulic tailings re-mining (After Robinson, 2008)

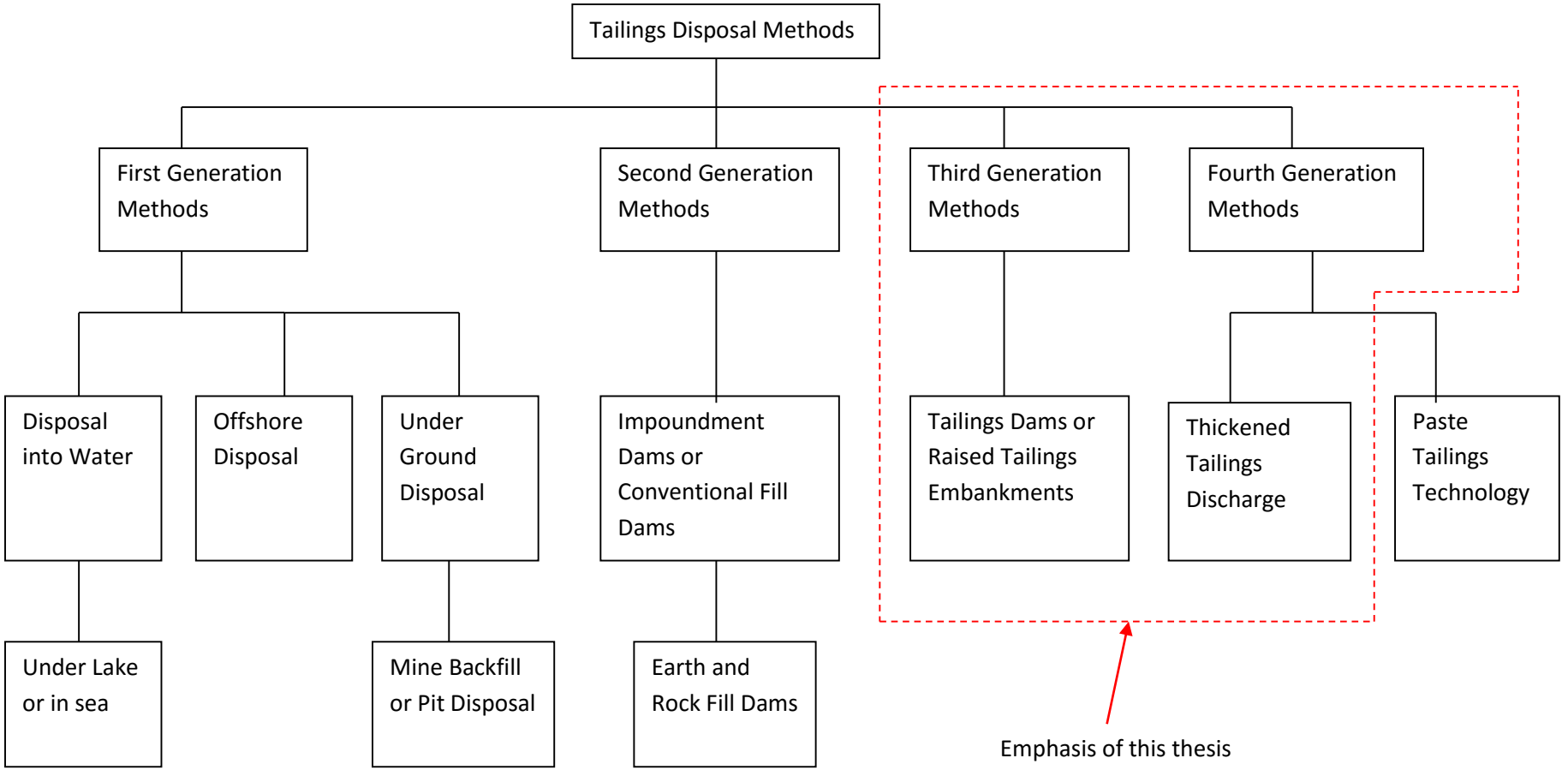

Figure 2.5: Generations of tailings disposal methods

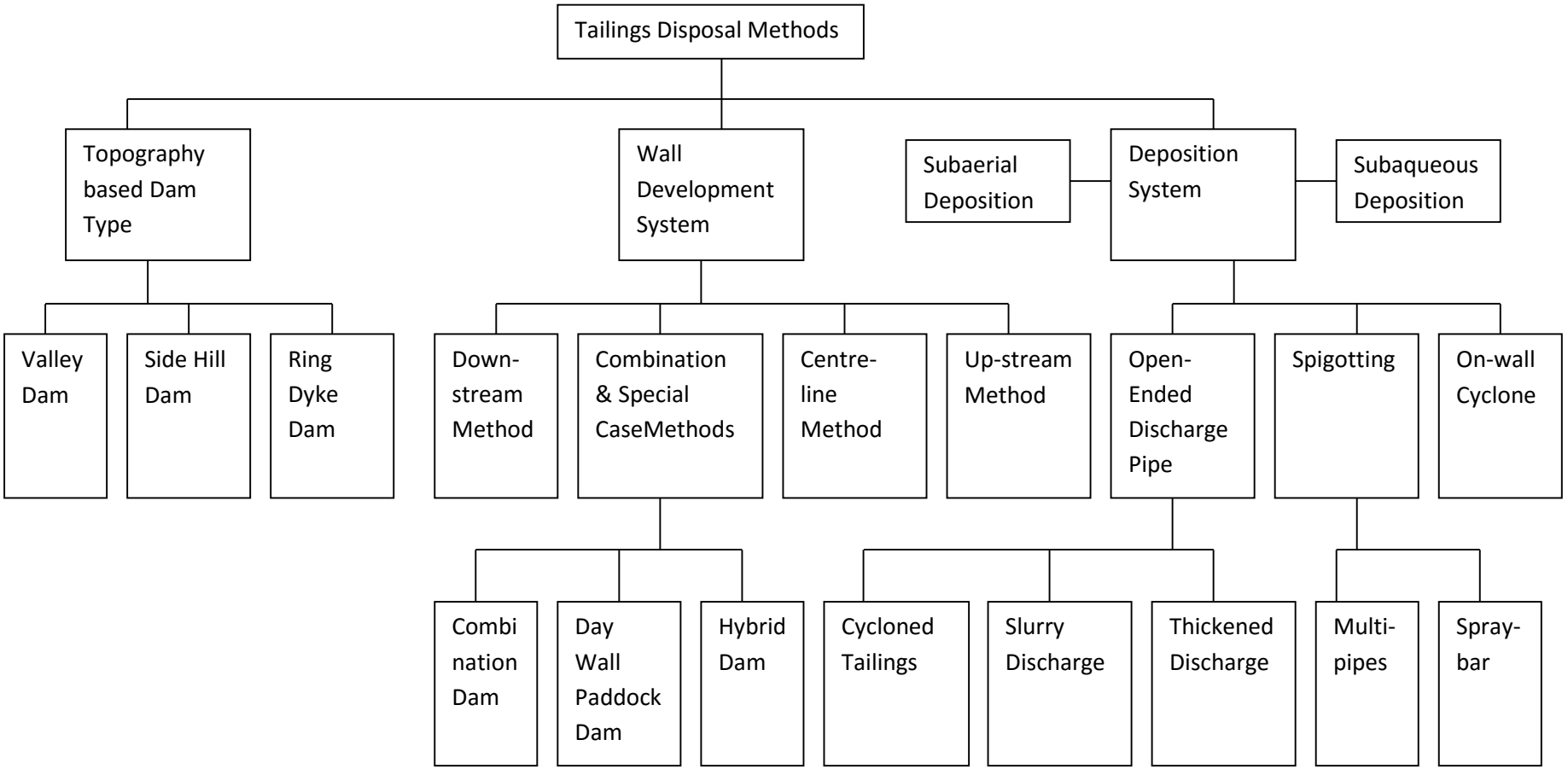

Figure 2.6: Classification of tailings disposal methods

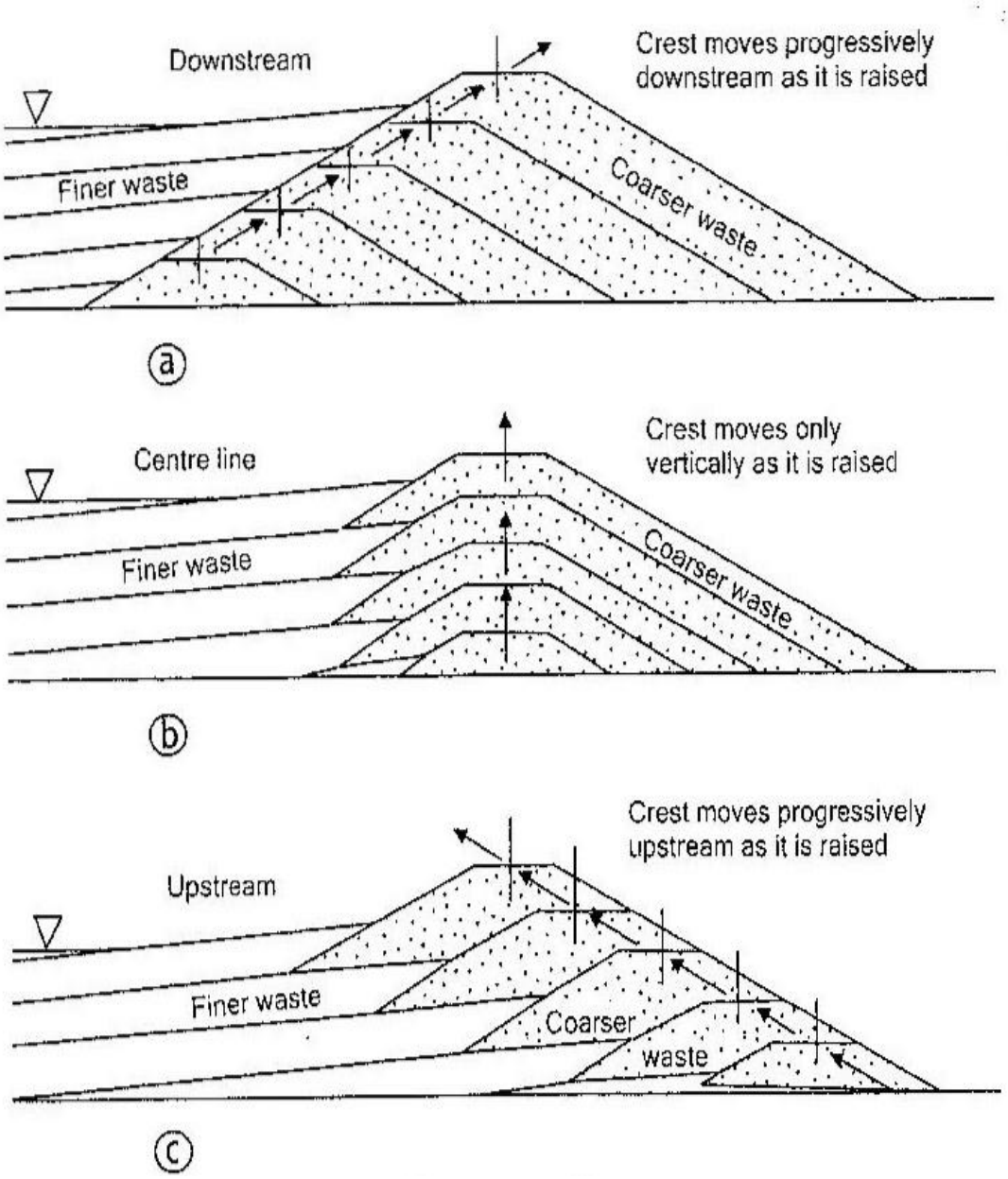

Figure 2.7: Main wall development systems for tailings dams (After Blight, 2010)

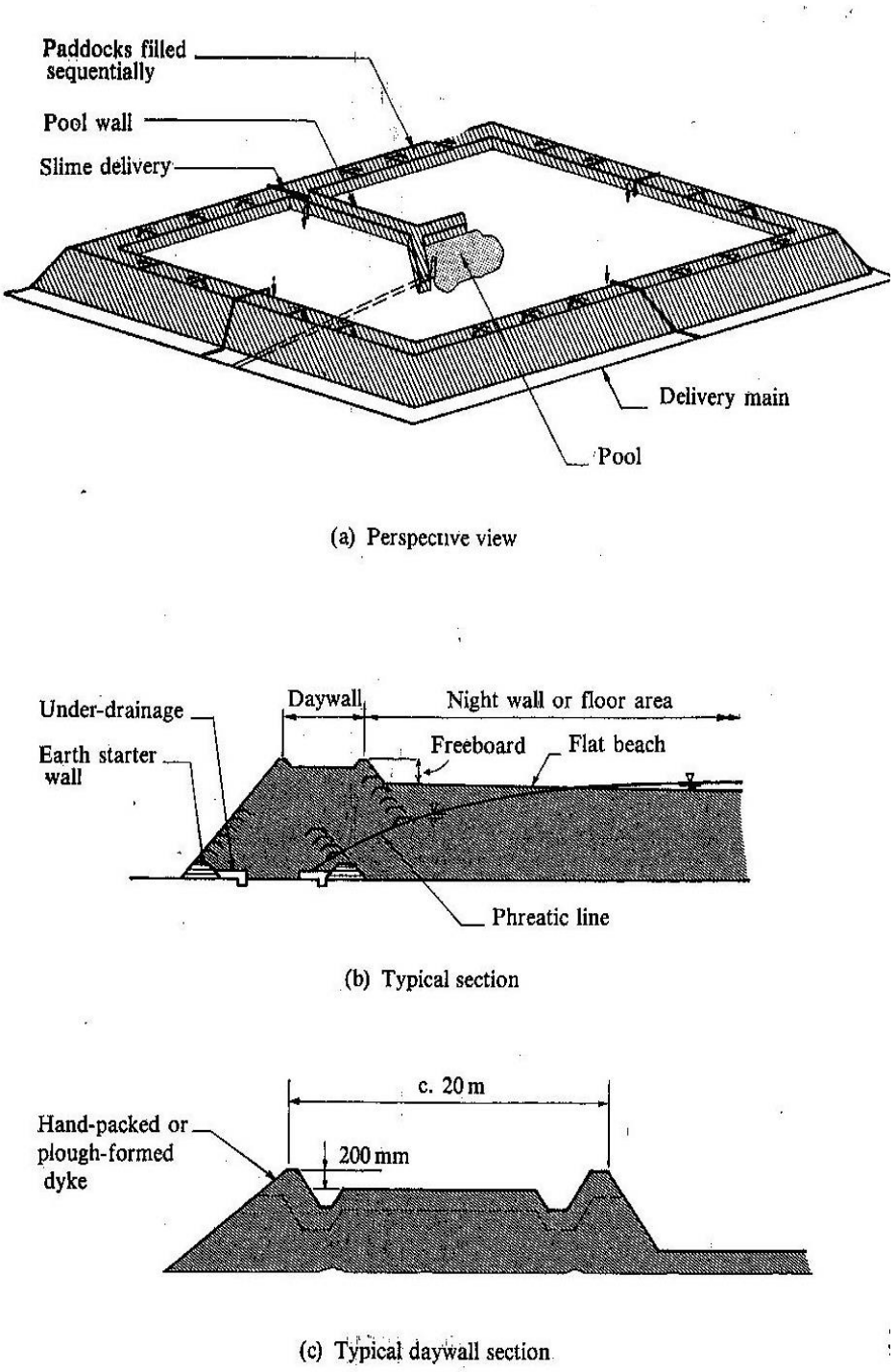

Figure 2.8: Paddock system of dam construction (After McPhail and Wagner, 1989)

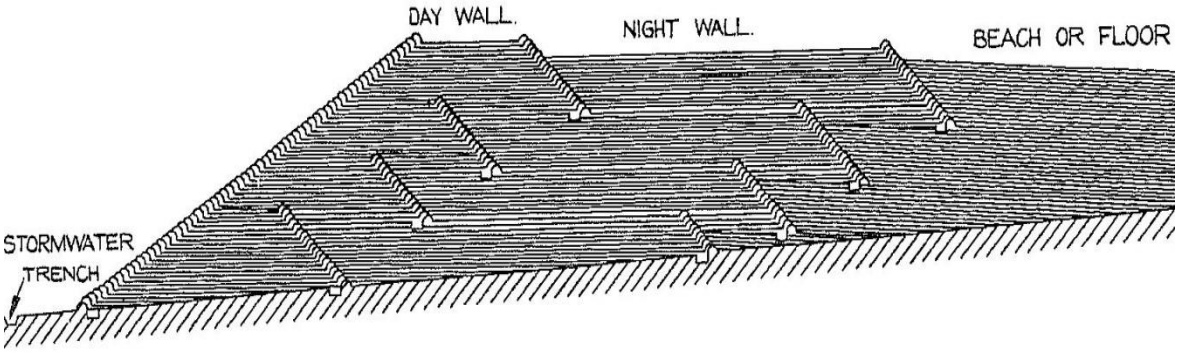

Figure 2.9: Paddock system of dam construction showing daywall and nightwall (NBRI, 1959)

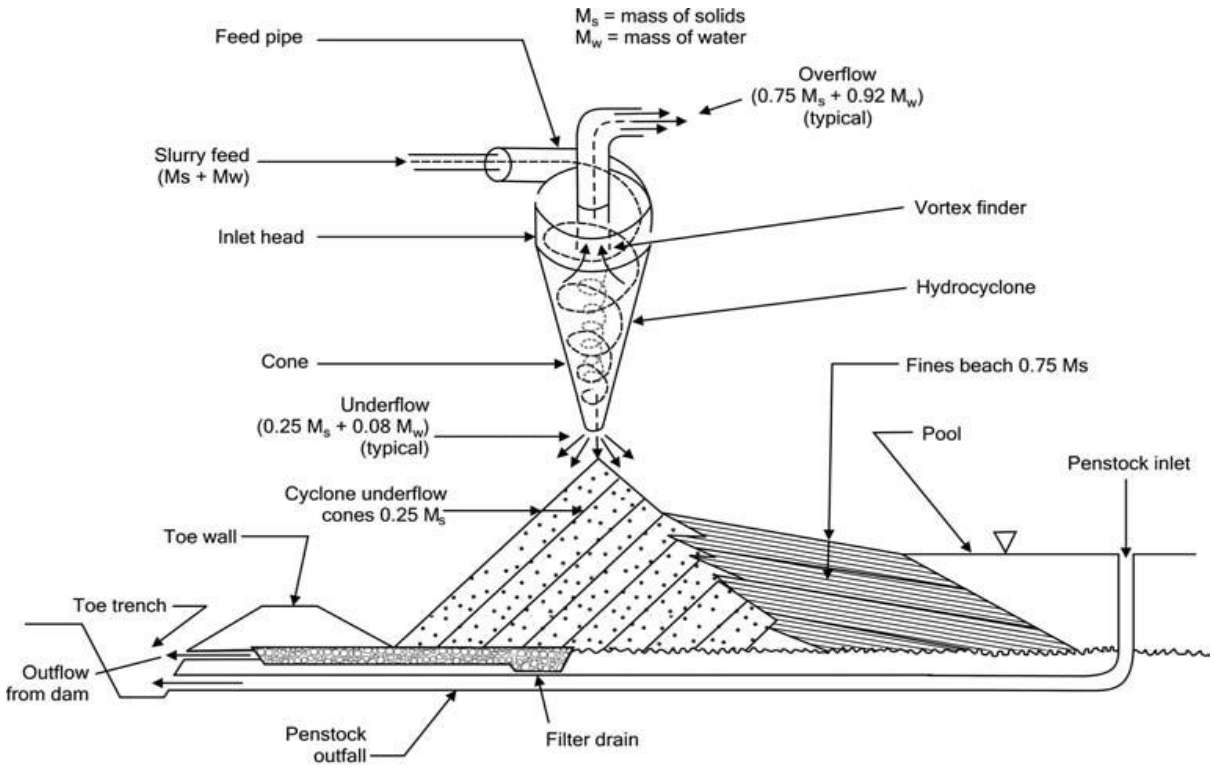

Figure 2.10 Dam construction using on-wall cycloning (Blight, 2010)

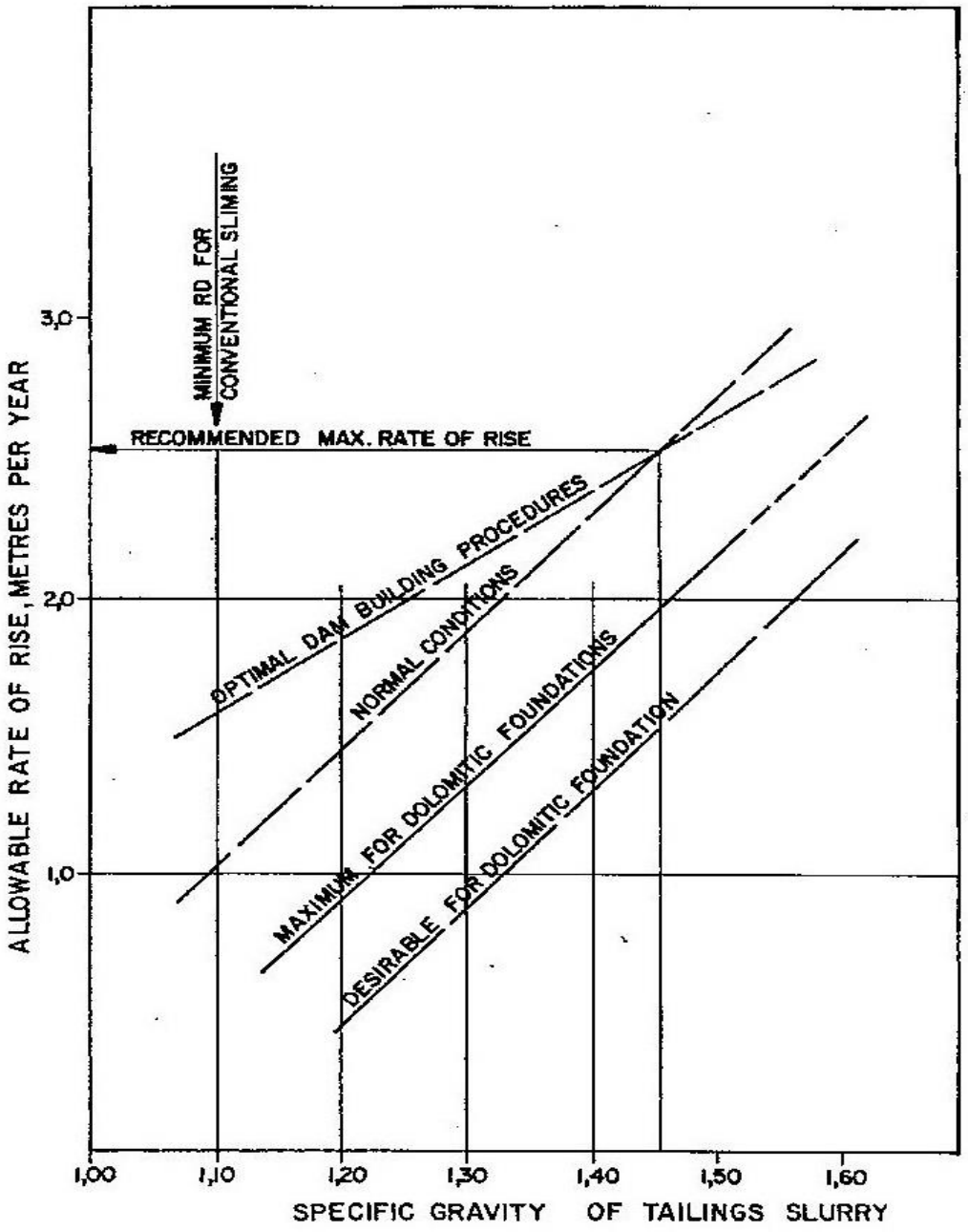

Figure 2.11 Allowable rate of rise versus specific gravity of slurry (Wates, 1983, 1988)

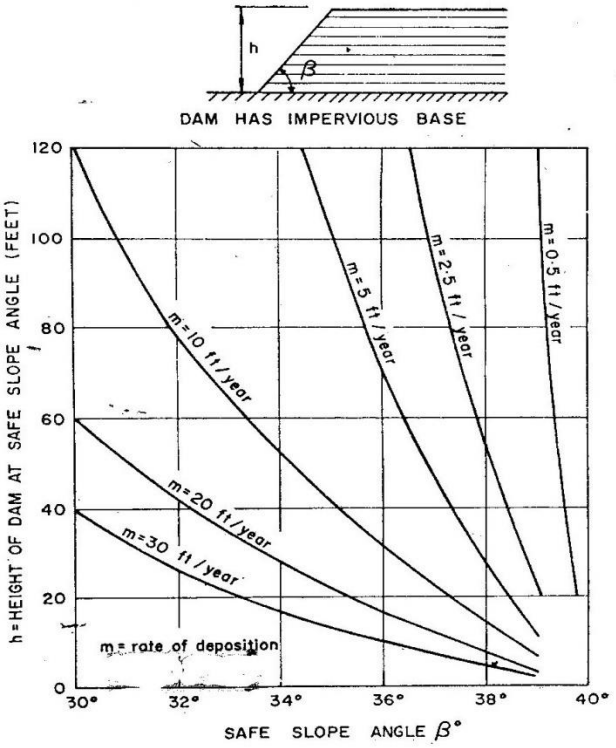

(a)

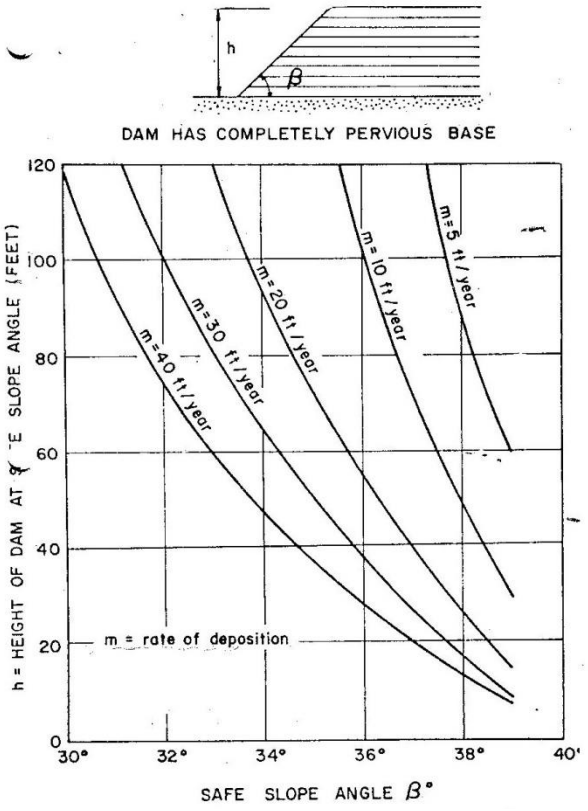

(b)

Figure 2.12 Height of dam versus wall slopes for various rates of rise (Blight, 1969)

Void ratio of tailings undergoing deposition and representing a deposition rate equivalent state in void ratio terms e=1.45

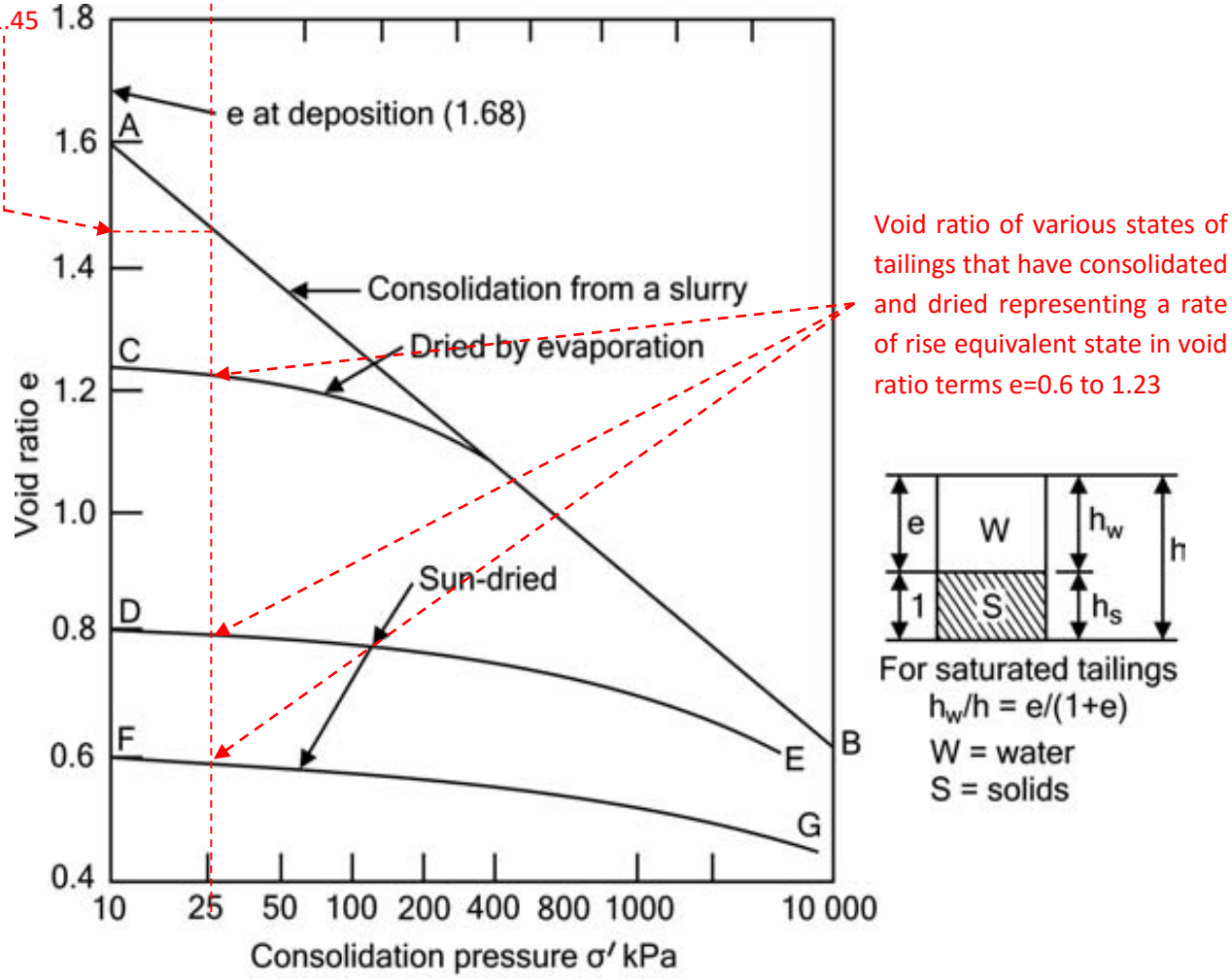

Void ratio of various states of tailings that have consolidated and dried representing a rate of rise equivalent state in void ratio terms e=0.6 to 1.23

Figure 2.13 Void ratio - Consolidation pressure relation for slurry and dried gold tailings states (Chamber of Mines, 1996)

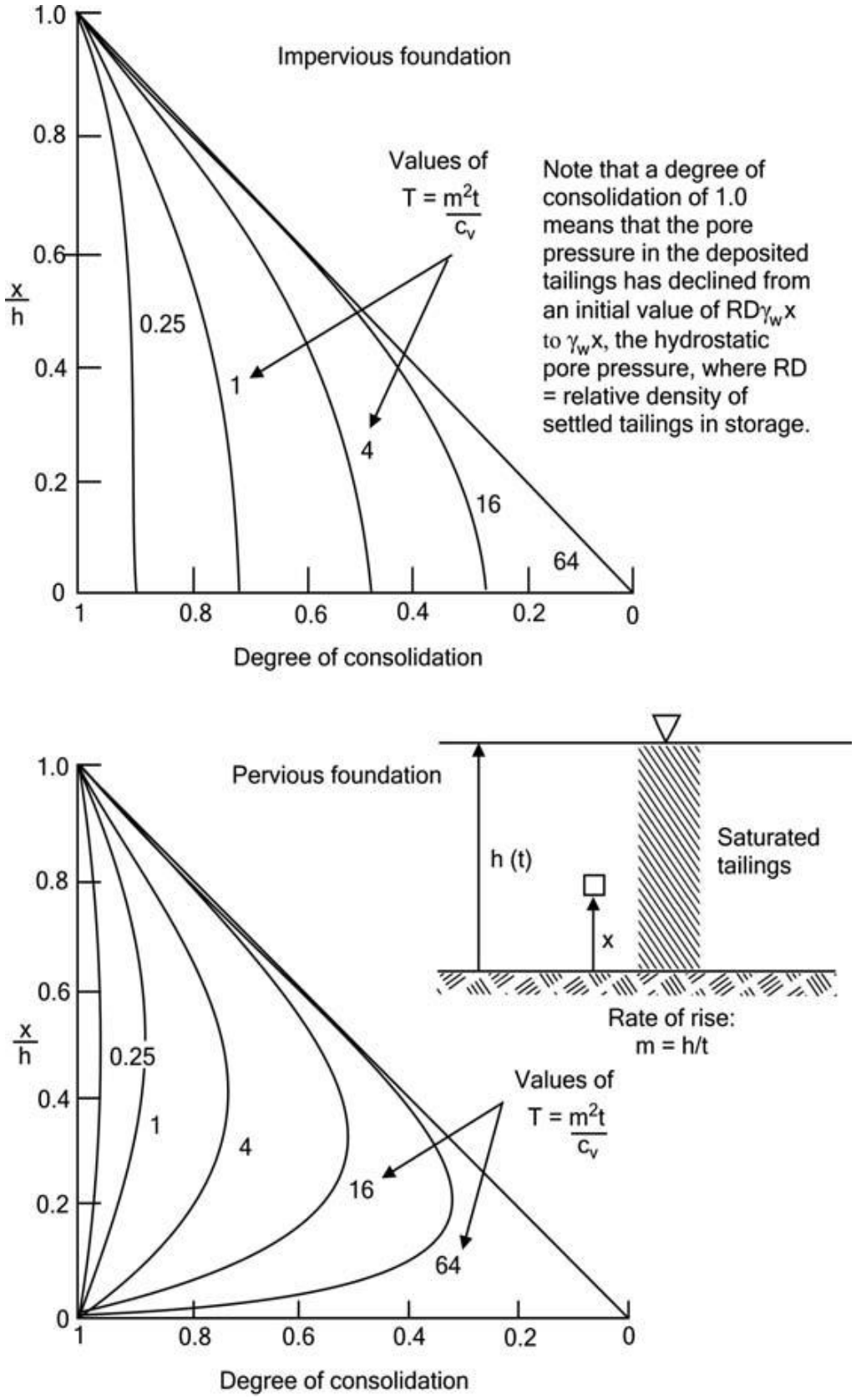

Figure 2.14 Gibson's (1958) Consolidation rate of rise design chart [h=mt case] (Blight, 2010)

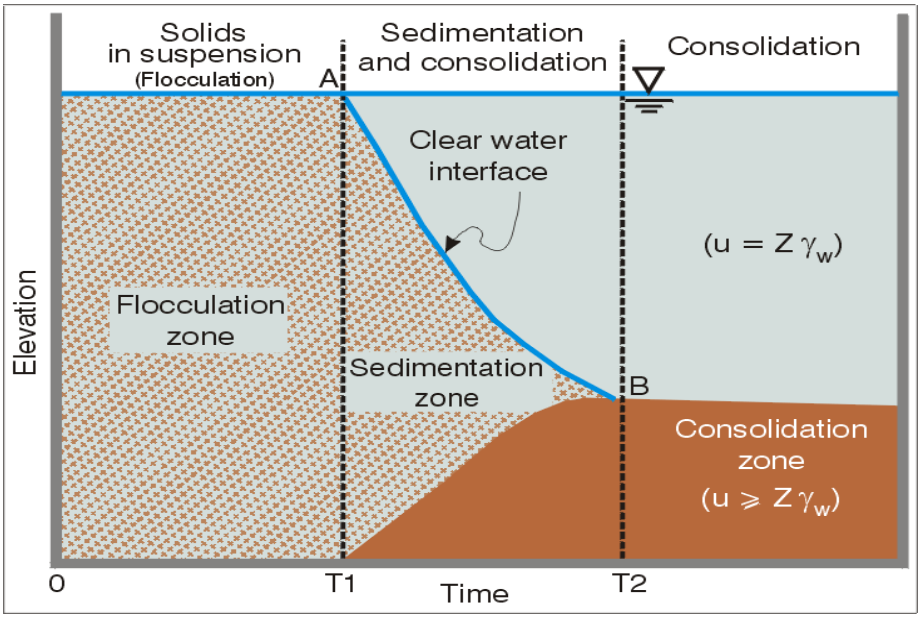

Figure 2.15 Schematic representation of flocculation, sedimentation and consolidation in a vertical column (Pedroni et al., 2006)

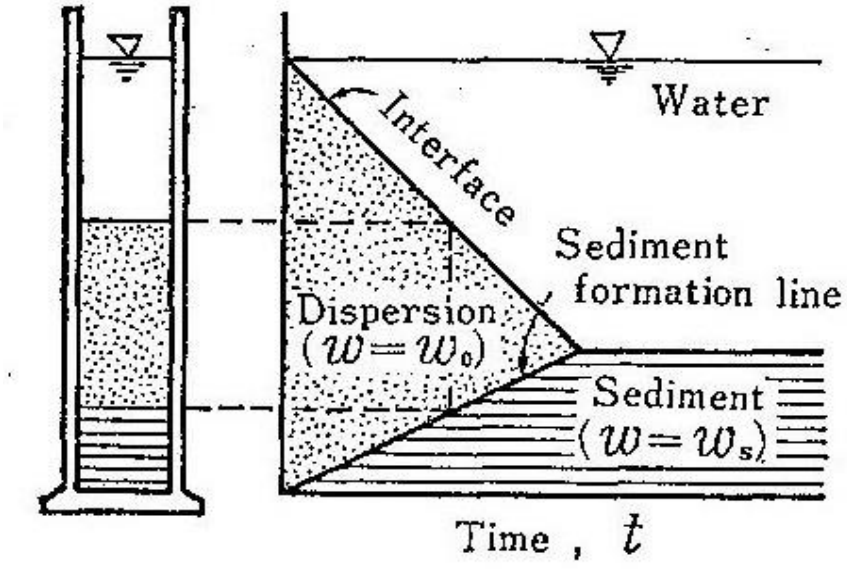

Figure 2.16 Idealized hindered settling typical of sandy materials (Imai, 1981)

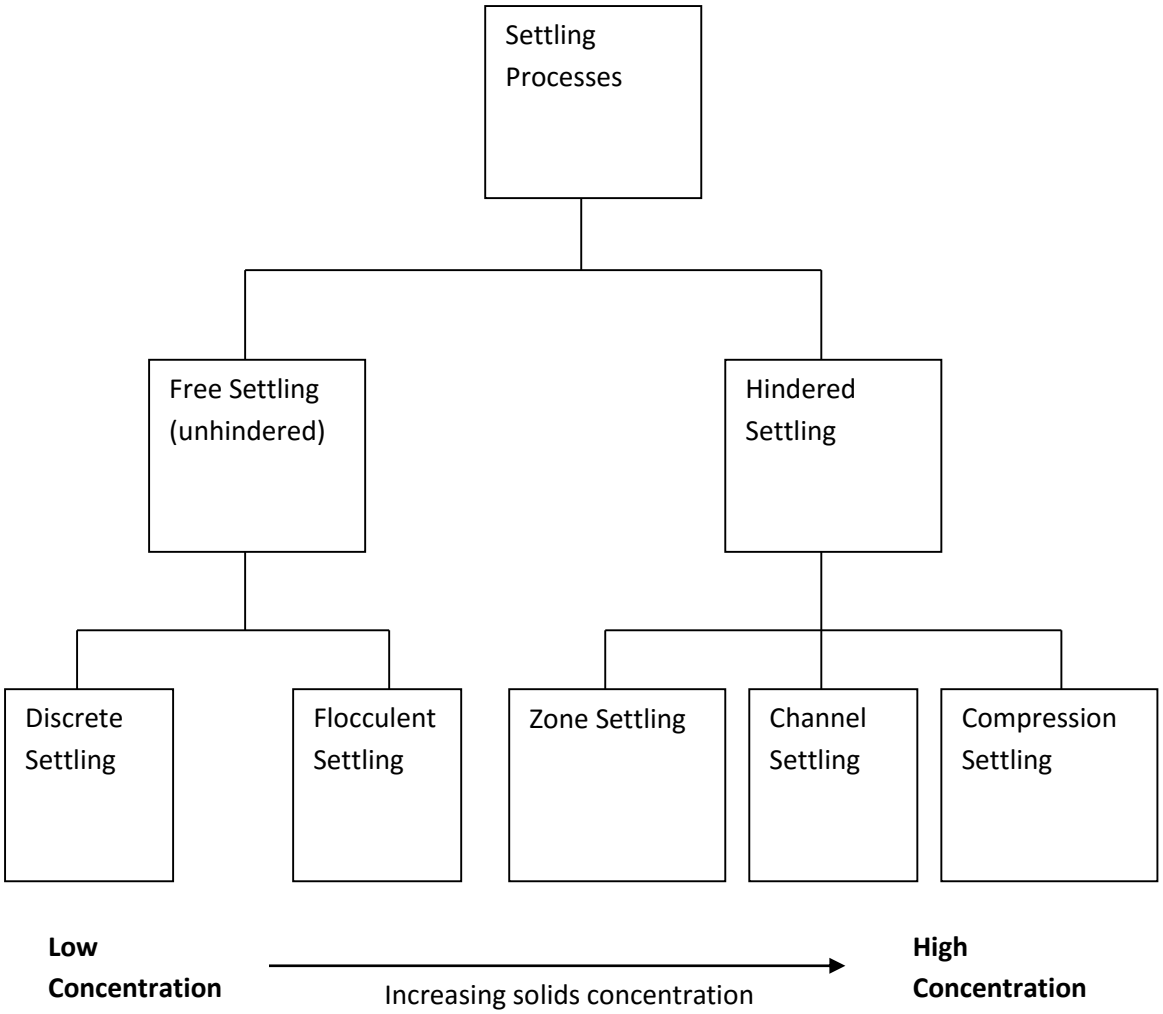

Figure 2.17: Classification of settling processes

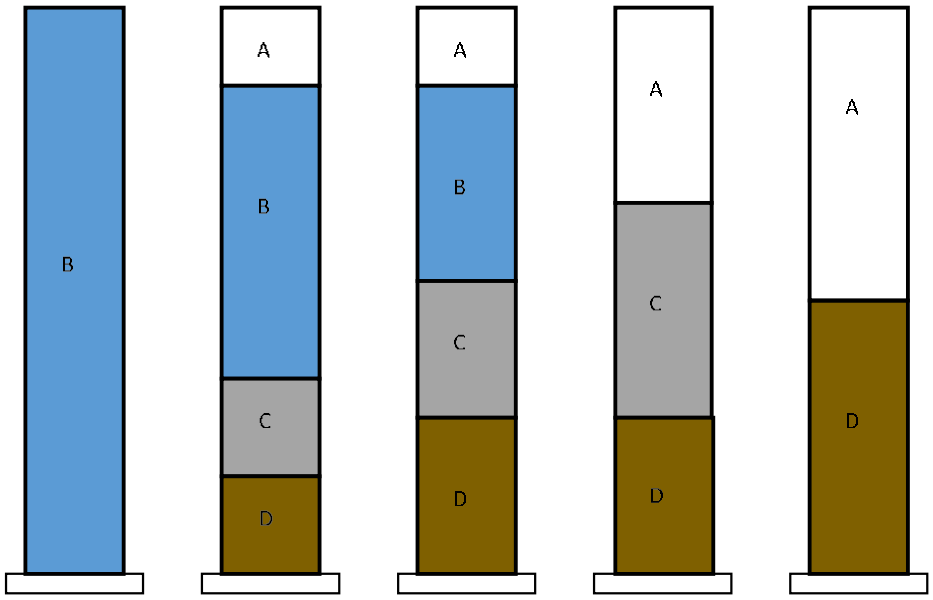

A	Clear liquid	C	Variable concentration
B	Initial concentration	D	Settled bed

Figure 2.18: The 5 stage batch settling process (Kurt, 2006)

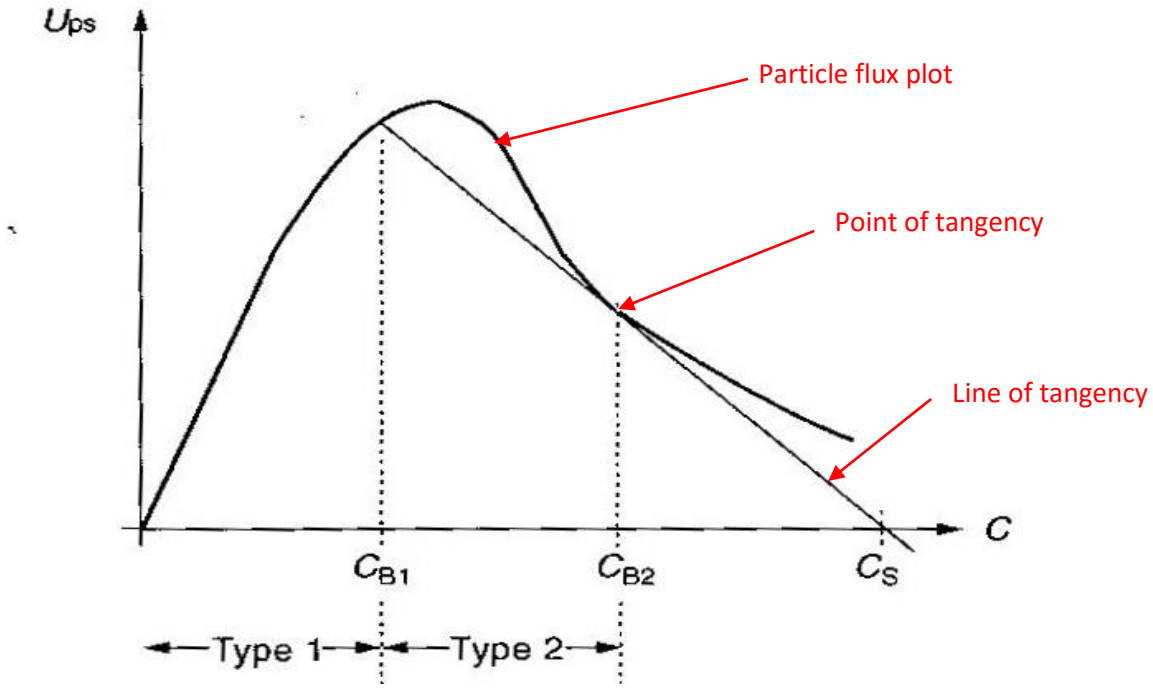

Figure 2.19 Suspension concentration - settling type relation (Rhodes, 2008)

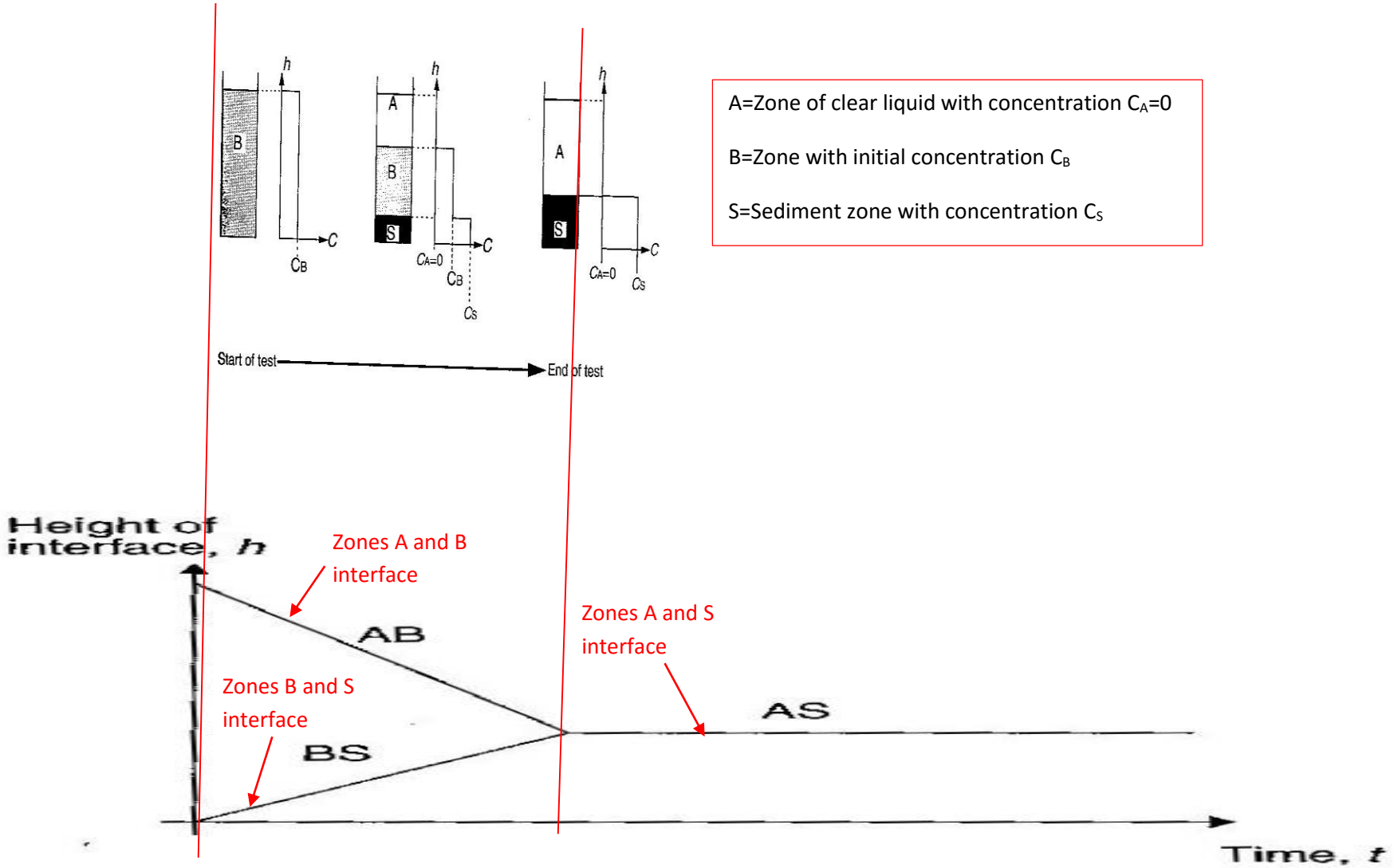

Figure 2.20 Concentration defined Settling type 1 plot (Rhodes, 2008)

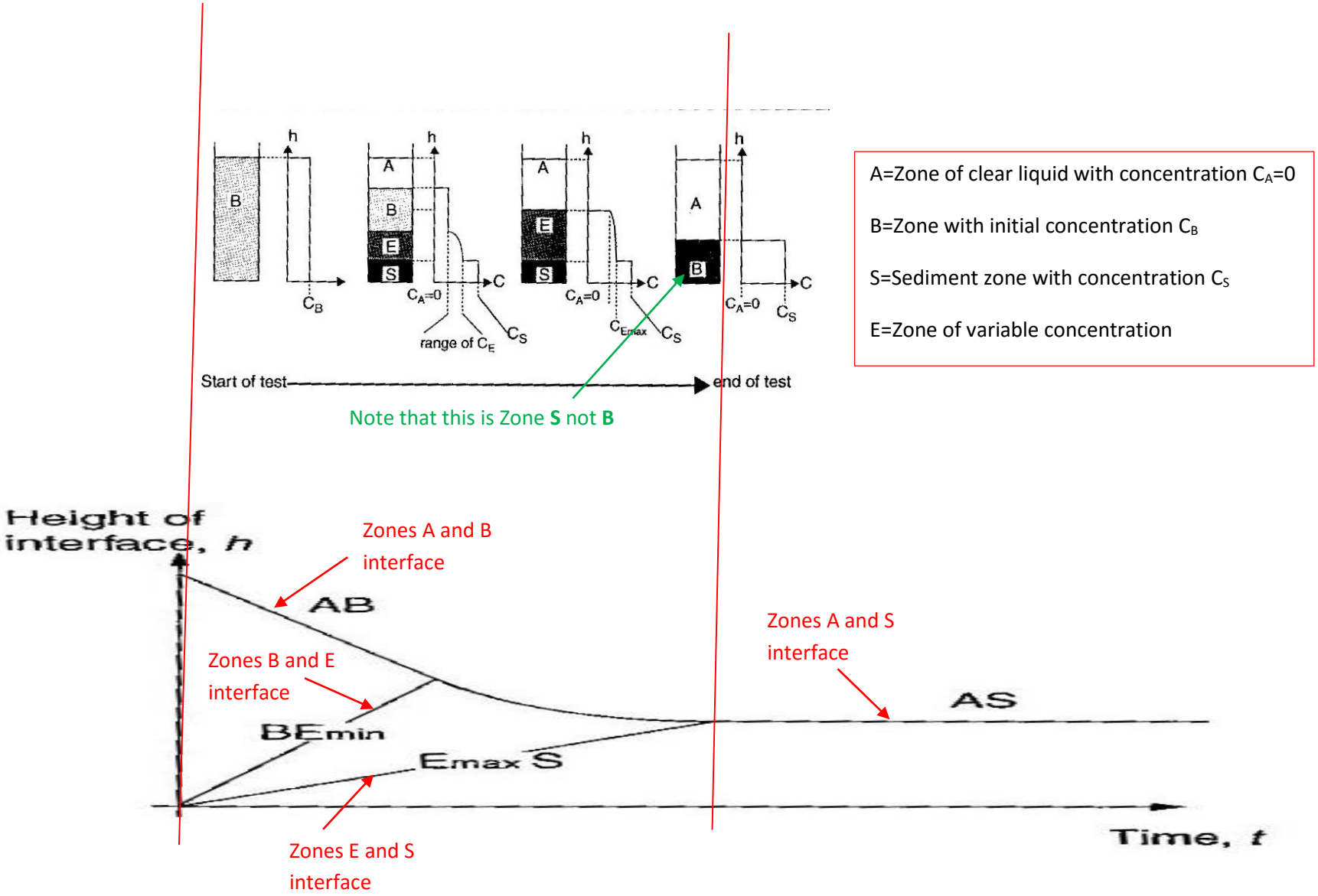

Figure 2.21 Concentration defined Settling type 2 plot (Rhodes, 2008)

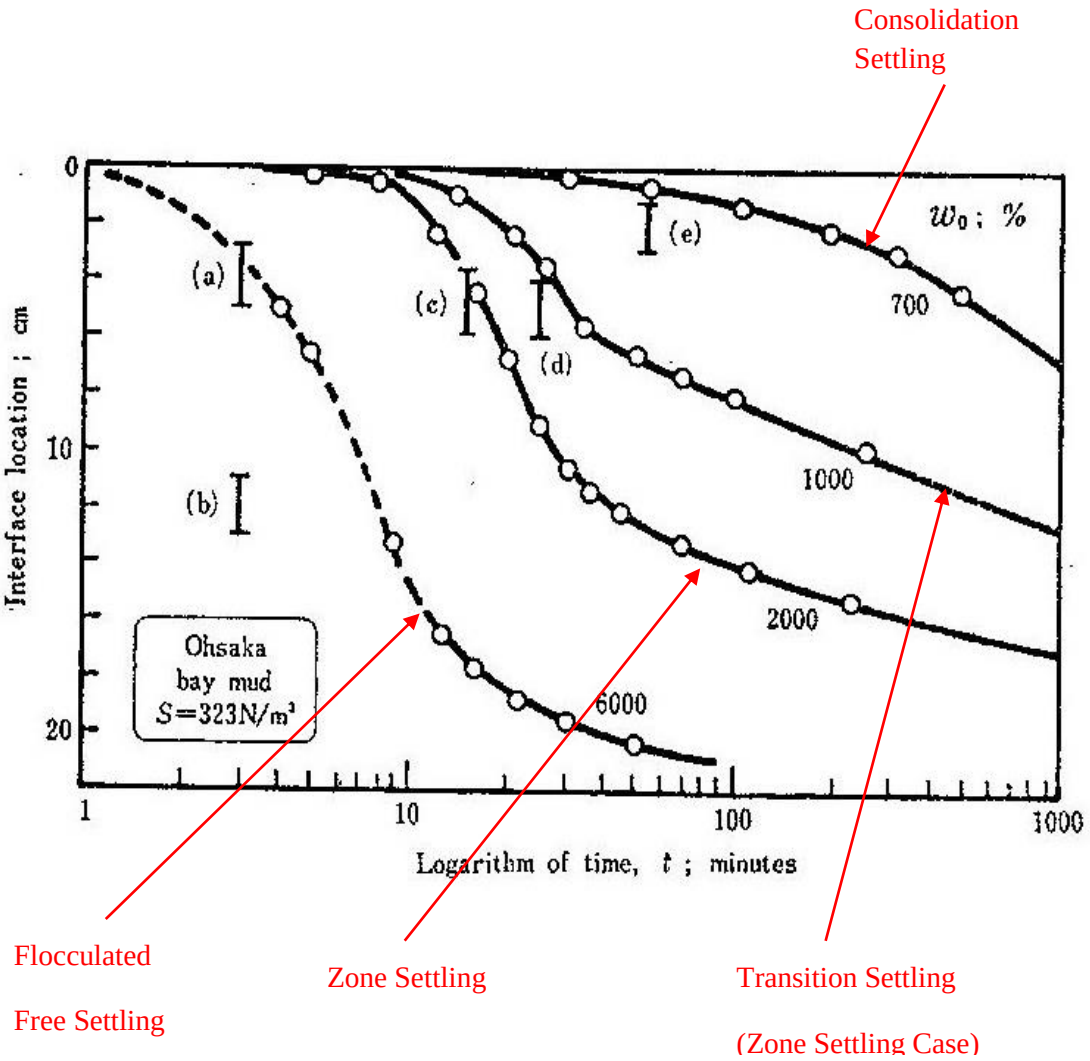

Figure 2.22: Variation of settling plots with suspension concentration (Imai, 1980)

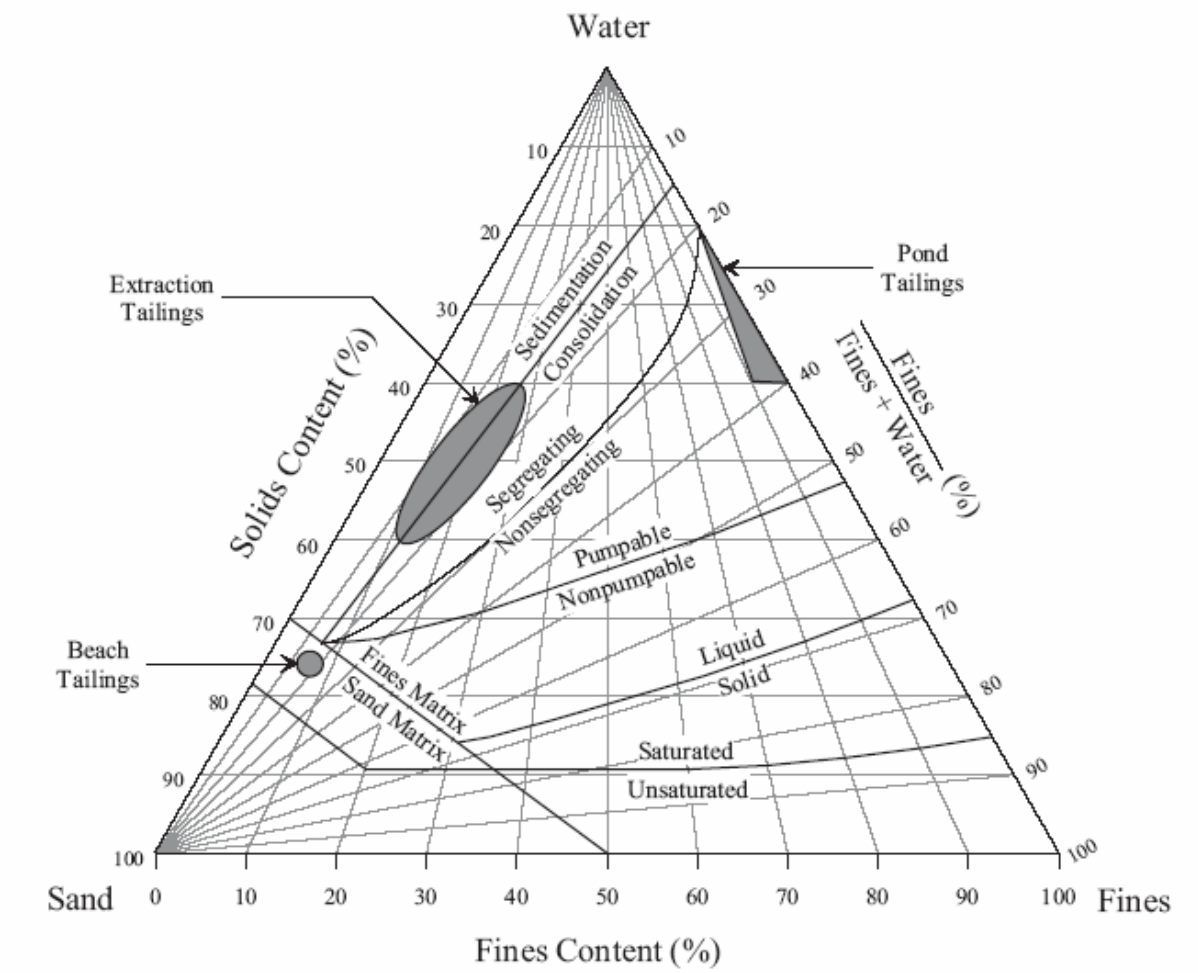

Figure 2.23: Tailings properties diagram of oil sands tailings (Jeeravipoolvarn, 2010)

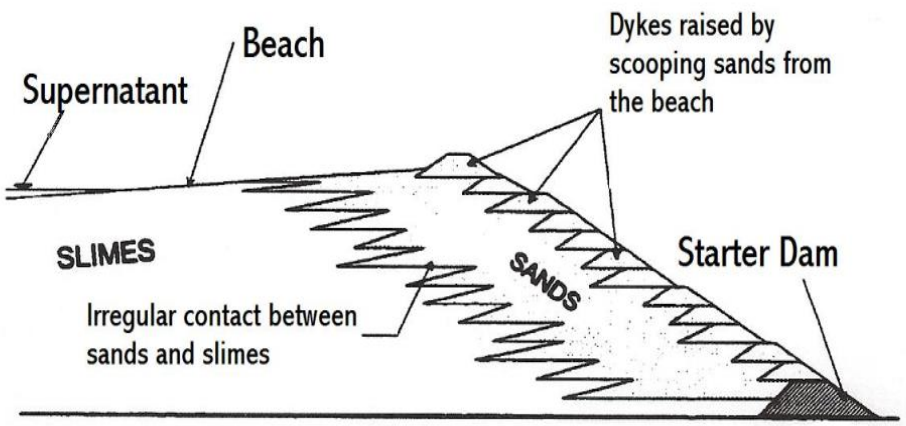

Figure 2.24: Raised embankment by upstream method (Priscu, 1999)

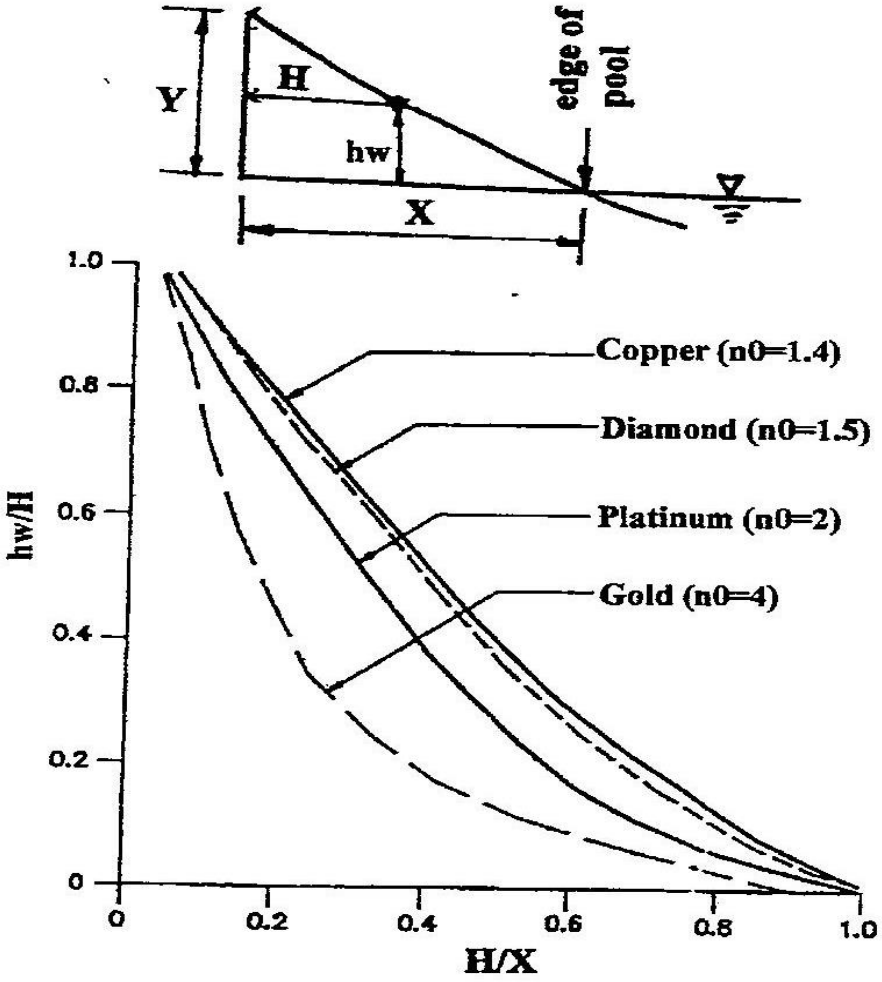

Figure 2.25: Beach profiles for dams of various types of tailings (Modified from Blight 1987 by Qiu, 2000)

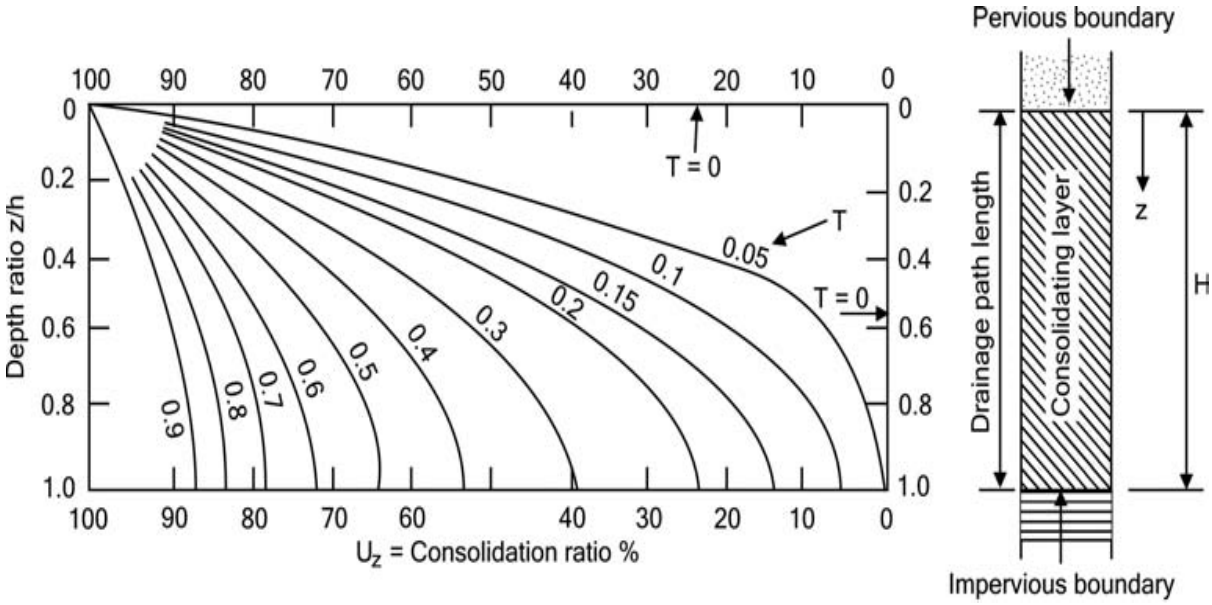

Figure 2.26 Graphical solution of Terzaghi's one dimensional consolidation equation (after Blight, 2010)

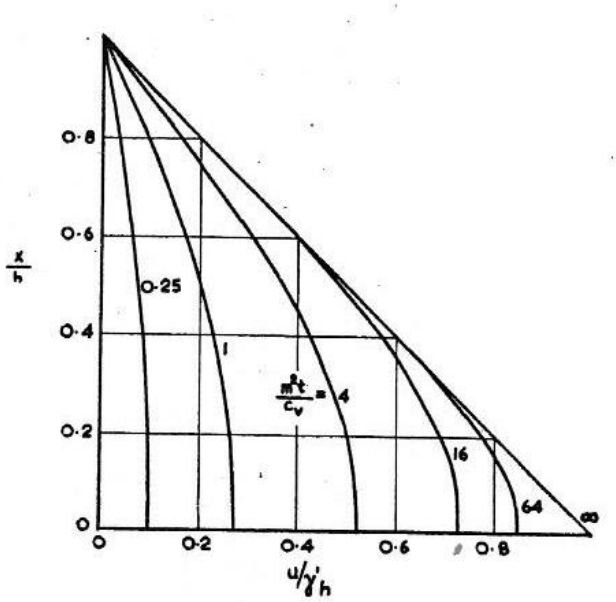

Figure 2.27: Graphical solution of Gibson's (1958) consolidation equation for impermeable base at deposition rate h=mt (Gibson, 1958)

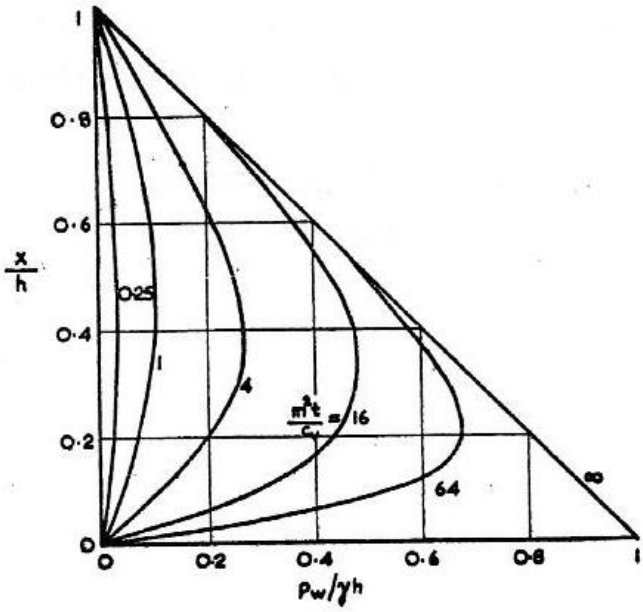

Figure 2.28: Graphical solution of Gibson's (1958) consolidation equation for permeable base at deposition rate h=mt (Gibson, 1958)

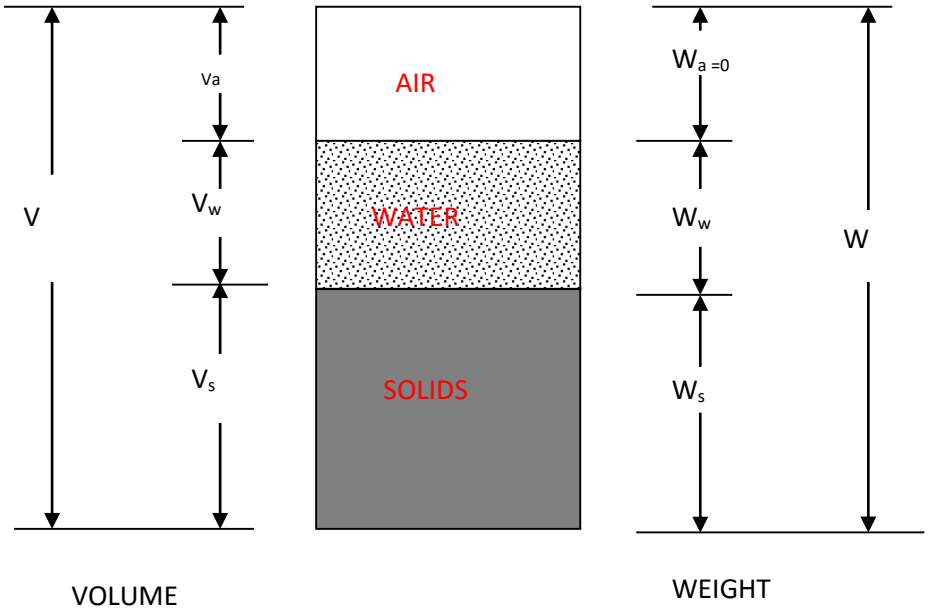

(a) 3 PHASE SOIL DIAGRAM

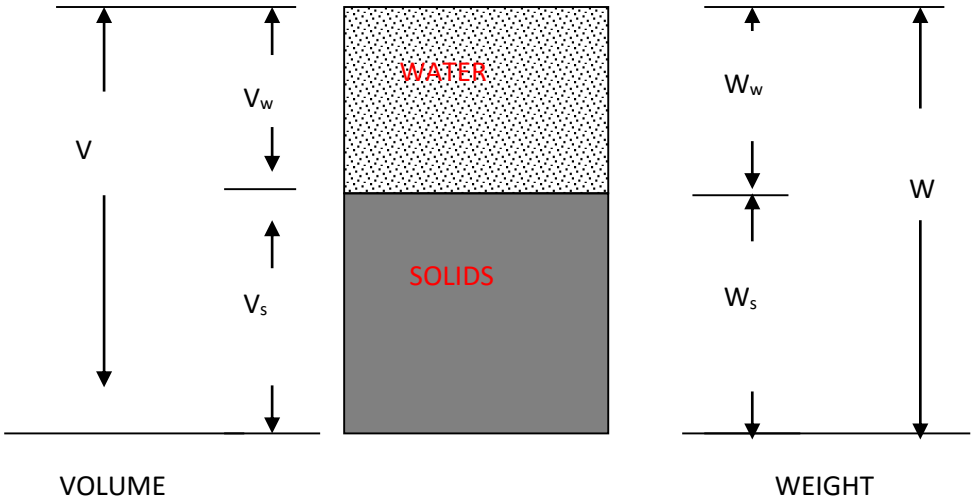

(b) 2 PHASE SOIL DIAGRAM

Figure 2.29 Soil phase diagrams representing (a) 3 phase diagram and (b) 2 phase soil diagram

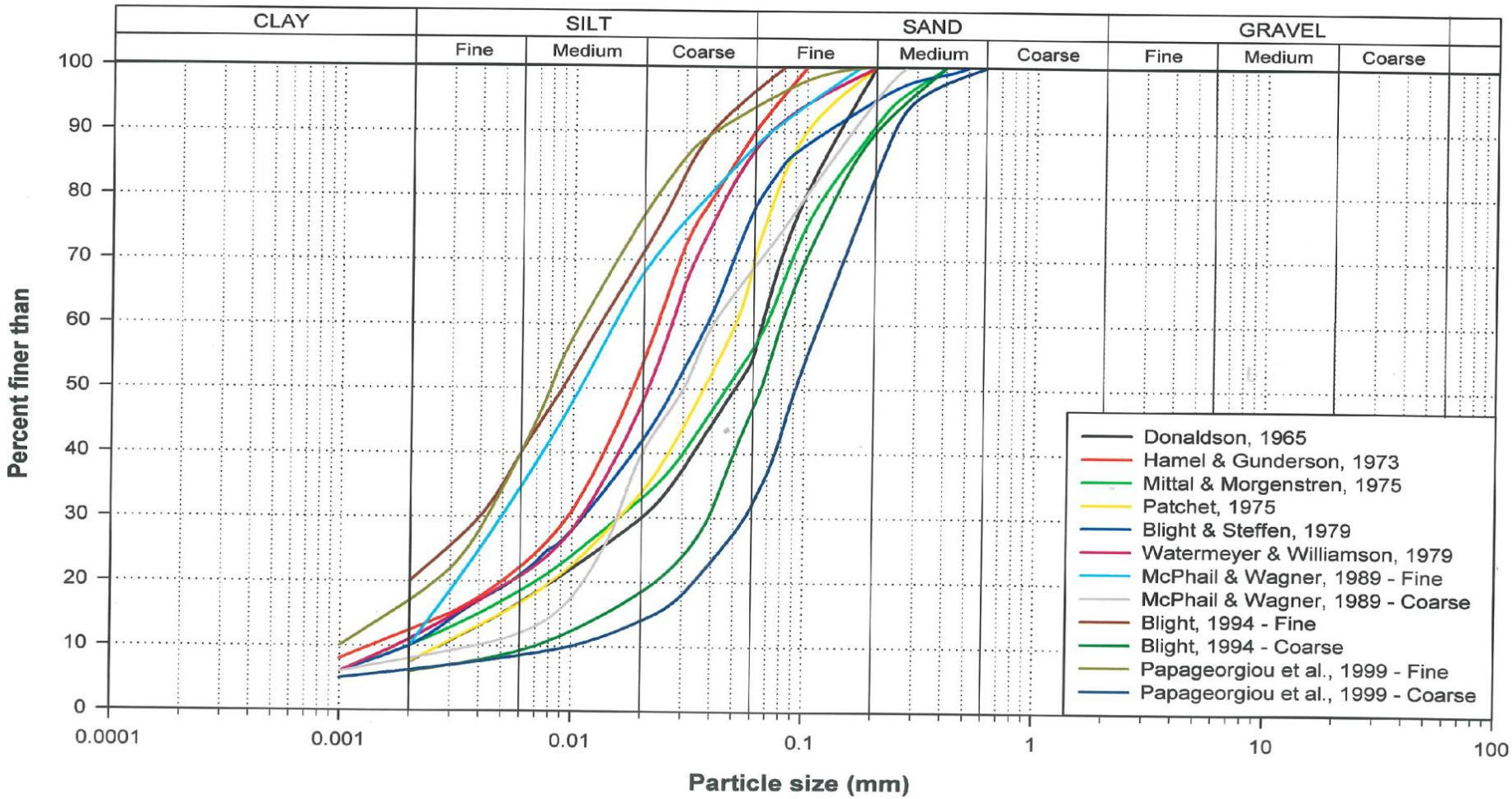

Figure 2.30: Grading curves for gold tailings (after Vermeulen, 2001)

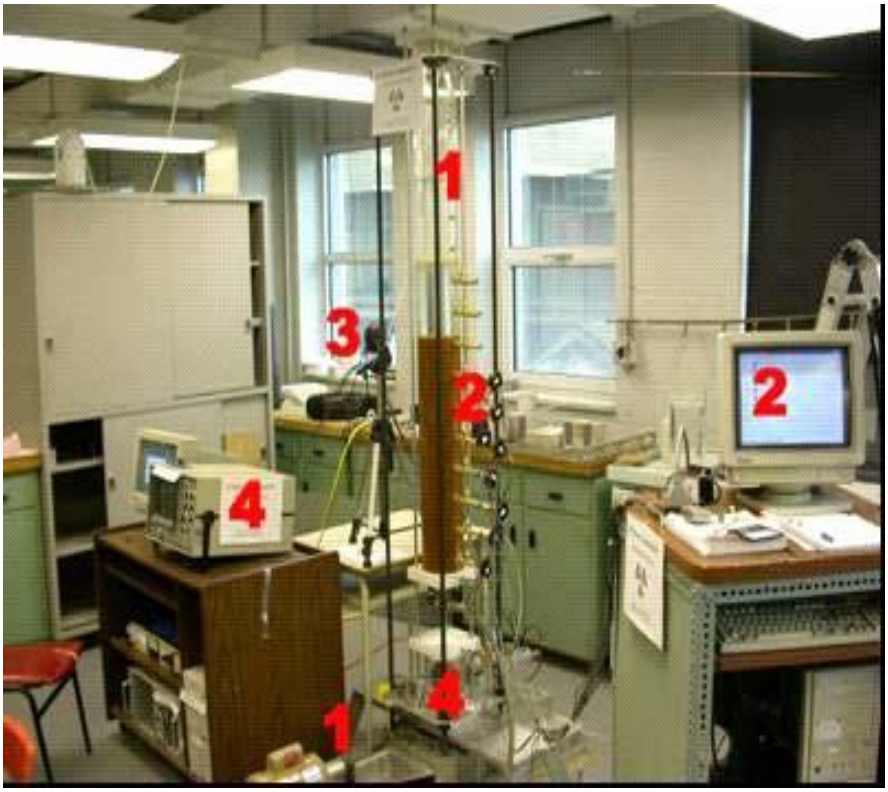

Figure 2.31: Settling column showing the main components (after Dromer, 2004; Dromer et al., 2004 and Pedroni et al., 2006)

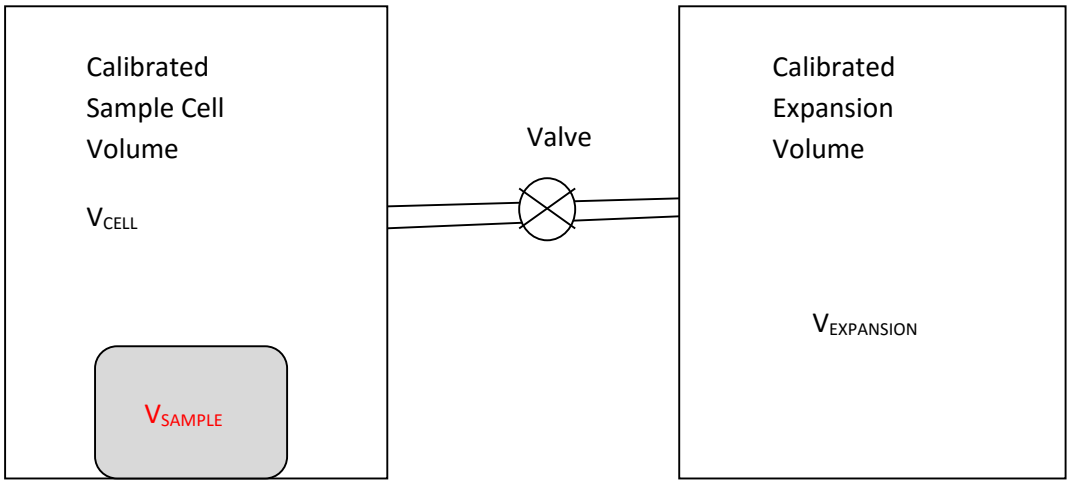

Figure 2.32: Principle of the gas pycnometer density test

Chapter 3

EXPERIMENTAL WORK

3.1 Introduction

This chapter describes the experimental methodology that was applied to achieve the objectives of the study. The methodology comprised of; characterisation of tailings and the slurry made from mixing tailings with distilled water, measurement of pore water pressures and slurry interface height from the settling column apparatus, determination of the saturated permeability of the settled tailings and evaluation of both fabric and gradation characteristics of the recovered settled tailings columns. Figure 3.1 summarises the experimental methodology.

The study aims at examining tailings deposition, sedimentation and consolidation together with the attendant properties of tailings. The properties of tailings included permeability, compressibility, density and fabric under different rate of rise scenarios. The study required an assembly of equipment and instruments that were not readily available and therefore an apparatus was designed and purpose built at the University of Pretoria laboratories.

One of the objectives of this research was to study particle size segregation and the development of pore water pressure when tailings are deposited. Specifically tailings particle size segregation and permeability of tailings were to be quantified as well as to investigate the widely held notion that excess pore water pressures limit rate of rise of tailings dams. Subject to the permeability of the tailings, a high rate of rise is believed to result in the build-up of excess pore water pressures and possible collapse of the tailings dam while a low rate of rise on the contrary would allow dissipation of excess pore water pressures and thus result in safe tailings dam walls being constructed.

The chapter presents the testing programme adopted, describes the samples used for the research and details the making of slurries for the study. The chapter briefly describes the laboratory tests used to characterise the gold tailings before and after settling column experiments. The processes of fabricating and assembling the apparatus are summarised. The calibration of various components of the apparatus together with the testing procedures for the

experiments that were carried out are also discussed. The presentation of the experimental results is made in the next chapter.

3.2 Testing Programme

The testing programme adopted to achieve the aim and objectives of the research involved the selection of tailings dams from which to source samples, rate of rise scenarios, slurry testing apparatus and testing methods and techniques to fully characterise tailings to enable a comprehensive analysis of the excess pore water response of tailings in a laboratory set up. The experimentation necessary to answer the research questions concerning particle size segregation, tailings permeability and excess pore water pressure, required a good appreciation of the processes and procedures of building tailings dams. The common methods of construction of tailings dams in South Africa, which are, the day night paddock wall system and the on-wall cyclone tailings dam construction system were the methods focussed on for the purposes of this research. Each of the two tailings dam construction systems is summarised below with an emphasis on aspects relevant to developing a testing programme and an experimental apparatus for this research.

Day night paddock wall system

The construction procedure for the day night paddock wall system in South Africa entail deposition of a thin layer of 150mm thickness of whole tailings slurry on the paddock during the day and the same slurry deposited in thicker layers on the beach at night. The day's deposition was then allowed time, usually a two weeks rest period without any tailings deposition at the specific location, while deposition was carried out at other parts of the paddock system. During the two weeks rest period the tailings solids settle and the tailings fluid is allowed to drain into the pond. Some amount of evaporation and desiccation also takes place given the abundant sunshine and a dry climate with a moisture deficit. A subsequent deposition is placed when the previous layer is "firm enough to walk" on it. This is a scenario where the previously deposited layer has gained strength through suctions. From a geotechnical engineering perspective the scenario described above is very complex to model. The complexity arises from the size of a tailings dam as a structure whose foot print averages 500 hectares and a height in the range from 60 metres to 100 metres. The state of tailings materials in the dam walls which are under suction also make analysing the state of the tailings complex.

The stress paths of a tailings dam wall therefore cannot be easily modelled or reproduced experimentally. In order to simulate a high rate of rise scenario in an actual tailings dam wall for instance, one is forced to confine the tailings in a container of finite dimensions yet in the actual tailings dam the wall tailings are retained by previously deposited tailings placed further away from the slurry being deposited in the paddocks which are usually around 10 meters wide.

On wall cyclone tailings dam construction system

The on wall cyclone tailings dam construction system entail building of the dam wall using the coarse fraction of the tailings or underflow. The deposition of the fine fraction of the tailings or overflow into the interior of the tailing dams comprise the beach and pond parts of the tailings dam. Under this construction system, since the wall is built with coarse tailings materials or the faction with good drainage properties, usually a higher rate of rise can be used. In as far as modelling of the on dam cyclone tailings dams therefore a dam wall model could be adopted for the exterior of the dam whilst a pond and beach model could be used for the interior of a tailings dam.

Settling column and tailings materials testing

For this research whose major aim was to prove or disprove the linkage of excess pore water pressure with rate of rise, to determine particle size segregation and to evaluate the saturated permeability of tailings, a model was desirable that would simulate a wall built under a scenario of high excess pore water pressures and where tailings deposition was likely to allow particle size segregation. The requirement of high pore water pressures dictated that fine tailings form part of the materials to be used in the research. In order for particle size segregation to take place a reasonable height of passage for the slurry and high moisture content were required. There was a need to deposit thick layers during the research so that a high rate of rise could be easily achieved as well as generating adequate magnitudes of excess pore water pressure to enable addressing the research question on excess pore water pressures. It was important that pore water pressures could be measured and that processes similar to those of wall formation which yields varying rates of rise that was necessary for addressing the research questions could be easily achieved.

Transparent settling column experiments were the most amenable to the requirements of the objectives of the research. In order to observe and to visually examine tailings slurry deposition, sedimentation and consolidation, a container that was transparent was necessary so that slurry undergoing the different processes of soil formation could be observed. The container also had to be of such a size in which reasonable and manageable amounts of tailings could be studied.

The basic measurements required to answer the study questions necessitated a means to measure height, instruments to measure pore water pressures within tailings and a method to determine the permeability of the settled layers.

The fittings for the instruments required to measure pore water pressures in particular were to be such that they did not interfere with the formation processes of the tailings sediment from the slurry. This meant that the fittings would be best placed on the side of the slurry container. The requirement also dictated that the slurry container be such a size that it caused none or minimal edge or wall effects. This meant that the containers diameter or aspect ratio had to be of the appropriate size in order to minimise the effects (section 2.7 under Literature Review).

In order to examine and to characterise the deposited materials, different layers formed during sedimentation were to be recovered at the end of the experiments. The particle sizes, shapes, fabric and mineralogy as well as the soil index properties of the recovered samples were to be determined. Soil index testing, scanning electron microscope (SEM) viewing, X Ray Diffraction (XRD) tests and X ray Fluorescence Spectroscopy (XRF) tests were therefore carried out to complement settling column tests (see Figure 3.1). This required that the container in which the tailings were deposited as slurry was to be made of a material that could be cut open easily so that a sample could be recovered with minimal disturbance to the sample (sacrificial settling column). This meant a container with a small thickness of 3mm and PVC was selected as the appropriate material because PVC was easy to cut with readily available tools.

For the measurement of permeability, the settling column apparatus needed to be modified so that the permeability of the material in the settling column could be measured. The settling column as is could easily yield data required for determining tailings permeability under the

falling head permeability test conditions. After a water exit tank and a reservoir were added to the settling column apparatus, a constant head permeability test could also be carried out.

Different shapes of containers could be used which satisfied the requirements of the preceding section of this chapter. Circular PVC and Perspex pipes were preferred due to the availability of pipes of different diameters and heights. Machines and equipment to cut and drill PVC and Perspex were available at University of Pretoria Laboratories. As discussed in the literature review section of this thesis, there was also a lot of experience gained worldwide where various researchers had used circular settling columns to study aspects of the sedimentation-consolidation phenomenon which provided published data against which to compare the results of the research.

On the basis of the work of previous researchers (Been, 1980; Elder, 1988; Dimitrova, 2011 amongst others) an exploratory settling column tube 190mm ID and 500mm height was constructed and used to explore the suitability of the apparatus to the research work. The inside diameter of 190mm would not result in edge effects which would not adversely affect pore water pressure measurements and a height of 500mm was adequate to execute reasonable sized exploratory experiments within a short period of time. The exploratory experiments were used to gain experience for the experimental methods and the behaviour of gold tailings as slurry. Though the results of the exploratory experiments do not form part of this thesis; the lessons drawn from the experiments are captured within this research owing to their value in informing the execution of experiments reported in the thesis.

3.3 Sample Description

Gold tailings samples used in the research were sourced from a tailings dam in the Klerksdorp-Orkney-Stilfontein-Hartbeesfontein area in the Witwatersrand Basin in South Africa. The three main samples used for the research comprised the tailings underflow sample collected in 2010, the underflow sample collected in 2011 and the catwalk fines sample of 2011. Figures 3.2a and 3.2b show the locations of the two tailings dams where the samples were collected. Figures 3.3 to 3.8 show the different parts of the Chemwes Dam 5 and Mooifontein tailings dams with relevance to the samples obtained. The 2010 coarse tailings sample was collected on the beach area near a hydrocyclone (see Figures 3.3 and 3.4). A penstock tailings sample collected from the Mooifontein tailings dam in 2009 plays a role in the research. Figures 3.3 and 3.4 show the

tailings dam wall with underflow tailings deposited by hydrocyclones near the wall. The sample was a cyclone underflow obtained at a distance of 10m from the dam wall crest where the tailings were deposited. All the materials for the sample were scooped from the surface without digging deeper into existing layers that were deposited before. It is to be noted that this was the best accessible area for collecting fine tailings owing to the wetness of the dam at the time of sampling (see Figure 3.5). Figure 3.5 illustrates the practical difficulty arising from the softness of the tailings that limited obtaining of samples to distances within 20m from the dam wall down the tailings beach area towards the tailings dam pool area. The 2011 coarse sample which was collected 7m from a cyclone towards the tailings pool area. The third sample was a fine tailings sample which was collected from under the catwalk at a distance of 20m from the pool where the penstock was located (see Figure 3.6a). Figure 3.6a shows part of the catwalk where the tailings overflow that had segregated over the beach area were within reach under the catwalk where the tailings were extracted using the bucket and rope technique to obtain the required catwalk tailings fine grained samples. Figures 3.6b and 3.6c show other parts of the penstock area together with the pool that was immersed in water. No sample could be obtained from there. The sample comprised the fines from the cyclone overflow which had settled the furthest from the discharge point and was carried by the tailings water towards the penstock. Figure 3.7 shows deposition of tailings overflow and channel formation from the depositing tailings at the pipe discharge point. Overflow tailings samples were obtained at these locations.

For purposes of obtaining a broader picture of the properties of the gold tailings used in the research, additional samples were collected and tested. The additional samples included whole tailings and tailings overflow from Chemwes dam 5 as well as penstock tailings from the Mooifontein dam of the Crown Mine tailings complex which was used in the exploratory experiments. The Mooifontein tailings dam was located nearer to University of Pretoria and at this tailings dam, the penstock tailings sample was directly accessible at the time of sampling due to non-deposition at the tailings dam (Figure 3.8). The additional samples were therefore tested together with the three samples for this research.

3.4 Sample Preparation

This section describes how the samples were prepared before testing in the settling columns as well as reports on initial cylinder sedimentation tests that were carried out to determine appropriate slurry mixtures to use with the experiments. The samples for the settling column experiments were oven-dried at 110°C temperature and then mixed with distilled water to obtain slurry of specific gravity of 1.3, a moisture content of 172% and a void ratio of 4.67. Figure 3.9 shows oven-dried tailings that were sieved using the 2mm sieve for use in making slurry for the experiments. Equation 2.29 (Hagan, 2009) was used to calculate quantities of tailings solids and distilled water required for each test. A specific gravity of slurry of 1.3 was selected so that the slurry deposited in the settling column was within the range of relative densities at which deposition takes place in gold tailings dams in South Africa (Robinson, 2008 and Lebitsa et al., 2009). The selected specific gravity of slurry was also to result in slurry that was easy to work with within the apparatus used in the research.

$$G_{slurry} = \left(\frac{1+m}{\frac{1}{\rho_s}+\frac{m}{\rho_w}}\right)/1000 \qquad 2.32$$

In order to obtain quantities of tailings slurry required to be deposited to simulate a given rate of rise in the settling column apparatus, a preliminary 500mm full depth slurry deposition test was carried out in the 190mm ID 500mm height settling column with a transparent window (exploratory settling column). The test was continued until consolidation was completed followed by a sun-drying period of 14 days of the tailings slurry sample inside the settling column. Decant water was removed following the completion of consolidation so that as much sun drying of tailings would have taken place by the end of 14 days drying period. A rate of rise factor was calculated from the experiment. Rate of rise factor was taken as the ratio of the slurry height immediately after deposition to the height of settled tailings. In a study of dredged materials deposited in confined disposal areas, Johnson (1976) reported bulking or design factors similar to rate of rise factor used in this research. Johnson (1976) reported bulking factors for clays, silts and sands in the range of 1 to 3. A rate of rise factor of 1.73 for the slurry of specific gravity of 1.3 and the consolidated tailings was obtained for this research. The rate of rise factor was applied to slurry volumes to calculate equivalent slurry volumes to be deposited to yield a targeted rate of rise for each experiment. The oven-dried tailings sample

was characterised to determine its grading and Atterberg limit properties. Distilled water was used for making tailings slurry rather than using tailings fluid. Tailings fluid is reported to contain both flocculants and dispersants which change both the behaviour and properties of tailings (Vermeulen, 2001 and Villar *et al*., 2009). It was decided to use distilled water for the tests when making tailings slurry because the objectives of the research emphasised understanding of tailings slurry behaviour within the context of the study hypothesis without bringing in the complex behaviour of tailings arising from the chemistry of the tailings fluids.

Cylinder sedimentation tests

1000ml capacity measuring cylinders were used to carry out tailings sedimentation and consolidation tests in order to gain experience of tailings slurry behaviour when deposited. The tests helped to determine sedimentation rates and to establish workable slurry concentrations at which the experiments could be carried out. Additionally slurry properties were determined and experience gained on the use of gold tailings as a geotechnical material. Figure 3.10 (a) and (b) show the cylinder sedimentation tests. Gold tailings sample sourced from the Mooifontein tailings dam was used for the exploratory settling tests. It was decided to obtain penstock tailings fines in which high excess pore water pressures were most likely to be generated compared to a coarse grained tailings sample that drained very quickly.

Ten cylinder sedimentation tests were carried out at different slurry concentrations ranging from 50g/L to 2330g/L during which visual observations were made of the slurry from the start of deposition until sedimentation ceased. Measurements of the tailings water interface (TWI) over time were made. On the basis of cylinder sedimentation tests, it was decided that a slurry with solids concentration of 470g/L be adopted for the experiments because it was workable and fell within the slurry deposition specific gravity range used in tailings dams in South Africa. A detailed discussion of the cylinder sedimentation tests results is given in Lebitsa *et al.* (2009).

3.5 Laboratory Tests

Laboratory tests were required to characterise gold tailings used in this research. The laboratory tests carried out to characterise gold tailings were specific gravity test, gradation tests and Atterberg limits tests. Each of the tests is described briefly below. The physical properties of

the samples and their gradation characteristics obtained from the test results are reported in Chapter 4.

3.5.1 Specific Gravity Test

The densities of gold tailings solid particles were determined using displacement methods to obtain the volumes of the particle solids which together with the respective masses of the solids yielded the densities of the solid particles. The water displacement method tests were carried out by the author while the helium gas displacement test methods were undertaken by the Civil Engineering Department of the University of Pretoria technician. The salient points of the two tests methods are described below.

Density Bottle Tests

The particle densities of the gold tailings were determined in accordance with the procedures of the British Standard BS 1377: Part 2:1990: 8.3. Archimedes principle is applied in this test to obtain the volume of the solid particles in the density bottle from the volume of de-aired distilled water that the solid particles displaced.

Since the resultant particle densities are dependent on both the accurate determination of the mass of the particles and the volume of the solid particles obtained from water displacement, the quantity of solid particles used in the test were just as important as the adherence to the set procedures and the required calibrations for the test.

In this regard both 50ml and 100ml pycnometers were used during the tests as well as carrying out three density determinations per sample as called for by Head (1992). It is believed the 100ml pycnometer which allowed for the use of double the mass of solid particles compared to the 50ml pycnometer resulted in fewer errors in the resulting particle density measurements.

It is worth noting that literature dating back to the days before BS 1377:1990 and some recent ones stipulate the use of density bottles of capacity as high as 500ml (Taylor, 1948; Lambe, 1951; Liu and Evett, 1984; Wray, 1986; and Bardet, 1997) because using large masses of solid particles entails less sensitivity to errors than when small quantities are used with the 50ml density bottles.

AccuPyc II 1340 Gas Pycnometer Test

The test determines the solid particle density by obtaining the volume of a given mass of solid particles from the volume of helium gas that the sample displaces which it uses together with the supplied mass of the sample in the calculation of particle density. The AccuPyc II 1340 gas pycnometer is connected to a computer which carries out the computations and returned a specific gravity of the solids. The method therefore is a helium gas displacement method as opposed to the water displacement principle employed by the density bottle method described above. The principle of the test was illustrated in Figure 2.31 under the literature review.

The procedure for the test took 10 minutes on average. The test entailed weighing a dry sample (40g to 90g) in the sample cell and placing the sample into the testing apparatus which was then tightly closed so that there was no gas leakage when the system was under pressure. The machine was set to make an average of three density determinations. A report was generated which listed an average volume of 15cm^3 to 33 cm^3 for gold tailings samples as well as the temperature of the tests which was from 19° C to 22° C for all the tests. Three density determinations were reported for the conditions described. The machine was calibrated every six months by determining the density of a steel spherical ball of known density which was provided for purposes of calibration.

3.5.2 Particle Size Grading Tests

The distribution of the gold tailings particle sizes was determined using a wet sieving method, a hydrometer sedimentation method and a laser diffraction method. The wet sieving test and hydrometer tests were carried out by the author while the laser diffraction tests were carried out by a laboratory technician with the author observing the test procedures. The following subsections describe each of these tests.

Sieve Analysis and Hydrometer Analysis Tests

Figure 3.11 summarises the procedure that was followed for the determination of gradation properties of the tailings. The wet sieving tests and hydrometer tests were carried out in accordance with British Standard BS 1377: Part 2: 1990: 9.2 and 9.5 respectively. The wet

sieving method yielded a "mesh sieve diameter" and a corresponding percentage mass of tailings passing the specific mesh sieve diameter. The sieve apertures were square in shape.

The hydrometer method relied on the sedimentation principle and applied Stokes's Law for the terminal velocity of unhindered spherical particles in a liquid medium. The test therefore yielded an equivalent sphere diameter of gold tailings having the same diameter as the sphere falling unhindered through a suspension under the same conditions together with an estimate of the percentage smaller than the equivalent spherical diameter based on the suspension density at the hydrometer depth of measurement of 140mm.

The gold tailings are essentially a silt and therefore a 50g representative sample obtained through quartering was used for the hydrometer test. In order to obtain valid results satisfying the requirement for unhindered settling spheres in a liquid medium and to be able to apply Stokes Law, a hydrometer test suspension concentration of less than 50g/L was used.

The same 50g sample was also used for the wet sieving test part of the particle size determination. Several wet sieving tests were also performed on a 100g sample as stipulated by British Standard BS 1377: Part 2 for silt sized particles and were compared with the gradation curve obtained from the 50g sample. It was found that the coarse fraction of the particle size distribution for the 50g sample and that for the 100g sample were essentially coincident. This was expected owing to the narrow range of particle sizes in the gold tailings samples under this research.

The stack of sieves used was the British Standard full set of sieves (Head, 1992). Hydrometer 151H was used in all the experiments. Calibrations and hydrometer corrections for meniscus, dispersant (datum reading) and temperature were carried out as stipulated in British Standard BS 1377:Part 2: 1990:9.5.

A maximum of six hydrometers were carried out at a time in a warm water temperature bath set at 25^{o}C. Each set of hydrometer tests were run for at least four days to obtain a full particle size distribution up to the clay size of 2µm. The gold tailings particles in suspension were dispersed using a 40g/L solution comprising 33g of sodium hexametaphosphate (calgon) ($NaPO_4$) and 7g of sodium carbonate ($NaCO_3$). The schematic diagram of Figure 3.11 summarises the procedure used for particle size analysis in this thesis. Whilst it is reported that

the hydrometer test is less accurate than the pipette test (Clayton et al.,1995) the hydrometer test was used in this study because of its availability and amenability to the large volume of tests that had to be carried out within a short space of time since the test is easier and quicker (Lewis, 1984). Were it not for the constraint of the small warm water temperature bath, up to 21 hydrometer tests could be carried out all at once within a given day (Lewis, 1984). Lewis (1984) also argued that any particle size method is an indirect measurement of particle size and so different results will always be obtained from different methods. He concluded from a comparison of six analyses that the hydrometer method like the pipette method gave reproducible results and that the two methods compared very well with each other.

Mastersizer Test

The procedure followed to test samples using the Mastersizer laser diffraction method under this research was as follows:

1. The Mastersizer machine was run with sample holder filled with distilled water only first to obtain the background reading.

2. A small sample of gold tailings ranging between 2g to 3g was extracted from the bulk sample. The sub-sample was made into slurry by adding distilled water. The small amount of slurry was added to the test cylinder a little at a time while the distilled water in the test cylinder continued to be agitated using a stirrer. The more fine the gold tailings sample the smaller the mass of the sample that was be added to the test cylinder. During the test 5% to 25% of the 2g to 3g selected initially for the tests was used in the actual test.

3. Under step 2 when the slurry was made from the small sample by adding distilled water, caution was exercised so that only sufficient water was added to make a slurry consistency that could easily be added to the distilled water without the sample segregating.

4. The tailings slurry was then added to the sample dispersion unit with distilled water in it. While the sample was being added the sample stirrer was continuously mixing in the measuring cylinder. The amount of slurry added was automatically controlled by the computer as it had to fall within the obscuration range set for the test. Obscuration was defined as the portion of light that was lost from the analyser beam when the sample was added to the distilled water in

the sample dispersion unit (Malvern Instruments Ltd., 2004). The computer screen displayed the obscuration indicator and displayed the message to the effect that enough sample was added which signalled the operator to either add more slurry or to stop slurry addition.

5. The Mastersizer then measured and carried out an analysis displaying the outcome on the computer screen.

6. The ultrasonics were then turned on and another measurement and analysis was carried out for comparison with the test carried out without ultrasonics to establish if there was any segregation, flocculation or if the stirring that took place during the first test procedure was adequate to keep the gold tailings particles dispersed during the particle size test.

7. The Mastersizer equipment was then rinsed and made ready for the next test. Each test cycle lasted 2 minutes.

3.5.3 Atterberg Limits Tests

A limited amount of indicator testing on gold tailings was carried out for classification purposes as well as to compare consistency limits of gold tailings samples in this research with results available from the literature studied.

The tests carried out were the liquid limit test and the plastic limit test from which the plasticity index was determined. The tests were carried out according to British Standard BS 1377:Part2:1990:4 and 5.

For the liquid limit test, both the cone penetrometer method BS 1377:1990:4 and the Casagrande method BS 1377:1990:5 were used. Whilst the cone penetrometer method was reported to be fundamentally more satisfactory and was said to yield more reproducible results, both methods were deemed to be satisfactory for this research more so that testing was limited and involved one operator for both tests.

3.6 Settling Column Tests

This section describes the settling column tests that were carried out under the study. The section gives a summary of the lessons and experience gained from exploratory settling column tests. Appendix A describes the exploratory settling column tests. The experience gained from the tests were used as the basis for carrying out the final experiments of the thesis. This section also details the construction of settling column apparatus and concludes with a summary of the six experiments reported under the research.

3.6.1. Lessons from Exploratory Settling Column Tests.

The lessons from the exploratory settling column tests are summarised in categories as; lessons for standpipes, transducers, settling columns and procedures for carrying out settling column tests.

Standpipes

i. A standpipe piezometer board with a graduated grid was to be used in order to eliminate systematic and parallax errors inherent in reading individual standpipes mounted by themselves.

ii. Standpipe piezometer tubes with the smallest inside diameter of 2mm had the least response time compared to the large diameter standpipes whilst at the same time having similar air bubbles problems as the larger standpipes which had slower response times. A summary of typical response times measured and those estimated using Penman (1960), Brand and Premchitt (1980) and Premchitt and Brand (1981) are listed in Table 3.1. The large standpipe's low response time in the extreme manifested as negative excess pore water pressures.

iii. Standpipes tubes with inside diameters of 2mm used in conjunction with sintered bronze filters (see Figures 3.12 and 3.13) measured pore water pressures in the experiments adequately and warranted their use in final experiments.

iv. Capillary effects were minimal on the plastic standpipes. Capillary effects on the 2mm ID plastic standpipes were in the range of 5mm to 7mm compared to the estimated capillary rise of 15mm for glass standpipes of the same diameter (Holtz and Kovacs, 1981 and Barnes, 2000).The differences between the free water levels inside the large diameter settling column and the 2mm ID standpipes levels were consistently between 5mm and 7mm.

v. A need to use colorants to enhance visibility of piezometric heights within standpipes was identified and trialled but was discontinued because the improvements were minimal.

Table 3.1: Standpipe Piezometer Response Times.

Standpipe Inside Diameter (mm)	Response Time (minutes)			
	Measured Values		Calculated Values using k=3m/yr Blight(1980)	
	(minutes over total varying heights)	(minutes per centimeter)	Brand & Premchitt (1980)	Penman (1960)
2	2	0.25	0.5	0.05
3	23	0.56	0.8	0.1
5	50	1.59	2.1	0.3
6	90	2.54	3.2	0.4
9	165	8.25	7.2	1.0

Transducers

i. Transducers were to be used with sintered bronze filters. Transducer plumbing was to be as short as possible to enhance transducer pressure response. Summary of salient features of transducers are summarised in Table 3.2 and Figures 3.14, 3.15(a) to (c).

ii. Pore pressure response was quick especially immediately following deposition which resulted in much loss of data when data was collected manually. The need for continuous data capture through the use of more electronic transducers and a data logger was justified. There was also a need for the transducer and data logger system to have a resolution equal to or better than the resolution of the standpipes which was at 1mm.

Piezometers (Standpipes and Transducers)

i. The use of valves with piezometers to control water flow and to easily measure response times was found to be a useful improvement to the apparatus.

ii. Piezometers were to be concentrated at the bottom one metre height of the settling column at intervals of between 50mm and 100mm where significant pore water pressure changes took place and the height within which sediment would be located for the slurry properties selected for the experiments. The upper portion of the settling column was observed to be occupied mostly by the supernatant water.

Table 3.2: Salient Features of Transducers.

Transducer No	Make	Serial No	Transducer Height (mm)	Depth To Diaphragm (mm)	Max. Output	Full Scale (kPa)	Resolution	Accuracy	Gauge Factor	Operating Temperature Range (°C)
0	WIKA S10	11028555	58	21	10V	40	0.001V	0.5%span	0.33V/V-0.71V/V	-30-100
1	GEMS	AO33513	73	34	10V	100	0.001V	0.25%FS	0.29V/V-1.42V/V	-40 - 125
2	GEMS	BO84043	72	30	10V	100	0.001V	0.25%FS	0.29V/V	-40 - 125
3	GEMS	YO78291	71	30	10V	100	0.001V	0.25%FS	0.29V/V	-40 - 125
4	GEMS	8084054	72	31	10V	100	0.001V	0.25%FS	0.29V/V	-40 - 125
5	WIKA A10	0012612w35	36	21	20mA	100	0.01mA	0.5%span	0.13mA/V-0.67mA/V	-30-100

Settling Columns

i. A need to use a video camera to capture the air water interface (AWI) and the tailings water interface (TWI) as well as other experimental parameters was identified.

ii. Deposition of thin layers of gold tailings slurries of 150mm to 200mm at a time (as practiced and occurs in real tailings dams) into settling columns generated very small and insignificant excess pore water pressures. Much thicker deposition layers were therefore adopted.

iii. The surface of the tailings sediment inside the settling columns as viewed through the transparent window as well as from above the settling column tubes appeared level and uniform which was indicative of the absence of edge and wall effects in the 190mm inside diameter settling column.

iv. The exploratory settling column that utilised a lot of adhesive experienced more water leaks with the progress of experiments which indicated a need for an apparatus that was more robust in construction and that did not entail the use of windows or adhesives. It was thus decided to use sintered bronze filters and associated fittings in subsequent settling column tubes. The sintered bronze filters had water flow rates greater than 93ml/min (with a head of up to 150mm) which was more than adequate for gold tailings. The only disadvantage was that the sintered bronze filters protruded into the inside of the settling tube by 10mm. The disturbance caused to the sediment formation from slurry and to the measurements were considered minimal.

Settling Column Test Procedures

Test procedures for the settling column experiments were established from the exploratory experiments and in summary the procedures entailed the following steps:-

i. Saturation of transducers using de-aired water deposited at the required depth of the settling tube without re-introducing air into the de-aired water.

ii. calibration of transducers, settling columns and standpipes using tap water.

iii. determination of response times for transducers and standpipes.

iv. preparation of tailings slurry for deposition.

v. deposition of tailings slurries with small time interval data capture at commencement of deposition followed by large time interval data capture during latter stage of the experiments.

vi. decanting supernatant water just before the next deposition cycle, when tailings were deposited in stages to simulate rate of rise. Decanting was necessary to avoid segregation of a deposited slurry layer which would have occurred if the deposited layer had to pass through a layer of water overlying the already settled tailings sediment.

vii. calibrations and determination of response times of piezometers both before and after the experiment to evaluate filter blockage during an experiment which assisted with identification of erroneous data.

viii. incorporation of permeability test with the settling column test so that permeability testing could commence after full dissipation of excess pore water pressures.

3.6.2 Settling Columns

Six settling column experiments were carried out and are reported in the thesis. The experiments were carried out using the 190mm ID 1535mm height settling column (permanent settling column) and three separate 154mm ID 2000mm height settling columns which after each experiment were split open (sacrificial settling columns) to recover intact tailings samples. The permanent settling column was repeatedly used for various experiments (series "A" experiments, sacrificial columns on the contrary were used only once for an experiment (series 'B" experiments) and split open after each test. Figures 3.16 and 3.17 show schematic diagrams comparing the permanent and sacrificial settling columns in terms of the transducers and standpipes used and their locations along the height of the settling columns. A third settling column of 154mm ID with a height of 500mm to be used as overflow reservoir for the permeability test was also constructed.

A schematic diagram of an instrumented settling column used in the experiments is shown in Figure 3.18. The annotated schematic diagram of the apparatus shows that it comprises three main parts. The first part is made up of either a 154mm ID translucent PVC settling column (sacrificial settling column) or 190mm ID PVC settling column with a transparent window

(permanent settling column). The settling column is fitted with four 100kPa full scale strain gauge based electronic pressure transducers (1a) in the case of the permanent settling column (all voltage based) or six transducers in the case of the sacrificial settling column. It is to be noted that in the case of the sacrificial settling columns, five of the transducers were voltage based while one was current based. The five voltage based pore water pressure transducers were logged onto a Graphtec electronic data logger which was set to take readings at a sampling rate of 2 seconds intervals at the start of each experiment. Later in the test, the sampling rate was reset to less frequent sampling rate which reflected the slow pore water pressure response as the experiment progressed when the excess pore water response was no longer rapid. Seven 2mm ID standpipe piezometers with maximum tubing pressure rating of 10 bar (1b) were installed opposite to and at the same height with the transducers on the settling column. The locations of the standpipes along the height of the settling column are shown in Figure 3.18. The second part is made up of: a water supply reservoir, a de-aired water supply tank, a constant head water supply tap, an exit water tank with a graduated measuring cylinder for collecting expelled water from the permeability test component of the experiment. The third main component is the power supply and a recording system which includes an uninterrupted power system (UPS) to stabilise the mains 220 Volts electricity power supply, a 35Volts dc power supply for exciting the transducers as well as a 20 channel data logger to display and record voltage data measured by the transducers. Data collected manually using standpipes was recorded together with transducer data displayed on the data logger display unit and the settling column interfaces data at the same times that the standpipe readings were taken at.

A 30mm thick soil filter made up of two successive wire meshes (2.0mm and 0.5mm aperture) sizes, a uniform sand layer with grain sizes between 2mm and 0.075mm sizes, a Whatman filter paper and a non-woven geotextile was added at the bottom of the settling column. The soil filter was to retain tailings during the permeability test. The 190mm ID 1535mm height permanent settling column and the three 154mm ID 2000mm height sacrificial settling columns are described in the next section.

190mm ID permanent settling column

The 190mm ID diameter 1535mm height permanent settling column is shown in Figure 3.19. Figure 3.20 shows the exploratory settling column prior to its modification into the permanent settling column.

The permanent settling column comprised seven standpipe piezometers and four pore pressure transducers as well as a provision for the measurement of permeability of the settled tailings using both the falling head and constant head permeability tests. Figure 3.21(a) and (b) show a close up views of the 190mm ID 1535mm height and the 154mm ID 2000mm height apparatus respectively with transducers connected. Descriptions of aspects of permeability testing and decanting of tailings which also apply to the permanent settling column are given in the next section covering the sacrificial columns. These are listed as items 7,9,10 and 11.

154mm ID sacrificial settling columns

Three settling columns 154mm ID and height ranging from 1500mm to 2000mm were constructed using translucent PVC pipes. A fourth and shorter settling tube of height 900mm is included under this section because it was constructed the same way as the sacrificial settling columns. The shorter column was used as the constant head permeability test exit water tank. The construction sequence of the settling column tubes is summarised below and illustrated with the help of Figure 3.22:-

1. The settling column was cut to the appropriate height using a grinder leaving both ends flat, even and uniform since both ends were to provide support at the base and at the top end of the columns connected through threaded steel rods. The flatness and evenness of the ends of the settling tubes were required as their fitting with the base and top plates would determine how good the water seal would be.

2. A circular top cap 15mm thick and diameter 270mm was cut from a translucent PVC plate. The 270mm diameter PVC plate was dictated by the lathe available for use in making the settling column tubes. A 130mm diameter hole was machined into the centre of the top cap to allow pouring in of tailings slurry. A 4mm diameter groove was cut into the top cap for holding the 160mm diameter settling tube in place (see Figure 3.22).

3. A circular base plate 30mm thick and 270mm diameter was cut from a grey PVC plate. A 4mm diameter hole was drilled at the centre of the base plate for a transducer fitting. Another hole of 20mm was drilled for provision of an exit tap for water during permeability testing. A groove 4mm thick and 4mm deep was provided to hold both the PVC tube and a

3mm thick 153mm diameter o-ring to seal the base plate to make the settling column base plate connection water tight.

4. Four diametrically opposite 13mm diameter holes were drilled near the edges of both the base plate and the top cap. Four threaded 12mm diameter steel rods with nuts were secured for connecting the settling tube between the bottom and top plates at the 13mm diameter drilled holes.

5. 4mm diameter holes were drilled and tapped for the five transducer fittings and seven similar holes were drilled and tapped for the standpipe fittings. Additional holes were made at 60mm depth from base of the tube for a saturation tap and several taps for permeability test at 100mm intervals from the top up to a depth of 800mm down the settling column (see Figure 3.23). A hydraulic gradient of 1 was targeted for the constant head permeability test Blight (2010) argued that for soft materials such as gold tailings used in the experiments, permeability tests should be carried out at hydraulic gradients near unity because high hydraulic gradients changed the compressibility characteristics of the material. A decision was taken to have fittings at the same locations as in the 190mm ID permanent settling column so that data from all the settling column experiments could be compared. Figures 3.21 and 3.22 show the transducers and the standpipes as well as the permeability test setup. Figure 3.23 also gives both the 190mm ID and 154mm ID settling columns side by side for ease of comparison. The figure displays the various optional height locations along settling columns where water could be exited during permeability testing to assist with attaining a hydraulic gradient of 1.

6. One meter high timber platforms were used to place and secured base plates using threaded rods that bound both the end plates with the settling tubes.

7. A 100 litres capacity PVC tank was secured for use as a constant head permeability test water reservoir. A 4mm diameter hole was made at a height of 10mm from the base of the water reservoir to fit a valve for water supply from the reservoir to the settling column during the permeability test. This is shown in Figure 3.24. The same type of fittings used for transducers and standpipes were used for the water supply. The water supply tank was located at a height of 2.9m from the ground to provide sufficient head for water flow. The final height of the sediment, L, was used to estimate the hydraulic gradient.

8. A slurry pouring tremie pipe to attenuate the energy of incoming slurry in order to minimise disturbance of the already settled tailings sediment by subsequent layers of slurry was used during the deposition of rate of rise experiments. Figure 3.25(a) shows the slurry deposition tremie pipe inserted into a settling column. The tremie pipe was made up of a funnel into which slurry was poured, a 110mm ID PVC pipe and a 10mm aperture wire mesh at the base of the pipe. Both the wire mesh and the steel funnel were wide enough not to segregate the slurry. Table 3.3 shows tailings sediment heights from the rate of rise experiments (20m/yr and 10m/yr) which were used to determine the length of the tremie pipe and the location of holes drilled to suit the deposition depths of the experiments at depths 100mm, 350mm and 460mm from the top end of the tremie pipe.

Table 3.3: Slurry Pouring Tremie Pipe Lengths.

Experiment	Sediment Height (mm)			Pipe Length Required (mm)	
	Lift 1	Lift 2	Lift 3	Lift 2	Lift 3
RoR20A and RoR20B	333	589	853	1176	911
RoR10A and RoR10B	238	469	698	1262	802

9. A 30mm thick soil filter was designed and assembled for use with the settling column for carrying permeability tests on deposited tailings. The filter comprised of a 2mm mesh wire sieve, followed by 0.5mm mesh wire sieve, two layers of 0.03mm thick geotextile used with roof waterproofing chemicals, two sheets of 0.02mm thick Whatman 100 cycles filter paper and a 26mm thick layer of dry sand passing a 2mm sieve and retained on 75µm sieve with the sand freely poured from the top of the settling column.

10. A de-aired water supply tank was constructed from 110mm diameter PVC pipe of height 940mm. A PVC plate 10mm thick, 210mm long and 210mm wide onto which a 3mm groove was made was used as a base plate for the de-aired water tank. PVC glue was used to attach the base plate and the pipe. A 4mm hole was drilled at a height of 7mm from the bottom of the 110mm diameter pipe where a fitting similar to fittings used for transducers

and standpipes was used. Figure 3.20 showed the de-aired water supply tank with the 190mm ID 1535mm height exploratory settling column.

11. A venturi tube shown in Figure 3.25b was used with 12mm diameter tubing with suction from a tap water supply to decant tailings between depositions where rate of rise was simulated in the experiments.

The supports on which the settling tubes together with the base and top plates for Experiments FDB, RoR20B, and RoR10B were fixed onto were not exactly the same height whilst the same piezometer board height and the constant head permeability test water exit tank were used for all the experiments. There were as a result, height differences between the zero readings of the piezometer board and those of the settling columns. There was therefore a need to make corrections for the elevation differences in the readings. There was also a need to make adjustments for height differences brought about by the filters added in settling columns to enable carrying out permeability tests following settling column tests. Table 3.4 summarises the elevation corrections that were made to readings for both calibrations and experimental data collected.

Table 3.4: Settling Apparatus Calibrations and Experimental Data Height Corrections.

Experiment	Correction Made (mm)		
	Piezometer Board and Settling tube Elevation Difference (mm)	Filter Height (mm)	Total Correction Made (mm)
FDA and FDB	2	30	32
RoR20A and RoR20B	31	31	62
RoR10A and RoR10B	22	30	52

3.6.3 Apparatus Calibration

Introduction

Each settling column experiment commenced with calibration of the various components of the settling column apparatus. The components calibrated included the settling column, the standpipes and the pore pressure transducers. The three components of the apparatus required calibration to establish the level of confidence of the data to be measured with the apparatus.

Standpipe piezometers and pore pressure transducers calibrations were undertaken prior to carrying out each experiment and after completing the experiment. This was required in order to establish if there was any blockage of the conduits to the standpipes and pore pressure transducers which would have adversely affected the readings. The settling columns were calibrated first followed by the calibration of standpipes and transducers which required the use of the settling column tubes for their calibrations. The calibrations of the standpipes and pore pressure transducers and the settling columns are described below.

Settling Columns Calibration

The two main settling column types used in the study were the permanent settling column (190mm ID 1535mm height with a 55 mm wide transparent window) and the sacrificial settling columns (154mm ID 1500mm to 2000mm height).

The calibration of the settling columns entailed determining the volume of the columns as a standard against which both standpipes and pore pressure transducers were to be calibrated. The calibration procedure for the settling columns compared the actual volume of the water added to the settling column using a 5 Litre graduated measuring cylinder and the volume of water calculated basing on the height of water inside the settling column which was read from the measuring tape fixed to the settling column. It was ensured that a given calibration exercise was undertaken within a period of 30 minutes over which both room and water temperatures were recorded and observed to remain within a 5˚C temperature range during the calibration period.

The settling column calibrations commenced with calibrating the 5 Litre capacity measuring cylinder using a 250 ml capacity measuring cylinder. The 250 ml measuring cylinder had a minimum reading value of 30 ml and was graduated in steps of 20 ml while the 5 Litre measuring cylinder had a minimum reading of 500 ml and was graduated in steps of 250 ml.

Standpipe Calibration

The settling column was instrumented with seven standpipes whose length varied according to the specific location of the standpipe on the settling column and its location on the standpipe piezometer board. The standpipes were mounted on a graduated board from which piezometric height of rise of water inside the tubes was read.

The calibration of the standpipes comprised the response times of the standpipes, the relationships between standpipe piezometric height and the water height in the settling column as well as observations of the compliance effects of the standpipes. Varying heights of water in settling column were recorded with respective piezometeric heights in the standpipes. The time it took for the standpipes to attain the same height as the water in the settling columns were collected together with the height of water in the settling columns at the commencement and at the end of the response time measurements. Appendix B lists average response times and typical calibrations for standpipes which were carried out in all the settling columns used during the study.

Electronic Pore Pressure Transducers Calibrations

The six strain gauge based pressure transducers used in the experiments were calibrated. The calibrations of the transducers included measurement of response times and the determination of calibration factors used to convert voltage or current responses of the transducers into pressures units.

As was observed from Table 3.2, the four GEMs transducers (1 to 4) had full scale reading of 100kPa while the two WIKA transducers (0 and 5) were 40kPa and 100kPa full capacity respectively. The low pressure range of the pressure transducers made it difficult to calibrate the transducers using the conventional methods such as the dead weight tester which had been shown to be less accurate at low pressures (Chang, 2009).

The five voltage based transducers were connected to a Graphtec data logger which captured pore pressure changes during the experiment. The wire connections to the data logger and the excitation power supply of the transducers formed a part of the transducer measurement system and were calibrated with the transducers in-situ (Cable, 2005).

The electronic pore pressure transducers were calibrated using varying column heights of water in-situ as connected with the associated electronics. Appendix B gives calibration charts for the transducers. The calibration trends over the time period of the research as well as calibration factors and zero readings for the transducers are also listed. It was observed that both calibration factors and zero readings changed over time. The transducers used in the research were of the vented gage pressure type. The openings of the transducers to atmospheric barometric pressure enabled the sensors to adjust to the changing barometric conditions with the result that there was no barometric pressure related drift in the transducer measurements (see Appendix B). On the contrary whilst the transducers were temperature compensated, Appendix B shows that there was a variation in voltage response of the transducers with temperature. The data plotted was taken while the settling column was filled with de-aired water only and each measurement was therefore a transducer zero reading.

Three calibration procedures were carried out for the pore pressure transducers which complemented each other. The three calibrations were the calibration using the permanent settling column, the sacrificial settling column and the 12mm diameter 5m height calibration column. The calibrations in the settling columns established the status of the transducers and other fittings before and after each experiment. The 5m calibration method sought to calibrate the transducers to within 50% of their full working capacity.

3.6.4 Settling Column Experiments

Six final experiments undertaken using both the coarse and fine tailings samples form a basis for this thesis. Three of the experiments were carried out using the permanent settling column (series “A” experiments) while the other three used sacrificial settling columns (series “B” experiments). In each experiment tailings slurries were poured into the settling columns using 20 litre capacity buckets. The six experiments comprised two full depth deposition experiments (Full Depth A and B) and two experiments each simulating rate of rise at 20m/yr (RoR 20m/yr

A and B) and 10m/yr (RoR 10m/yr A and B) respectively. The coding of the six experiments is summarised in Table 3.5. More detailed information on each of the experiments is given in Table 3.6.

Table 3.5: Coding of Settling Column Experiments

Experiment	Abbreviation	Settling Column Type
Full Depth A	FDA	Permanent
Full Depth B	FDB	Sacrificial
Rate of Rise 20m/yr A	RoR20A	Permanent
Rate of Rise 20m/yr B	RoR20B	Sacrificial
Rate of Rise 10m/yr A	RoR10A	Permanent
Rate of Rise 10m/yr B	RoR10B	Sacrificial

It is noted that for Experiments RoR20A and RoR10A as shown in Table 3.6 a total slurry height exceeding the settling column was deposited into the column as a result of decanting supernatant water. This created extra storage capacity to deposit more tailings slurry. Under Experiments RoR20B and RoR10B however, total tailings slurry deposited was confined to the total capacity of the settling column. In these latter cases the total slurry height deposited is less than the total settling column height. The durations of the different experiments shown in Table 3.6 depended on the time it took to reach full dissipation of excess pore water pressures for the deposited slurry layer. Experiments RoR20B and RoR10A were observed for longer periods of time to enable the evaluation of transducer flactuations over time. The saturated sediment densities shown in the table were approximated from the initial mass of the slurry deposited into the column less the mass of water decanted during the experiment divided by the volume of the settled tailings inside the settling column. The design of tailings dams require information such as amount of tailings solids that can be stored in a given site, an estimate of the density of the tailings in a storage facility as well as the amount of water that can be recovered from a tailings dams to reuse at processing plants. Although the design of tailings dams does not fall within the objectives of this study, the results of the settling column tests (Table 3.6) suggest some aspects of tailings dam that are significant and are worth noting. These include an estimate of saturated density of materials following consolidation (column

6), sediment depth (column 5) and height of decanted water (column 4 minus column 5). The results of settling columns can thus facilitate obtaining dam storage capacity, material density and estimates of recoverable quantities of water from tailings dams.

3.6.5 Settling Column Permeability Tests

When the deposited tailings had fully consolidated and all pore water pressures were hydrostatic in a given experiment, a constant head permeability test was undertaken for Experiments FDA, FDB, RoR20A, RoR20B and RoR10B. Both falling head and constant head permeability tests could be carried out, however constant head permeability tests were carried since the tailings materials were very soft and the test was relatively less transient and likely not to affect the permeability values. Figure 3.18 demonstrated the principle of the permeability test where the supply tank (2c), the supply tap (2d) and the exit tap (2e) helped to maintain the required constant head.

Steady state conditions were necessary for the proper determination of the coefficient of permeability of the tailings under the different experiments. The determination of the coefficient of permeability was to be evaluated when the tailings were subjected to no other flow except for the flow caused by the imposed head difference required for permeability test at a hydraulic gradient of unity (Blight, 2010). In order to measure the permeability at a hydraulic gradient of 1 ($\Delta H/L=1$), the height of the settled tailings, L, was used to estimate the appropriate water exit tap (2e) to use from among the optional taps (see Figure 3.23).

Once the settling column test had been completed with the excess pore water pressures dissipated, a constant head permeability test could be carried out at the prevailing steady state conditions. At this stage there would be no flow and no potential difference thereby rendering the experiment conditions ready for permeability test. However, the equilibrium conditions reached under the respective experiments did not correspond with a hydraulic gradient of 1 required for permeability testing of soft materials. Therefore prior to the commencement of the constant head permeability test it was necessary to raise or lower the water level within the settling column to adjust the head to achieve a hydraulic gradient of 1. The process of raising or lowering the water level within the settling column itself occasioned new transient conditions which required time to reach steady state before the permeability test could start.

Once hydrostatic conditions were re-established at a hydraulic gradient of 1, the constant head permeability test was carried out. The water discharged over time was recorded as well as both transducer and standpipe readings which gave change in head at the instrumentation (standpipes and transducers) locations along the height of the settling column. Vertical saturated permeability values were inferred from flow rates using Equations 2-43 and 2-46. It is worth mentioning that the permeability of the tailings were not independently measured other than through the use of the settling column data.

3.7 Microscopy and Mineral Determination Tests of Tailings Samples

This section covers the scanning electron microscope (SEM) viewing of samples as well as the X-ray diffraction (XRD) and X-ray fluorescence spectroscopy (XRF) tests that were undertaken on the tailings samples. The preparations of specimen for SEM viewing, XRD and XRF analysis work are described together with brief summaries of how each test method was carried out.

3.7.1 Scanning Electron Microscope Viewing Tests

Introduction

The Scanning Electron Microscope was used to view prepared specimen from the tailings samples. This section summarises sample preparation and viewing methods as well as the tests carried out.

Sample Preparation for SEM Viewing

Gold tailings deposited for Experiments FDB, RoR20B, RoR10A, and RoR10B were decanted following the constant head permeability tests. After decanting the supernatant water, the settling column were moved from the testing location inside the laboratory to a fenced area outside the laboratory where the settled tailings were exposed to sun, air and wind in order to dry the tailings inside the settling column. Experiment RoR10B was disturbed from its original horizontal level to the sloped level observed in the photograph shown later in this section. It is also likely that the sample was not level during the drying period. Because of disturbance to this test only grading information was used from this test and not particle orientation data. A

cover at the top of the settling column with a one meter gap between the top of the settling column and the cover was provided to minimise ingress of rain water into the drying tailings in case of rainfall. The one meter gap between the top of the settling column and the cover was provided so that the cover does not shade the drying tailings from sunlight which would delay the desired tailings drying process. Figure 3.26 shows the samples inside settling columns placed outside the laboratory for drying. It was observed from Figure 3.26 that as the tailings dried, the tailings materials shrunk and cracked inside the settling columns.

Table 3.6: Description of Experiments

Experiment	Duration (Days)	Settling Column Type	Tailings Type	Slurry Depth (mm)	Sediment Depth (mm)	Sediment Saturated Density (kg/m^3)	Remarks
FDA (Full Depth A)	6	Permanent 190mm ID 1500mm Height Column	Chemwes Dam 5 underflow 2010 sample	1455	622	1657 1710 1728	7 standpipes 4 transducers. Column 8 shows sediment density followed by densities after constant and falling head permeability tests.
FDB (Full Depth B)	10	Sacrificial 154mm ID 2000mm Height Column	Chemwes Dam 5 catwalk 2011fines sample	1915	889	1620 1678	7 standpipes 6 transducers. Column 8 shows sediment density followed by density after constant head permeability test.
RoR20A (RoR 20m/yr A, (3 layers deposited)	14	Permanent 190mm ID 1500mm Height Column	Chemwes Dam 5 underflow 2010 sample	1994	853	1590 1655 1679 1707	7 standpipes 4 transducers 660mm slurry layer every 4 days. Column 8 shows sediment density for each layer followed by density after constant head permeability test.
RoR20B (RoR 20m/yr B (3 layers deposited)	23	Sacrificial 154mm ID 1500mm Height Column	Chemwes Dam 5 catwalk 2011fines sample	1819	895	1530 1574 1585 1624	7 standpipes 6 transducers 660mm slurry layer every 4 days. Column 8 shows sediment density for each layer followed by density after constant head permeability test.
RoR10A (RoR 10m/yr A 3 layers deposited)	81	Permanent 190mm ID 1500mm Height Column	Chemwes Dam 5 underflow 2010 sample	1760	698	1699 1728 1729	7 standpipes 4 transducers 580mm slurry layer every 7 days. Column 8 shows sediment density for each deposited layer.
RoR10B (RoR 10m/yr B 4 layers deposited)	14	Sacrificial 154mm ID 1500mm Height Column	Chemwes Dam 5 underflow 2011 sample	1919	767	1616 1694 1721 1724 1741	7 standpipes 6 transducers 580mm slurry layer every 7 days. Column 8 shows sediment density for each layer followed by density after constant head permeability test.

Table 3.7 summarises information on the drying and recovery process of the tailings samples from the settling column experiments. Figure 3.27(a) shows a settling column after drying. As was expected the settled and dried tailings were intact inside the settling tubes and required careful removal from the settling tubes to secure recovered tailings samples with minimum disturbance.

A hand grinder with fine tooth was used to cut open the settling column into halves to expose the dried sample. Figure 3.27(a) and (b) show the sample recovery process. The tailings inside the settling columns were still intact due to the moisture that kept both the fine and coarse grained fractions of the tailings together. Figures 3.27 to 3.31 show the tailings profiles of the recovered tailings samples. Figure 3.29 shows the non-horizontal tailings layers caused by disturbance when the column was moved. Figure 3.32 is a schematic diagram representing the locations of the subsamples extracted from the recovered tailings samples for the determination of gradations, SEM micrographs, and specific gravity as well as showing the profiles of the estimated permeability values of the tailings profiles.

Once the sample had been recovered from the settling tubes, vertical and horizontal fabric specimen were extracted from each profile of the settling column. Figure 3.32 shows both horizontally oriented and vertically oriented samples along the height of the settling column. A horizontally oriented sample was prepared by taking a settling column specimen that was perpendicular to the height axis of the settling column and therefore parallel to the diameter axis of the settling column. A vertical sample on the other hand was a specimen that was aligned along the height axis of the column. Figure 3.33 illustrates both the horizontal and the vertical oriented specimen for SEM viewing. Each fabric examination sample was 100mmx100mmx40mm in size. The specimen were extracted, cut and trimmed using a laboratory spatula knife. Figures 3.34 (a), (b) and (c) show typical specimen of tailings prepared for viewing under the scanning electron microscope. The specimen were prepared by shaping and reducing the size of the sample so that it could be viewed under the microscope. Additional tailings samples of the profile were also kept for gradation tests.

It is worth noting that after drying outside the laboratory, the samples were further dried in the oven at 35°C. The samples were then cooled to room temperature inside the oven. Thereafter the samples were trimmed to the required smaller sizes. The properly sized samples were oven dried and cooled in the oven again. From the oven, the specimen were stored in desiccators.

The specimen was then fixed onto aluminium plate specimen stubs using conductive carbon glue as an adhesive. These specimens were sputter coated with 5 layers of gold (30nm each). The samples mounted on the substrate were fixed onto the microscope stage for viewing. Figure 3.35 (a) and (b) show tailings specimen for use with the scanning electron microscope before and after sputter coating with gold.

Three specimen preparation methods were used for specimen viewed under the SEM. The first preparation method entailed picking up a specimen in a loose state onto conductive carbon tape. The second method obtained the fabric of an intact tailings specimen whose surface was prepared to be uniform and hence disturbed (Figures 3.35a and 3.35b). The third method involved breaking and exposing an undisturbed tailings surface which was fixed to a specimen stub to hold it while the undisturbed surface is coated with gold and viewed under the SEM.

One set of micrographs were prepared by means of pressing a sticky carbon tape (CT) onto the sample which had been prepared and had a disturbed surface viewed under the SEM. The second set of micrographs was prepared by breaking up an undisturbed surface of the sample which was then mounted on a specimen stub using carbon glue (CG) and viewed in a relatively undisturbed state. Table 3.8 summarises the SEM micrograph preparations methods used and the samples or experiments to which they were applied.

Table 3.7: Drying and Recovery Process of Tailings Samples

Description	Drying Period (days)	Initial Sediment Height (mm)	Final Sediment Height (mm)	Percentage Reduction In Height (%)	Remarks
RoR 20m/yr B (3 layers of 2010 catwalk fines sample deposited)	109	807	775	4.0	Sample lost water and settled less relative to the other experiments whilst being moved from location of experiment inside the laboratory to outside for drying.
RoR 10m/yr B (4 layers of underflow sample deposited)	67	679	664	2.2	Sample underwent 66mm settlement due to water loss during movement to outside the laboratory for drying. Top most layers experienced tilting.
Full Depth B (deposition of 2010 catwalk fines sample)	47	737	724	1.8	Sample underwent 81mm settlement due to water loss during movement to outside the laboratory for drying. Top most layers experienced tilting.

Table 3.8: SEM micrograph specimen preparation methods

Specimen preparation	SEM micrograph method	Experiment/Sample used
Disturbed sample of tailings	Sticky Carbon tape (CT)	2010 & 2011 underflow and 2011 catwalk fines loose tailings
Sieved and dispersant treated	Sticky Carbon tape (CT)	2010 underflow loose tailings
Disturbed surface but intact	Sticky Carbon tape (CT)	FDB height profiles
Undisturbed intact surface	Specimen mounted on stub with carbon glue (CG)	FDB height profiles
Undisturbed intact surface	Specimen mounted on stub with carbon glue (CG)	RoR20B
Disturbed surface but intact	Sticky Carbon tape (CT)	RoR10A (no permeability test)
Undisturbed intact surface	Specimen mounted on stub with carbon glue (CG)	RoR10B

The different sample preparation methods were expected to affect the resultant micrographs. The carbon tape micrographs comprised of discrete particles stuck to the tape while the specimen stub carbon glue mounted samples were intact deposited tailings held together from the time of experimentation commencing from tailings deposition through both sedimentation and consolidation stages right through the seepage pressure inducing permeability testing and the effects of drying.

SEM Viewing of Tailings Specimen.

The two Scanning Electron Microscopes used in the research were the JEOL JSM-5800 LV and JEOL JSM-6010. Some of the typical settings of the microscopes were WD 12, SEI of 5kV and LC of 26µA. Microscope cross-hairs were used to navigate the whole specimen surface.

The microscope analysis undertaken was mainly at the macro level where the emphasis was to observe pores, particles shapes as well as to relate patterns depicting tailings fabric.

The structure of carbon tape and carbon glue used in securing the specimen were observed and noted under the scanning electron microscope. The sizes of the pores and cracks of the structure of both the carbon glue and carbon paper affected the fine and coarse tailings particles appearances differently on the viewed micrographs. The finer particles fell into the pores of the substrate leading to observation of "dimples" while coarse tailings particles tended to mask the pores. It was important to distinguish air pockets within the tailings specimen from the structure of the substrate.

The specimen prepared using the third preparation method where tailings specimen was broken up to expose undisturbed surfaces to be viewed under the microscope often resulted in uneven surfaces which were not entirely flat and horizontal. The exposed surface which was at varying elevations made it difficult to focus on the whole surface simultaneously resulting in micrographs that were partly focused with other portions blurred.

The fine tailings specimen generated a lot of charge build-up which resulted in poor quality micrographs with streak lines and large white patches obscuring parts of the image. Coarse tailings on the other hand resulted in very good quality micrographs. Magnification scales at x90, x350 and x1500 were adopted to enable a common micrograph analysis scale.

3.7.2 X Ray Diffraction Tests and X Ray Fluorescence Spectroscopy Tests

Gold tailings specimens were subjected to X-ray powder diffraction (XRD) and X-ray Fluorescence spectroscopy (XRF) testing. The XRD tests were undertaken to determine the crystalline mineralogical make-up of the tailings and the XRF tests to determine the chemical composition of the gold tailings. The XRD and XRF tests complement each other (Loubser and Verryn, 2008). In addition, specific gravity of the solids was estimated from the XRD and XRF data. Appendix C lists the samples that were tested to obtain mineralogy and specific gravity of solids.

Both the XRD and XRF analysis were not carried out by the author but by the personnel of the XRD and XRF Facility of the Geology Department of the University of Pretoria. The samples

were oven dried and provided in the form of powder whose maximum particle size was 2mm. The tests procedures used by the XRD and XRF facility on the samples provided were reported by Grote (2012) and Dykstra (2012) with the test results for the XRD and the XRF tests respectively and are summarised below.

For the qualitative and quantitative XRD tests the specimen were required to have a maximum particle size of 1mm. The specimen were therefore first milled to a much fine powder and placed into a sample holder using a back loading preparation method. The samples were analyzed using a PANalytical X'Pert Pro powder diffractometer with X'Celerator detector and variable divergence and receiving slits with Fe filtered Co-Kα radiation. The phases in the examined samples were identified using X'Pert Highscore plus software. The results were given in both tabulated form with proportions given as percentage weight and in graphical form depicting scattering angle against intensity. The measurement errors were reported to be on the 3 sigma level. The minerals identified using the XRD technique were therefore over 99% likely to be correct as identified assuming normal distribution. The relative phase amounts in percentage weight was estimated using the Rietveld method. Amorphous phases, if present were not taken into consideration in the quantification (Grote, 2012). The samples for the XRF tests were prepared as pressed powder briquettes. The ARL9400 XP+ Sequential XRF and Uniquant software was used for analyses. The software analysed for all elements in the periodic table between sodium (Na) and Uranium (U), but only elements found above the detection limits were reported. . The values were normalised, as no loss on ignition (LOI) was carried out to determine crystal water and oxidation state changes. All elements were expressed as oxides (Dykstra, 2012).

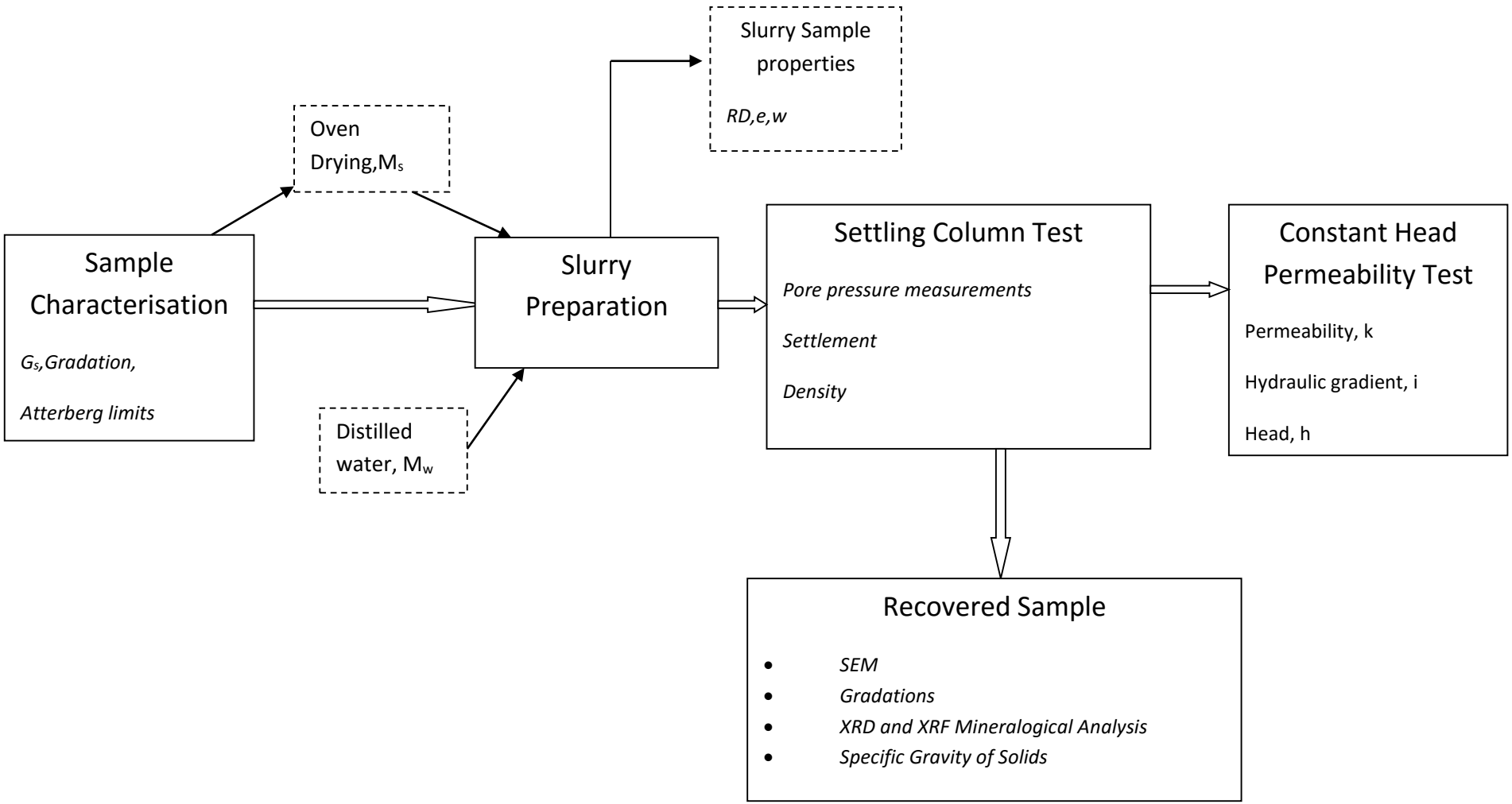

Figure 3.1: Summary of study methodology

Figure 3.2a: Location of Chemwes Dam 5 in Stilfontein, South Africa.

Figure 3.2b: Location of Mooifontein Dam, Crown Mines in Johannesburg, South Africa.

Figure 3.3: Chemwes Dam 5 dam wall and beach area

Figure 3.4: Chemwes Dam 5 hydrocyclones depositing underflow on dam wall

Figure 3.5: Chemwes Dam 5 sampling of underflow restricted (20meters) from dam wall

Figure 3.6a: Chemwes Dam 5 catwalk with deposited catwalk fines within reach for rope and bucket sampling. *Channelling visible.*

Figure 3.6b: Chemwes Dam 5 the start of catwalk leading to the penstock

Figure 3.6c: Chemwes Dam 5 dam penstock area under water

Figure 3.7: Chemwes Dam 5 overflow tailings depositing on the beach area with channelling forming at the discharge point and along the dam beach area.

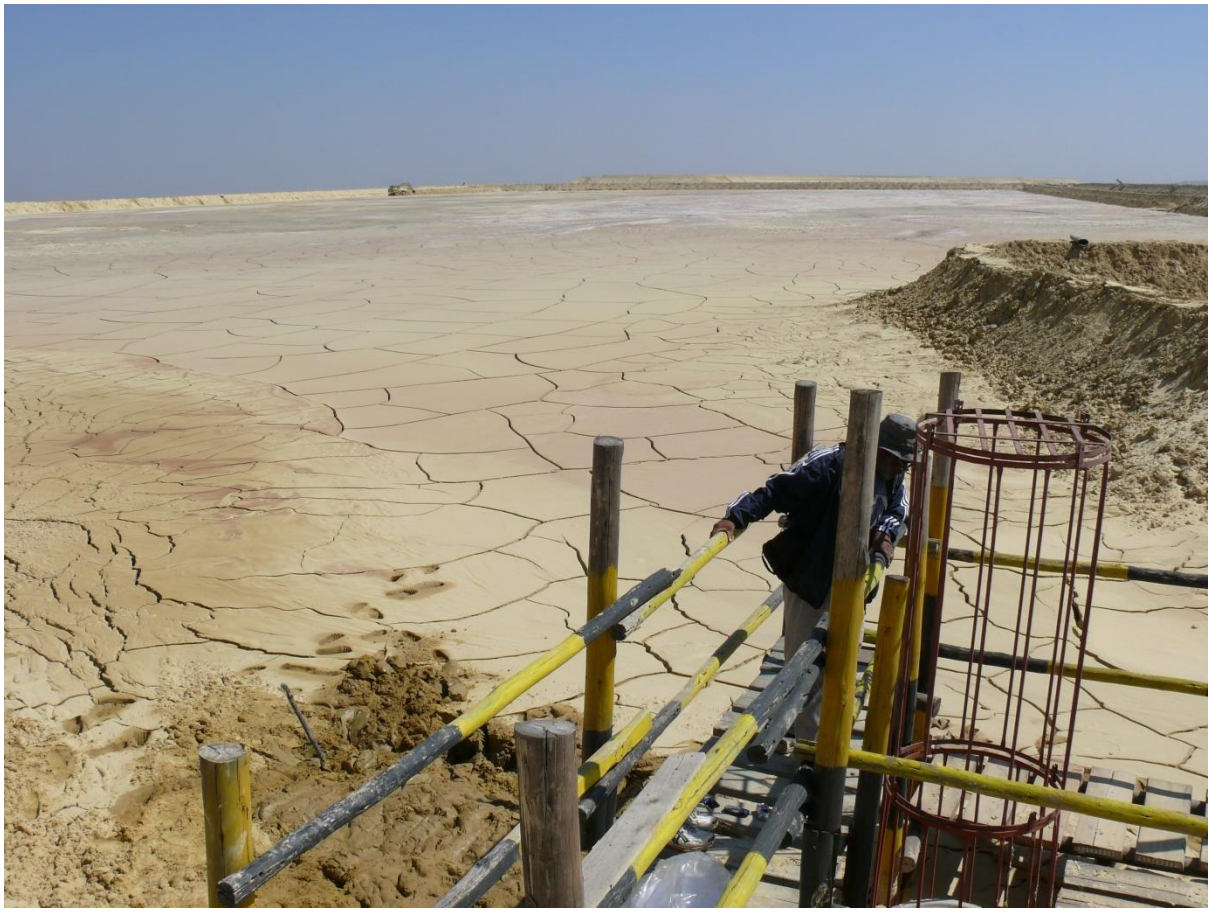

Figure 3.8: Crown Tailings Complex's Mooifontein Dam penstock area dry allowing extraction of penstock tailings samples directly using a shovel

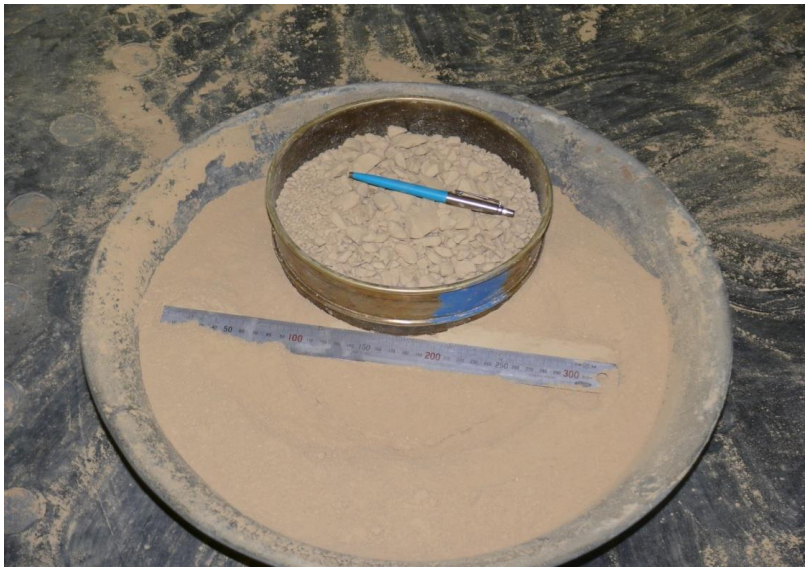

Figure 3.9: Oven-dried gold tailings pulverised by tamping and sieved by 2mm sieve ready for mixing with distilled water to make slurry.

Figure 3.10a: Cylinder sedimentation tests different cylinder sizes

Figure 3.10b: 1000ml Cylinder sedimentation tests

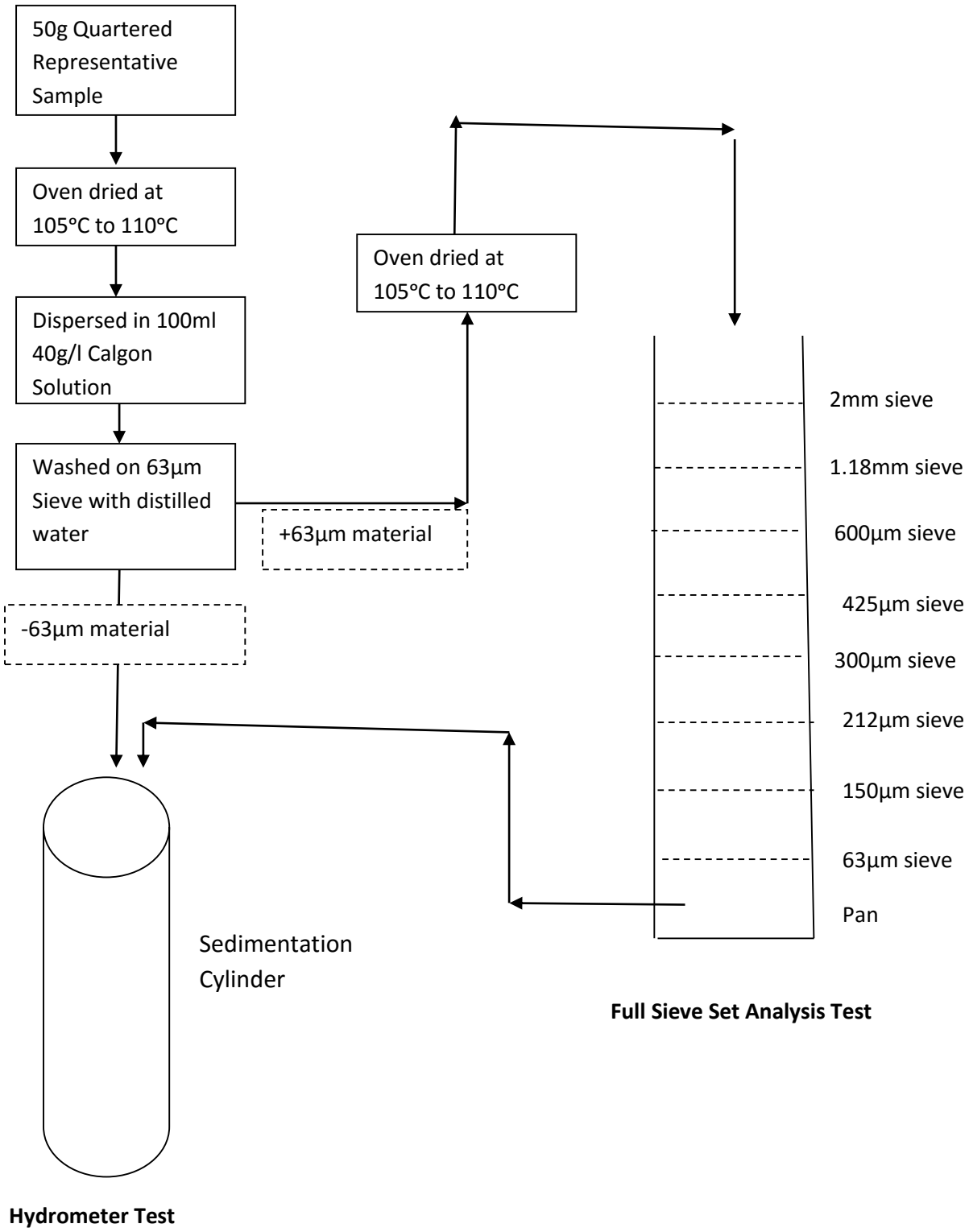

Figure 3.11: Summary of particle size analysis procedure

Figure 3.12: Sintered bronze filter

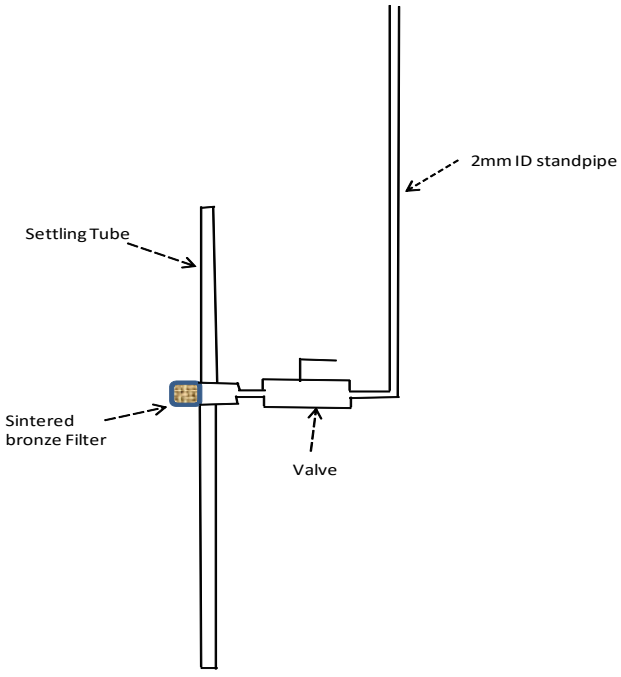

Figure 3.13: Standpipe piezometer fittings

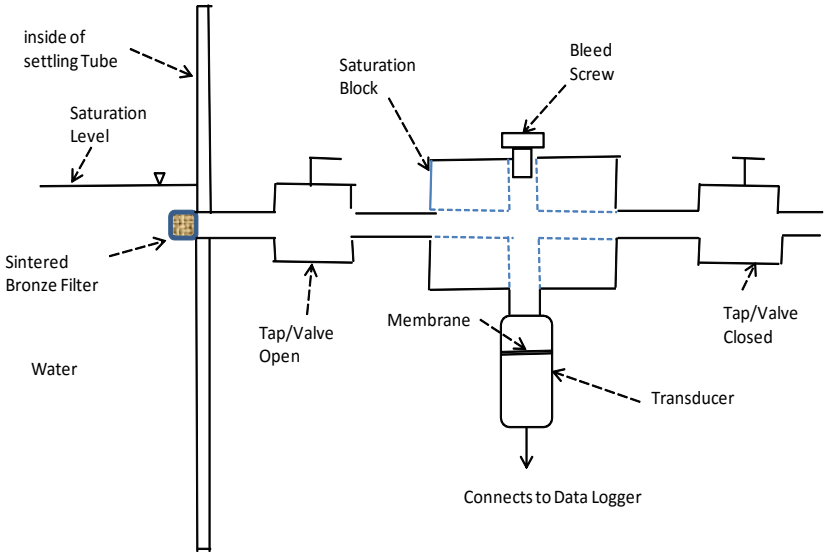

Figure 3.14: Pore pressure transducer fittings

Figure 3.15a: GEMS 100kPa transducer

Figure 3.15b: WIKA 100kPa transducer

Figure 3.15c: WIKA40kPa transducer

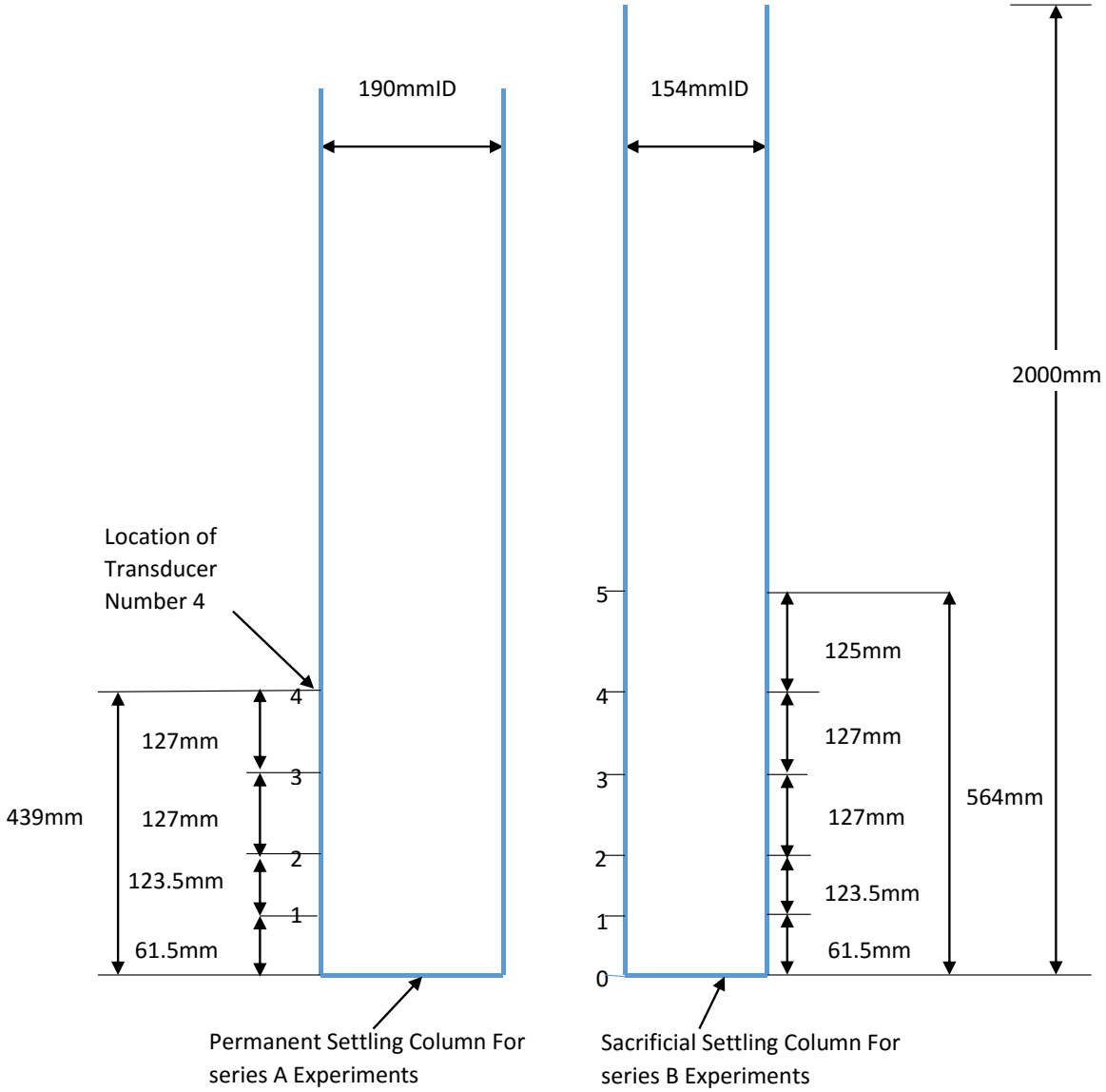

Figure 3.16: Location of transducers on settling columns

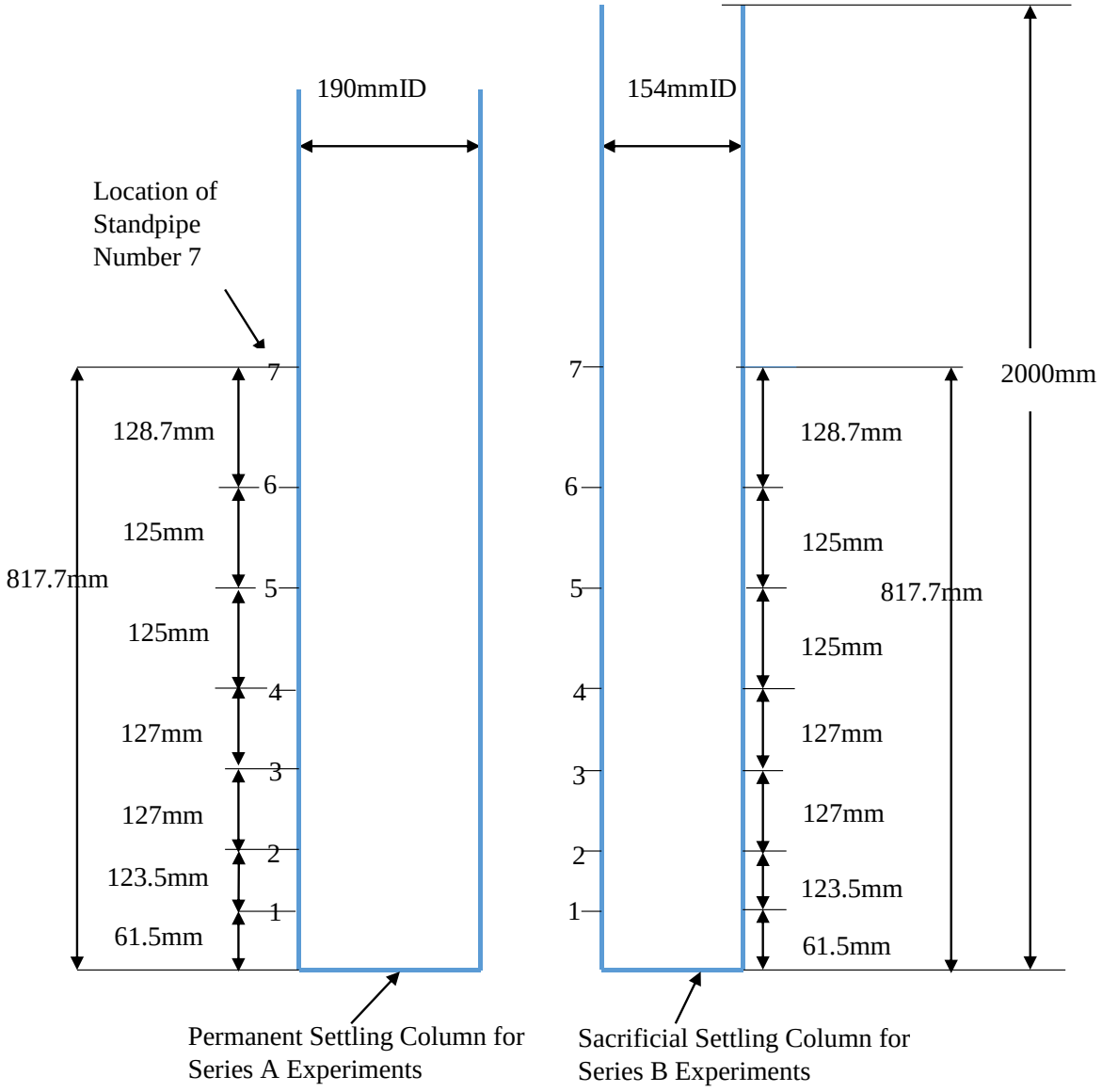

Figure 3.17: Location of standpipes on settling columns

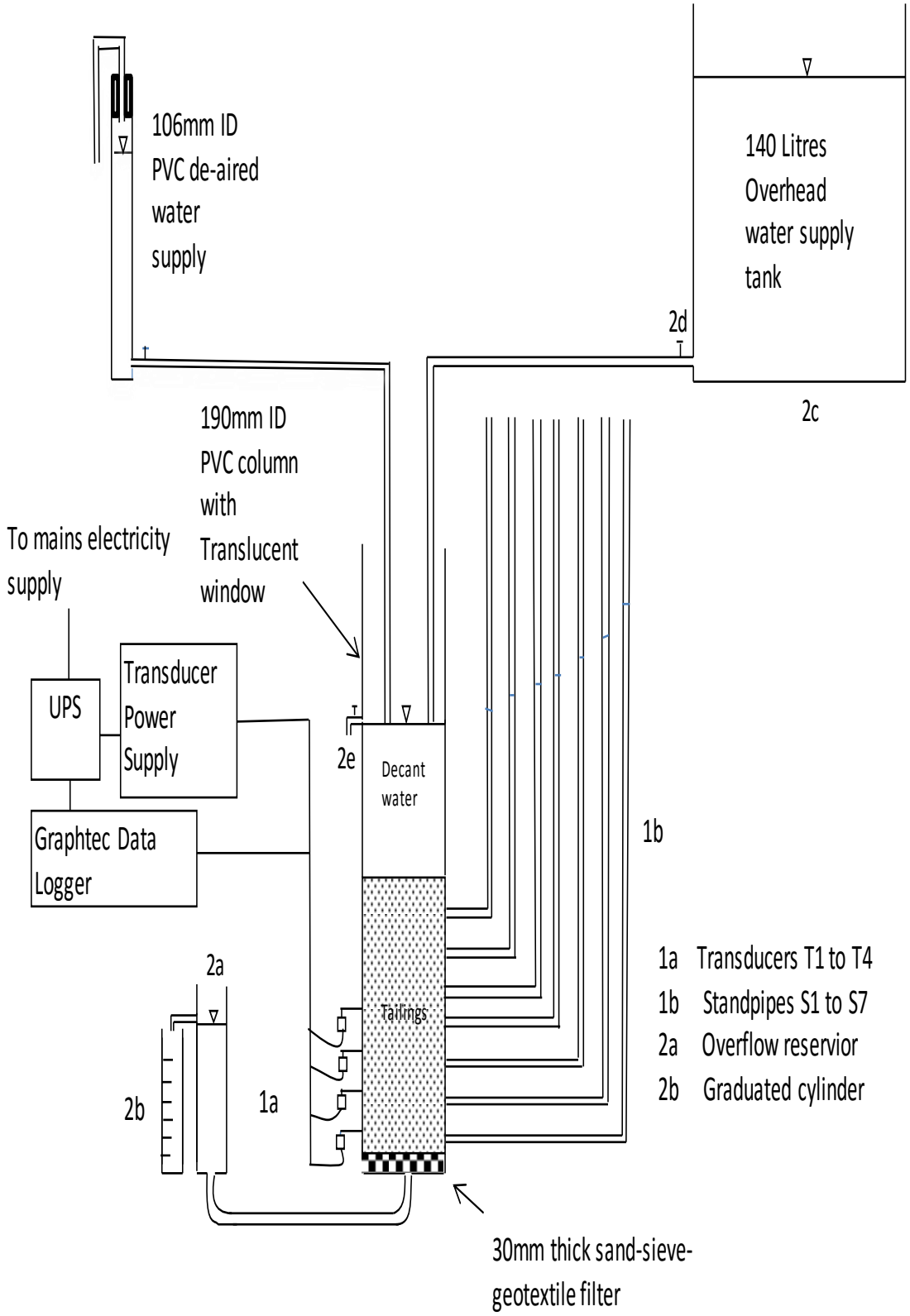

Figure 3.18: Instrumented settling column apparatus

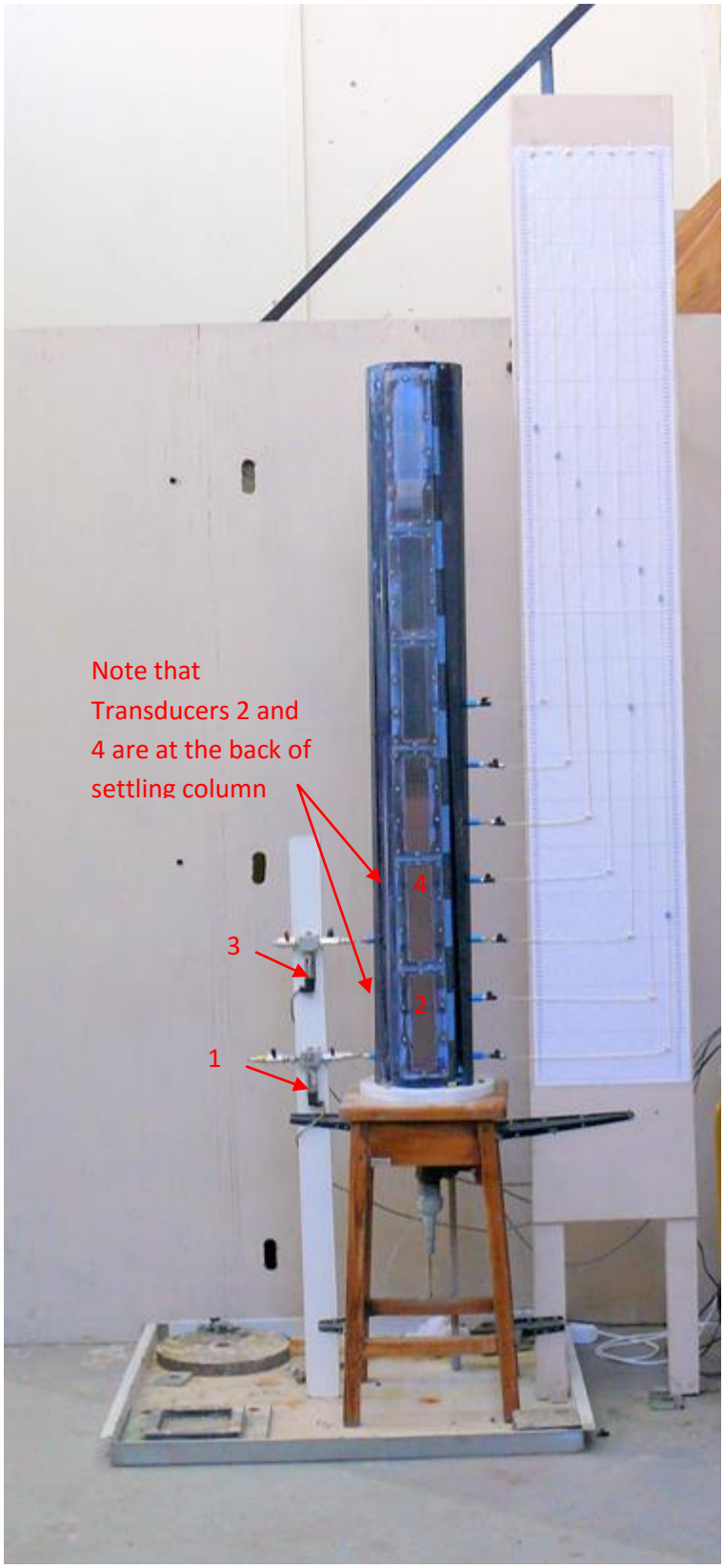

Figure 3.19: 190mm ID Settling column apparatus

Figure 3.20: 190mm ID exploratory settling column (prior to modification into permanent settling column) and de-aired water supply tank

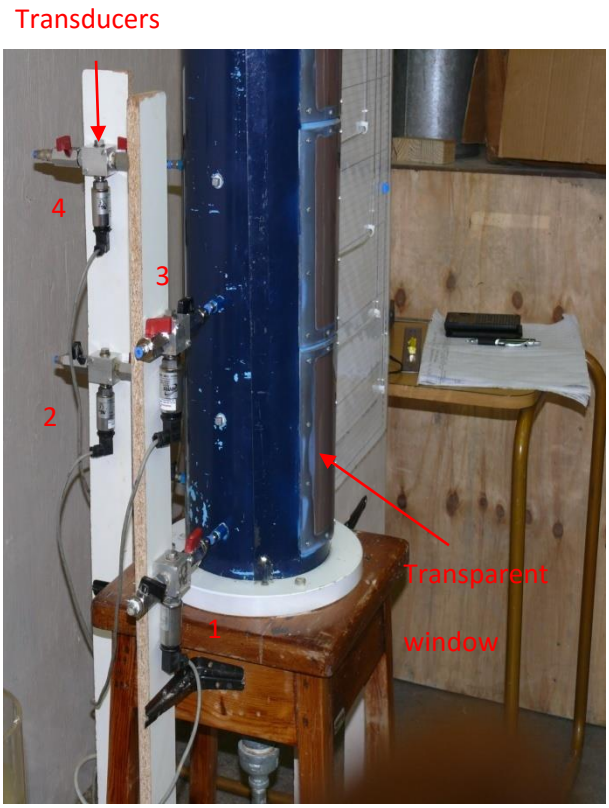

Figure 3.21a: Transducer connected to 190mm id settling column

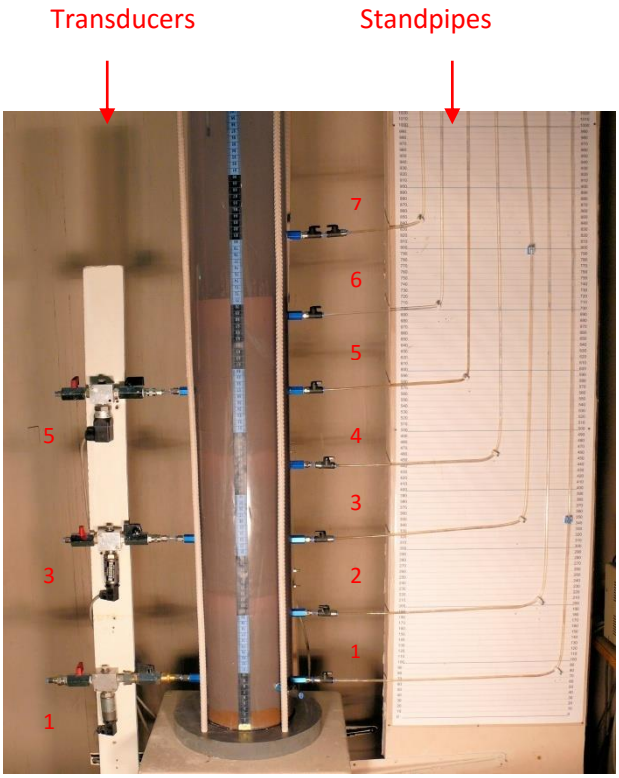

Figure 3.21b: 154mm ID Settling column with pore pressure instrumentation

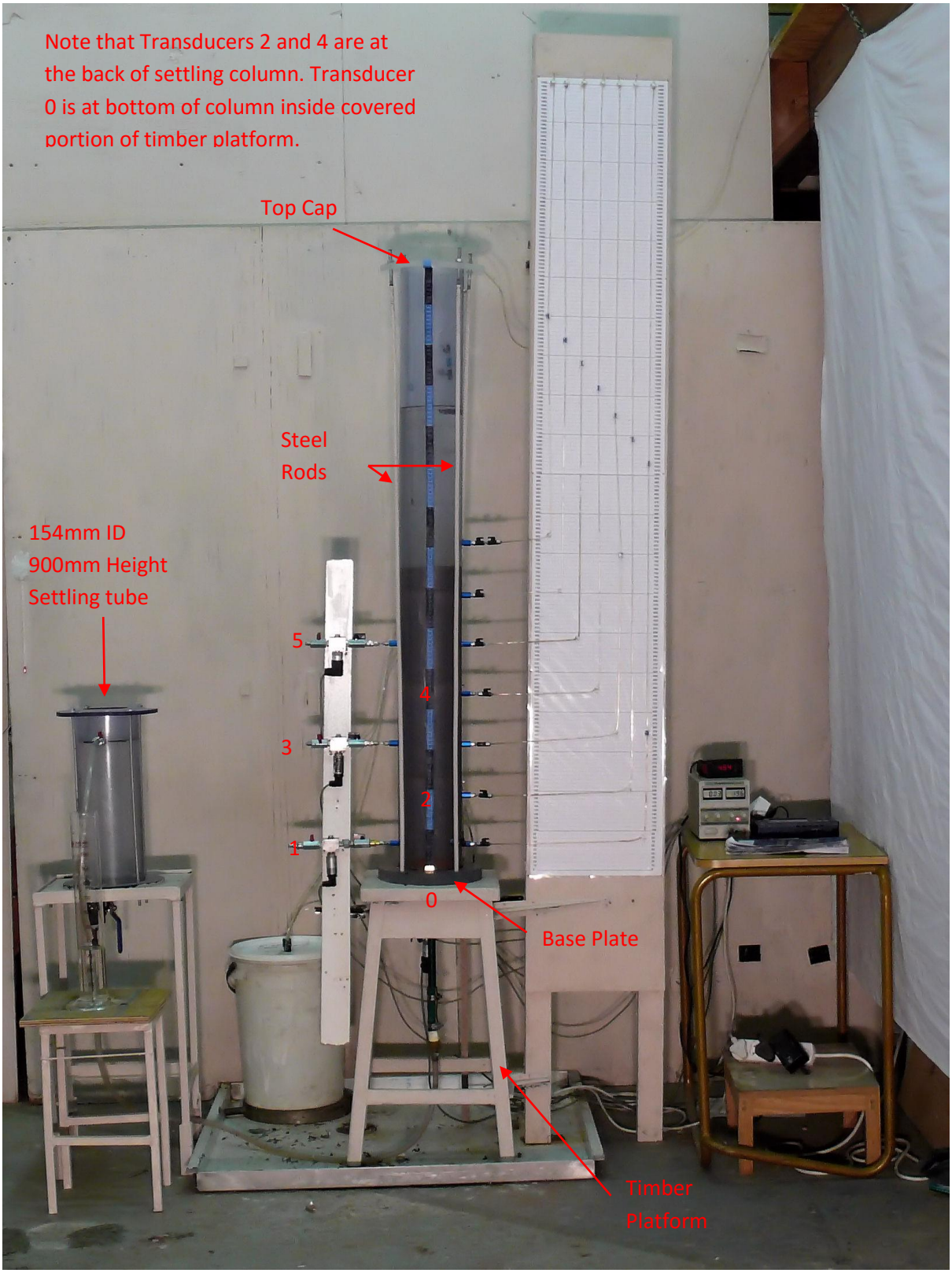

Figure 3.22: 154mm ID Settling column apparatus with permeability test setup

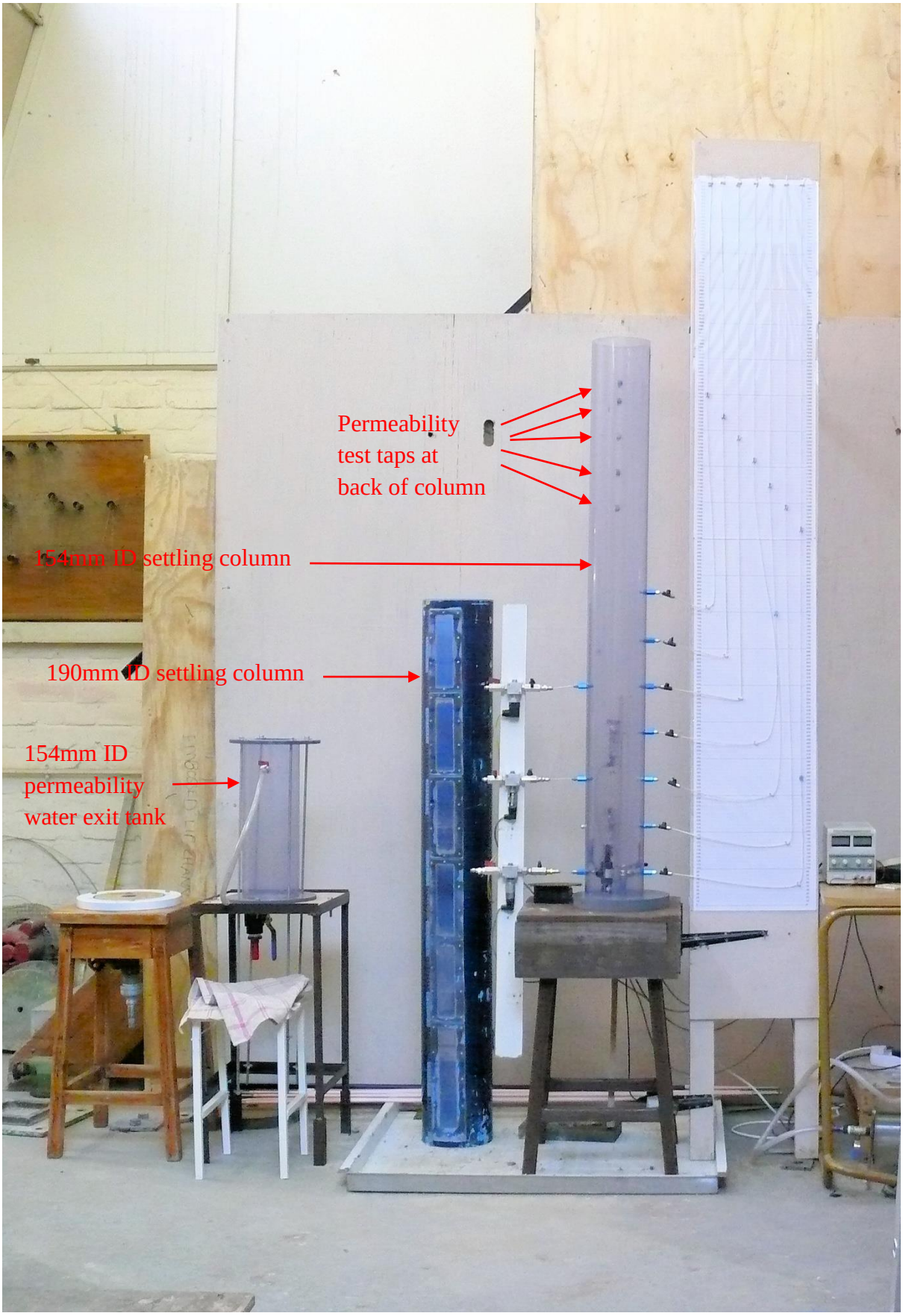

Figure 3.23: 190mm ID and 154mm ID Settling column apparatus

Figure 3.24a: Permeability 1000L water reservoir

Figure 3.24b: Permeability water reservoir with water supply value

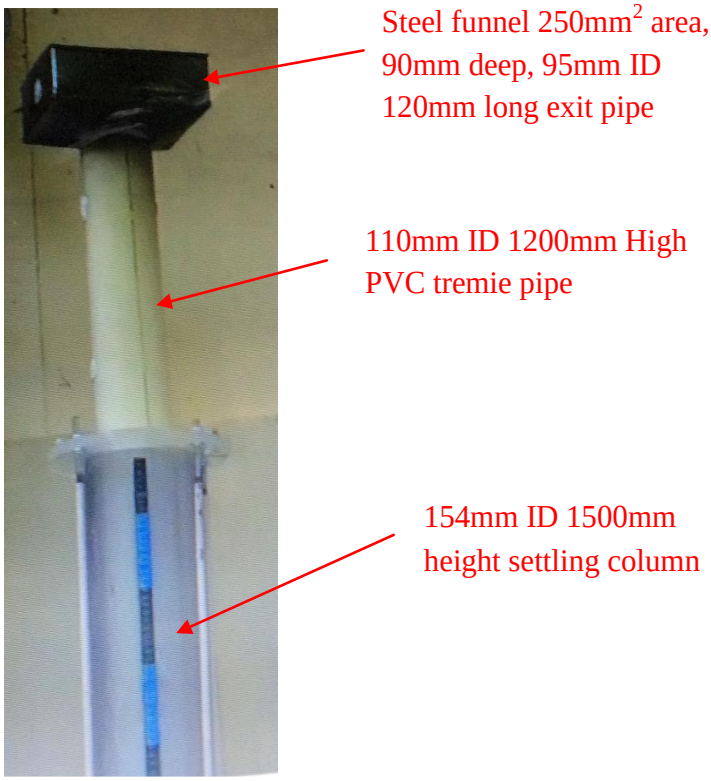

Figure 3.25a: Slurry pouring tremie pipe

Figure 3.25b: Venturi meter for decanting water from settled tailings

Figure 3.26: Experiments FDB, RoR20B and RoR10B settling columns tailings drying

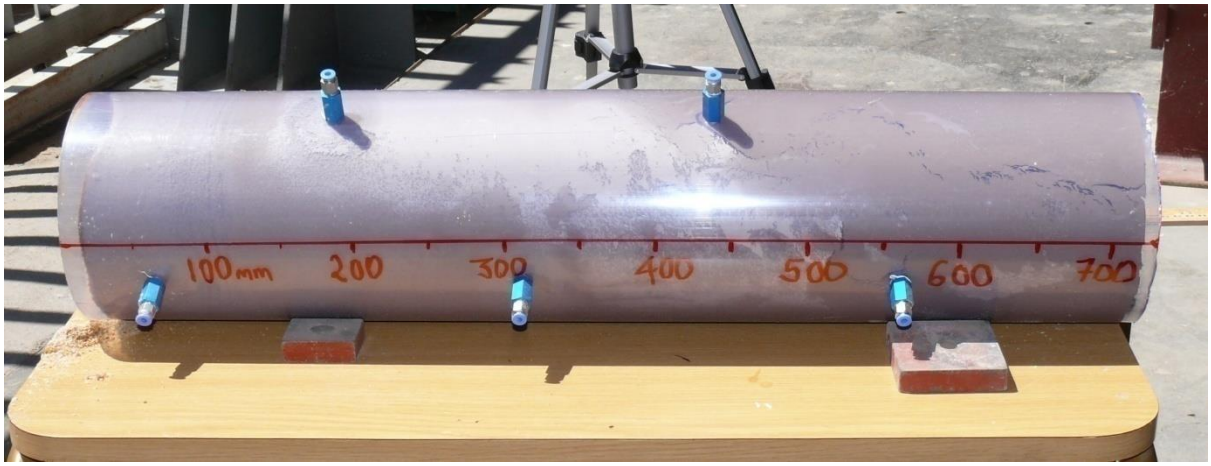

Figure 3.27a: PVC pipe containing dried tailings

Figure 3.27b: Cutting open PVC tube to recover dried tailings

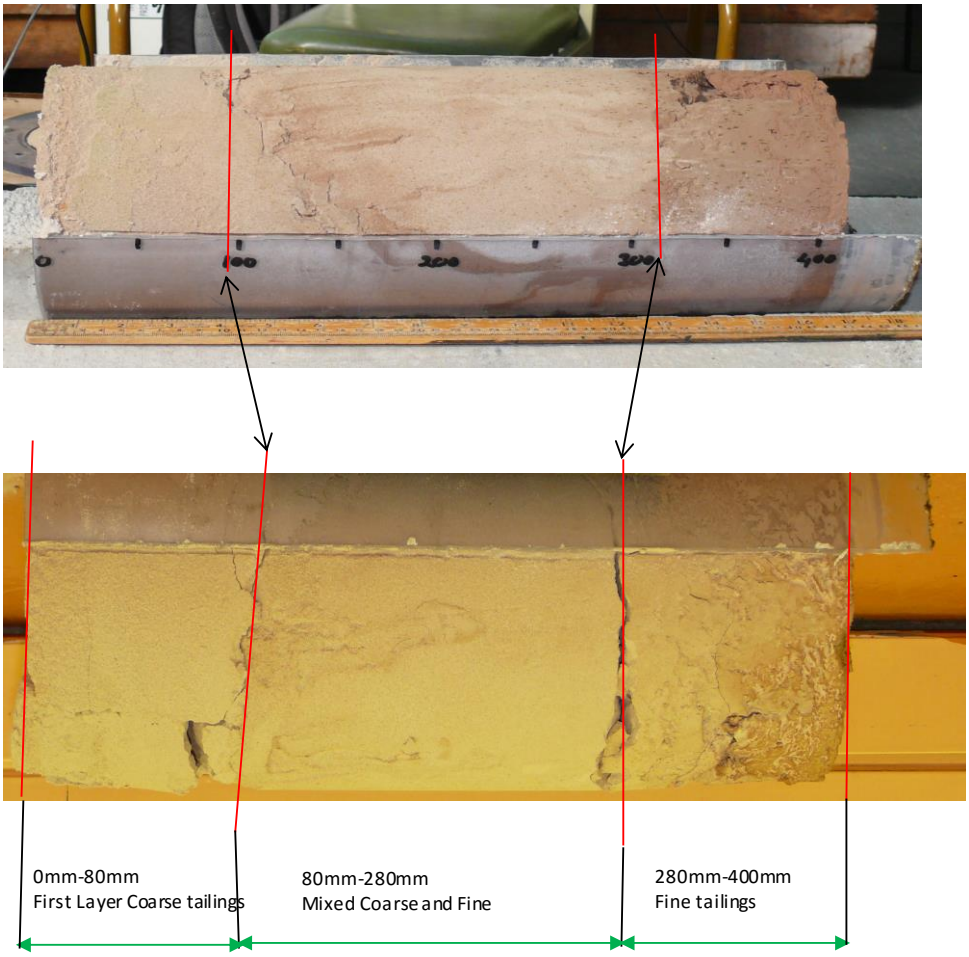

Figure 3.28: Recovered tailings RoR 10m/yr sample not subjected to permeability test

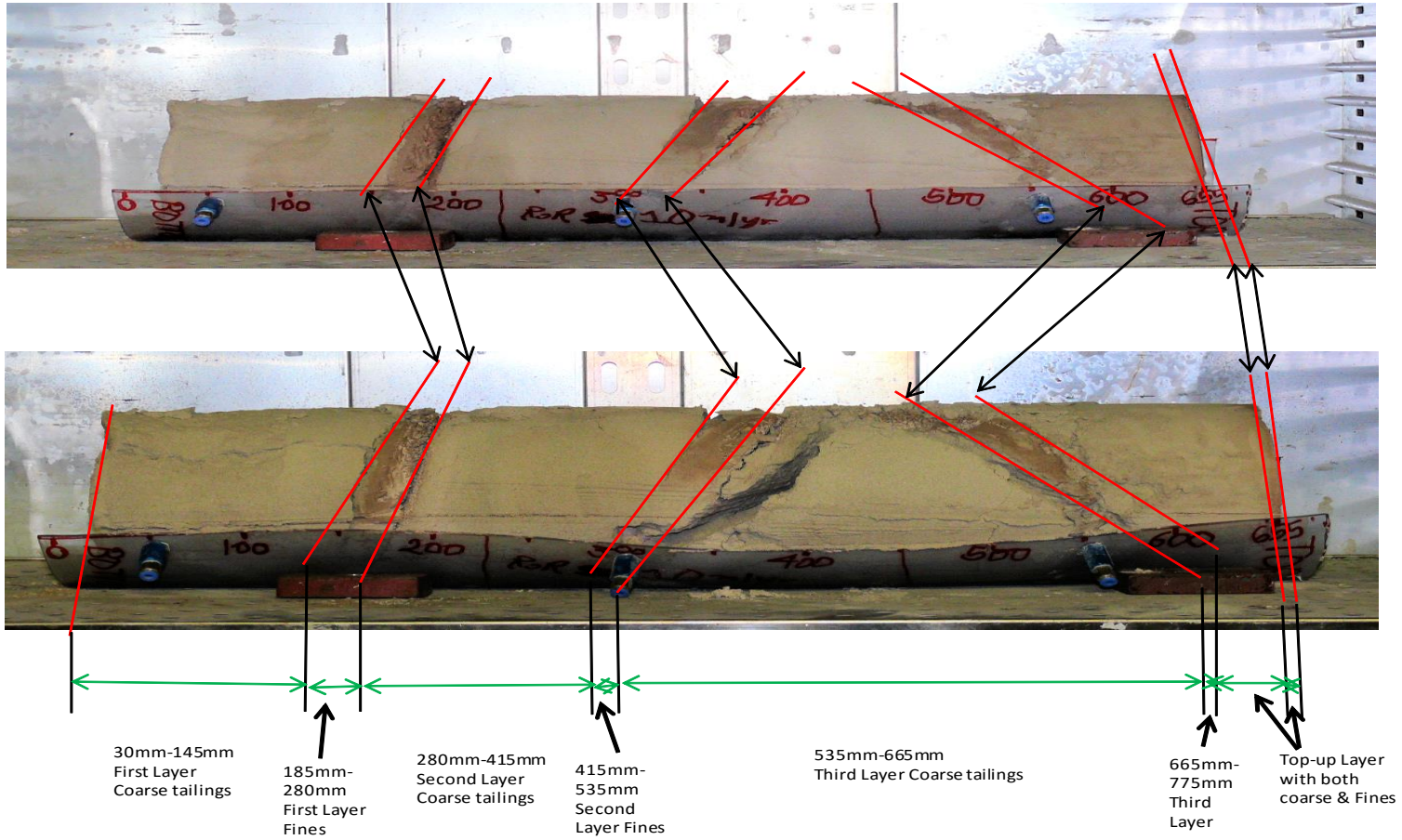

Figure 3.29: Recovered tailings sample Experiment RoR10B

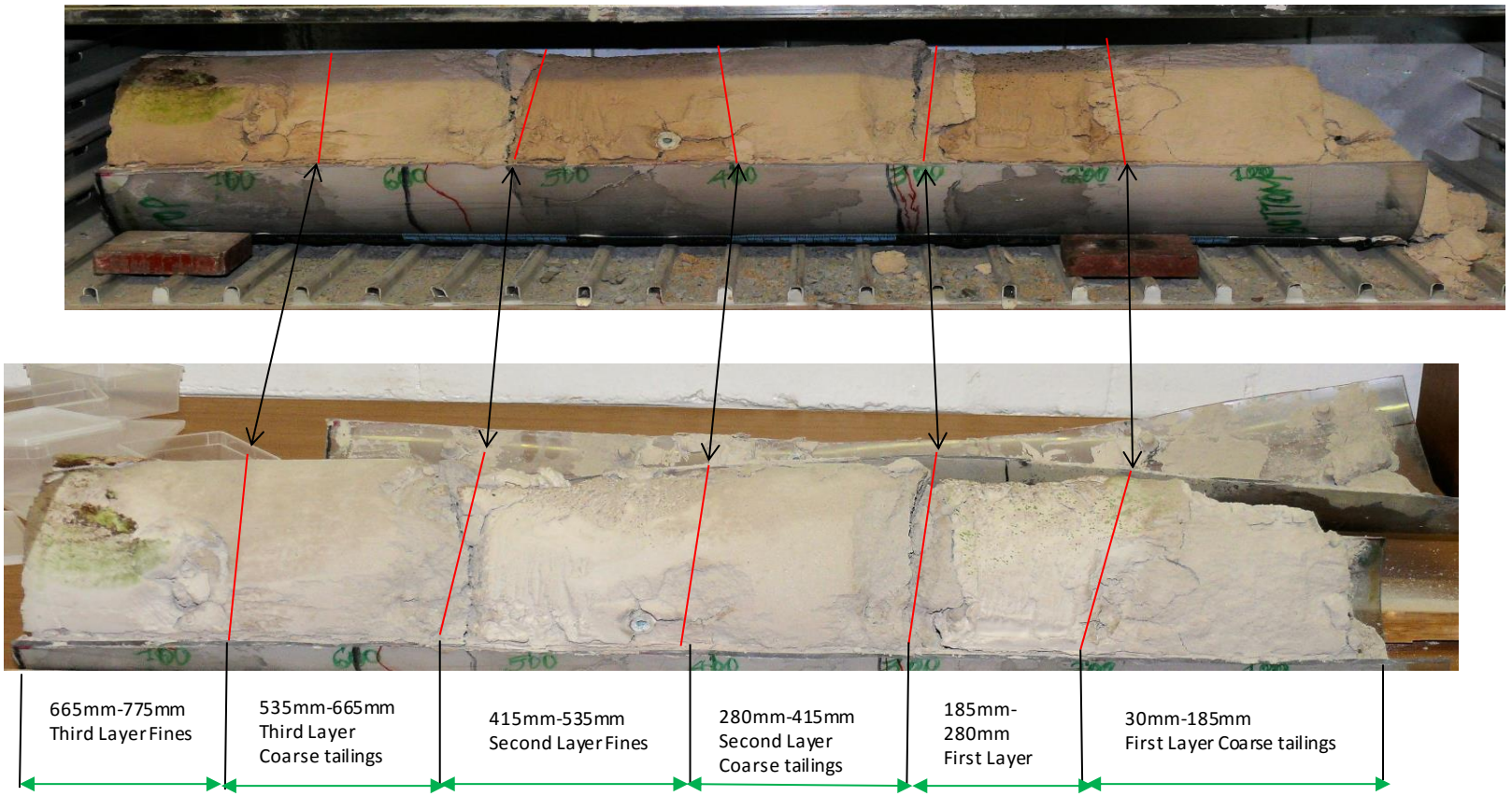

Figure 3.30: Recovered tailings sample Experiment RoR20B

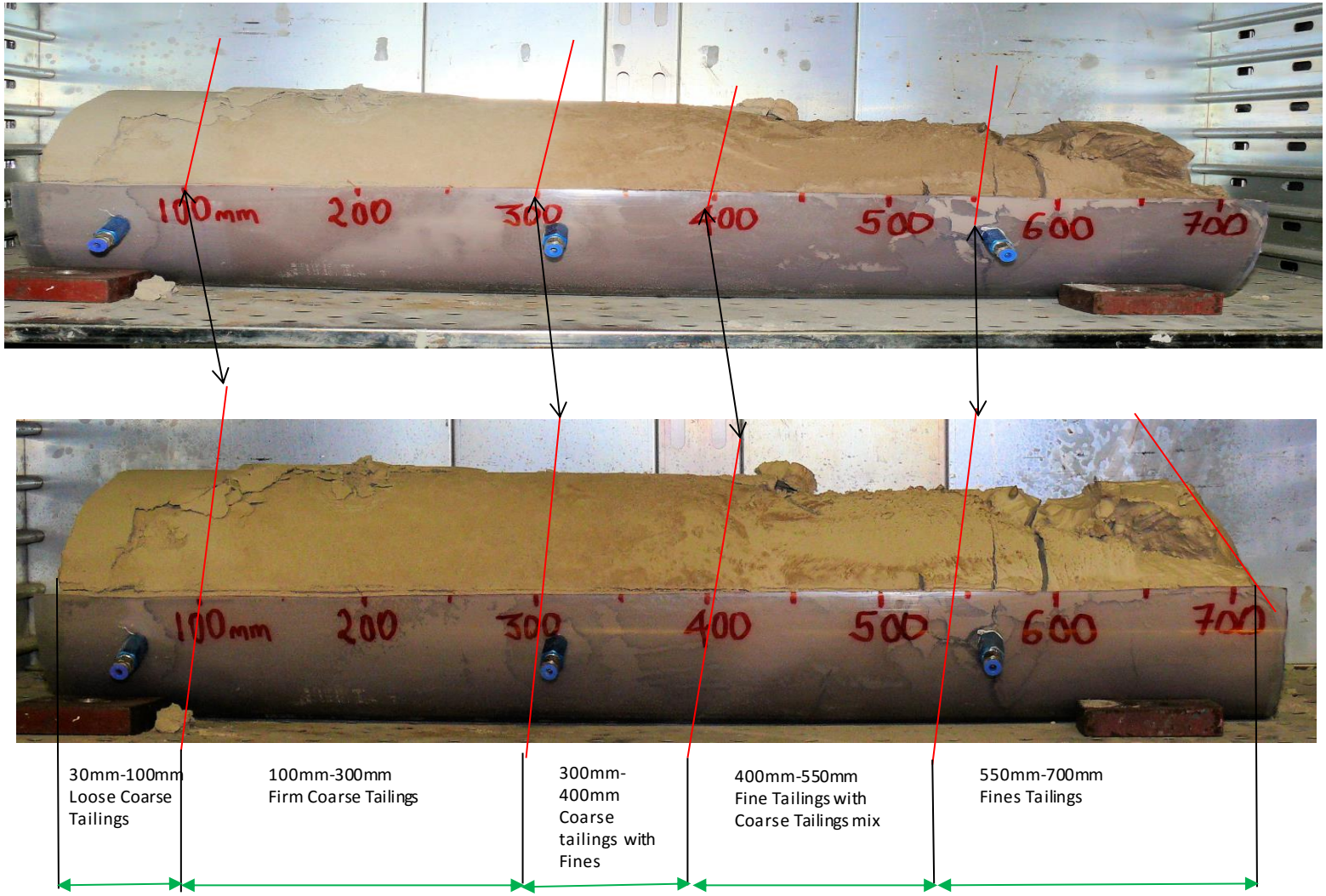

Figure 3.31: Recovered tailings sample Experiment FDB

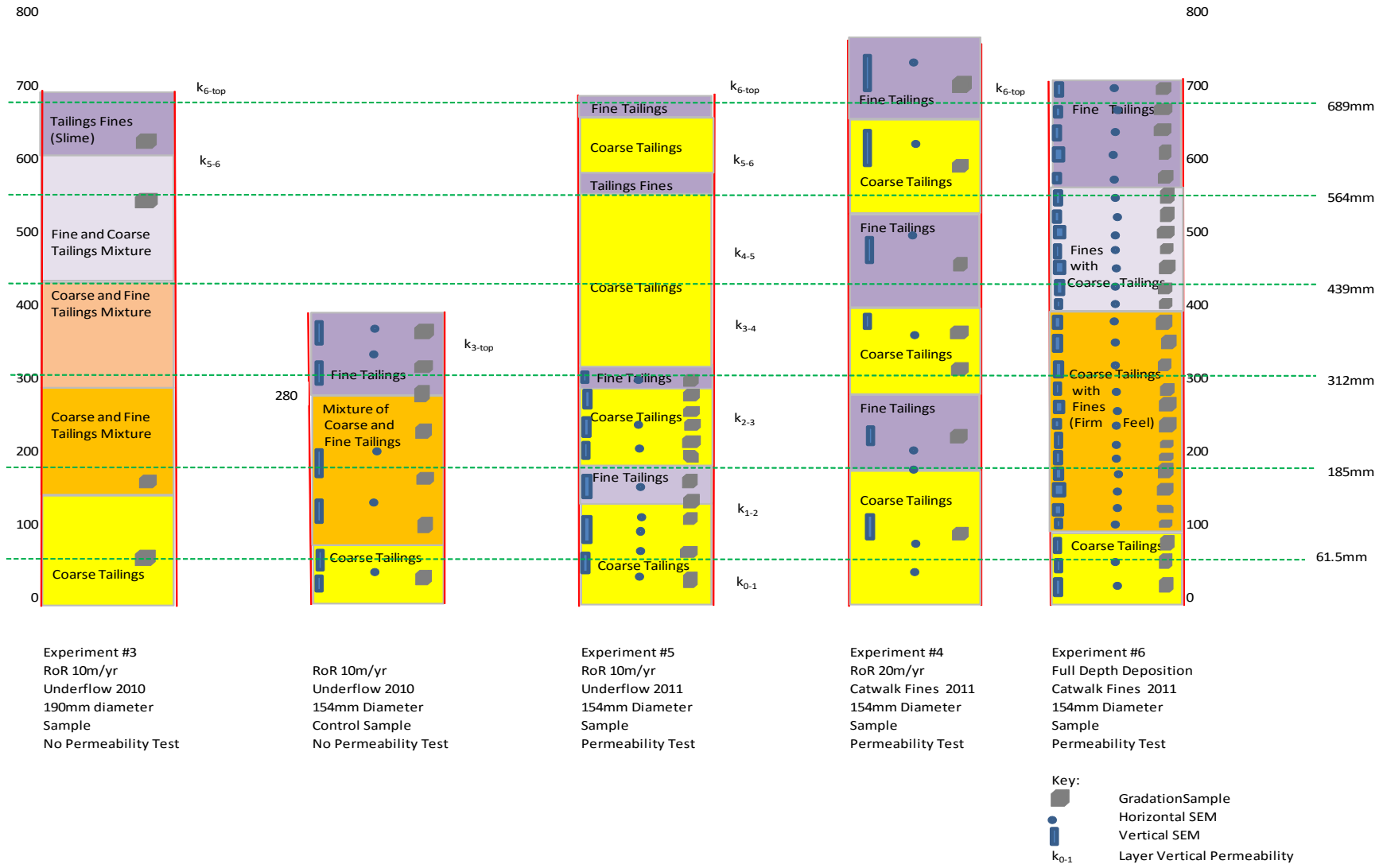

Figure 3.32: Schematic diagram of recovered tailings samples showing locations of specimen tested

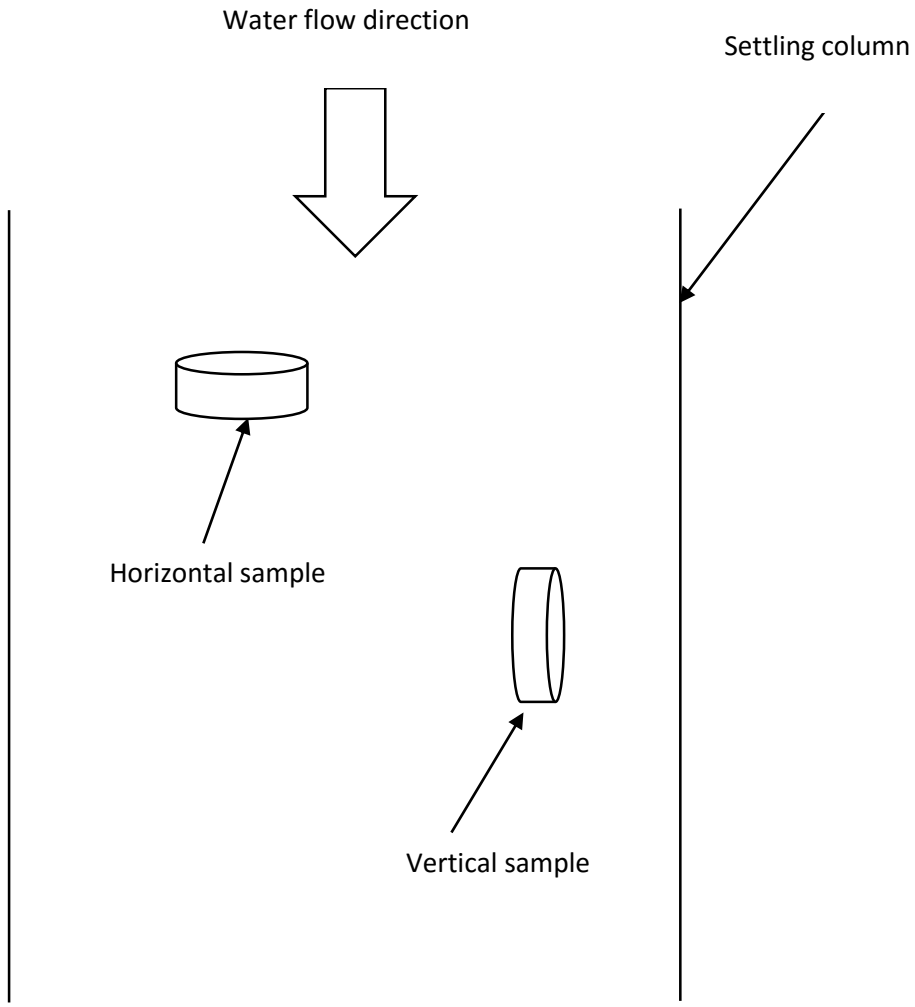

Figure 3.33: Horizontal and vertical SEM specimen in settling column

Figure 3.34a: SEM recovered tailings samples preparations

Figure 3.34b: Prepared SEM recovered tailings samples ready for desiccation

Figure 3.34c: Prepared SEM recovered tailings samples ready for desiccation

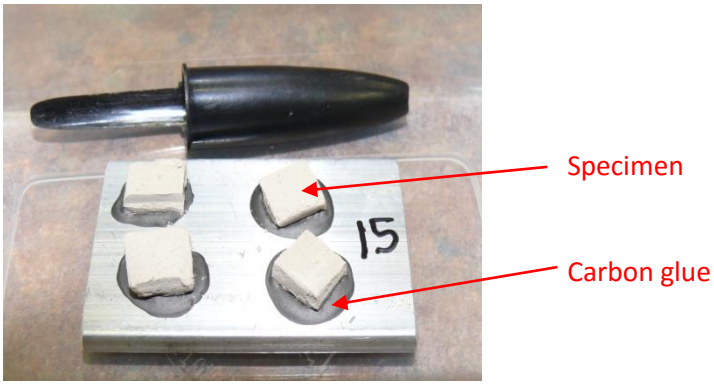

Figure 3.35a: Prepared SEM recovered tailings samples mounted on specimen stub using carbon glue (CG)

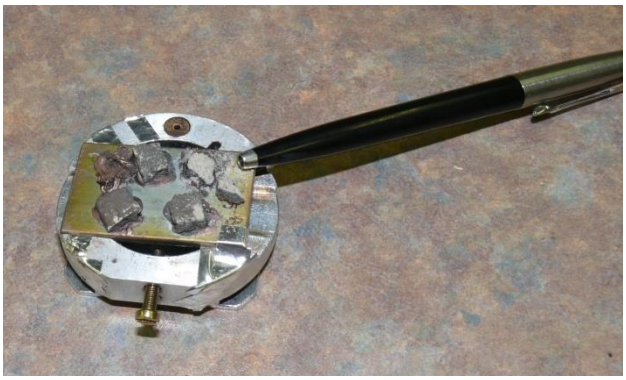

Figure 3.35b: Prepared SEM recovered tailings samples sputter coated with gold

Chapter 4

EXPERIMENTAL RESULTS

4.1 Introduction

This chapter presents results of the six experiments carried out to achieve the objectives of the research which sought to investigate particle size segregation, to evaluate layer permeability of tailings and to assess whether excess pore water pressures limit rate of rise in tailings dams. The tailings materials used in the research were characterised before and after experimentation. The experimental results comprise; physical properties of tailings and their slurry, tailings interface height time plots, changes of total heads with depth, pore water pressure changes with rate of deposition and with rate of rise, variation of tailings permeability with depth and tailings segregation. Tailings segregation was reported in terms of grading, specific gravity of tailings solids, mineralogical make-up and tailings fabric of tailings as displayed in SEM micrographs.

The experimental results are presented under subheadings designed to address the research study questions. Section 4.2 presents the physical properties of tailings and the slurry made from the tailings, section 4.3 tables the slurry interface height time plots for all the experiments which allows for an assessment of slurry deposition, sedimentation and consolidation rates. Section 4.4 captures the pore water pressure results for the different deposition phases which is the key aspect aimed at addressing the research question relating to rate of rise of tailings dams and excess pore water pressures generated. Sections 4.5, 4.6 and 4.7 deal with variation of vertical tailings saturated permeability with depth, particle size grading and specific gravity trends with settling column height and tailings fabric from SEM micrographs respectively. The last three sections of the experimental results *viz* sections 4.5, 4.6 and 4.7 address particle size segregation and their effects on properties of deposited tailings.

4.2 Tailings Physical Properties

The tests results on the samples are summarised in Table 4.1 and Figures 4.1 and 4.2. Table 4.1 summarises the physical properties of the tailings solids and tailings slurry as well as

properties of the complementary samples tested for completeness. Figure 4.1 shows the grain size distribution of the samples relative to the grading envelope of gold tailings in general (Vermeulen, 2001). Figures 4.2 depict the classification of the tailings samples under the Unified soil classification system. Figure 4.3 gives the mineralogical make-up while Figure 4.4 shows the SEM micrographs of the samples used in the experiments at magnifications of x90. Figure 4.5a depicts micrographs of particle size ranges extracted from the samples at magnifications of x90 and x350 for the sieved size ranges: -300µm+212µm, -212µm+150µm, -150µm+63µm and -63µm. Figure 4.5b illustrates the sieved size ranges.

4.3 Tailings Interface Height Data

Each of the experiments commenced with deposition of tailings slurry of specific gravity of 1.3 (or a suspension concentration of 467g/L). For each of the depositions, the solid tailings particles settled according to their sizes in the mixture and subject to the concentration of the slurry which evolved over time under the prevailing conditions within the settling column. The settling process and sedimentation continued over a period of time. Sedimentation and consolidation stages overlapped and eventually culminated in the consolidation of the settled bed of tailings solids.

In this section sedimentation and consolidation processes which unfolded and manifested as interfaces between a clear supernatant liquid and much darker coloured tailings slurry were recorded over time. The supernatant and settled slurry interface was referred to as the soil water interface (SWI). Additionally the interface between the supernatant liquid and the air at the surface of the settling tube was also recorded and referred to as the air water interface (AWI). Figure 4.6 shows a photograph with typical AWI and SWI values as captured for Experiment RoR20B after 45 minutes following tailings slurry deposition.

Figure 4.7 shows the change of tailings interface height (SWI) over time curves for Experiments FDA and FDB plotted together. The figure emphasises the different parts of the time-settlement processes of sedimentation and consolidation. It can be observed that the fine tailings slurry comprising catwalk fines (FDB) consolidated more than the coarse tailings slurry made from underflow tailings (FDA). This reflected a higher density for coarse tailings than for fine tailings as shown in Table 3.6.

Table 4.1: Physical properties of gold tailings samples

Physical Property	Underflow Sample 2010	Underflow Sample 2011	Catwalk Fines Sample 2011	Chemwes Whole Tailings Sample 2011	Chemwes Overflow Tailings Sample 2011	Mooifontein Penstock Tailings Sample 2009
Specific Gravity of Solids, G_s	2.69	2.66	2.71	2.71	2.73	2.75
Liquid Limit, LL	23	19	26			48
Plasticity Index, PI	NP	NP	2			13
D_{10} (mm)	0.0099	0.0145	0.00265	0.0015	0.016	0.0015
D_{30} (mm)	0.0538	0.058	0.0155	0.0100	0.050	0.0040
D_{50} (mm)	0.0825	0.0800	0.0405	0.062	0.052	0.0080
D_{60} (mm)	0.0998	0.1000	0.0585	0.062	0.060	0.0095
D_{90} (mm)	0.1825	0.1700	0.1350	0.1400	0.1300	0.029
Clay Fraction (%<0.002mm)	3	3	8	11	5	13
C_u	10.08	6.90	22.08	41.33	3.75	6.33
C_c	2.93	2.32	1.55	1.08	2.60	1.12
Grading Modulus, GM	0.54	0.48	0.23	0.3	0.28	0
AASHTO Class	A-4 Silty Soil	A-4 Silty Soil	A-4 Silty Soil	A-4 Silty Soil	A-4 Silty Soil	A-7-5 Clayey Soil
Unified Class	ML	ML	ML	ML	ML	ML and OL

Figure 4.8 shows the comparison of two underflow tailings samples of 2010 and 2011 deposited under Experiments RoR10A and RoR10B. The figure reflects that the two time settlement curves were similar as expected in contrast to the observation in Figure 4.7. Figure 4.9 shows the interface height change (SWI) with time data and the change of void ratio with logarithm of time for Experiment FDA. The plots show the various ways of presenting the time settlement data that demonstrates uses to which the data can be applied as well as emphasize other aspects of the data arising from the different data plotting approaches. The figures in addition identify the different phases of the sedimentation and consolidation process that the tailings slurry underwent to reach the dense consolidated layer thickness achieved at the end of the experiment. Appendix D gives settlement time data for the other experiments.

On the whole it was evident that coarse tailings slurry settled at rate of about 1mm/minute while fine tailings slurry settled at 0.633 mm/minute. The settlement rate was observed to comprise of two parts being the initial faster rate and a slower rate of settlement during the latter stages of the process of tailings consolidation (Figure 4.9a). This trend of faster deposition rates during sedimentation than the later slower consolidation rates was also observable from the rate of rise experiments which had three different deposition stages under each experiment.

4.4 Pore Water Pressure Results

4.4.1 Introduction

One of the objectives of the research was to investigate whether excess pore water pressure in deposited tailings limited rate of rise. With regard to this objective, pore water pressure within the deposited tailings in the settling column apparatus was measured. This section presents the results of the pore water pressure measurements.

The presentation of the test results starts with a description of the pore water pressure data collected and examines the effects of temperature, barometric pressure and settling column disturbances on experimental data. Excess pore water pressures observed in the experiments are also summarised.

4.4.2 Standpipe Excess Pore Water Pressure Trends

The top surface of the settling column base was taken as the datum for the settling column as well as for the measurement of total heads of the respective standpipes. The total heads in each of the standpipes were recorded at five minute intervals which was sufficient time for a whole cycle of recorded readings for the seven standpipes and up to a maximum of six transducers. The total heads were recorded together with the top surface of the settling slurry (SWI) and the supernatant water in the settling column apparatus (AWI). The temperature of the room and that of the water within the settling column were also recorded with other manually collected data. The manually collected data complemented the logged transducer data.

Excess pore water pressures at each standpipe location were calculated as the difference between the piezometric head in the standpipe and the air water interface (AWI) level in the settling column. The calculated excess pore water pressures were plotted over time. Figure 4.10 shows typical plots for Experiment FDA while Figure 4.11 shows the same data for Experiment RoR20A. The two figures represent standpipe data for full depth and rate of rise experiments respectively. Appendix E shows the results of the excess pore water pressure trends over time from the manually collected standpipe data for the rest of the experiments. Because the standpipes had a response time ranging from 2 to 5 seconds, the maximum excess pore water pressures obtained from standpipes were lower than the corresponding values obtained from transducers located at the same height on the settling column. The transducers had a response time of 0.5 seconds on average in water only. As noted in the next section, even though transducer zero readings and calibration factors were affected by temperature changes, the data collected was constant and reliable.

4.4.3 Transducer Excess Pore Water Pressure Trends

The transducer readings in units of Volts (V) were divided by calibration factors which were expressed in (V/mm) to calculate pore water pressures recorded by the transducers. The calculated pore water pressures in units of millimetre (mm) were used to calculate excess pore water pressures as the difference between transducer readings in mm and the air water interface (AWI) in the settling column also expressed in mm. Figure 4.12 gives the results for Experiment FDA while Figure 4.13 gives results for Experiment RoR20A. The two figures

show typical data for full depth and rate of rise experiments. Appendix E lists results of the rest of the experiments.

It was observed that some of the transducers yielded data that contained fluctuation of pore pressure measurements (Figure 4.14). The causes of the fluctuation is unclear, but it may be seen that the amplitude of the fluctuation is small relative to the magnitude of pore pressure measurement and therefore did not impact on the conclusions. Three trends of data are shown in Figure 4.14 as follows: data with fluctuation, data with the fluctuation removed from the data over a short period of 2 days and data with effects removed over the entire duration of the experiment. The fluctuations were corrected for resulting in a very good match of data between the transducers and standpipes collected data. Corresponding transducer data alongside standpipe data plotted together assisted in identifying the fluctuations within the data. Figures 4.15a to 4.15d show transducer and standpipe data pairs for Experiment FDA. The results of the paired data for other experiments followed a similar trend and can be found in Appendix E.

Manually collected transducer data yielded maximum excess pore water pressure values which were lower than the data logged transducer data. The analysis in this work was therefore based on logged transducer data while the manually recorded data served to validate logged transducer data as well as guided in obtaining the appropriate calibration factors and zero readings for transducers where data had the fluctuations cited above.

Figures 4.16a and 4.17a show deposition trend Experiments FDA and FDB. The insert within Figure 4.16a represents the early deposition trend covering the first 3 minutes of the slurry sedimentation following deposition. The insert depicts the deposition made during the 2 minutes duration using four 20 litre capacity buckets containing slurry. Figure 4.16b details tailings sedimentation and consolidation processes within the first 10 hours since the tailings slurry deposition commenced. It is worth noting that Figure 4.16a and 4.16b as well as Figure 4.17a show a series of vibrations which probably took place during the experiments. On Figure 4.16a the vibrations took place at the following times: 500 minutes, 1400 minutes, 1900 minutes, 2800 minutes and 3000 minutes. At these times the excess pore water pressures seemed to have suddenly increased at the same time for all the transducers. It took 20 minutes for the excess pore water pressures to revert back to levels that existed before the vibrations occurred. The behaviour where excess pore water pressures increased suddenly was also

observed when the settling column was shaken to induce vibrations. It is believed that the sudden “spike-like” increases of excess pore water pressures was attributable to vibrations arising from other uses of the laboratory around the room where the experiment was being conducted.

This included movements on the stairs that was near to the experiment and the use of the milling machine located in the same room with the experiment. The vibrations however caused effects that were easy to observe, to evaluate and to account for during the analysis of data. Similar disturbances to settling column experiments have been reported by other researchers (Been, 1980).

It is worth noting that the experiments under this research comprised a settling column filled with tailings slurry wherein the pore pressure readings as a result were very sensitive to any movements that affected the settling column apparatus. Because the slurry was fluid, disturbances that impacted on the slurry tended to increase excess pore water pressures. The disturbances mostly manifested as vibrations which generated excess pore water pressures. Once re-generated it took time to dissipate the excess pore water pressures to levels that existed prior to the vibrations that induced the excess pore pressures.

Figure 4.18a displays excess pore water pressure trends of the three slurry lifts deposited under Experiment RoR20A observed over a 14 days period. Figure 4.18b details the early excess pore pressure plots for the three slurry deposition lifts to focus attention on the transducer pore pressure rapid changes at the start of each deposition. It needs to be noted that in Figures 4.16 through to 4.18, the figures marked with the letter (a) showed the excess pore water pressure trends over the whole duration of the experiment while the figures marked with the letter (b) covered the first 3 hours to 2 days from the start of the experiments which focussed on the initial slurry deposition period. The figures marked with the letter (b) reveal more detailed pore pressure trends at the start of the experiments when the pore pressures changed rapidly.

Appendix E contains the logged transducer data for the other experiments. In the appendix the figures marked (a) and (b) are maintained as for Figures 4.16 to 4.18.

The excess pore water pressures generated at the different locations within tailings samples in the settling column were expected to be proportional to the weight of the tailings slurry

deposited. The bucket method of deposition used in this research did not deposit tailings instantaneously. The magnitude of the generated excess pore water pressures were therefore suspected to be lower than their actual values. The series of steps observed in the insert figure 4.16a represent the four containers that were used to store tailings slurry prior to deposition. The figure insert demonstrates the build-up of total pore water pressures as tailings slurry was deposited. It can be noted on the insert deposition chart that pore water pressures increased with deposition time up to the deposited slurry depth of 1450mm. Since instantaneous deposition did not occur, a starting time (time t =0) was selected for each experiment for purposes of data analysis. A choice of a starting time depended on the total slurry deposition time and the time to reach maximum generated excess pore water pressure values which occurred just prior to the commencement of pore pressure dissipations. Table 4.2 shows the start times selected for the experiments. The start times for rate of rise experiments were taken as the average times for the deposited lifts.

Table 4.2: Slurry deposition starting times for experiments

Experiment	Start Time (seconds)
FDA	89
FDB	47
RoR20A	44
RoR20B	23
RoR10A	46
RoR10B	35

Figure 4.19 summarises excess pore water pressure trends at transducers 1 for all the experiments. The figure shows that the full depth deposition experiments (FDA and FDB) generated relatively higher excess pore water pressures than the rate of rise experiments. In addition, fine tailings generated higher excess pore water pressures than coarse tailings. As regards the rate of rise experiments, however, excess pore water pressures from the rate of rise experiments at both RoR 20m/yr and 10m/yr were similar. Excess pore water pressure comparisons for Transducers 2 and 3 are given in Appendix E.

4.4.4 Pore Water Pressure Isochrones

Introduction

In order to address the research question regarding whether excess pore water pressure limit rate of rise, isochrones were plotted for the experiments. For each experiment, total heads and pore water pressures as well as degree of consolidation and remaining excess pore water pressure isochrones and their ratios were considered. The results of the different types of pore pressure isochrones plots were considered together with a greater emphasis on excess pore water pressures. Experiments FDA and FDB are reported first, followed by Experiments RoR20A and RoR20B and ending with Experiments RoR10A and RoR10B under each of the above listed pore pressure types.

Total Pore Pressure Isochrones

Figures 4.20 and 4.21 show the trends of total pore pressure isochrones along the depth of the settling columns for Experiments FDA and FDB. In these figures the isochrones designated as t=0 represent the maximum theoretical pore pressures expected. The values were calculated as the difference between the maximum pore pressures equivalent to the weight of slurry deposited (u_o) and the pore pressures under hydrostatic conditions (u_∞). The plots in Figures 4.20 and 4.21 show that all the excess pore water pressures dissipated within 26 hours and 10 days for both the 1450mm thick underflow tailings slurry and the 1900mm thickness of catwalk fines tailings slurry respectively. The maximum excess pore water pressures recorded for catwalk fines was 6kPa under Experiment FDA while under Experiment FDB a maximum of 4kPa was reached. The effect of the different internal diameters of the settling columns on pore water pressure results was deemed to have been minimal. It is noted that data points around zero (0) excess pore water pressure were obtained by assuming that since the points lie at a zone of clear water with no tailings, excess pore water pressure was zero at the respective heights which were the Air Water Interface (AWI).

Figures 4.22 and 4.23 show total pore water pressure trends for Experiments RoR20A and RoR20B. Whereas the two tailings types deposited in the experiments differed, the excess pore water pressure dissipation rates were very similar at a rate of 0.2kPa/hr of excess pore water

pressure decay. However, the times of dissipation as well as the maximum excess pore water pressures generated differed. The coarse underflow tailings dissipated between 2kPa and 4kPa in 15hrs while the fine catwalk tailings dissipated from 2kPa to about 6kPa in 25 hours.

Figures 4.24 and 4.25 show the total pore pressure isochrones trend for Experiments RoR10A and RoR10B. These two experiments used underflow tailings slurries prepared from the 2010 and 2011 samples collected at different locations of the Chemwes Dam 5 tailings dam. Even though the two experiments used coarse underflow tailings, excess pore pressure dissipation rates as well as total dissipation periods varied over a wide range. The dissipation rates ranged from 0.1 to 0.2 kPa/hr with between 2kPa and 5kPa maximum excess pore water pressures dissipated over a 13hrs to 43hrs time period.

Considering all the experiments, a dissipation rate of 0.2kPa/hr was observed in which 2kPa to 6kPa of excess pore water pressures were dissipated within 12hrs to 43hrs' time period. Trends of total pore pressure decay throughout the duration of the experiments were also obtained in terms of the variation of total heads with time. These trends are summarised under Appendix F.

Degree of Consolidation Isochrones

Figures 4.26 and 4.27 show the degree of consolidation plots for Experiments FDA and FDB while Figures 4.28 to 4.29 give the same data for Experiments RoR20A and RoR20B. Figures 4.30 to 4.31 show the data trends for Experiments RoR10A and RoR10B. Degree of consolidation plots were obtained from Equation 2.10. For Experiment FDA 100% degree of consolidation (Figure 4.26) corresponds with isochrones (t=1560 minutes) while 90% degree of consolidation corresponds with isochrones (t=360 minutes). The times to reach the respective degree of consolidation in hours are given in Table 4.3 as 26 hrs and 6 hrs. Similar approximations were carried out for the other experiments. Tables 4.3, 4.4 and 4.5 summarise the degree of consolidation isochrones data for 50%, 90% and full dissipation of excess pore water pressures for Experiments FDA and FDB (Table 4.3), RoR20A and RoR20B (Table 4.4), and RoR10A and RoR10B (Table 4.5) for the respective deposition lifts. The degree of consolidation results showed total dissipation times of 26hrs (1560minutes) and 10 days (14979minutes) respectively for Experiments FDA and FDB. The time to reach 90% and 50% consolidation for Experiments FDA and FDB were as follows: 6hrs for 90% and 2hrs for 50%

for FDA, for FDB 90% degree of consolidation was achieved after 3 days whilst it took 3hrs to reach 50% dissipation.

It is worth noting that while 90% of excess pore water pressure dissipated in 3 days for the catwalk fines tailings, it took an additional week to achieve near 100% dissipation. This indicated the disproportionate slow rate at which the remaining excess pore water pressures dissipate during the stages of consolidation following the initial faster dissipation of 90% of the excess pore water pressures.

Under Experiment RoR20A (Table 4.4) 50% dissipation of excess pore water pressures occurred within 0.25hrs to 0.5hrs lift 1, 1.5hrs to 9hrs for lift 2 to reach 90% dissipation and from 10hrs to 1.5 days for 100% dissipation of excess pore water pressures to be achieved. This is also consistent with the asymptotic nature of consolidation behaviour. In Table 4.5 it was observed that the times to reach degree of consolidation of 100%, 90% and 50% for Experiment RoR10A were more than double the corresponding values for Experiment RoR10B yet underflow tailings slurries were used in both experiments. Furthermore, the degree of consolidation times were greater than equivalent values for Experiments FDA and RoR20A. This was contrary to the trend of degree of consolidation times (100%, 90% and 50%) observed from Experiments FDB, RoR20B and RoR10B. The results indicate that excess pore water pressure dissipation was slower in the coarse tailings compared to in fine tailings comprising thicker layers (Experiments FDB and RoR20B). On the basis of one dimensional consolidation theory this could not be possible. The dissipation time data of Experiment RoR10A most likely contains errors. These could arise from the fact that the experiment was carried out over a much longer period of time (81 days although it was done for other reasons discussed in the thesis). Clogging of filters does not sound as a plausible an explanation of the odd results because permeability test was carried out after the consolidation stage yielding permeability tests results that were reasonable. The possibility of the filters all clogging up and all opening up again makes clogging of filters a remote possible explanation of the erroneous results. The results from Experiment RoR10B which was a replica of Experiment RoR10A can be considered to be correct in relation to Experiment RoR10A results.

As expected consolidation in terms of dissipated excess pore water pressure magnitudes and the dissipation durations were higher for catwalk fines than for coarse tailings since the fine tailings consolidated much slower. All the three deposition lifts reached 50% dissipation within

1hr to 3hrs, 90% dissipation was reached in 1 day and close to full dissipation was reached between 2 and 4 days.

Table 4.3: Degree of consolidation for Experiments FDA and FDB

Experiment	Degree of Consolidation (%)	Time to Reach $\overline{U}$ (Hours)
FDA	50	0.33
	90	6
	100	26
FDB	50	2.4
	90	53.1
	100	240

Remaining Excess Pore Pressure Ratio Isochrones

Figures 4.32 and 4.33 show the remaining excess pore water pressure isochrones for the full depth deposition experiments. Experiment FDA plot show both the remaining total excess pore pressure isochrones ratio $\left(\frac{u}{u_o}\right)$ in Figure 4.32a and the remaining excess pore pressure isochrones in Figure 4.32b. Figures 4.32b(i) and 4.32b(ii) show the sedimentation/consolidation phase and the consolidation phase respectively. Figure 4.33 shows remaining excess pore water pressures for Experiment FDB. Figures 4.34a(i) through to 4.37 show the normalised remaining excess pore water pressure ratio isochrones for respective deposition lifts under Experiments RoR20A, RoR20B, RoR10A and RoR10B. The data for the rest of the deposition lifts are given in Appendix E. It needs to be noted that excess pore water pressure values shown in Figure 4.35 at the base of the settling column are low are low (Experiment RoR10B). The isochrones based on the low values seem to suggest double drainage under this experiment which was not the case. In Figures 4.33 and 4.37 correctly recorded excess pore water pressure values at Transducer 0 are shown for Experiments FDB and RoR10B respectively. A possible cause of the low readings that resulted in the low excess pore water pressure values in Transducer 0 under Experiment RoR20B could be an unnoticed small leakage of water at the bottom of the

settling column. Openings at the bottom of the column included permeability test outlet tap as well where unnoticed water leakage could have taken place.

Table 4.4: Degree of consolidation for Experiments RoR20A and RoR20B

		Time to Reach $\bar{U}$ (hours)		
Experiment	Degree of Consolidation (%)	Lift 1	Lift 2	Lift3
RoR20A	50	0.25	0.5	0.25
	90	7	9	1.5
	100	10	16	38
RoR20B	50	1	3	3
	90	25	24	20
	100	98	45	89

Table 4.5: Degree of consolidation for Experiments RoR10A and RoR10B

		Time to reach $\frac{u}{u_o}$ (hours)			
Experiment	Degree of Consolidation (%)	Lift 1	Lift 2	Lift3	Lift3 Top-up
RoR10A	50	1	2	2	
	90	79	199	20	
	100	79	288	48	
RoR10B	50	0.07	0.42	0.25	0.25
	90	48	5	2	1
	100	48	12	11	18

Table 4.6 shows the remaining excess pore water pressure ratio data for Experiments FDA and FDB. Experiment FDA had dissipated 20% excess pore water pressures within 5 minutes and

70% excess pore water pressures in the first half hour. In contrast Experiment FDB took over an hour to dissipate 50% of the excess pore water pressures while the balance of the remaining excess pore water pressures were fully dissipated after two and a half days.

In general for both coarse and fine tailings under the full depth deposition experiments, the first 50% of the excess pore pressures dissipated very quickly while the remaining 50% of the excess pore pressures took a much longer time period to dissipate. It was observed that the remaining 50% of the excess pore pressures took much longer time to dissipate than the observed dissipation times for the first 50% of excess pore water pressures even though the drainage path lengths reduced.

Experiments RoR20A and RoR20B results (Table 4.7) showed that the underflow tailings had dissipated 67% excess pore water pressures compared to 50% for the catwalk fines tailings within the first five minutes.

An observation was also made that after 5hrs of dissipation the coarse tailings had reached 93% dissipation compared to 72% dissipation for the fine catwalk tailings. In each of the depositions lifts under the experiments the dissipations of the first 50% of the excess pore pressures took place within the first half hour while the remaining 50% of the pore pressures dissipated in 5hrs and 20hrs respectively for the coarse and fine tailings. For both experiments the latter lifts excess pore pressure dissipation rates were again slower than the dissipation rates for the earlier pore pressure dissipations. Table 4.7 shows remaining percentage excess pore water pressure summary data derived from the isochrones for Experiments RoR20A and RoR20B for lifts 1 to 3.

Table 4.6: Experiments FDA and FDB Percentage Remaining Excess Pore water Pressure Ratios, $\left(\frac{u}{u_o}\right)$

	Percentage Remaining Excess Pore water Pressure Ratio, $\left(\frac{u}{u_o}\right)$ (%)	
Time (minutes)	FDA	FDB
5	80	94
10	60	
15	45	
30	30	70
60		55
85	18	
180	15	37
300		31
600	8	23
900		17
1200		12
1800		8
3600		<1

Table 4.7: Experiments RoR20A and RoR20B percentage (%) remaining excess pore pressure ratio.

	Percentage Remaining Excess Pore Pressure Ratio, $\left(\frac{u}{u_o}\right)$ (%)					
Time (min)	RoR20A			RoR20B		
	Lift1	Lift2	Lift3	Lift1	Lift2	Lift3
1	27	33			50	
5	27	40	40		40	40
15	27	25	30			
30	23	36	16	59	58	40
60	17	26	8			
120	14	12				
180				32	37	32
300	8	6		27	32	26
900		0		14	14	12
1200				7	10	8
1800					5	

Table 4.8 shows remaining percentage excess pore water pressures based on isochrones for Experiments RoR10A and RoR10B for the three deposition lifts under each experiment including the top-up layer of lift 3 under Experiment RoR10B.

Under these experiments, 80% dissipation had occurred within the first 25 minutes for all the deposition lifts with full dissipation of excess pore water pressures achieved within a 15hrs time period. In these coarse tailings experiments as well, the latter stages dissipation rates of excess pore water pressures were also at a much slower rate than the earlier stages excess pore water pressure dissipations, which followed the same trend observed in the previous experiments.

Table 4.8: Experiments RoR10A and RoR10B percentage (%) remaining excess pore pressure ratio.

	Percentage Remaining Excess Pore Pressure Ratio, $\left(\frac{u}{u_o}\right)$ (%)							
Time(min)	RoR10A				RoR10B			
	Lift1	Lift2	Lift3		Lift1	Lift2	Lift3	Lift3 top -up
1	18		40		20			
5						50	35	
10								14
25					12	25	21	13
60		54					13	3
90						9	7	
120			20					0
180	8	24				5	3	
240			11		4			
600		17						
900					0	0	0	
1872		5						
21600			0					

4.5 Permeability Test Results

4.5.1 Introduction

In this section the results of the permeability tests carried out on the consolidated soil columns are reported. First the results of the variation of total head over time during the constant head permeability test are summarised. The coefficient of permeability of the tailings throughout the settling column height as inferred from flow rates and hydraulic heads measured during the permeability testing is then presented.

4.5.2 Permeability Tests Total Head Trends

The results of the total head trends over time at the instrumentation locations during permeability testing are pertinent because they present the actual prevailing total heads during the *constant* head test. Figures 4.38 and 4.39 show the results for Experiments FDA and FDB. The results of the rate of rise experiments are listed in Appendix G together with total heads for a falling head permeability test carried out at the end of Experiment FDA to show the difference of total head behaviour under the variable head test.

4.5.3 Coefficient of Permeability Test Results

Figures 4.40, 4.41 and 4.42 show the results of the change in saturated vertical coefficient of permeability, k_v, with depth for Experiments FDB and RoR20B. The figures comprise permeability values derived from standpipe data and transducer data respectively for Experiment FDB and a comparison of the pairs of permeability values for Experiment RoR20B from the corresponding standpipes and transducers. The vertical permeability trends for Experiments FDA, RoR20B, RoR20A and RoR10B are given in appendix G. Table 4.9 summarise vertical permeability values along the height of the settling column at height ranges defined by the elevation of the pore pressure instrumentation for the respective experiments. The permeability values attained after steady state discharge time was reached are reported in the table.

4.6 Particle Size Grading and Specific Gravity of Solids Test Results

4.6.1 Introduction

In order to address the secondary objective of the research which was to investigate particle size segregation, particle size analysis, specific gravity of solids and mineralogical compositions tests were carried out. The tests were carried out on samples recovered from Experiments FDB, RoR20B, and RoR10B as well as for the 10m/yr rate of rise test without a permeability test (see Figures 3.28 to 3.32). The section presents particle size grading, specific gravity of the solids and mineralogical composition results. It is to be noted that the distances shown in mm with the results refer to distances in mm measured from the bottom of the settling column.

4.6.2 Particle Size Grading

Figures 4.43 to 4.45 give particle size grading charts for the coarse and fine tailings samples respectively. Figure 4.43 shows data for Experiment RoR10B whereby only two deposited layers of the three deposited layers are shown because the third layer results duplicated the results from the first two slurry depositions layers. Figure 4.44 shows the gradation curve for Experiment RoR20B. The catwalk fines which was the source material together with tailings gradation envelope are also plotted to enable a comparison of the segregated particle sizes in relation to the source material as well as to the gold tailings gradation envelope from published literature. The gradations shown were sampled at 20mm to 60mm intervals. Figures 4.45 shows gradation curves for Experiment FDB. The figure shows plots for gradation samples taken at 30mm intervals along the column height.

Figure 4.46 shows the gradation curves for FDB experiment obtained from the Mastersizer apparatus shown side by side with the hydrometer analysis grading based on samples obtained at the same elevations. The Mastersizer grading curves are labelled while the sieve/hydrometer grading curves are not labelled but show the same elevations as the corresponding Mastersizer grading curves. Appendix H shows particle size grading for Experiments FDA, FDB, RoR20B and RoR10B. The appendix also summarises gradation parameters (D_{10} to D_{90}, C_u, C_c and GM) for the samples tested under the study. Gradation parameters for Experiment FDB are discussed in the next chapter.

4.6.3 Mineralogical Composition and Specific Gravity of Solids

The results of specific gravity and mineralogy are summarised in Appendix I. The XRF elemental analysis and the XRD mineral composition analysis results are in good agreement. This aspect is discussed further in Chapter 5.

Appendix I also lists specific gravity values obtained from the density bottle method (BS 1377: Part 2:1990:8.3), Accupyc 1340II Gas Pycnometer method and specific gravity values estimated from XRD data using the respective minerals' specific gravity values obtained from literature.

4.7 Scanning Electron Microscope (SEM) Micrographs

Gold tailings fabric was characterised in its dry state which is amenable to the use of scanning electron microscope technology which worked with dry materials that are conductive. The resulting SEM micrographs are summarised in Appendix J which include micrographs for Experiments FDB, RoR20B, RoR10B and rate of rise 10m/yr test without permeability. During permeability testing the settling column underwent an increase in effective stress which was believed to be reflected in the resulting SEM micrographs.

The results of specimen viewed under the SEM microscope for purposes of comparison included micrographs of the tailings samples used in the three experiments *viz* FDB, RoR20B and RoR10B, micrographs of sieved and dispersant treated experiment sample specimen and micrographs of rate of rise 10m/yr recovered samples that was not subjected to a permeability test. Figures 4.4 and 4.5 showed the experimental samples micrographs. Figures 4.47 to 4.49 depict SEM micrographs for Experiment FDB. Figure 4.47 and 4.48 show micrographs obtained using the carbon tape preparation method (CT) while Figure 4.49 shows those obtained from the carbon glue method (CG). Figure 4.50 represents micrographs obtained from the 10m/yr rate of rise test carried out without permeability test. The sets of micrographs were selected to show both coarse and fine grained tailings particles. Figure 4.49 also shows SEM micrographs of the specimen viewed on the plane perpendicular to the direction of water flow (horizontal prints) on the left hand side of the figure (Left) while the vertical prints or the micrographs obtained from viewing the specimen along the plane that was parallel to the direction of water flow is shown on the right hand side of the figure (right). Appendix J shows the remaining SEM micrographs for the Experiment FDB as well as those for Experiments RoR20B and RoR10B.

Table 4.9: Measured vertical coefficient of permeability values.

Description	Height Range (mm)	Experiment Permeability Values (cm/sec)				
		FDA (Underflow)	FDB (Catwalk Fines)	RoR20A (Underflow)	RoR20B (Catwalk Fines)	RoR10B (Underflow)
k_{0-1}	0-6.15		$9.72x10^{-6}$		$7.63x10^{-6}$	$1.53x10^{-3}$
k_{1-2}	6.15-185	$1.53x10^{-3}$	$6.11x10^{-4}$	$2.44x10^{-4}$	$1.57x10^{-5}$	$6.93x10^{-4}$
k_{2-3}	185-312	$6.93x10^{-4}$	$8.91x10^{-4}$	$2.18x10^{-4}$	$6.19x10^{-5}$	$1.25x10^{-4}$
k_{3-4}	312-439	$1.25x10^{-4}$	$1.10x10^{-4}$	$8.15x10^{-5}$	$9.70x10^{-5}$	$1.89x10^{-5}$
k_{4-5}	439-564	$1.89x10^{-5}$	$2.78x10^{-5}$	$1.25x10^{-4}$	$1.90x10^{-5}$	$5.12x10^{-5}$
k_{5-6}	564-689		$1.46x10^{-5}$	$1.40x10^{-4}$	$7.81x10^{-5}$	$9.37x10^{-5}$
k_{6-7}	689-818		$2.10x10^{-5}$	$7.28x10^{-5}$	$2.59x10^{-5}$	
k_{top}	564 upwards	$6.66x10^{-6}$	$2.52x10^{-4}$	$6.85x10^{-7}$	$2.85x10^{-6}$	$2.52x10^{-4}$
$(k_v)_{Average}$		$5.25x10^{-5}$	$2.44x10^{-5}$	$8.15x10^{-5}$	$2.04x10^{-5}$	$8.22x10^{-5}$

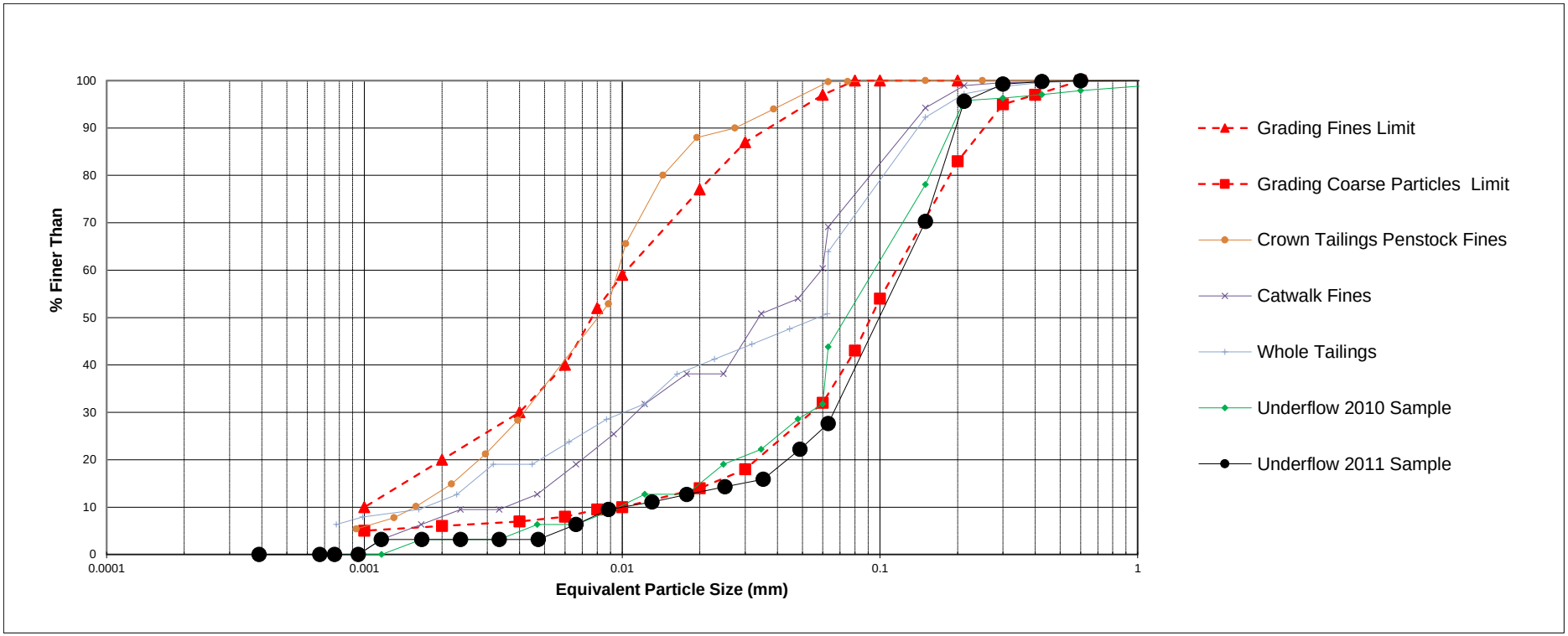

Figure 4.1: Typical gradations of tailings sample relative to grading envelopes

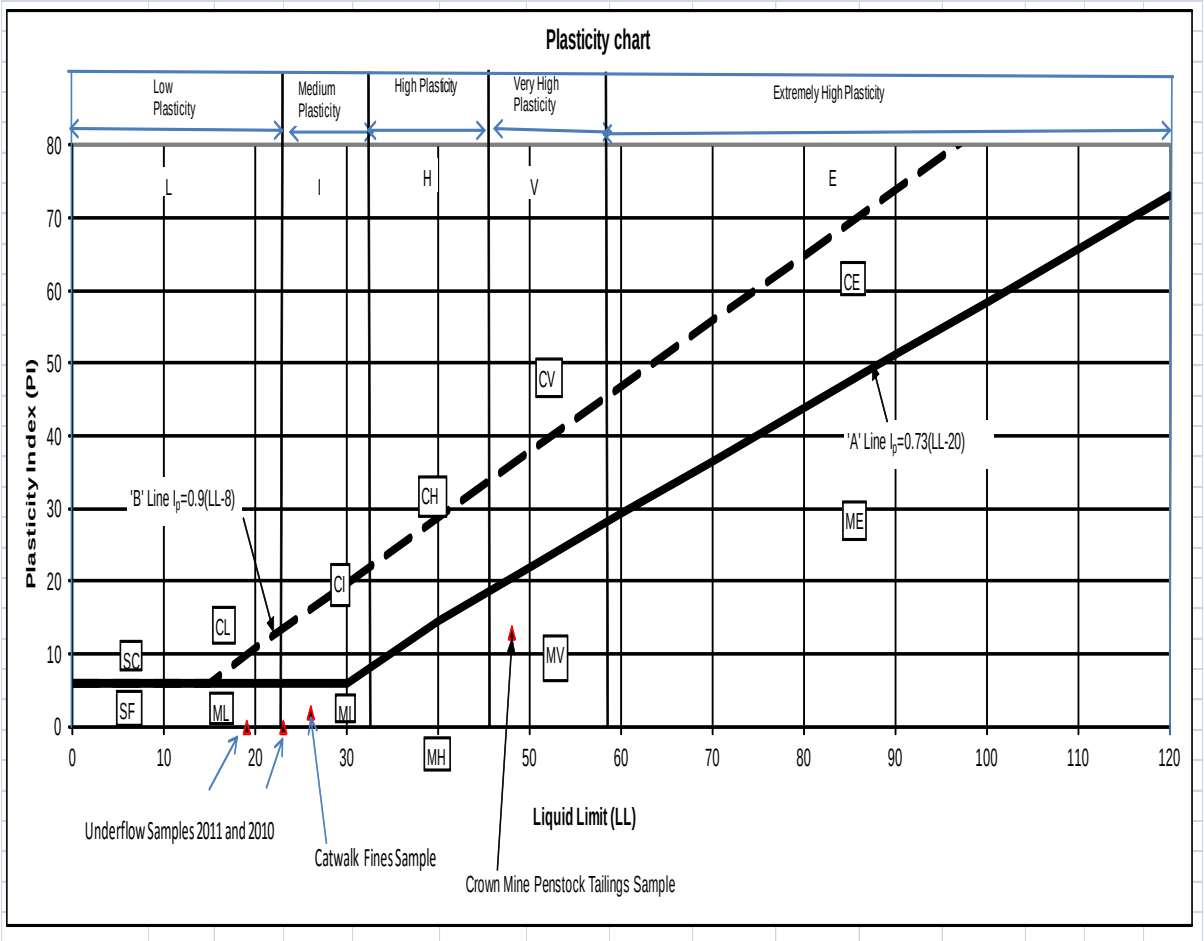

Figure 4.2: Unified classification of tailings samples

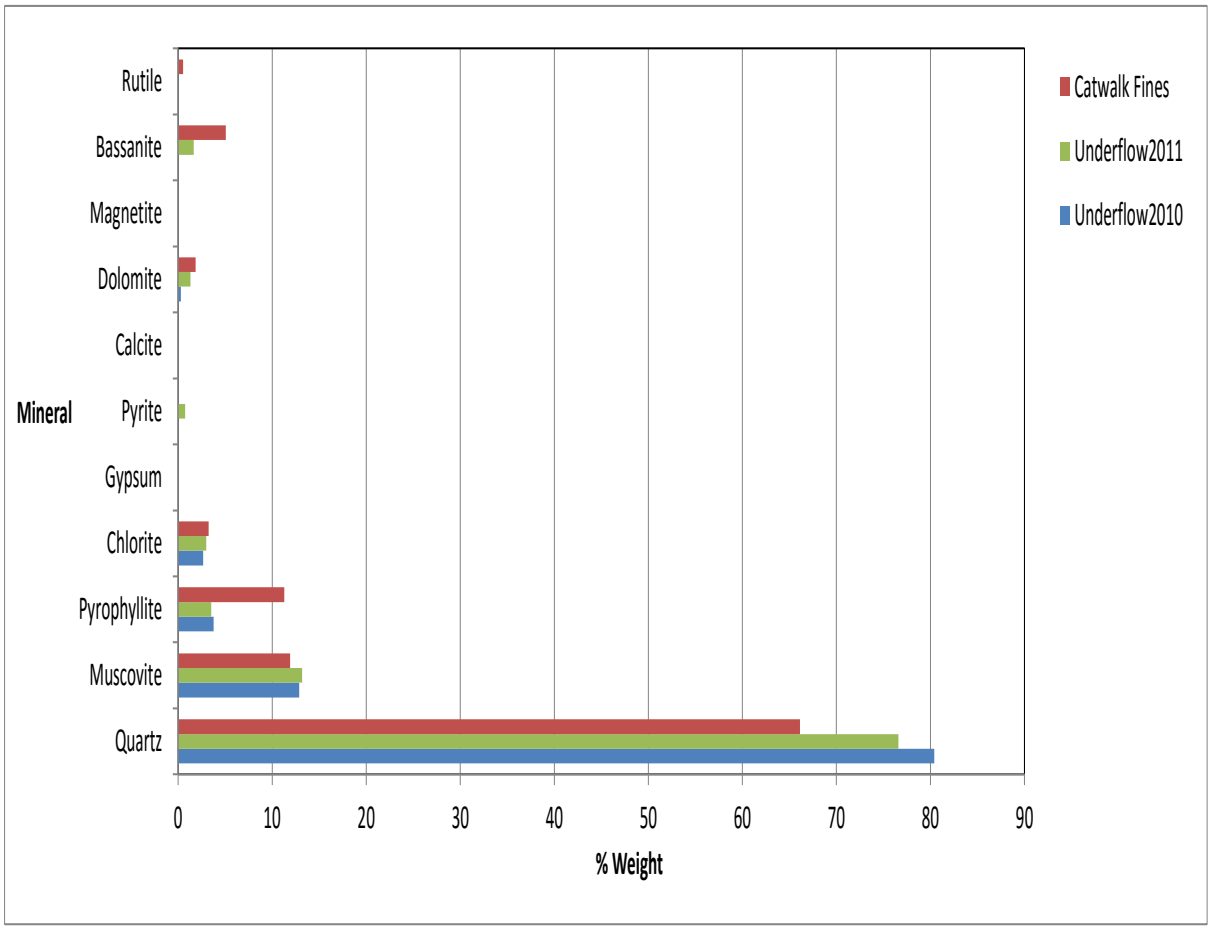

Figure 4.3: Mineralogical make-up of gold tailings samples

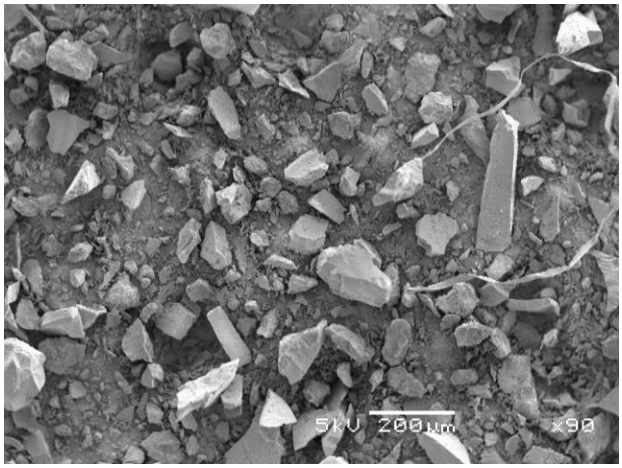

Underflow Coarse Tailings Sample 2010

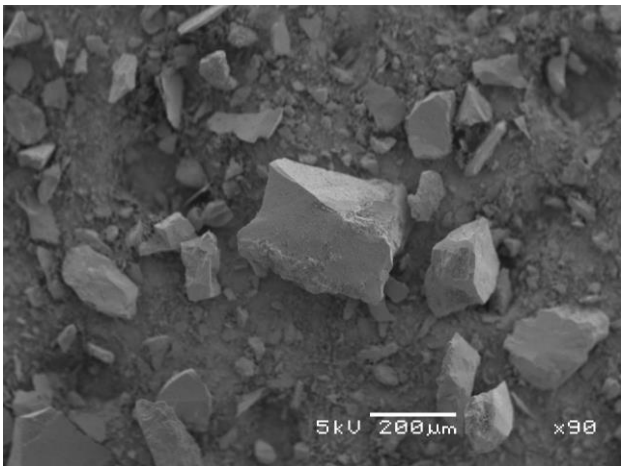

Underflow Coarse Tailings Sample 2011

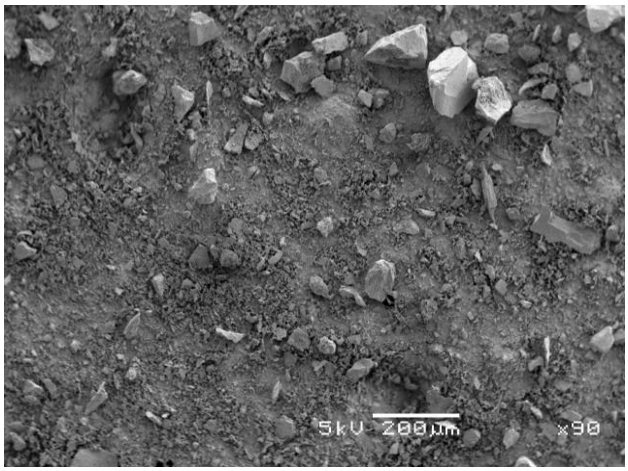

Catwalk Fine Tailings Sample 2011

Figure 4.4: SEM micrographs of experiment samples

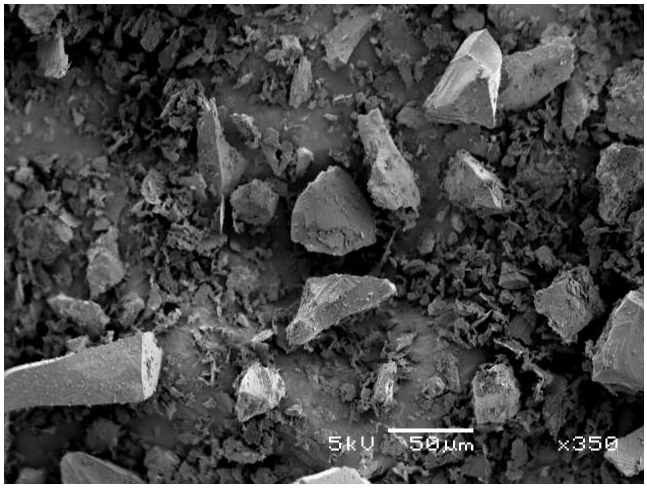

minus 63µm

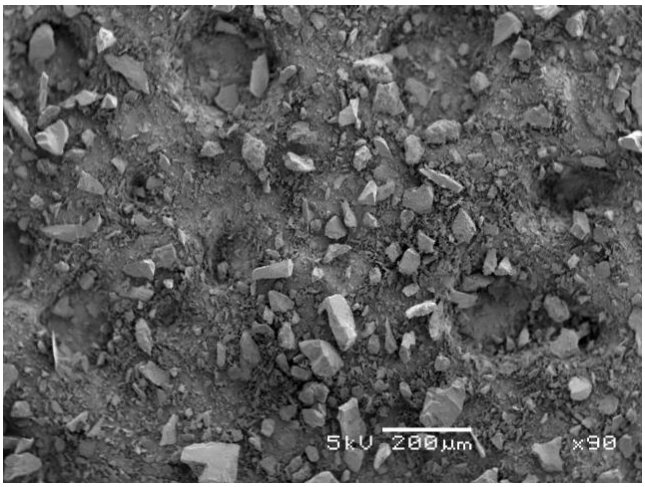

minus 63µm

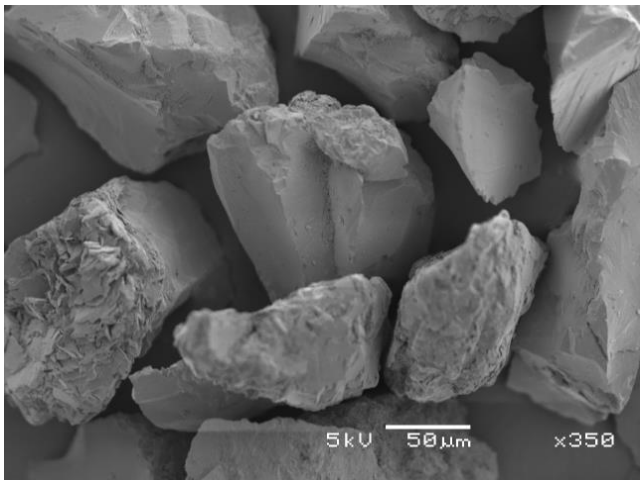

minus150µm+63µm

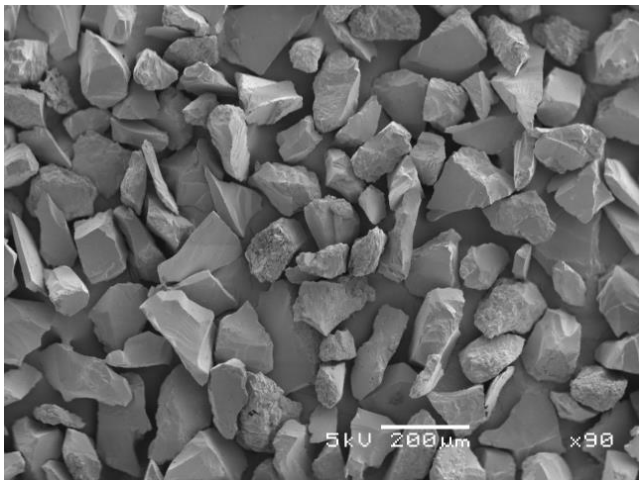

minus150µm+63µm

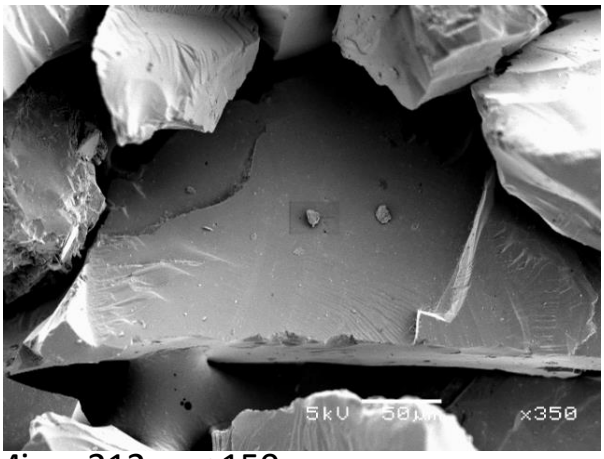

Minus212µm+150µm

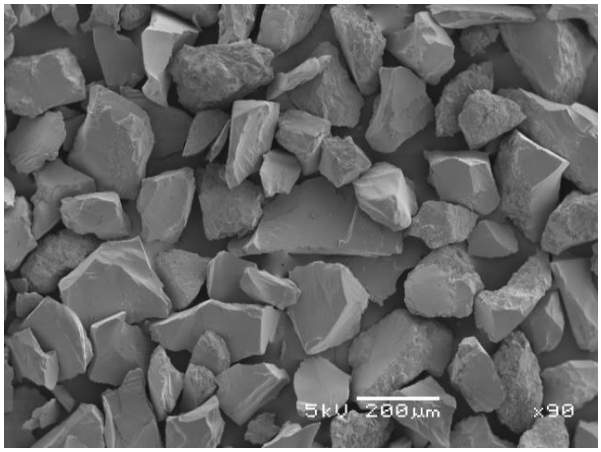

Minus212µm+150µm

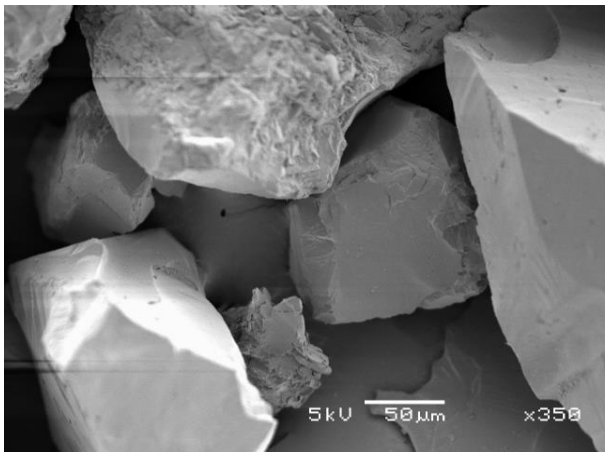

Minus300µm+212µm

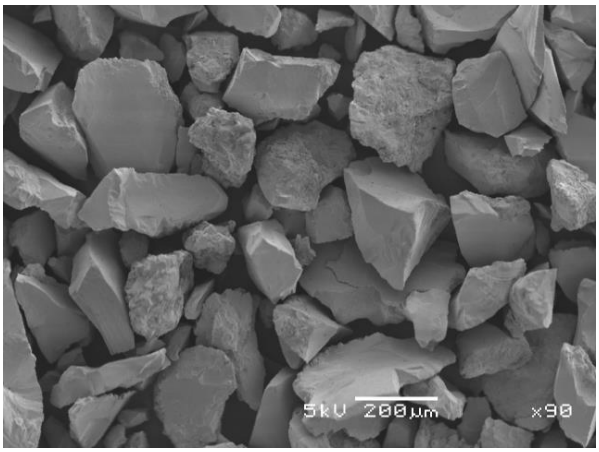

Minus300µm+212µm

Figure 4.5a: SEM micrographs of sieved and dispersant treated tailings samples

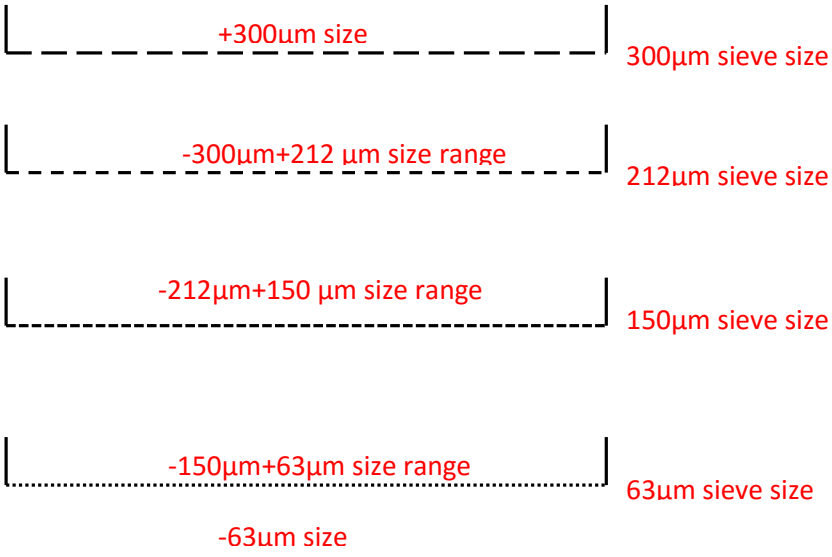

Figure 4.5b: Sieve size and size ranges of dispersant treated tailings samples

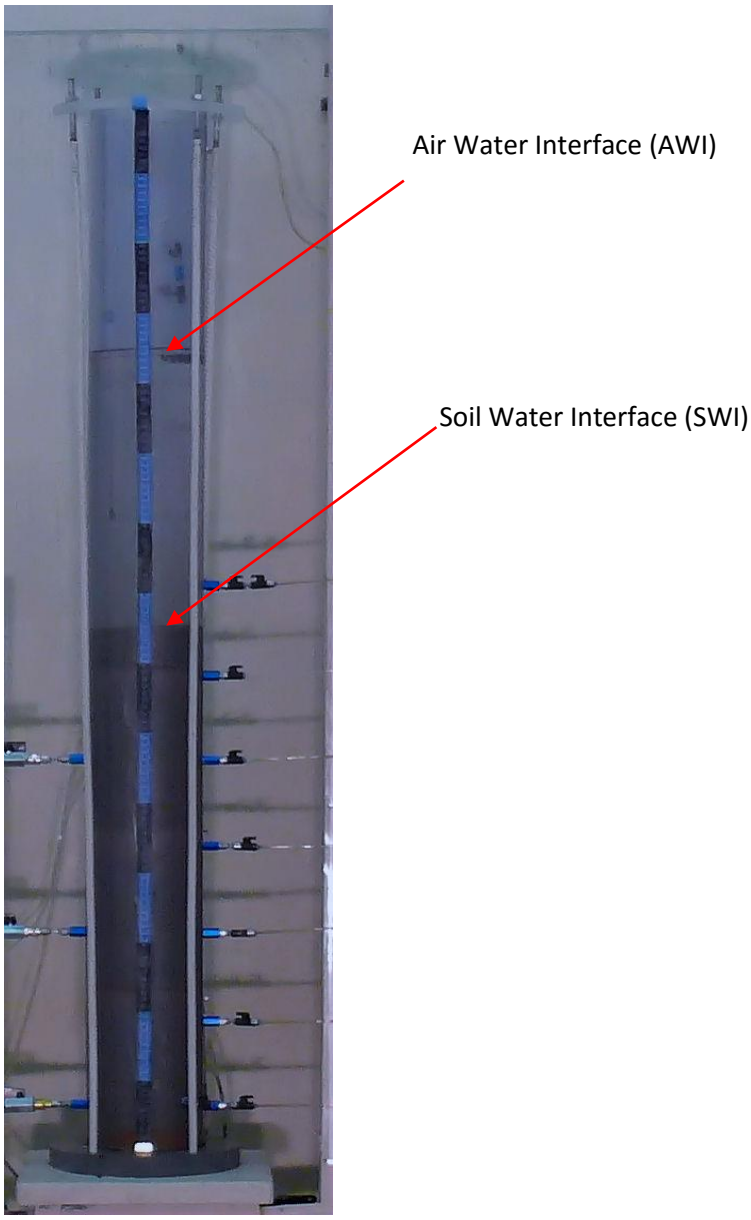

Figure 4.6: Experiment RoR20B Lift 3 deposition after 45 minutes showing AWI and SWI

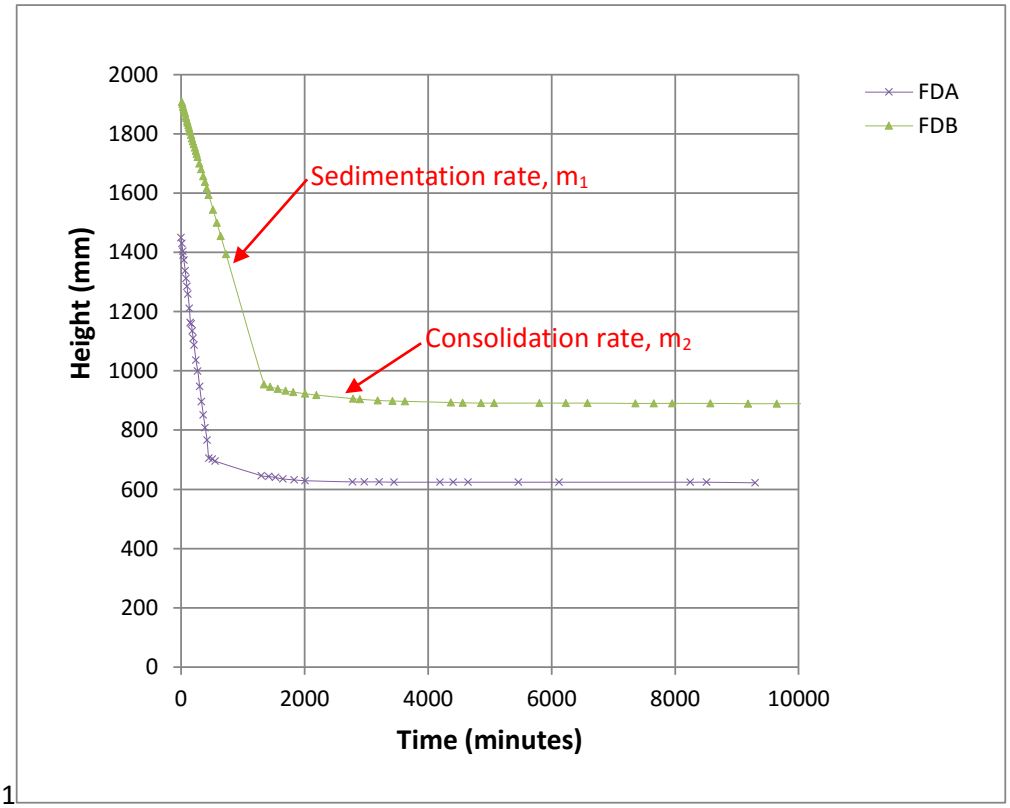

1

Figure 4.7a: Settlement (SWI) time plots Experiments FDA and FDB

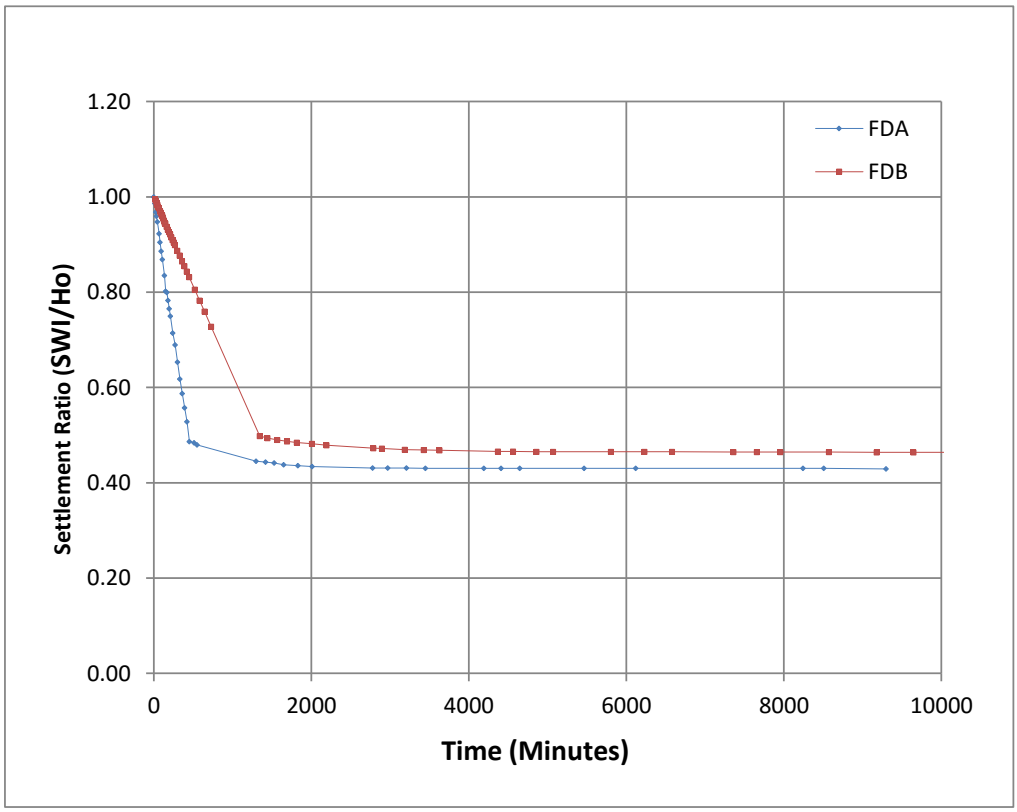

Figure 4.7b: Normalised settlement (SWI) time plots Experiments FDA and FDB

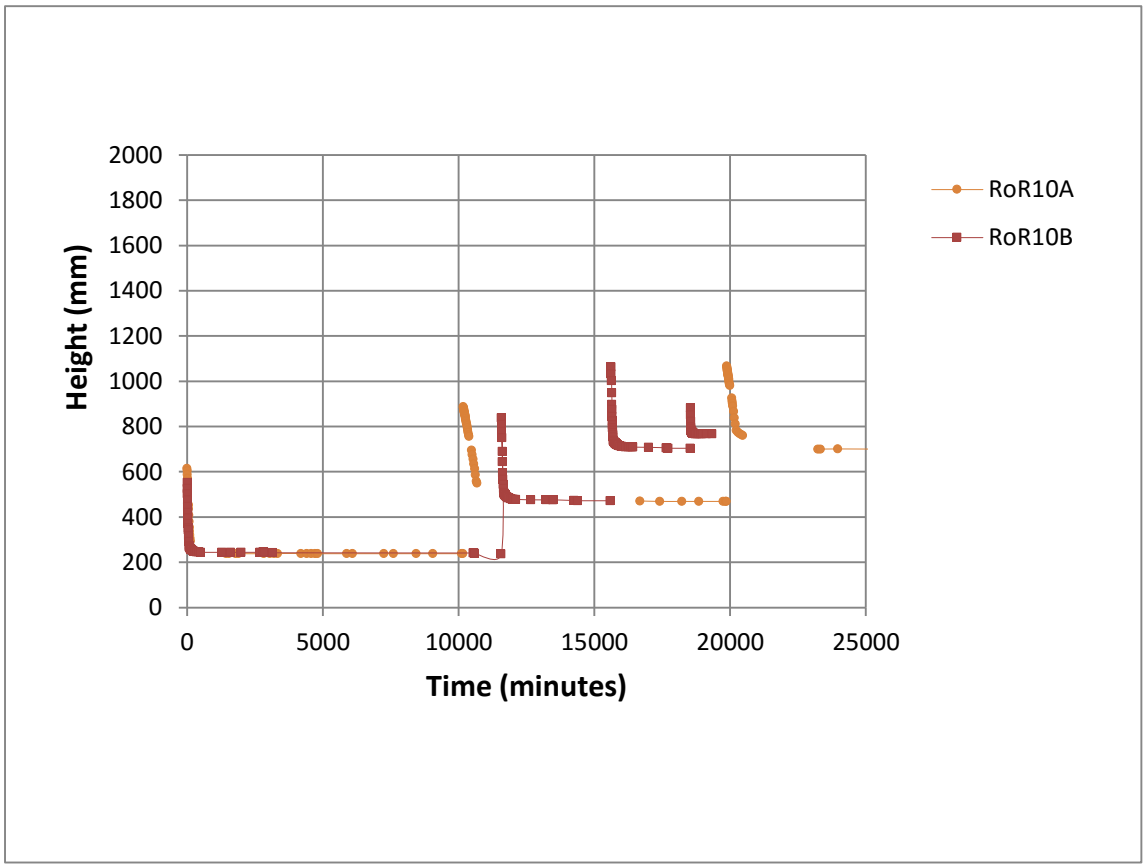

Figure 4.8: Settlement (SWI) time plots Experiments RoR10A and RoR10B

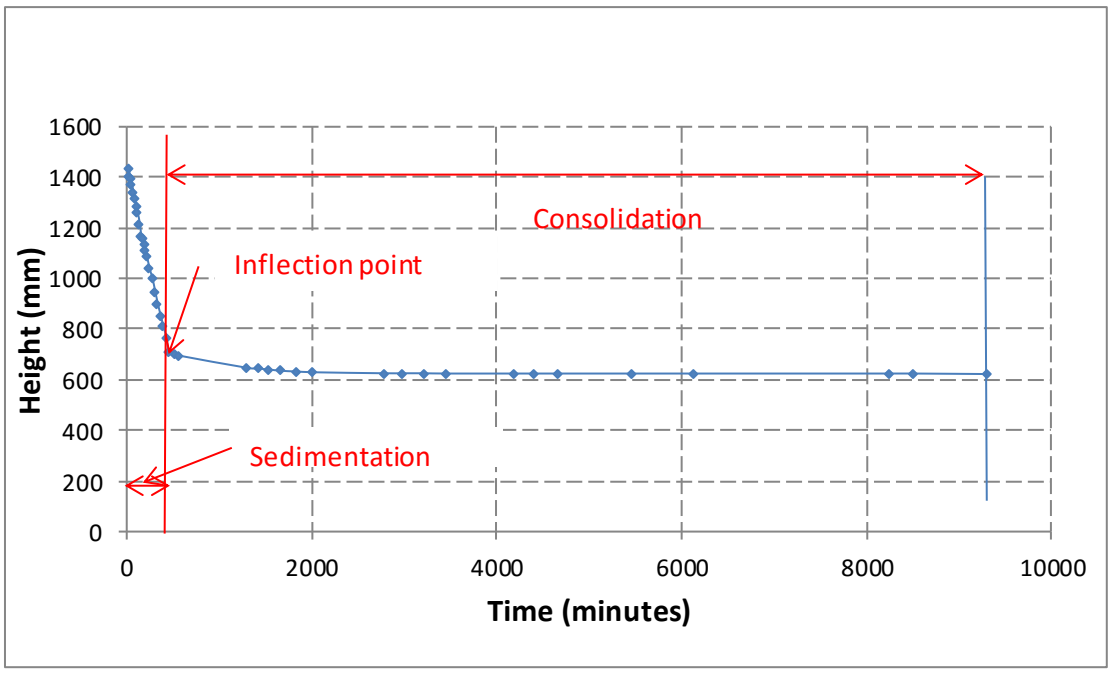

Figure 4.9a: Soil interface height (SWI) vs time plots Experiment FDA

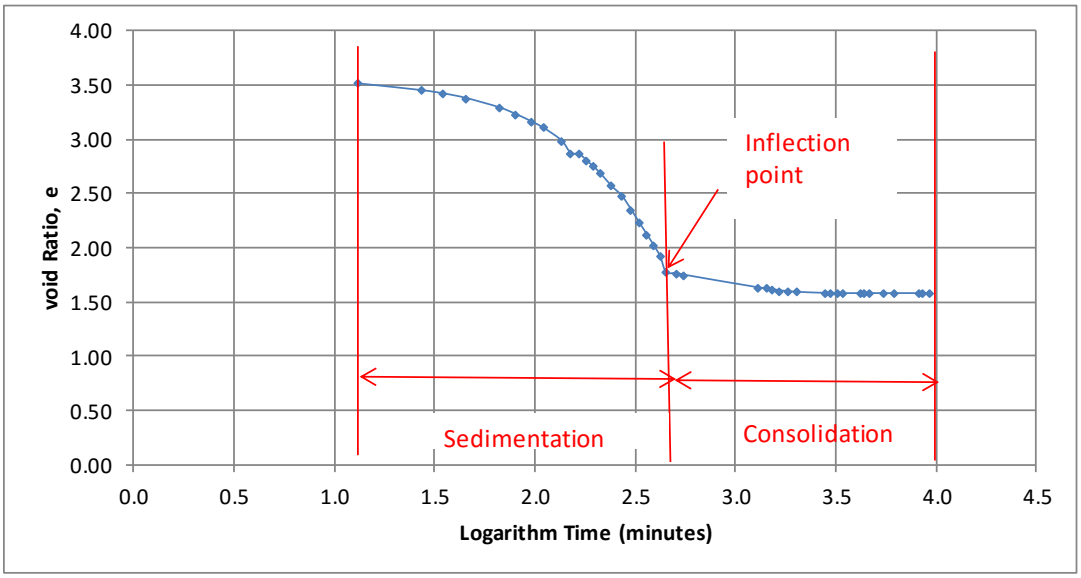

Figure 4.9b: Void Ratio time plots Experiment FDA

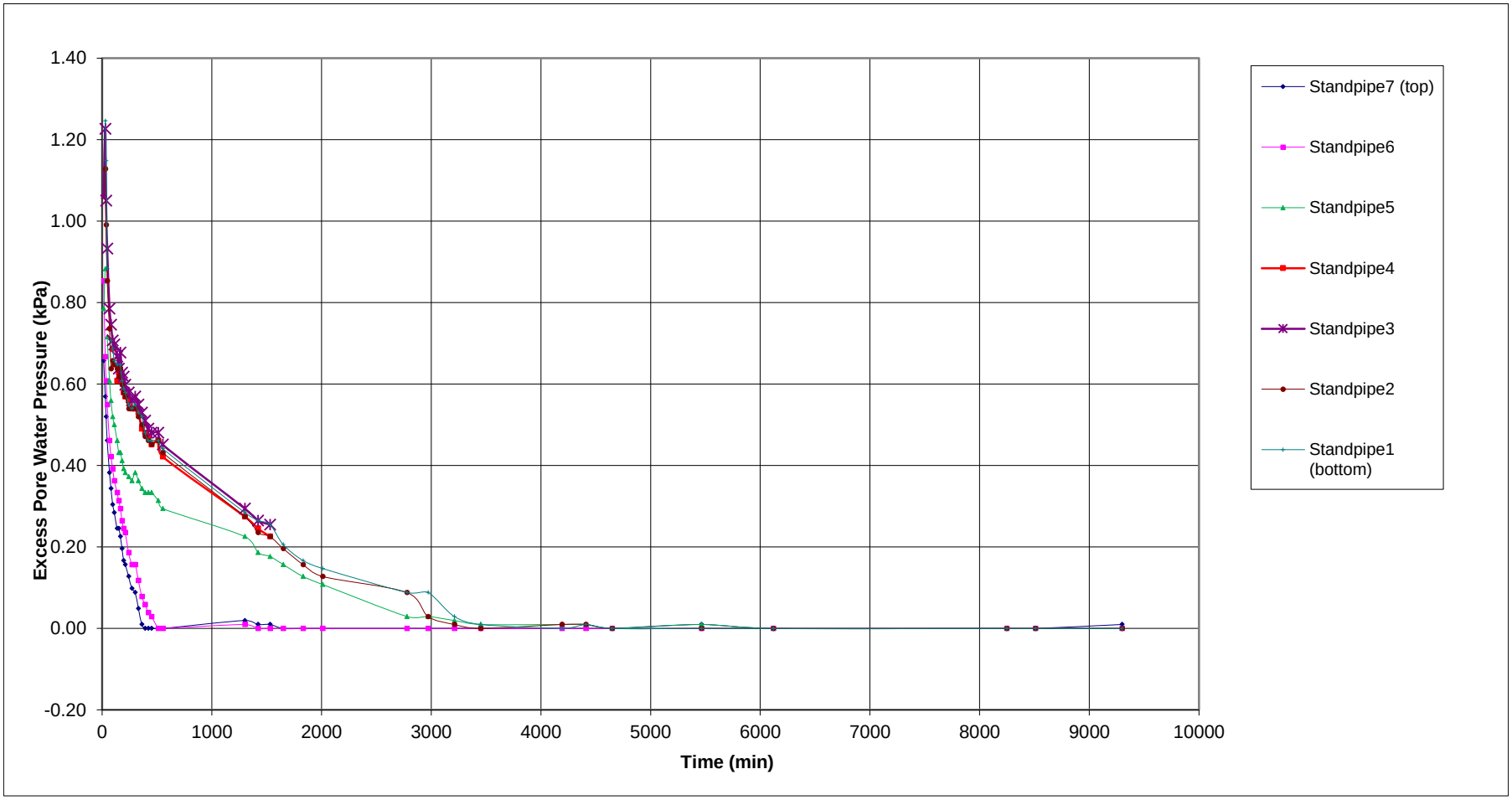

Figure 4.10: Excess pore water pressure Experiment FDA standpipe data

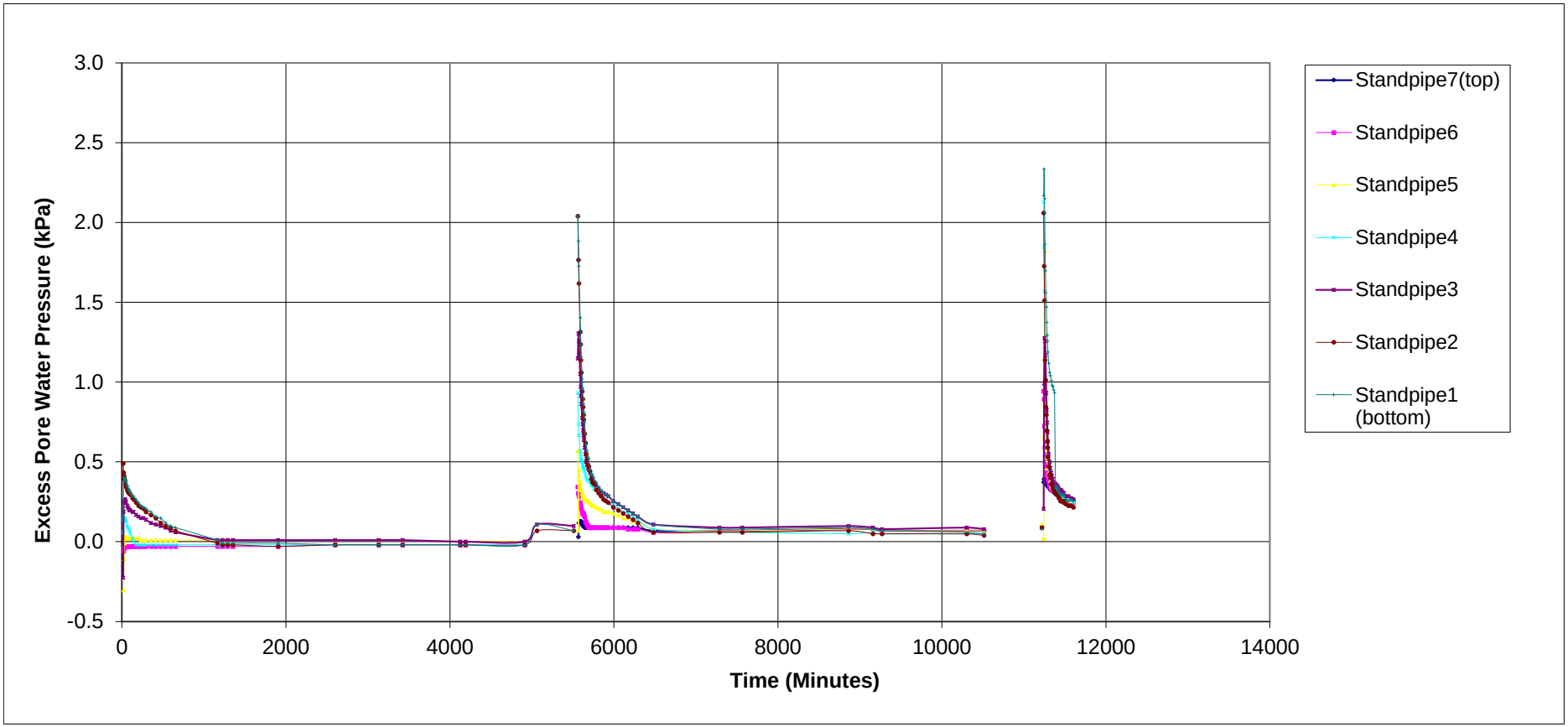

Figure 4.11: Excess pore water pressure Experiment RoR20A standpipe data

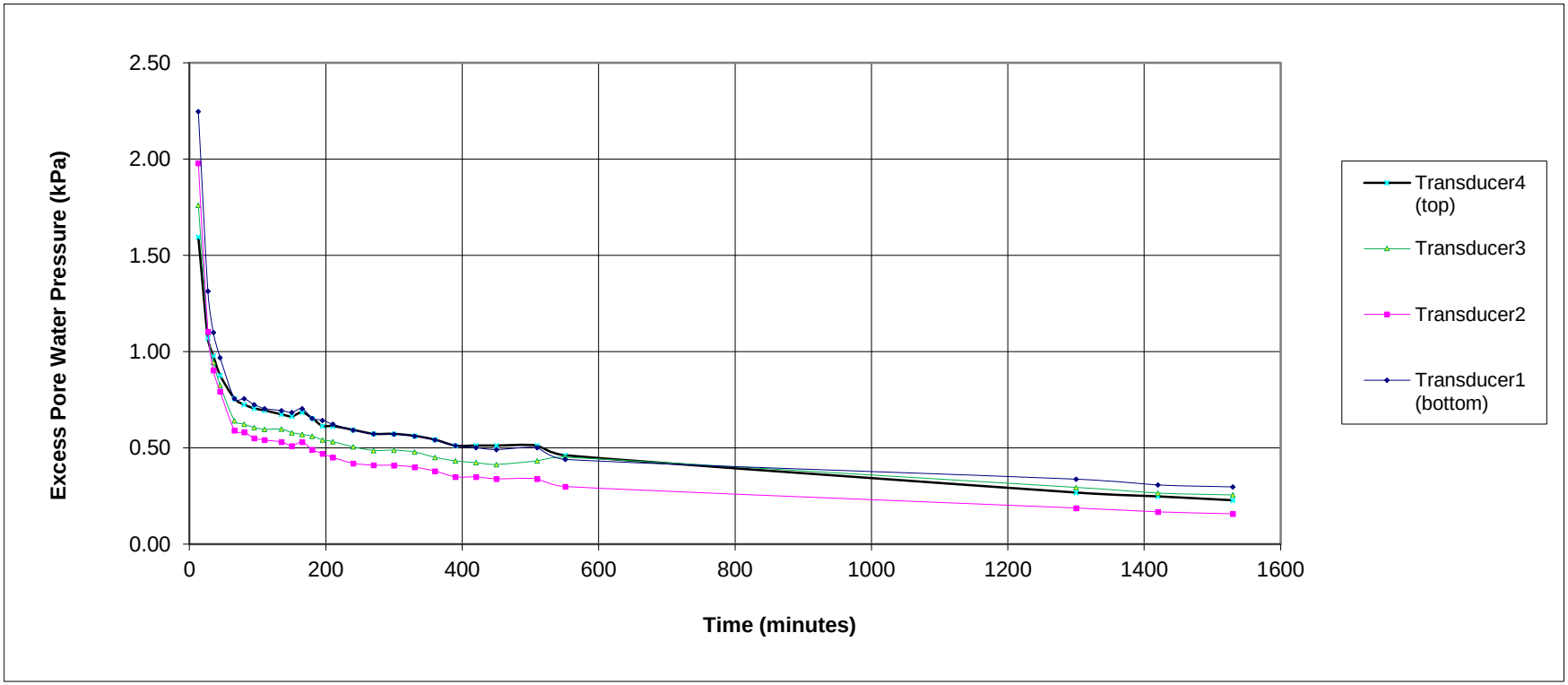

Figure 4.12: Excess pore water pressure Experiment FDA transducer data

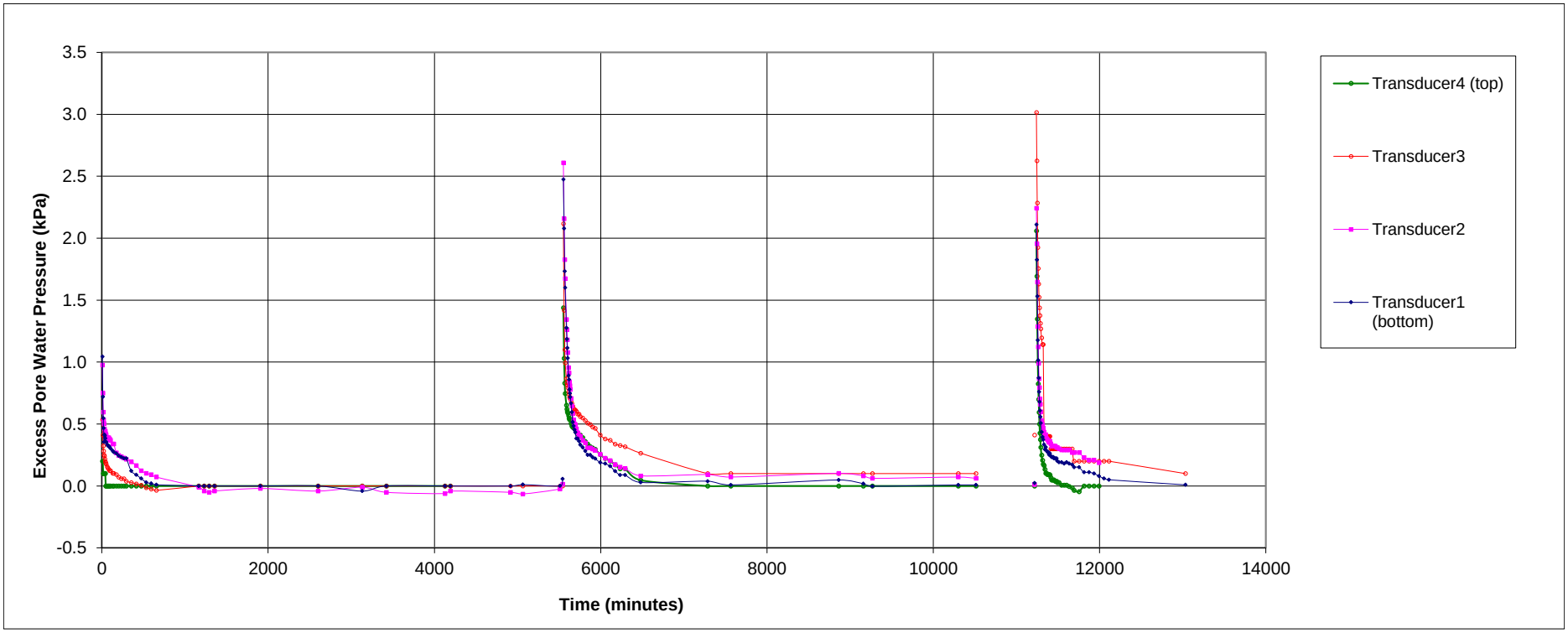

Figure 4.13: Excess pore water pressure Experiment RoR20A transducer data

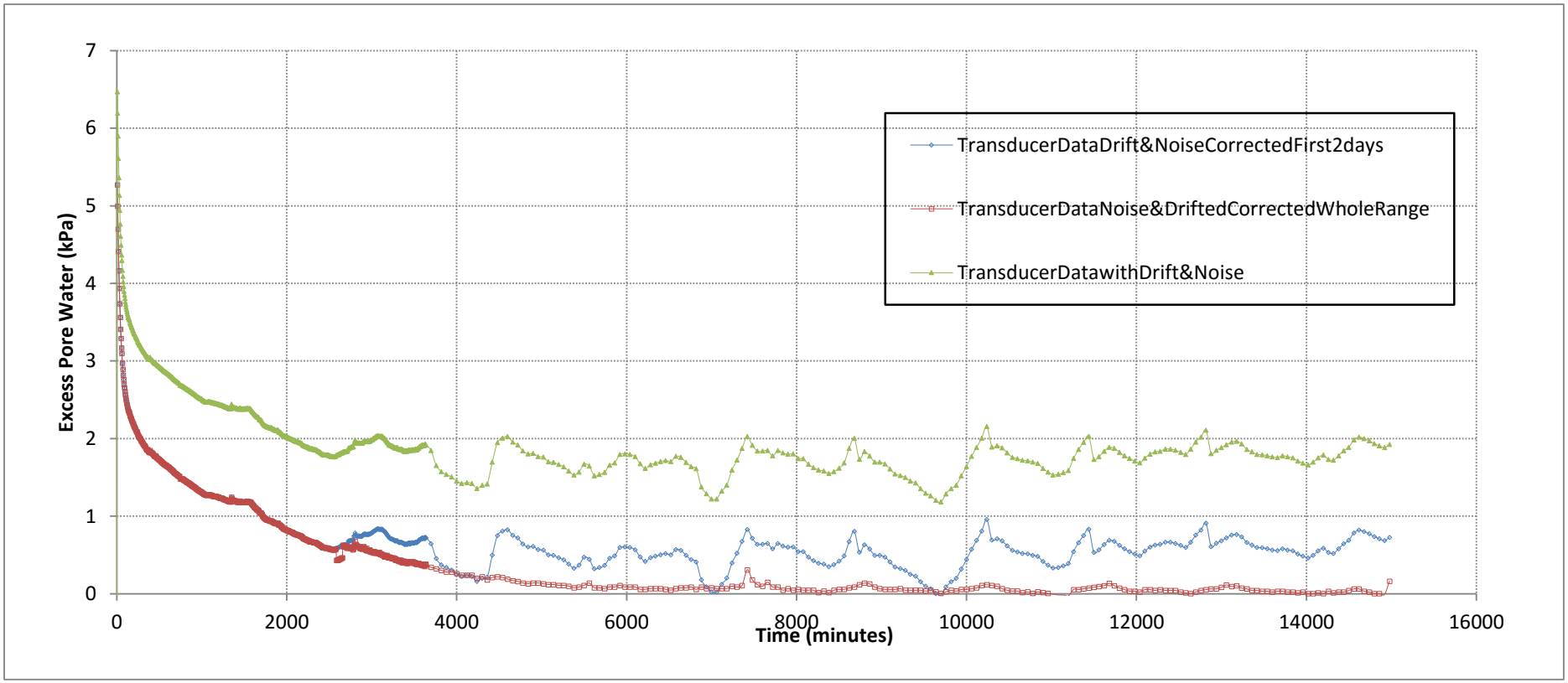

Figure 4.14: Experiment FDB transducer 0 excess pore water pressure data showing corrections for fluctuations in data

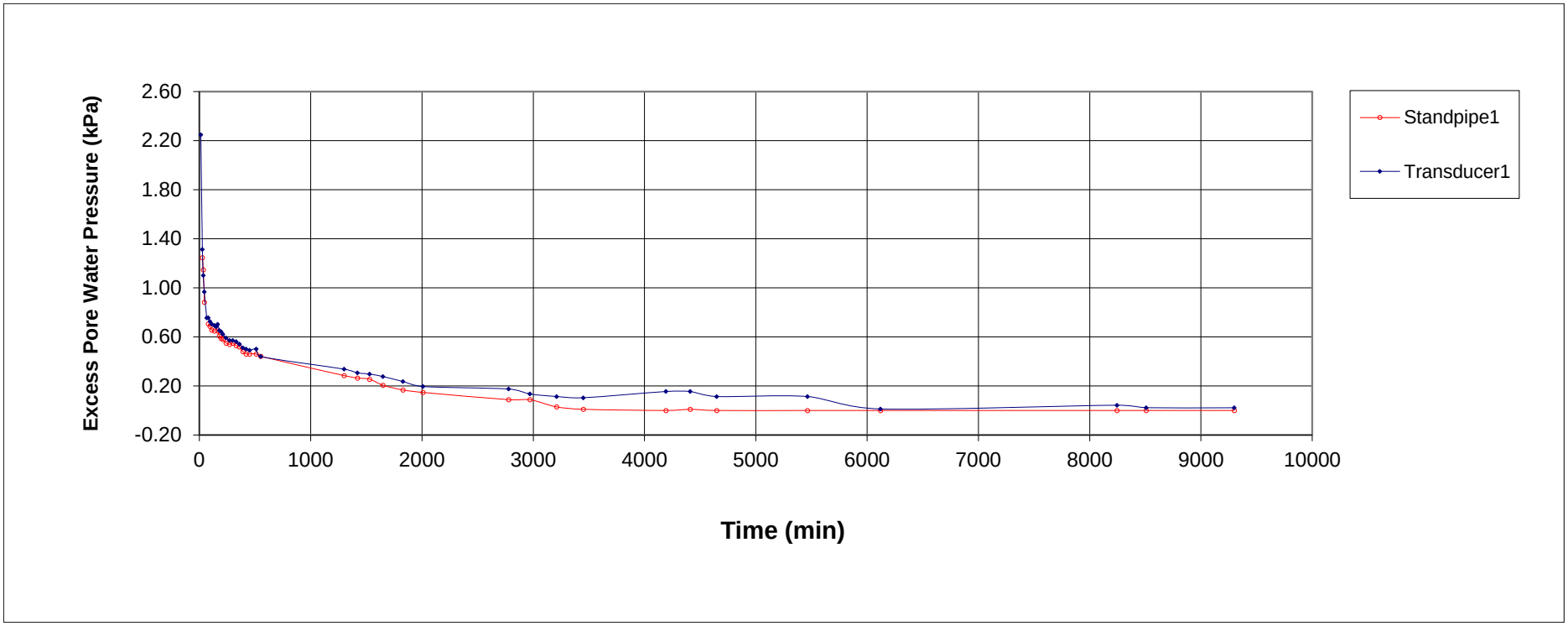

Figure 4.15a: Standpipe 1 and Transducer 1 pair excess pore pressure comparisons Experiment FDA

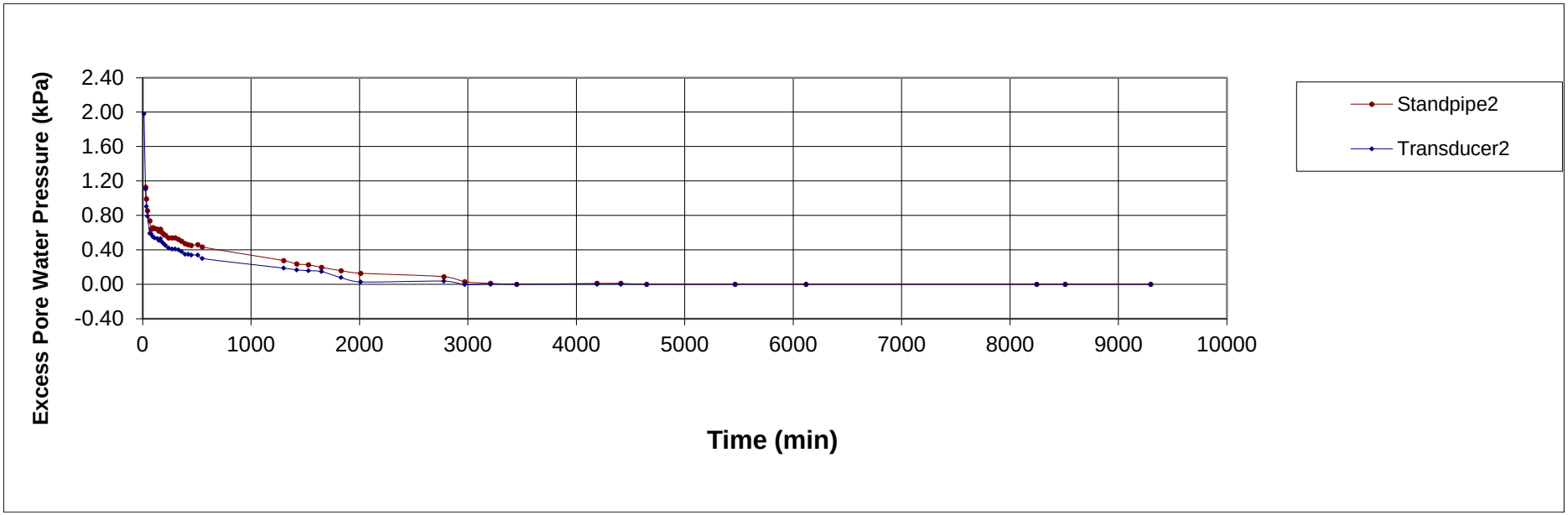

Figure 4.15b: Standpipe 2 and Transducer 2 pair excess pore pressure comparisons Experiment FDA

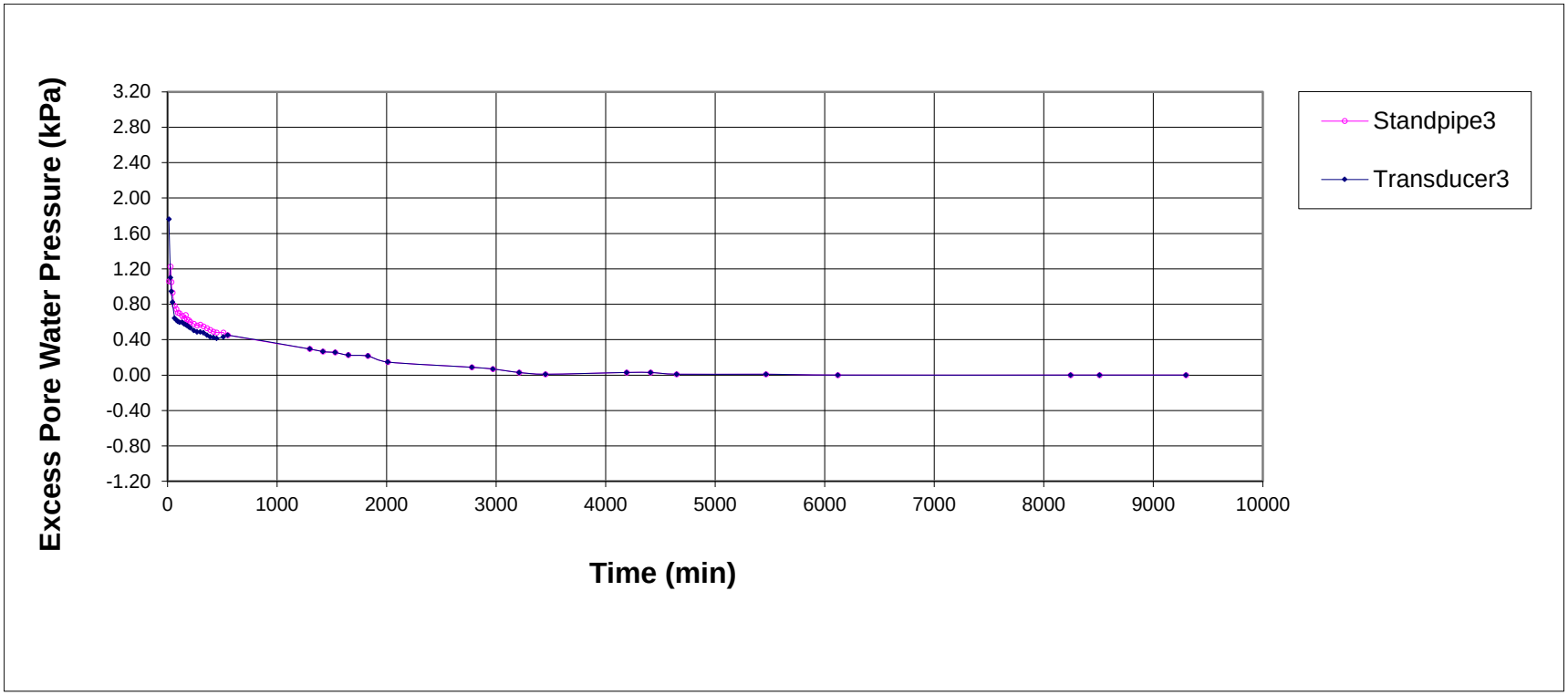

Figure 4.15c: Standpipe 3 and Transducer 3 pair excess pore pressure comparisons Experiment FDA

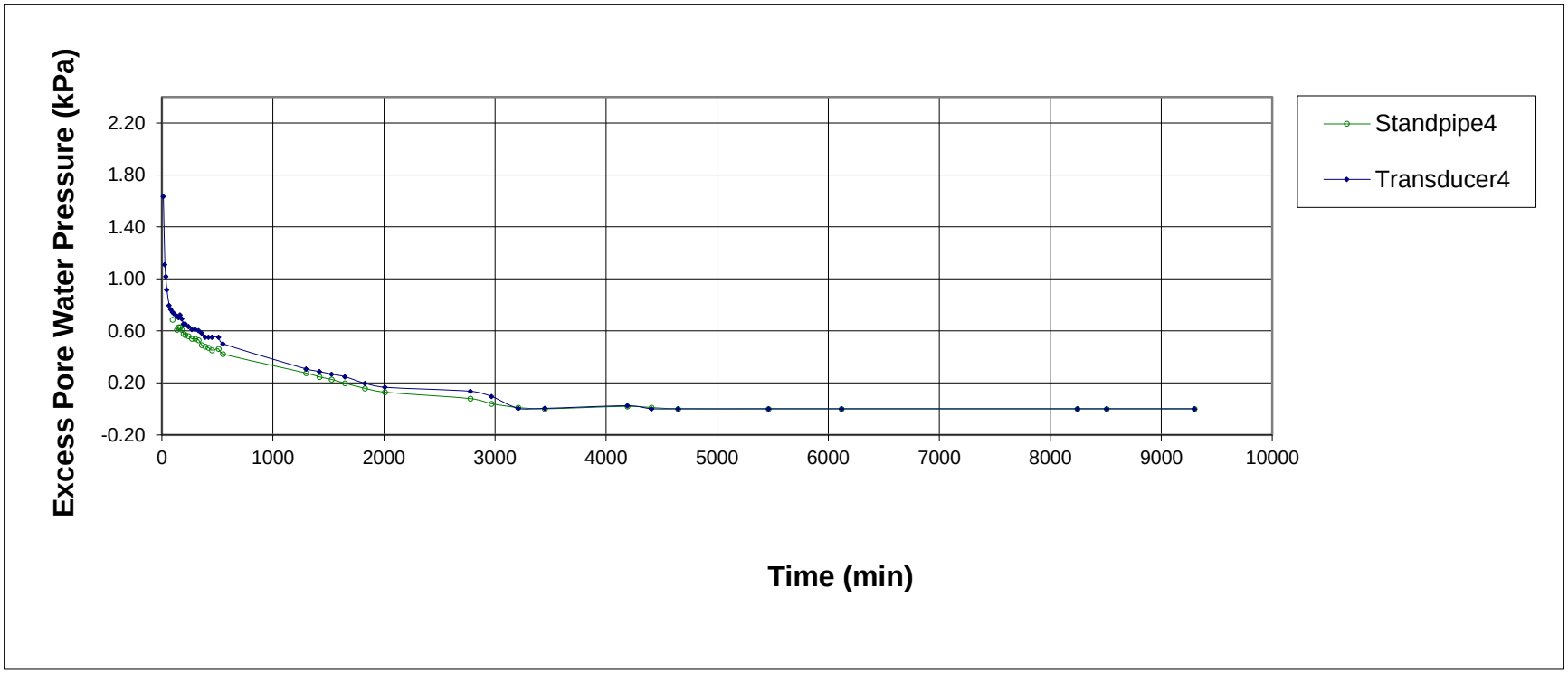

Figure 4.15d: Standpipe 4 and Transducer 4 pair excess pore pressure comparisons Experiment FDA

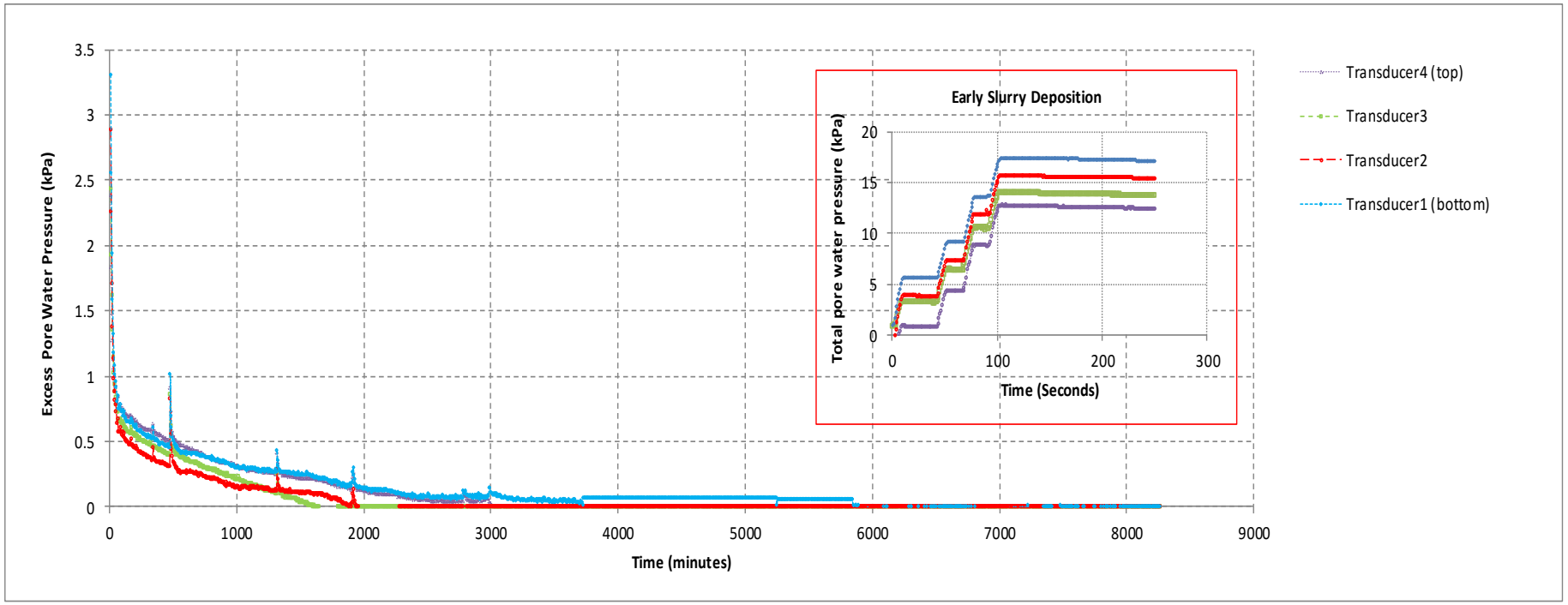

Figure 4.16a: Graphtec logger data Experiment FDA

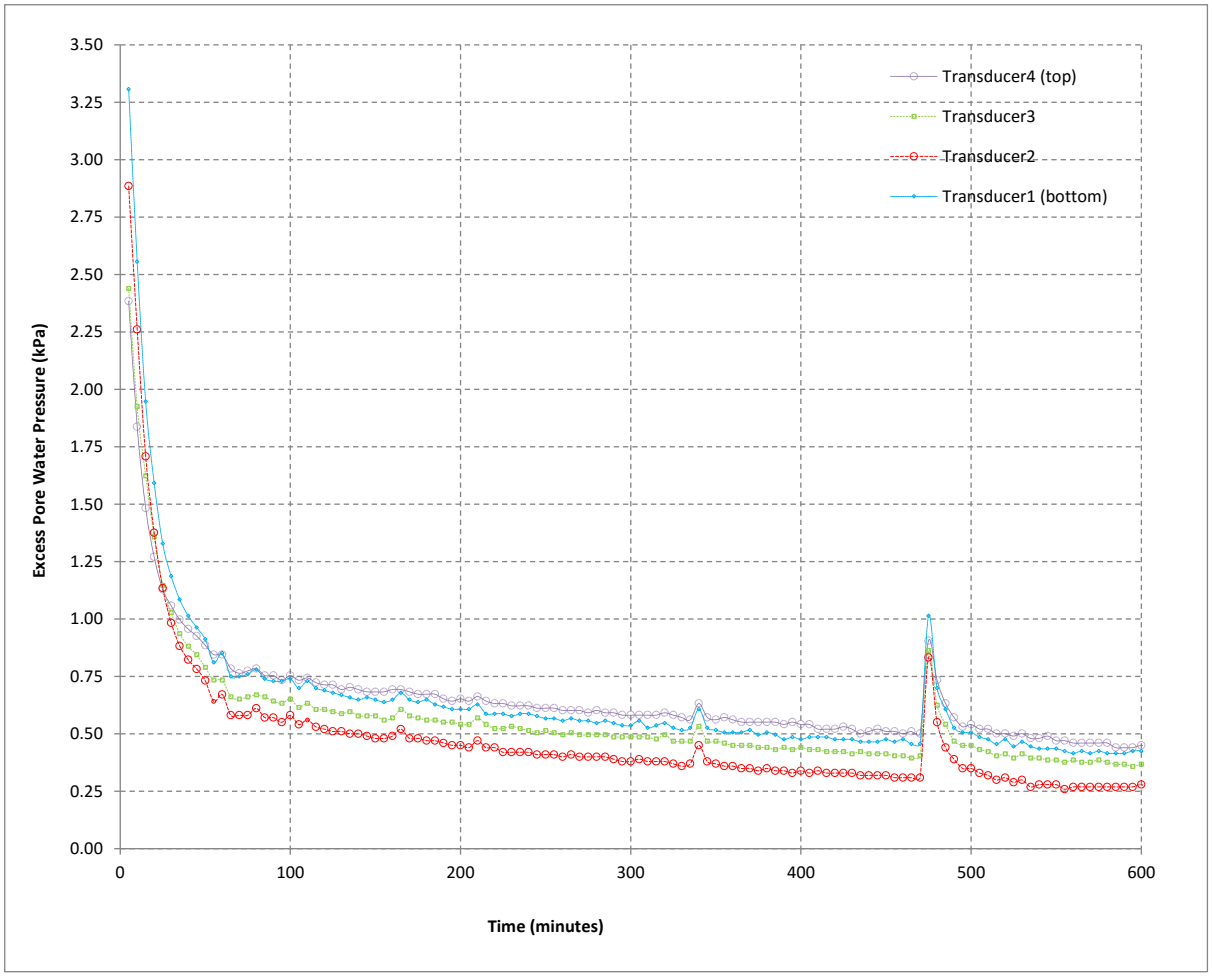

Figure 4.16b: Graphtec logger data Experiment FDA start of deposition

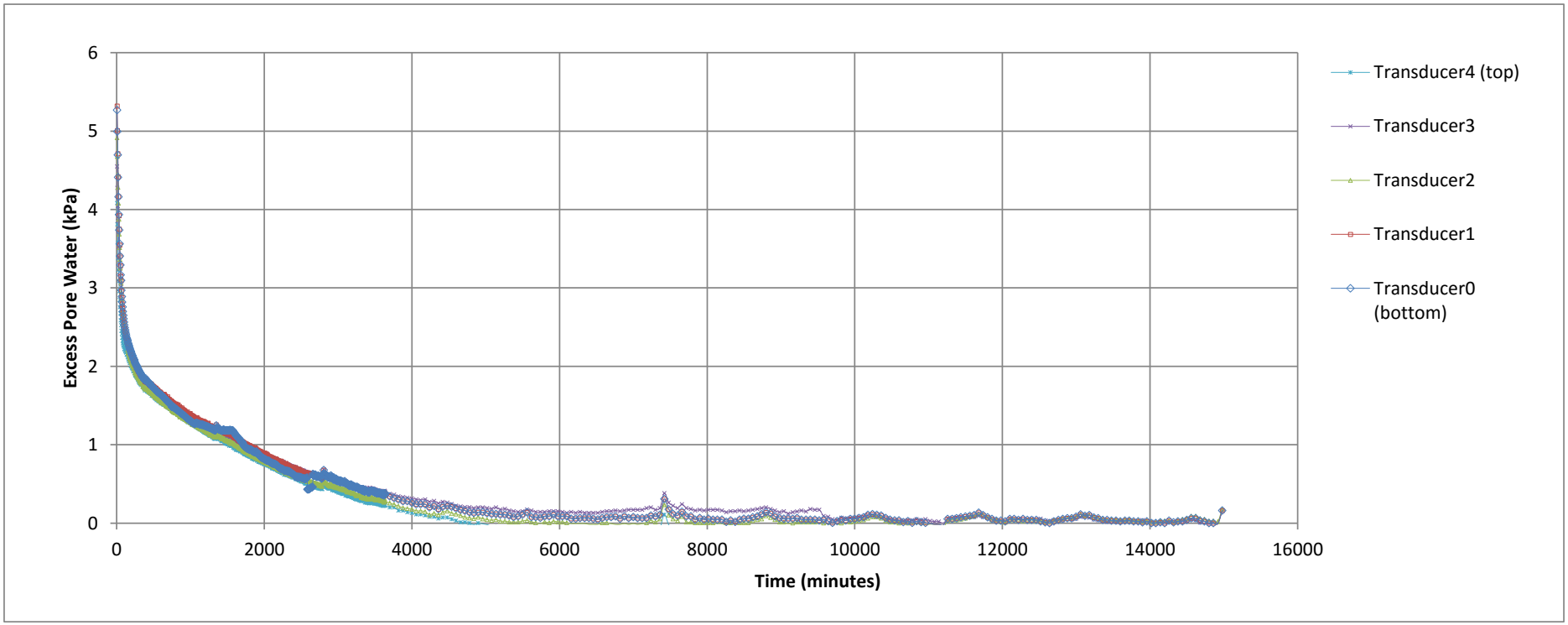

Figure 4.17a: Graphtec logger data Experiment FDB

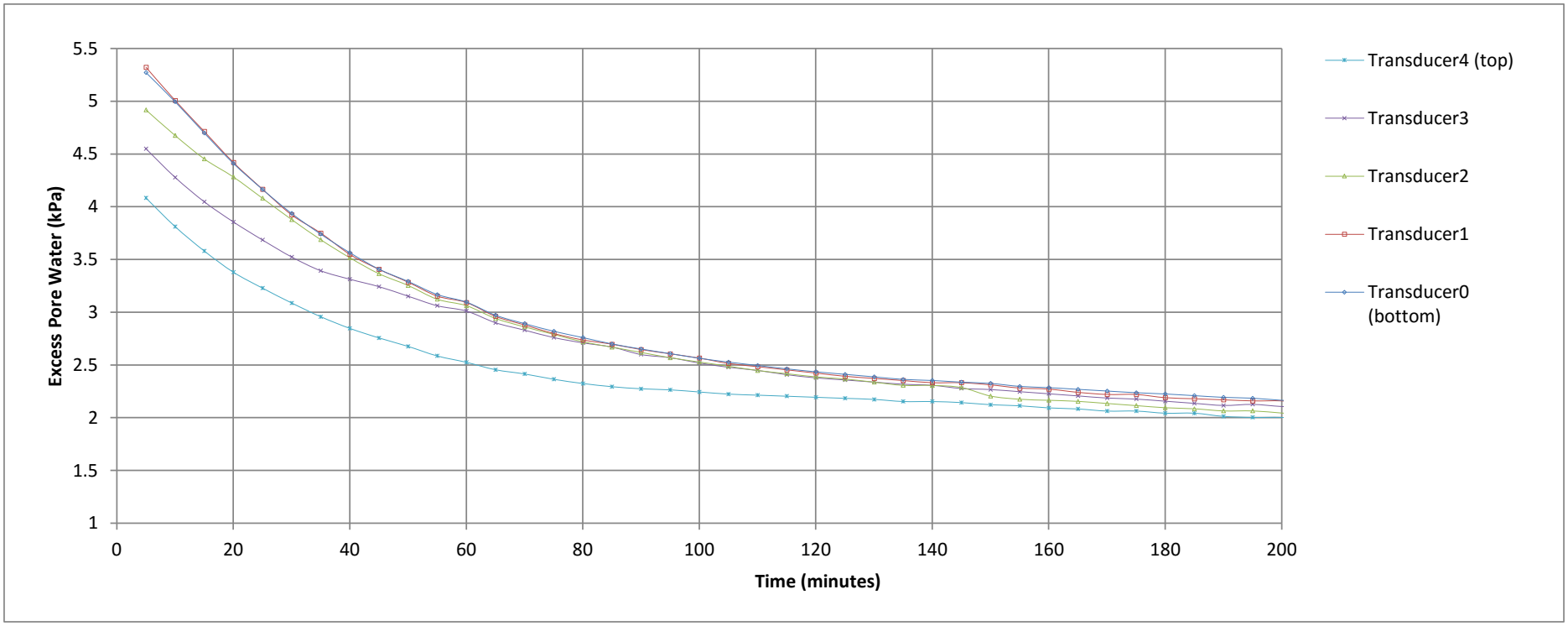

Figure 4.17b: Graphtec logger data Experiment FDB early pore pressure lift trend

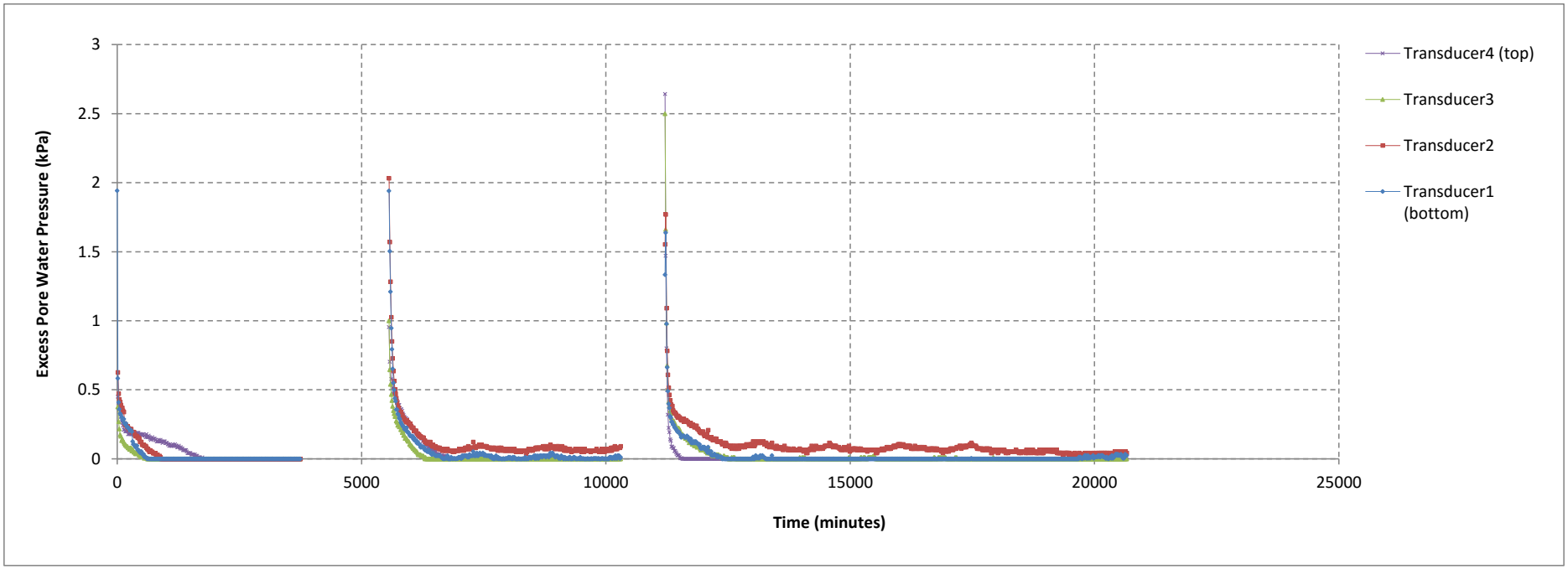

Figure 4.18a: Graphtec logger data Experiment RoR20A

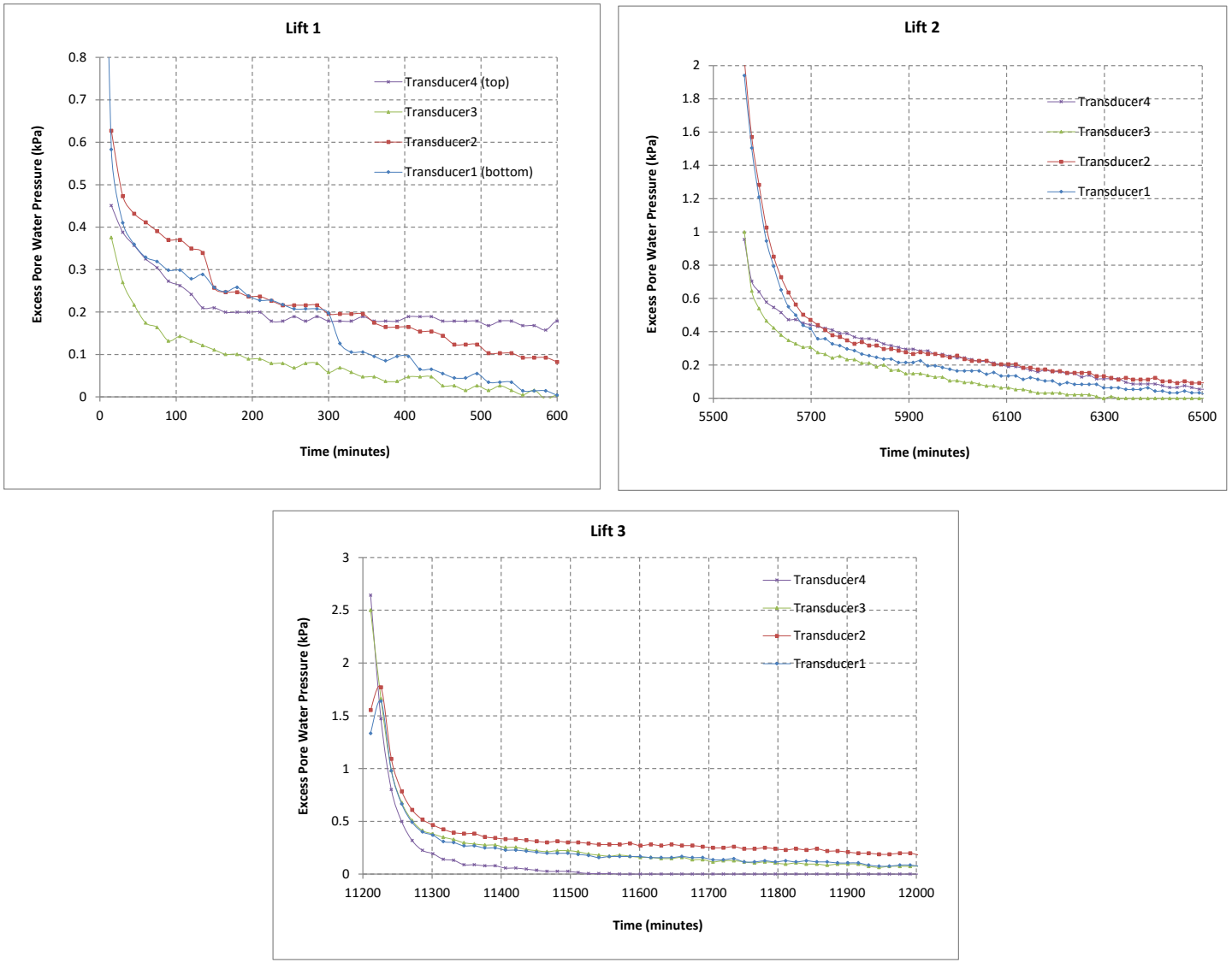

Figure 4.18b: Graphtec logger data Experiment RoR20A early pore pressure lift trend

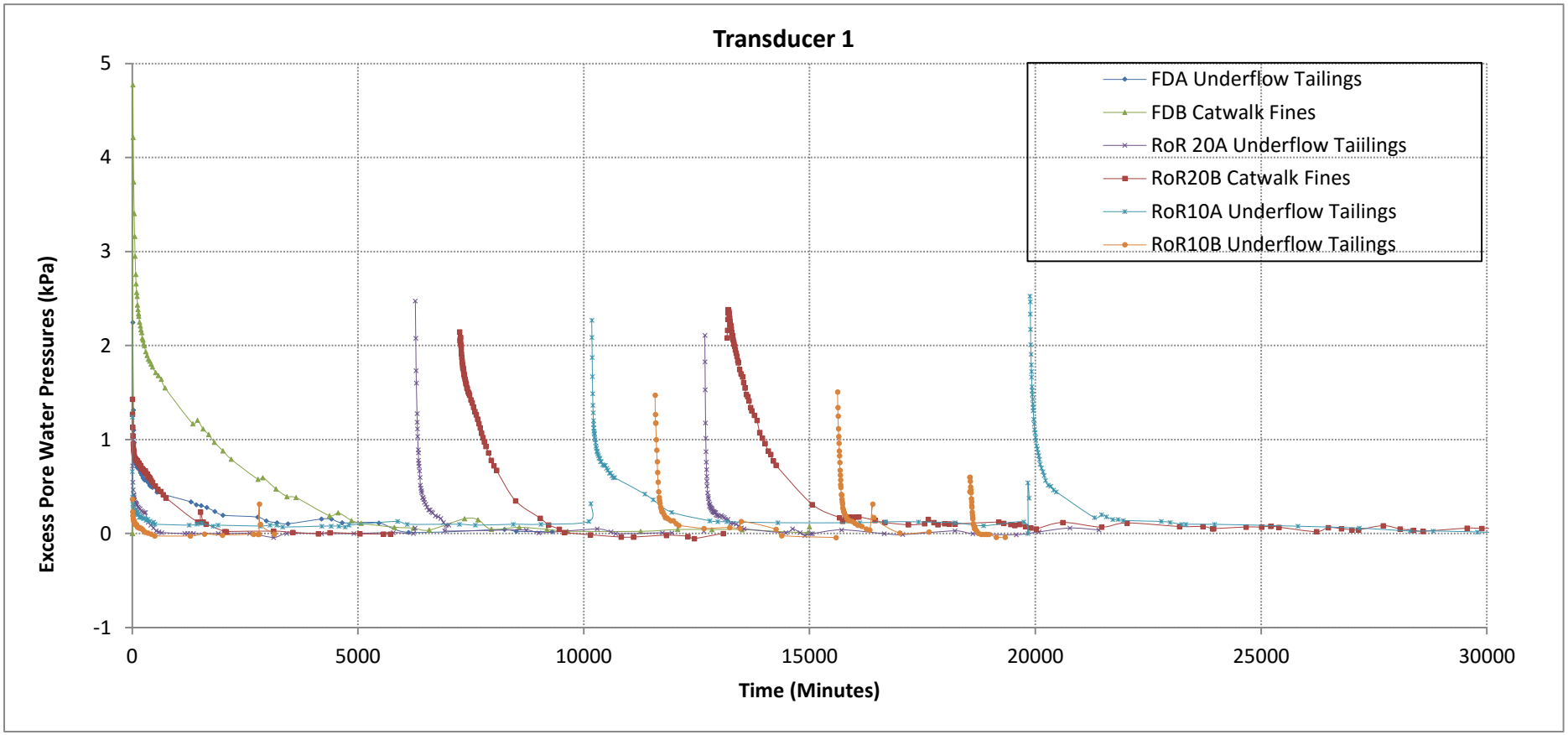

Figure 4.19: Excess pore pressures dissipation with time at transducer 1 - all experiments

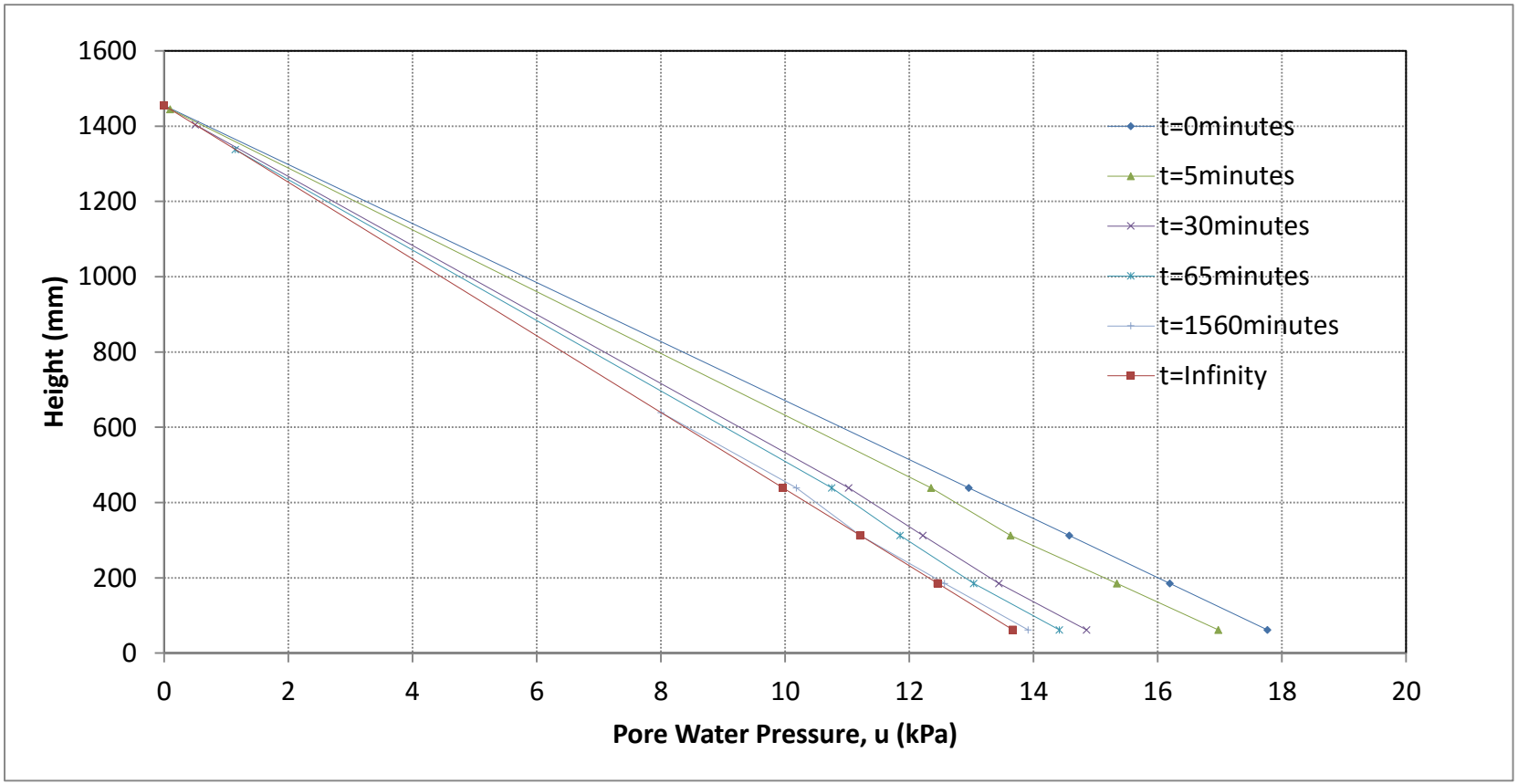

Figure 4.20: Depth vs pore pressure Experiment FDA

Excess pore pressures dissipation with time at transducer 1 - all experiments

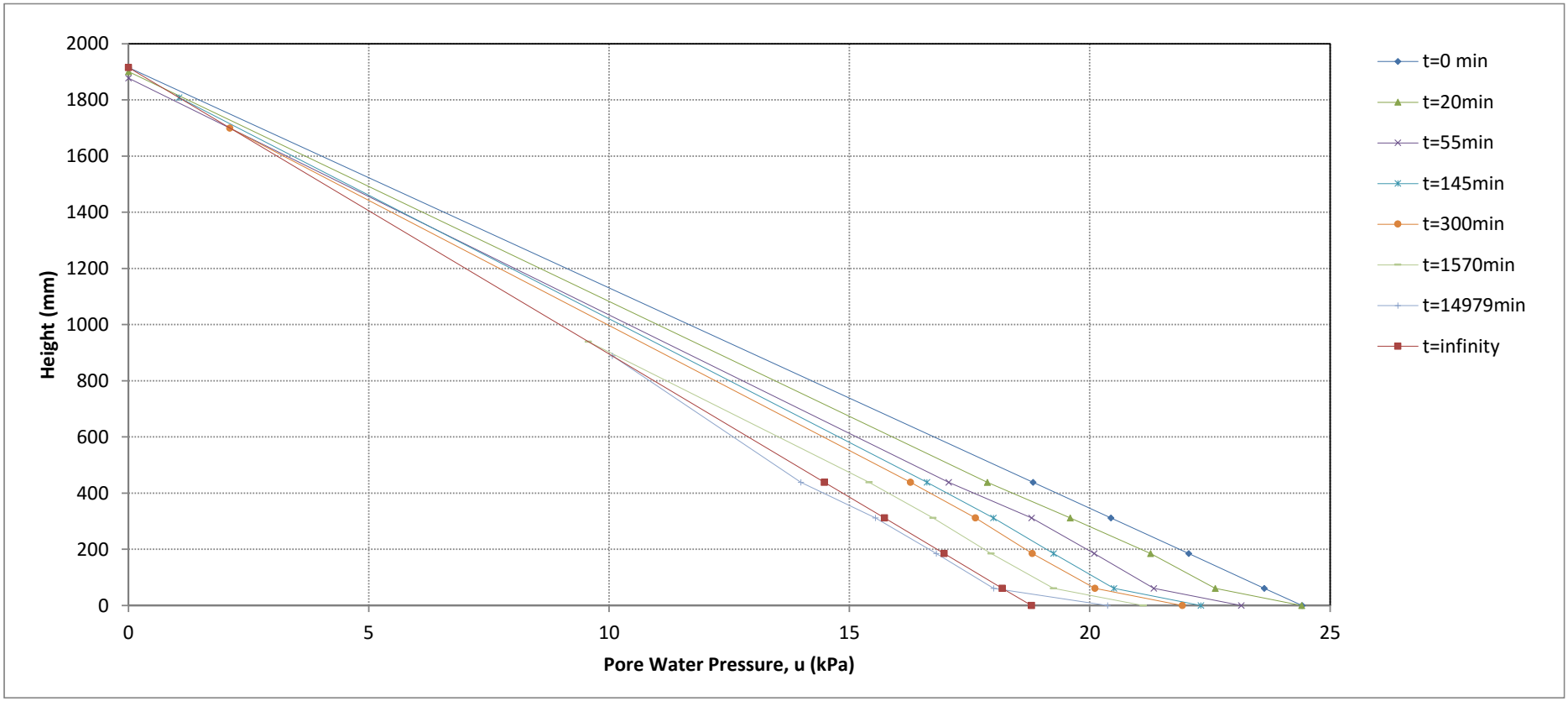

Figure 4.21: Depth vs pore pressure trend Experiment FDB

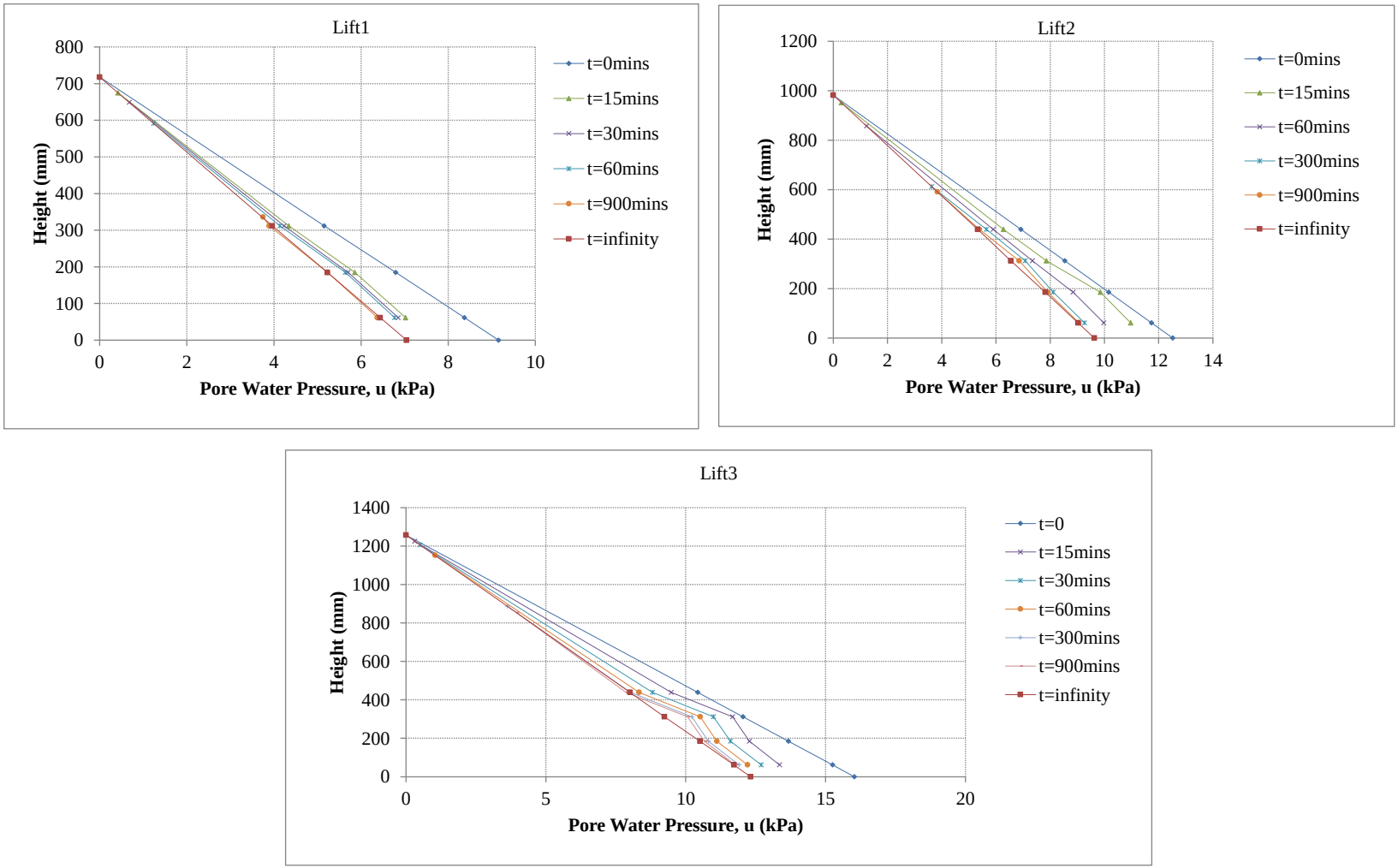

Figure 4.22: Depth vs pore pressure trend Experiment RoR20A

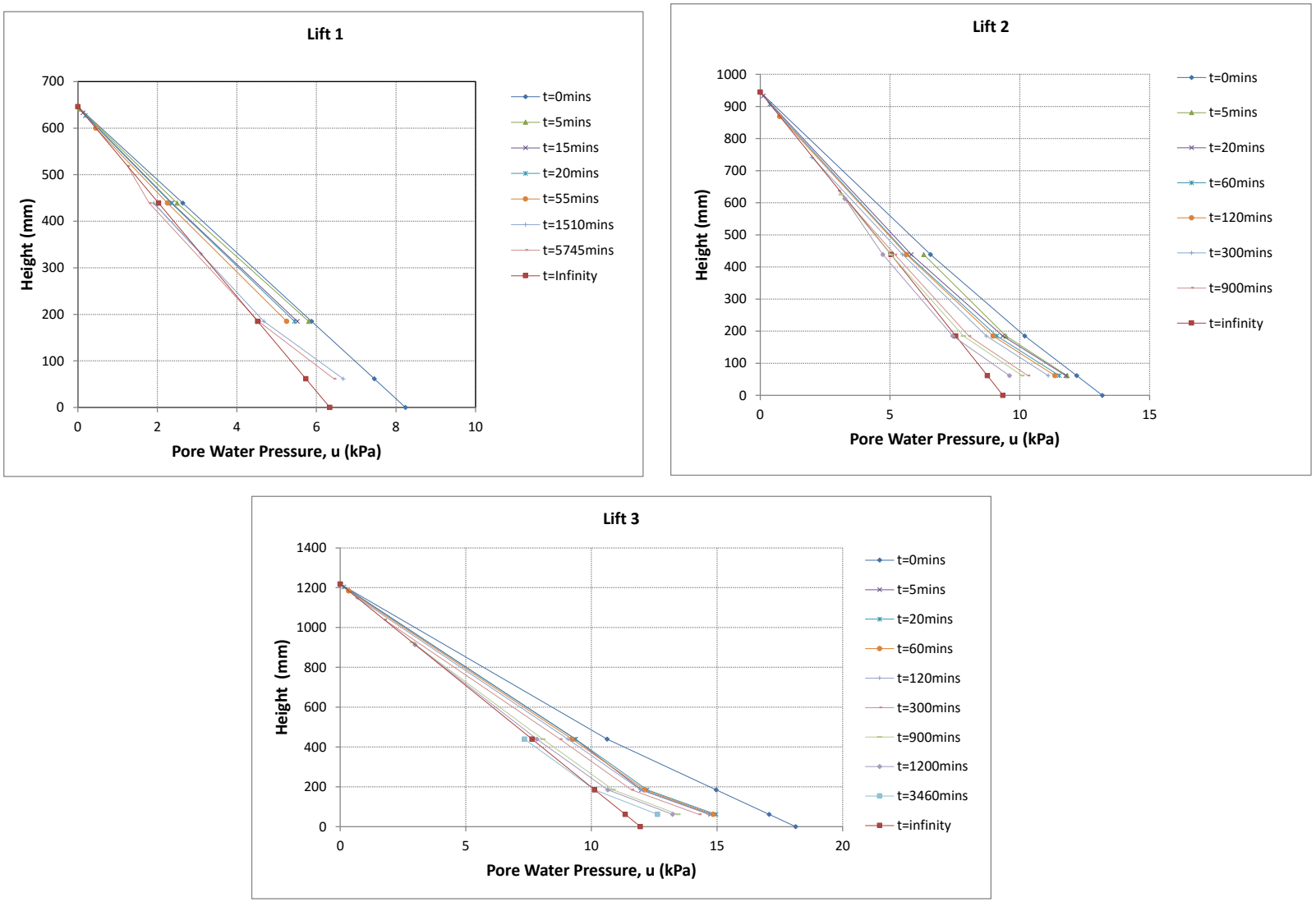

Figure 4.23: Depth vs pore pressure trend Experiment RoR20B

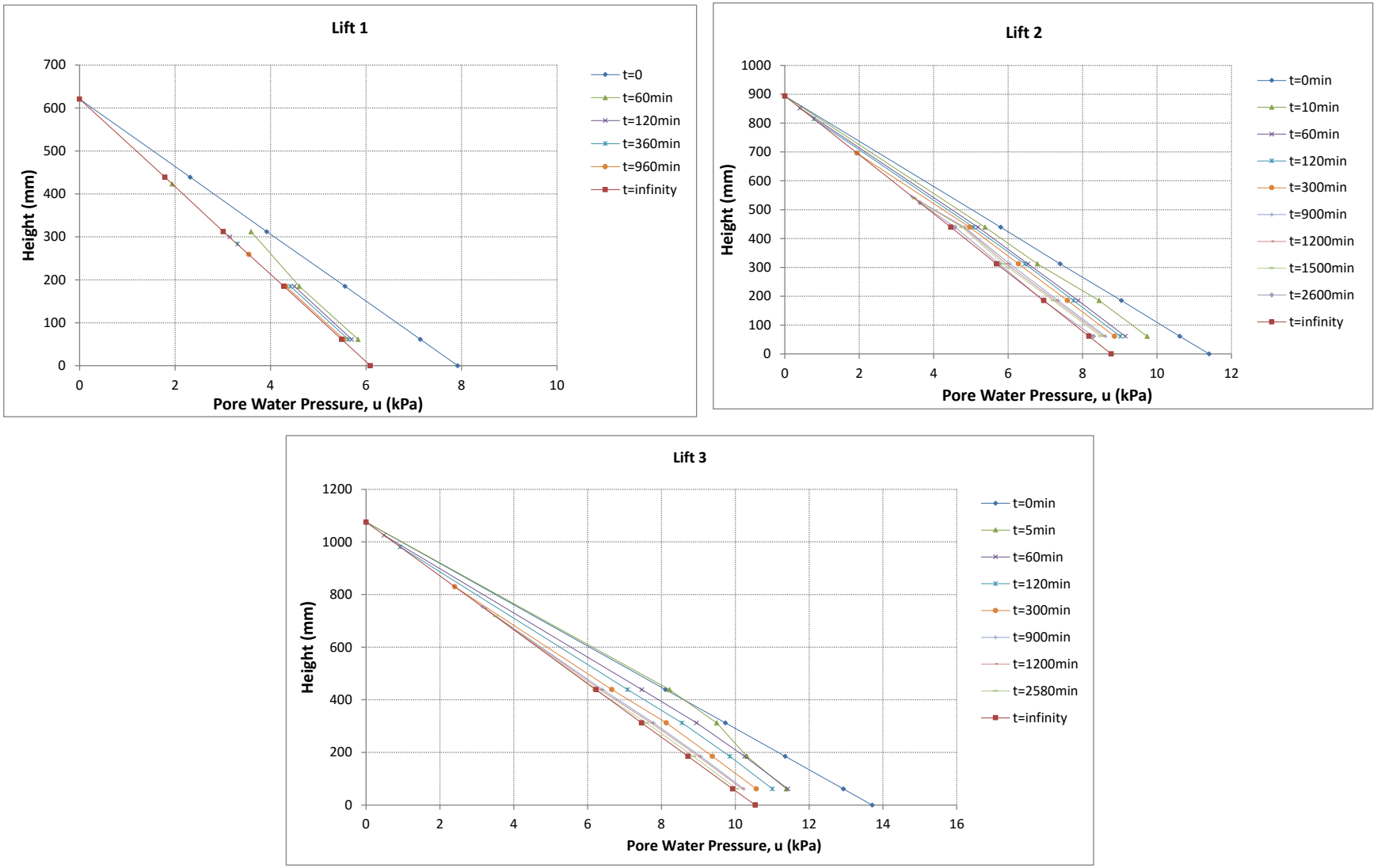

Figure 4.24: Depth vs pore pressure trend Experiment RoR10A

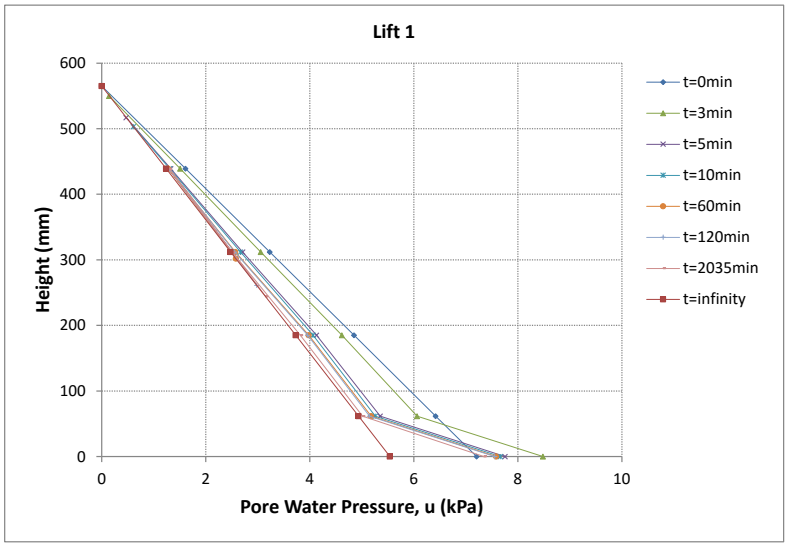

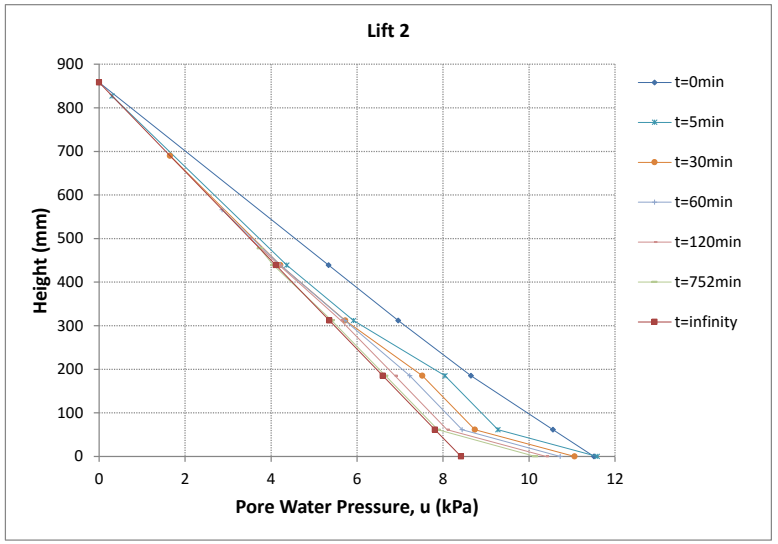

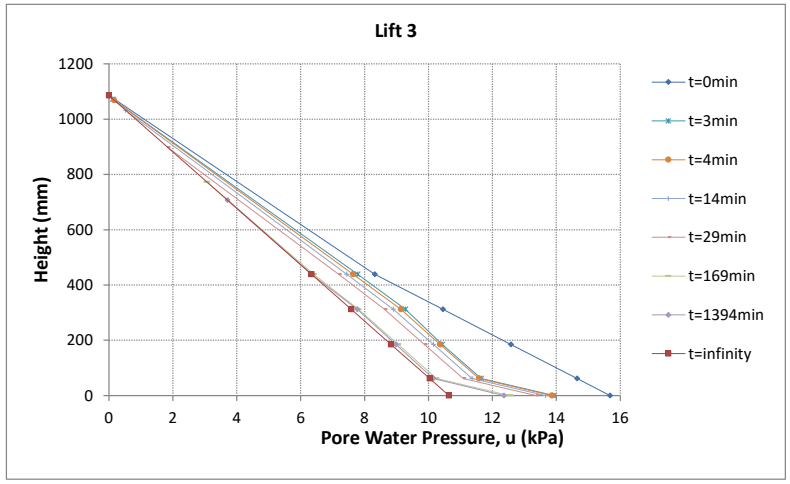

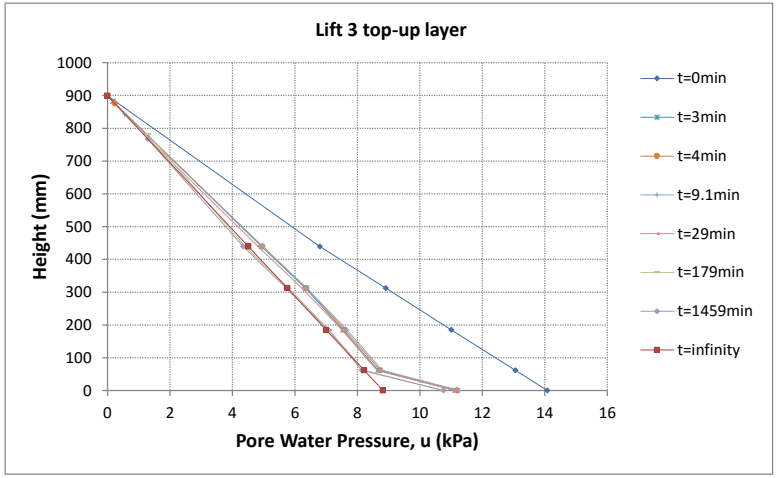

Figure 4.25: Depth vs pore pressure trend Experiment RoR10B

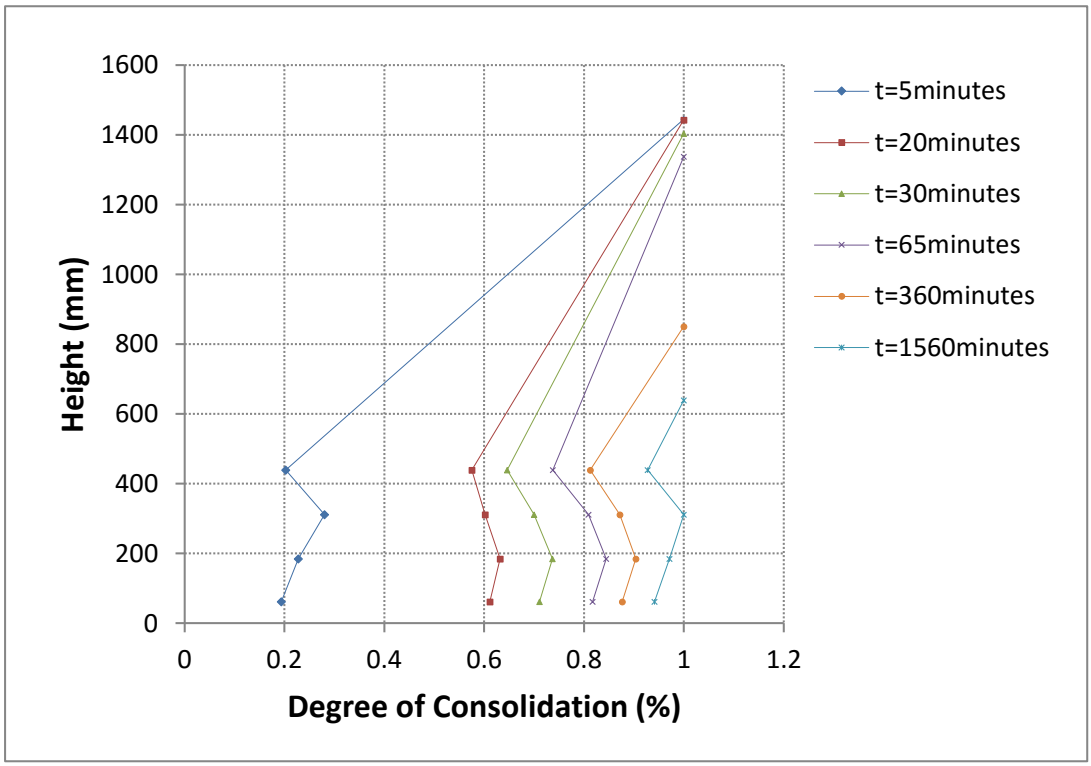

Figure 4.26: Degree of consolidation Experiment FDA

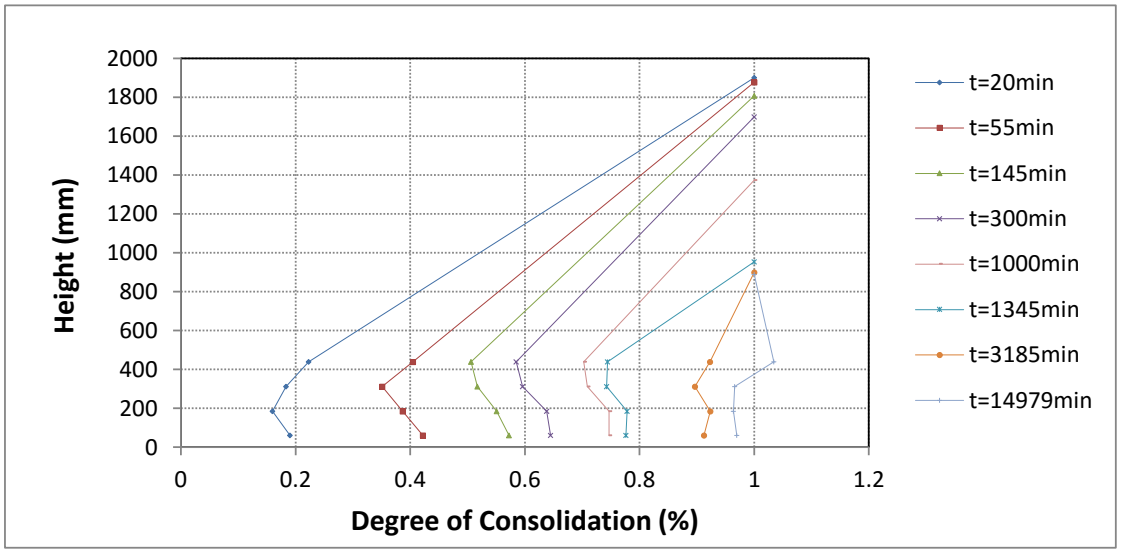

Figure 4.27: Degree of consolidation Experiment FDB

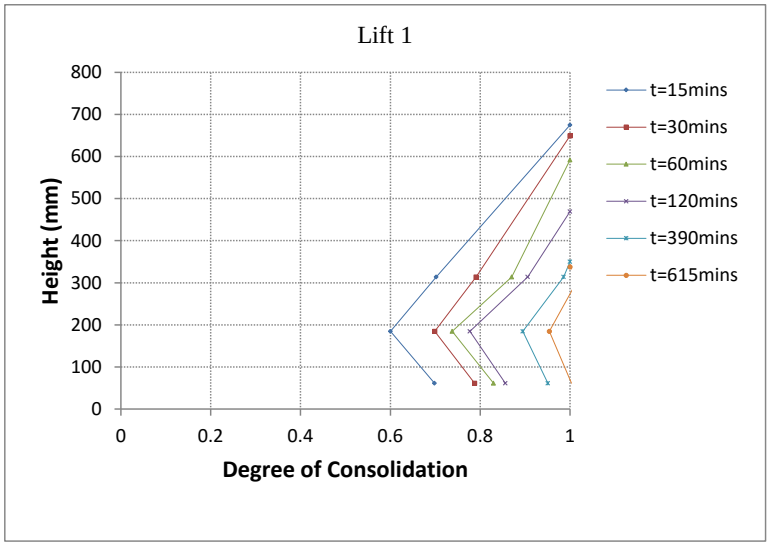

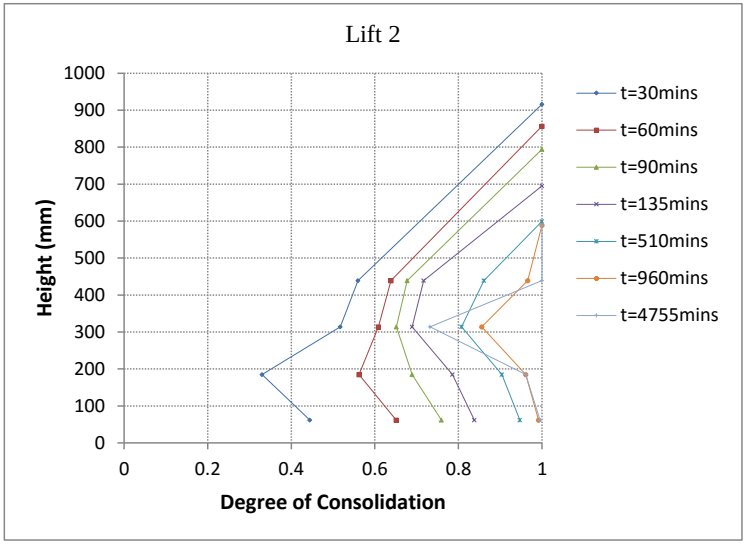

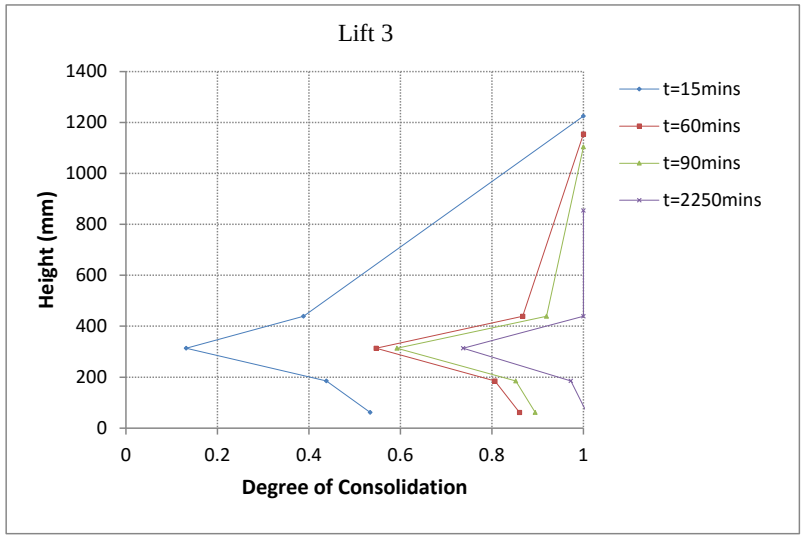

Figure 4.28: Degree of consolidation Experiment RoR20A

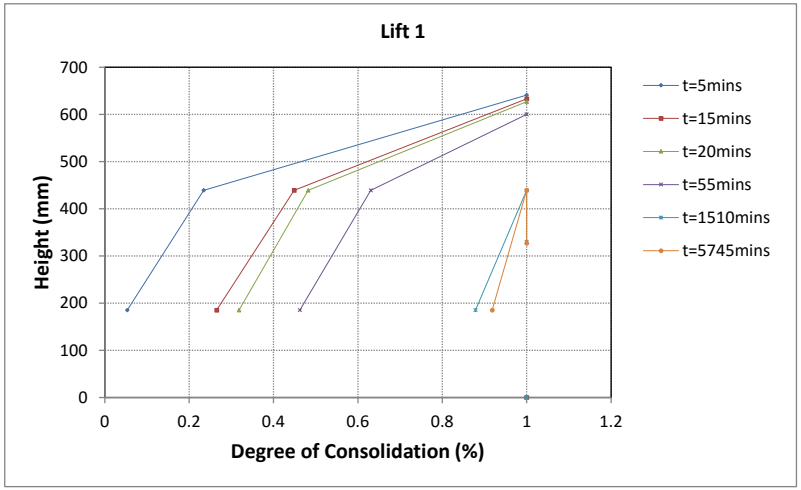

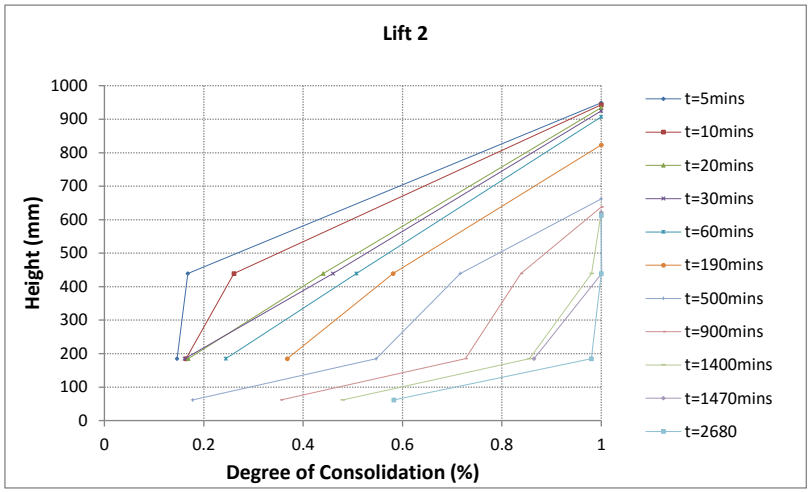

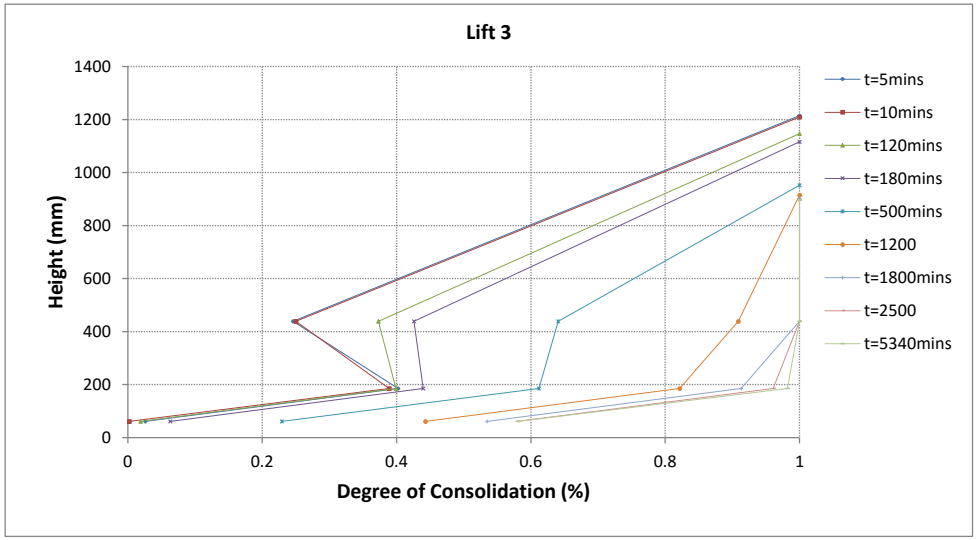

Figure 4.29: Degree of consolidation Experiment RoR20B

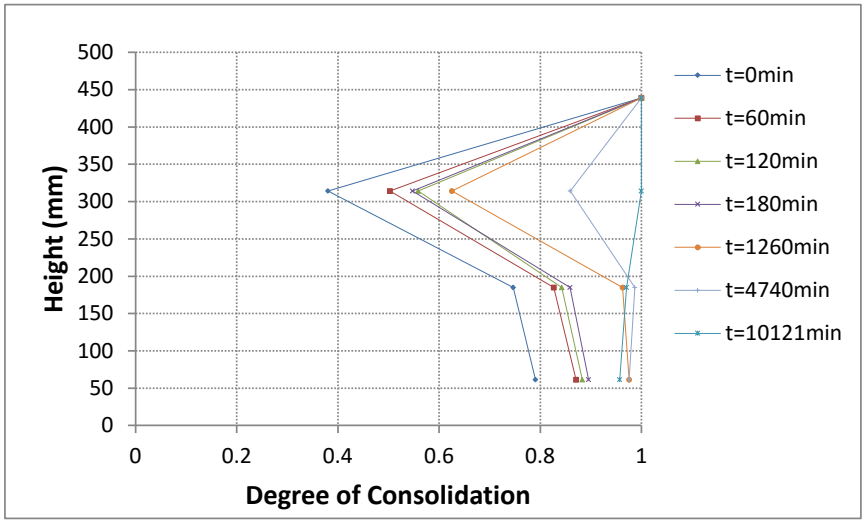

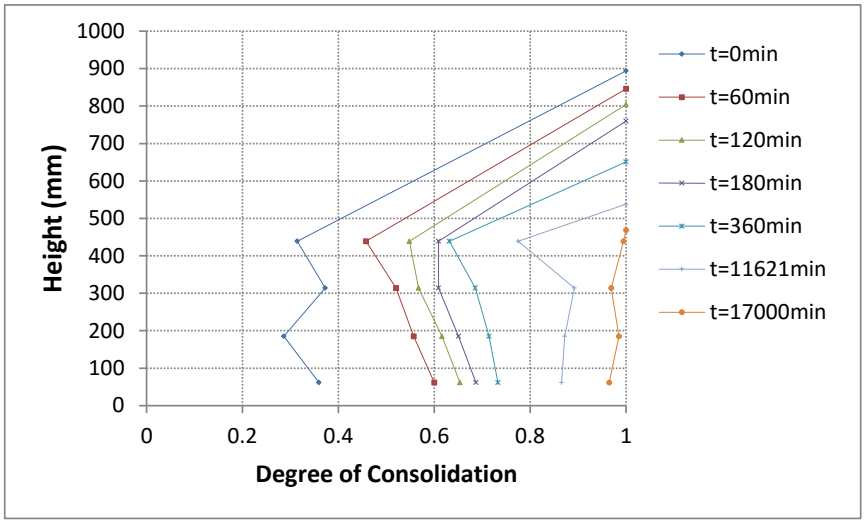

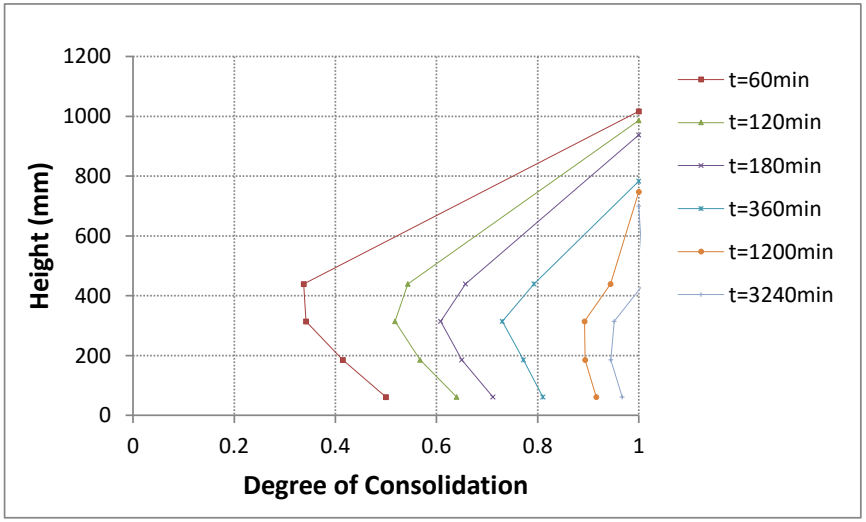

Figure 4.30: Degree of consolidation Experiment RoR10A

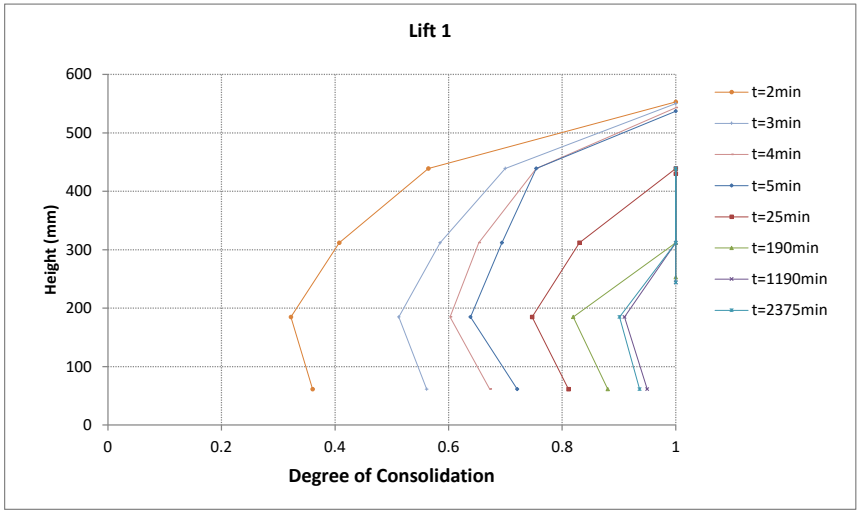

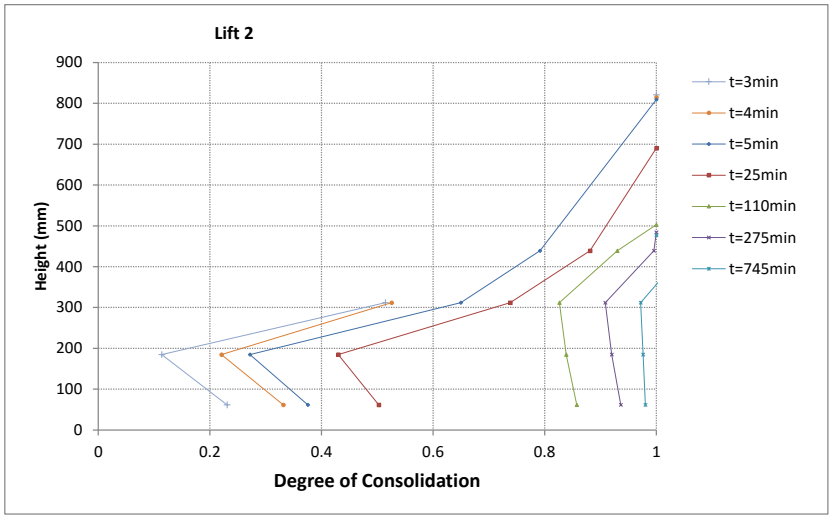

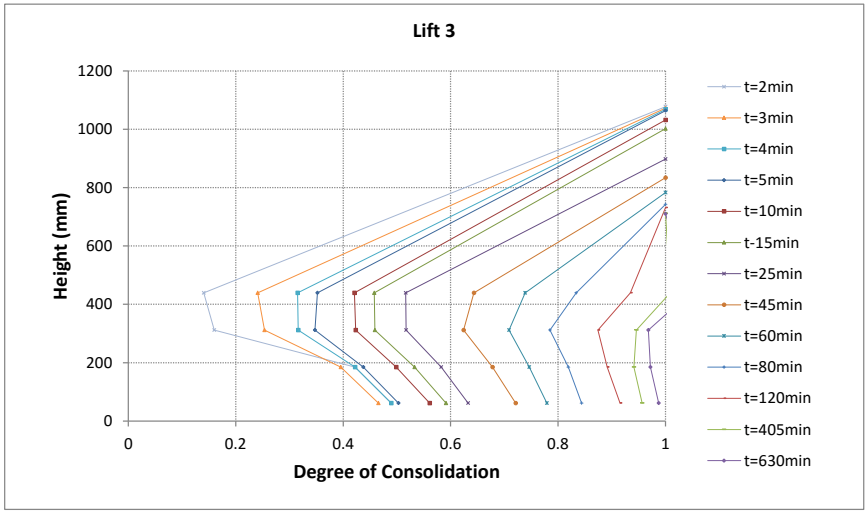

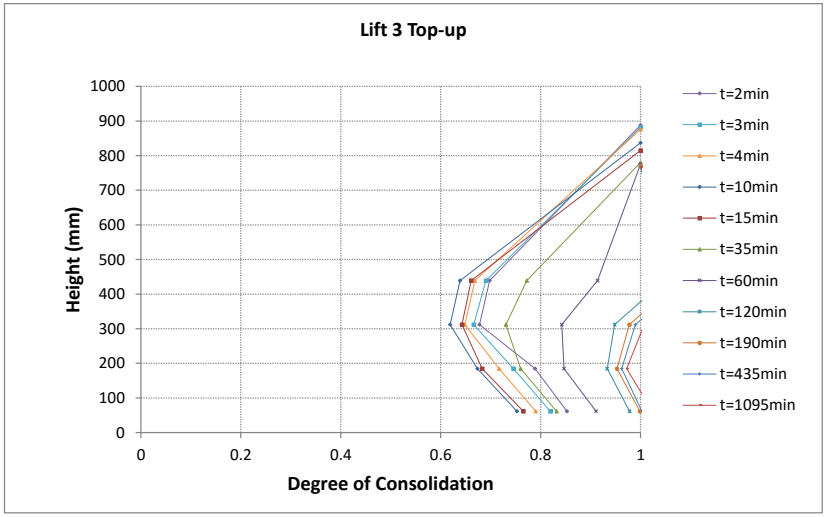

Figure 4.31: Degree of consolidation Experiment RoR10B

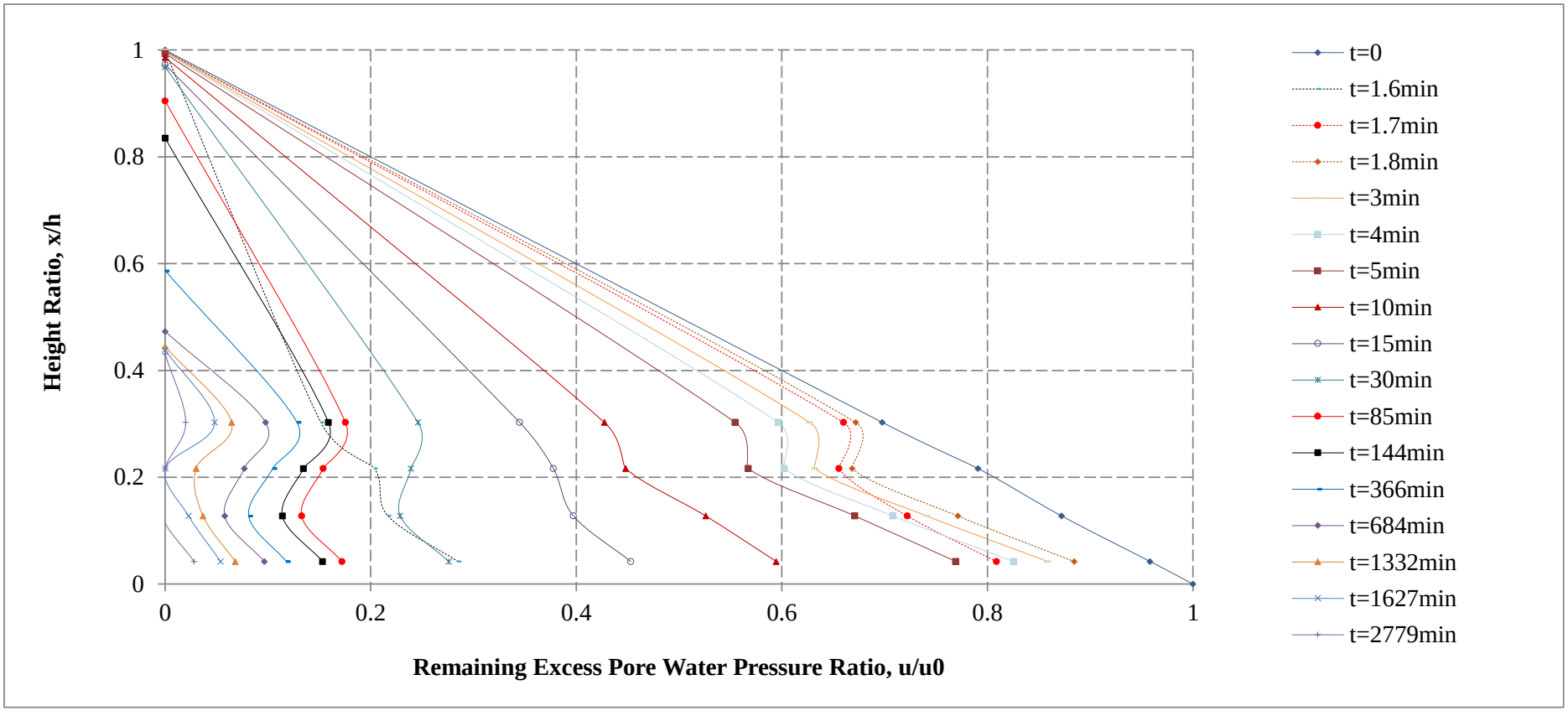

Figure 4.32a: Remaining excess pore pressures Experiment FDA

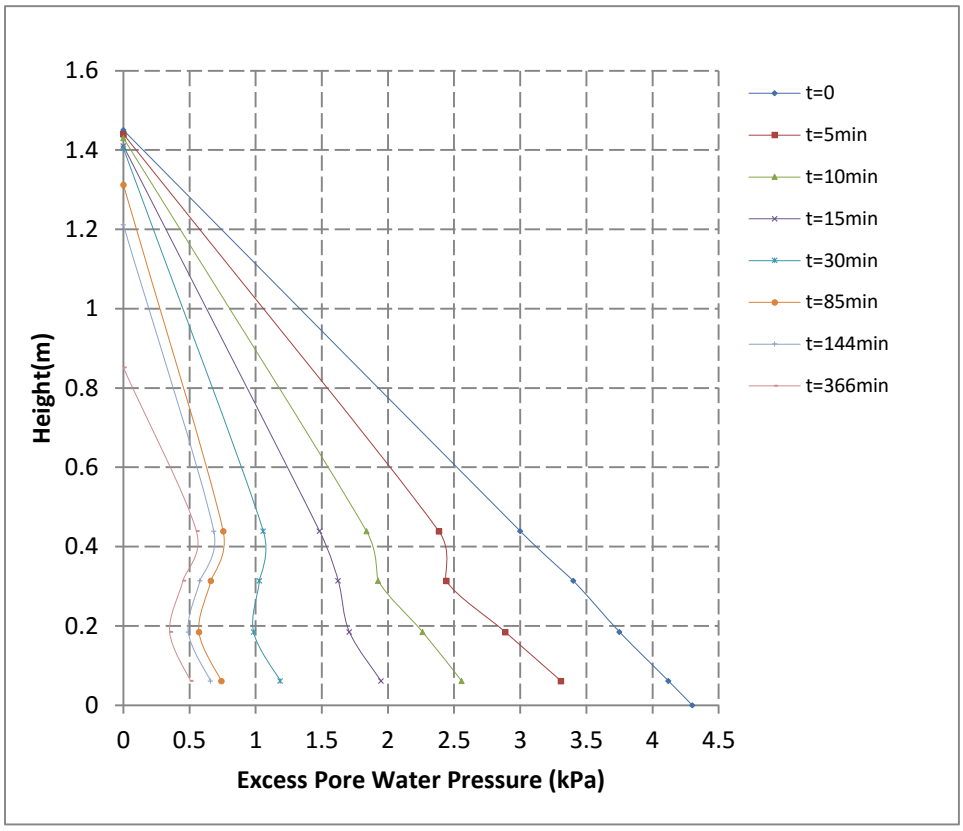

Figure 4.32b(i): Remaining excess pore pressures sedimentation/consolidation stage Experiment FDA

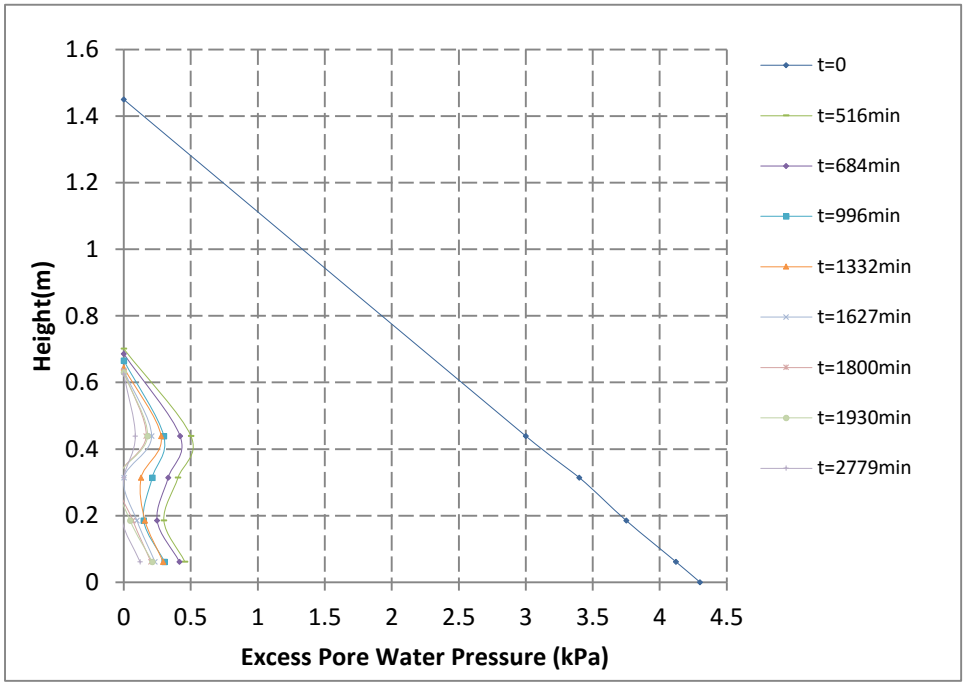

Figure 4.32b(ii): Remaining excess pore pressures consolidation stage Experiment FDA

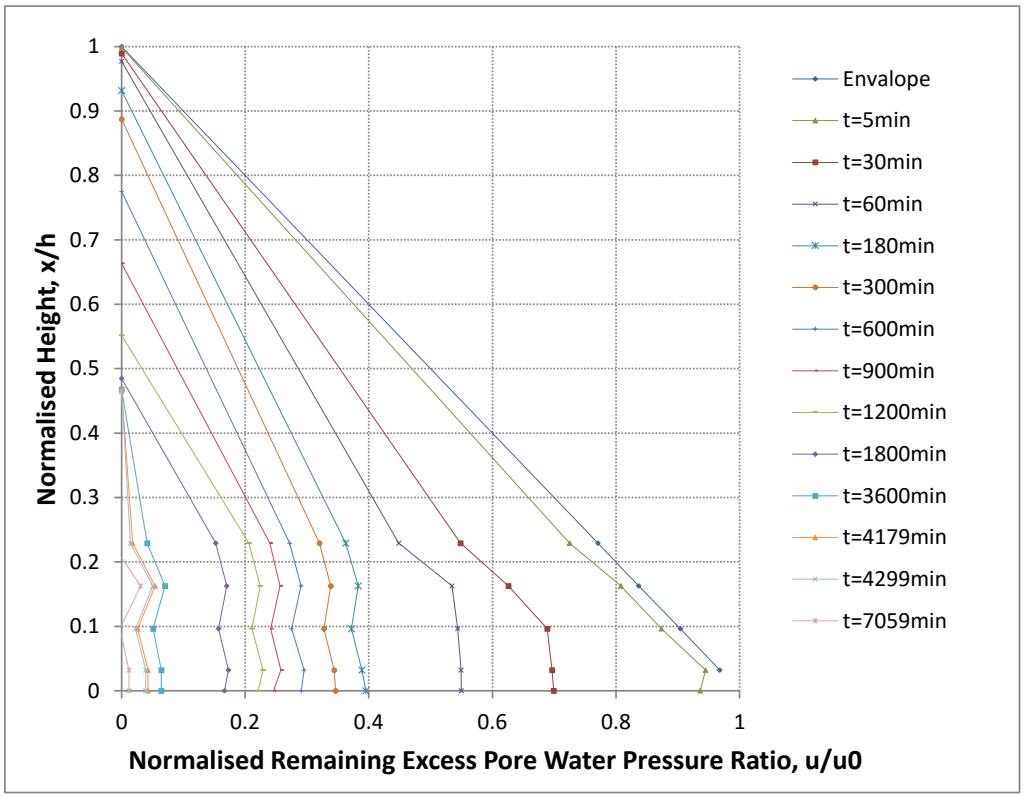

Figure 4.33: Remaining excess pore pressure ratio Experiment FDB

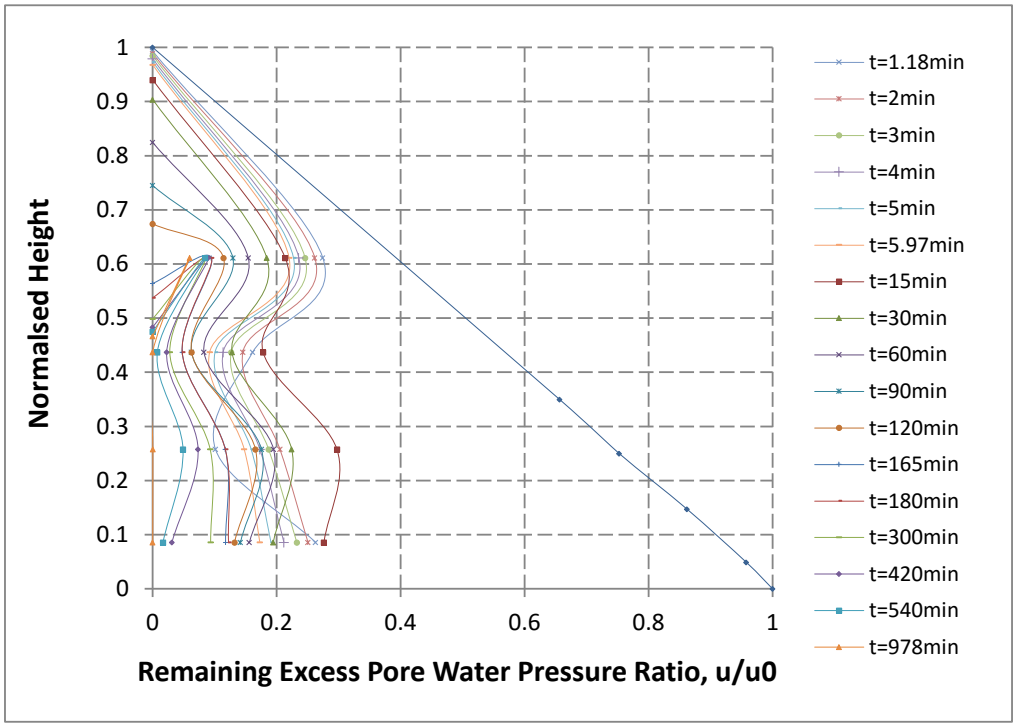

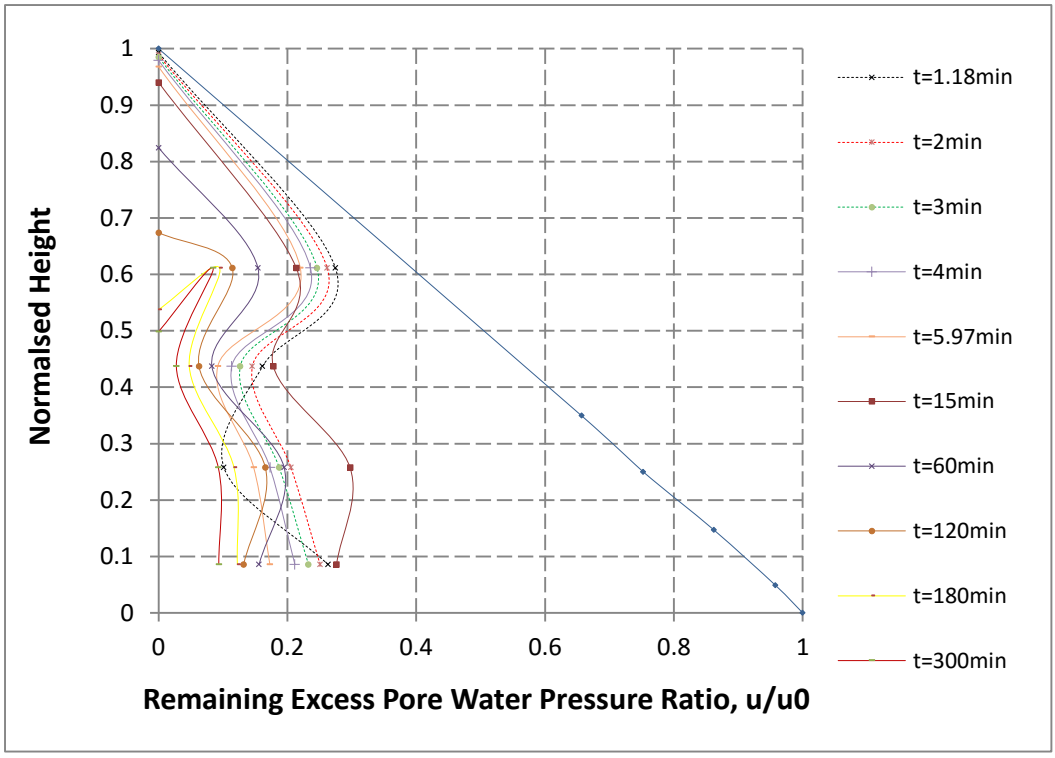

Figure 4.34a(i): Remaining excess pore pressures ratio Experiment RoR20A all isochrones - Lift 1

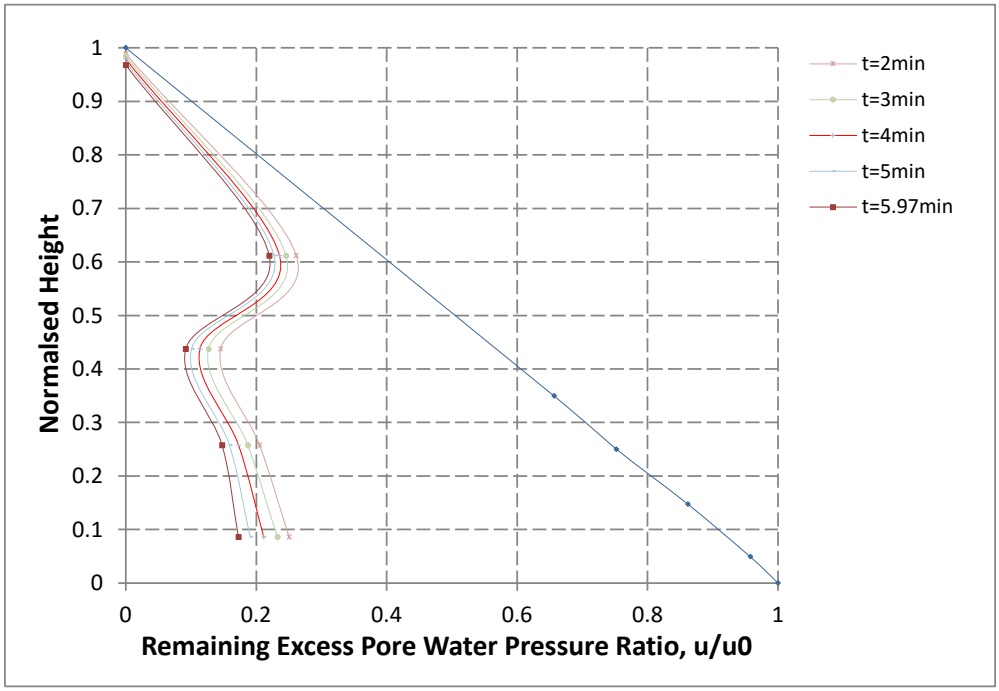

Figure 4.34a(ii): Remaining excess pore pressures ratio Experiment RoR20A pattern 1 isochrones *after first hour of deposition* - Lift 1

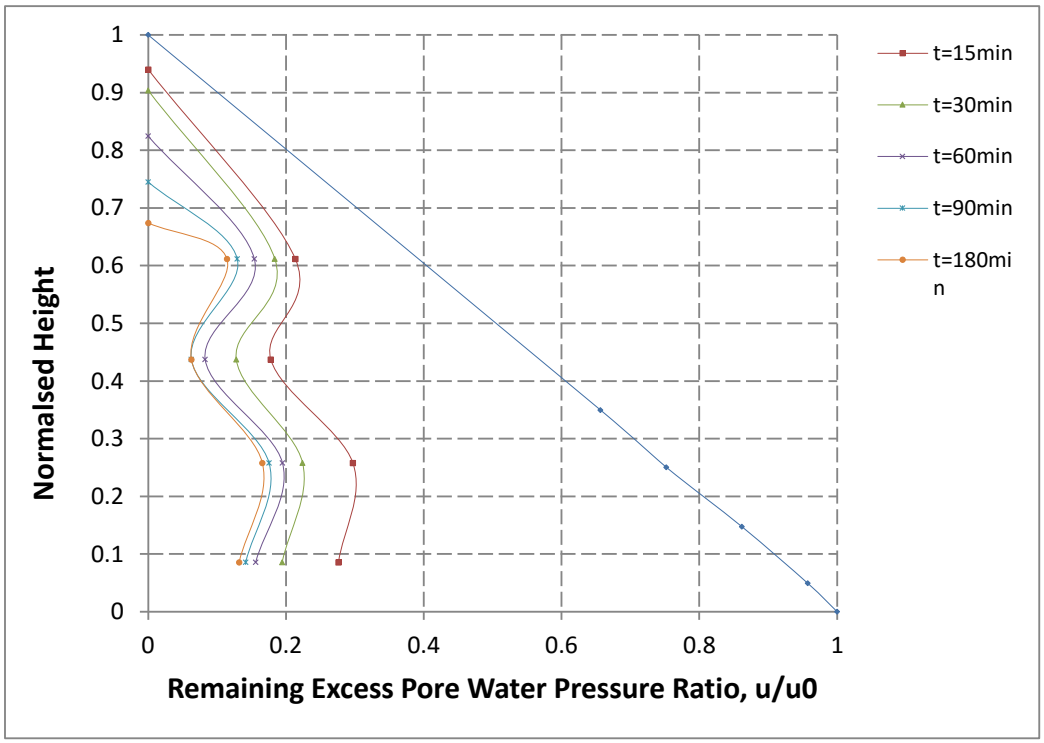

Figure 4.34a(iii): Remaining excess pore pressures ratio Experiment RoR20A pattern 2 shaped isochrones *after 2 hours from deposition* - Lift 1

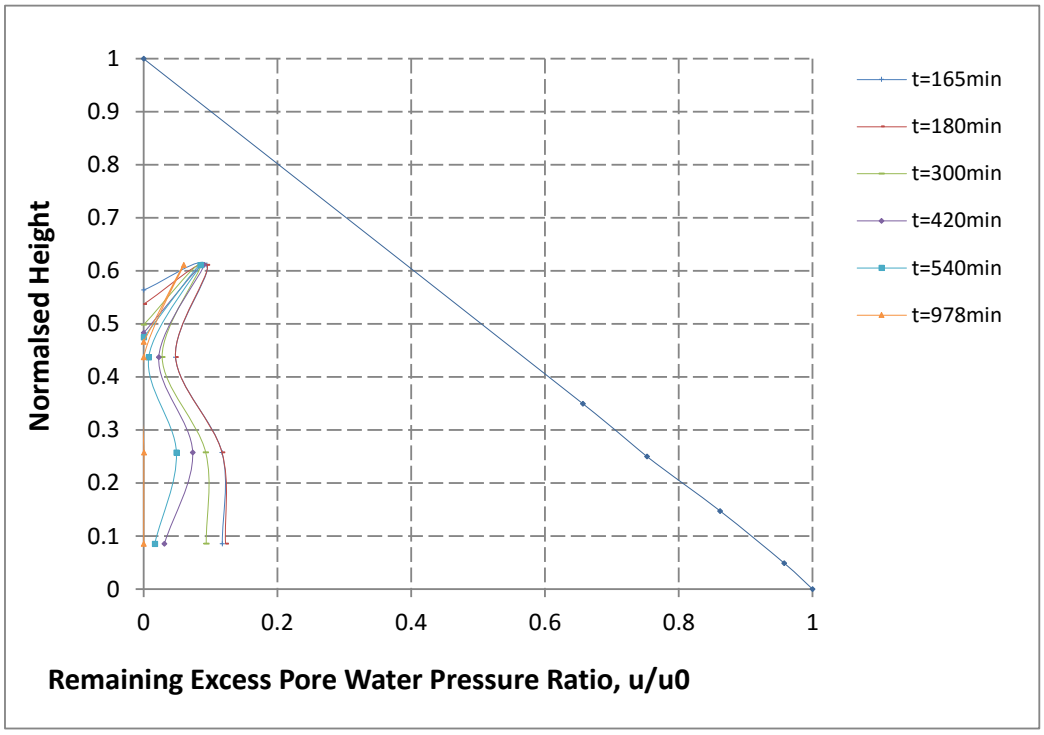

Figure 4.34a(iv): Remaining excess pore pressures ratio Experiment RoR20A pattern 3 isochrones *during consolidation stage* - Lift 1

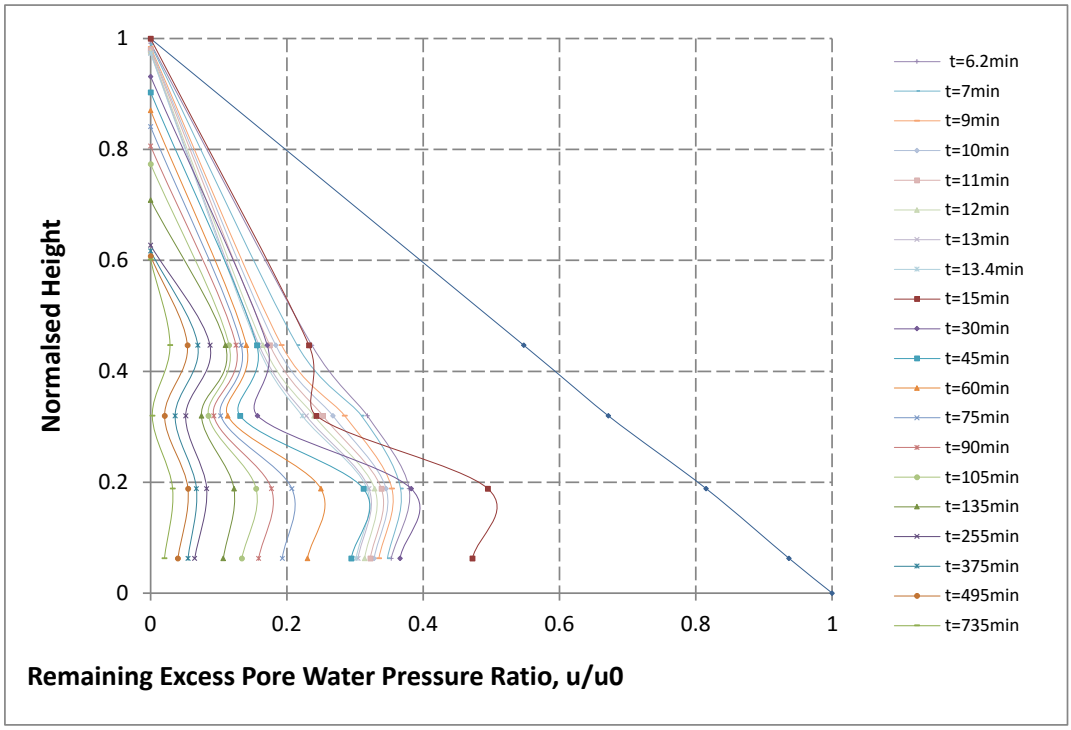

Figure 4.34b(i): Remaining excess pore pressures ratio Experiment RoR20A all isochrones - Lift 2

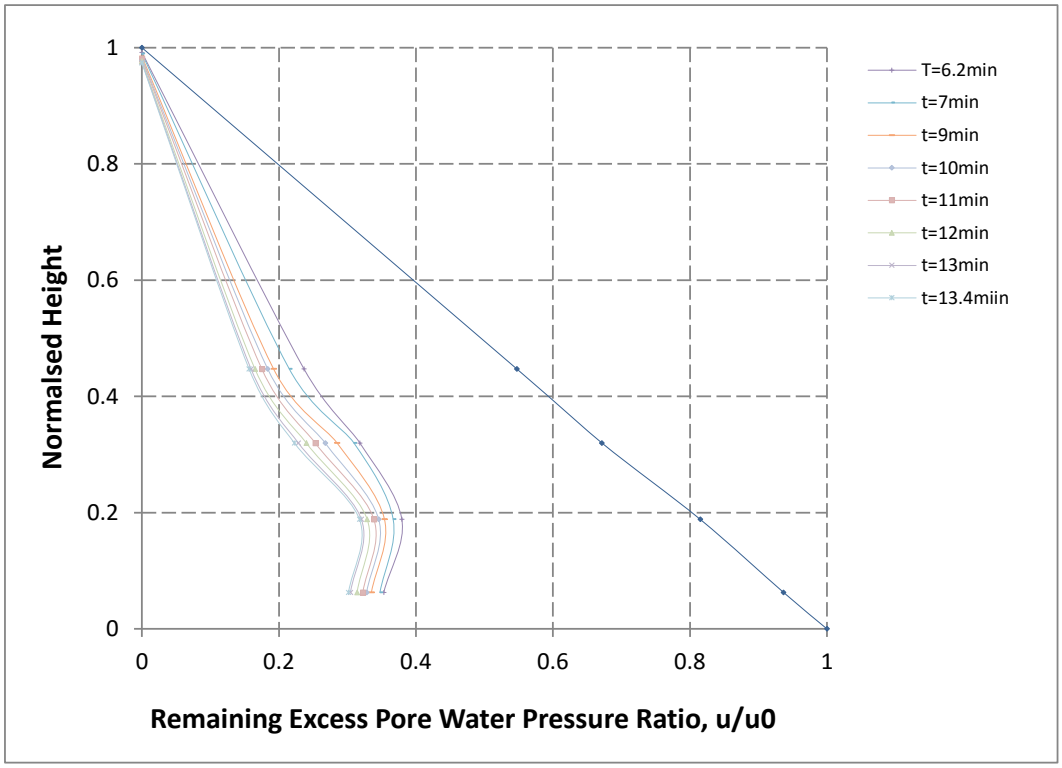

Figure 4.34b(ii): Remaining excess pore pressures ratio Experiment RoR20A pattern 1 isochrones *after first hour of deposition* - Lift 2

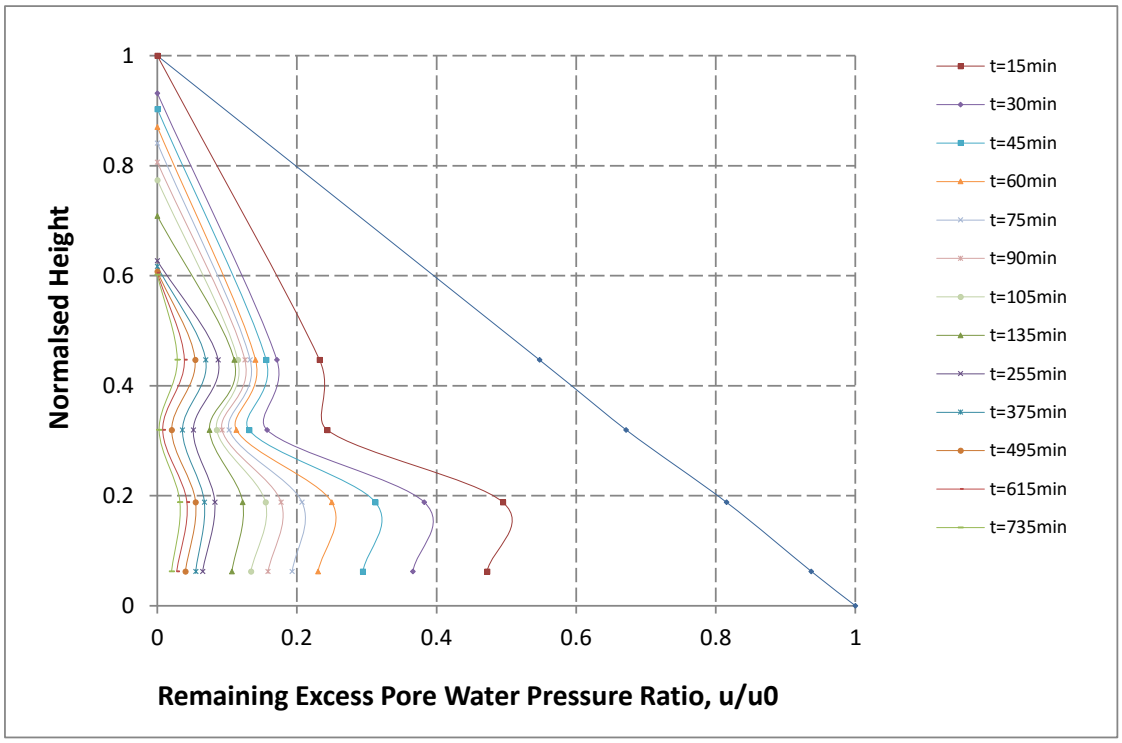

Figure 4.34b(iii): Remaining excess pore pressures ratio Experiment RoR20A pattern 2 shaped isochrones *after 2 hours from deposition* - Lift 2

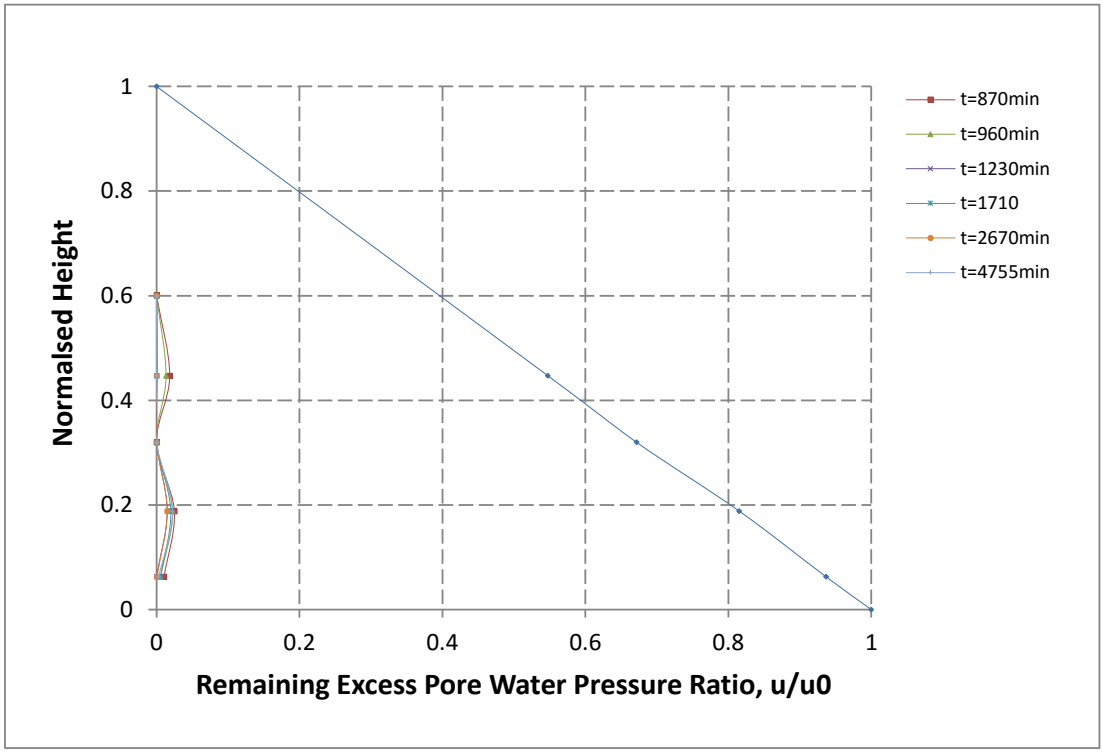

Figure 4.34b(iv): Remaining excess pore pressures ratio Experiment RoR20A pattern 3 isochrones *during consolidation stage* - Lift 2

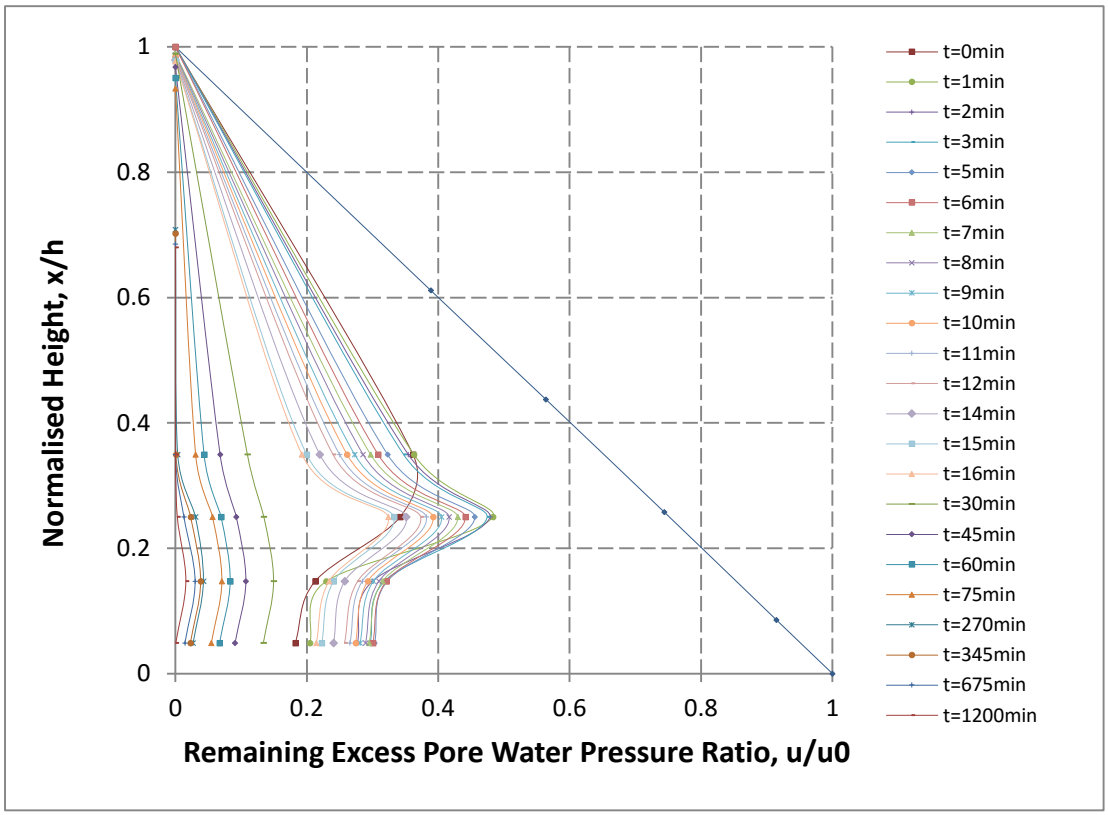

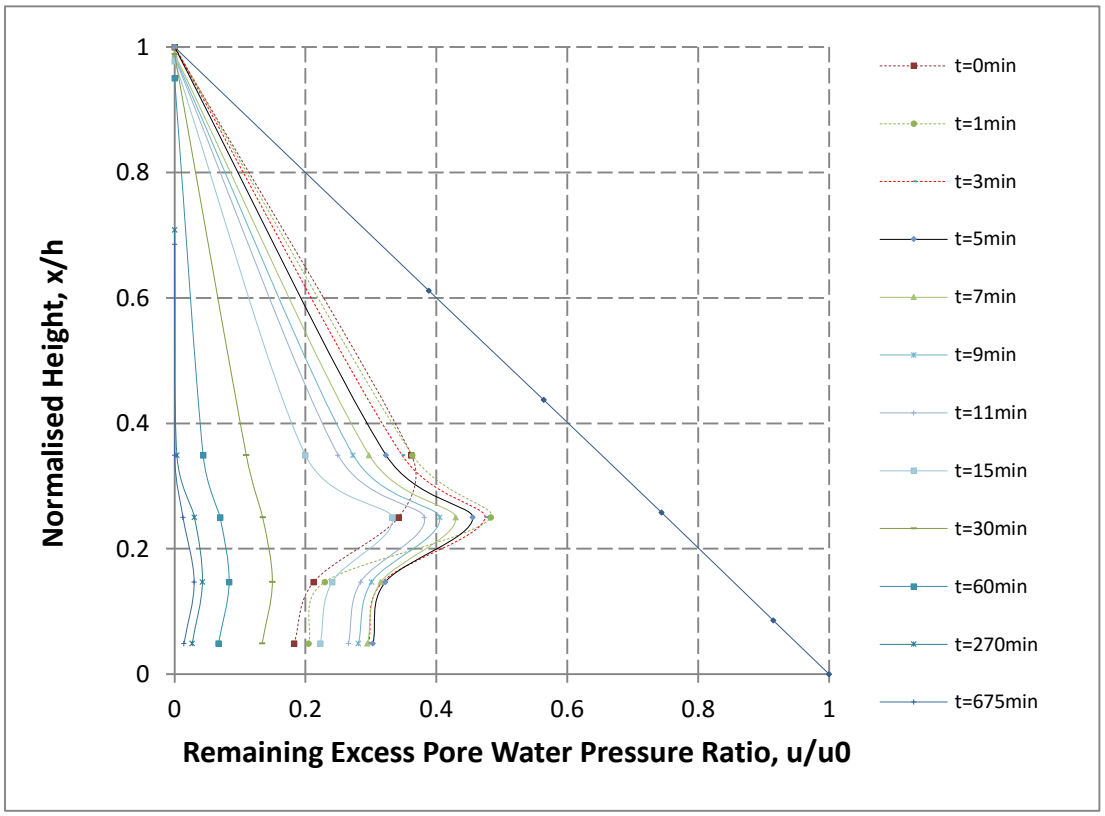

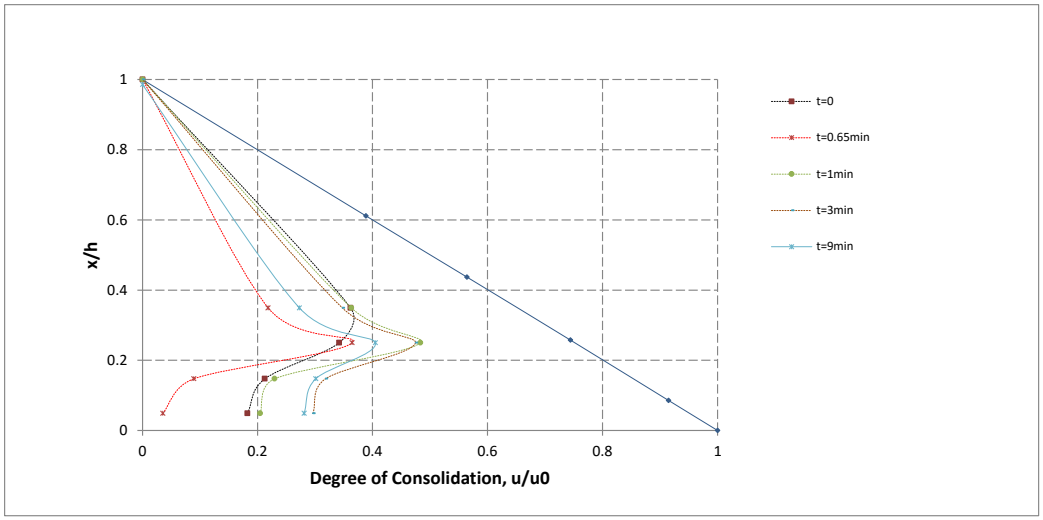

Figure 4.34c(i): Remaining excess pore pressures ratio Experiment RoR20A all isochrones - Lift 3

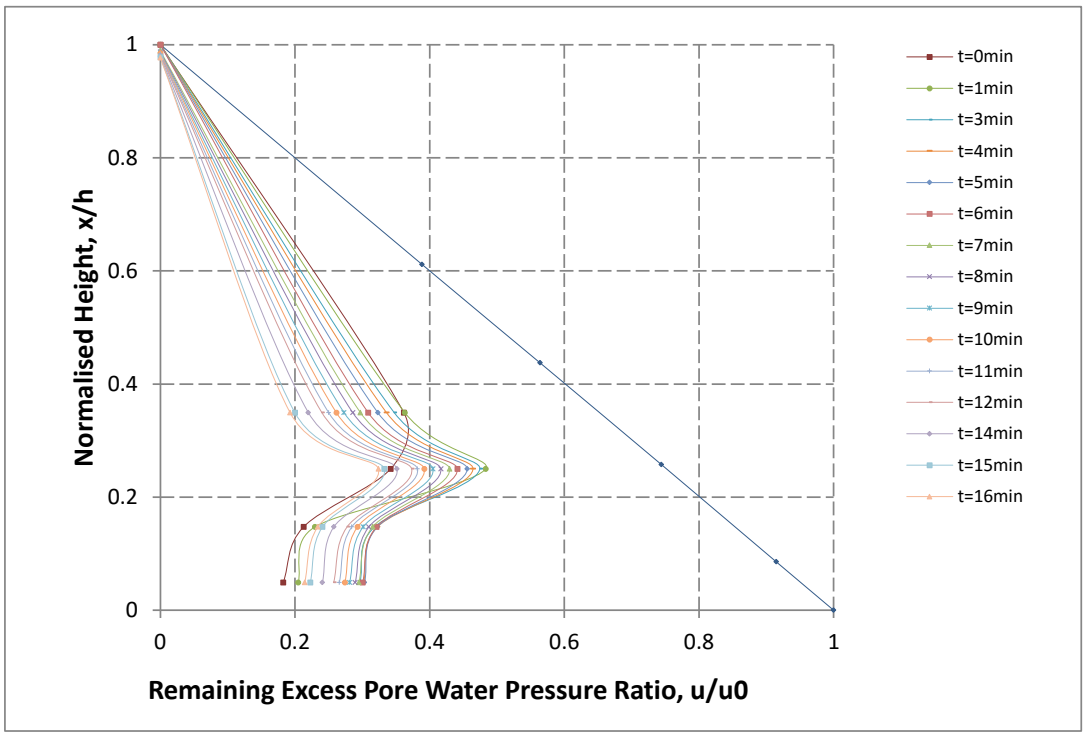

Figure 4.34c(ii): Remaining excess pore pressures ratio Experiment RoR20A pattern 1 isochrones *during first hour after deposition* - Lift 3

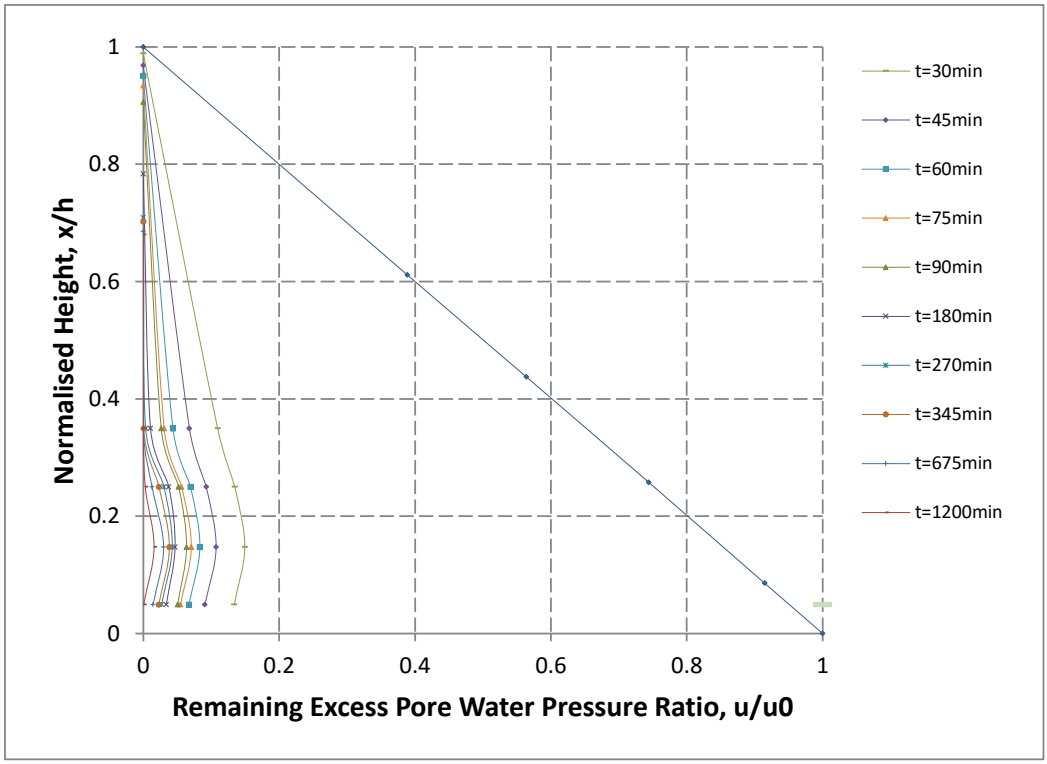

Figure 4.34c(iii): Remaining excess pore pressures ratio Experiment RoR20A pattern 2 shaped isochrones *1 to 2 hours after deposition* - Lift 3

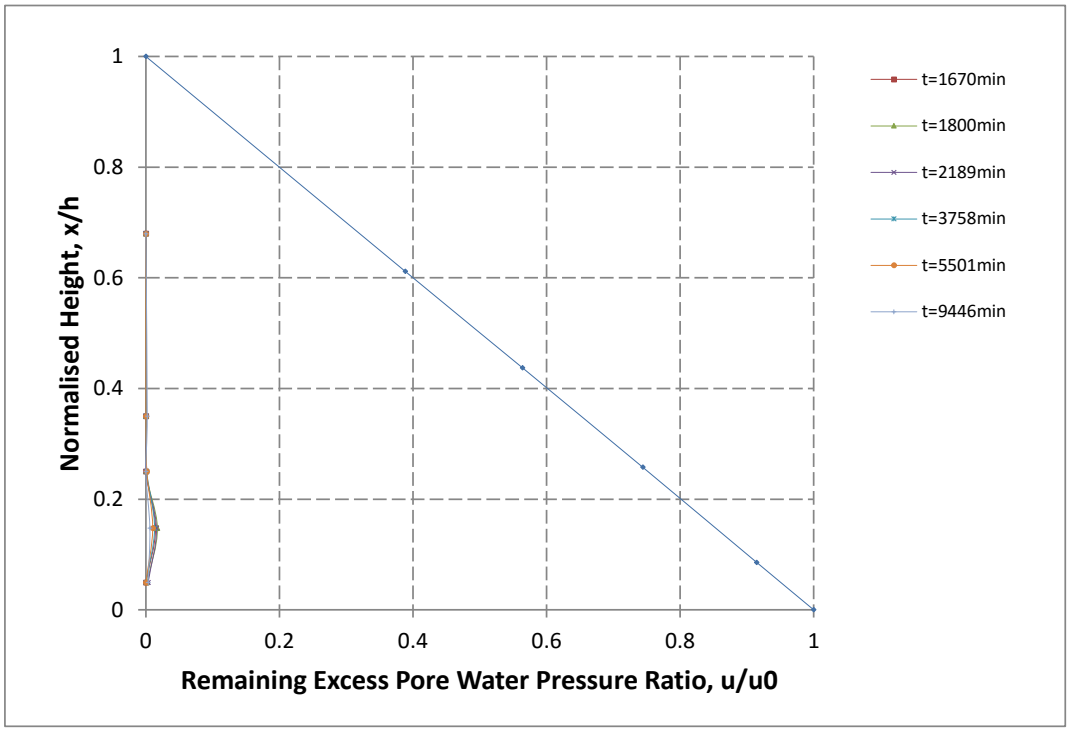

Figure 4.34c(iv): Remaining excess pore pressures ratio Experiment RoR20A pattern 3 isochrones *during consolidation stage* - Lift 3

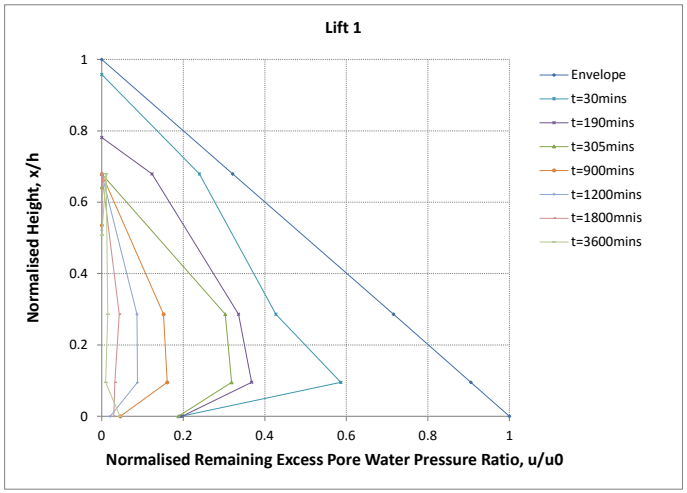

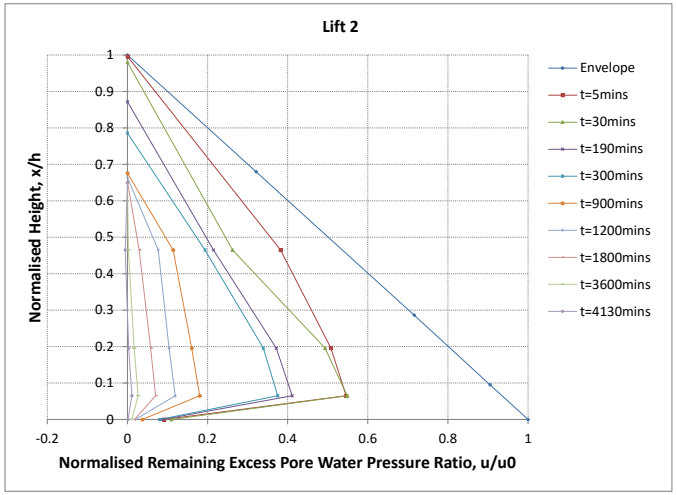

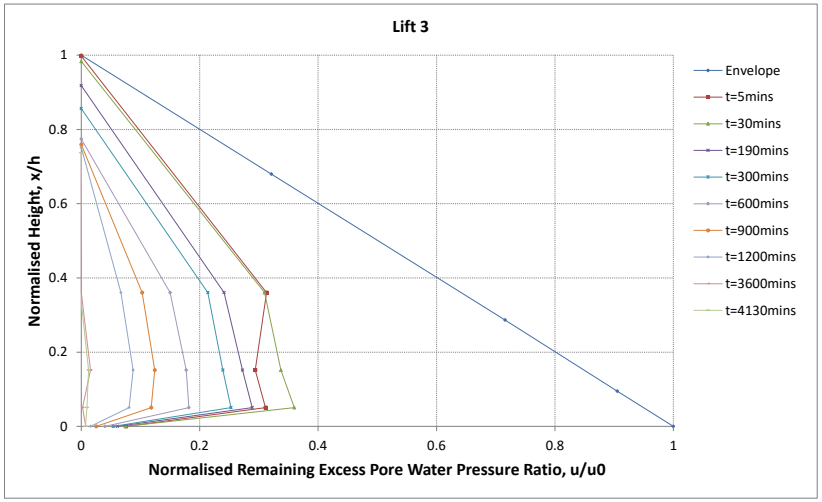

Figure 4.35: Remaining excess pore pressures ratio Experiment RoR20B

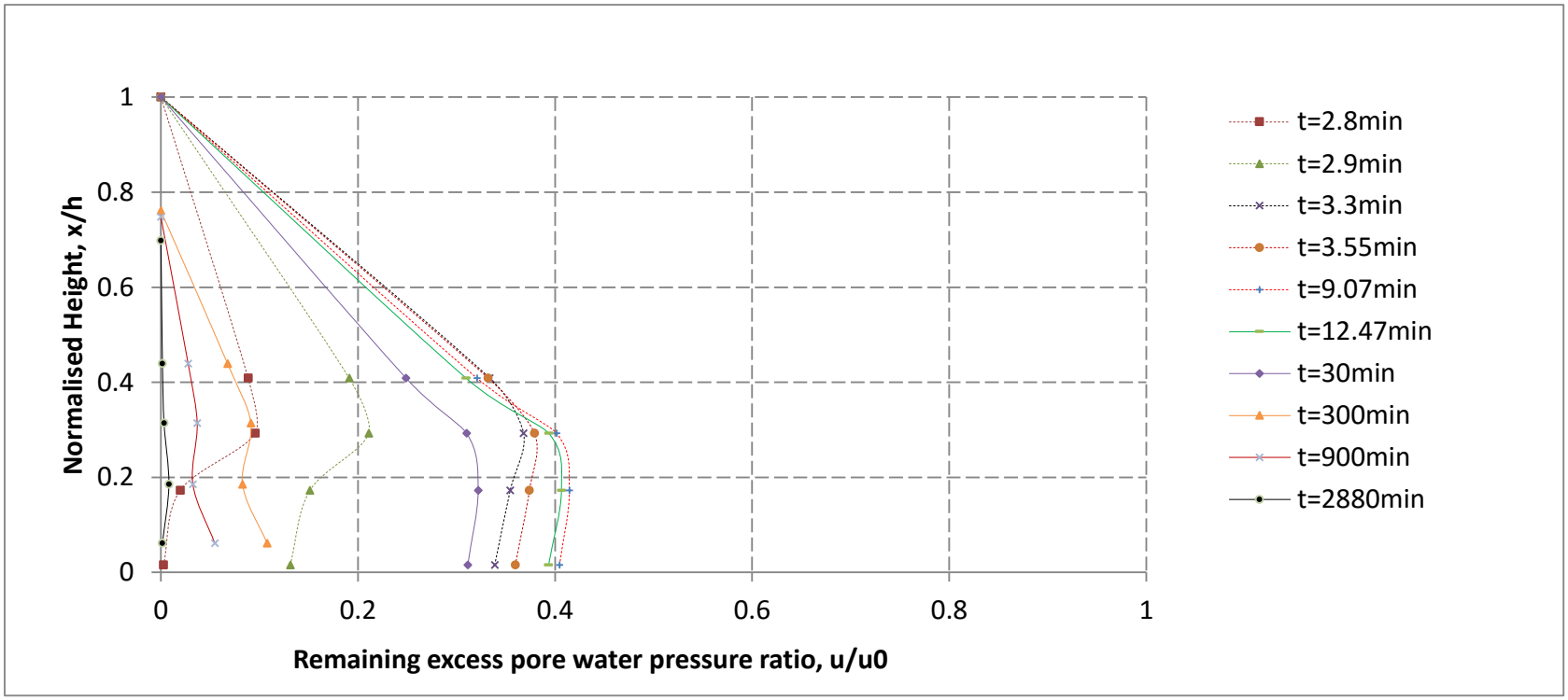

Figure 4.36a(i): Remaining excess pore pressures ratio Experiment RoR10A Lift 1 early stages

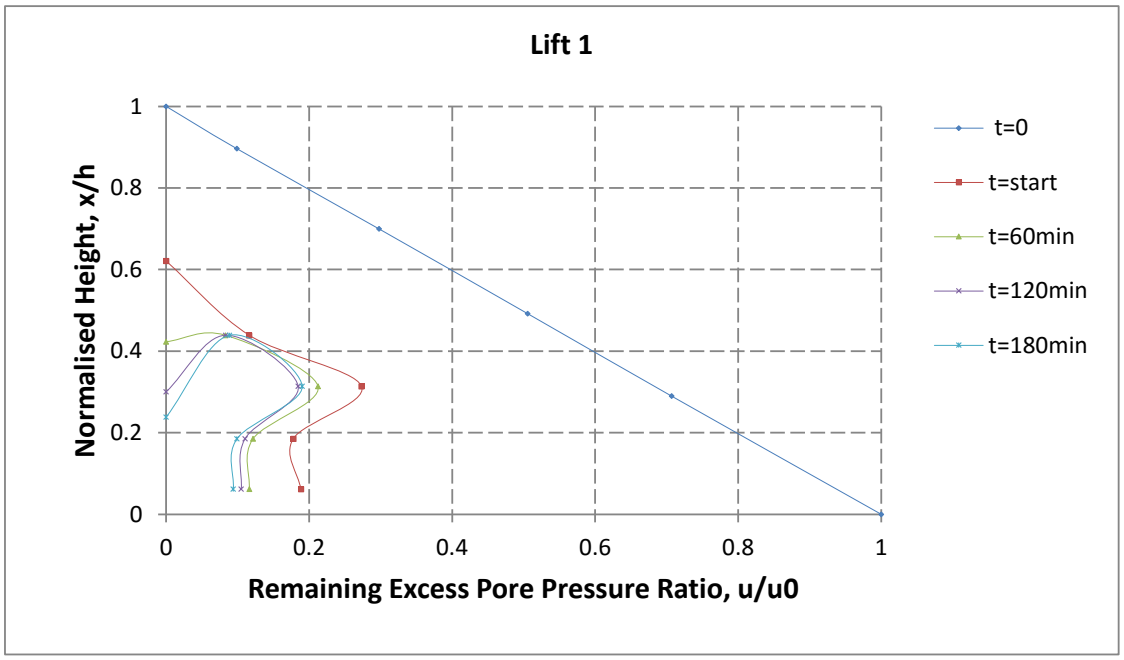

Figure 4.36a(ii): Remaining excess pore pressures ratio Experiment RoR10A Lift 1 consolidation stage

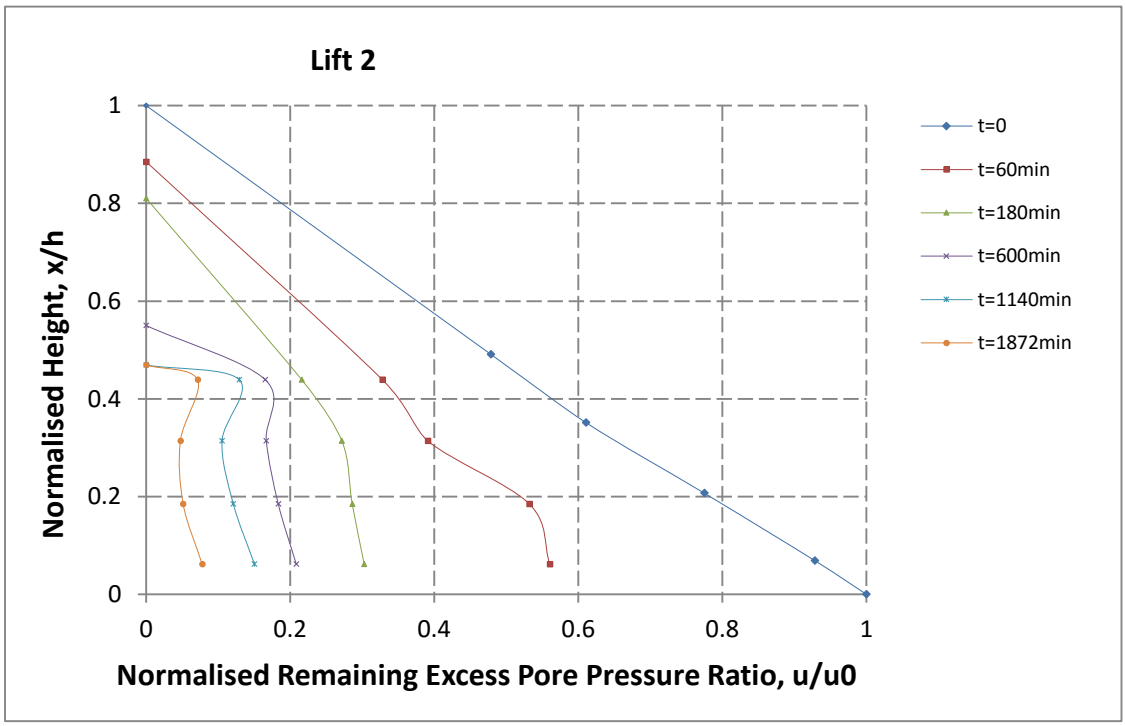

Figure 4.36b: Remaining excess pore pressures ratio Experiment RoR10A

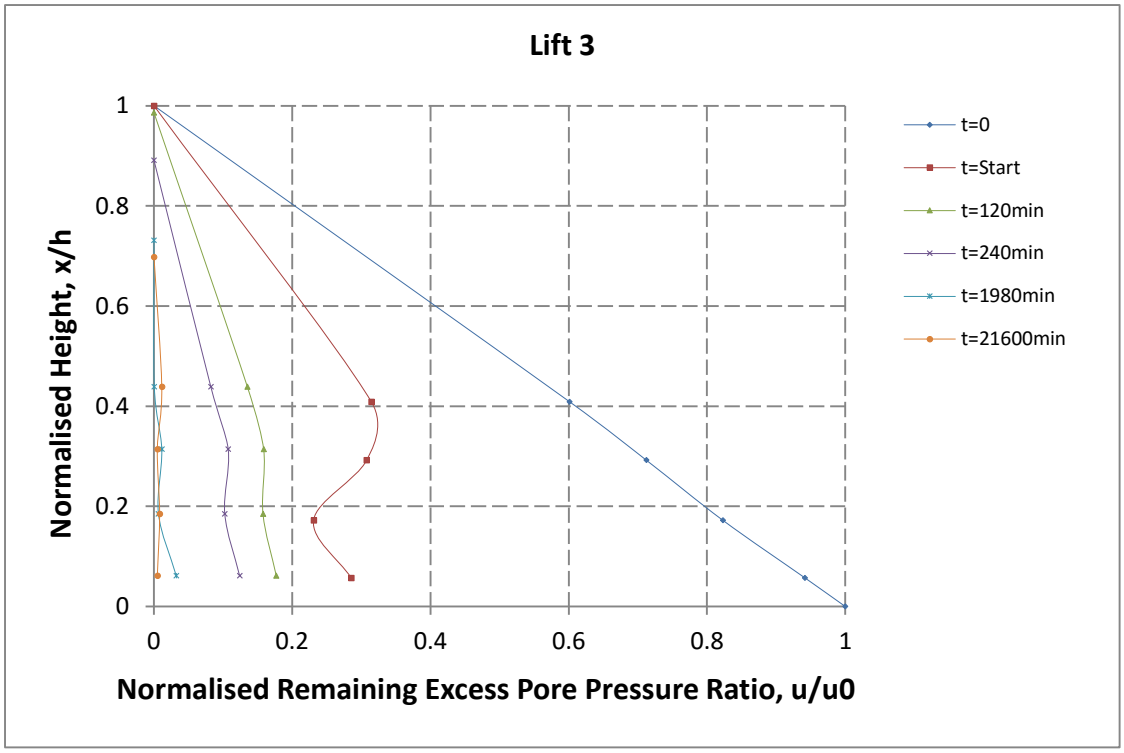

Figure 4.36c: Remaining excess pore pressures ratio Experiment RoR10A

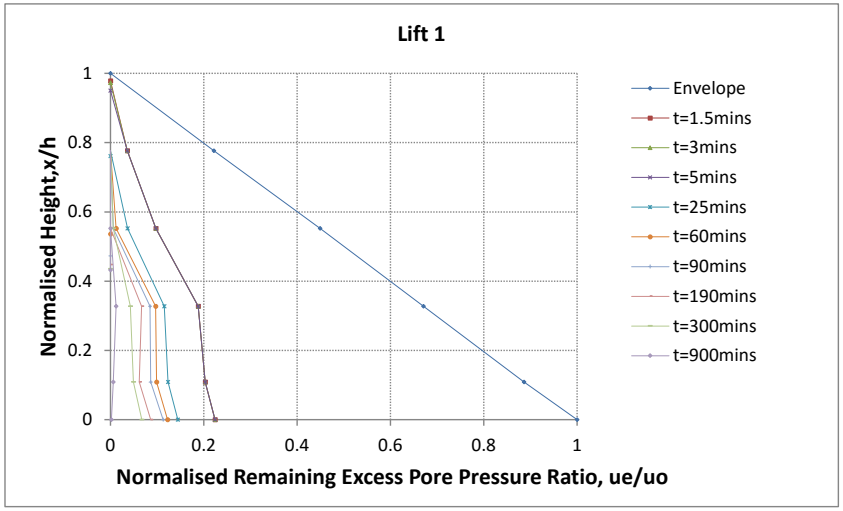

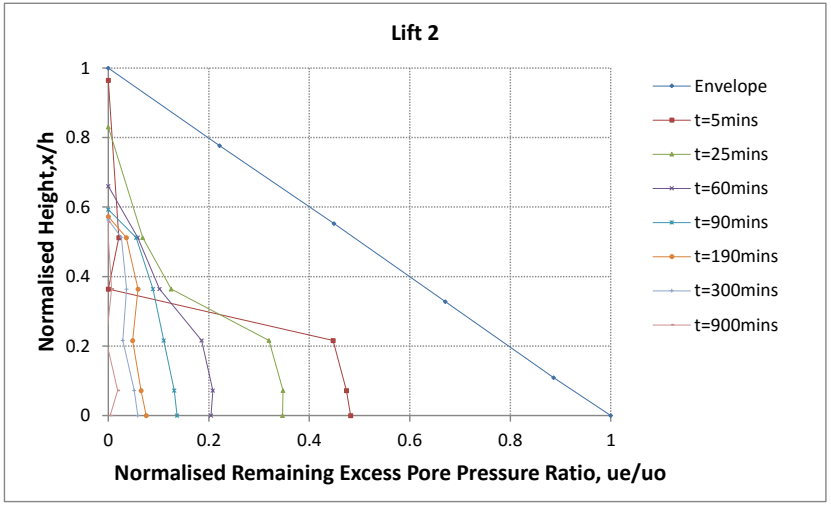

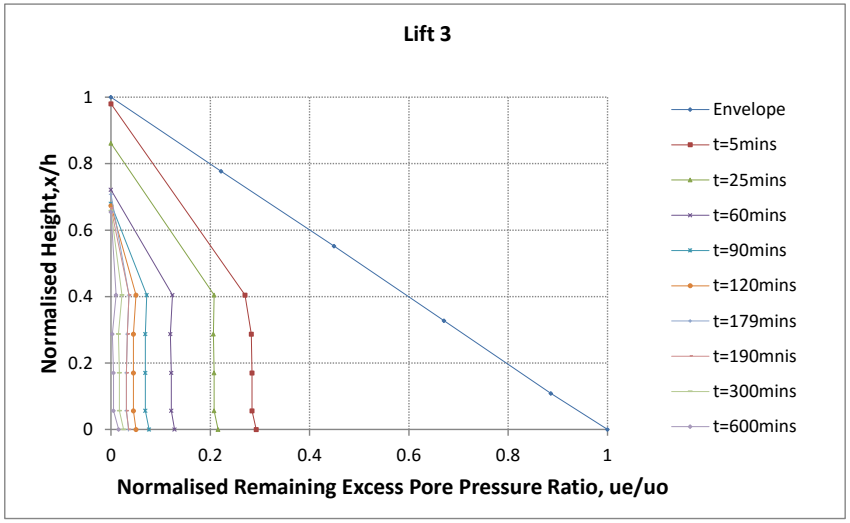

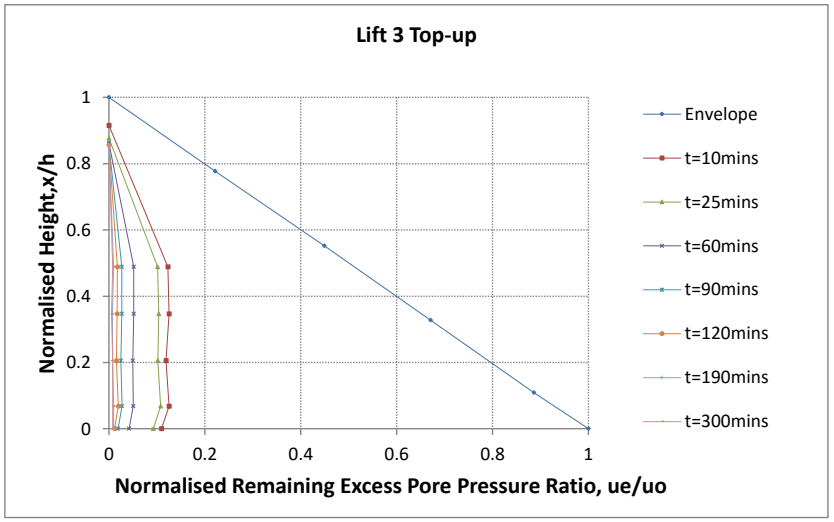

Figure 4.37: Remaining excess pore pressures ratio Experiment RoR10B

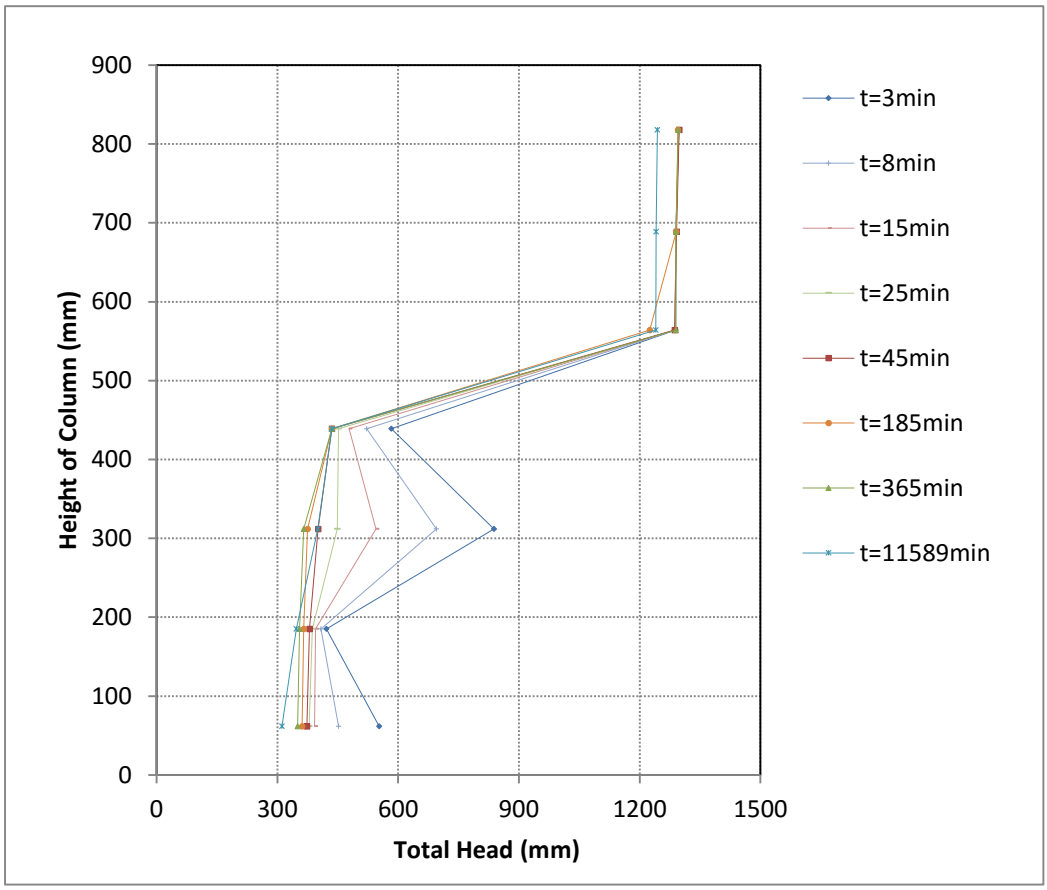

Figure 4.38: Change of constant head permeability test total head with depth Experiment FDA

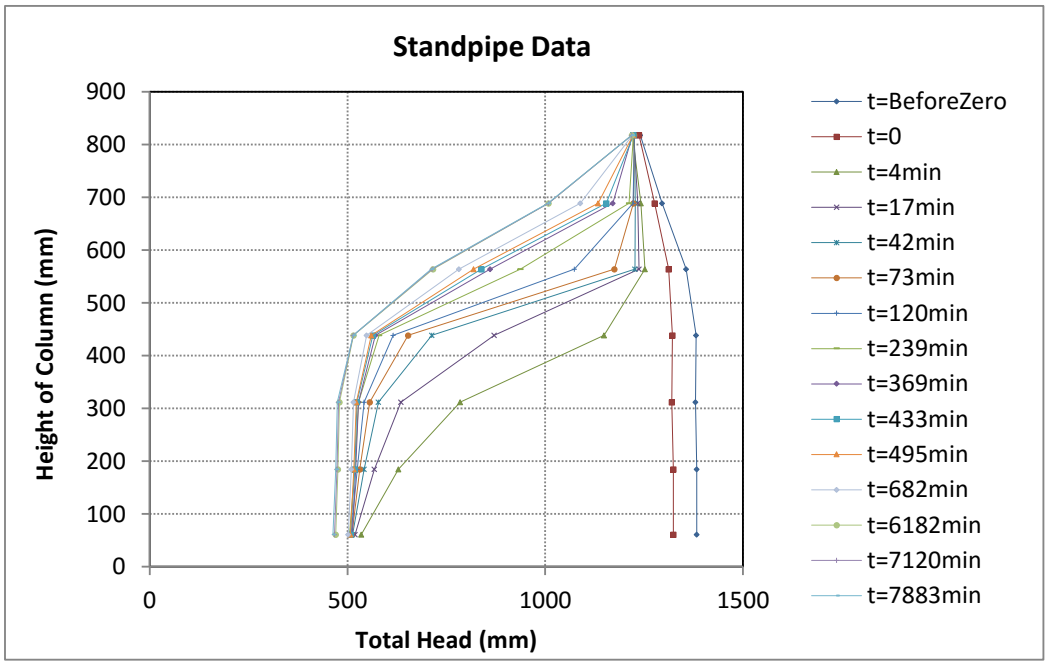

Figure 4.39: Change of constant head permeability test total head with depth Experiment FDB

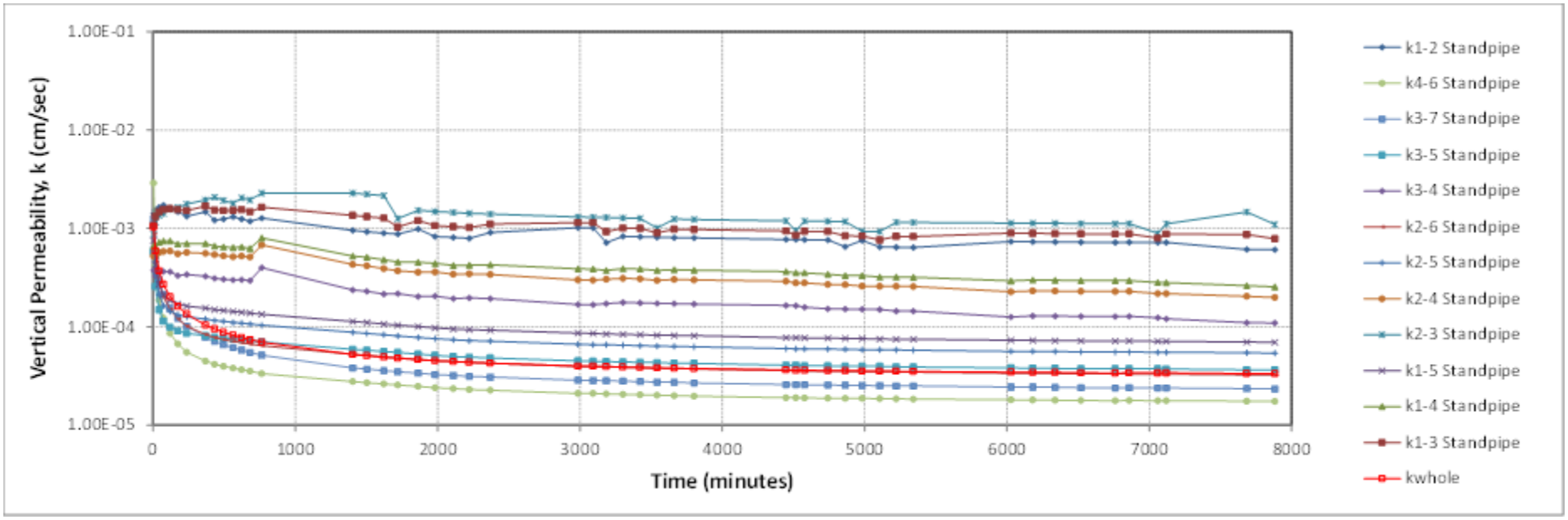

Figure 4.40: Change of permeability with depth over time Experiment FDB – standpipes data

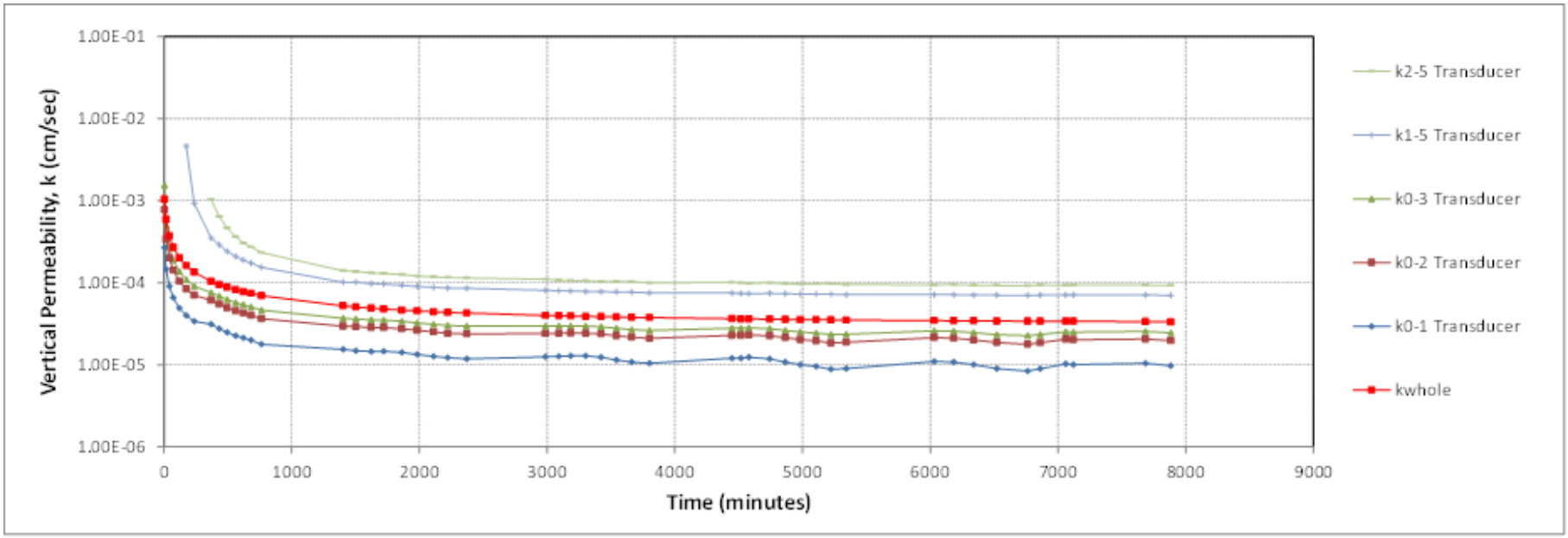

Figure 4.41: Change of permeability with depth over time Experiment FDB – standpipes and transducers data

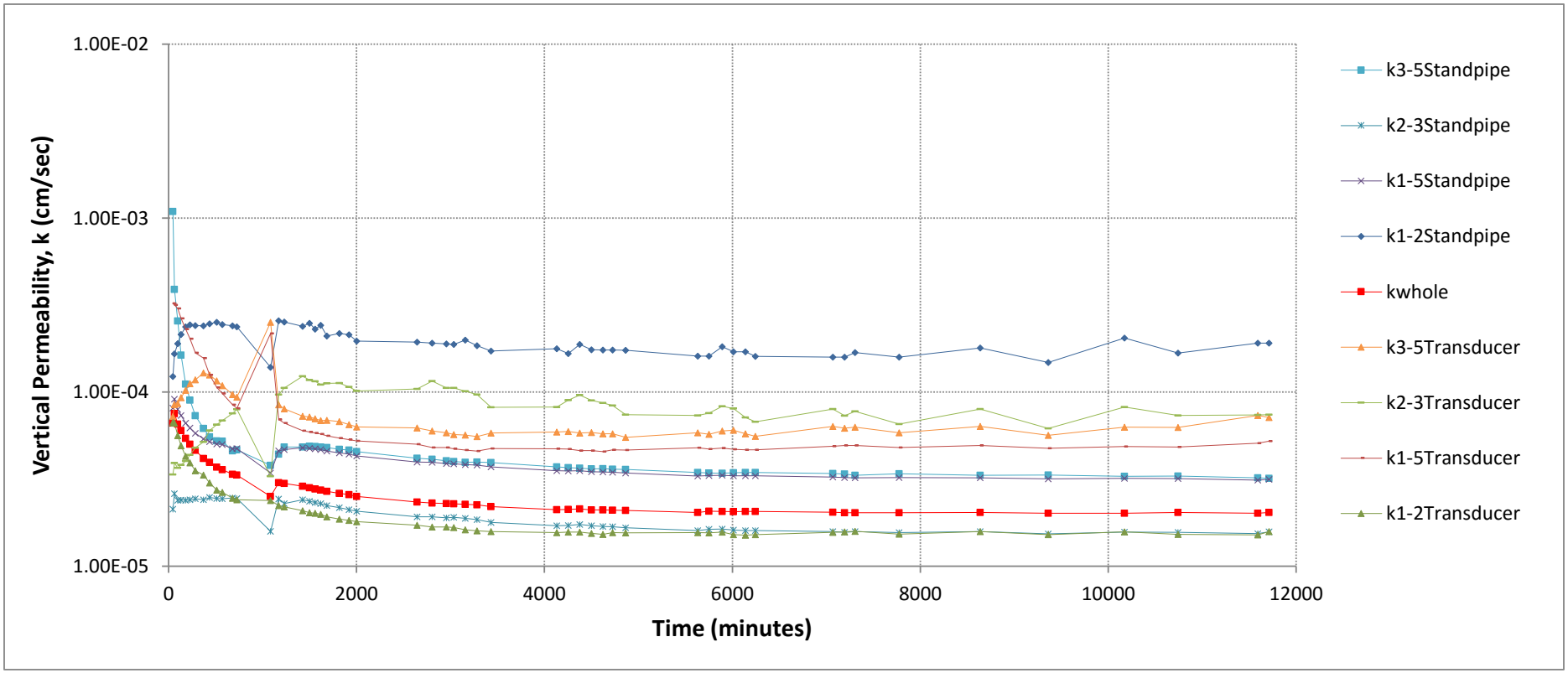

Figure 4.42: Change of permeability with depth over time Experiment RoR20B: standpipe and transducer data

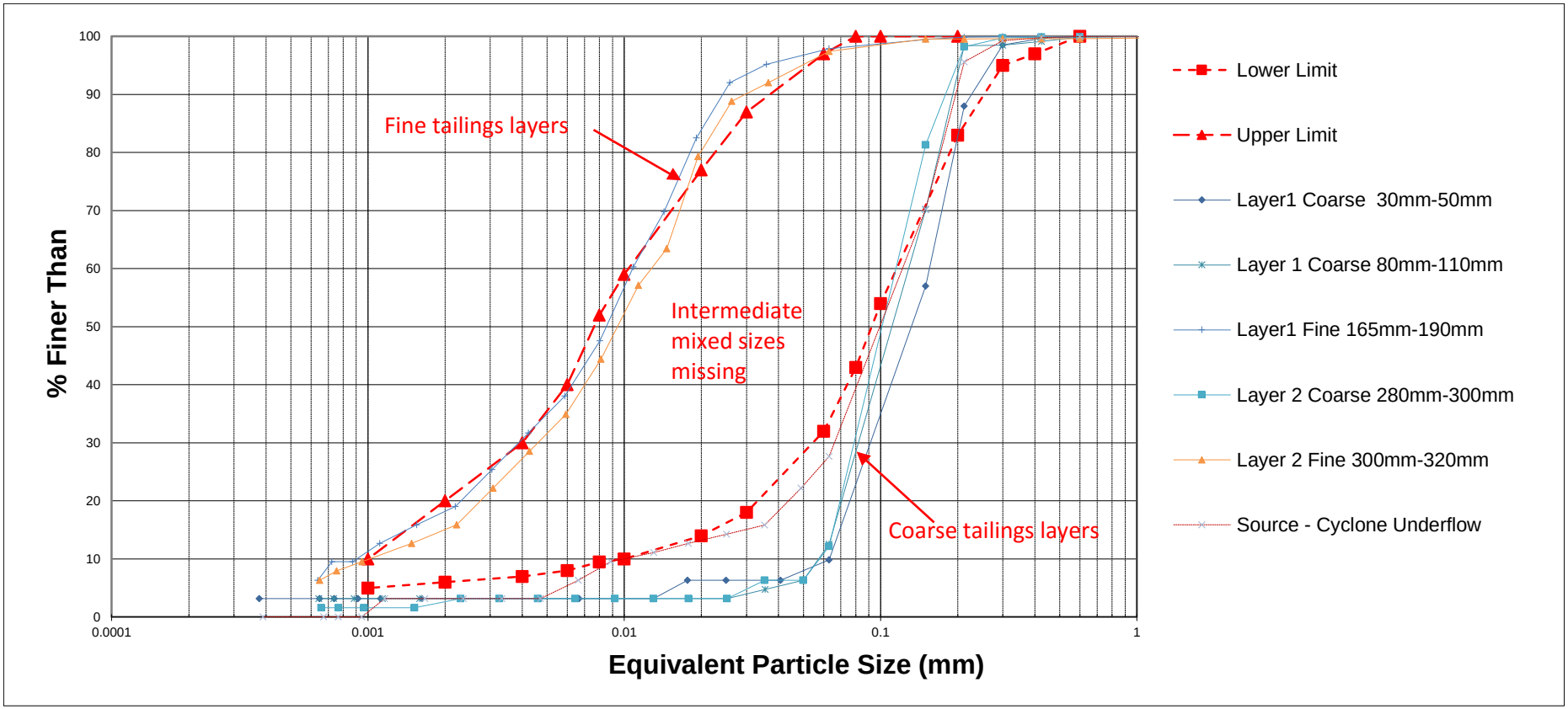

Figure 4.43: Gradations of recovered sample large interval (100mm) specimen spacing Experiment RoR10B

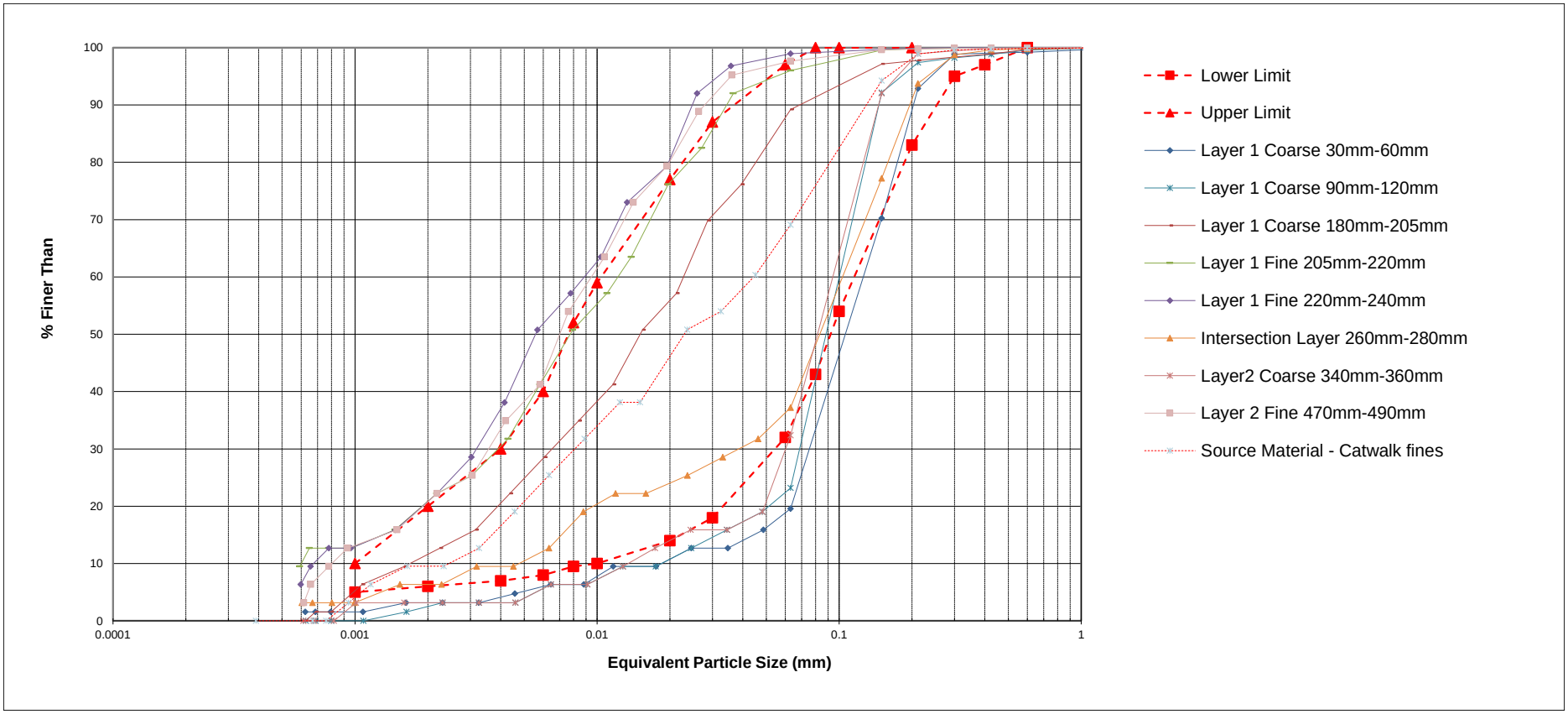

Figure 4.44: Gradations of recovered sample small interval (30mm) specimen spacing Experiment RoR20B

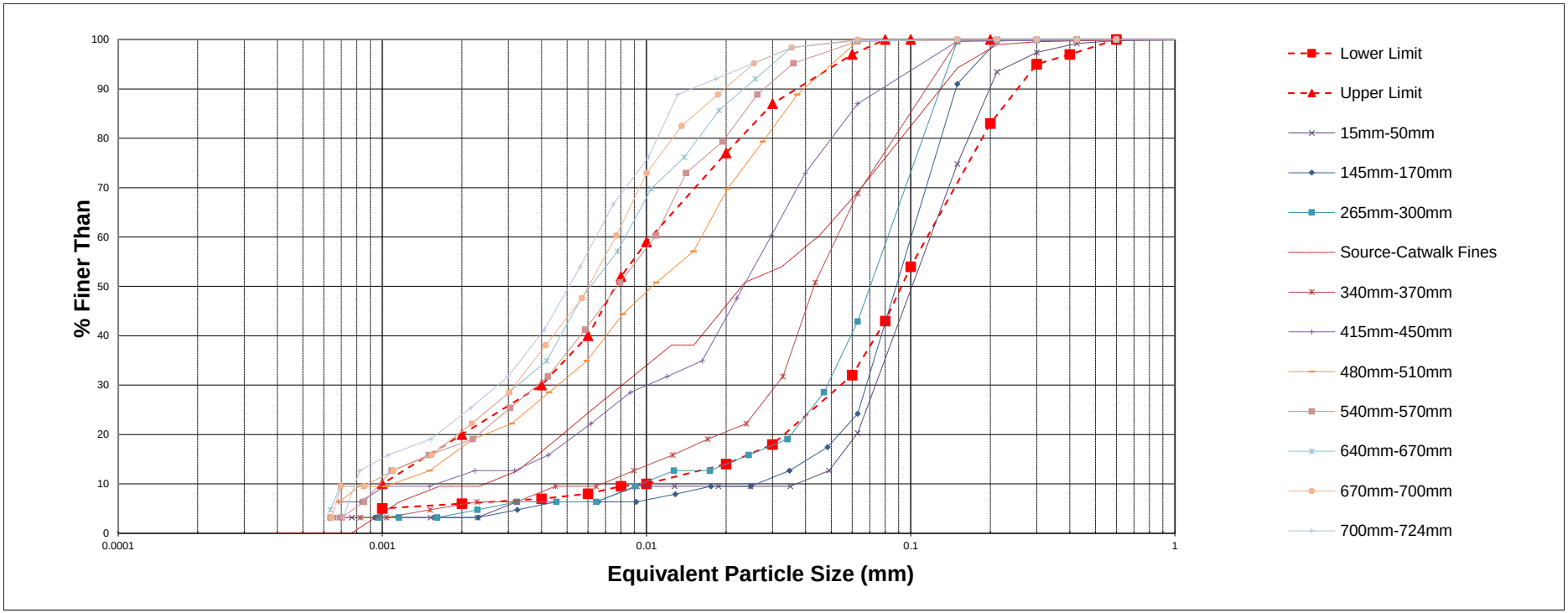

Figure 4.45: Gradations of recovered sample small interval (30mm) specimen spacing Experiment FDB

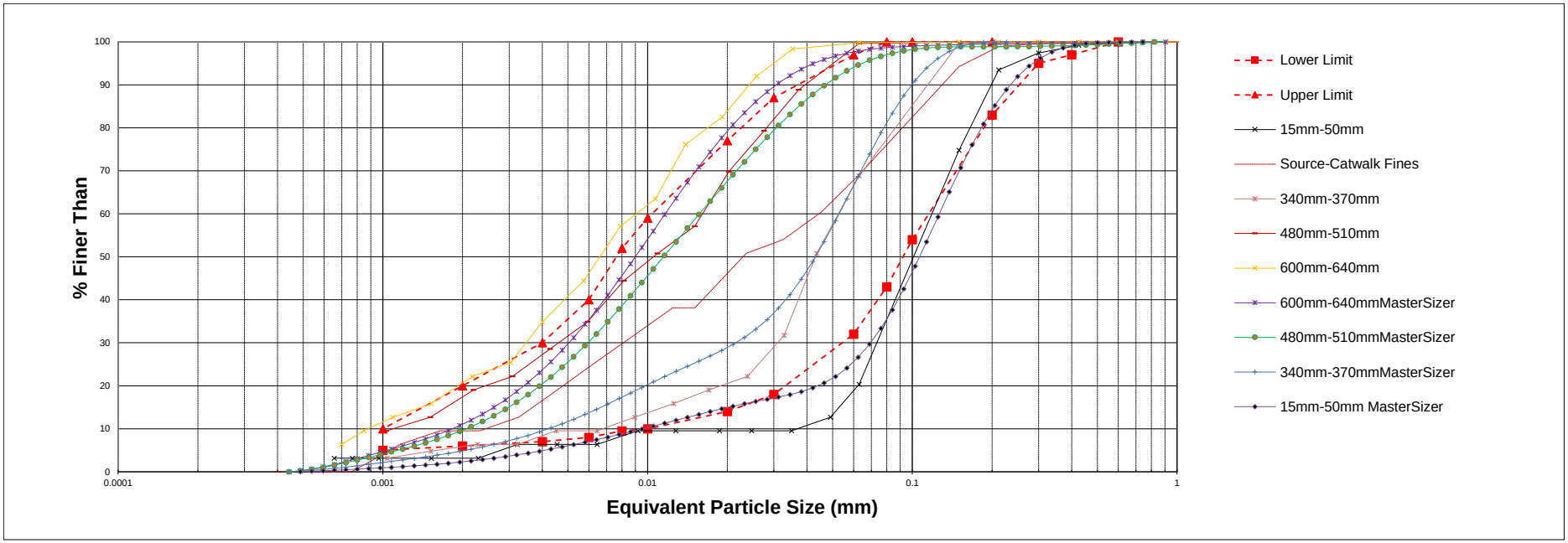

Figure 4.46: Sieve & hydrometer and Mastersizer diffraction analysis gradations of recovered sample Experiment FDB

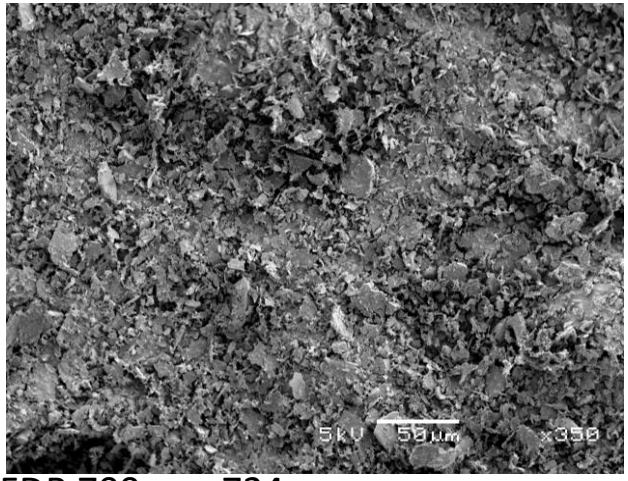

FDB 700mm-724mm

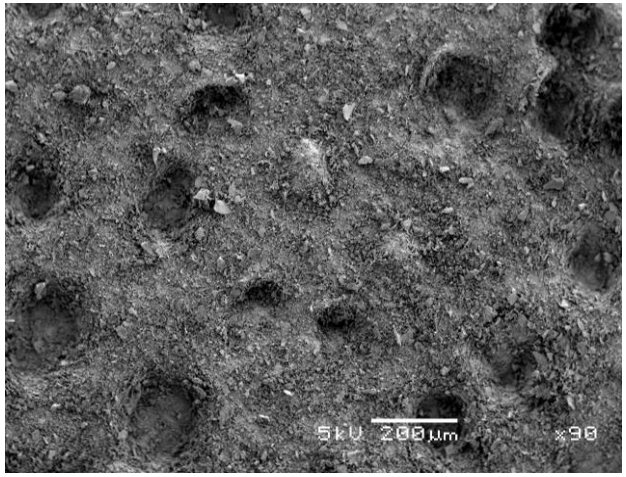

FDB 700mm-724mm

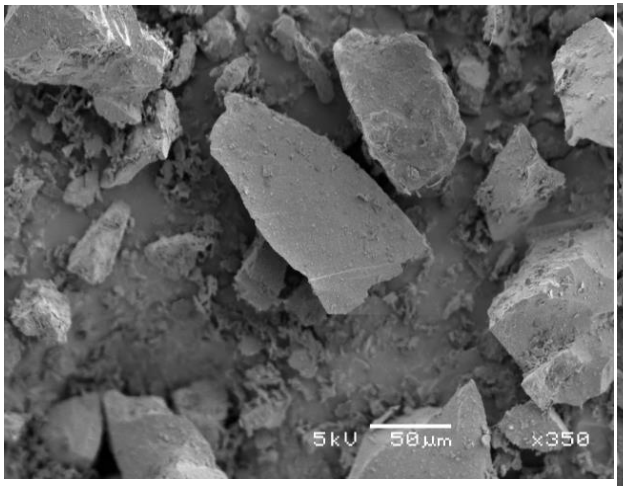

FDB 300mm-340mm

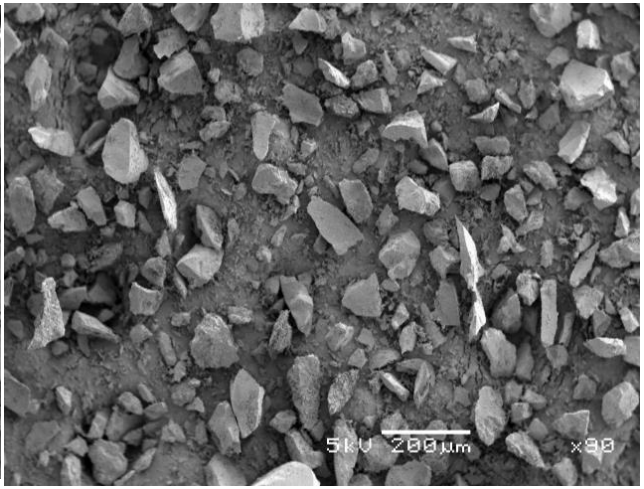

FDB 300mm-340mm

Figure 4.47: Experiment FDB SEM micrographs using carbon tape method (CT)

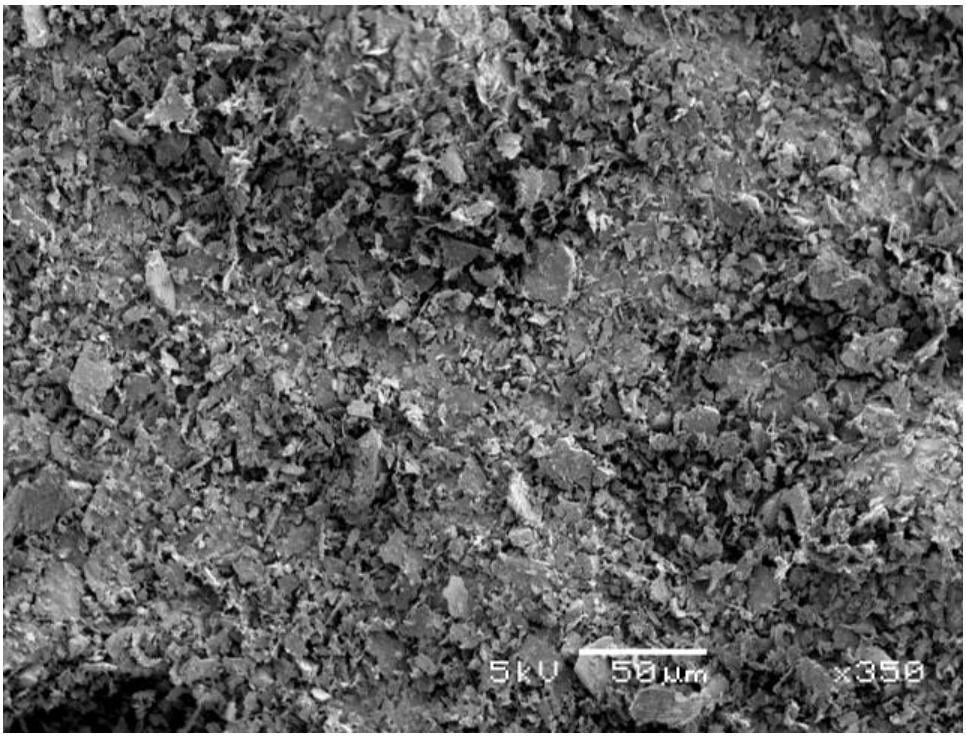

FDB 700mm-724mm

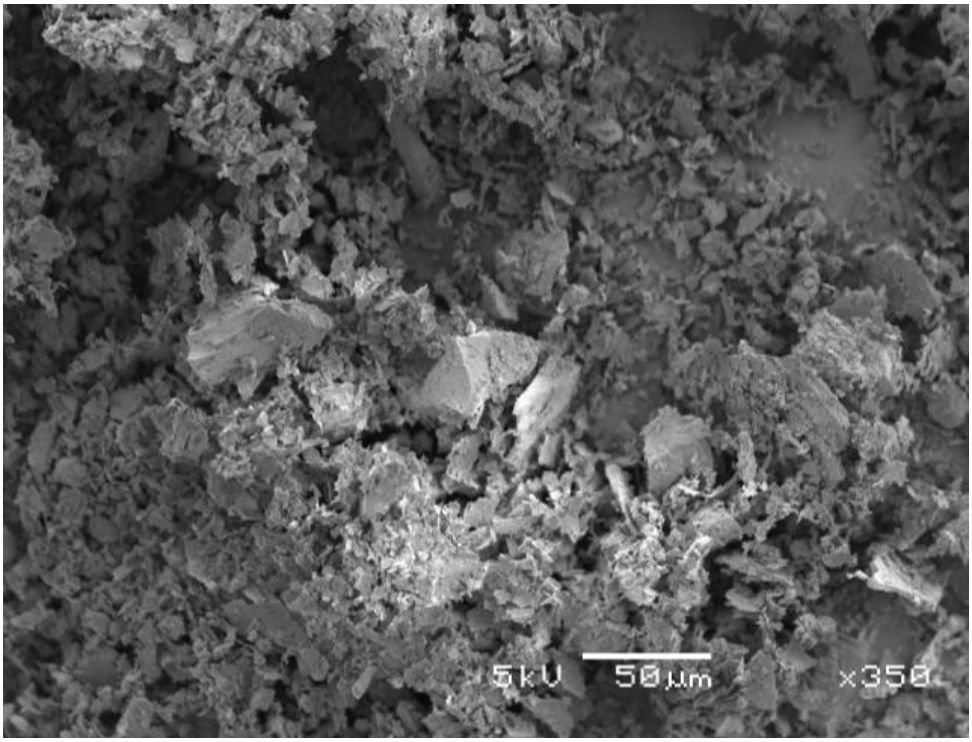

FDB 510mm-540mm

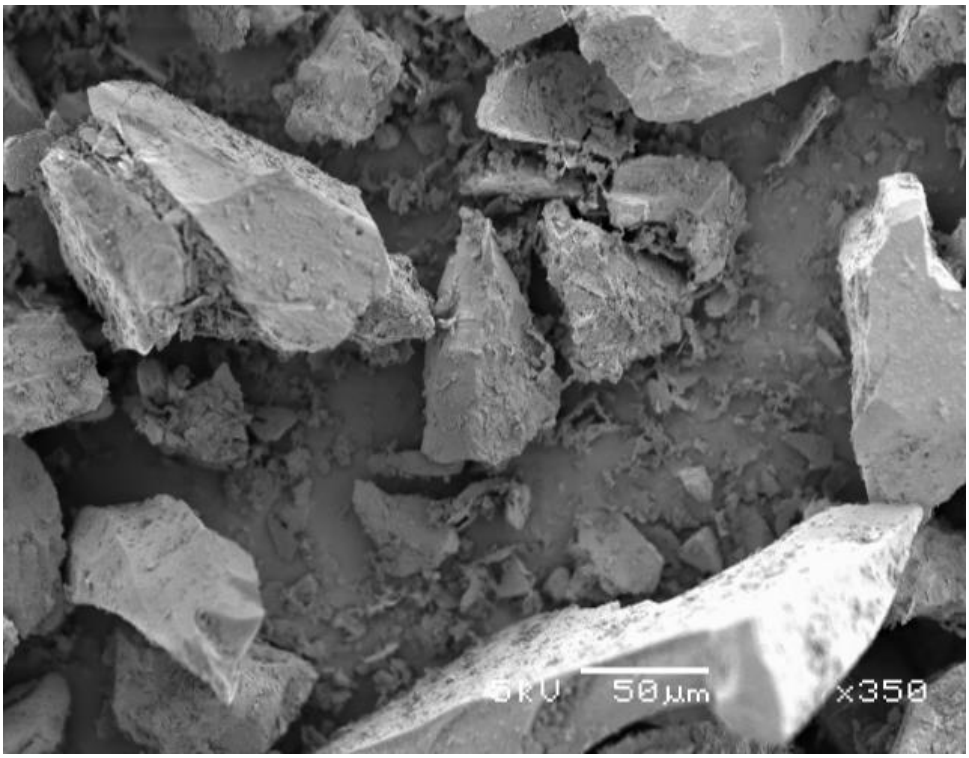

FDB 265mm-300mm

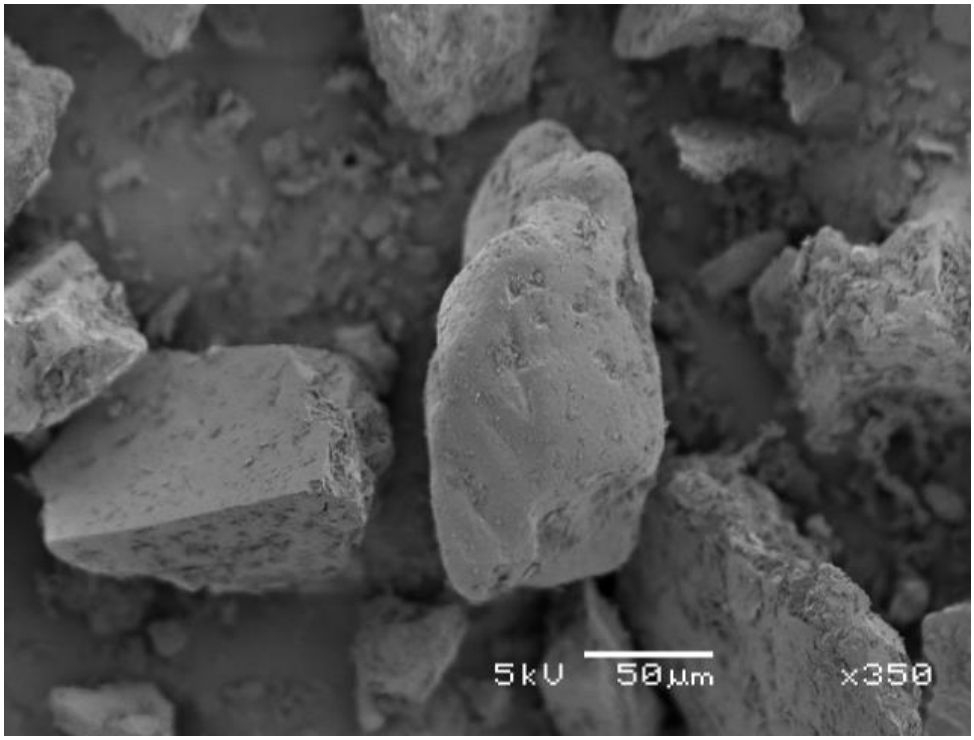

FDB 15mm-50mm

Figure 4.48: Experiment FDB micrographs (CT) depicting particle size segregation

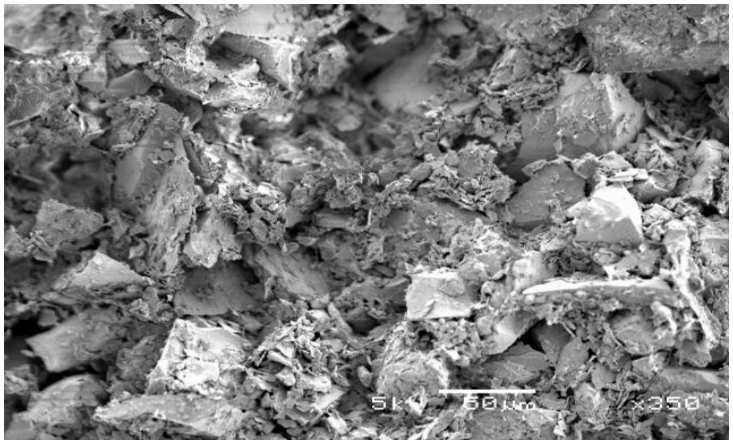

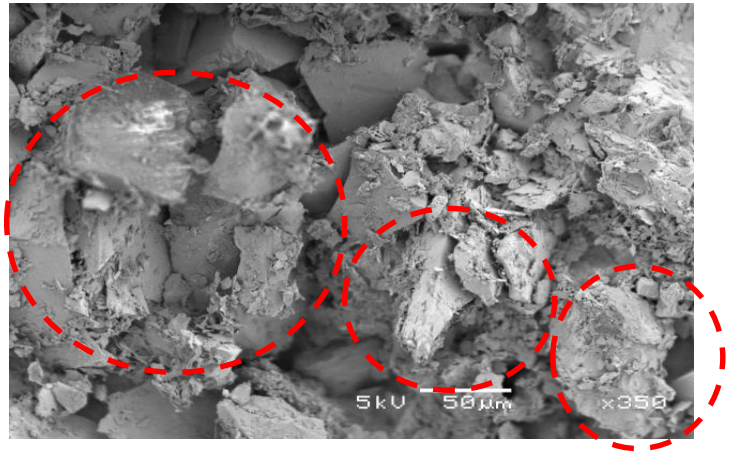

Height 300mm-340mm

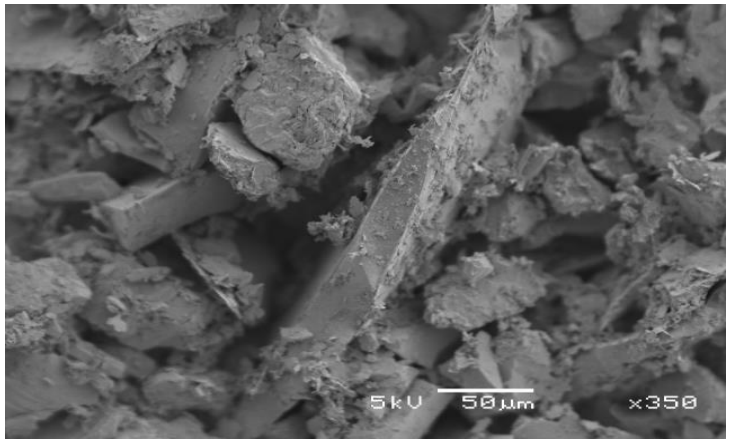

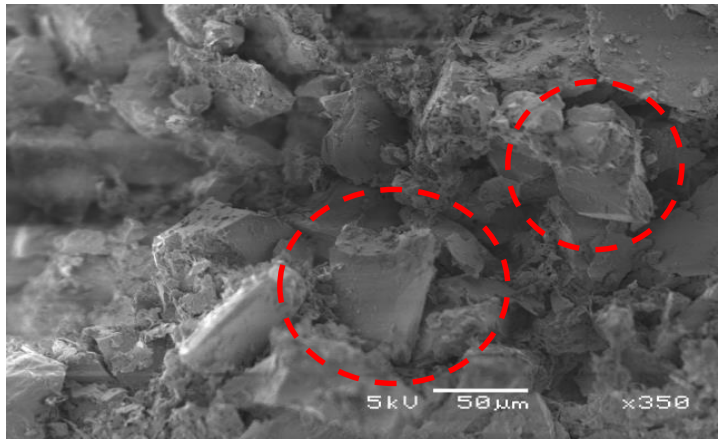

Height 265mm-300mm

Figure 4.49: Experiment FDB micrographs using carbon glue method (CG) showing horizontal (left) and vertical Prints (right)

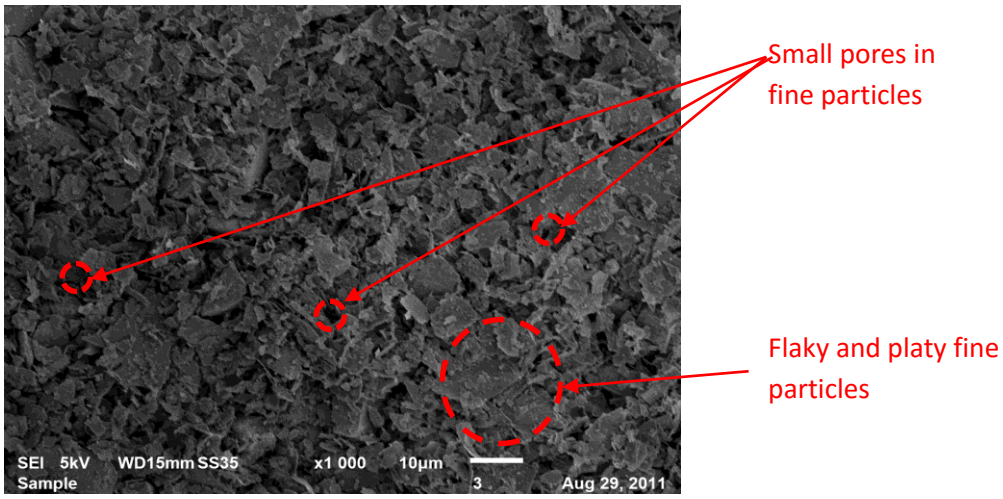

RoR10A 350mm-400mm

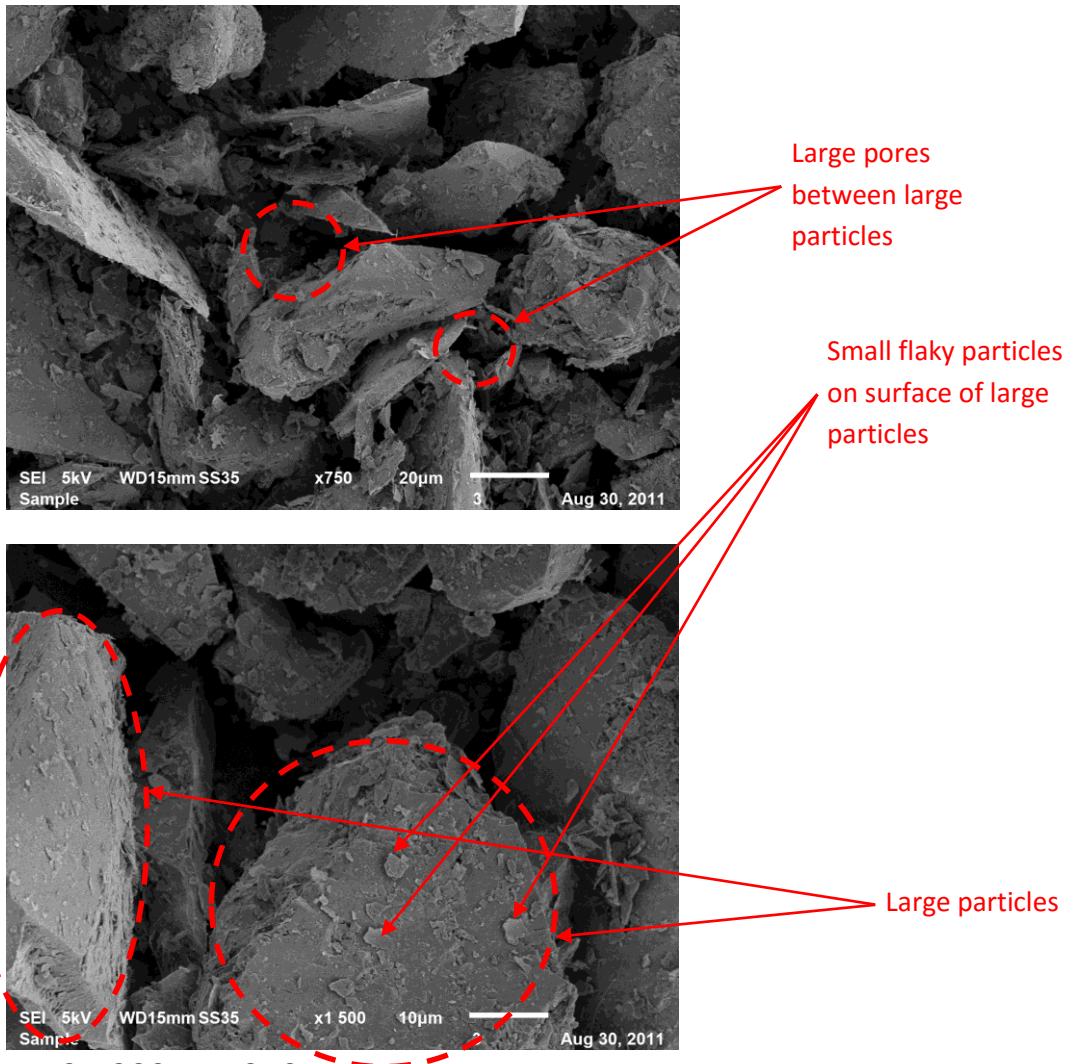

RoR10A 300mm-350mm

Figure 4.50: Experiment RoR10A micrographs (CT) depicting particle size segregation

Chapter 5

ANALYSIS OF RESULTS AND DISCUSSIONS

5.1 Introduction

The purpose of this chapter is to analyse and discuss the experimental results of the research which were tabled in Chapter 4. The analysis and discussions under this chapter aim specifically to answer the research questions concerning the linkage between excess pore water pressure and rate of rise in tailings dams and the characterisation of tailings parameters such as particle size segregation, saturated density and saturated coefficient of permeability through the use of instrumented settling column apparatus.

Chapter 5 starts with a brief discussion of the physical properties of gold tailings samples. Owing to the importance of excess pore water pressures and its relevance to the rate of rise in tailings dams for this research, the pore pressure response as a whole is analysed and discussed at length for all the experiments. The discussion and analysis covers total pore water pressure trends, degree of consolidation isochrones and normalised remaining excess pore water pressure ratio isochrones. The results of excess pore water pressure trends in relation to the time-settling characteristics of the tailings slurry are also discussed. The comparison of excess pore water pressure values with both Terzaghi (1923) and Gibson (1958) theories are also undertaken.

Chapter 5 ends with an examination of experimental results relating to particle size distribution, recovered tailings settling column fabric and the resultant permeability characteristics of the gold tailings.

5.2 Tailings and Slurry Physical Properties

The samples used in this research had a range of specific gravity of solids of 2.63 to 2.76, a liquid limit of between 19 and 48 with a non-plastic coarse tailings and a relatively high plasticity index of 13 for the Crown mines penstock tailings sample. The samples classified as ML or rock flour under the Unified soil classification system and as a silty soil A-4 under the AASHTO system.

The target relative density of the slurry prior to deposition was 1.3. The results of random samples of the slurry prepared for use in the research that was tested yielded moisture content range of 172% to 177%, a slurry specific gravity from 1.25 to 1.30 and a void ratio of 3.97 to 5.35. The coarse and fine tailings samples gradation curves straddled both the lower and upper boundaries of gold tailings gradation envelopes reported in the literature (Vermeulen, 2001 and Blight, 2010). The results of the random sampling of the tailings slurry prepared for the settling column experiments confirmed that the targeted moisture content of 172%, relative density of 1.3 and a void ratio of 4.67 were well representative of the slurries used in the experiments since the results of the random samples were close to the targeted values. The wide range in void ratio was acceptable since it only reflected the extent of segregation that took place in the samples collected for the determination of volume of the solids. The variation in void ratio therefore showed the differences in the volume of solids. This was especially so in the case of the 2010 underflow tailings sample where the coarsest fraction settled almost instantaneously.

The mineralogical compositions of the three samples depicted the predominance of the quartz mineral at around 75% by weight, followed by muscovite at 12% by weight, pyrophillite at 4%, chlorite at 3% with the remaining 6% weight made up of pyrite, dolomite, bassanite and rutile in varying quantities in the different samples.

It was observed from Figure 4.3 which analysed the mineral composition of the tailings samples that the 2010 underflow sample had slightly more quartz than the 2011 underflow sample whilst both the 2010 and 2011 samples contained smaller amounts of pyrophillites and chlorites. The 2011 sample also contained pyrites, dolomites and bassanites which were not detected in the 2010 underflow sample. The catwalk fines sample had smaller amounts of quartz and muscovites. It contained more pyrophyllites, chlorites, dolomites and bassanites than those found in the underflow samples. It however contained rutile which was not detected in either of the samples used in the research. Figure 5.1 summarises the specific gravity of solids data for the 2010 and 2011 samples. The variation in mineralogy and consequently in the specific gravity of the solids between the 2010 and 2011 samples reflects the variation of tailings materials reported by Robinson (2008). It was to be expected therefore that in a tailings dam the waste product is not uniform but changes from time to time (Robinson, 2008 and Blight, 2010).

From the particle size grading comparisons, the three samples comprised a size range starting from clay size of 0.002mm up to a medium and a coarse sand size of 0.6mm. The results indicated that what distinguished the fine catwalk tailings sample from the coarse underflow tailings samples was the particle size distribution. This meant that the size range proportions distinguished the samples rather than the maximum and minimum particle sizes of the respective samples. Table 5.1 summarises these observations. The underflow tailings comprised of almost two thirds sand and a third made up of silt which was of a coarse texture. The catwalk fines sample consisted of 75% slimes (particle sizes smaller than 75µm) and 25% sands wherein the sand was fine (38%) whilst the silt was medium to coarse (54%) in texture and a small amount of clay sized particles (8%). The penstock tailings were 100% slimes comprised mainly of medium sized silt particles. Tables 5.1 and 5.2 summarise particle size distributions of experiment and complementary samples.

The scanning electron microscope (SEM) micrographs from the three samples used in the research were viewed at selected magnifications of x90, x350 and x1500. The micrographs showed comparable particle size ranges across all the samples as well as similar particle shapes ranging from platy to rotund with some elongated particle shapes (Figure 4.4). The micrographs of the tailings that were sieved into particle size ranges shown in Figure 4.5a also confirmed the presence of various shapes within the tailings samples. The figure brought into focus the sharp edges of the tailings particles which resulted from blasting, crushing and milling of ore rock which preceded mineral processing to extract the gold valuables.

The particle size grading curves of the experiment samples (two underflow tailings samples and catwalk fines sample) as well as the complementary penstock tailings sample (Mooifontein dam in the Crown mines tailings complex) fell within and along the outer boundaries of gradation envelopes for gold tailings (Vermeulen, 2001; Blight and Bentel, 1979; Blight, 2010 and Chang, 2009). The underflow samples fell on the coarse side of the grading envelope and had very little clay (3%). It ranged through the silt and sand sizes up to medium/coarse sand size. The catwalk fines sample fell into the middle of the gradation envelope with the penstock tailings sample close to tailings gradation envelope's fine particles boundary (grading fines limit). The grading fines limit defines the grading envelope on its side with the smallest particle sizes as defined in published literature. The grading coarse particles limit was defined in a similar manner (Figure 4.1). The penstock tailings and the catwalk fines ranged from clay size (7-13%) through silt sizes up to fine sand size. The penstock tailings clearly represented the

worst case scenario in terms of a fine tailings sample located along the particle size distribution's fines limit. In a well-constructed dam, however, such fine tailings should be found in the pond and well away from the daywall. The underflow and catwalk tailings samples selected for use in this research were however more representative of gold tailings found on the beach and at the daywall of gold tailings dams. The outcomes of the research should therefore adequately answer the posed research questions since the samples are reasonably distributed within the gradation envelope of gold tailings as widely reported in literature.

Table 5.1: Particle size range proportions of sample (%)

	Tailings Samples					
Particle Size Range (mm)	Underflow Tailings 2010	Underflow Tailings 2011	Catwalk Tailings 2011	Penstock Tailings 2009	Overflow Tailings 2011	Whole Tailings 2011
>0.6mm (Coarse sand)	0	0	0	0	1	0
0.2mm-0.6mm (Medium sand)	10	10	4	0	2	3
0.06mm-0.2mm (Fine sand)	58	63	34	0	46	34
0.02mm-0.06mm (Coarse silt)	19	15	25	12	40	23
0.006mm-0.02mm (Medium silt)	7	7	20	47	7	17
0.002mm-0.006mm (Fine Silt)	6	2	9	28	3	13
<0.002mm (Clay)	0	3	8	14	0	10
Totals	**100**	**100**	**100**	**100**	**100**	**100**

Table 5.2: Gradation composition of tailings samples

	Underflow Tailings 2010	Underflow Tailings 2011	Catwalk Fines 2011	Penstock Tailings 2009	Overflow Tailings 2011	Whole Tailings 2011
Sand	68	73	38	0	50	37
Silt	32	24	54	87	50	53
Clay	0	3	8	13	0	10
Slimes	54	38	72	100	76	75
Coarse Tailings	46	62	28	0	24	25

The coefficient of curvature, C_z, of all the samples fell within the range of 1 to 3 which showed that the samples were well-graded (Knappett and Craig, 2012 and Chang, 2009). The uniformity coefficient, C_u, of all the samples used in the research were below a C_u of 36 which according to Chang (2009) meant the voids between the coarse particles were filled with fines whereby there was limited coarse particles contact in the samples. Chang (2009) also pointed out that Fullers curve was applicable to spherical particles whilst tailings particles tended to be platy and elongated as seen from SEM micrographs. It was more likely therefore that in the tailings samples coarse particles contact was predominant given their shapes.

The specific gravity of the tailings solid particles, the plasticity index and the classification of the tailings samples for this research agreed well with those reported by Vermeulen (2001) and Chang (2009). The samples used were therefore representative of gold tailings.

5.3 Excess Pore Water Pressure Response

5.3.1 Introduction

The subsection discusses the excess pore water pressure response observed from the experimental results and undertakes comparison of the results with approximations obtained

from Terzaghi's one dimensional consolidation theory. Excess pore water pressure build-up times, excess pore water pressure trends and excess pore water pressure dissipation isochrones shapes are evaluated. Correlation between soil interface height changes over time with excess pore water pressure dissipation was examined. Settling column results were also compared with Terzaghi (1923) consolidation theory. No comparisons were made with Gibson (1958) consolidation theory. The values of the increasing deposition rate (m) specified in the Gibson (1958) theory could not be determined from the settling column test results carried out under this research.

5.3.2 Excess pore water pressure build up times

When all the required slurry was deposited into the settling column for a given experiment it was noted that both transducers and standpipes did not immediately record maximum excess pore water pressures. The excess pore water pressures were observed to initially build up to maximum values following which excess pore water pressure dissipation became apparent. This section discusses the build-up of excess pore water pressures prior to excess pore water pressure dissipation.

Figures 4.32a, 4.34c(i) and 4.36a(i) show excess pore water pressure build up for Experiments FDA, RoR20A and RoR10A. Experiment FDA excess pore water pressure build-up was complete in about 3 minutes. Experiments RoR20A and RoR10A third deposition lifts of slurry had excess pore water pressure build-up times of slightly more than 3 minutes and 9 minutes respectively. The build-up time of excess pore water pressure for Experiment RoR10A was longer. The longer time taken for the excess pore water pressures to build-up in the latter deposition of the experiment is speculated to have arisen from reduced response times of the standpipes and transducers due to previously deposited layers.

In Figure 4.32a it is shown that from the start of the experiment following the deposition of the tailings, excess pore water pressures built-up with the isochrones at 1.6 minutes and 1.7 minutes showing the very fast excess pore pressure build up from 23% to 89% of the total excess pore water pressures. The percentage excess pore water pressure build up is calculated as the area under the isochrones in Figure 4.32a. It is shown that at 3 minutes dissipation of the excess pore water pressure had started. The dissipation of the excess pore water pressures then continued with 38% of the excess pore water pressures dissipated in 10 minutes and 68%

dissipation after 30 minutes measured from the start of the experiment. Dissipation rate of excess pore water pressures was observed to have slowed down significantly with 82% dissipated after 2.4hrs and 90% dissipation of excess pore water pressures occurring after 10hrs. The remaining 10% of excess pore water pressures dissipated after 2 days. After 1.93 days 2% of the excess pore water pressures had not dissipated.

In Figure 4.34c(i) which shows data for Experiment RoR20A Lift 3, the excess pore water pressure build-up went up to the 3rd minute from the start of the experiment. Dissipation started during the 3rd minute and is shown to be in progress by the 9th minute. Figure 4.36a(i) shows Experiment RoR10A Lift 3 where the excess pore water pressure build-up is depicted to have been in progress between the 2nd and the 9th minute. Dissipation of excess pore water pressure is shown to have commenced by the 12th minute. In relating the results from the study with consolidation theories it was noted that consolidation theories emphasise dissipation of excess pore water pressures rather than excess pore pressure build up which is considered to take place instantaneously. It is noted from the results that whilst excess pore water pressure builds up quickly it is also likely to overlap with dissipation in tailings dams.

Following the build-up of pore water pressure, maximum excess pore water pressures were attained. Figure 5.2 shows the relative magnitudes of the maximum excess pore water pressures generated in Experiments FDA, FDB, RoR20A, RoR20B and RoR10A. The figure shows maximum excess pore water pressures reached following slurry deposition under the experiments. Figure 5.2a compares the maximum initial excess pore water pressures in the 2010 underflow tailings (Experiments FDA, RoR20A and RoR10A). Figure 5.2b shows similar data for the 2011 catwalk fines tailings sample (Experiments FDB and RoR20B). The full depth deposition experiments generated higher excess pore water pressures followed by the 20m/yr rate of rise deposited tailings at 50% of the excess pore water pressures generated in the full depth deposition. The 10m/yr rate of rise deposited tailings generated less than 30% of the magnitudes of excess pore water pressures generated by the full depth deposition. In Figure 5.2b it is also apparent that maximum excess pore water pressures generated at 20m/yr rate of rise reach 50% of the full depth deposition excess pore water pressures for fine tailings as well. A lower rate of rise of 2m/yr to 3m/yr as specified in the South African Chamber of Mines Guidelines (1996) and currently used in practice would generate far much less magnitudes of excess pore water pressures under similar experimental conditions. The implication for tailings dams construction practice, where tailings layer thickness of up to 250mm are deposited at a

given time, is that maximum excess pore water pressures will be generated within less than 15 minutes of their deposition. This effectively means that the generation of maximum excess pore water pressures which is completed within the short time following layer deposition is not likely to limit both rate of rise and deposition rate.

5.3.3 Excess Pore Water Pressure Trends

Excess pore water pressure trends were observed to change continuously over time for all experiments (Figures 4.16 to 4.19 and Appendix E). Arbitrary times were therefore selected at which to compare excess pore water pressure values of the experiments. Excess pore water pressure trends were analysed for the first 10hrs of slurry deposition lift under each experiment. It was noted that excess pore water pressure of high magnitudes dissipated within the first 10hrs after slurry deposition. The excess pore water pressure trends were evaluated at 1hr, 4hrs and at 10hrs from the start of slurry deposition for comparison purposes. It was expected that the excess pore water pressure trends were to follow a pattern where Transducers 1 and 2 showed the highest excess pore water pressures in that order while Transducers 3 and 4 showed the lowest excess pore water pressure magnitudes (See Figures 3.16 and 3.17 for elevations of pore pressure transducers and standpipes). Transducer 3 was expected to record high excess pore water pressures than Transducer 4. This pattern of excess pore water pressure was expected because transducers located at the bottom of the settling column (Transducers 1 and 2) measured voltages that were representative of high pore water pressures experienced by the pore water due to the weight of slurry above the transducers located at the bottom of the settling column. The pore pressure measurements by the transducers located at the top half of the settling column (Transducers 3 and 4), on the contrary corresponded with pore water experiencing less weight of deposited tailings that should generate low pore pressures by virtue of less weight of deposited tailings at these locations. In this thesis excess pore water pressures where the values of the excess pore water pressures are proportional to the weight of tailings slurries above a given elevation in the settling column constituted expected pore water pressure trends. The expected trends were therefore in accordance with Terzaghi (1923) consolidation theory. The pore water trends contrary to the above described pattern were considered unexpected trends. In the unexpected excess pore water pressure trends, the transducers placed high up on the settling column depicted voltages reflecting high excess pore pressures which could not be explained in terms of the weight of the slurry at the given elevations. Under unexpected trends low excess pore water pressures were associated with transducers located

near the bottom of the settling column which corresponded with more tailings slurry weight and should have reflected high excess pore water pressures.

Figures 4.16a and 4.16b showed excess pore water pressure response from four transducers of Experiment FDA under which both expected and unexpected excess pore water pressure trends were observed. Figure 4.16b show excess pore water pressure trends for the first 600 minutes of the experiment. During the first 40 minutes the four transducers exhibited expected excess pore water pressure trends where Transducer 1 placed near the bottom of the settling column recorded one of the highest excess pore water pressure values. Transducers 2 and 3 trends closely followed Transducer 1 trend as expected if weight of slurry at a given settling column elevation was proportional to the excess pore water pressure developed at the given elevation.

Experiment FDA the pattern of unexpected excess pore water pressures was exhibited by some of the transducer data in Figures 4.16a and 4.16b (the scale of the Figure 4.16b make it difficult to observe some of the trends described). Transducer 4 (Figure 4.16b) showed the highest excess pore water pressures up to 600 minutes. This transducer recorded excess pore water pressures that were greater than those recorded by Transducer 2 and 3 yet it was located at a high elevation on the settling column in relation to the others. It was expected that Transducer 4 would record low excess pore water pressures because it corresponded to an elevation with the least weight of tailings applying pressure on the pore water at its elevation. A summary of the excess pore water pressure dissipation trends after 600 minutes is described below. After 600 minutes Transducer 4 excess pore water pressures dropped below those of Transducer 1 until the end of the experiment. Transducer 3 which at the start of the experiment closely followed Transducers 1 and 4, showed unexpected trends when it dropped below Transducer 2 which it lagged from the start of the experiment. Transducer 2 surpassed Transducer 3 (expected trend) after 1000 minutes but remained below Transducers 1 and 4 until the end of the experiment. The standpipe excess pore water pressure trends also showed unexpected excess pore water pressure trends. The pattern shown by the standpipe data however differed from the pattern shown by the corresponding transducers. The trends of the standpipes in general followed the order described below. Standpipe 3 followed by Standpipe 1 followed by standpipe 4 and Standpipe 2. Standpipe 2 had the lowest excess pore water pressure magnitudes. Whilst the magnitudes of the excess pore water pressures of the standpipes were not exactly the same as those of the transducers in the experiment, the standpipes trends were similar to those of the transducers.

In Figure 5.3 expected excess pore water pressure trends which corresponded with the weight of the tailings slurry at the elevation of the standpipes and transducers under consideration is depicted for Experiment RoR10A Lift 2. In the figure all the transducers show expected excess pore water pressure trends from the start of the deposition lift up to 16.7hrs from the start of the lift. During the 17hrs significant excess pore water pressures in terms of high magnitudes were dissipated (>0.4kPa). It is noted that beyond 17hrs from the commencement of slurry deposition, unexpected excess pore water pressure trends were observed where Transducer 4 excess pore water pressure magnitudes exceeded those of Transducers 2 and 3 which should not have been the case. It is interesting to note that the changeover in excess pore water pressure trends occurred after deposition of the tailings and consequently after the tailings had segregated by particle size among others.

Experiments RoR10A Lift 2 and RoR10B Lift 1 show trends of maximum excess pore water pressures for all transducers which corresponds with the magnitudes of the self-weight loads at the respective transducer elevations. One would expect this type of excess pore water pressure trend because an imposed load should be proportional to the pore water pressure experienced within the soil pores at a given location according to consolidation theory. Experiment RoR20B on the other hand shows the expected trends of excess pore water pressures for Transducers 1, 2 and 4 for all the three lifts. Transducer 0 recorded low excess pore water pressures due to a suspected unnoticeable leak at the base of the settling column. Experiments FDB showed expected trends for Transducers 1 to 4. For Experiment FDA Transducers 3 and 4 recorded relatively high excess pore water pressures since both transducer were located within fine tailings materials at the top of the tailings column. Transducer 2 which was located within coarse tailings showed low excess pore water pressures. The excess pore water pressures at Transducer 1 however do not follow the logic used to explain the behaviour pattern shown by the other transducers. Under Experiment FDB Transducer 0 which like Transducer 1 was located within coarse tailings yielded similar maximum excess pore water pressures values at 5.30kPa. Considering the predominant size of particles at a given elevation on the settling column helps advance explanations of excess pore water pressure trends for most of the transducers.

Other unexpected excess pore water pressure trends were observed under Experiments RoR20A and RoR10A Lift 1. On the whole 60% of the excess pore water pressure dissipations

results depicted expected trends while 40% indicated unexpected excess pore water pressure trends. Because of the prevalence of unexpected excess pore water pressure trends at various transducers, it is speculated that the segregation of deposited tailings could have contributed to the unexpected behaviour of the excess pore water pressure trends. It had been observed (Figure 5.4) that the fine and coarse segregated tailings comprised of different minerals. The different minerals together with varying particle sizes could have influenced excess pore water pressure trends causing unexpected trends which were at variance with pore pressures arising from applied loads only.

5.3.4 Excess Pore Water Pressure Magnitudes and Dissipation Times

Excess pore water pressure dissipated in 26 hrs and 10 days respectively for Experiments FDA and FDB. For Experiments RoR20A and RoR20B the dissipation times were 16hrs and 98hrs in that order. In Experiments RoR10A and RoR10B dissipation of excess pore water pressure was complete in 48hrs. In all the experiments coarse tailings dissipated excess pore water pressures within shorter times compared to fine tailings. It must be noted that significant magnitudes of the generated excess pore water pressures dissipated in much shorter times than those listed above. 90% of the maximum magnitude of the generated excess pore water pressures dissipated between 1hr and 20hrs for Experiments RoR20A and RoR20B, between 2hrs and 29hrs for Experiments RoR10A and RoR10B and between 10hrs and 30hrs for Experiments FDA and FDB. It has been observed from the research that maximum excess pore water pressure magnitudes did not exceed 6kPa. Of these maximum excess pore water pressures, a significant portion dissipated to within 10% of their initial magnitudes in shorter periods of time not exceeding 30hrs. Excess pore water pressure build-up as well as high excess pore water pressure values therefore cannot be the mechanism that limit the construction of tailings dams to rate of rise of 20m/yr. It is noted however that they may be other mechanisms that limit rate of rise. Currently there are examples of well managed and constructed cyclone gold tailings dams on the West Rand that have been built safely at a rate of rise of 10m/yr.

The excess pore water pressure trends of the standpipe piezometers compared well with those of the pore pressure transducers. It is to be noted however that when standpipe data was compared to the transducer data, the standpipes maximum excess pore pressure values were lower than the corresponding values of the transducers (see Figures 4.14a to 4.14d and Appendix E). The differences in initial maximum excess pore water pressure values was

expected since the standpipes had a relativley slower response time of 2 to 5 seconds compared to the transducers with a response time between 0.5 seconds and 0.9 seconds.

Figure 5.5 shows excess pore water pressure magnitudes over time for Transducer 1 and Standpipe 1 for Experiment FDA. Figure 5.5a shows the excess pore water pressure throughout the duration of the experiment while Figure 5.5b focuses on the first 600 minutes of the experiment at a small scale to show the differences and similarities between the pore pressure trends. The graphs show standpipe data, transducer data that was collected manually and transducer data that was captured through the data logger. It is observed from this figure that transducer data and standpipe data are comparable especially when observations were made for sufficiently long periods of time. The long periods of data collection tended to discount the effects of the initial lower maximum excess pore water pressures recorded by standpipes. It is evident from the figure that excepting the initial lower maximum values, standpipe and transducer excess pore water pressure values were comparable.

Figure 5.6 compares excess pore water pressure values for Experiments FDA, RoR20A and RoR10A at transducer 1. In the figure Experiment FDA exhibited the highest excess pore water pressures followed by Experiment RoR20A and Experiment RoR10A. Tables 5.3a and 5.3b summarise the maximum excess pore water pressures for the full depth deposition and the rate of rise experiments respectively. Experiment RoR10A shows expected trends of maximum excess pore water pressures at all transducer locations for all the deposition lifts. Experiment RoR20A on the other hand shows the expected trends of excess pore water pressures only for Transducers 3 and 4 under all the deposition lifts. Transducers 1 and 2 under the experiment do not show expected trends of excess pore water pressures with Lift 2 excess pore water pressures exceeding the Lift 3 maximum excess pore water pressures. In the expected maximum excess pore water pressure trends, pore pressure patterns show transducers located at the bottom of the settling column with high excess pore water pressures than transducers located high up the settling column. The transducers located at high elevations in the settling column show low excess pore water pressures because weight of tailings at their locations are of a low magnitude. Unexpected trends show the opposite trends (see also Section 5.3.3).

Table 5.3a: Maximum excess pore water pressures for full depth deposition experiments

Experiment	Maximum Excess Pore Water Pressure, ue, (kPa)				
	Transducer Number				
	0	1	2	3	4
FDA		3.38	3.33	2.88	2.90
FDB	5.44	5.50	5.29	4.69	4.25

Table 5.3b: Maximum excess pore water pressures for rate of rise experiments

Experiment	Transducer Number	Maximum Excess Pore Water Pressure, ue, (kPa)			
		Lift 1	Lift 2	Lift 3	Lift 3 top up
RoR20A	1	1.94	2.6	2.30	
	2	1.59	2.79	2.38	
	3	1.2	2.40	3.60	
	4	1.5	1.80	2.70	
RoR20B	0	2.45	0.38	0.52	
	1	2.04	2.26	2.59	
	2	1.46	2.10	2.40	
	3	0.30	1.08	2.66	
	4	0.76	1.55	2.35	
RoR10A	1	0.4	1.6	2.56	
	2	0.4	1.5	2.63	
	3	0.6	1.2	2.57	
	4	0.3	1.0	2.11	
RoR10B	0	1.10	2.38	1.58	0.58
	1	1.08	2.40	1.61	0.67
	2	0.82	2.20	1.60	0.64
	3	0.53	0.78	2.46	0.94
	4	0.24	0.37	2.20	0.92

On the basis of Figures 4.20 to 4.25 as well as Tables 4.3, 4.4 and 4.5, the cycle time of the RoR 20m/yr experiments was 4 days while close to 100% degree of consolidation was reached in a time ranging between 1 day (underflow tailings) and 4 days (catwalk fine tailings). For the RoR 10m/yr experiments the cycle time was 7 days. The underflow tailings which were used in both the RoR 10m/yr experiments reached close to 100% degree of consolidation in 3 days. The average time for degree of consolidation of 100% for the RoR 20m/yr experiments was 43hrs and for RoR 10m/yr was 72hrs. The cycle times for the two rate of rise experiments were 96hrs for RoR 20m/yr (660mm layer every 4 days per lift) and 168hrs for RoR 10m/yr (580mm thick slurry layer every 7 days per lift). The current tailings dam practice deposit thin layers of slurry (100mm to 300mm thick) every fortnight which translates to a cycle time of 336hrs and a rate of rise of 2m/yr to 3m/yr. Since the cycle times for the experiments were greater than the times in which full dissipation of excess pore water pressures was reached it therefore, follows that excess pore water pressures do not limit rate of rise of tailings dams. It needs to be noted that Experiment RoR10A (coarse tailings) yielded longer consolidation times that were greater than the times for Experiment RoR20A. This indicates that the time values for Experiment RoR10A are not reasonable and likely to be incorrect. These large values have been considered in the analysis leading to more conservative conclusions.

A consideration of remaining excess pore water pressures shown in Figures 4.32a to 4.37 and summarised in Tables 4.6, 4.7 and 4.8 shows that less than 10% of the generated excess pore water pressures remained after 30hrs from the deposition time of tailings slurry for the rate of rise experiments (RoR20A, RoR20B, RoR10A and RoR10B). If remaining excess pore water pressure of less than 10% are considered insignificant, it can be argued that excess pore water pressure dissipate within a quarter of the tailing slurry deposition cycle time. It is to be noted that this observation is based on experimental results carried out on 2m height settling column. The extrapolation of this observation to greater heights of tailings might not be justifiable. It is however believed that if permeability values of the tailings do not increase by an order of magnitude coupled with possible reduction of overall drainage path lengths by segregated coarse tailings layers interspersed with fine tailings layers, that the findings of this study could be applicable even at higher loading stresses than those in the 2m high settling column.

5.3.5 Shapes of Excess Pore Water Pressure Dissipation Isochrones

The shapes of excess pore pressure dissipation isochrones changed throughout the duration of the experiments. Excess pore water pressure isochrones for Experiments FDA, FDB and RoR20A Lift 2 are shown in Figures 4.32a, 4.33 and 4.34a(i) to 4.34c(iv) respectively. Each set of isochrones for a given experiment can be subdivided into three distinct shapes of isochrones consisting of similar patterns of isochrones. The first pattern comprise of relatively linear isochrones which generally depicted excess pore water pressure build-up and the early dissipation of excess pore water pressures in the first 15 minutes of the experiments. A second pattern of isochrones which were more curved and bent followed. The second pattern of isochrones showed the development of the layering profiles that continued with time up to about 20hrs from start of the experiment. Beyond 20hrs of excess pore water pressure dissipation, a third and last pattern of isochrones appeared. The last pattern of isochrones showed the very slow dissipation of excess pore water pressures of very small magnitudes. The isochrones were also observed to be compound curves which changed in shape as excess pore water pressure dissipation was taking place.

Figures 4.32a and 4.33 represented hindered settling that occurred under Experiments FDA and FDB respectively. In these figures both sedimentation and consolidation were taking place under hindered settling with sedimentation believed to be occurring in a fluid without effective stress (Tan et. al, 1990). In this study excess pore water pressure were recorded early after deposition of tailings slurry. In Experiment FDA excess pore water pressure in the range 0.65kPa to 1.22kPa were recorded between Transducers 1 to 4 after 2 minutes. Corresponding values of excess pore water pressure for Experiment FDB at depths of 0.0615m to 0.439m were 4.08kPa to 5.32kPa after 5 minutes from slurry deposition. The values at Experiment FDB were close to the maximum excess pore water pressures recorded under the experiment which was 5.5kPa. From both Figures 4.32a ad 4.33 the sedimentation of the fine fraction of the tailings slurry can be identified by the remaining excess pore water pressure isochrones with a varying height ratio on the y axis of the figures. The end of sedimentation and commencement of the last part of consolidation (that is with no or very insignificant sedimentation taking place) is depicted by isochrones with a relatively constant height ratio. The height ratios occurred at 0.43 and 0.46 for Experiments FDA and FDB respectively.

From Figure 4.7 it can be noted that sedimentation was completed after 450 minutes and 1300 minutes for Experiments FDA and FDB. It must be emphasised that the presence of excess pore water pressures as early as 5 minutes in the experiments relative to the completion times of sedimentation (450 minutes and 1300 minutes) taken together with Figure 2.16 as well as observations made by several workers (Tan et. al., 1990; Schiffman et al., 1988; Been and Sills, 1981; and Imai, 1981) signals the fact that in the sedimentation region (Figure 4.9) consolidation was taking place alongside the sedimentation of the fine tailings segregated from the initial slurry deposited. It is believed that due to the segregating nature of the slurry used in the research, coarse tailings fraction of the slurry settled quickly with the tailings fractions that hindered its settling. The consolidation of the settled tailings continued with sedimentation of the fine tailings. The sedimentation-consolidation transition zone and linkage represented by Equation 2.20 is speculated to be wide and more complex under these experiments. This aspect has not been dealt with in detail under this work whose emphasis was whether excess pore water pressures limited rate of rise.

5.3.6 Excess Pore Water Pressure Dissipation and Slurry Interface Change

The bulk of the dissipation of excess pore water pressures were observed to have occurred within the sedimentation and consolidation region when the slurry interface height change with time (SWI) was steep. Large changes in slurry interface height coincided with rapid excess pore water dissipations (see Figures 5.7 and Appendix K). It can be observed from these figures that the most rapid dissipation of excess pore water pressures took place during the period when the slurry interface height change with time was also changing rapidly. The figures further show that very little excess pore water pressure dissipation took place when the slope of the tailings interface change (SWI) with time was flat (that is when the bulk of consolidation was taking place). It was noted that the more significant excess pore water pressures are generated and dissipated within the shorter sedimentation/consolidation phase rather than during the much longer last part of the consolidation phase. It can be inferred from this observation that excess pore water pressure build up does not limit rate of rise because by the time the bulk of consolidation commences the excess pore water pressures would have dissipated. Rate of rise encompasses not only sedimentation and the early stages of consolidation but the whole of consolidation and desiccation by sun drying as well, all of which take place over a relatively long period of time compared to the sedimentation/consolidation phase where significant excess pore pressure seem to dissipate.

It is worth noting from Figures 4.7 and 5.7 and Appendix K that changes of slurry interface height over time for the experiments occurred at a sedimentation rate with a constant slope of soil water interface which reflected the similar initial slurry concentration used in the experiments.

Table 5.4 summarises changes in tailings water interface height and excess pore water pressure with time for all experiments during sedimentation and consolidation phases. The table lists the ratios of the change in soil water interface and excess pore water pressure dissipation during the two phases of slurry settlement. The ratio of the soil water interface rate of the sedimentation/consolidation to the consolidation phase varied by over two orders of magnitude while the excess pore pressure dissipation rate differed by one order of magnitude. The table shows that the dissipation of excess pore water pressures occurs during the sedimentation and initial consolidation phases.

Table 5.4: Soil water interface and excess pore water pressure dissipation rates

	Sedimentation/ Consolidation Phase		Consolidation Phase		Sedimentation/Consolidation Phase Ratios	
Experiment	ΔSWI/Δt (mm/min)	$u_e/\Delta t$ (kPa/min)	ΔSWI/Δt (mm/min)	$u_e/\Delta t$ (kPa/min)	$\left(\frac{(\Delta SWI/\Delta t)sed}{(\Delta SWI/\Delta t)cons}\right)$	$\left(\frac{(\Delta u_e/\Delta t)sed}{(\Delta u_e/\Delta t)cons}\right)$
FDA	1.50	0.0062	0.0064	0.00005	233	119
FDB	0.81	0.0037	0.0072	0.000070	112	51
RoR20A L1	1.60	0.0035	0.0061	0.000212	264	17
RoR20B L1	1.08	0.0058	0.0222	0.00022	49	26
RoR20BL2	0.37	0.0013	0.0097	0.000146	38	9
RoR20BL3	0.70	0.0012	0.0086	0.000428	82	3
RoR10AL1	3.50	0.0025	0.0082	0.000071	429	35
RoR10AL2	0.75	0.0010	0.0040	0.000070	189	14
RoR10AL3	0.38	0.0005	0.0029	0.0000513	130	10
RoR10BL1	3.56	0.0018	0.0392	0.000431	91	4
RoR10BL2	2.19	0.0069	0.0294	0.000588	74	12
RoR10BL3	4.00	0.0040	0.200	0.003667	20	1
				Average	143	25

5.3.7 Settling Column Results and Terzaghi Consolidation Theory

Introduction

This section compares results obtained from settling column experiments with approximations from Terzaghi (1923) consolidation theory. The section evaluates consolidation rates and compares excess pore water pressure from Experiments FDA and RoR20A Lifts 2 and 3 with pore pressures estimated using Terzaghi's theory. The disparity between settling column results

and Terzaghi's one dimensional consolidation theoretical approximations are expected to be large owing to the simplifying assumptions used in the theory which differ from the settling column experimental conditions.

Coefficient of consolidation

Table 5.5 shows the values of coefficient of consolidation, c_v, obtained using the consolidation rate, (m_2) (Figure 4.7a). The sedimentation/consolidation phase as shown in Figure 4.7a applied mostly to fine fraction of the tailings which segregated and settled later. The mechanism of sedimentation which forms a significant portion of this phase differs from the consolidation mechanism in the settling column experiments and in common laboratory consolidation tests such as the oedometer test. Whilst consolidation involves application of stress to strain a soil, sedimentation is dominated by deposition of soil particles. Experiment FDA data was used to calculate the c_v values. The c_v values were calculated using Equations 2.9 and 2.17 from Terzaghi's one dimensional consolidation theory. Taylors square root of time method, $(c_v)_{90}$, and the Casagrande logarithm of time method, $(c_v)_{50}$ (Knappett and Craig, 2012) were used. It is noted from Table 5.5 that the c_v values were reasonable though relatively low compared to values published in the literature. The initial and generally large magnitude excess pore pressure dissipations fell within the sedimentation/consolidation region of the graph where sedimentation behaviour dominated rather than consolidation behaviour. Very large values could be obtained if the determination of c_v values was carried out in this region and such values would be meaningless. Beyond the inflection point separating the completion of sedimentation from consolidation (see Figures 4.9a and 4.9b), c_v values were obtained based only on the consolidation phase. For the data in Table 5.5 the inflection point occurred at a time of 450 minutes (the boundary between completion of sedimentation and consolidation). It needs to be noted that the calculation of both $(c_v)_{50}$ and $(c_v)_{90}$ in the consolidation region was undertaken with the inflection point considered to be the new origin for the measurement of the c_v values. It must be also be pointed out that while the $(c_v)_{50}$ and $(c_v)_{90}$ values are usually comparable for a material that was sufficiently stiff such as under oedometer tests, the two values varied for the settling column tailings. In the settling column the material changed continuously as it evolved from a soft deposited tailings to a more consolidated firm settled column of tailings. With this level of change in material properties large variations in c_v values were expected.

Table 5.5: Experiment FDA coefficient of consolidation results

		Consolidation Rate, c_v (m^2/yr)
Terzaghi (Equation 2.9)	$(c_v)50$	37-61
	$(c_v)90$	32-306

The comparison of experimental excess pore water pressure data with those obtained from Terzaghi's (1923) theory, was undertaken using Experiment RoR20A Lifts 2 and 3 data. Because Terzaghi's theory ignores self-weight effects and emphasises imposed external loads, Lift 2 was considered a load on settled tailings of Lift 1 while Lift 3 an imposed load on Lifts 1 and 2 tailings. Theoretical approximations of excess pore water pressure were obtained at equivalent pore pressure transducer elevations from Figure 2.26. Respective values of time factor, T_v, were calculated from Equation 2.9. The c_v values in the range 109m^2/yr to 3,850m^2/yr were used in the calculations, however the value of 109m^2/yr was used for the comparisons. Table 5.6 summarises the comparison of the results. From the table it can be observed that Terzaghi's theory (values shown within square breackets) overestimated excess pore water pressures compared to the measured values. The measured values were 30% of the theoretical values in Lift 2 with a drainage path length of 0.333m. Under Lift 3 with a drainage path length of 0,589m the measured values were 15% of the theoretical values.

Table 5.6: Experiment RoR20A excess pore pressure comparison with Terzaghi (1923) theory values

Transducer	Lift 2 Excess Pore Pressure (kPa)			
	Time (min)			
	3	45	190	
1	2.5 [8.12]	1.2 [7.53]	0.4 [4.26]	
2	2.6 [7.94]	1.3 [5.73]	0.4 [2.62]	
3	2.1 [7.29]	0.8 [1.64]	0.6 [0.66]	
	Lift 3 Excess Pore Pressure (kPa)			
		Time (min)		
	6	16	78	218
1	2.1 [8.67]	1.5 [8.67]	0.4 [8.51]	0.2 [7.81]
2	2.2 [8.59]	1.6 [8.51]	0.5 [8.25]	0.3 [6.94]
3	3.0 [8.51]	2.3 [8.33]	1.1 [7.64]	0.3 [5.64]
4	2.1 [8.42]	1.3 [8.07]	0.2 [5.03]	0 [3.30]

5.4 Particle Size Analysis

5.4.1 Introduction

This section starts with a discussion of the effects of sedimentation and segregation on particle size distribution of gold tailings. The section then analyses particle size results of experiment samples and recovered samples from Experiments FDB, RoR20B, RoR10B and a RoR 10m/yr sample that was not subjected to a permeability test. The segregation of tailings and the particle size grading of underflow tailings is discussed first, followed by a discussion of catwalk fines sample. The discussion of the particle size analysis of recovered tailings from the experiments and sample without permeability test concludes the section.

5.4.2 Effects of Sedimentation and Segregation

In the context of this study particle size segregation took place under and as a part of the sedimentation stage. Given the high initial slurry concentration of the tailings (467g/L), sedimentation of the tailings solids was of the hindered type (Figure 2.17). It is unlikely that free settling (unhindered settling and Stokes' Law) could be applicable under the experimental conditions of this study because the high initial slurry concentration violated some of the conditions under which Stokes' Law operates. Stokes' Law conditions as summarised in Chapter 2 include the requirement of a low slurry concentration where particles can fall freely independent of each other. Under this study, however a slurry concentration greater than 50g/L (used for hydrometer particles size analysis) was used whereby Stokes Law does not apply. The modified Stokes' Law (Richardson and Zaki, 1954) and the extended Kynch theory (MacRoberts and Nixon, 1976) were also not applicable to this work owing to the theories's emphasis on spherical particles and an assumption that segregation does not take place respectively. It is believed that tailings slurries progressed from zone settling to compression settling as the tailings underwent settling (Figure 2.17). It is worth noting that flow channels in the form of flow paths, volcanoes and craters (Kurt, 2006) were observed during the settling column experiments which would be expected in the context of zone and compression settling types. The results of the particle size analysis in the next sections demonstrate that vertical segregation occurred in settled columns. The segregated profiles are believed to be dominated by grain size distribution of solids, slurry concentration as well as by the effects of the finer fraction of the solids as suggested by Kupper, (1999).

5.4.3 Underflow Tailings Grading

Figure 3.32 shows the height profiles of the recovered underflow tailings samples whose particle size analysis is considered in this section. These are Experiment RoR10A recovered samples on the left hand side of Figure 3.32, followed by the RoR 10m/yr recovered tailings column which was not subjected to a permeability test and Experiment RoR10B recovered column sample. Figure 3.28 shows the recovered tailings column not subjected to permeability test while Figure 3.29 shows Experiment RoR10B recovered tailings sample. Experiment RoR10A samples were obtained from the permanent settling column apparatus when it was emptied. The recovery of this sample was therefore different from those of the other samples

which were recovered by splitting the sacrificial column. This recovery method entailed a high likelihood of contamination of different height profiles with tailings from other heights of the column as the samples were accessed from the ends of the column.

Figures 5.8, 5.9 and 4.43 show the particle size distribution curves of samples from Experiments RoR10A, RoR 10m/yr without permeability test and RoR10B respectively. In Figure 5.10 the three samples were plotted together on one particle grading chart for ease of comparison. In the Figures 5.8 and 5.9 it was noted that the grading of the tailings where the slurry pouring process entailed the subsequent disturbance of the previously deposited tailings layers by the incoming slurry, the grading pattern of coarse layers of tailings at the bottom of the recovered settled column were followed by tailings particle sizes in between the coarse layer and the top most layer of the column made up of fine tailings particles. There was therefore an intermediate grading curve caused by mixing of two deposition slurry lifts. In the case where mixing took place due to the impact of incoming slurry a gradual variation in particle sizes was observed as the settled column was vertically traversed upwards. A mixture of coarse and fine tailings occurred between the coarse and fine particles grading curves. The mixed coarse and fine tailings particle sizes affected sedimentation and deposition of the tailings solids. Under this scenario tailings segregation was mitigated by re-mixing with the previously deposited slurry layer's fine tailings particles.

Figure 4.43 shows the gradations of the tailings under Experiment RoR10B where the underflow tailings were deposited with the help of a tremie pipe. The tremie pipe was meant to prevent re-mixing and disturbance of previously deposited layers of tailings which mitigated the resultant segregated particle size distribution pattern. A distinctly segregated tailings gradation pattern of the settled column comprising a fine tailings layer at the top of the settling column and coarse tailings at the bottom of each deposited tailings lift was observed (Figure 4.43). In this case coarse and fine layer particle size distributions are separated from each other with no intermediate grading curves.

From Figure 5.10 in which all the underflow tailings sample particle size distribution curves were compared it was observed that the 2011 underflow tailings sample contained more fine grained particles than the 2010 underflow sample. The coarse tailings particles of the two samples were comparable as the coarse particles fractions plotted very close to each other. The fine tailings fractions on the other hand differed and separated noticeably from each other.

5.4.4 Catwalk Fines Tailings Sample Grading

In this section the catwalk fines tailings particle size grading characteristics from sieve and hydrometer test results are compared with particle size grading curves from the Mastersizer method.

Particle size distribution curves were plotted for Experiment RoR20B at large sampling interval (100mm) and at a smaller interval of 30mm respectively (Figures 4.44 and Appendix H). The large sampling interval resulted in grading curves that straddled several height profiles of segregated tailings which contained a wide range of particle sizes leading to overlapping particle size distribution curves. The particle size grading pattern was similar to the grading curves obtained when slurry pouring remixed settled tailings from the previous slurry deposition lifts. Particle size segregation was more pronounced at the top and bottom of the settled tailings column where the samples displayed a predominantly uniform size range. The grading curves obtained from the small sampling interval (30mm) demonstrated that segregation most likely took place during the sedimentation of the tailings with the different depth sampling profiles yielding particle size grading curves that were distinct from each other. Based on the small sampling interval particle size grading curves, the intersection between consecutive tailings profile grading curves depicted limited amount of mixing of coarse tailings and fine tailings. The limited mixing of layers observed in this sample (deposited with the help of a tremie pipe) indicated that even though the fine tailings particles at the top of the preceding layer had already settled, the incoming layer of slurry deposited coarse grained tailings particles which contaminated the settled fine tailings layer at the top of the previous deposited layer. By virtue of the two layers being adjacent to each other this was expected.

Experiment FDB particle size distribution plots at the large sampling interval (100mm) and at the small sampling interval (30mm) are shown respectively in Appendix H (Figure H5) and Figure 4.45. The particle size distribution curves depicted similar patterns to those for Experiment RoR20B (Figures 4.44 and H4). This was to be expected since the 2011 catwalk fines sample were used in both experiments. The differences that one would have expected would be the extent of particle size segregation since in Experiment FDB the slurry settled over a greater height of fall (1900mm) compared to 660mm in Experiment RoR20B. This could mean that for a slurry concentration of 467g/L and the given catwalk fines tailings gradation

the height of fall (660mm to 1900mm) was less significant than the particle hindrance of each other in effecting a difference in particle size segregation. In tailings dams multiple layers of alternating fine and coarse particle sizes have been documented. The rationale behind particle size distribution sample specimen at different thicknesses (100mm and 30mm) was thus to observe the effect of the layers. Figure 5.11 (based on the 30mm specimen spacing) showed the segregation of the catwalk fines as comprising of three groups of gradation curves. These were the grading curves of the depth profiles finer than the source tailings (labelled A), the intermediate graded particle size grading curves that criss-crossed the source tailings and were located near the centre of the settled tailings column (B) and the coarse grained tailings which were coarser than the source tailings (C).

Figure 4.46 compared particle size distribution curves for catwalk fines obtained from the sieve/hydrometer analysis and from the Mastersizer diffraction analysis for Experiment FDB. Additional particle size distribution curves comparing sieve/hydrometer grading with the Mastersizer particle analyser can be found in Appendix H. The Mastersizer uses scattering angles and particle volume to obtain particle sizes. The Mastersizer showed large particles (>0.008mm) that were relatively smaller than the corresponding sieve and hydrometer tests sizes. For the small particles sizes the Mastersizer particle sizes were either the same as those from sieve and hydrometer particle determination techniques or the Mastersizer determined sizes were greater than the sizes from the sieve/hydrometer tests. The large tailings particles are well known to be mostly rotund with isolated platy and flat sizes attached to them (Chang, 2009). The fine tailings particle sizes on the contrary are known to be flaky and platy in shape. In a comparison of results of the single optical sizing (SPOS) method with dry sieving for sands, White (2003) observed that the SPOS method yielded particle sizes that were 20-40% larger than the dry sieving sizes. White (2003) noted that none of the methods could be considered to yield correct particle sizes relative to the other because the methods emphasised different aspects of the dimensions of a given particle. In another study where a review of particle sizing methods was undertaken, Abbireddy and Clayton (2009) highlighted the importance of particle shape on particle size distributions obtained from different particle sizing methods. They showed that the sedigraph (automated sedimentation based particle sizing method), pipette and laser diffraction methods yielded comparable particle size distribution results when spherical particles (glass ballotini) were considered. They however noted that the particle size distribution varied when flaky and platy particles (classified tailings, mica and kaolin) were compared. In this research it is believed that the flaky shapes of the small size

tailings particles contributed to the variation in the sizes between the Mastersizer and the sieve and hydrometer test particle size distribution curve results. The variations between the different particle size determination methods were however considered insignificant with regard to their overall effects on particle size segregation and the related generation of excess pore water pressures.

5.4.5 Grading Parameters

Grading parameters and the hydrometer sample concentrations were evaluated to complement the assessment of the tailings particle size grading results. The parameters included size percentiles (D_{10}, D_{30}, D_{50}, D_{60}, and D_{90}), grading coefficients (Cu and C_z) and grading modulus (GM). Similar trends of the listed grading parameters were observed in both the rate of rise experiments and the full depth deposition experiments for both coarse and fine tailings. Figure 5.12 shows the variation of the above parameters with the depth of tailings in the settling columns. All the plots show fine particles at the top of the settled tailing column and coarse particle sizes at the bottom with a gradual change in particle sizes through the height of the settling column which reflected particle size segregation.

The hydrometer sample concentrations (Figure 5.12) were low for coarse grained tailings particles and gradually increased as the tailings particles became finer in size. The low concentration for coarse tailings reflect the fact that some of the coarser tailings particles settled quickly in relation to the other particles (segregation). This meant that by the time a sample was collected for the determination of sample concentration the particles had settled. This resulted in a reduced mass of the coarse tailings which led to concentrations below 50g/L. The particle size percentile trends (D_{10}, D_{30}, D_{50}, D_{60} and D_{90}) and the grading modulus (GM) depict similar trends in all the experiments regardless of the deposition type (full depth deposition *vs* rate of rise) and the nature of the sample used (whether fine or coarse grained). As expected the percentiles (D_{10} to D_{90}) were high for coarse tailings (0.02mm to 0.15mm) and low for fine tailings (0.01mm to 0.02mm) The individual trends therefore were high for coarse tailings and the trends tended to reduce as particles sizes became smaller along the depth of the settled tailings columns. The coefficient of uniformity, C_u, and the coefficient of curvature, C_z, gave results which did not correlate well with tailings particle sizes. The C_z trend was largely inconsistent with particle size. In general a high C_z value indicated coarse grained tailings while a low value reflected fine grained tailings. The C_u trend also varied but indicated an average

C_u value of around 10 with a range in values between 1.8 and 52. The major variations in the values of C_u occurred at locations within the settled column of tailings where two separate slurry depositions took place and at depths where there was a mixture of a range of particle sizes.

5.5 Specific Gravity and Mineralogy of Tailings

5.5.1 Introduction

This subsection discusses the results of the specific gravity of the solid tailings particles as well as the results from the XRD and XRF analysis which describe the mineralogy of the samples. The specific gravity of the solid particles from different test methods were compared. The estimates of specific gravity from mineralogy based on both XRD and XRF analysis are also considered. The gold tailings mineralogy is examined from the perspective of its relevance to the properties of tailings which are applicable to the research questions. This includes its possible use in explaining observations relating to the fabric of settled tailings column which affects permeability and pore water pressure response of tailings. The discussion is followed by a consideration of the same properties for Experiment FDB recovered settling column samples.

5.5.2 Experiment Source Samples

The specific gravity of solids results discussed in this section comprise results obtained from tailings samples from site as is before the tailings were used in settling column experiments, the results of tests carried out on samples recovered from settling column tests as well samples that were dispersed using calgon and sieved into particle size ranges. The samples used in the experiments had an average specific gravity of solids of 2.67 while the average was 2.74 for fine tailings (Table 4.1).

The 2011 tailings samples were visually observed to contain significant and easily noticeable contamination of flocculated globules which comprised mainly bassanite (60%), quartz (16%), muscovite (16%) with traces of calcite (3%) which were not present in the 2010 tailings samples. The globules were believed to have been lumped together due to a strong flocculent used by the mining industry during the mineral processing to extract gold from ore. Most of

the globules could not be dispersed by calgon used in the hydrometer testing for particle size analysis but were observed to be crushed to minus 2mm size when the gold tailings were prepared for making a slurry that was used in the research thus leading to higher specific gravity of the solids of tailings in the 2011 samples.

A close examination of the mineral composition of the 2010 and 2011 samples using both the XRD and XRF analysis results indicated that both samples contained similar quantities of quartz (70%), muscovite (13%), pyrophillite (4-12%) and chlorite (4%). The 2011 samples in addition contained bassanite (2-4%), more dolomite (3%) and traces of rutile and pyrite which were not detected in the 2010 samples which again led to the expectation of a relatively higher specific gravity of the solids value in the 2011 samples than in the 2010 samples.

A portion of the combined experiments samples that was dispersed with calgon and later sieved into size fractions showed a composition of the sand fraction made up of quartz (87%) and phyllosilicates (13%) which agreed quite well with findings on gold tailings by Vermeulen (2001) who reported a split in the sand size fraction made up of quartz at 90% and Phyllosilicates at 10%. Rösner (1999) also reported sand fractions made up of 89% quartz and 11% phyllosilicates. The slimes (minus 75µm) on the contrary showed a composition of 70% quartz and 30% phyllosilicates as opposed to 50% split reported by Vermeulen (2001). The difference was however not considered to be significant because only a limited amount of testing was carried out in the current work. There was a good agreement between the XRD and XRF derived constituents' parts of the related minerals and oxides of the elements that the two analysis methods used.

5.5.3 Experiment FDB Recovered Column Samples

The specific gravity of the solids of the recovered column samples showed an increase in the specific gravity values as the particle sizes reduced from coarse tailings to fine tailings particle sizes. The samples at the bottom of the settled column of tailings up to a height of 145mm had a specific gravity value of 2.70, whilst from height 145mm up to 415mm had a value of 2.71, with the 415mm height up to 640mm having a value of 2.73 and the rest of the column up to its total height of 724mm with a value of 2.75 (Refer to Figures 5.13 and 5.14). The XRD and XRF data corroborated the above specific gravity value trends. It was apparent from the XRD and XRF data that the different minerals that constituted the coarse and fine tailings changed

along the height of the settling column which accounted for the observed trends of the measured specific gravity values. The main component, quartz, with a specific gravity of 2.66 changed from 83% to 54% as a proportion of the whole sample, muscovite with a SG of 2.83 changed from 9% to 25%, pyrophillite with an SG of 2.78 changed from 2% to 11% with chlorite changing from 2% to 4% while its SG was 2.81 (Figures 5.15). It was noted that while the other minerals' amounts changed by smaller percentages their specific gravity values were higher in value than the SG value for the main constituent, quartz, which impacted significantly on the overall SG value leading to higher SG values when ascending up the settled tailings column.

The SG values became smaller as tailings particles got coarser (Figure 5.16 and Appendix I). It was observed that with the exception of the sample at column height 700mm-724mm, all the other samples showed comparable SG values determined from the density bottle method and the SG values estimated from the XRD determined minerals theoretical SG values. The SG values obtained from the different methods were comparable.

5.6 Recovered Settling Column Fabric

5.6.1 Introduction

This subsection examines tailings fabric as observed from SEM micrographs of the recovered samples (Experiments FDB, RoR20B, and the ROR 10m/yr without permeability test). The micrographs were examined and compared with the aim of identifying tailings fabric patterns in the directions perpendicular to water flow and parallel to the water flow during the experiments as well as effects of different specimen preparation methods. The subsection discusses results in the order listed above and concludes with a summary.

5.6.2 Experiment FDB Recovered Tailings Fabric

Introduction

The fabric of the catwalk fines are discussed in the context of the micrographs obtained from viewing specimen prepared using three different preparation methods. Micrographs depicting dispersed and sieved tailings are examined, followed by micrographs obtained by viewing specimen prepared using the carbon tape (CT) preparation method and the specimen stub

carbon glue (CG) prepared micrographs. It was expected that the dispersed and sieved tailings particles fabric would show discrete tailings particles displaying the varying specified size ranges. The carbon tape based fabric would reveal the wide particle size ranges at any given recovered settled column tailings height but less about the structure of the recovered settled tailings in the column. The particle to particle contacts and inter-particle contact together with depth of field view would be limited. The carbon glue based micrographs were expected to capture the full fabric of the tailings along the column height inclusive of meaningful depth of field offered by the SEM technique which should facilitate answering the research questions relating to fabric of the tailings materials.

Sieved and Dispersant Treated Particles Micrographs

The dispersant treated and sieved tailings fractions had smooth surfaces devoid of tailings fines usually attached to the surfaces of tailings. This was observed in Figure 4.5. In all the size ranges considered the particle shapes ranged from rotund, angular and elongated to platy/flaky. The particle shapes also varied significantly especially at the small magnification of x90 which covered a wide range of tailings particle sizes in a given area of the specimen being examined under the microscope. There was clear size reduction in the four size ranges considered (-300µm+212µm, -212µm+150µm, -150µm +63µm and -63µm). It was observed that almost all the particle sizes were present within any of the above specified size ranges. This was not surprising as it demonstrated the weakness of the sieving technique which allowed a wide range of particle sizes to pass through a particular sieve aperture. The particle size that goes through a given size aperture depends on the orientation of the particle at the time it went through the sieve opening even though the given particle has different size dimensions depending on the side it is oriented at. This was more pronounced on elongated particles whose shape has more than one size dimension. The flaky and platy tailings fines were not observed under the dispersant treated and sieved particle size range micrographs because the dispersant had disaggregated these fines from the coarse tailings particles during pre-treatment of the sample. It is believed that the bulk of the -63µm fraction which was drained to waste contained most of the fine and flaky particles. In other words, the dispersant successfully washed off fines from the surfaces of larger particles.

Recovered Catwalk Fines Fabric

The fabric of recovered tailings column specimen (Experiment FDB) prepared using the carbon tape pick up preparation method showed a range of particle sizes throughout the column height. A correlation emerged where the large particle sizes were predominant at the base of the settled column and the fine particles concentrated at the top of the column. Table 5.7 summarises particle size grading throughout the full depth of the settled recovered tailings column examined at x350 and x90 magnifications as depicted in Figures 4.47 and 4.48. The trend supported the belief of the segregated settling process by particle size and weight preference as expressed by Stokes law. The variation in sizes at the different elevations of the settling column suggested hindered settling. The larger particles seemed to have carried along with them fine particles which under unhindered settling conditions would have settled at a much later time. In turn the fine particles would be located at the top of the settling column rather than at the base of the settling column with the heavier and larger particle sizes.

The observed structure of the tailings in this subsection is based on a micrographs prepared from the carbon glue preparation method which differs from the micrographs of the preceding paragraph which were based on the carbon tape preparation method. The carbon glue preparation method based fabric showed more depth of field and particle interaction than was observed under the carbon tape pick up method. Both the magnifications analysed (x90 and x350) showed an increase in particle sizes as the settled tailings column was traversed from its top towards its base. Table 5.8 summarises the size changes throughout the depth of the settled tailing column (Figure 4.49 and Appendix J). The whole settled column SEM micrographs are shown in Appendix J. The tailings fabric at an orientation perpendicular to water flow and the fabric parallel to water flow were compared. On the whole it was observed that the tailings were oriented randomly.

Table 5.7: Experiment FDB summary micrographs observed particle size grading through depth column (using carbon tape method)

Settling Column Depth (mm)	Micrograph Based Descriptions of Size Ranges
600-724	Fine particles of maximum size of 70µm predominate. Very fine layer of tailings such that the pores of the carbon tape reflect through the tailings fabric.
510-600	A transition layer between fine tailings and coarse tailings whereby fine tailings are more numerous yet isolated large tailings particles are present. The maximum diameter of the large sized particles around 110µm.
415-510	The number of large particle sized tailings cover of 45% of the whole viewed micrograph area. The maximum size of the large particles still around 110µm.
170-415	The matrix of large particles more predominant. The voids between the particles also large. The approximate maximum diameter of the large particles at about 225µm.
15-170	The viewed area of the micrograph occupied by large tailings particles with a maximum diameter of around 400µm. The particle shapes were still the same as that of the layers up the settled tailings column.

Table 5.8: Summary of particle size changes in settled column observed from micrographs (using carbon glue method)

Settling Column Depth (mm)	Description of Fabric Size Range Changes
570-724	Fine particles predominate with many voids probably worsened by water evaporation when the tailings were drying inside the settling tube.
480-570	A more pronounced appearance of large sized tailings particles.
300-480	Large tailings particles with large voids between them. There was also a presence of fine tailings particles attached to the surfaces of the large tailings particles.
15-300	Large particles in contact with fine particles stuck to their surfaces. Voids between the large particles were clearly visible.

5.6.3 Rate of Rise 10m/yr Underflow Tailings Fabric

Introduction

The SEM micrographs of recovered tailings deposited at 10m/yr rate of rise without permeability test are discussed in this section. It was expected that the carbon tape preparation method based samples of the coarse underflow tailings sample of 2010 would result in porous fabric with very little fine tailings particles. This is because the SEM micrograph preparation method did not allow for viewing of the whole intact sample specimen. It was worth noting that the fabric of specimen was sampled from the more coarse grained underflow tailings of 2010.

RoR 10m/yr Experiment Without Permeability Test Fabric

SEM micrographs oriented along and perpendicular to the vertical axis of the settling column are given in Figure 5.16 magnification x25 and x160. The figure showed a distinct change in particle size from fine tailings at the top of settling column, through a mixture of fine and coarse grained tailings particles sizes in the middle of the settling column and coarser tailings at the base of the column. The gradual change in particle sizes along the height of the settling column showed that segregation by particle size occurred during sedimentation following slurry deposition. Disturbance of deposited settled layers of tailings by subsequent slurry depositions were shown by the presence of particles of different sizes at the interface of coarse and fine tailings of the two adjacent layers representing the deposition lifts.

From the SEM micrographs captured at magnification of x750 and at magnification of x1500 it was observed that the large tailings particles had fine and flaky shaped particles stuck to the surfaces of the large tailings particles (Figure 4.50). It was further noted that some of the large particle sizes were angular in shape whilst the bulk of the fine tailings particles were flaky and platy. Both the large and fine particles had pore spaces in between them which differed only in size (Figure 4.50).

5.6.4 Experiment RoR20B Tailings Fabric

Figure 3.30 shows Experiment RoR20B profile. The SEM micrographs are given in Appendix J. Figure 3.32 shows the location of the specimen used for SEM viewing. Considering micrographs at all the magnifications scales of x90, x350 and x1500 the particles were oriented randomly. The micrographs showed the larger particles being regular to rotund in shape with the fine particles mostly flaky and platy. There was also the presence of bigger voids spaces between the large tailings particles even though fine tailings were again observed sticking to the surfaces of the coarse tailings particles. Despite segregation by particle size, the fine particles on the surfaces of the larger particles and the fine tailings in between some of the void spaces indicated hindered settling that occurred during sedimentation. The fine tailings also had smaller void spaces in between the small particles which made the fine tailings mat porous as opposed to it being a closed mosaic of platy particles (Appendix J2). This observation was expected within the context of the relatively high permeability values for fine particles in relation to permeability values of layers with similar particle sizes but comprising of clay

minerals. The SEM viewing of fine tailings which formed the top layer of each deposited slurry lift caused charge build up under the SEM which resulted in poor quality micrographs.

5.6.5 Tailings Fabric Analysis Summary

SEM micrographs were analysed for catwalk fines tailings (Experiment RoR20B and FDB) and underflow tailings (Experiment RoR 10m/yr without permeability test). The fabric of the underflow tailings showed subtle changes from fine tailings layers to coarse tailings layers. Catwalk fines tailings fabric displayed distinct fine tailings layers and coarse tailings layers. The coarse tailings layers were contaminated with fine tailings particles which arose from the abundant amount of tailings fines coupled with short distance of fall of 660mm in Experiment RoR20B. Under this scenario sedimentation took place under hindered settling which assisted in forming the matrix of fine and coarse tailings observed in the micrographs. Experiment FDB micrographs showed evidence of segregation with distinct fine tailings fabric at the top of the column and a coarse tailings structure at the bottom of the column. The 2m high settling column allowed adequate distance of fall during which significant segregation could take place. The difference between the micrographs of the coarse fraction from the underflow tailings and the coarse fraction of the fine catwalk tailings micrographs was that the catwalk tailings coarse layer was mixed with a significant amount of fines while the coarse layer from the underflow tailings contained less fine tailings.

5.7 Tailings Permeability

5.7.1 Introduction

The section discusses the saturated vertical coefficient of permeability of the tailings researched under this thesis. The total heads comprising elevation and pressure heads developed during sedimentation and consolidation phases of the experiment and the total heads developed during the constant head permeability test stage were both examined. Following the examination of the total heads under the experiments, the permeability trends in the different profiles of the settled tailings column are presented and discussed.

5.7.2 Sedimentation-Consolidation and Permeability Test Total Heads

Experiments Steady State Hydraulic Conditions

Steady state conditions were necessary for the proper determination of the coefficient of permeability of the tailings under the different experiments. The determination of the coefficient of permeability was to be evaluated when the tailings were subjected to no other flow except for the flow caused by the imposed head difference required for permeability test at a hydraulic gradient of unity (Blight, 2010).

When the settling column test commenced, excess pore water pressures were generated and were later dissipated leading to steady state conditions. At this stage there was no flow and no potential difference thereby rendering the experiment conditions suitable for permeability test. The equilibrium conditions reached under the respective experiments corresponded with the type of tailings especially the fines content of the tailings samples as well as the deposition scenario of the experiment.

Prior to the commencement of the constant head permeability test, it was necessary to ensure that permeability test was carried out under hydraulic conditions where the hydraulic gradient was equal to one (1). Blight (2010) recommends that permeability testing for soft materials such as gold tailings be undertaken when a hydraulic gradient of unity was achieved. For experiments undertaken for this research, the total head of supernatant water above the settled tailings layer imposed hydraulic gradients greater than one. Water was therefore decanted to achieve hydraulic gradient of one (1). Because of lowering the existing head by removing water from the settling column, new steady state conditions were required for the measurement of tailings permeability following the adjustment of the hydraulic head. The experiments were therefore allowed to re-establish hydrostatic conditions. It is noted that under the new transient conditions occasioned by the commencement of the constant head permeability test, seepage pressures were set up which altered the permeability of the tailings. The tailings became more dense as a result of downward water flow.

Sedimentation-Consolidation Total Heads

Total heads decreased over time in all the experiments during the sedimentation and consolidation phases of the experiments (Appendix F). During the first hour following slurry deposition total heads isochrones crossed each other which indicated the prevailing transient conditions in the experiments at the time. At this time concurrent build-up and dissipation of pore water pressures occurred at the different elevations within the settling column. Appendix F depicts this behaviour. Table 5.9 summarises the total sedimentation and consolidation heads trends under all the experiments in terms of the total heads quantities and the times required to reach steady state conditions under the respective experiments.

It is evident from Table 5.9 that Experiments FDA and FDB whose height of slurry varied from 1450mm to 1900 mm respectively reached equilibrium within 6 to 10 days. Experiments RoR20A and RoR20B and RoR10A and RoR10B in which 660mm to 580mm height of slurry was deposited per lift respectively reached steady state conditions between 1 day and 4 days. In both cases fines tailings took longer times than coarse tailings. In the rate of rise experiments, the tailings deposition lifts which were deposited after the first and earlier lifts (Lifts 2 and 3) showed responses that appeared to suggest latter lifts were thicker than the earlier lifts. The times to reach steady state conditions for these lifts were longer. The coarse grained tailings slurries reached equilibrium faster than the slurries made with the fine grained catwalk tailings in general. From the results of the total heads of the experiments as captured in Table 5.9, Experiment RoR10B dissipated total heads in the shortest time followed by Experiment RoR20B. The longest times to dissipate total heads occurred in Experiments FDA and FDB.

Experiments RoR20A and RoR20B in which both fine and coarse tailings were tested showed that while the more fine grained catwalk tailings generated higher total heads than the coarse grained underflow tailings samples, the dissipation times for the total heads to reach hydrostatic conditions did not vary widely and were within a 3hr period of each other. The plots of the total heads for the RoR20B and RoR10B indicated that successive slurry depositions led to cumulative total heads that increased the time to reach steady state for the subsequent deposited slurry layers.

Constant Head Permeability Test Total Heads

The total head steady state condition of the constant head permeability test was used as an indicator of the appropriate stage at which to evaluate the saturated vertical coefficient of permeability of the tailings in the settling column. Since during the constant head permeability test the water discharged was collected during a given time interval, the plot of the discharged water versus time was also used as an additional indicator of the attainment of steady state conditions. This meant that the two conditions could be used to judge the most appropriate condition at which to determine a more reliable vertical permeability value. Figures 4.38, 4.39 and Appendix G present the height profile versus total head plots for the constant head permeability tests. In Figure 4.39 it is to be noted that the total head just before permeability commenced was recorded (t=BeforeZero). The total head was compared with heads immediately after starting the test (t=0). The change in total head was noted to take place gradually which was acceptable for the soft materials being tested.

Figure 5.17 shows the discharge rate versus time plots for the experiments. The insert within the figure compares the discharge rates for all the experiments at a finer scale than the main figure. Table 5.10 summarises total head decay and water discharge rate data used to identify the appropriate permeability values for each experiment. It was observed from the table that the time to reach steady state conditions of flow based on total head decay (column 5) and the time extracted from the water discharge time curve varied (column 4). The trends of the two respective times to reach steady state conditions were however observed to be consistent with respect to the different experiments. The time differences between the two sets of trends varied significantly with a difference ranging from 15hrs to 48hrs. The steady state times based on the water discharge time curve were the greater of the two set of values. These results indicated that whilst based on observations of total heads alone the experiment might seem to have reached steady state conditions (which would be appropriate for the determination of coefficient of permeability values), the actual state of the tailings in the column could be such that the material remained soft. Seepage forces resulting from permeability testing could rapidly make the tailings more dense leading to large variations in permeability values within a very short time with imposition of small seepage pressures. The data captured in Table 5.9 show variations in maximum head difference at isolated specific depths in the settling column in the ranges of 50mm to 300mm (which may seem negligible in terms of discharge rates in the segregated and very soft tailings layers), but the overall discharge rates for the whole

tailings layer might still have not stabilised. On the basis of this data it means that depending on which steady state times are selected, the time differences for the appropriate value of permeability could vary by between 15hrs and 2 days at the very small seepage pressures experienced during the experiments which could lead to large variations in permeability values.

From Table 5.10 it was observed that on the basis of total heads decay the coarse underflow tailings reached steady state conditions between 0.5hrs and 2hrs while fine tailings (catwalk fines) required between 8hrs and 24hrs to reach the same state of equilibrium.

Considering the tailings samples on the basis of particle size, a similar pattern emerges for discharge rates observed during the permeability tests in that underflow tailings which were coarse, discharged water at rates between 1.5 and 3.5 mm/min, while the more fine grained catwalk fines discharged water at lower rates of just 1mm/min.

It is noted that the constant head permeability test total heads at steady state varied throughout the depth of the settled column of tailings. The total heads varied between 200mm and 1450mm with the heads distributed in a step-wise pattern. The total heads with a greater value were high up the soil column and the heads of lower values at the base of the column which reflected the downward flow of water caused by the potential difference required for the permeability test.

It was further observed that the height versus total head plots comprised the segregated thicknesses of the settled tailings layers. The slopes of the plots compared well with the results of tailings permeability values computed from the permeability data obtained when the experiments were carried out. This was however expected as Equation 2-46 represents the slopes of the height of column *vs* total head plot.

5.7.3 Tailings Permeability Trends

This section discusses the vertical permeability trends of the different profiles of the settling columns and compares permeability values based on standpipes data with values obtained from transducer data. Figures 4.40 to 4.42 and Appendix G summarised the vertical permeability trends over time for the respective experiments. From examining the figures the initial permeability values were observed to decrease rapidly with time until at a much later time when the steady state permeability values which remained relatively constant were established.

In all the experiments the tailings in the settling columns were very soft and the permeability values changed rapidly during the initial stages of measurement due to the downward seepage forces and increase in effective stress that made the tailings more dense in the process reducing their permeability. It was observed that in the permeability trends (Figures 4.40 to 4.42 and Appendix G the average vertical permeability (Global k_v) was in the middle of the trends in only 20% of the cases. In 80% of the cases the average permeability values were at the bottom or in the bottom part of the trends. In the case where water flow was across bedding planes, as is the case with the settling columns, overall permeability (average in this case) is expected to be governed by the layers with the lowest permeability values. The majority of the results under this study are in agreement with this expectation.

The plots of permeability value against time (Figure 5.18) indicated that when the total heads steady state conditions were established in each experiment as shown in Table 5.10 (column 5), the permeability values were still changing rapidly and that it was only when the steady state water discharge rates (column 4) were reached that permeability values became relatively constant. Tailings permeability values were therefore taken as those permeability values obtained at the condition of the water discharge rate threshold values rather than the values based on the total heads steady state condition. Table 5.10 shows the upper and lower limits of steady state total head are as follows. The total head change indicates the head before permeability test was started (maximum head). The minimum head observed under steady state discharge conditions (at standpipe 1) is the lower limit. The variable head from the standpipes indicated flow. The head across the settling column was kept fairly constant but the head at different standpipes on settled column profiles were variable. The times between Experiments FDB and RoR20A could indicate that FDB with effectively one low permeability layer was less permeable than RoR20B which had three such layers.

Figure 5.18 demonstrates permeability values obtained using both the steady state total head and steady discharge rate conditions. The initial permeability values based on both conditions are indicated in the figure with the total heads based values lower than the water discharge rate values. The total heads conditions based initial permeability values fall within the region of rapidly changing values while the water discharge rate based values indicate initial permeability values at the time when the values had become more stable.

Vertical permeability values based on pore pressure transducer measured data and the values obtained from standpipe piezometer data were also compared. The comparisons showed that the permeability values of coarse tailings deduced from transducer data were one order of magnitude higher than the counterpart standpipe permeability based values. For the fine tailings layers the permeability values were similar to each other.

Table 5.9: Summary of total heads and times of reaching steady state conditions

Experiment	Initial Total Head (mm)	Steady State Total Head (mm)	Time to Reach Steady State (Days)	Average Head Loss (mm/day)
FDA	1565	1450	6.5	17.69
FDB	2400	1900	10	50
RoR20A Lift1	760	710	4	17.65
RoR20A Lift2	1120	1000	2.6	5.13
RoR20A Lift3	1475	1280	2.4	27.46
RoR20B Lift1	790	650	4	35
RoR20B Lift2	1170	950	2.6	84.6
RoR20B Lift3	1500	1200	2.4	125
RoR10B Lift1	633	580	2	26.5
RoR10B Lift2	1020	900	2	60
RoR10B Lift3	1255	1120	2	45
RoR10B L3 Top Up	1005	760	0.63	392

The observed trends were the same for all the experiments in which both the more coarse underflow tailings samples and the fine tailings catwalk samples were used. The observed trend was expected since both underflow tailings and catwalk fines tailings segregated by particle size into zones wherein the only difference was the extent of fineness or coarseness of the respective settling columns.

The variation of the standpipe data based permeability values observed in coarse grained layers was believed to reflect the relatively slow response times of the standpipes at 2 to 5 seconds in relation to the more rapid response time of pore pressure transducers at 0.5 to 0.9 seconds. Since large values of the peizometric heights were involved in the coarse grained tailings there were high volumes of water flow which reflected in permeability values obtained from the two systems. The standpipes which are a slower response time system had a time lag relative to the transducers which were very sensitive to pressure changes and recorded pressures at the instance of occurrence (despite being slowed down by the data logger sampling rate). For the tailings layers comprising fine particles the relatively low quantities of water flow resulted in low piezometeric heights measured by the standpipes and therefore less height changes for the standpipes. The reduced piezometric heights minimised the effects the slower measuring standpipes could have had. The negligible differences between transducer and standpipe measurements resulting from the low volume of water flow through the standpipes brought the two sets of permeability values close to each other. The opposite was true for coarse grained tailings where large volumes of water in the standpipes coupled with the low response times of the standpipes resulted in large disparity between the two sets of values. It needs to be noted that with tailings the response time of standpipes and transducers were probably greater than the response times values in water only.

Table 5.10: Constant head permeability test steady state discharge rates and times

Experiment.	Steady State Total Head (mm)	Steady State Discharge Rate (ml/min)	Time To Reach Steady State Discharge Rate (Days)	Time to Reach Total Head Steady State (Days)
FDA	400-1300	2.65	0.79	0.8-8
FDB	500-1450	1.02	0.96	0.3-5.5
RoR20A	200-1300	3.26	0.75	0.1-2
RoR20B	700-1200	0.43	3	1-8
RoR10B	620-1170	1.54	2	0.6-4.3

Table 5.11 summarises the average permeability values obtained from the study. An assessment of the permeability of the segregated fine and coarse fractions of the tailings

recovered from the settled column yielded permeability values as follows: 10^{-5} cm/sec to 10^{-6} cm/sec for fine tailings and 10^{-3} cm/sec to 10^{-5}cm/sec for coarse tailings. These indicated differences of up to three orders of magnitude.

Table 5.11: Average vertical permeability of gold tailings

Experiment	Average Vertical Permeability (cm/sec)
FDA	$5.25x10^{-5}$
RoR20A	$8.15x10^{-5}$
RoR20B	$2.04x10^{-5}$
RoR10B	$8.22x10^{-5}$
FDB	$2.44x10^{-5}$

The vertical permeability values of the experiments computed using the slopes of the settling column depth profile versus the total heads plots agreed well with the permeability values obtained from the permeability tests. Using the slopes of the plots the coarse tailings fraction (sand) resulted in permeability value of 10^{-3} cm/sec to 10^{-5} cm/sec. The more mixed tailings fractions in the middle of the settled column of tailings up to the very fine tailings fractions at the top of the settling column gave permeability range of 10^{-5} cm/sec to 10^{-7} cm/sec. Few exceptions were observed where the permeability values of layers that contained very thin layers of fine tailings could not be determined successfully. Figure 5.19 present variation of vertical permeability values with height of column. The results from Experiments FDA and FDB show a gradual decrease in permeability as the settling column is traversed upwards reflecting the deposition of coarse tailings at the base and fine tailings at the top of the respective column with a gradual change in particle size grading in-between the two extremes. The vertical permeability plot pattern for the rate of rise experiments for its part reflected the alternating coarse and fine tailings profiles of the successive layer depositions which had segregated. Figure 5.20 summarises the vertical permeability values obtained under this study for all the experiments. The figure shows the segregated fine and coarse tailings fractions as well as their mixtures along the height of the settling column based on particle size distribution and visual observations in addition to permeability value results.

5.8 Discussion Summary

Gold tailings samples used for this research were characterised and shown to be representative of gold tailings properties in general. An analysis and discussion of excess pore water pressure trends and magnitudes was undertaken which indicated low magnitudes excess pore water pressures that dissipated within short periods of time for all slurry deposition scenarios of the experiments.

Particle size analysis, specific gravity tests and saturated tailings permeability tests results as well as fabric analysis of recovered dried gold tailings showed that tailings segregated in settling column experiments.

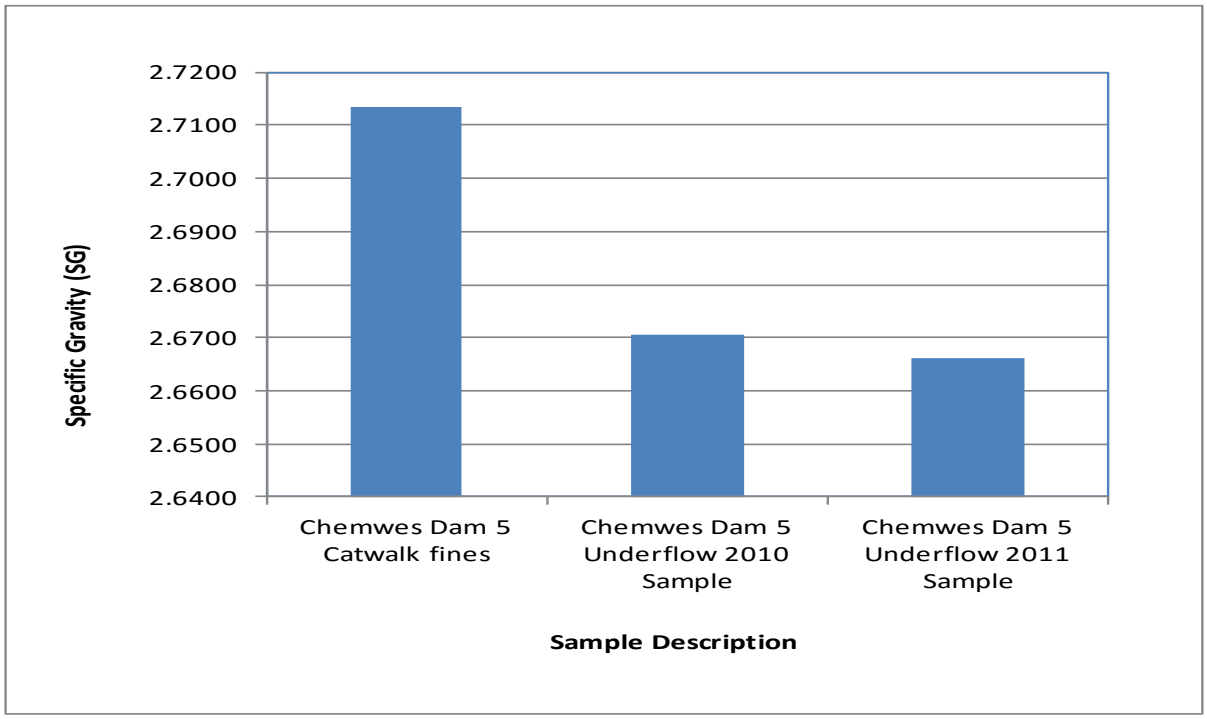

Figure 5.1: Specific gravity of solids comparisons

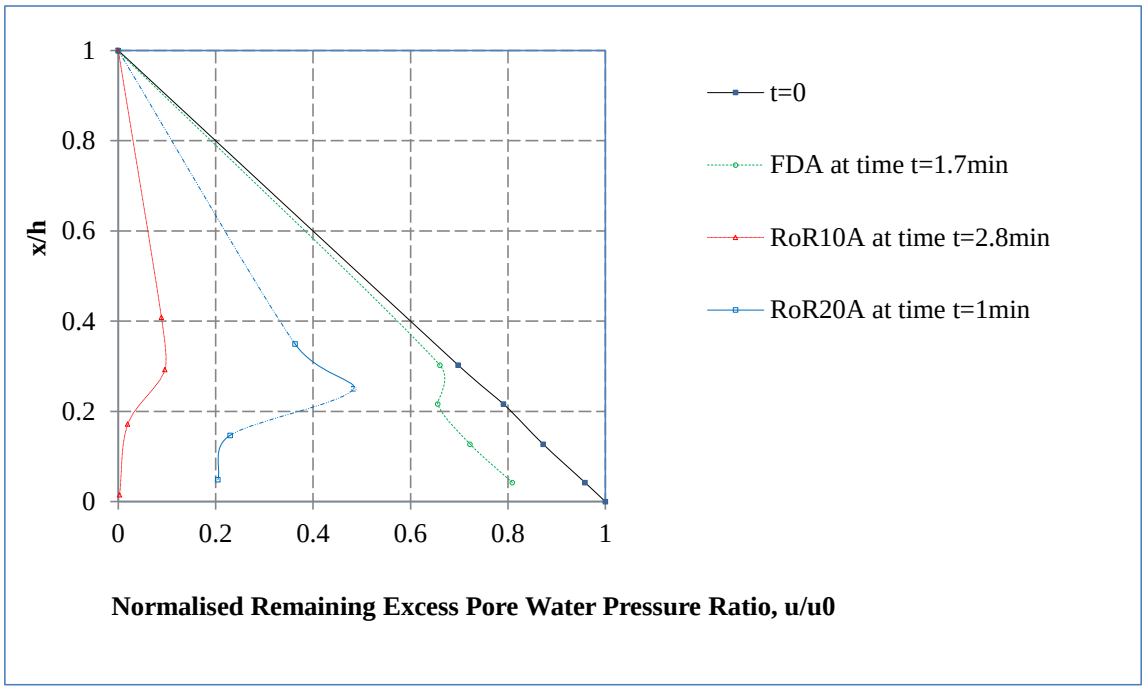

Figure 5.2a: Relative magnitudes of initial maximum excess pore water pressure in underflow tailings

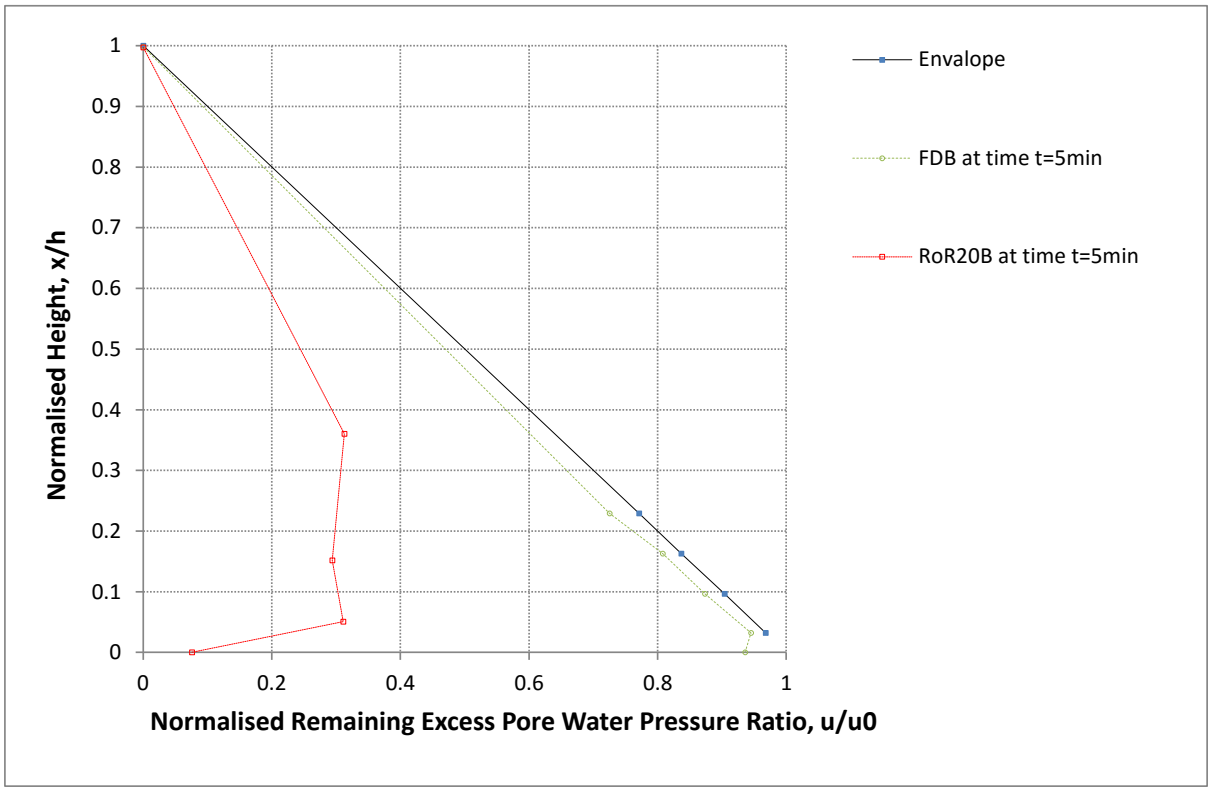

Figure 5.2b: Relative magnitudes of initial maximum excess pore water pressure in catwalk fines tailings

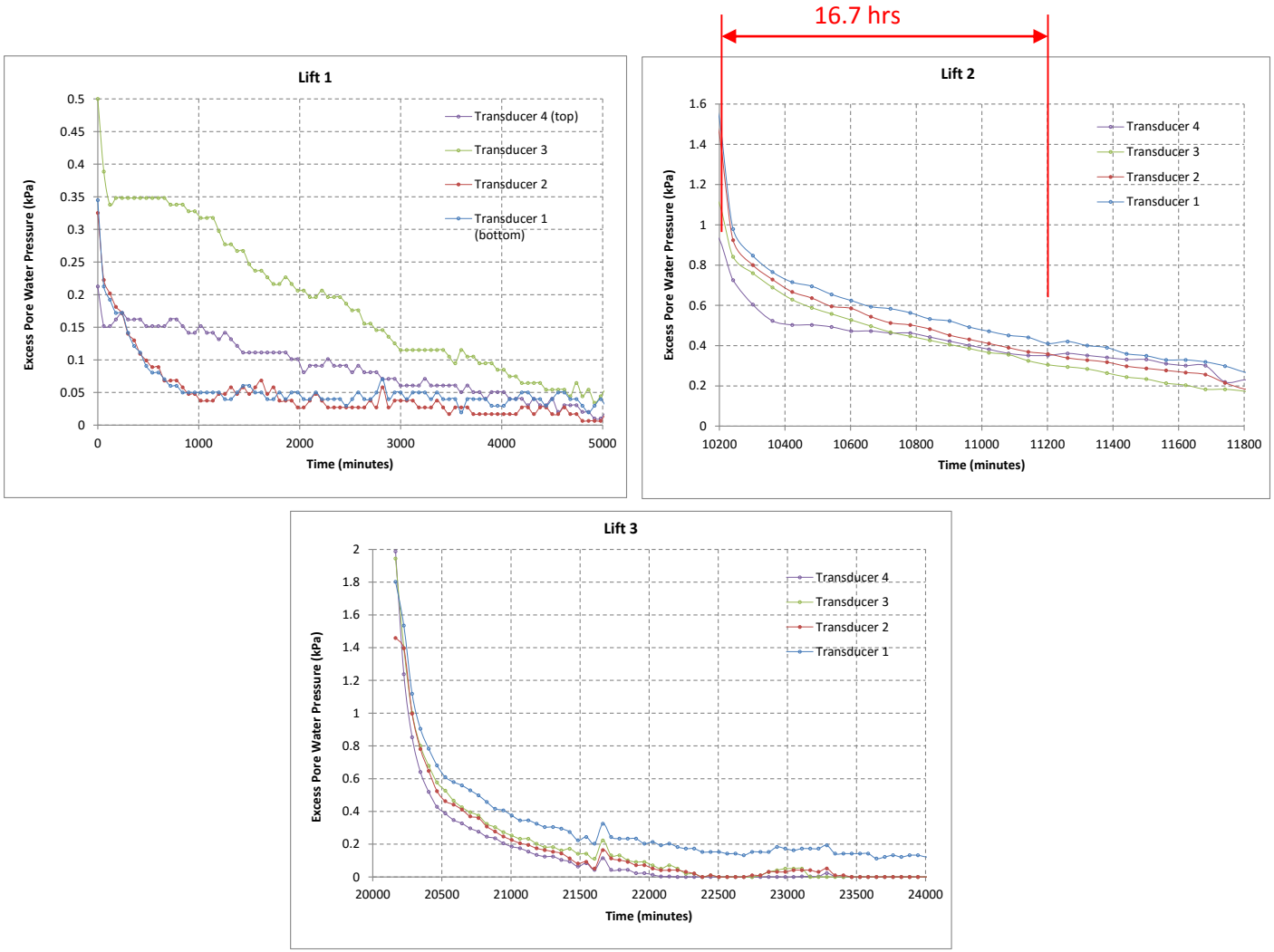

Figure 5.3: Data logger Experiment RoR10A early pore pressure lift trend

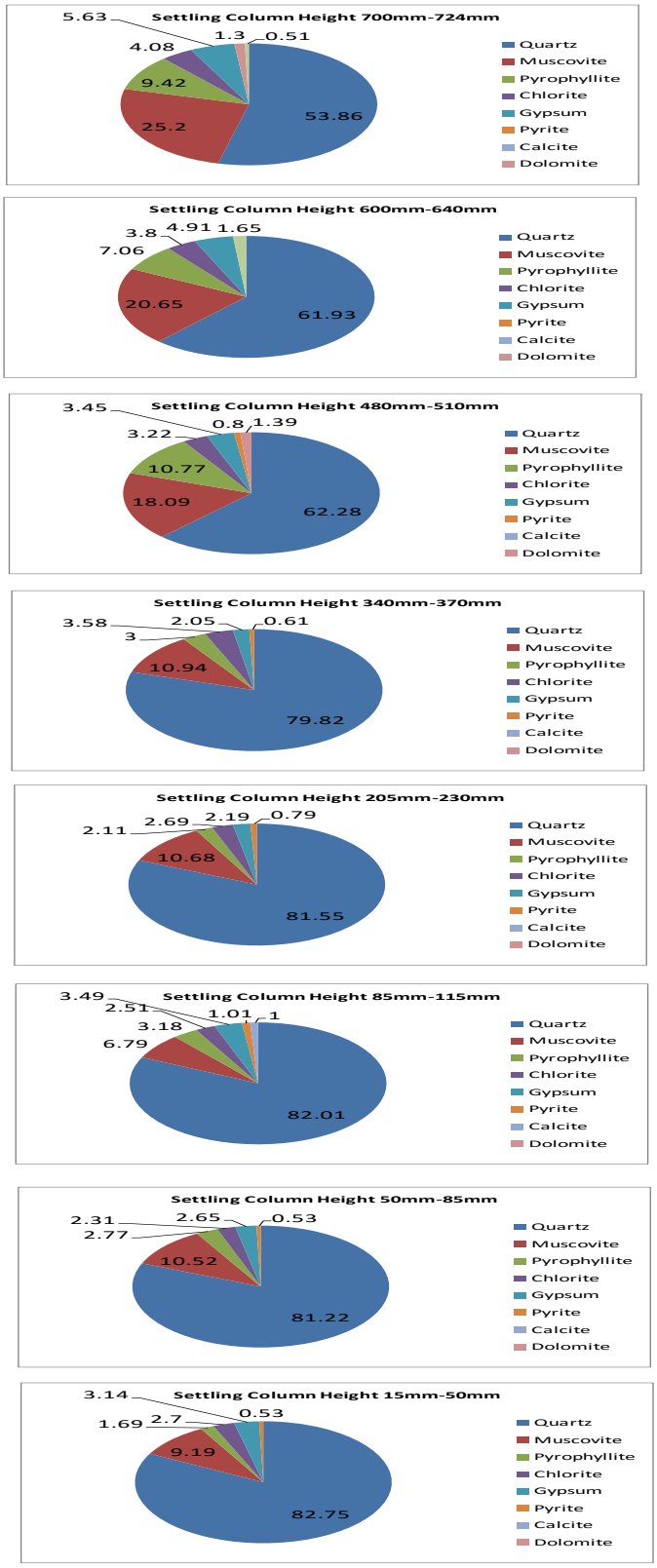

Figure 5.4: Experiment FDB depth profile samples XRD derived minerals comparisons

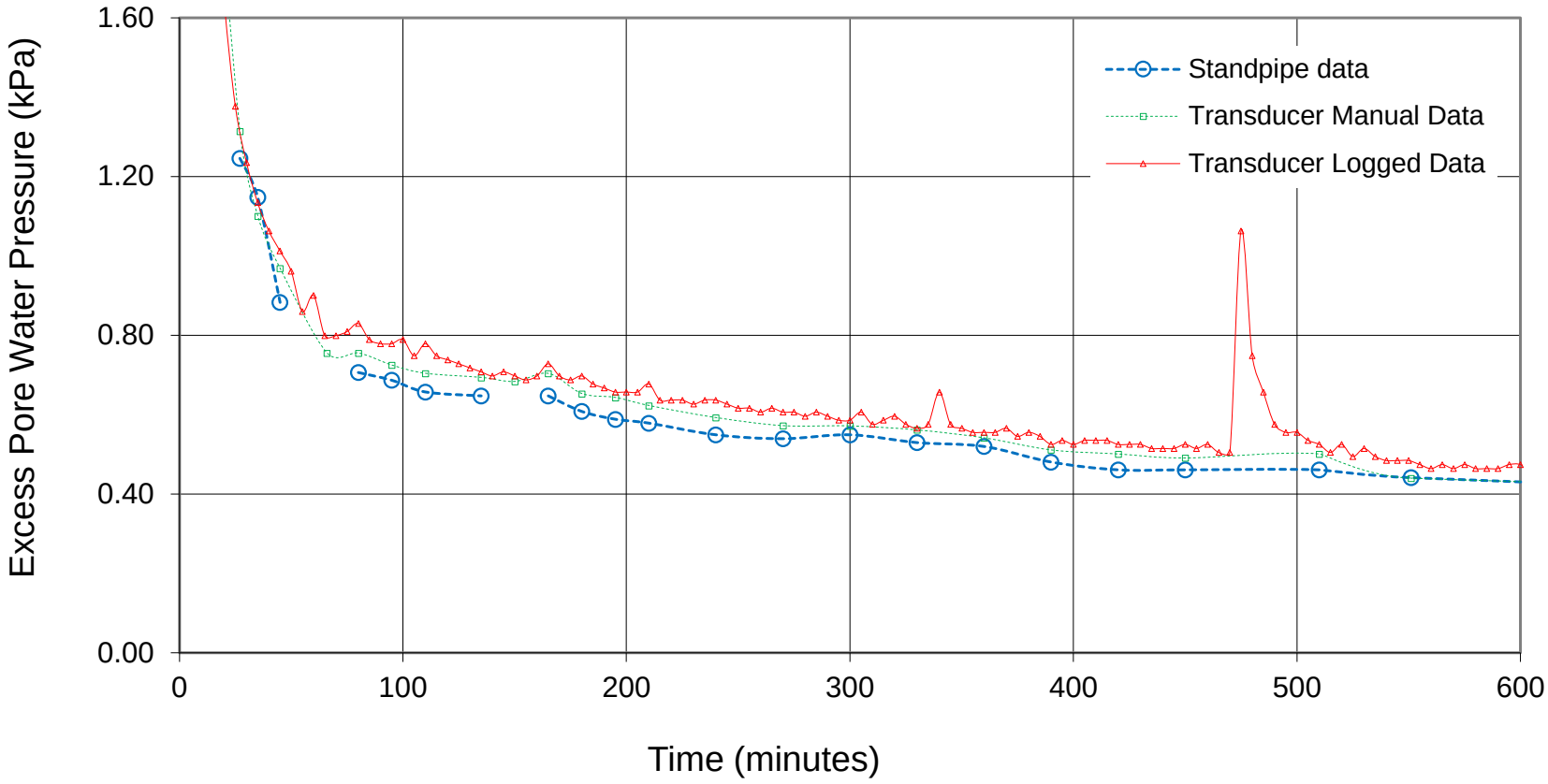

Figure 5.5a: Comparison of excess pore water pressure at depth 61.5mm Experiment FDA – large scale

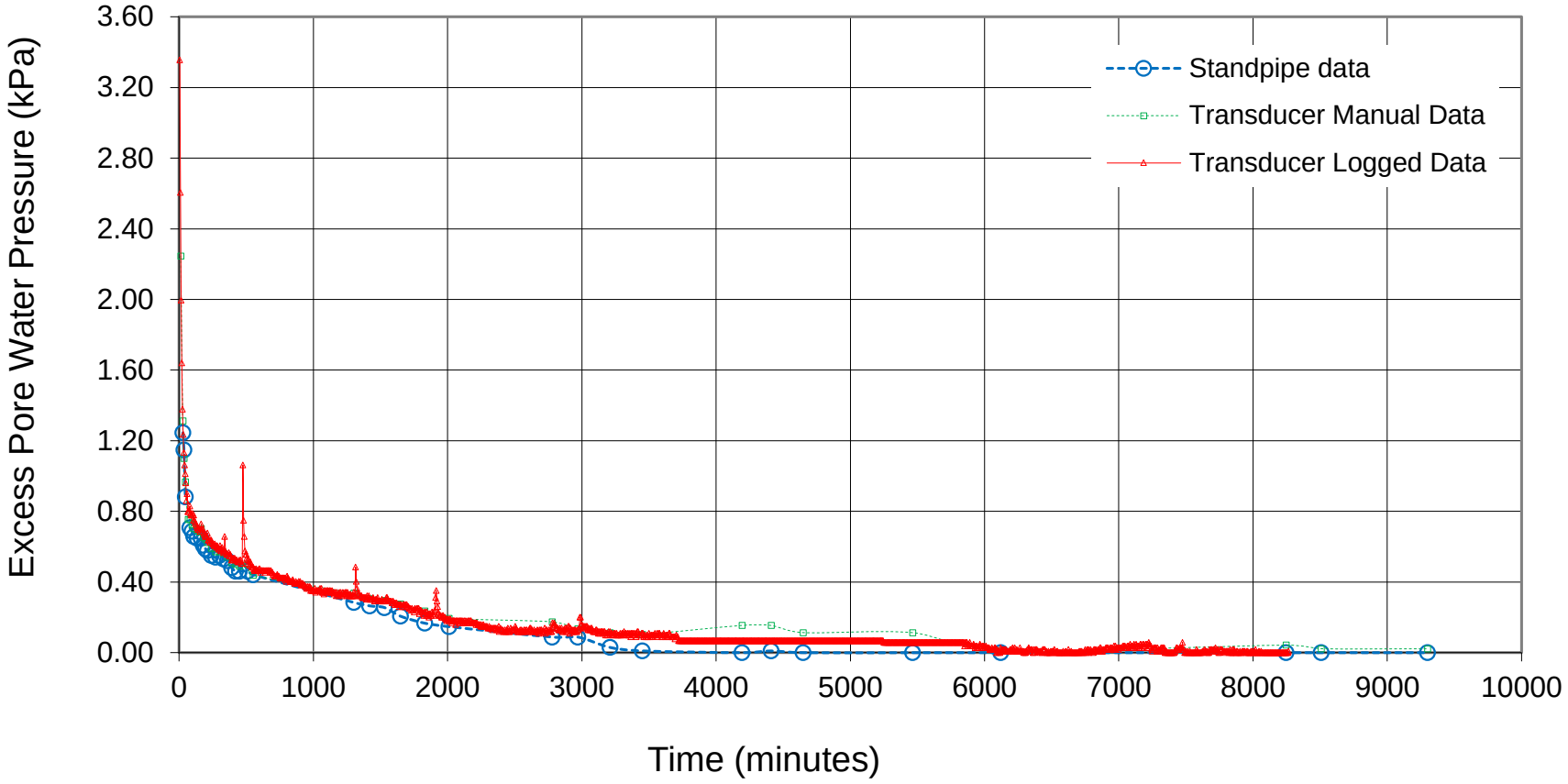

Figure 5.5b: Comparison of excess pore water pressure at depth 61.5mm Experiment FDA - small scale

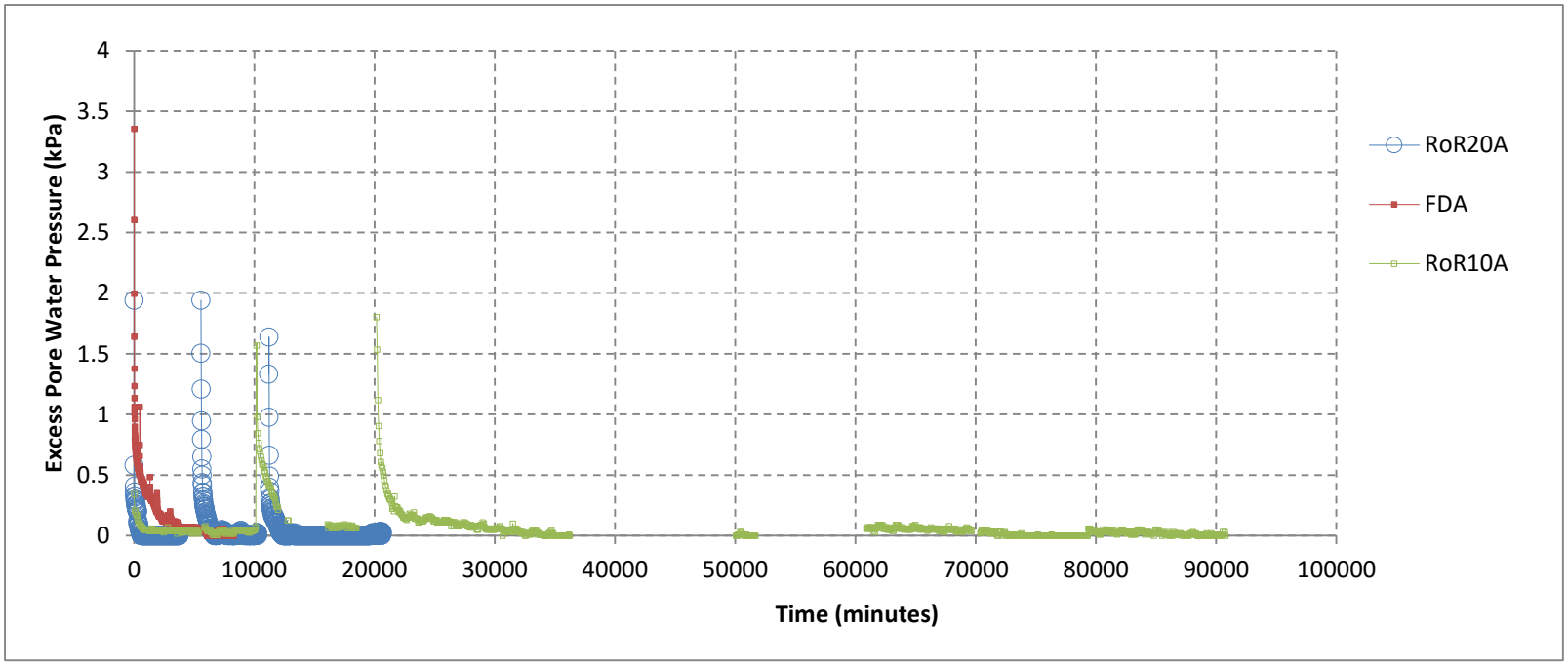

Figure 5.6: Comparison of Transducer 1 excess pore water pressure in underflow tailings Experiments FDA, RoR20A and RoR10A

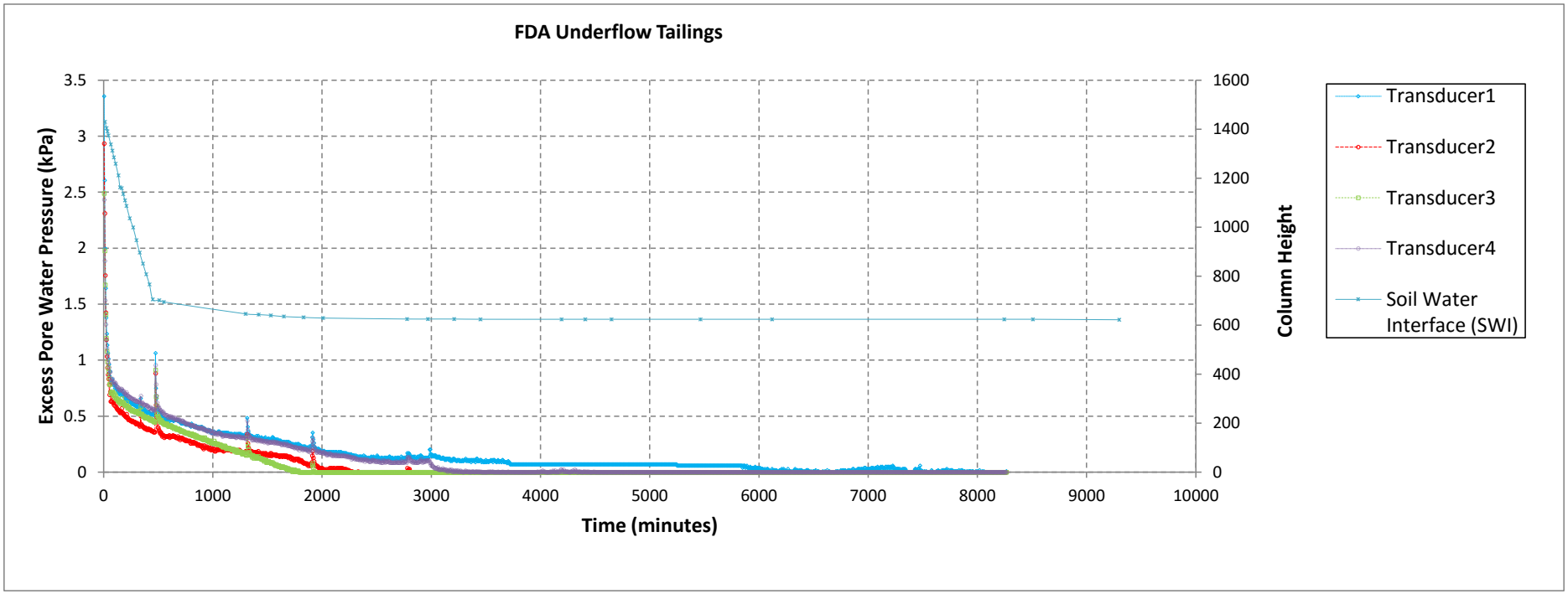

Figure 5.7a: Soil water interface and excess pore pressure change over time - Experiment FDA

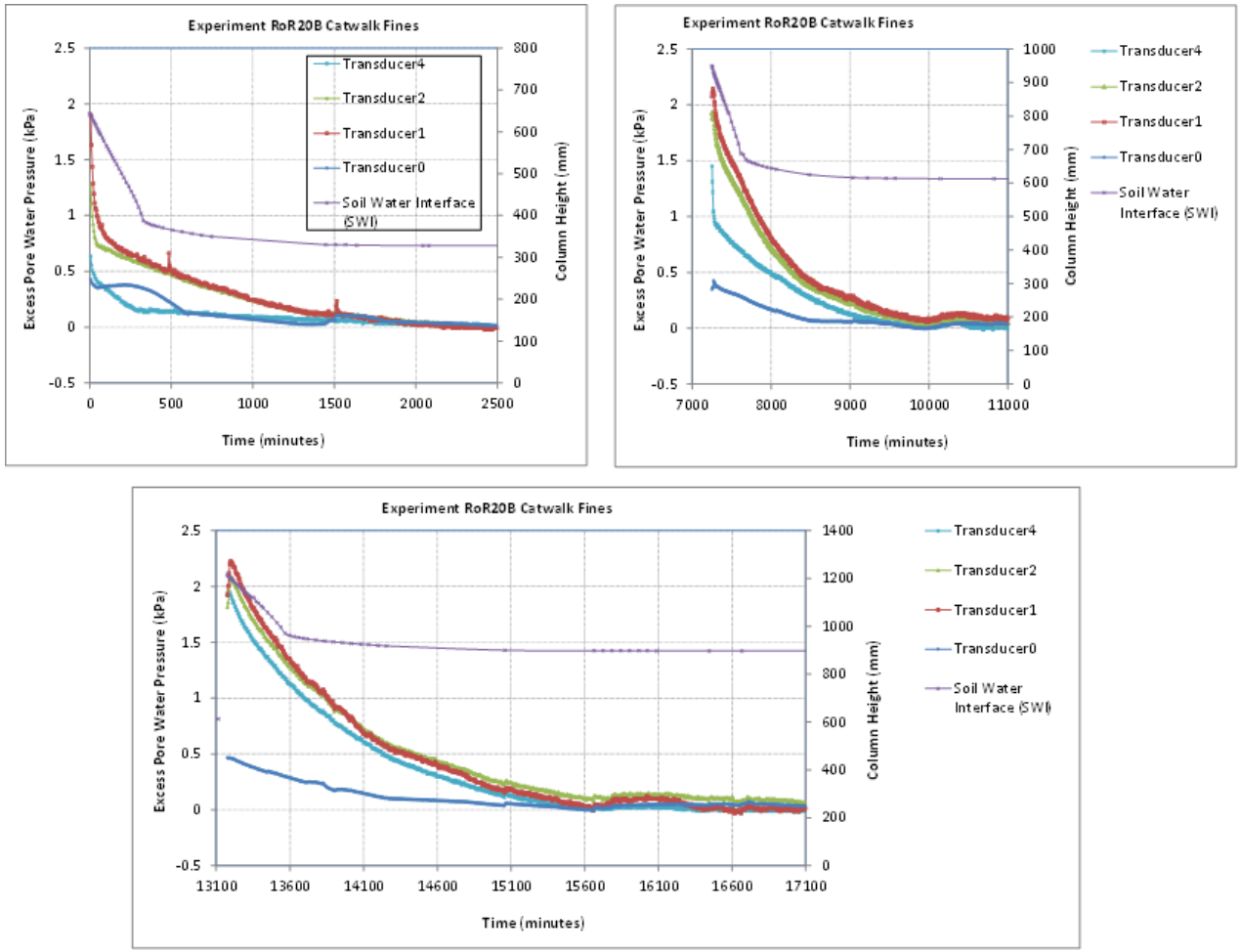

Figure 5.7b: Soil water interface and excess pore pressure change over time – Experiment RoR20B

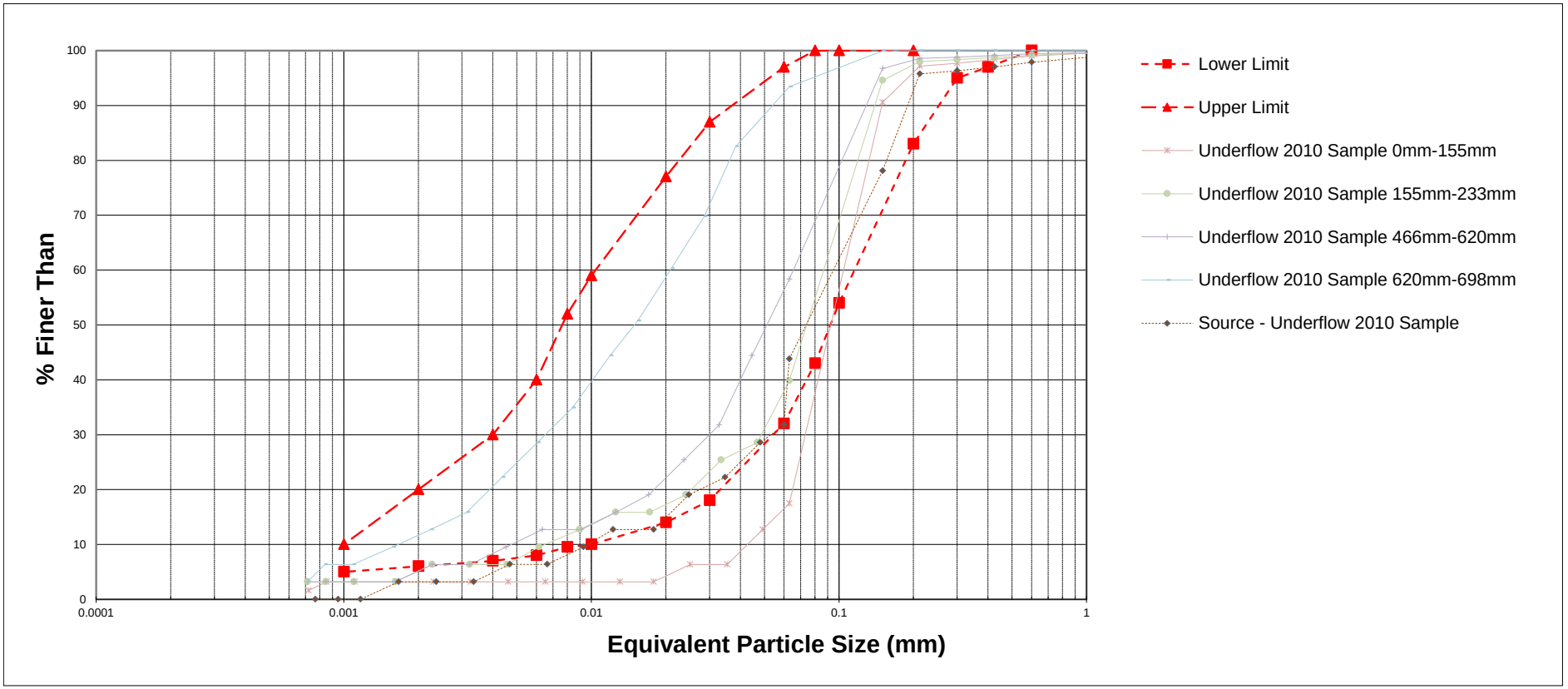

Figure 5.8: Gradations of recovered Experiment RoR10A sample at large interval (100mm) specimen spacing

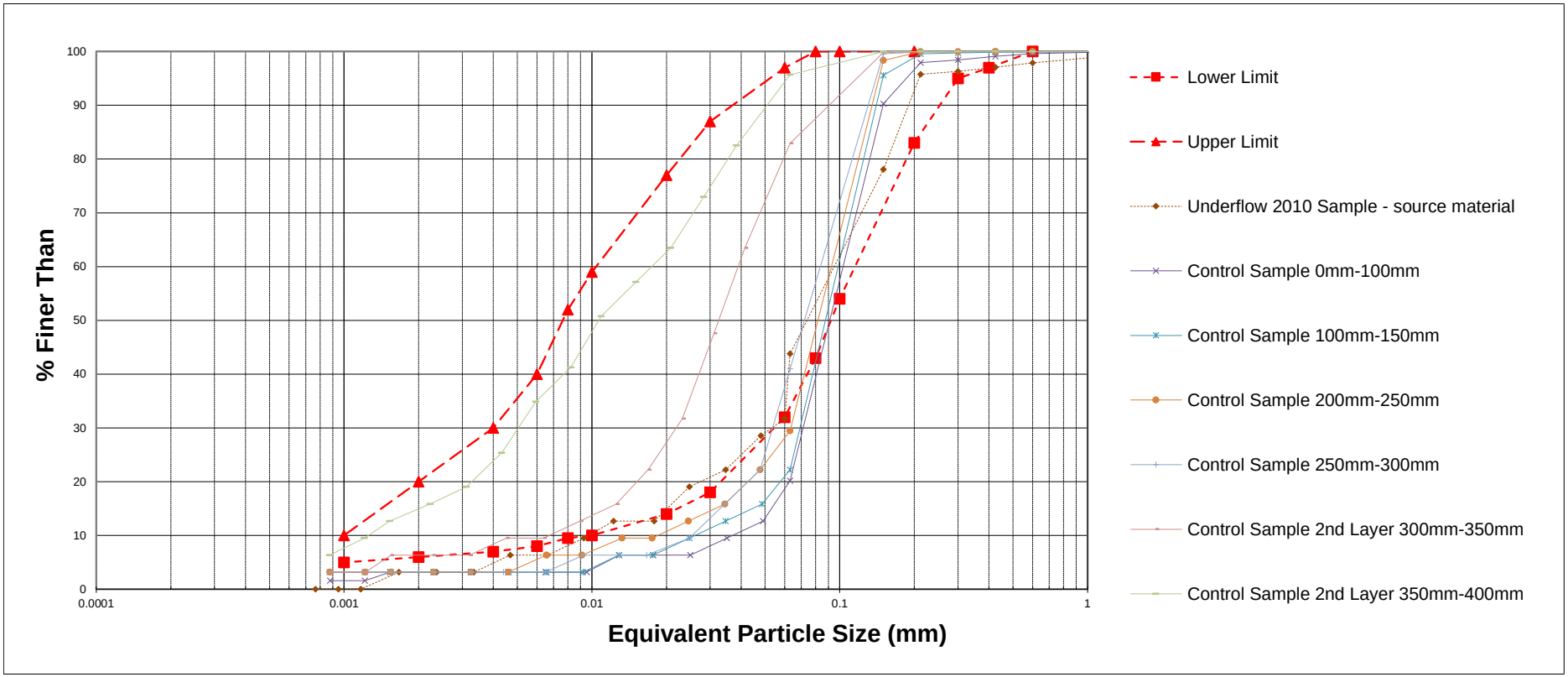

Figure 5.9: Gradations of recovered RoR 10m/yr sample not subjected to permeability test -large interval (100mm) specimen spacing

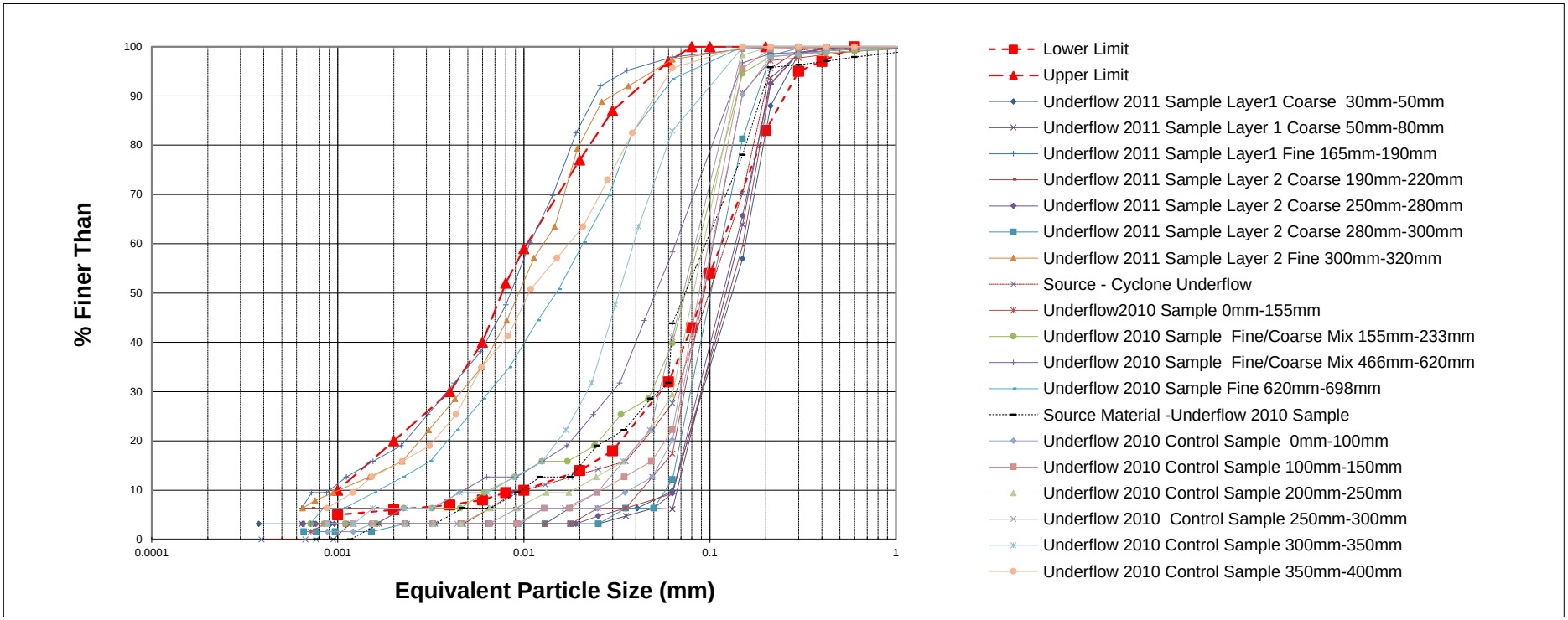

Figure 5.10: Gradations of recovered Experiment RoR10A and RoR10B samples

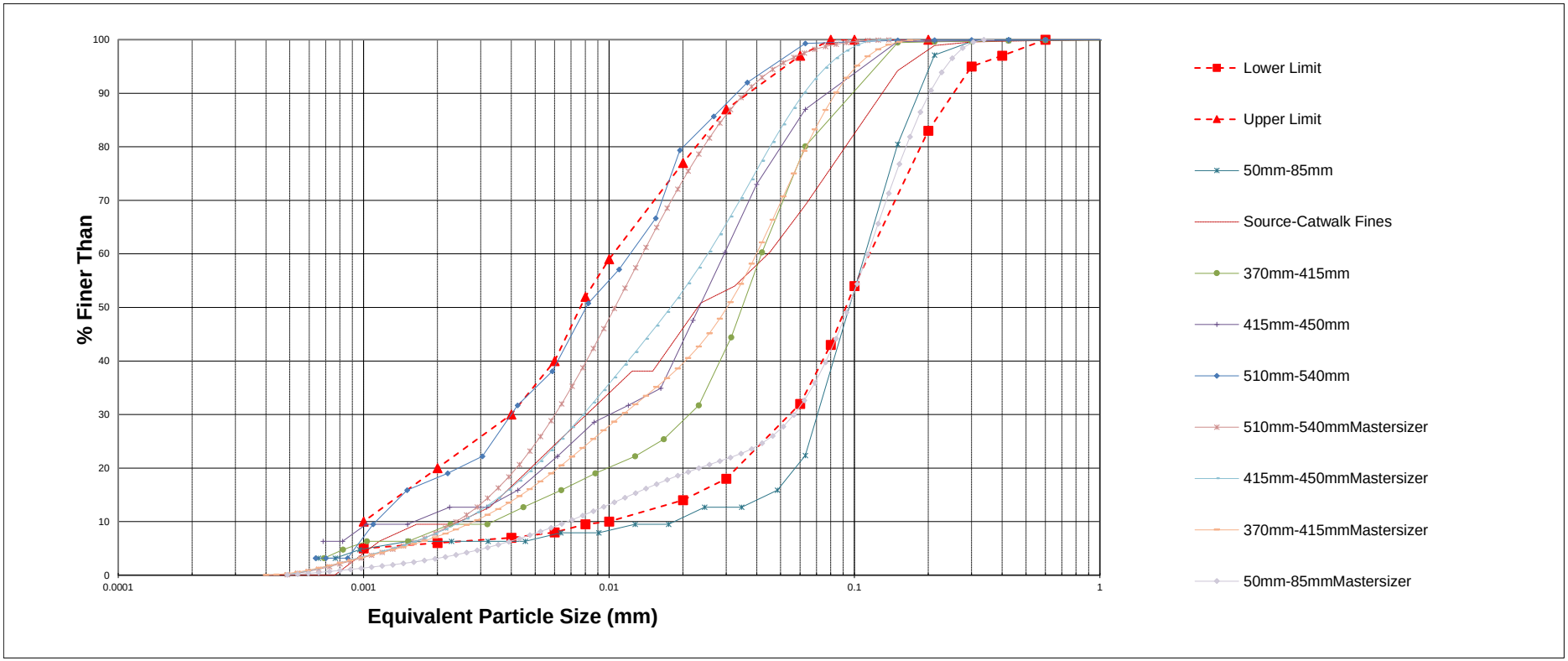

Figure 5.11: Sieve and hydrometer & Mastersizer diffraction analysis gradations of recovered Experiment FDB sample at small specimen intervals

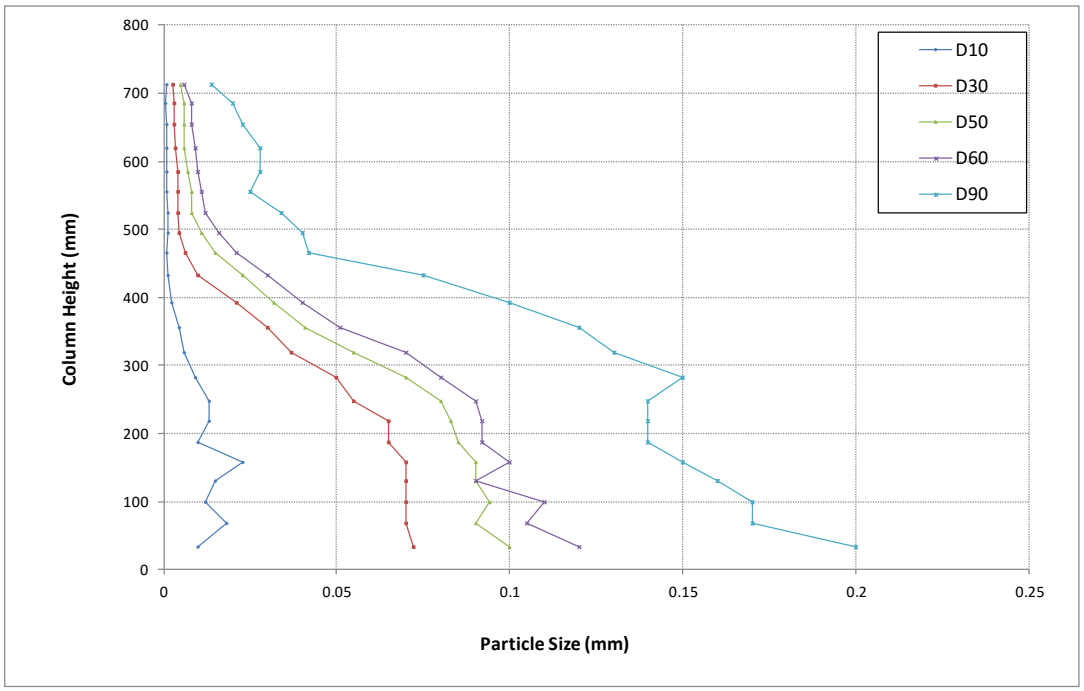

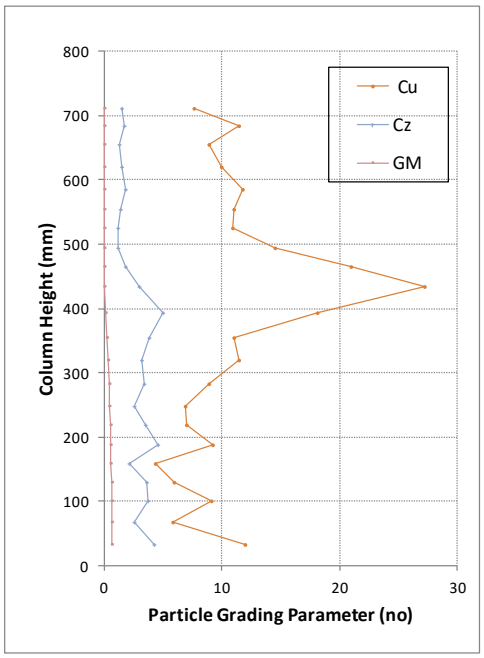

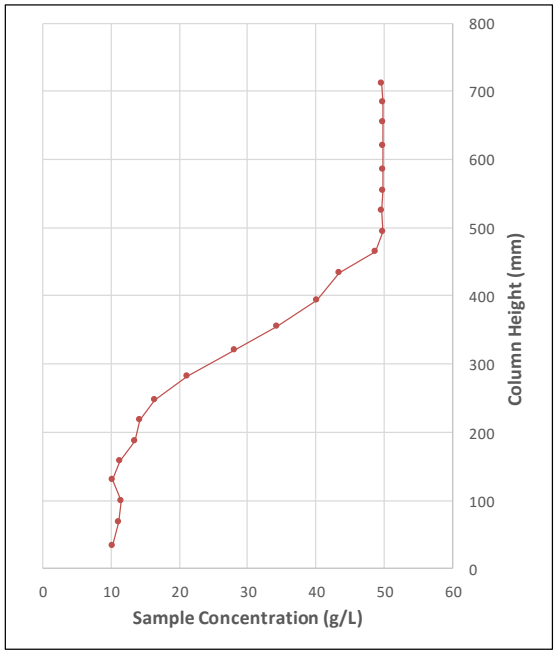

Figure 5.12: Variation of particle size parameters with column height – Experiment FDB

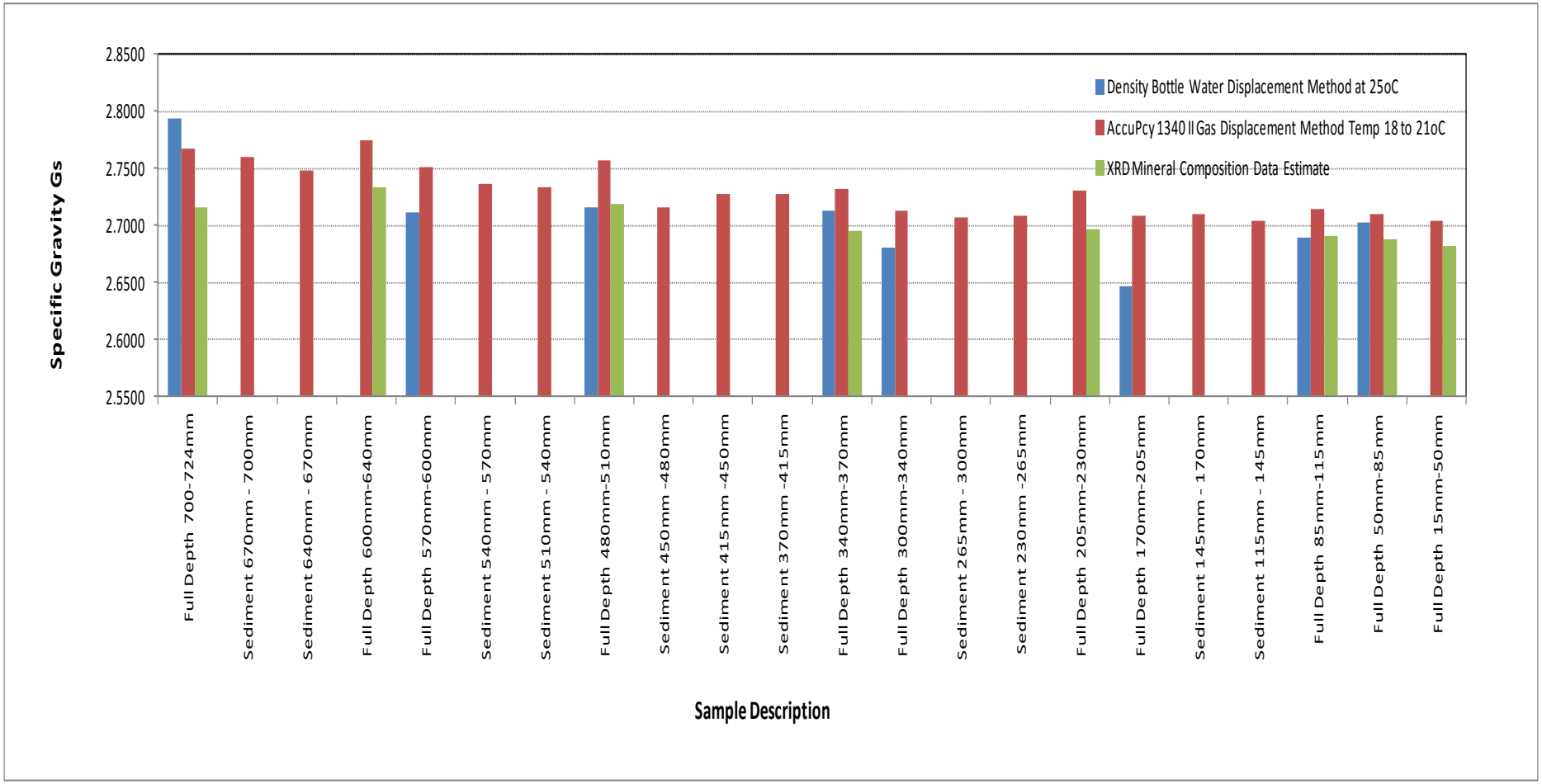

Figure 5.13: Comparisons of specific gravity of solids determined by different methods: density bottle, AccuPyc 1340 II gas displacement and XRD composition estimated values – Experiment FDB

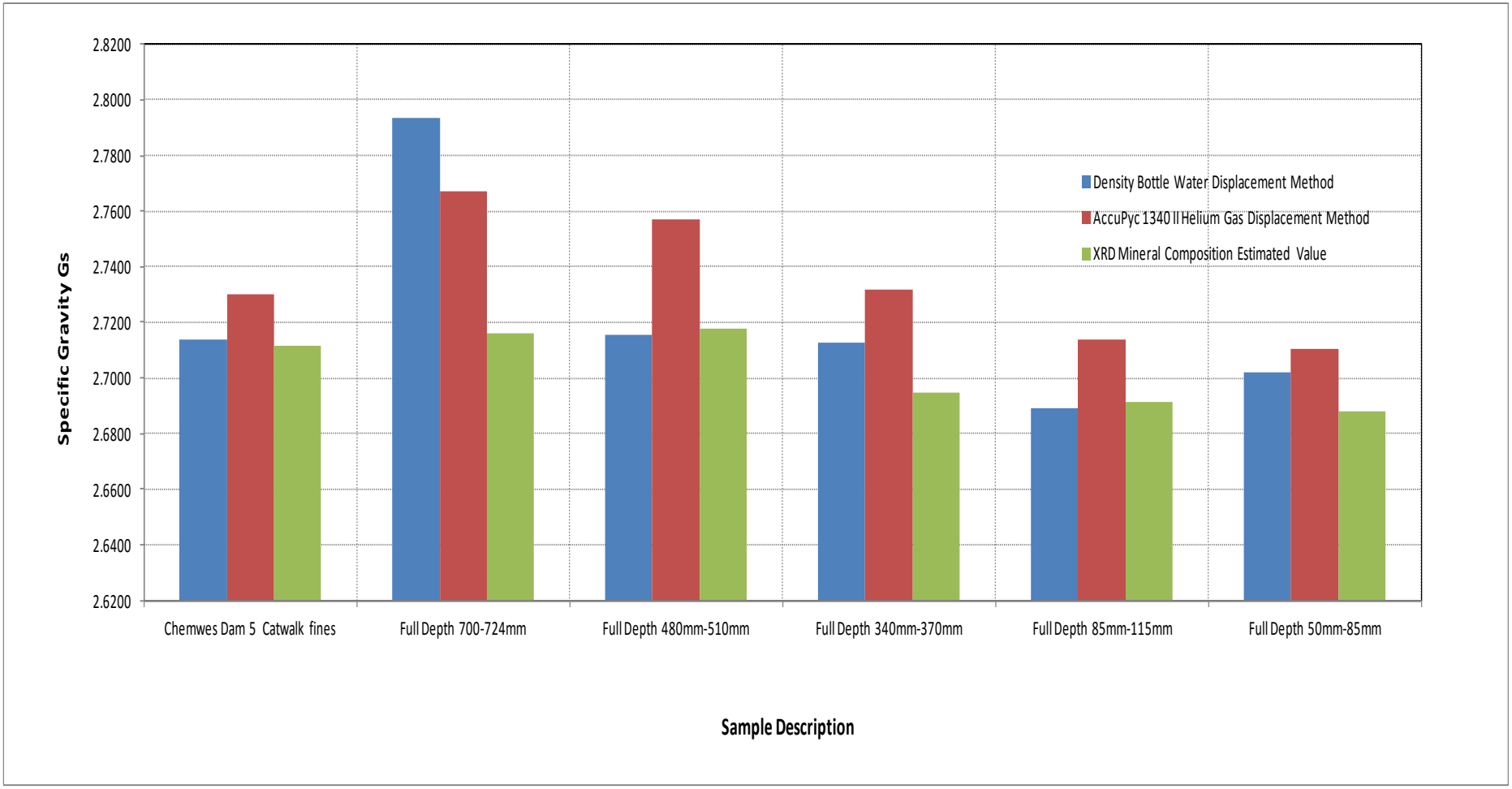

Figure 5.14: Comparisons of specific gravity of solids determined by different methods: density bottle, AccuPyc 1340 II gas displacement and XRD composition estimated values -Experiment FDB

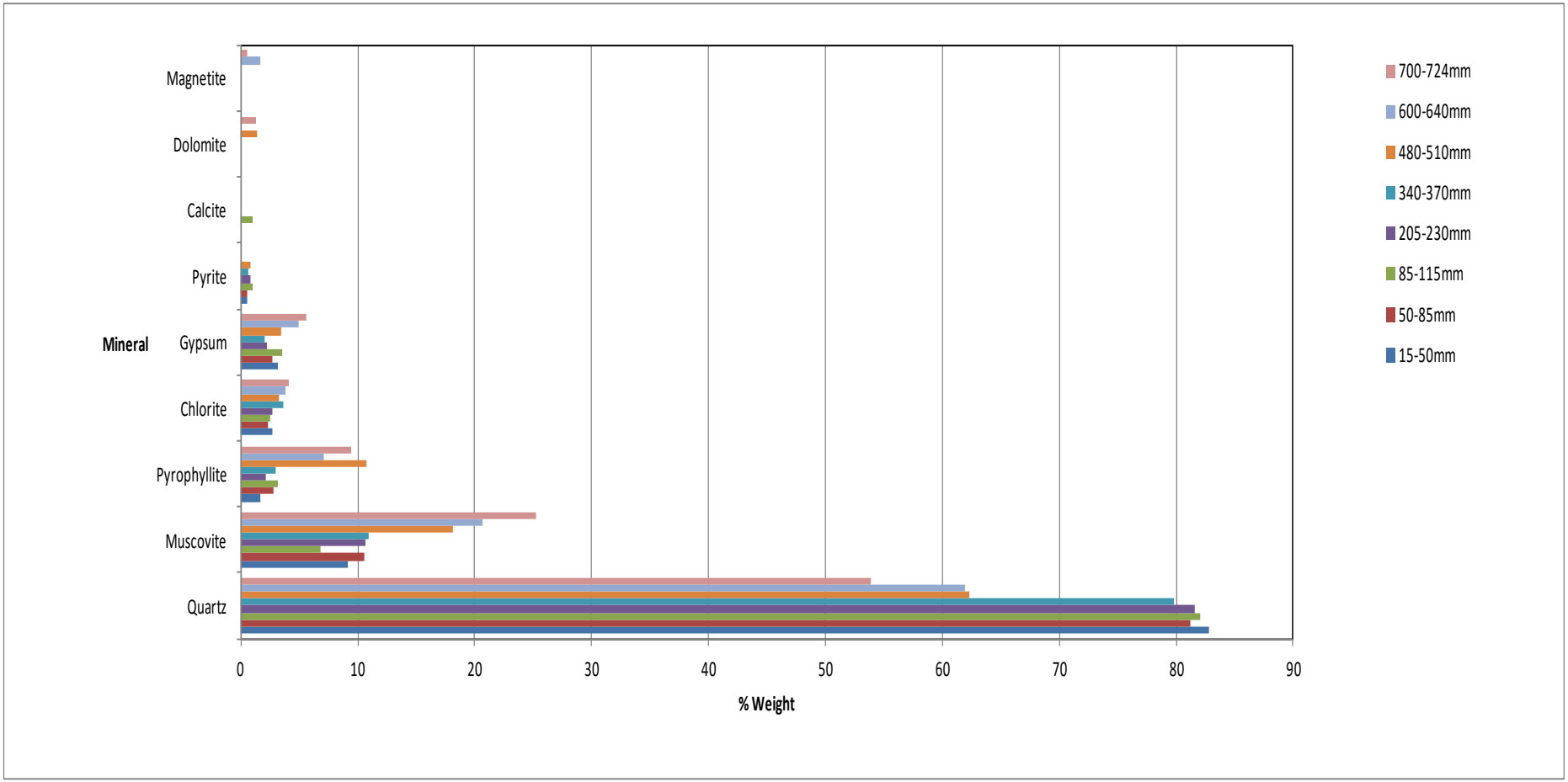

Figure 5.15: Experiment FDB depth profile samples XRD derived minerals comparisons

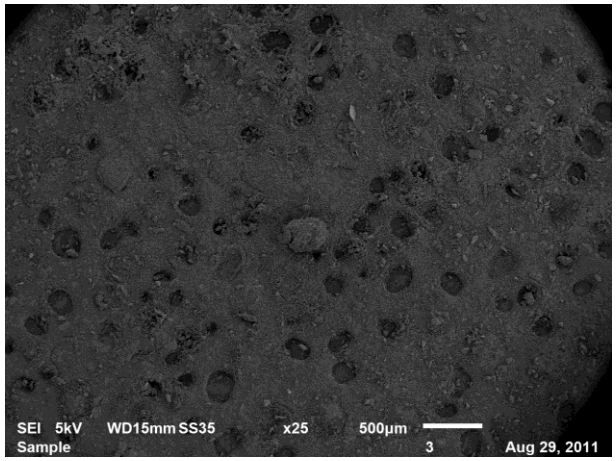

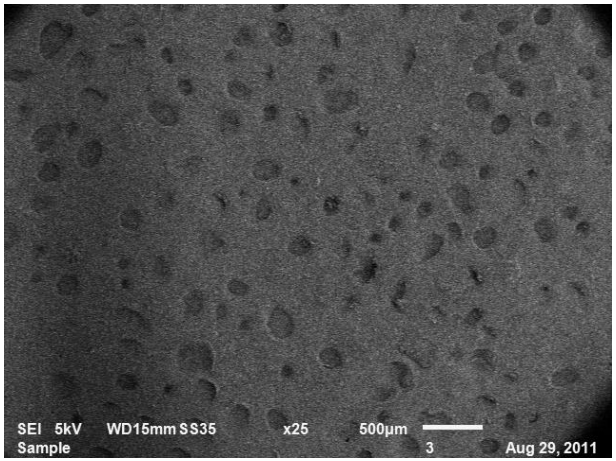

RoR10mA 350mm-400mm

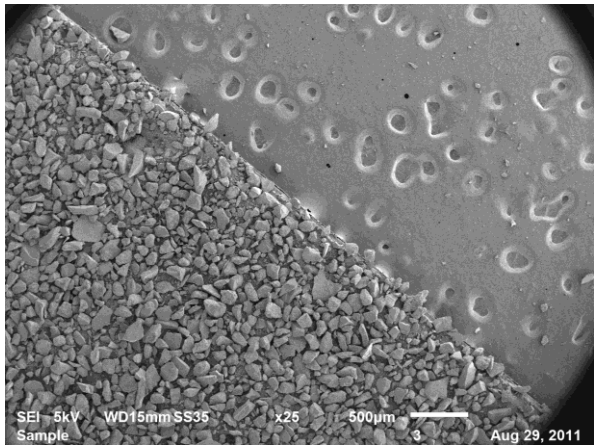

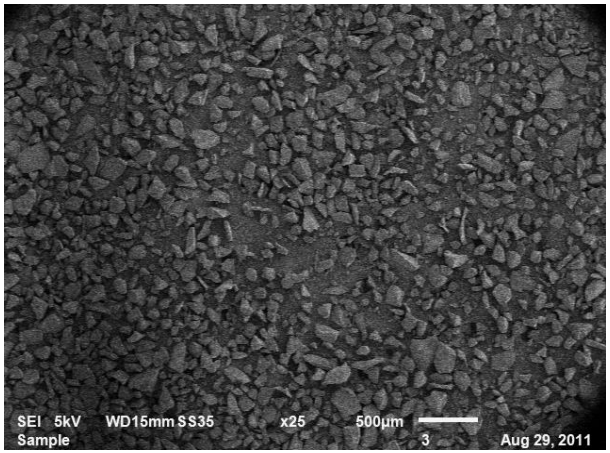

RoR10A 150mm-200mm

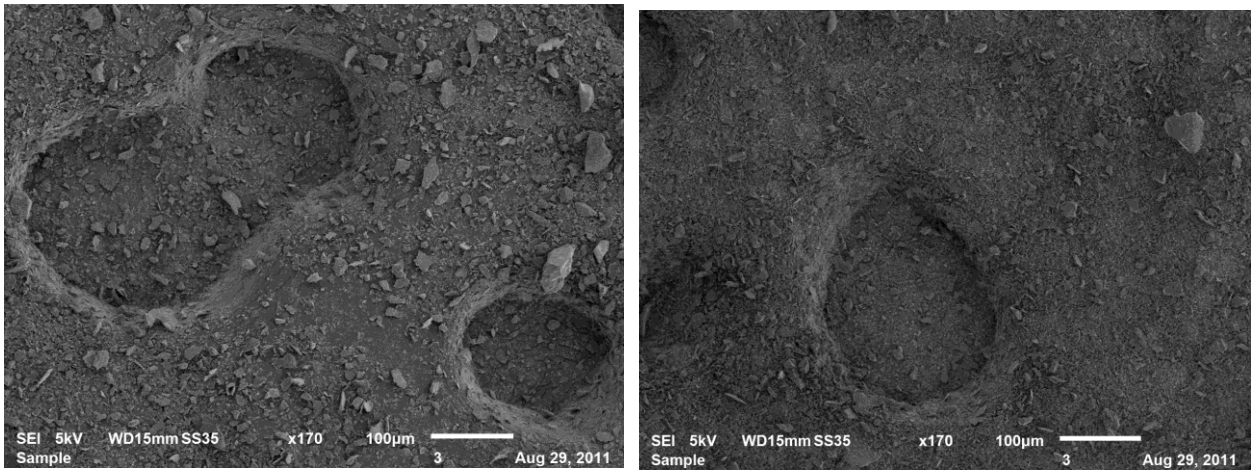

RoR10A 350mm-400mm

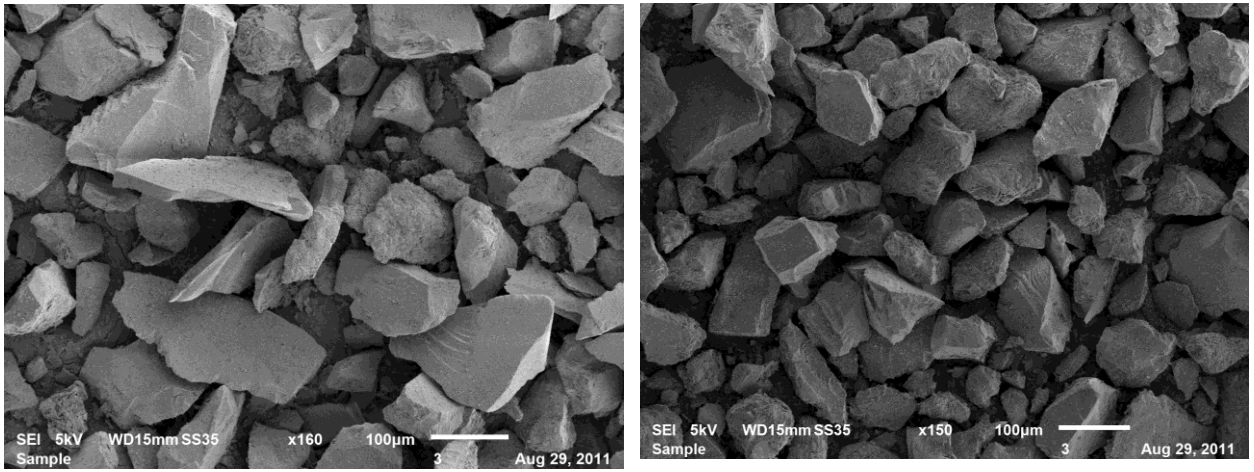

RoR10A 125mm-150mm

Figure 5.16: Experiment RoR10A (without permeability test) SEM micrographs (CT) -horizontal prints

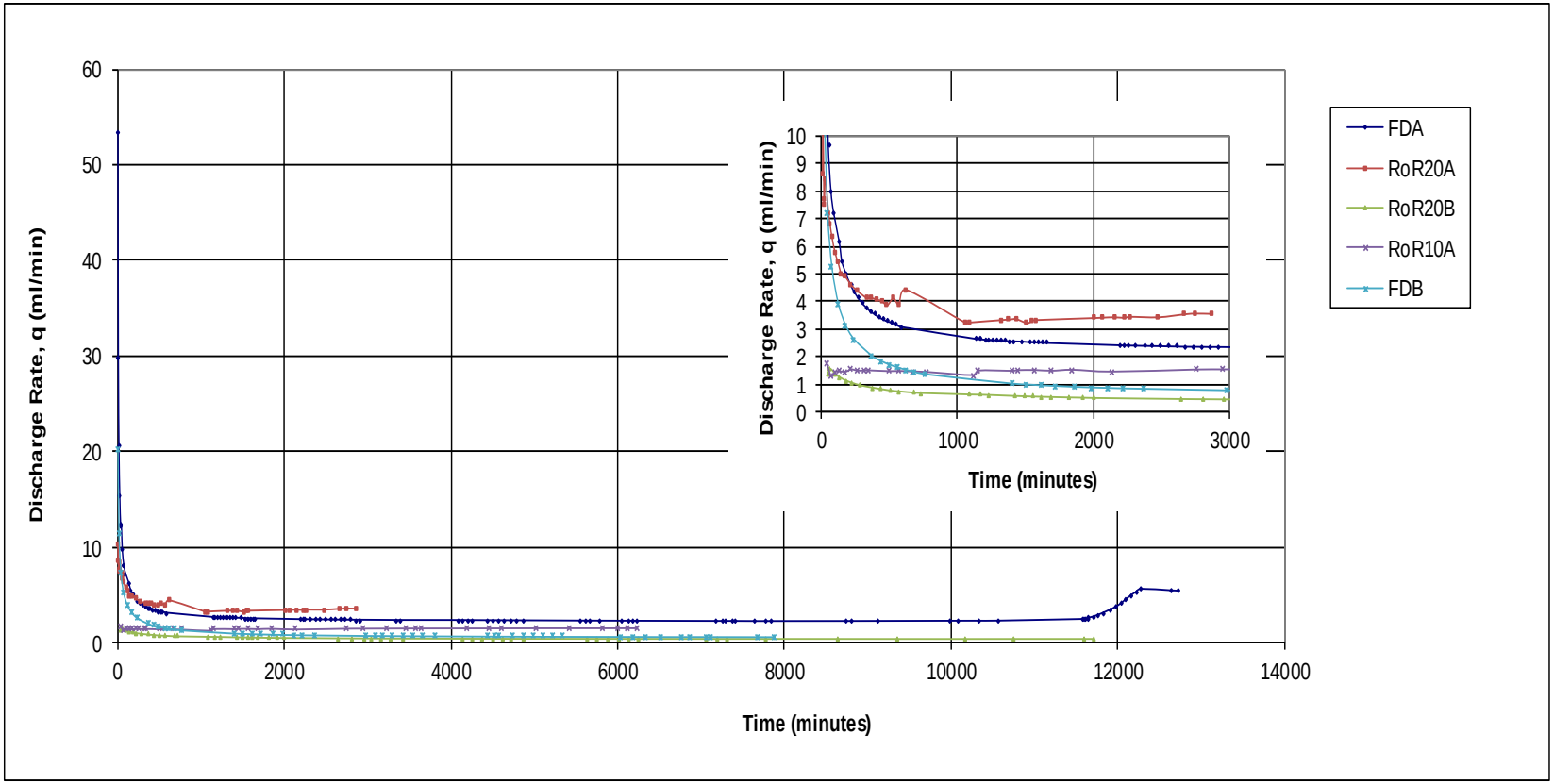

Figure 5.17: Permeability discharge rates - all experiments

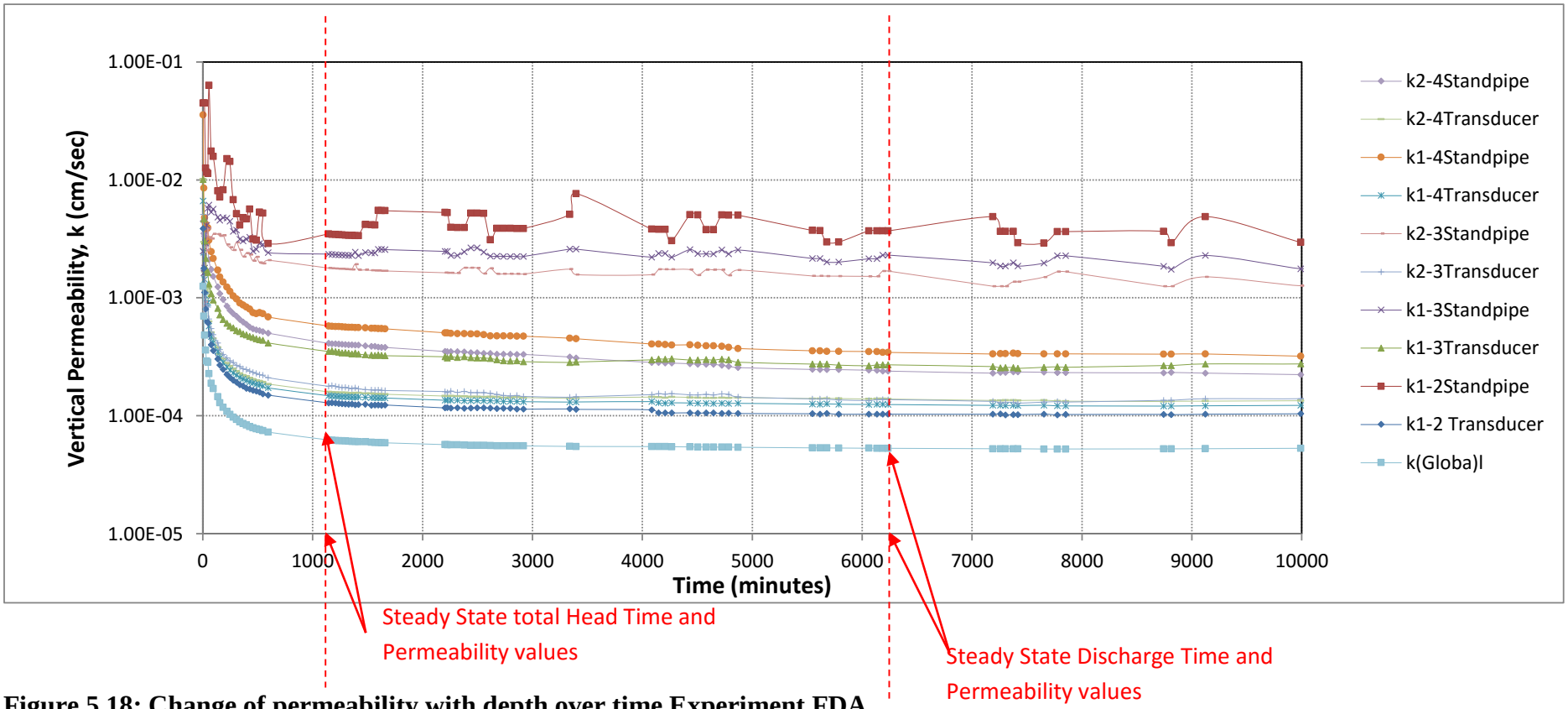

Figure 5.18: Change of permeability with depth over time Experiment FDA

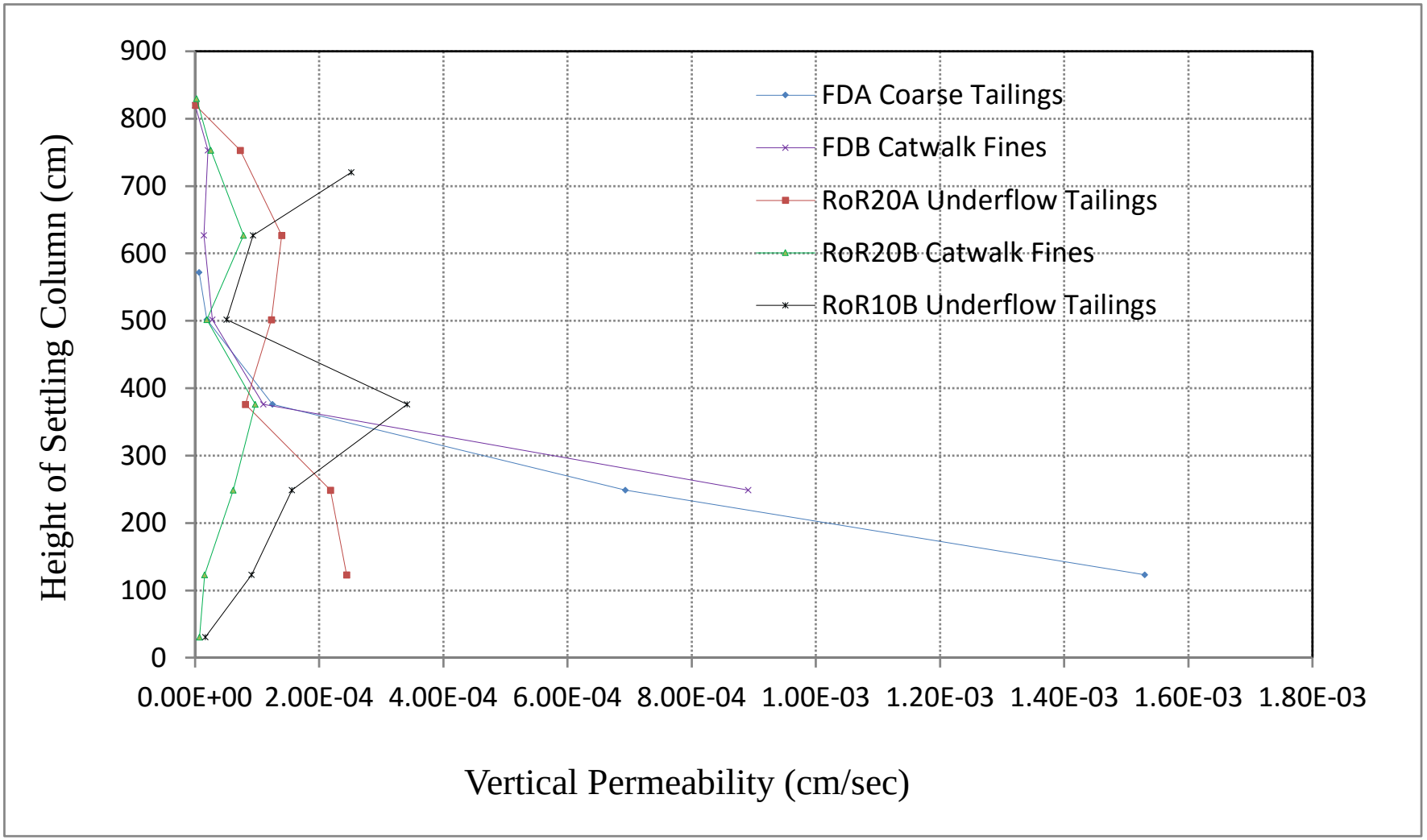

Figure 5.19: Variation of tailings permeability with depth - Experiments FDA, FDB, RoR20A, RoR20B and RoR10B

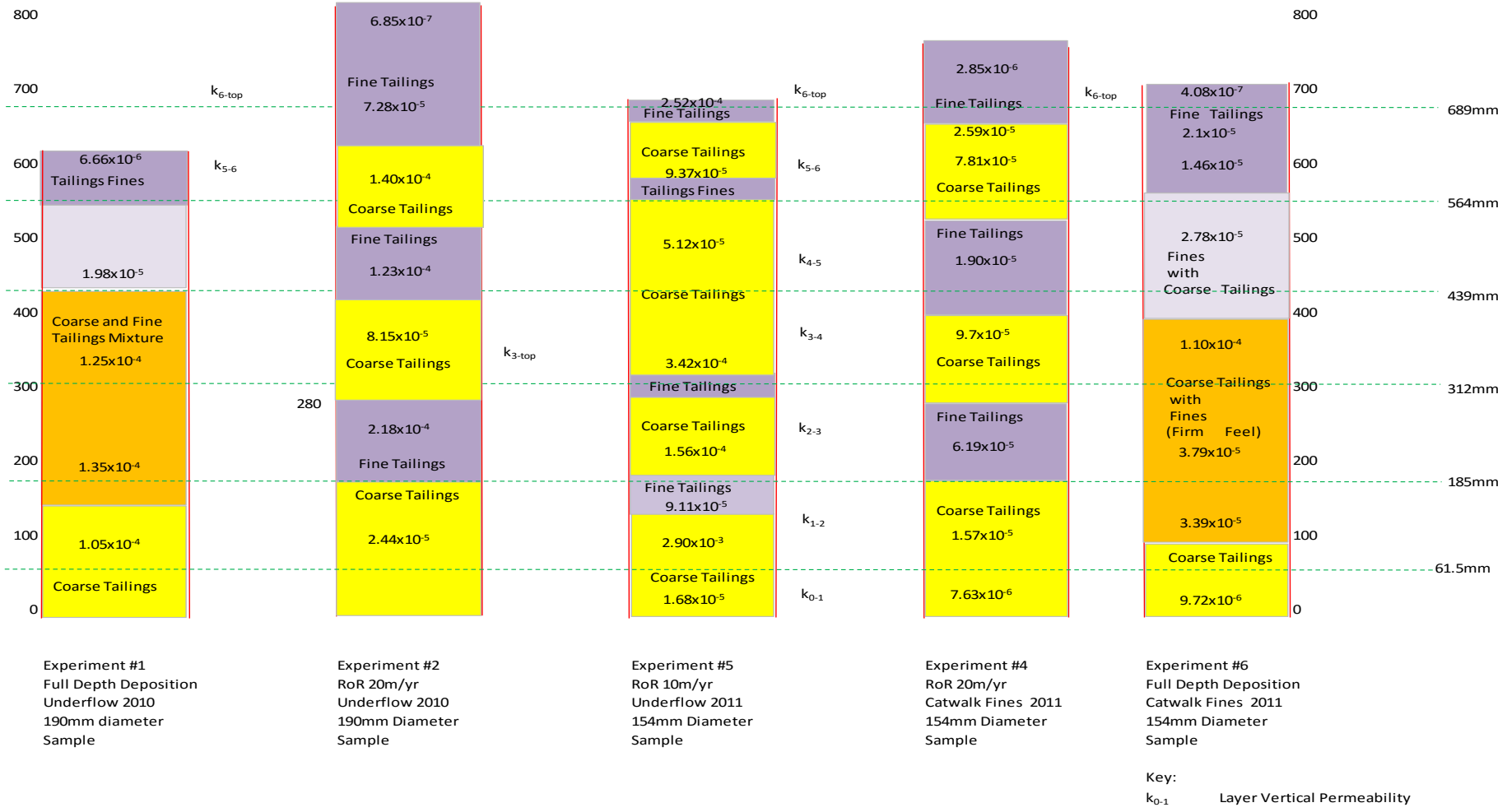

Figure 5.20: Tailings layer permeability values - Experiments FDA, FDB, RoR20A, RoR20B and RoR10B

Chapter 6

CONCLUSIONS AND RECOMMENDATIONS

This chapter presents conclusions of the research as well makes recommendations for future research. First the main conclusions are listed followed by subsidiary conclusions from the study. The chapter ends with recommendations for further research.

6.1 Main Conclusions

The main conclusions emanating from this research are:

1. Excess pore water pressures generated in tailings dams simulated at rate of rise of 10m/yr and 20m/yr as well as the pore water pressures generated from full depth deposition of tailings all dissipated in 2 days compared to a typical tailings dam wall construction deposition cycle of 14 days. Tailings dam wall construction cycle using low plasticity tailings silts deposited every 2 days to a depth of up to 600mm, subject to the practical deposition paddock height limit, translates to a rate of rise of close to 1km/year if permeability of tailings does not change significantly (one order of magnitude) and the dissipation of excess pore water pressures is the only consideration. This means that excess pore water pressure is not the mechanism that limit rate of rise of tailings dams. There are however other known factors which govern rate of rise of tailings dams which fall outside the scope of this research that must be taken into consideration when specifying rate of rise of tailings dams.

2. Particle size segregation of tailings is influenced by particle shape, particle density and particle size.

3. The settling column test has been used to evaluate vertical permeability of undisturbed layered gold tailings material. Vertical permeability values in the range of 10^{-7}cm/sec to 10^{-3}cm/sec were determined for fine and coarse gold tailings respectively.

6.2 Subsidiary Conclusions

1. Following the pouring of tailings, excess pore water pressures first built up within the first 4 minutes up to 9 minutes followed by dissipation of excess pore water pressures. The solids concentration of 467g/L of the slurry was high and interparticle contact within the slurry developed rapidly. The excess pore water pressures were always less than the total applied self weight stresses (effective stress in the tailings from early on).

2. Tailings deposited in a segregated manner in settling columns with the particle size gradation profile ranging from fine to coarse particles descending down the settling column height. This led to excess pore water pressure trends which were not proportional to the self-weight of the tailings overlying the elevation of the settling column under consideration. The fine tailings generated high excess pore water pressures while coarse tailings dissipated excess pore water pressures.

3. Sedimentation/consolidation region excess pore water pressure isochrones (consolidation taking place within the sedimentation region) which have not been reported adequately in literature have been determined experimentally under this research.

4. Both fine and coarse gold tailings settled very little but dissipated high magnitudes of excess pore water pressures rapidly during the initial stages of sedimentation. Excess pore water pressure dissipation slowed down followed by very large settlements during the latter part of the sedimentation phase (consolidation concurrent with sedimentation). During the last stage of consolidation, amount of settlement and excess pore water dissipation were of very small magnitudes relative to the same values during the sedimentation stage (Refer to Figures 5.7 and K1 to K4 as well as Table 5.4).

5. The excess pore water pressure isochrones from the experiments comprised more than one curve. Excess pore water pressure isochrones changed in shape during the sedimentation-consolidation processes. The first pattern comprise linear isochrones which depict excess pore water pressure build-up and early dissipation of excess pore water pressures in the first fifteen minutes of the experiment. The second pattern of isochrones were curved and bent showing the particle size segregation layering that develops with time to about twenty hours from start of the experiment. Beyond twenty hours the third and last pattern of isochrones shapes comprised more than one curve. These dissipated very small magnitudes of excess pore water pressures very slowly.

6. The initial sedimentation mechanism observed with the slurry solids concentration of 467g/L was of a compression sedimentation type where the coarse tailings fraction settled soon within 3 minutes of slurry pouring. The subsequent phase of sedimentation which lasted beyond 2 hours (concurrent with consolidation of settled tailings) was the typical suspension sedimentation type which involved very fine tailings fraction with a low solids concentration which had resulted from the reduction of initial solids concentration by particle segregation. The fine tailings fraction settled at decreasing rates over time.

7. Both coarse (underflow) and fine tailings (catwalk fines) whether placed at full depth (Experiments FDA and FDB) or placed in stages (Experiments RoR20A, RoR20B RoR10A and RoR10B) achieved similar final saturated densities under self-weight consolidation ranging from 1600 kg/m^3 to 1700 kg/m^3 (Table 3.6). However, fine tailings settled 7% more compared to coarse tailings.

8. The settling column apparatus can be used in tailings dam design process to obtain dam storage capacity and achievable densities as well as decant water quantities.

9. Both strain gauge based transducers and standpipes piezometers have been shown to be good pore water pressure measuring devices each with its own strengths and weaknesses. Transducers yield continuous data which are subject to fluctuation especially for measurements taken over long periods of time. Measurements are also adversely affected by temperature variations. Standpipes give visual results which are easy to interpret. Standpipes have a slow response time of 2 to 5 seconds in water only;

standpipes suffer compliance effects and are affected by air bubbles. The data obtained is also less frequent and subject to human error.

10. Both transducer zero readings and calibration factors changed over time with temperature changes and with low amplitude fluctuations during the duration of an experiment (a month on average). The best calibration procedure was in-situ calibration both before and after every experiment rather than bench calibrations.

11. The response time for standpipes should include both time and a specified piezometric height to give complete and specific response values for the standpipe piezometer system. It is the response time of the standpipes with the settling column filled with tailings that is more important than the response times with settling column filled with water only. Response time with column filled with tailings is expected to be greater than with water only leading to even slower response times.

6.3 Recommendations for Further Research

1. It is recommended that a digital photography interface detection system be utilised to continuously record both the soil-water and air-water interfaces during sedimentation so that pore water pressures in standpipes could be recorded by detecting the meniscus and the interfaces within the settling column and the manometer tubes. This would improve the performance of standpipes as a pore water pressure measuring system.

2. It is recommended that much smaller pore pressure instruments spacing intervals of 30mm to 50mm be used in settling column apparatus with objective of determining the saturated permeability of the very thin fine tailings layers which result from segregation of tailings slurry deposits. Normal spacing of 100mm are too coarse for the thin layers.

3. It is recommended that a model be developed to explain the observed excess pore pressure trends from the settling column apparatus. Such a model could be used to estimate excess pore water pressures in tailings dams.

4. It is recommended that both vertical and horizontal saturated permeability of tailings in settling column be independently measured to compare the values with inferred flowrates and hydraulic gradients from the actual column tests.

REFERENCES

Abbireddy, C.O.R., and Clayton, C.R.I. (2009) A review of modern particle sizing methods. Proceedings of the Institution of Civil engineers, Geotechnical Engineering 162, GE4: 193-210.

Adamson, R.J. (1973), Gold metallurgy in South Africa. Johannesburg Chamber of Mines of South Africa.

Bardet, J.P. (1997), *Experimental Soil Mechanics*. New Jersey: Prentice Hall Inc.

Barnes, G. (2000), *Soil Mechanics: Principles and Practice*, Chippenham, Wiltshire, Great Britain: Antony Rowe Ltd.

Bartholomeeusen, G. (2003) *Compound shock waves and creep behaviour in sediment beds*, PhD thesis, Oxford University, England.

Bates, R.C., and Wayment, W.R. (1967), Laboratory study of factors influencing water flow in mine backfill, *U.S. Bureau of Mines, Report RI 7034*.

Been, K. (1980) *Stress Strain Behaviour of a Cohesive Soil Deposited Under Water*, PhD thesis, University of Oxford, UK.

Been, K. and Sills, G.C., (1981) Self-weight consolidation of soft soils: an experimental and theoretical study. *Geotechnique*, 31(4):519-535.

Blight G.E. (1980) Properties of pumped tailings fill, *Journal of the South African Institute of Mining and Metallurgy*, 79(15):446-453.

Blight G.E. (1981), Assessment for environmentally acceptable disposal of mine wastes, *The Civil Engineer in South Africa*, 23(10):480-499.

Blight G.E. (1988), Some less familiar aspects of hydraulic structures, *Hydraulic Fill Structures*, ASCE Geotechnical Special Publication No. 21, 1000-1027.

Blight G.E. (1989), Erosion losses from the surfaces of gold-tailings dams, *Journal of the South African Institute of Mining and Metallurgy*, 89(1):23-29.

Blight G.E. (2008) "Estimating Beach Profiles for Hydraulic Fill Tailings Impoundments". 4th International Mining and Industrial Waste Management Conference, Rustenburg.

Blight, G. (2010), *Geotechnical Engineering for Mine Waste Storage Facilities*, Taylor and Francis Group, London, U.K.

Blight G.E., (1987) The Concept for the Master Profile for tailings dam beaches: Prediction and performances in Geotechnical Engineering, Joshi and Griffiths editors, A.A. Balkema, P.O. Box 1675 3000 BR Rotterdam, Netherlands, pp. 361-365.

Blight G.E., Thomson, R.R. and Vorster, K. (1985) Profiles of hydraulic-fill tailings beaches, and seepage through hydraulically sorted tailings. *Journal of the South African Institute of Mining and Metallurgy*, 85(1):157-161

Blight, G.E. (1969) Shear Stability of dumps and dams of gold mining waste. *The Civil Engineer in South Africa*, Republished in the *Commemorative Journal of the Geotechnical Division of the South African Institution of Civil Engineering, first edition, first impression*, pp 247-252.

Blight, G.E., and Steffen, K.H.(1979) Geotechnics of gold mining waste disposal, *Current Geotechnical Practice in Mine Waste Disposal*, ASCE, New York, 1-53.

Blight, G.E.and Bentel, G.M. (1983) The Behaviour of mine tailings during hydraulic deposition. *Journal of the South African Institute of Mining and Metallurgy*. 83():73-86.

Bowden, R.K. (1988), *Compression behaviour and shear strength characteristics of a natural silty clay sedimented in the laboratory*, PhD thesis, University of Oxford, Oxford, England.

Brand, E.W., and Premchitt, J., (1980a), Shape factors of cylindrical piezometers, *Geotechnique*, 30(4):369-384.

BS 1377-2:1990:3.2, 4 and 5, Methods of test for soils for civil engineering purposes. Classification tests. British Standards Institution, London.

BS 1377-2:1990:8.3, Methods of test for soils for civil engineering purposes. Classification tests. British Standards Institution, London.

BS 1377-2:1990:9.2 and 9.5, Methods of test for soils for civil engineering purposes. Compressibility, permeability and durability tests. British Standards Institution, London.

BS 1377-2:1990:9.2 and 9.5, Methods of test for soils for civil engineering purposes. Compressibility, permeability and durability tests. British Standards Institution, London.

Bürger, R., and Wendland, W. (2001) Sedimentation and suspension flows: Historical perspective and some recent developments, *Journal of Engineering Mathematics* 41: 101-116, Kluwer Academic Publishers. Printed in the Netherlands.

Cable, M. (2005), *Calibration A Technician's Guide*. ISA, 67 Alexander Drive, Research Triangle Park, NC 27709, USA.

Cargill, K.W. (1984) Prediction of Consolidation of Very Soft Soil. *Journal of Geotechnical Engineering*, ASCE, 110(6):775-795.

Carrier III, W.D., Bromwell, L.G. and Somogyi, F., (1983) Design Capacity of Slurried Mineral Waste Ponds. *Journal of Geotechnical Engineering*, ASCE, 109(5):699-716.

Caughill, D.L., 1992, *Geotechnics of non-segregating oil sand tailings*, MSc thesis, University of Alberta, Edmonton, AB.

Chamber of Mines of South Africa 1996. *The Engineering Design, Operation and closure of Metalliferous, Diamond and Coal Residue Deposits. Guidelines for Environmental Protection*. Johannesburg: The Chamber.

Chang, H.N. (2009), *The effect of fabric on the behaviour of gold tailings*, PhD thesis, University of Pretoria, RSA

Chen, H.W., and Yamamoto, L.D., (1987) Permeability tests for hazardous waste management with clay liners. Geotechnical and Geohydrological Aspects of Waste Management. USA: Lewis Publishers pp. 229-243.

Cincilla, W.A., Landriault, D.A., and Verburg, R., (1997) Application of paste technology to surface disposal of mineral wastes, *Tailings and Mine Wastes '97*, Balkema, Rotterdam ISBN 905410 857 6.

Clayton, C.R.I., Matthews, M.C., and Simons, N.E. (1995), *Site Investigation, Second Edition*, Blackwell Science.

Coe H.S., and Clevenger G.H., (1916) "Methods for determining the capacities of slime-settling tanks" Transactions of the American Institute of Mining, Metallurgical and Petroleum Engineers, 55, 356-384.

Craig, R.F. (2004), *Craig's Soil Mechanics, Seventh Edition*, London: Spoon Press.

Cullity, B.D. (1978) *Elements of X-ray Diffraction 2nd Ed.*, Addison-Wesley Publishing Company, Inc., Reading, Massachusetts.

Cullity, B.D. and Stock, S.R., (2001) *Elements of X-ray Diffraction, 3rd Ed.*, Prentice Hall, Upper Saddle River, New Jersey, USA.

Das, B.M. (1983) *Advanced Soil Mechanics*, Washington. Hemisphere Publishing Corp

Day, S.R., and Daniel, D.E., (1985) Hydraulic conductivity of two prototype clay liners, *ASCE Journal of Geotechnical Engineering*, 111 (8):957-970.

De villiers, Ina Mari, *The theoretical determination of excess pore water pressure in an accreting layer of tailings in collaboration with a laboratory simulation*, University of Pretoria, Bachelor of Engineering(Civil Engineering) report July 2010 (unpublished)

Dearnaley, M.P., Roberts, W., Jones, S, Leurer, K.C., Lintern, D.G., Merckelbach, L.M., Sills, G.C., Toorman, E.A. and Winterwerp, J.C, (2002) Measurement and Modelling of the Properties of Cohesive Sediment Deposits: In: *Fine Sediment Dynamics in the Marine Environment*. Editors: Wintererp and Kranenburg. Elsevier Science B.V., pp57-73.

Dimitrova, R. (2011) *Geotechnique, physico-chemical behaviour and a new erosion model for mine tailings under environmental loading*, PhD thesis, The University of Western Ontario, London, Ontario, Canada.

Don Scott, J., Dusseault, M. B. and David Carrier, III, W. (1985) Large-scale Consolidation Testing, in Consolidation of Soils: Testing and Evaluation, ASTM Special technical Publication 892, Yong and Townsend editors, 1916 Race Street, Philadelphia, PA, pp. 500-515.

Donaldson,G.W. Theoretical and engineering aspects of slimes-dam construction. *Journal of the South African Institute of Mining and Metallurgy*, 74:175-177, 1973.

Donaldson, G.W. The Stability of Slimes Dams in the Gold Mining Industry. *Journal of the South African Institute of Mining and Metallurgy*, Vol., pp.183-199, 1960.

Dromer, J.-B., Aubertin, M. Kennedy, G. Pedroni, L., and Bussiere, B. (2004). A New Testing System to Investigate the sedimentation and Consolidation of sludge and slurry. 57th Canadian Geotechnical Conference.

Dunn, I.S., Anderson, L.R., and Kiefer, F.W., (1980) *Fundamentals of Geotechnical Analysis*, John Wiley & Sons, Inc., New York, U.S.A.

Dykstra (2012), Personal Communication.

East, D.R., Ransone, J.W., and Cincilla, W.A. (1988), Testing of the Homestake mine tailings deposit, Proceedings, 2nd International Conference on Case Histories in Geotechnical Engineering, 495-502.

Elder, D.McG. (1985) *Stress strain and strength behaviour of very soft sediment*, PhD thesis, University of Oxford, England.

Fahey, M., Helinski, M. and Fourie, A. (2010) Consolidation in accreting sediments: Gibson's solution applied to backfilling of mine stopes. *Geotechnique*, 60(11):877-882.

Fell, R., MacGregor, P. & Stapledon, D. (1992), *Geotechnical Engineering of Embankment Dams*, A.A. Balkema, Rotterdam, Netherlands.

Fuller, W.B., and Thompson, S.E. (1907), The laws of proportioning concrete, Transactions of the American Society of Civil Engineers, Vol. 59.

Gassner, F.W., and Fourie, A.B. (1998) Optimising the allowable rate of deposition on tailings dams. Proceedings, *Tailings and Mine Waste '98*, Fort Collins, Colorado, pp. 241-247.

Gaudin, A.M., and Fuerstenau, M.C. (1958) The transviewer- x-ray to measure suspended solids concentration, *Engineering and Mining Journal*, 159(9):110-112.

Gibson, R. E. (1958) The progress of consolidation in a layer increasing in thickness with time. *Geotechnique*, 14(3):171-182

Gibson, R.E., and Morgenstern, N., (1962) A note on the Stability of cuttings in normally consolidated clays. *Geotechnique*, 12():212-216.

Gibson, R.E., England, G.L. and Hussey, M.J.L. (1967) The theory of one-dimensional consolidation of saturated clays. *Geotechnique*, No.17, 261-273.

Gibson, R.E., Schiffman, R.L. and Cargill, K.W. (1981) The theory of one-dimensional consolidation of saturated clays. II. Finite nonlinear consolidation of thick homogeneous layers. *Canadian Geotech. Journal*, 18, 280-293.

Gibson, R.E., Schiffman, R.L. and Whitman, R.V., (1989) On two definitions of excess pore water pressure. *Geotechnique*, 39(1):169-171.

Gottchalk, L.C. (2006), Nature of Sedimentation Problems, chapter 1, in V.A. Vanoni (ed.), Sedimentation Engineering, ASCE Manual and Reports on Engineering Practice No. 54, USA, pp 1-10.

Grote, W., (2012), Personal Communication.

Gulhati, S.K., (1978) *Engineering Properties of Soils*, Tata McGraw-Hill Publishing Co. Ltd., New Delhi, India.

Hamel, J.V., and Gunderson, J.W. (1973), Shear strength of Homestake slimes tailings, ASCE *Journal of the Soil Mechanics and Foundation Engineering Division*, 99(SM5):427-431.

Hagan, F. (2009), Personal Communication.

Hazen, A. (1892), Physical properties of sands and gravels with reference to their use in filtration, *Report, Massachusetts State Board of Health*.

Head, K.H. (1986), *Manual of Soil Laboratory Testing Volume 3: Effective Stress Tests*, New York: John Wiley and sons.

Head, K.H. (1992), *Manual of Soil Laboratory Testing Volume 1: Soil Classifcation and Compaction Tests*, London: Pentech Press

Head, K.H. (1994), *Manual of Soil Laboratory Testing Volume 2: Permeability, Shear Strength and Compressibility Tests. 2nd Ed.* London: Pentech Press.

Holtz, D. and Kovacs, W.D. (1981), *An Introduction to Geotechnical Engineering*. New Jersey: Prentice-Hall, Inc. Englewood Cliffs. Pp 733.

Legge, G.H.H., L'Heriteau, G, Penman, A.D.M. and Wahler, W.A. (1982) *Manual on Tailings Dams and Dumps*. Bulletin 45. Published by the International Commission on Large Dams, Paris 237pp.

Imai, G. (1980), Settling behaviour of clay suspensions, *Soils and Foundation*, 20(2):61-77.

Imai, G. (1981), Experimental studies on sedimentation mechanisms and sediment formation of clay materials, *Soils and Foundation*, 21(1):7-20.

Jeeravipoolvarn S., (2006) *Compression behaviour of thixotropic oil sand tailings*, MSc thesis, University of Alberta, AB, Canada.

Jeeravipoolvarn S., (2010) *Geotechnical Behaviour of In-Line thickened Oil Sands Tailings*, PhD thesis, University of Alberta, Edmonton, Alberta, Canada.

Jenkins, R and Snyder, R.L. (1996) *Introduction to X-ray Powder Diffractometry*, John Wiley and Sons, Inc., New York, USA.

Jerabek, F., and Hartman, H., (1965) Investigation of segregation and compressibility in discharged fill slurry, Trans. SME March, pp 18-24.

Johnson, L.D., U.S. Army Engineer Waterways Experiment Station, Mathematical Model For Predicting Consolidation of Dredged Materials in Confined Disposal Areas. Technical Report D-76-1. January 1976.

Jones & Wagener (Pty) Ltd. Consulting Civil Engineers. *Risk Assessment of South Residue Slimes Dam*, Vaal Reefs Exploration and Mining Co. Limited, RSA. Report No. AA1/96/4934. January 1996.

Jones & Wagener (Pty) Ltd. Consulting Civil Engineers. *Risk Assessment of West Slimes Dam Complex*, Vaal Reefs Exploration and Mining Co. Limited, RSA. Report No. AA6/96/4934. March 1996.

Kealy, C.D., and Busch, R. (1971) Determining seepage characteristics of mill-tailings dams by the finite element method, *U.S. Bureau of Mines, RI 7477*.

Keshian, B., Ladd, C.C., and Olson, R.E., (1977) Sedimentation-consolidation behaviour of phosphatic clays, ASCE Proceedings of Speciality Conference on Geotechnical Practice for Disposal of Solid Waste Materials, 188-209, Ann Arbor, Michigan.

Knappett, J.A., and Craig, R.F., (2012) *Craigs's Soil Mechanics, 8th Ed.*, Spon Press, New York, New York.

Kupper, A.M.A.G. (1991) *Design of hydraulic fill*, PhD thesis, Department of Civil Engineering, University of Alberta, Edmonton.

Kurt N. (2006) *A study of channelling behaviour in batch sedimentation*, PhD thesis, REMIT University, Sydney, Australia. 2006.

Kusuda, T., Koga, K., and Awaya, Y. (1980) Gravity thicknening of sludge, Proceedings, *JSCE*, Hydraulic and Sanitary Eng. Div., 12():294.

Kynch, G.J. (1952) A theory of sedimentation. Transcations of the Faraday Society, vol. 48, 166-176.

Lambe, T.W. (1951), *Soil Testing for Engineers*, New York: John Wiley & Sons, Inc. Pp 165.

Lambe, T.W. and Whitman, R.V. (1969), *Soil Mechanics*. New York: John Wiley & Sons, Inc. Pp 553.

Lebitsa, G, Heymann, G and Rust, E.Laboratory measurement of pore pressures using transducers and standpipes, Proc. 13thBiennial Conference Botswana Institution of Engineers, Gaborone, Botswana, pp.116-123, 15-18 October 2013.

Lebitsa, G., Hagan, F., Heymann, G. and Rust, E. Assessment of Excess Pore Pressures in Gold Tailings. *Proc. 11th BIE Biennial Conference*, Gaborone, Botswana, pp. 273-280, 7-9 October 2009.

Lecasse, S.M., Lambe, T.W., Marr, W.A., and Neff, T.L., (1977) Void ratio of dredged material, Proc., ASCE Conf. Geotech. Practice for Disposal of Solid Waste Materials, Ann Arbor, Michigan.

Lee, I.K., White, W. and Ingles O.G. (1983), *Geotechnical Engineering*, Marshfield, Massachusetts, Pitman Publishing Inc.

Leeder, M.R. (1982) *Sedimentology - process and product*, Gorge Allen and Unwin Publishers, Sydney, Australia. 344p.

Lewis, D.W., (1984) *Practical Sedimentology*, Hutchinson Ross, Stroudsburg, PA.

Lin, T.W., and Lohnes, R.A., (1984) Sedimentation and self weight consolidation of dredge spoil. Sedimentation consolidation models: predictions and validation: In Proc. of a Symposium, R.N. Yong and F.C. Townsend Eds. ASCE, New York: 464-480.

Liu, C. and Evett, J.B., (1984) *Soil Properties: Testing, Measurement and Evaluation*, New Jersey: Prentice Hall Inc.

Loubser, M. and Verryn, (2008) Combining XRF and XRD analyses and sample preparation to solve mineralogicalproblems. *South African Journal of Geology*, 111():229-238.

MacArthur, R.C., Neill, C.R., Hall, B.R., Galay, V.I. and Shvidchenko, A.B. (2008) Overview of Sedimentation Engineering, chapter 1, in M.H. Garcia (ed.), Sedimentation Engineering, ASCE Manual and Reports on Engineering Practice No. 110, USA, pp 1-20.

Malvern Instruments Ltd. (2004) *Mastersizer 2000E Operators guide*, Worcestershire, United Kingdom

Martin, T.E., 1998. Characterisation of pore pressure conditions in upstream tailings dams. Proceedings, *Tailings and Mine Waste '99*, Balkema, Rotterdam, Netherlands, pp. 303-313.

McCarthy, T.S. (2006), The Witwatersrand supergroup, chapter 7, in Johnson, M.R., Anhaeusser, C.R. and Thomas, R.J. (Eds.), The Geology of South Africa. Geological Society of South Africa. Johannesburg/ Council of Geoscience, Prertoria, 155-186.

McPhail, G.I. and Wagner, J.C. (1989), Components of a Tailings disposal System. Disposal of Residues, Chapter 11, in G.G. Stanley(ed.), The Extractive Metallurgy of Gold in South Africa, The Chamber of Mines of South Africa, Volume 2, 655-707.

McRoberts, E.C., and Nixon, J.F. (1976), A theory of soil sedimentation, *Canadian Geotechnical Journal*, 13():294-310.

Mitchell, J.K. and Soga, K. (2005) *Fundamentals of Soil Behaviour, 3rd edition*, New York: Wiley

Merckelbach, L.M. (2000), *Consolidation and strength evolution of soft mud layers*, PhD thesis, Deft University of Technology, The Netherlands.

Mrost, M. (1974) Slimes disposal at South African gold mines. *Journal of the South African Institute of Mining and Metallurgy*, 74(7):285-291.

Michaels, A.S., and Bolger, J.C., (1962), Settling Rates and sediment volumes of flocculated kaolin suspension, *Industrial and Engineering Chemistry Fundamentals*, 1(1):24-33.

Micromeritics, (2008) *AccuPyc II 1340 Operators's Manual V1.05*

Migniot, C., (1968) A study of the physical properties of variuos forms of very fine sediments and their behaviour under hydrodynamic actions. La Houille Blanche 7: 591-620.

Miller, W. G., Scott, J. D., & Sego, D. C. (2011). Effect of extraction water chemistry on the self-weight consolidation of oil sands fine tailings. *CIM Journal*, *2*(1):40-54.

Mittal, H.K.and Morgenstern, N.R.(1976) Seepage control in tailings dams. *Canadian Geotechnical Journal*, 13:277-293.

Mittal, H.K., and Morgenstern, N.R. (1975) Parameters for the design of tailings dams. *Canadian Geotechnical Journal*, 12:235-261.

Owen, M.W., (1970) A detailed study of the settling velocities of an estuary mud. Report no. Int. 78. H.R.S. Wallingford. U.K.

Owen, M.W., (1970) Properties of a consolidating mud, Hydraulic Research Station, Report No. Int. 83. H.R.S. Wallingford, U.K.

Pane, V., and Schiffman, R.L., (1985) A note on sedimentation and consolidation. *Geotechnique*, 35(1): 69-72.

Pane, V., and Schiffman, R.L., (1995) "Letter to the editor", *Int. J. Num. Anal. Meth. In Geomech.* 19():149-151.

Papageorgiou, G. (2004) *Liquefaction Assessment and Flume Modelling of the Merriespruit gold and Bafokeng platinum Tailings*, PhD thesis, University of the Witwatersrand, South Africa.

Papageorgiou, G.P., Fourie, A.B., and Blight, G.E. (1999) Static liquefaction of Merriespruit gold Tailings dams, Proceedings, 12th Regional Conference for Africa on Soil Mechanics and Geotechnical Engineering, Durban, South Africa, 61-72.

Pedroni L., Dromer J.-B., Aubertin M. and Kennedy G. (2006) Properties of treatment sludge during sedimentation and consolidation tests. *7th International Conference on Acid Rock*

Drainage (ICARD). American Society of Mining and Reclamation. St. Louis MO. 26-30 March 2006. http://www.imwa.info/docs/imwa_2006/1531-Pedroni-QC.pdf.

Pedroni, L., (2011), *Étude experimentale Et Numerique de la sedimentation et de la consolidation des boues de aitement des eaux acides*, PhD thesis, Ecole Polytechnique De Montreal, Canada.

Pedroni, L., and Aubertin, M. (2008). Evaluation of sludge consolidation from hydraulic gradient tests conducted in large size columns. http:www.polymtl.ca/enviro-geremi/pdf/articles/edmonton2008_112.pdf Obtained online on 02/09/09.

Penman, A.D.M. (1956) A Field Piezometer apparatus. *Geotechnique*, 6:57-65.

Pettibone, H., and Kearly, D. (1971) Engineering properties of mine tailings, ASCE, *Journal of the Soil Mechanics and Foundations Division*, 97(SM9):1207-1225.

Premchitt, J. and Brand, E.W. (1981) Pore pressure equalisation of piezometers in compressible soils. *Geotechnique*, 31:105-123.

Priscu, C. (1999) *Behavior of mine tailings under high tailings deposition rates*. PhD thesis, McGill University, Montreal, Canada.

Qiu, Y. (2000) *Optimum deposition for sub-aerial tailings disposal*, PhD thesis, University of Alberta, Edmonton, Alberta.

Qiu, Y., and Sego, D.C. (2001) Laboratory properties of mine tailings, *Canadian Geotechnical Journal*, 38(1), 183-190.

Reed, S.J.B., (1993), *Electron Microprobe Analysis 2nd Ed*. Cambridge University Press, Cambridge, Great Britain.

Rhodes, M. (1998) *Introduction to particle technology*, John Wiley & Sons Ltd., Chichester, England.

Rhodes, M. (2008) *Introduction to particle technology 2nd Ed.*, John Wiley & Sons Ltd., Chichester, England

Richardson, J.F., and Zaki, W.N., (1954) Sedimentation and fluidisation: Part 1, *Transactions, Institution of chemical Engineers*, 32, 35-53.

Richardson, J.F., Harker, J.H., and Backhurst, J.R., (2002) *Coulson and Richardson's Chemical Engineering Particle Technology and Separation Processes Volume 2 5th Ed.* Butterworth-Heinmann Elsvier Science, Oxford, MA 01801-2041.

Robinson, B.C.S. (2003) "Tailings Dam Rate of Rise – A Closer Look". 3rd International Mining and Industrial Waste Management Conference, Indaba hotel

Robinson, B.C.S. (2008) "Operating to Safety – The Crown Story". 4th International Mining and Industrial Waste Management Conference, Rustenburg.

Robinson, B.C.S. (2008) "The Fundamentals of on-wall Cyclone Tailings dams". 4th International Mining and Industrial Waste Management Conference, Rustenburg.

Rösner, T. (1999) *The environmental impact of seepage from gold mine tailings dams near Johannesburg, South Africa*, PhD thesis, University of Pretoria, South Africa.

Ruhmer, W.T. (1974) Slimes-dam construction in the gold mines of the anglo American Group. *Journal of the South African Institute of Mining and Metallurgy*, 74(7):273-284.

Rust, E. (1991) Development of a Piezometer Probe in South Africa. University of Pretoria.

Rust, E., Jacobsz, S. and Van der Berg, P. "Seepage analysis from piezocone dissipation tests". Proceedings of the International Symposium on Cone Penetration Testing CPT'95 Volume 2, Swedish Geotechnical Society, Linkoping, Sweden, October 4-5, 1995, pp 289-294.

Samadi-Boroujeni, H., Fathi-Moghaddam, M., Shafaie-Bajestan, M. and Mohammad Vali-Samani, H, W. (2008) Modelling of Sedimentation and Self-Weight Consolidation of Cohesive Sediments, In: *Sediments and Ecohydrualics INTERCOH 2005* Editors: Kusuda, Yamanishi, Spearman and Gailani. Elsevier B.V., pp.165-191.

Sauffer, P.A. and Obermeyer, J.R. (1988) "Pore water pressure conditions in Tailing dams'' Hydraulic Fill Structures, A.S.C.E. Geotechnical Special Publication No. 21, Van Zyl and Vick editors, Ft. Collins, CO, pp 924 -939.

Schiffman, R.L., (1980) Finite and Infinitesimal Strain Consolidation. *Journal of Geotechnical Engineering*, ASCE, 106(GT2):203-207.

Schiffman, R.L., Pane, V., and Gibson, R.E. (1984), The theory of one-dimensional consolidation of saturated clays: An overview of non-linear finite strain sedimentation and

consolidation, in R.N. Yong and F.C. Townsend (eds.), ASCE, Proceedings, Symposium on Sedimentation and consolidation Models, Montreal, Canada, 1-29.

Schiffman, R.L., Vick, S.G., and Gibson, R.E. (1988), Behaviour and properties of hydraulic fills, Hydraulic Fill Structures, ASCE Geotechnical Special Publication No. 21, 166-202.

Selly, R.C. (1982) *An introduction to sedimentology*, 2nd Ed., academic Press Inc. (London) Ltd., England.

Sherard, J.L.,Dunningan,L.P. and Talbot, J.R. (1984) Basic Properties of Sand and Gravel Filters. *Journal of Geotechnical Engineering*, ASCE, 110(6):684-700.

Sherard, J.L., Dunningan,L.P. and Talbot, J.R. (1984) Filters for Silts and Clays. *Journal of Geotechnical Engineering*, ASCE, 110(6):701-718.

Soderberg, R., and Busch, R., (1977) Design guide for metal and non-metal tailings disposal, U.S. Bureau of Mines, IC8755.

South African National Building Research Institute (NBRI): An investigation into the stability of slimes dams with particular reference to the nature of materials of their construction and the nature of their foundation, Pretoria, South Africa: the Institute, 1959.

Stanley, G.G. (ed.) (1987), The Extractive Metallurgy of Gold in South Africa, the S.A. Institute of Mining and Metallurgy Monograph Series M7, The Chamber of Mines of South Africa, Volume 1 and 2.

Steenkamp, P.F., Wagener, F von M. and van Ryssen, G.J. (2008) “Recent Experiences with Cycloning in Africa”. 4th International Mining and Industrial Waste Management Conference, Rustenburg.

Stone, K.J.L., Randolph, M.F., Toh, S., and Sales, A.A. (1994), Evaluation of consolidation behaviour of mine tailings, *Journal of Geotechnical Engineering*, 120(3), 473-490.

Sully, J.P. (1985), Geotechnical aspects of remedial design for a gold tailings dam, *International Journal for Numerical and analytical Methods in Geomechanics*, 9(6):589-598.

Tan, T.S., Yong, K.Y., Leong, E.C., and Lee, S.L., (1990) Sedimentation of clayey slurry, Journal of Geotechnical Engineering vol. 116 No. 6 pp 885-898.

Taylor, D.W. (1948), *Fundamentals of Soil Mechanics*, New York, John Wiley & Sons.

Terzaghi, K. (1943), *Theoretical Soil Mechanics*. John Wiley and Sons, New York.

TMH1 (1986), Standard Methods of Testing Road Construction Materials – Technical Methods for Highways TMH1, National Institute for Transport and Road Research of the council for Scientific and Industrial Research (CSIR), second edition.

Toorman, E.A. (1999) Sedimentation and Self-weight consolidation: constitutive equations and numerical modelling, *Geotechnique*, 49(6), 709-726.

Tory, E.M., and Shannon, P.T. (1965), Reappraisal of the concept of settling in compression, *Industrial and Engineering Chemistry Fundamentals*, 4, 194-203.

Twenhofel, W.H., (1961) *Treatise on sedimentation Vol. 1, 2nd Ed.*, Dover Publications Inc., New York.

Van der Berg, J.P. (1995), *Monitoring of the Phreatic surface in a tailings dam and subsequent Stability Implications*, MSc Dissertation, University of Pretoria.

Van Zyl, D. (1993), Mine waste disposal, in D.E. Daniel (ed.), Geotechnical Practice for waste disposal, Chapman Hall, 269-286.

Vermeulen, N J 2001. *The composition and state of gold tailings*, PhD thesis, University of Pretoria, RSA.

Vick, S.G. (1983), *Planning, design and analysis of tailings dams*, New York: Wiley.

Villar, L.F.S., Campos, T.M.P., Azevedo, R.F. and Zomberg, J.G. (2009) Influence of Laboratory Techniques on the Geotechnical Characteristics of Mining and Industrial Wastes. Proceedings of the 17th International Conference on Soil Mechanics and Geotechnical Engineering, Alexandria, Egypt, pp 186-189.

Wagener, F., Craig, H.J., Blight, G., McPhail, G., Williams, A.A.B., and Strydom, J.H. (1998), The Merriespruit tailings dam failure – A review, Proceedings, 5th International Conference on Tailings and Mine Waste, Fort Collins, 925-952.

Ward, H.T., and Kamermeyer, K. (1940) Sedimentation in the laboratory: Design data from laboratory experimentation, Industrial and Engineering Chemistry, 32, No. 5, 622-626.

Wates, J.A., (1983) The Disposal of mine tailings: the real cost of excess water in residues. Journal of the South African Institute of Mining and Metallurgy. Volume 83 pp 257-262.

White, D.J. (2003) PSD measurement using the single particle optical (SPOS) method. *Geotechnique*, 53(3): 317-326.

Work, L.T., and Kohler, A.S. (1940), Sedimentation of suspensions, *Industrial Engineering Chemistry*, 32():1329- .

Wray, W.K. (1986), *Measuring Engineering Properties of Soil*. New Jersey: Prentice Hall Inc.

Yong, R.N., and Elmonayeri, D. (1984) On the stability and settling of suspended solids in settling ponds. Part III. Diffusion Analysis of initial settling of suspended solids, *Canadian Geotechnical Journal*, 21():644-656.

Young, R.A. (1996) Introduction to Rietveld method, chapter 1, in R.A. Young, The Rietveld Method, International Union of Crystallography, Oxford University Press, New York, USA, pp 1-38.

APPENDIX A

Exploratory Settling Column Tests

A1. Objectives of the exploratory settling column tests

Exploratory settling column tests were carried out prior to the final experiments of the research. The objectives of the exploratory settling column tests were:-

1. to determine the appropriate inside diameter of standpipe piezometers to be used in terms of response times and compliance,

2. to compare pore water pressures measured with standpipes with pore pressures measured using a strain gauge based transducer and thence decide on the adequacy of the use of standpipes for the measurement of pore water pressures in the research,

3. to select an appropriate transducer to use given the anticipated low pore water pressures envisaged in the gold tailings used for this research,

4. to evaluate the type of filters and fittings to use with transducers and standpipes for this research,

5. to observe the response of slurry concentration piloted in cylinder sedimentation tests in the relatively large settling column tests.

6. to observe the range of excess pore water pressures generated by deposited slurry in settling column tests.

7. to compare tailings water interface (TWI) results from cylinder sedimentation tests with those from the exploratory apparatus with a view to predicting the large scale test results from the small scale tests.

A2. Exploratory settling columns design considerations

Prior to the selection and construction of exploratory settling columns, considerations were made regarding the need to observe the slurry inside the settling column which necessitated the use of a transparent window, the size of the column, the magnitudes of excess pore water pressures expected and appropriate instrumentation. This subsection describes each of the aspects listed above and concludes with a summary of the exploratory settling column tests.

A2.1. Inside diameter of settling columns

Based on the literature survey it was concluded that the use of a settling column of inside diameter greater than 100mm would not impart edge effects to pore water pressure measurements (Michaels and Bolger, 1962; Been, 1980; Elder, 1985 and Merckelbach, 2000).

A2.2. Pore water pressure magnitude and instrumentation.

Gibson equation (1958) on a clay layer that accretes over time was used to estimate excess pore water pressures for gold tailings. The estimation was made over a coefficient of consolidation range of $0.1m^2/yr$ to $300{,}000m^2/yr$ which covered permeability values for sands and silts (Blight and Steffen, 1979, Blight, 1980 and 1981, Vick, 1983 and Vermeulen, 2001) for a height of tailings slurry of 2m with a saturated density of gold tailings of $20kN/m^3$yielded total

pore water pressures of up to 40kPa. The 100kPa full scale electronic pressure transducers that were readily available within the South African market were therefore selected as the most appropriate and adequate for the required pore water pressure measurements. The decision was based on both availability, technical support and proven reliable measuring ability based on wide usage of the transducers within industry. Since only half the capacity of the transducer at 50kPa would be expected to be used during the research a small capacity transducer at full scale reading of 40kPa was used during the final experiments of the research for comparison purposes. In addition to pore pressure transducers standpipes were used. It was however noted that the strain gauge based transducer was a "stiff system" that responded well to small water volume changes while standpipe piezometer would need lots of water flow for the measurements which in turn may affect the slurry that was being monitored by the measurements therefore causing compliance effects. Head (1994) argued that the stiff system required little physical change in terms of water flow or movement and that it would be a better measurement system compared to "soft systems" such as standpipes. Typical fittings considered for use in the exploratory apparatus were discussed under Chapter 3.

The transducers also required full saturation to function properly. Saturation of the transducer entailed filling all the conduits of the transducer plumbing links with de-aired water. The saturation block facilitated the transducer saturation process as it enabled easy flushing of the various links with de-aired water as shown in Chapter 3.

A2.3. Selection of filters

Porous stone, porous disk, filter paper, needle punched geofabric, sponge and sintered bronze filters shown in Figure A1 were considered for use as filters for transducer and standpipes. It was noted that materials that other researchers have used as filters included even cigarette filters (Pedroni and Aubetin, 2008). The filters selected for this research were chosen initially because they could be installed flat against the sides of the settling tubes and thus not protrude onto the deposited tailings so as to have as little effect as possible on the sedimentation formation processes of the tailings from deposited slurry. The different filter alternatives were subjected to a water flow rate test to determine how fast each filter type let water through. The object of the test was to ensure that the filters selected for the experiments with tailings had a water flow rate that was much higher than the water flow rate of the gold tailings. The selected filter was to allow only water to pass through while retaining the solid tailings particles, the

filter was to be less susceptible to blockage by tailings and the filter was to assist in keeping the instrumentation and its associated conduits saturated. Water flow rate tests carried out comprised 500ml capacity bottles filled with tap water which was allowed to flow out through the filter material. The results of the water flow rate tests were summarised in Table A1.

From the water flow rate tests all the filter materials had water flow rate values of 1 to 272 ml/min which was much higher than the water flow rates of the gold tailings which ranged from 0.03ml/min to 0.20ml/min as observed from Table A1. It needs to be noted that the water flow rates of the filters had to be much higher than those of the saturated tailings. The values reported for the saturated tailings were the average slopes of the variation of water collected over time. The needle punched geofabric and the sponges allowed tailings solids to pass through the filter. The filter paper was discounted on the basis of not being durable enough for both the sedimentation and consolidation phases of the experiments which were expected to run for several weeks.

The porous stone and the porous disc required the use of adhesive which was prone to leakage over long periods of time. Although the porous disk, filter paper, needle punched geofabric, sponge and sintered bronze filters were selected for use as filters with the exploratory settling columns, sintered bronze filters were selected for use in the final settling columns.

In general the saturated tailings water flow rates started off being large in magnitude but progressively became small in magnitude with time as the tests progressed which indicated the blockage of the different filters over time by the tailings which did not occur with water only flow rate tests. The reduction in magnitude of the water flow rate values over time for the saturated tailings indicated a reduction of the permeability of the tailings which became denser as water seeped through the tailings.

For all the filter types used in the exploratory tests, water flow rates was more than 33 times higher than the water flow rates of the tailings. The slurry used in the exploratory tests was made from fine grained penstock tailings of the Mooifontein tailings dam of the Crown Mines Tailings Complex. All the filters were pervious enough to be used with the tailings slurry which was 33 times slower in terms of water flow rates. The consideration of the most favourable filters therefore centred on other factors other than the filter obstructing water flow to instrumentation used to measure pore water pressures.

A.2.4. Exploratory Settling Column Tests

Three settling columns were used in which six exploratory experiments were carried out. The first exploratory settling column comprised a 190mm ID 500mm height PVC pipe with a 100mm wide transparent window glued to the PVC pipe using adhesive. This apparatus is shown in Figure A2. The second settling column was a 190mm ID 1535mm height PVC pipe with a 55mm wide transparent window fixed onto the pipe by bolts as well as pipe glue which were all treated with heat to make the joints more water tight. The settling column was modified into the permanent settling column and is given in Chapter 3. The third exploratory settling column was a 450mm ID 2450mm height cold rolled mild steel tank with a 215mm wide transparent window. Figure A3 shows the settling column.

The first exploratory settling column experienced leaks both at the base and at the window when loaded with greater masses of tailings and had limited capacity with a maximum height of 500mm. The second and larger aspect ratio settling column at 450mm ID and 2450mm height was unable to take pressure when filled with tailings. The third and final exploratory settling column performed very well except for the large intervals of 250mm between standpipes and it demonstrated the need to use more than one pore pressure transducer in order to capture the initial and rapidly changing excess pore water pressures.

The six exploratory settling column tests carried out are summarised in Table A2.

Table A1: Porous Filter Assessment

Filter Material	**Description**	**Water flow rate (ml/min)**	**Saturated Tailings Water flow rate (ml/min)**	**Ratio of Saturated Tailings to Water only Flow rates**
Porous Stone	Porous stone used in other lab tests.	11.11	0.0373 (0.98%)	298
Porous Disk	Porous plastic disk from Porvair Technology Ltd., UK.	1.56	0.0298 (0.98%)	52
Filter paper	Whatmann No. 10 paper	0.87	0.0267 (0.86%)	33
Needle punched geofabric (Bidim)	A water soaking geofabric	272.48	0.0479 (0.94%)	5689
Sponge	Household sponge	214.13	0.1842 (0.96%)	1162
Sintered Bronze	A high water flow rate filter	93	0.0652	1427

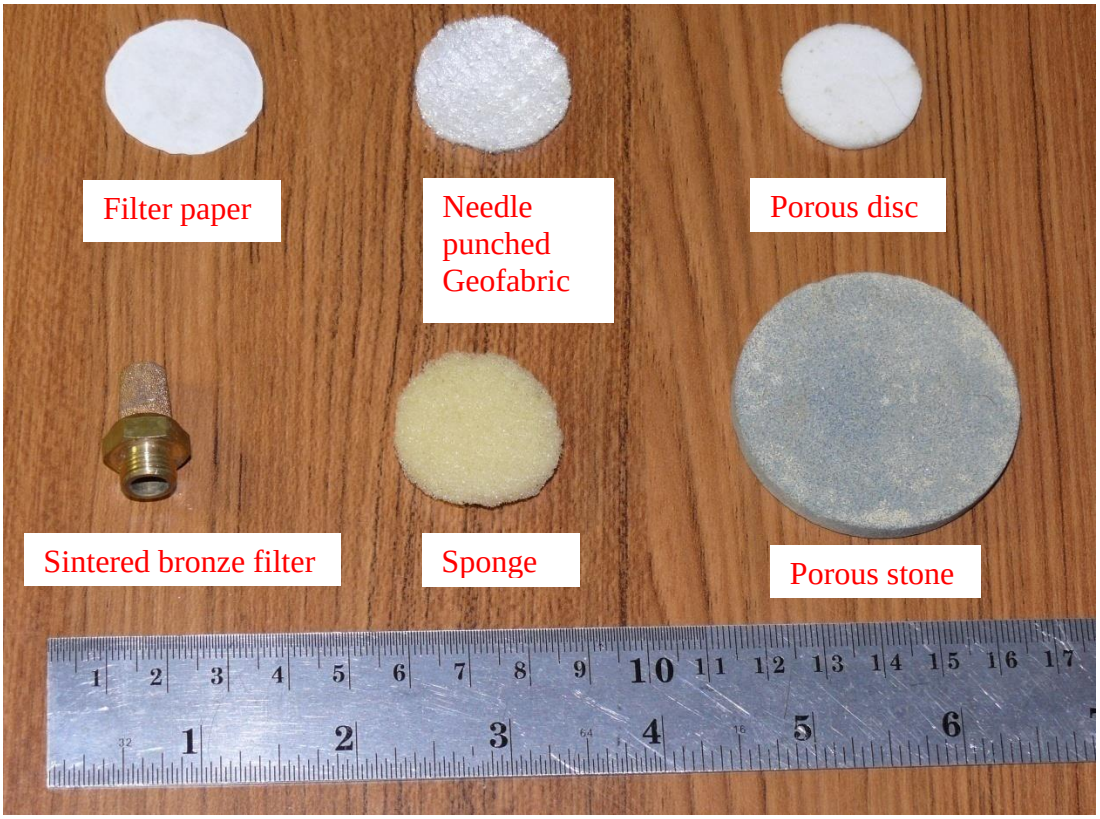

Figure A1: Exploratory Settling Column Filters

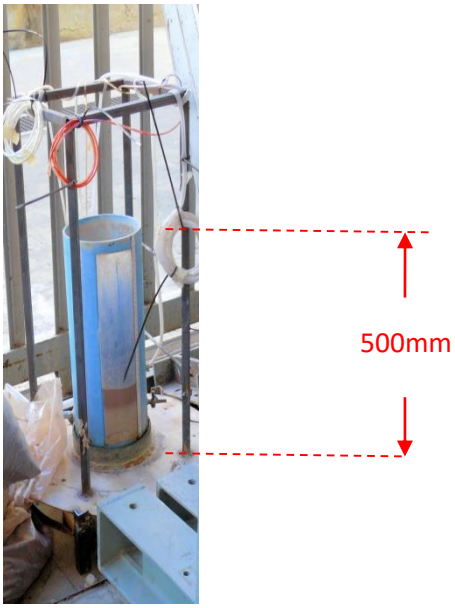

Figure A2: 190mm ID 500mm High Exploratory Settling Column Apparatus

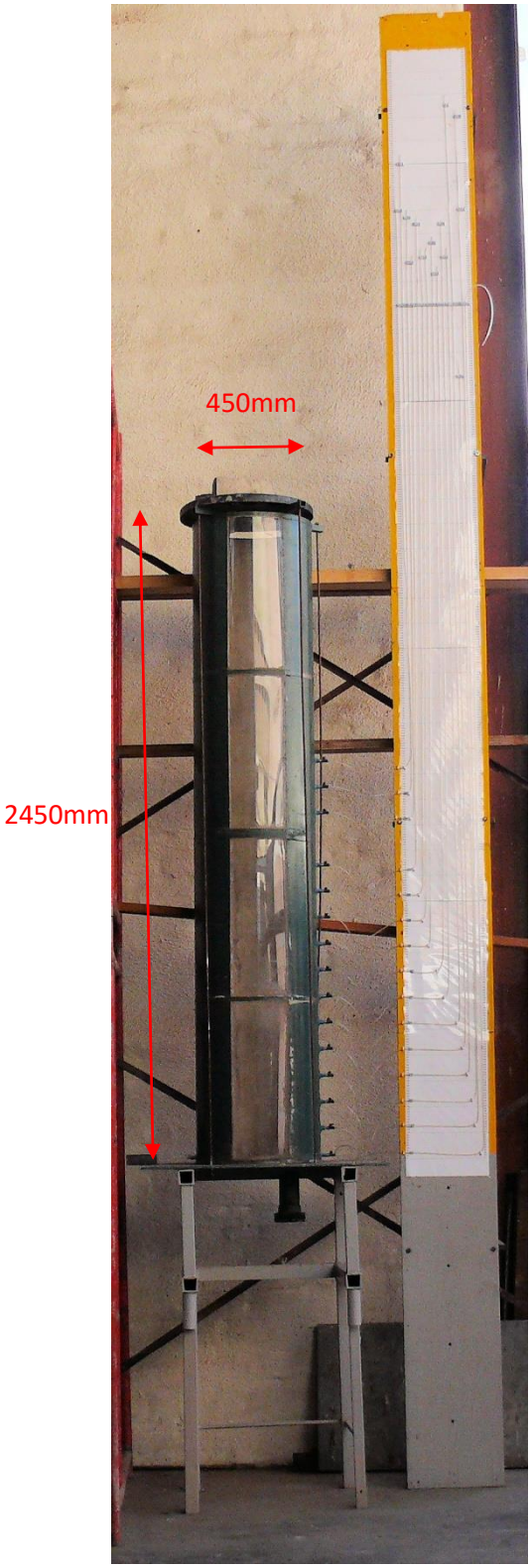

Figure A3: Large Settling Column apparatus

Table A2: Summary of Exploratory Settling Column Tests.

Test No.	Objective of Test	Description	Remarks
1	To observe excess pore water pressure magnitudes and effects of thickness of deposited slurry layers.	One 480mm layer deposited followed by 4 layers deposited after decanting in a 500mm height 190mm ID settling column with 1 transducer and standpipes of varying ID at 100mm intervals (2mm, 3mm, 5mm, 6mm and 9mm).	Short column apparatus had limited capacity and thus entailed low magnitude excess pore water pressures.
2	To observe effects of slow deposition rates and rest periods between slurry layer depositions in excess pore water pressure terms	Deposition of thick slurry layers allowed to achieve full dissipation followed by subsequent layer depositions.	Slow rate of rise deposition scenario.
3	To observe the effects of high rate of rise on generated excess pore water pressures.	200mm thick slurry layers deposited at hourly intervals.	Rapid rate of rise scenario. Thin layers of up to 200mm yielded minimal excess pore water pressures.
4	To compare strain gauge based pore pressure transducer performance in relation to 2mm ID standpipes in a high settling column apparatus.	Full depth slurry deposition in a 1500mm high settling column using 1 transducer and four 2mm ID standpipes at 250mm intervals.	Transducer recorded high initial excess pore water pressures than standpipes. Need for more transducers to capture early large magnitude excess pore water pressures and use of 100mm spacing between piezometers.

Test No	Objective of Test	Description	Remarks
5	To observe magnitudes of excess pore water pressures in high settling columns and to investigate the use of a venturi meter for decanting supernatant water in high settling columns.	Rate of rise 20m/yr deposition through 130mm thick slurry layers deposited daily.	130mm slurry layers generated minimal excess pore water pressures. Venturi meter successful in decanting water in high settling columns.
6	To establish the cause of shortfalls in piezometric heights of large ID standpipes in the short settling column apparatus and to evaluate effects of noise and/or drift on the data collected with the graphtec logger with the high settling apparatus.	500mm and 1500mm high settling column apparatuses both with 190mm ID filled with tap water only.	Large inside diameter standpipes response time very slow. Graphtec logger data contained either noise or drift effects or both.

APPENDIX B

Apparatus and Instruments Calibrations

This appendix summarises calibrations data collected during the research. The data includes response time measurements, calibration graphs, calibration factors and zero readings of pore pressure transducers. Change of transducer zero readings and the effects of both temperature and barometric pressure on zero readings over time are also listed. The Appendix shows Experiment FDB calibrations which was typical of the other experiments. The appendix reports the data as listed below.

B1 Standpipe Response Time Measurements

Table B1: Standpipe response time measurements

Measurement No.	AWI Average (mm)	Actual Height involved in Response Time Average (mm)	Percentage Actual Height involved in Response over AWI Average (%)	Response Speeds Averages (mm/sec)	Response times Averages (seconds)
1	836	398	48	61	10
2	1130	692	61	123	6
3	1093	656	60	135	6
4	1093	656	60	135	6
5	1053	615	58	129	6
6	1013	575	57	135	5
7	960	522	54	132	5
8	927	489	53	140	4
9	896	458	51	115	5
10	1356	919	68		3
11	1391	954	69	236	4
12	1394	956	69	227	4
13	1450	1012	70	151	7
14	625	313	50	49	6
15	1917	1480	77	285	6
16	1917	1480	77	367	5
Average	1191	761	61	161	**5**

B2 Standpipe Calibrations Data Charts

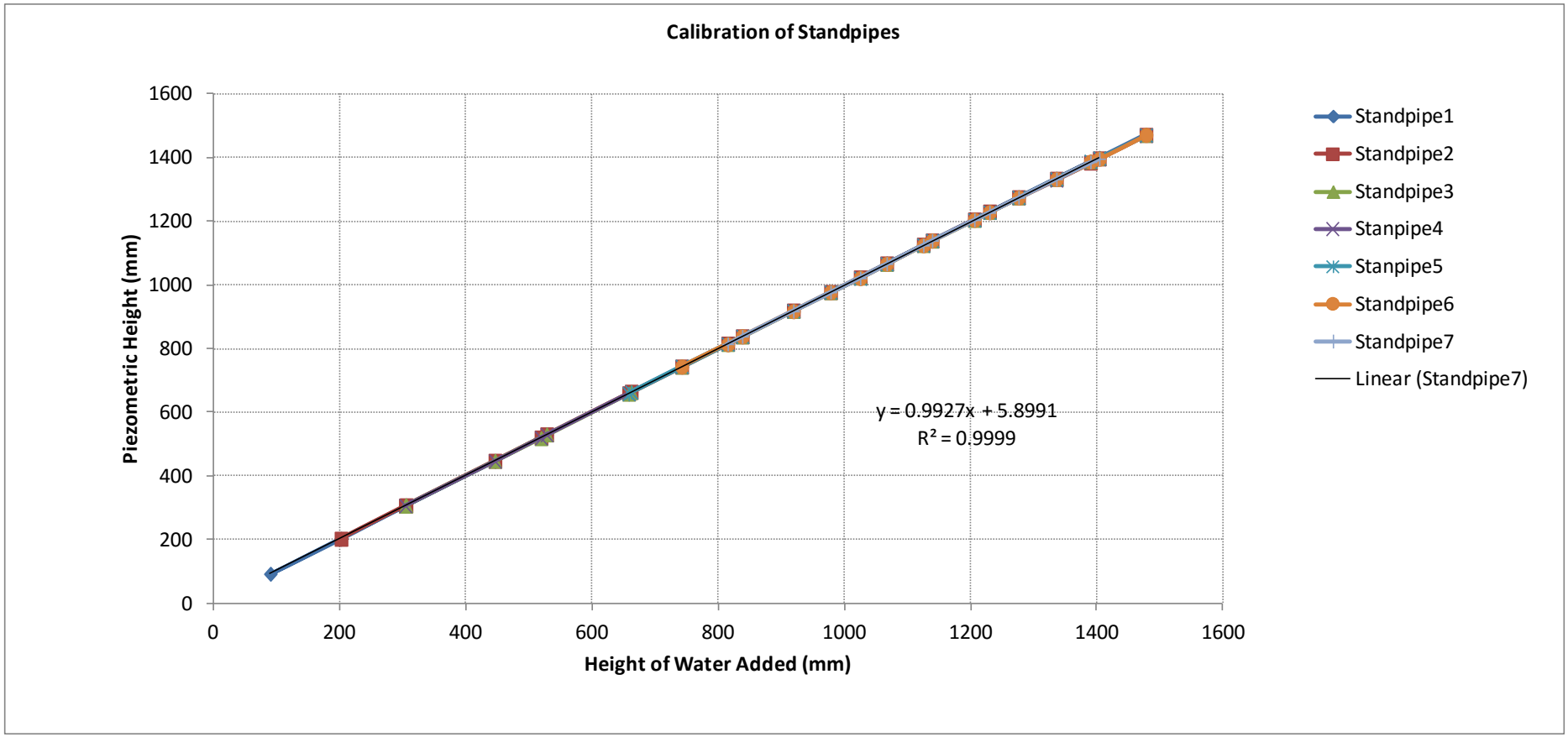

Figure B1: Standpipes calibrations data

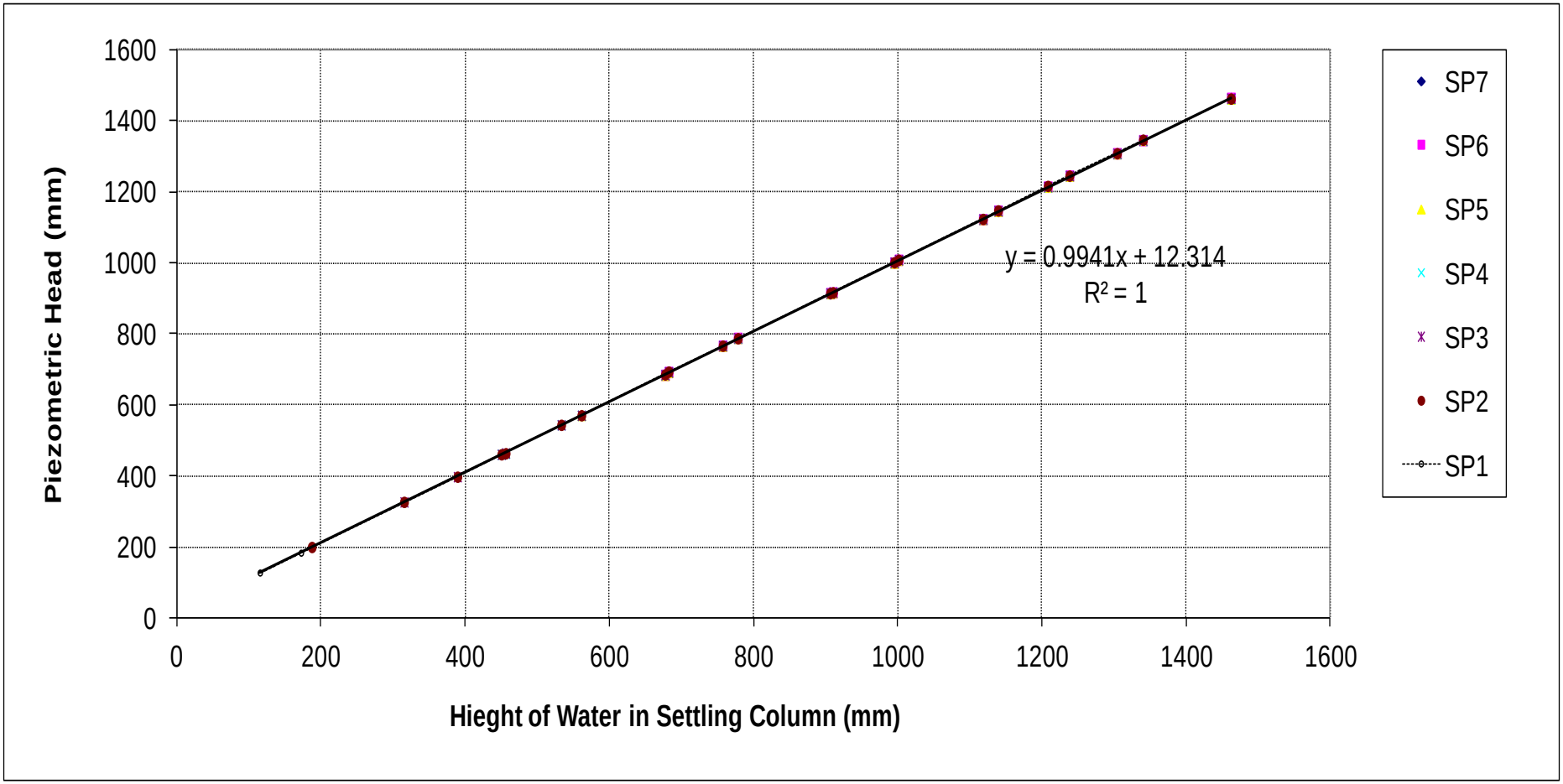

Figure B2: Calibration chart for standpipes

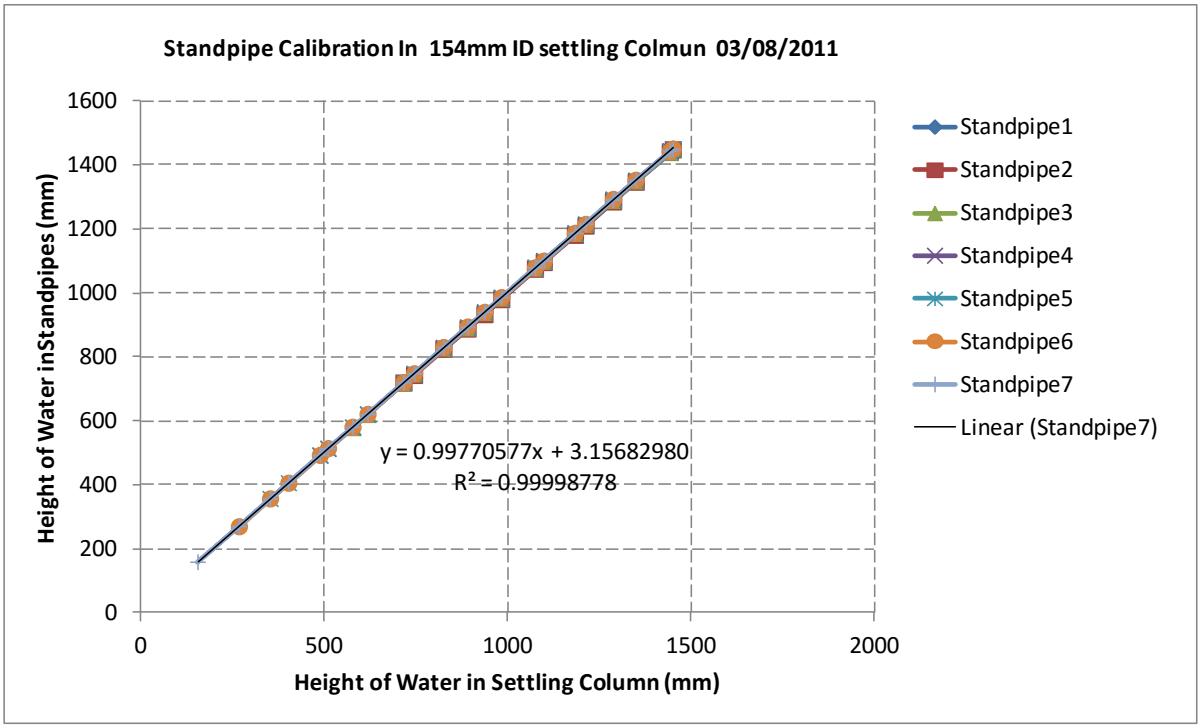

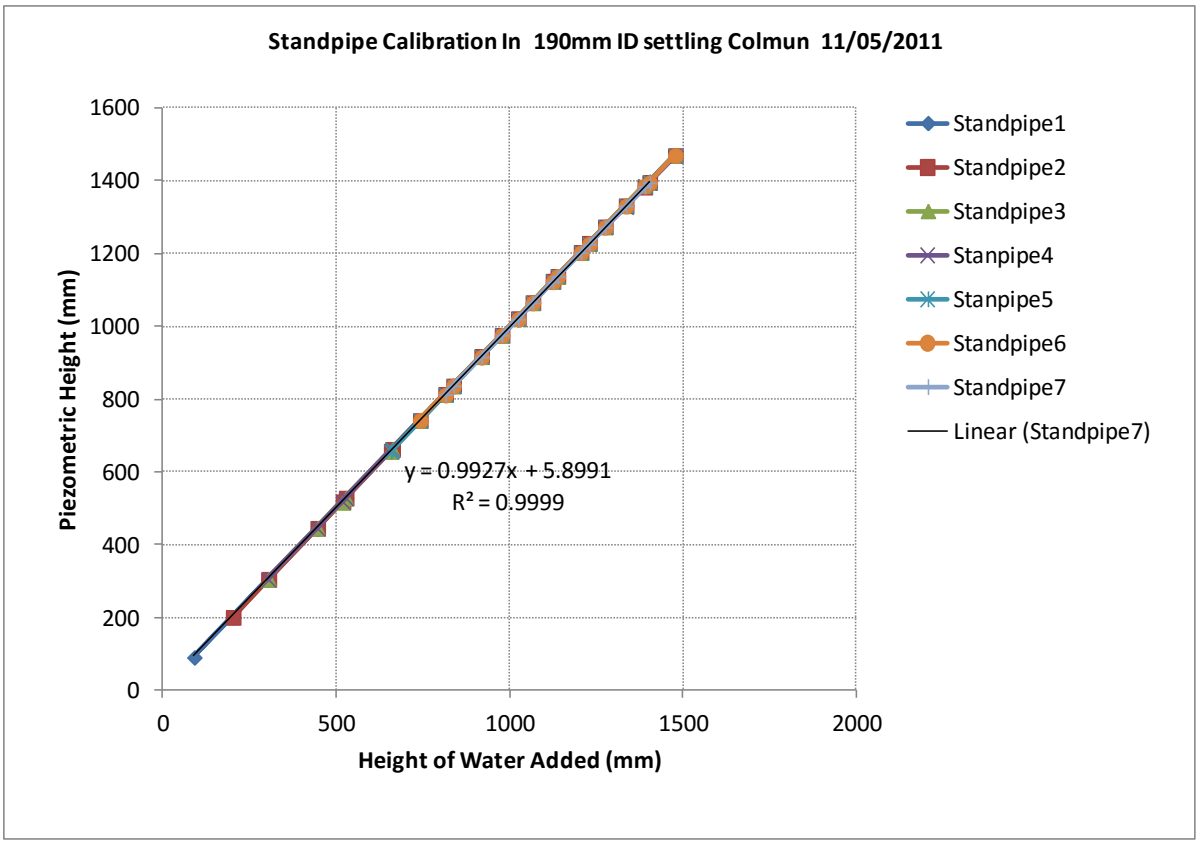

Figure B3: Calibration chart for standpipes

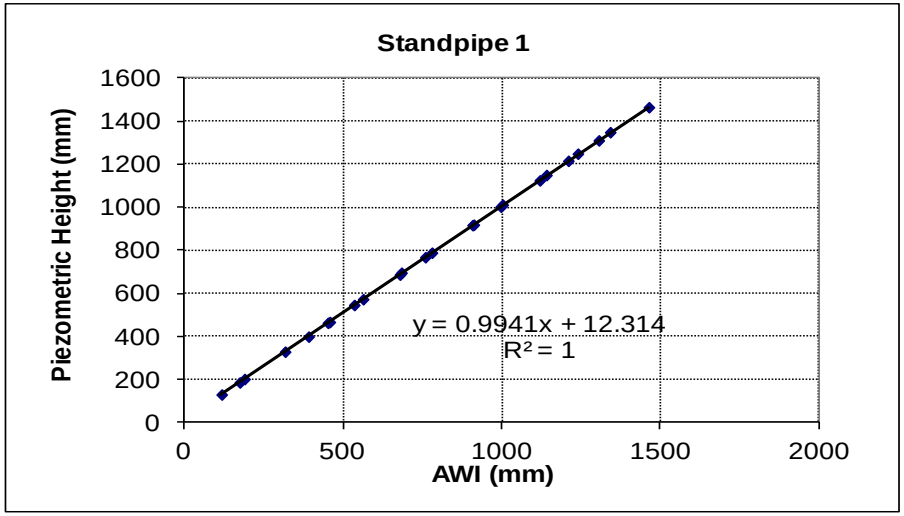

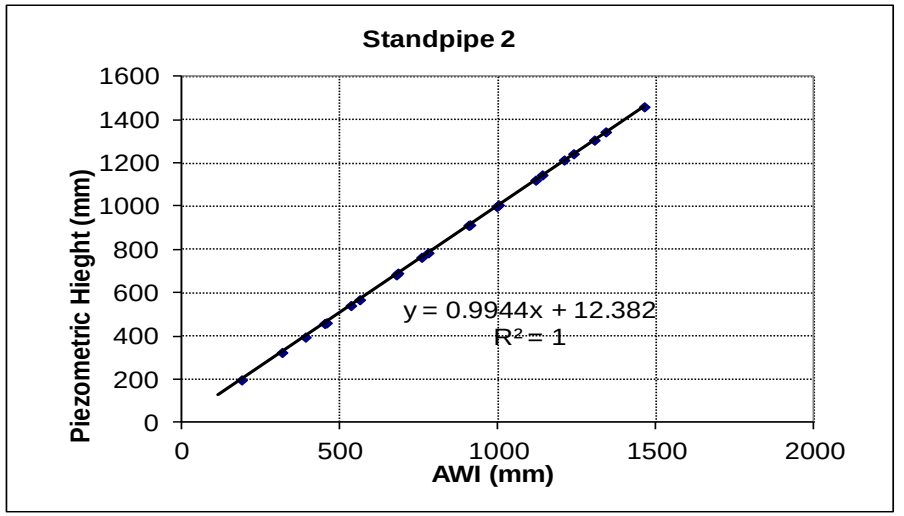

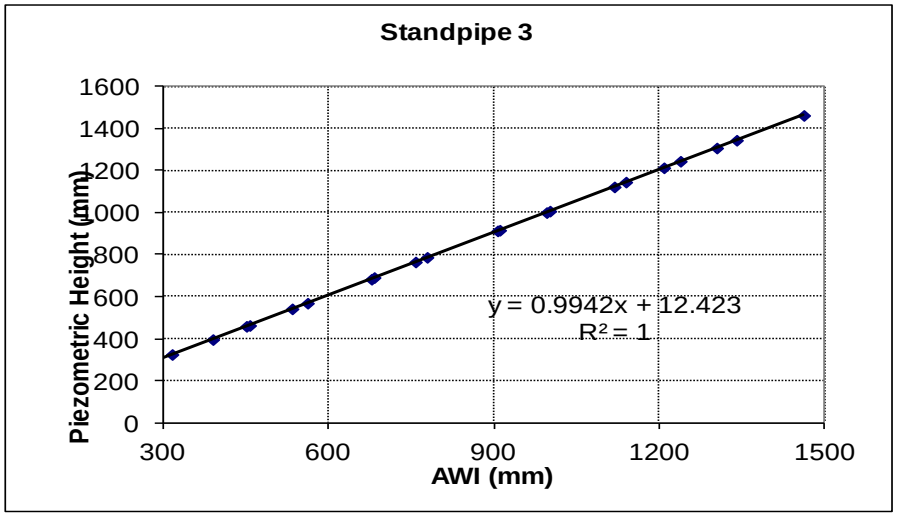

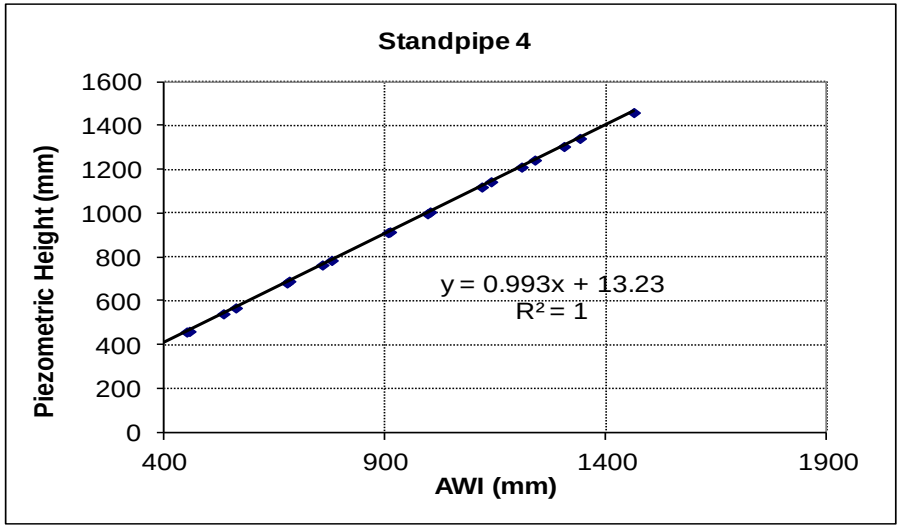

Figure B4: Standpipe calibration charts

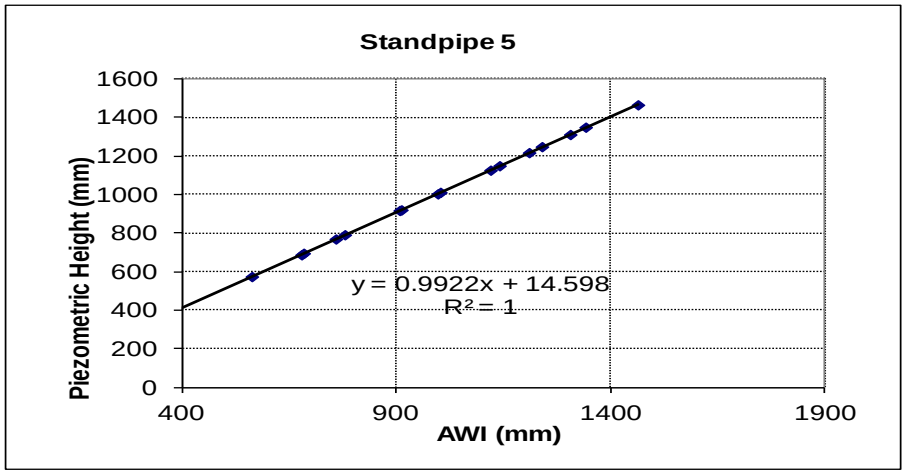

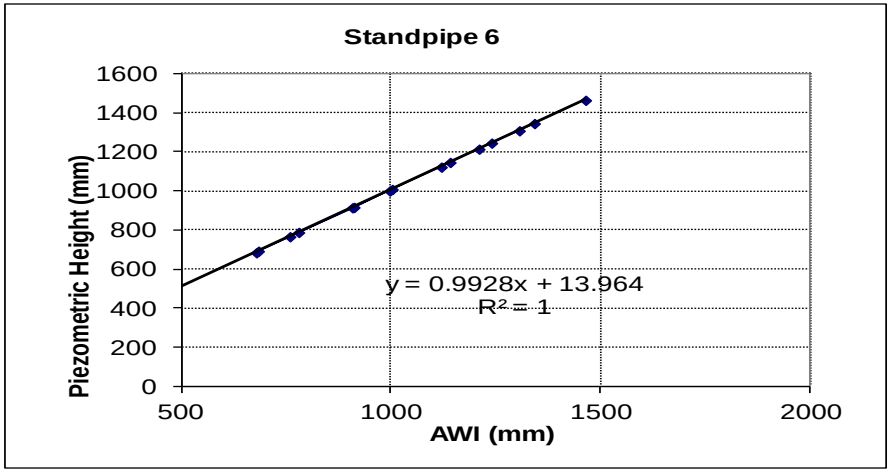

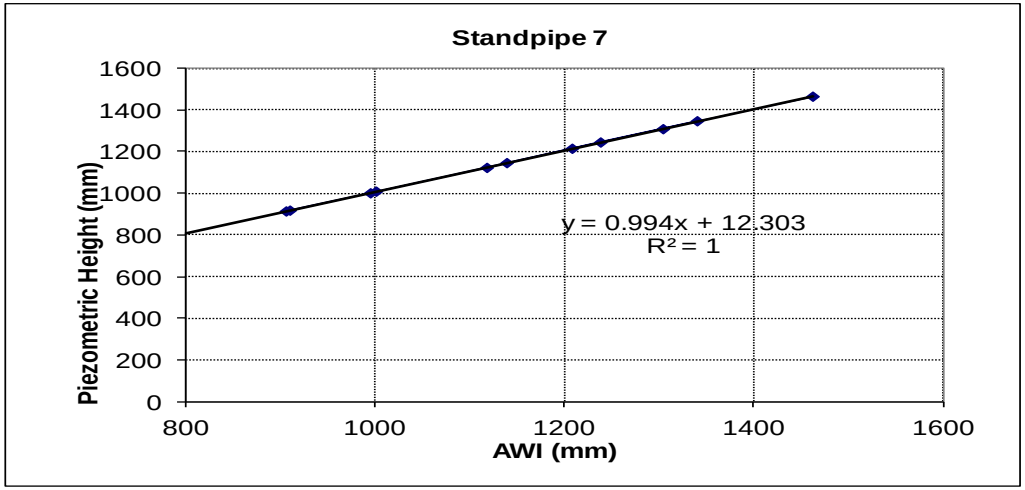

Figure B5: Standpipe calibration chart

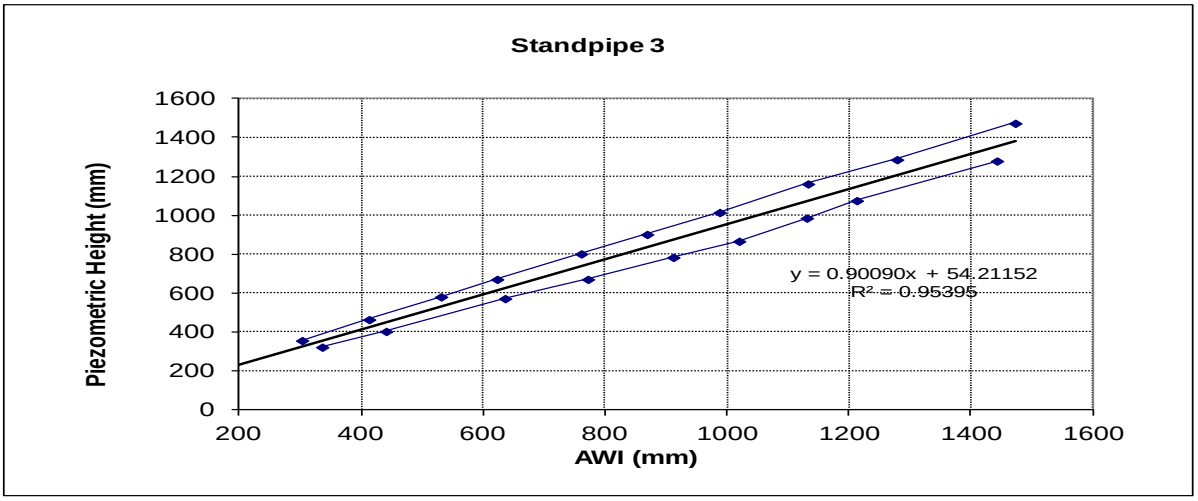

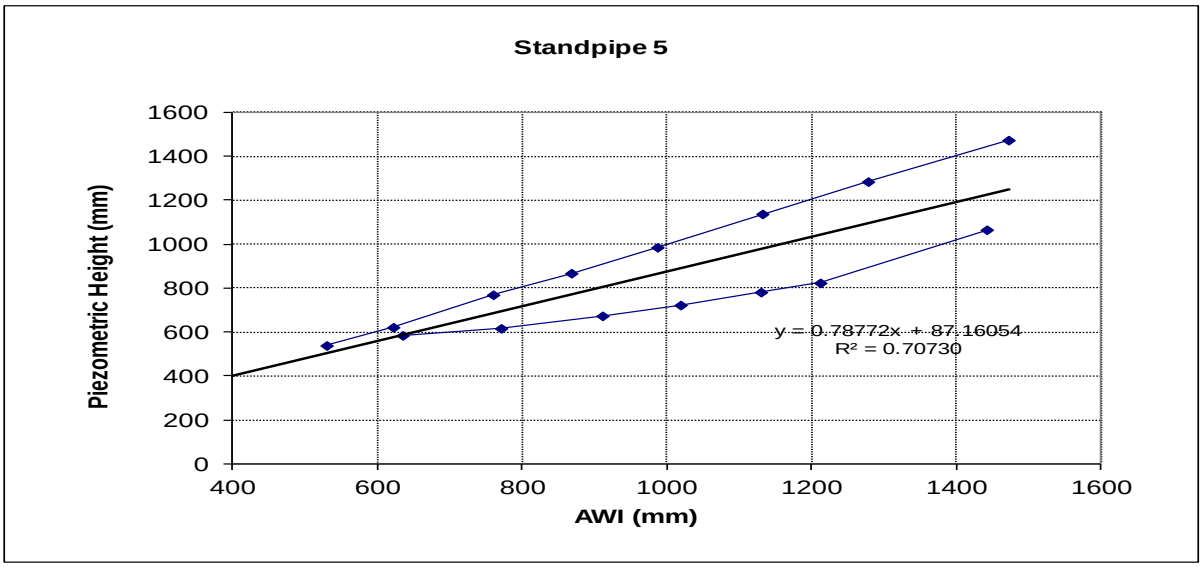

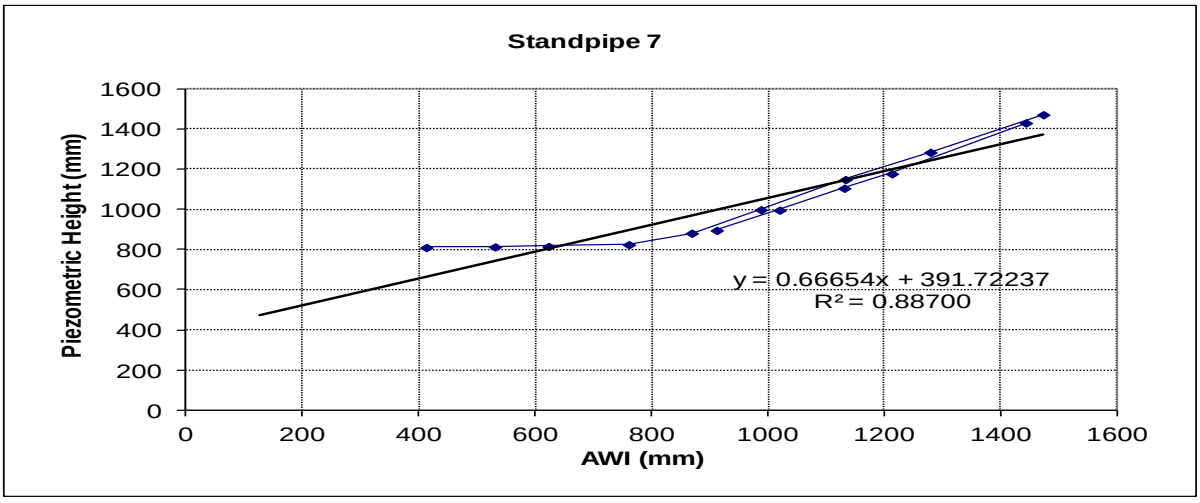

Figure B6: Standpipe calibrations

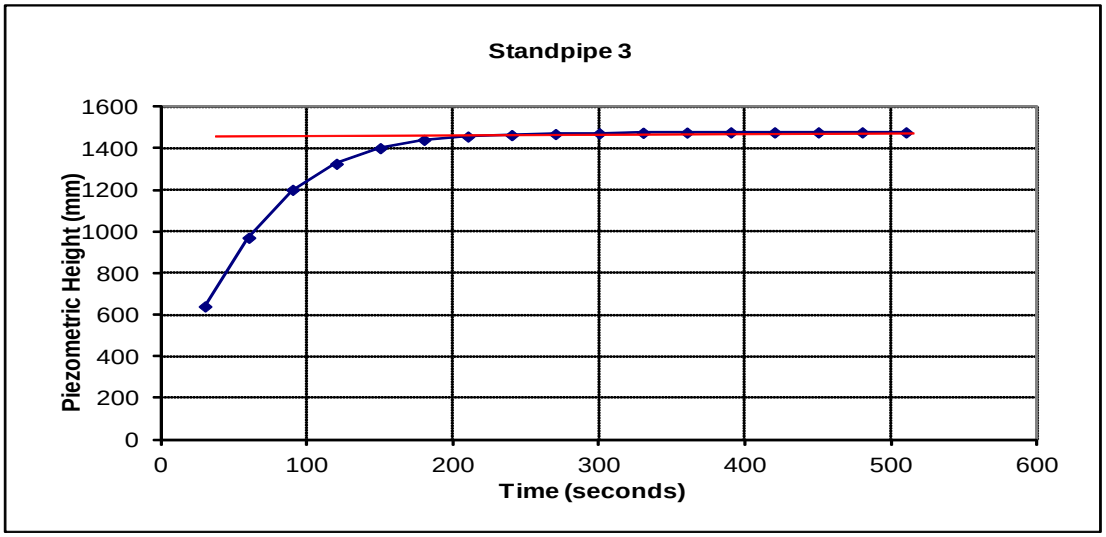

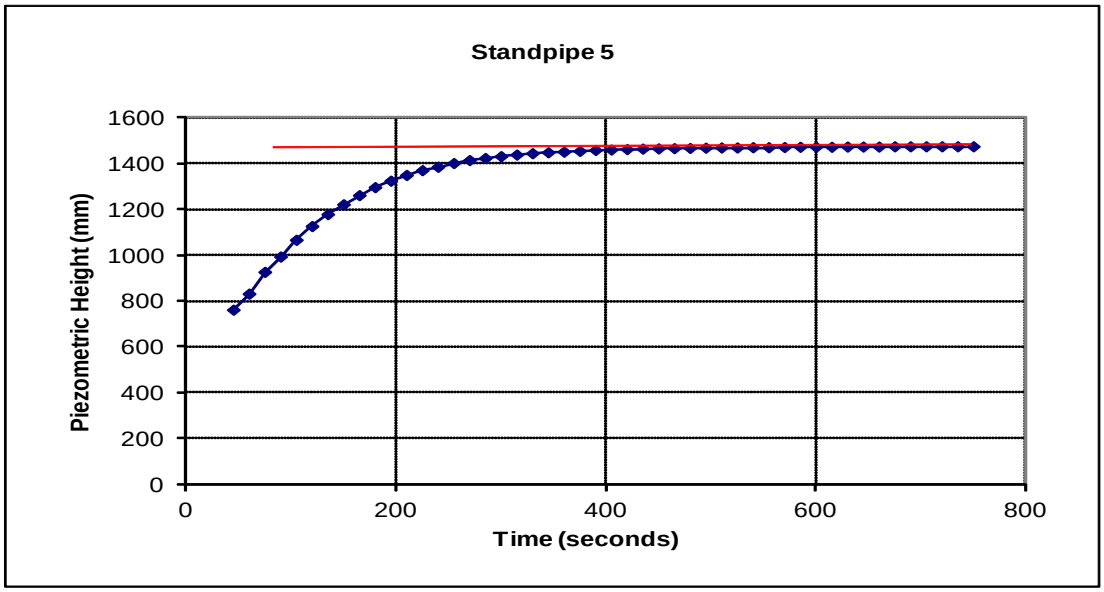

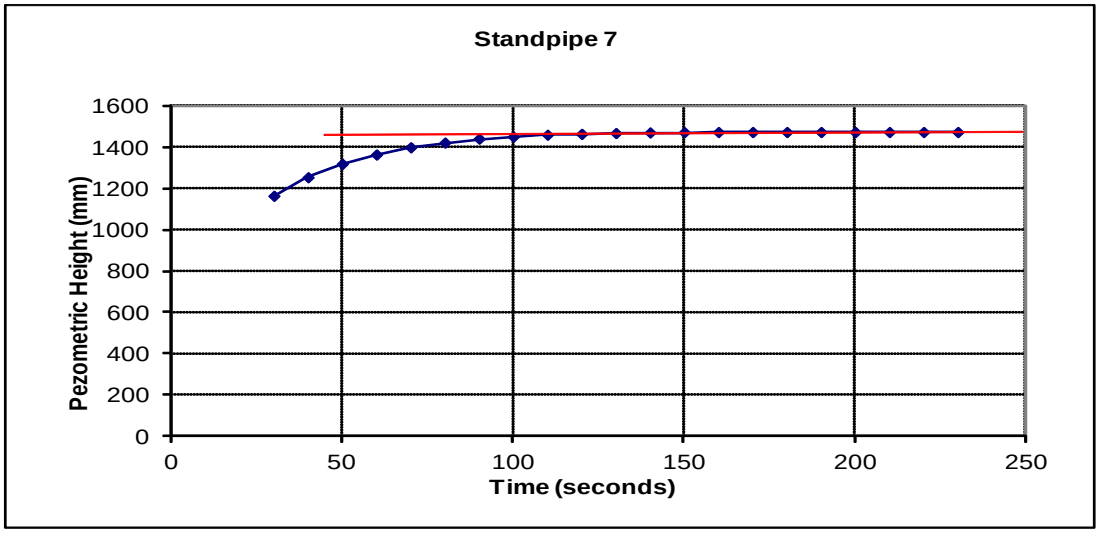

Figure B7: Standpipe calibrations

B3 Effects of Water Height on Standpipe Response Times

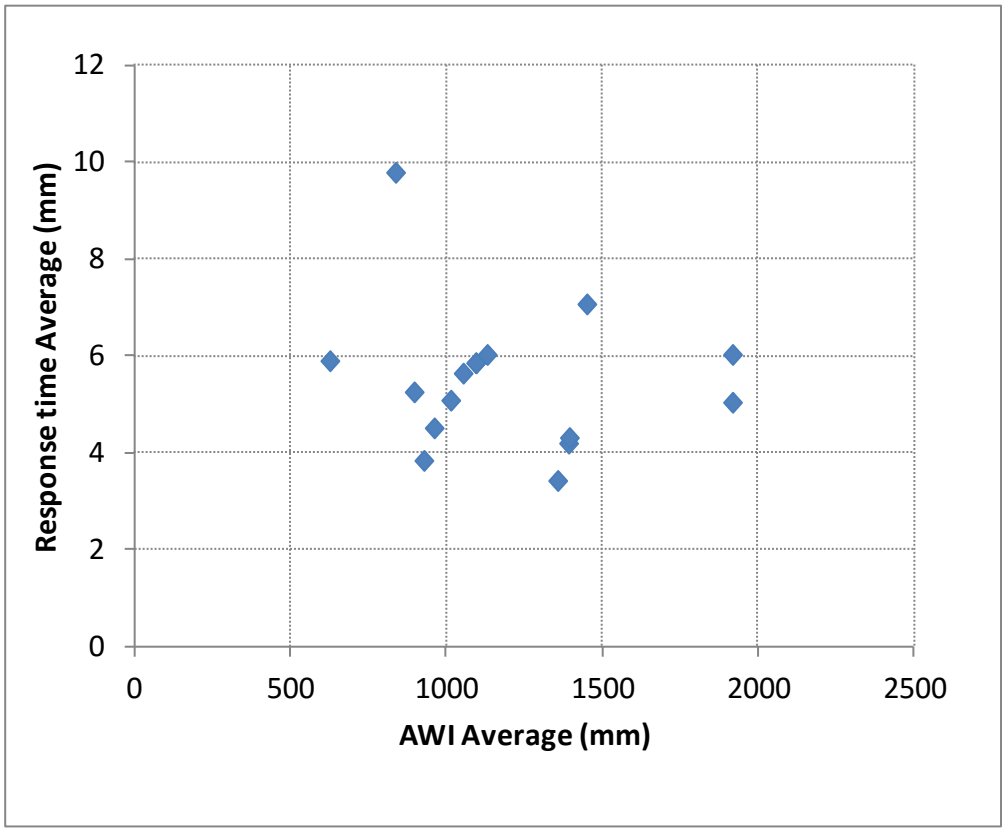

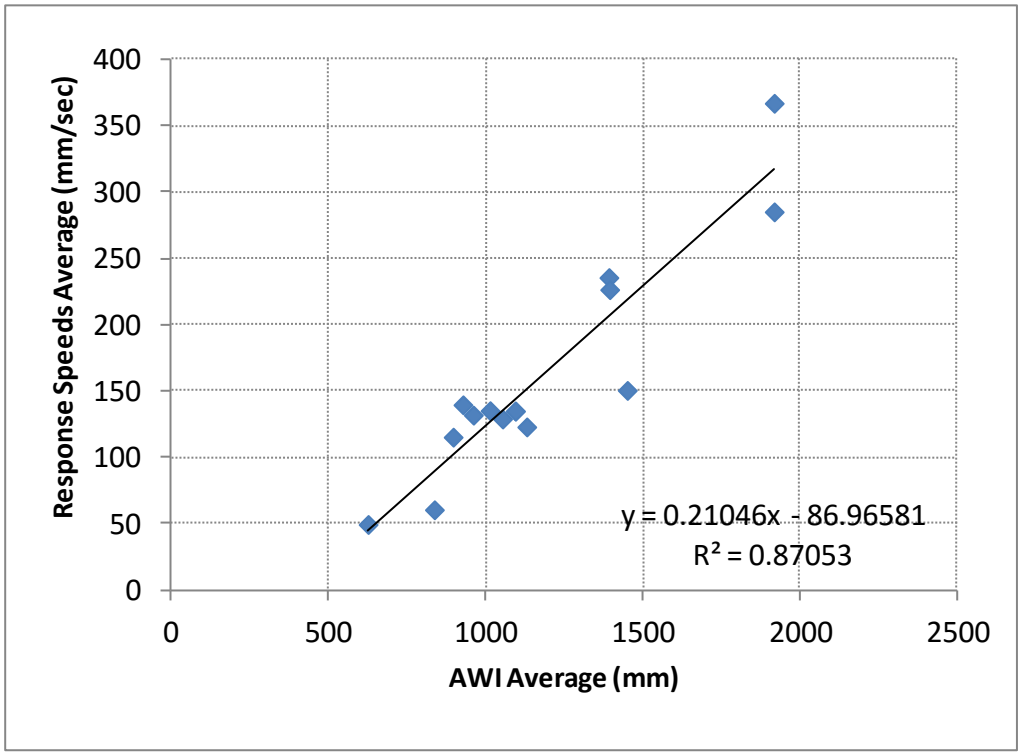

Figure B8: Effect of water height on standpipe response times

B4 Transducer Calibrations Data

TABLE B2: Transducer calibrations data

		#0 Wika 40kPa	#1 Gems 100kPa A033513		#2 Gems 100kPa Y078291		#3 Gems 100kPa B08404		#4 Gems 100kPa B084054		#5 Wika 100kPa
Date of Calibration	Number of Days	Calibration Factor (V/mm)	Calibration Factor (V/mm)	Zero Reading (V)	Calibration Factor (V/mm)	Zero Reading (V)	Calibration Factor (V/mm)	Zero Reading (V)	Calibration Factor (V/mm)	Zero Reading (V)	Calibration Factor (mA/mm)
2009-07-25	1		0.00084977	2.94							
2009-08-05	12		0.0009319								
2009-09-11	49		0.0009632								
2009-10-24	92		0.00089579								
2009-11-20	119		0.00090939								
2010-03-25	244		0.00096207								
2010-04-18	268		0.00096475								
2010-04-20	270		0.00095219								
2010-05-02	282		0.00096627								
2010-08-27	399		0.000954817								
2010-09-08	411		0.000925184								
2010-10-23	456		0.000967		0.000975		0.000973		0.000969		
2010-11-28	492		0.0009666	2.97	0.0009802	0.025	0.000927	-0.082	0.0009368	-0.006	
2010-12-17	511		0.00096733	2.98	0.00097264	0.024	0.0009688	-0.048	0.00097464	-0.128	
2011-02-12	568		0.00096528	2.919	0.00095493	-0.327	0.00097293	-0.045	0.00097539		
2011-02-13	569		0.0009657	2.955	0.0009657	0.004	0.00096584	-0.03	0.00097294	-0.221	
2011-02-14	570			2.778		0.004		-0.005		-0.037	
2011-02-19											0.00973731
2011-08-05		0.0024334	0.00096868		0.00097475		0.00097508		0.0009774		0.00964124
2011-10-26		0.00243406	0.00096748		0.00097387		0.00097387		0.00097442		0.00970953
2011-11-17		0.00245149	0.00096834		0.000973487		0.00097596		0.00097673		0.00974105
2011-12-20		0.0024317	0.0009658		0.0009715		0.0009686		0.0009598		0.0097387

B5 GEMs Transducer Calibrations

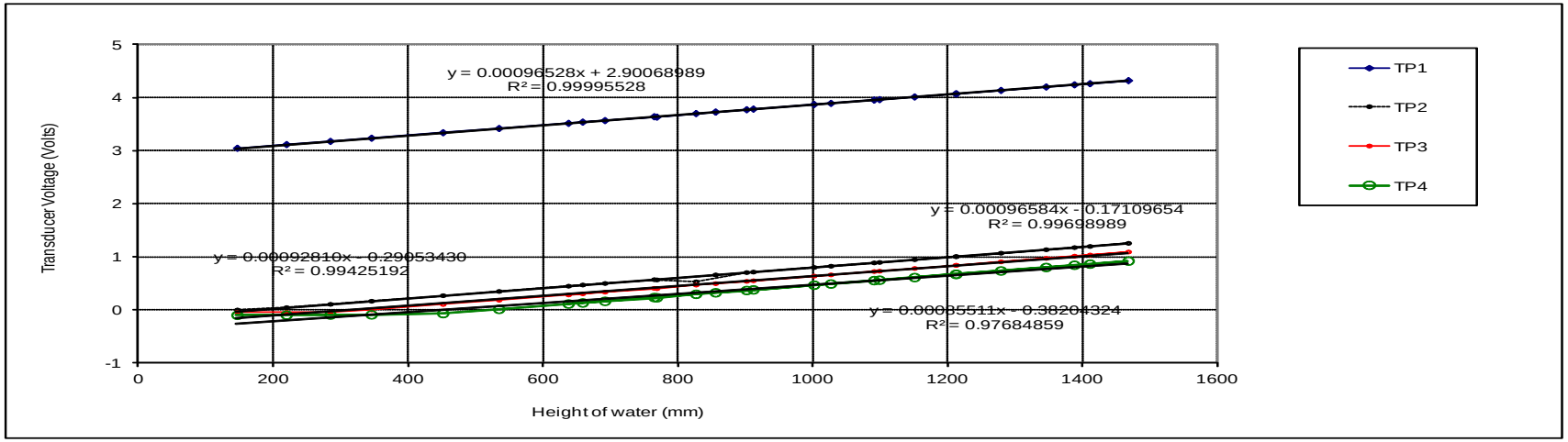

(a)

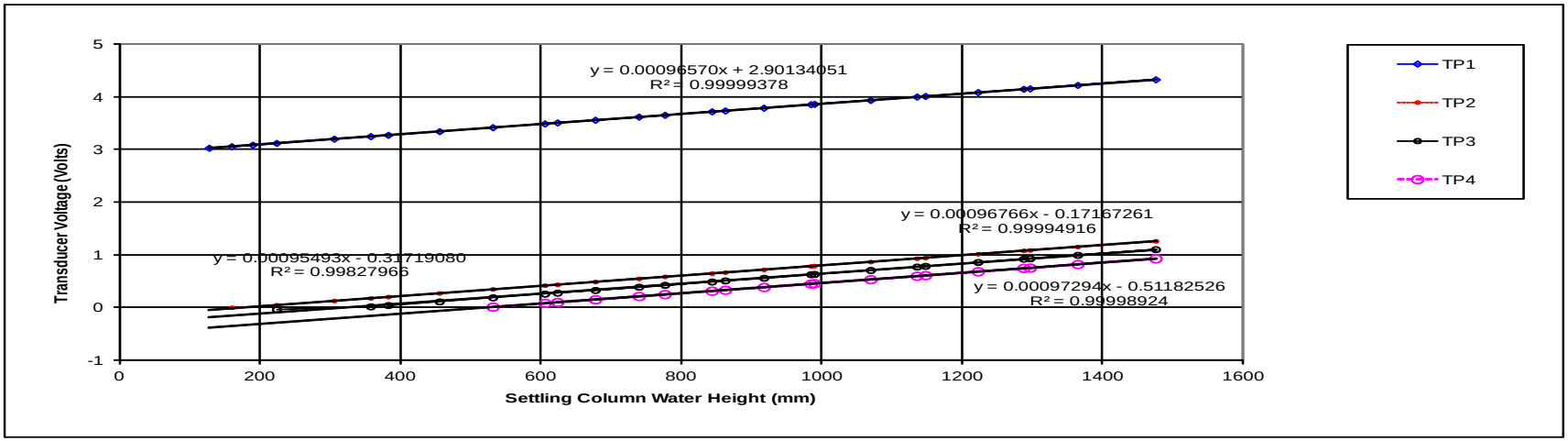

(b)

Figure B9: GEMs Transducers 1 to 4 calibrations

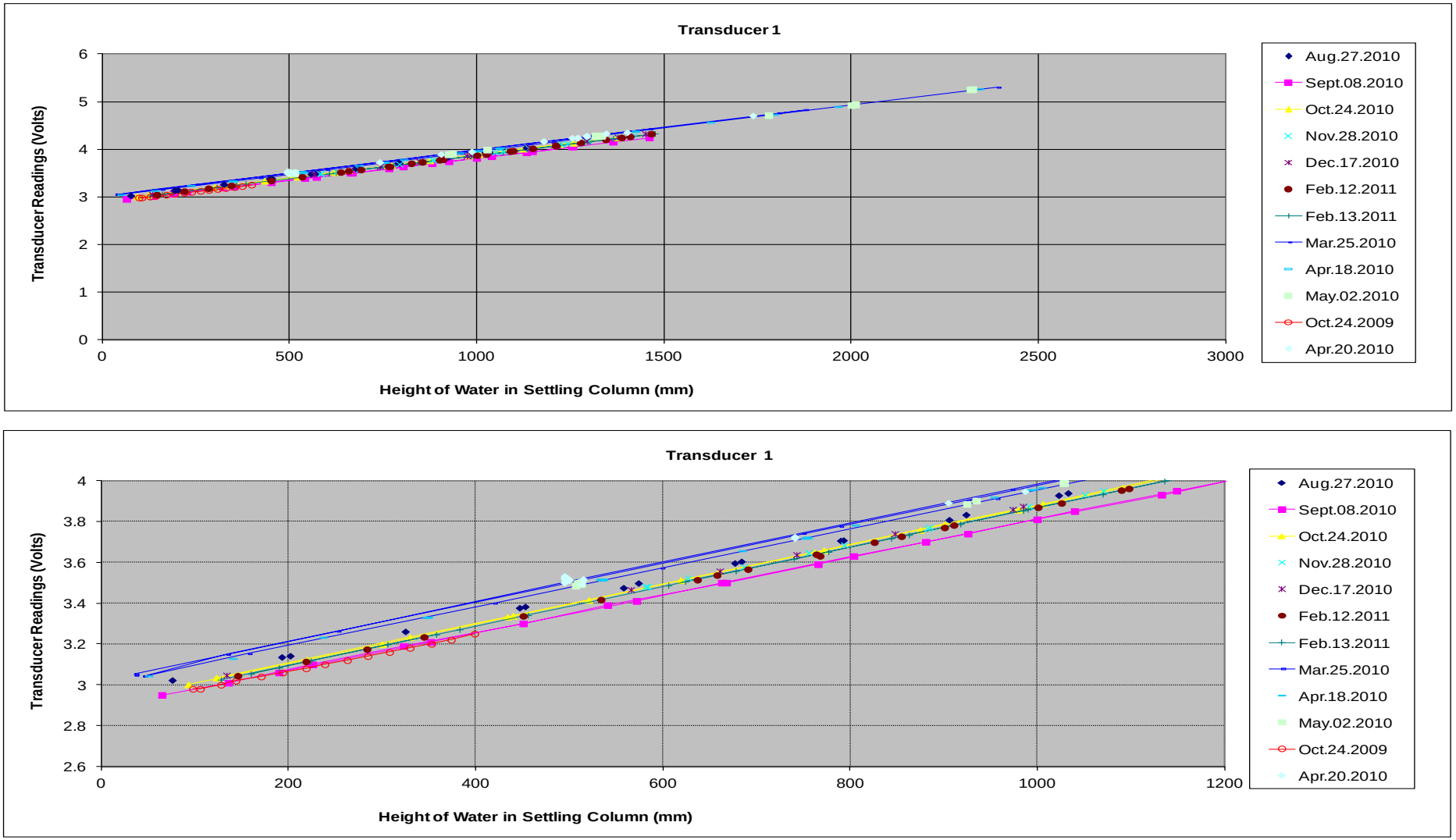

Figure B10: GEMs Transducers calibrations over time

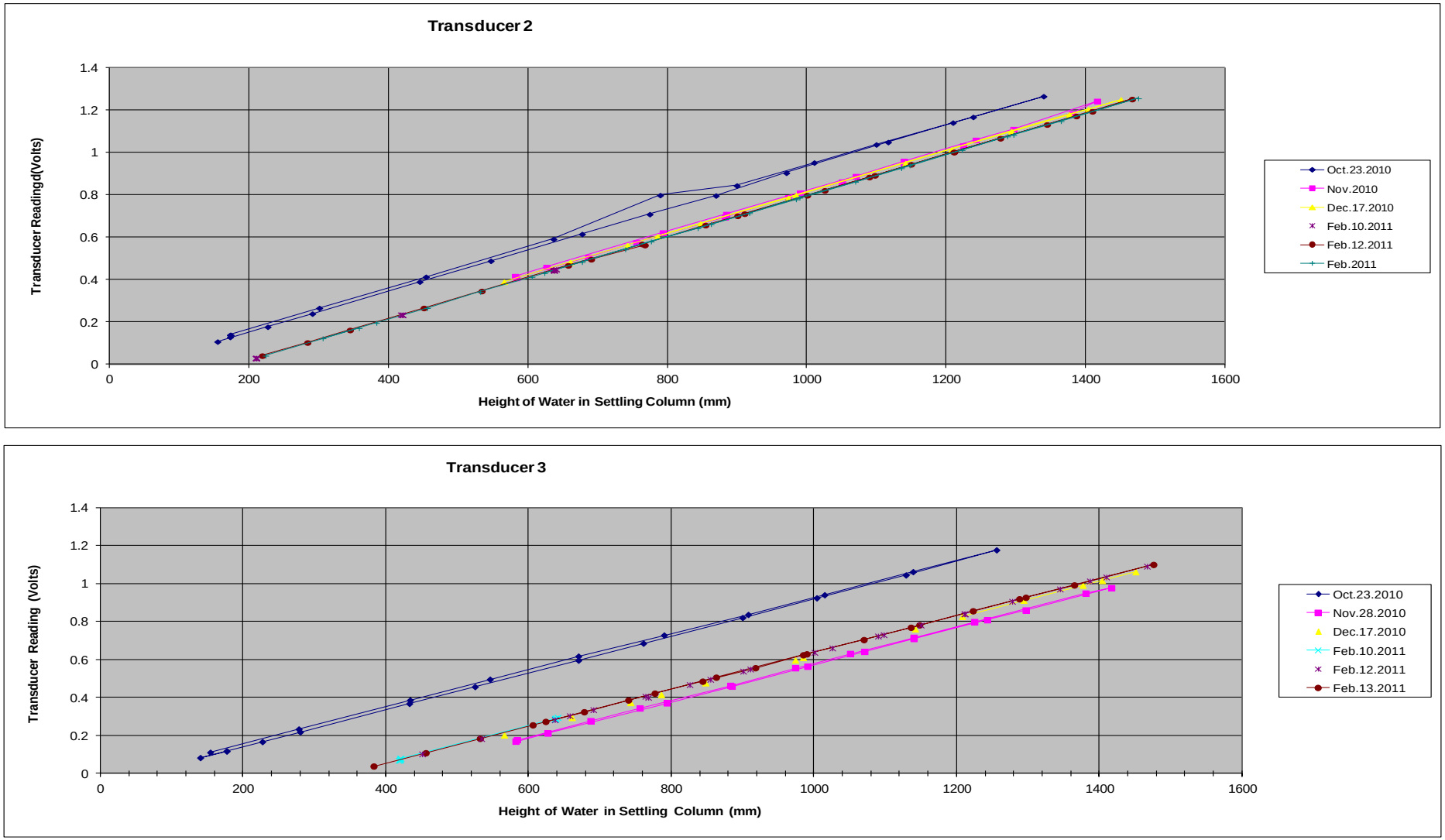

Figure B11: GEMs Transducers calibrations over time

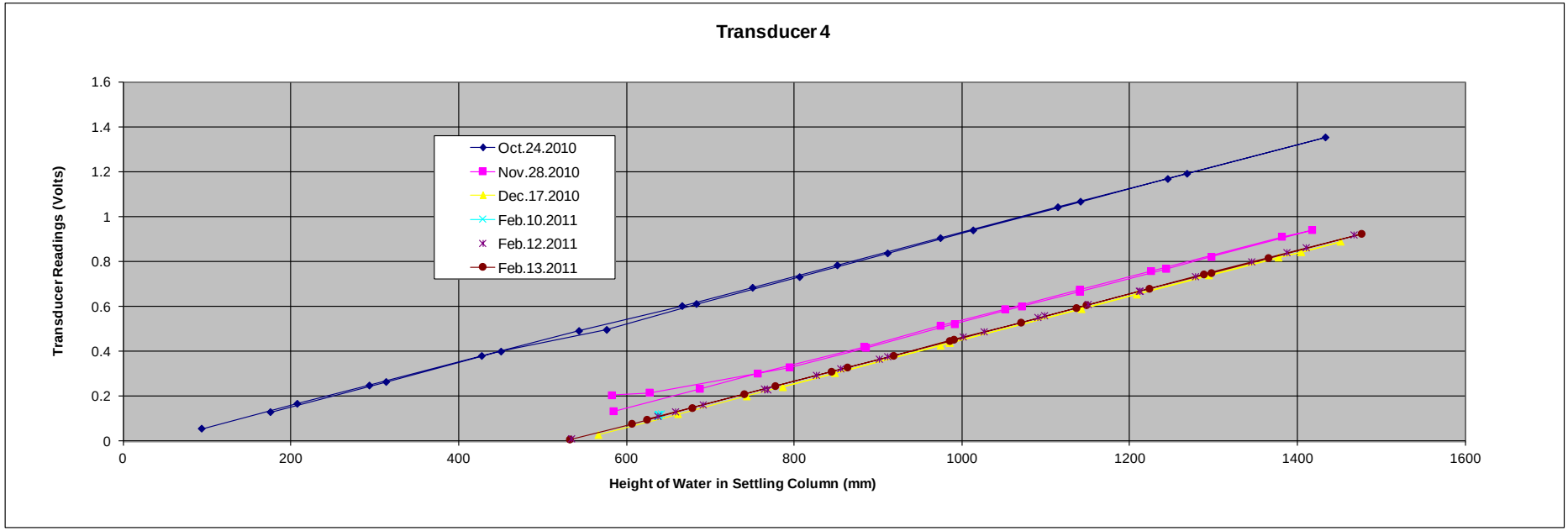

Figure B12: GEMs Transducers calibrations over time

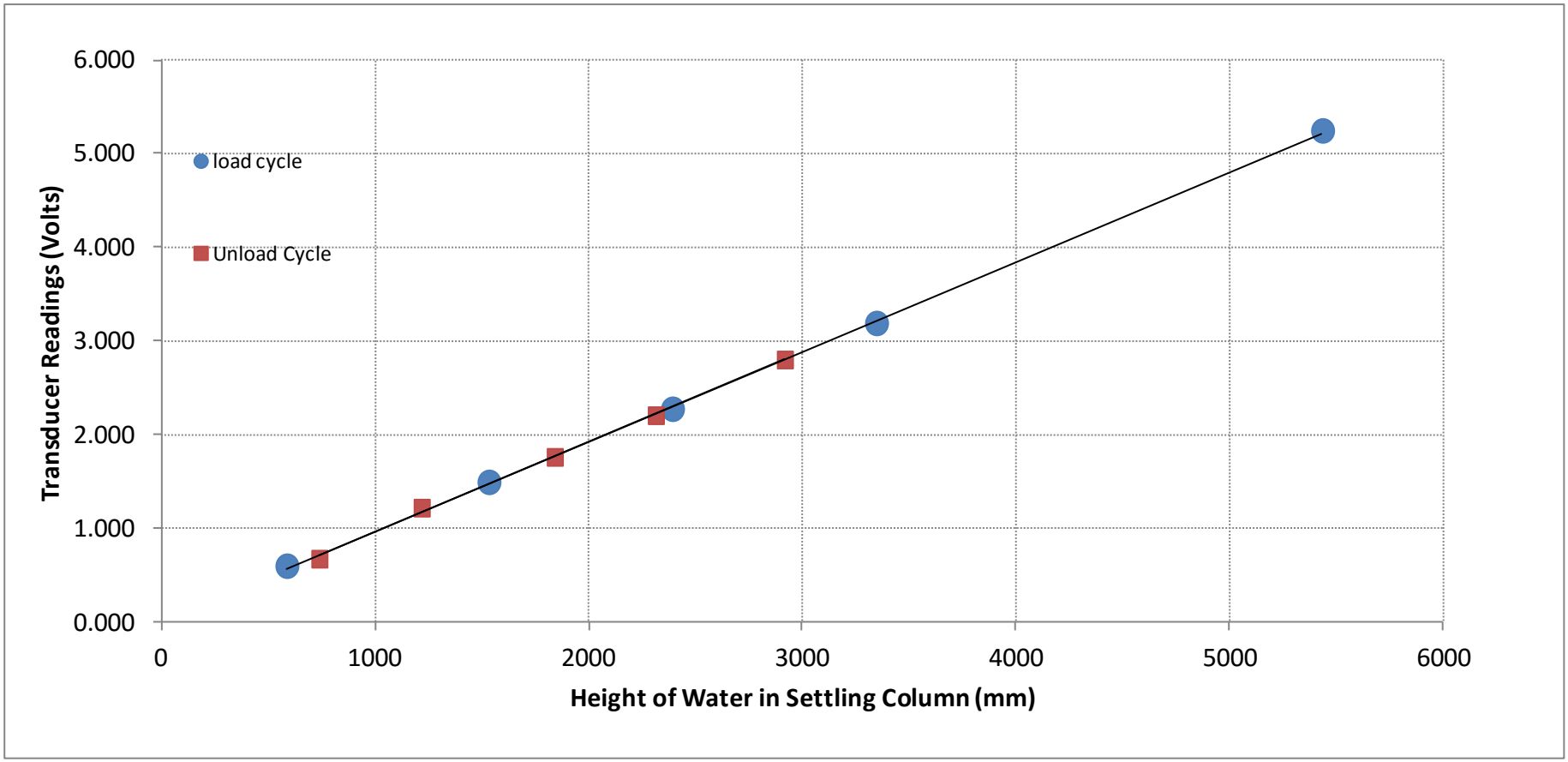

Figure B13: Transducer 4 calibration load and unload cycles

B6 Transducer Calibrations with 5 Metres High Column of Water

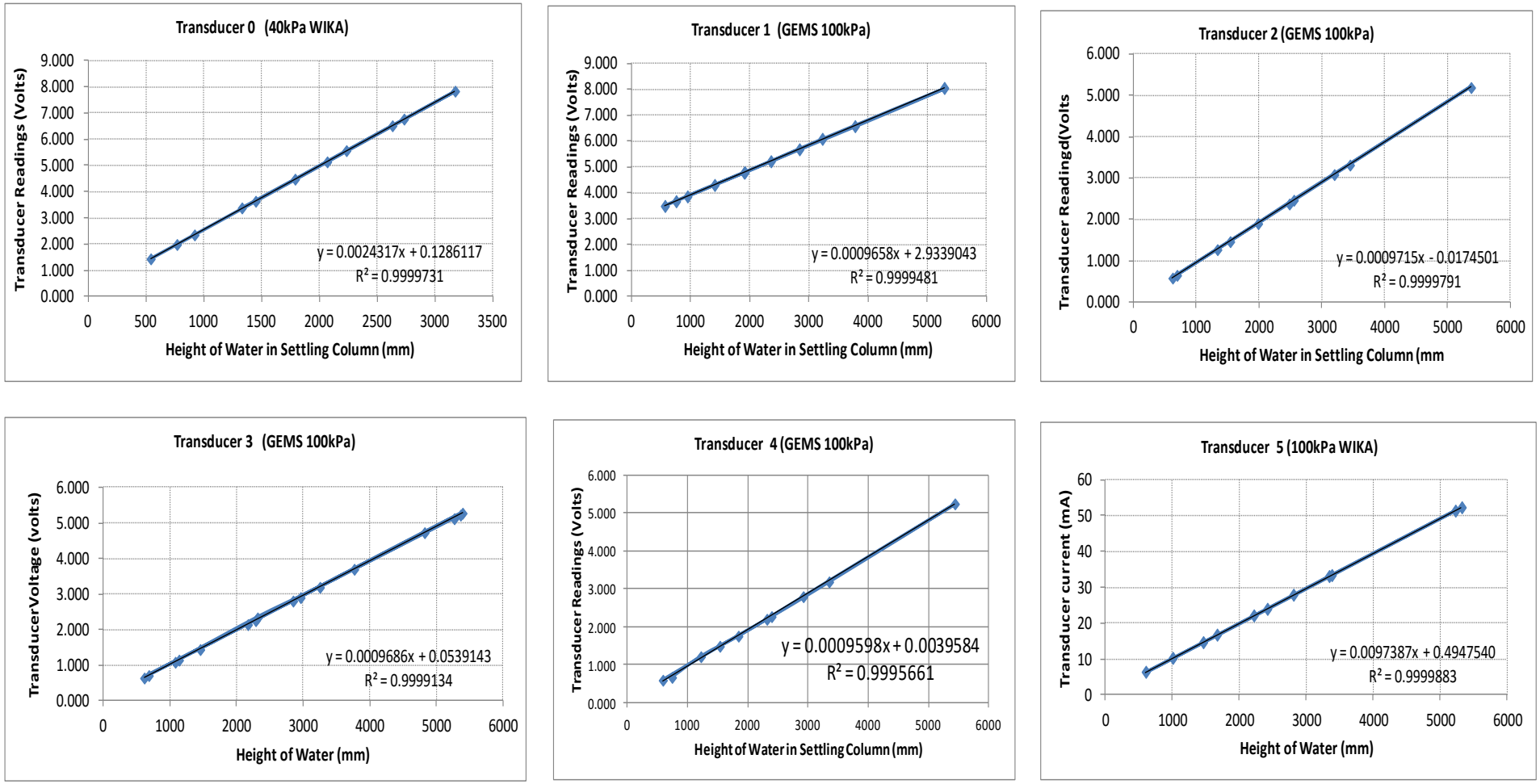

Figure B14: Transducer calibrations with 5 metres high column of water

B7 Change of Transducer Zero Readings Over Time

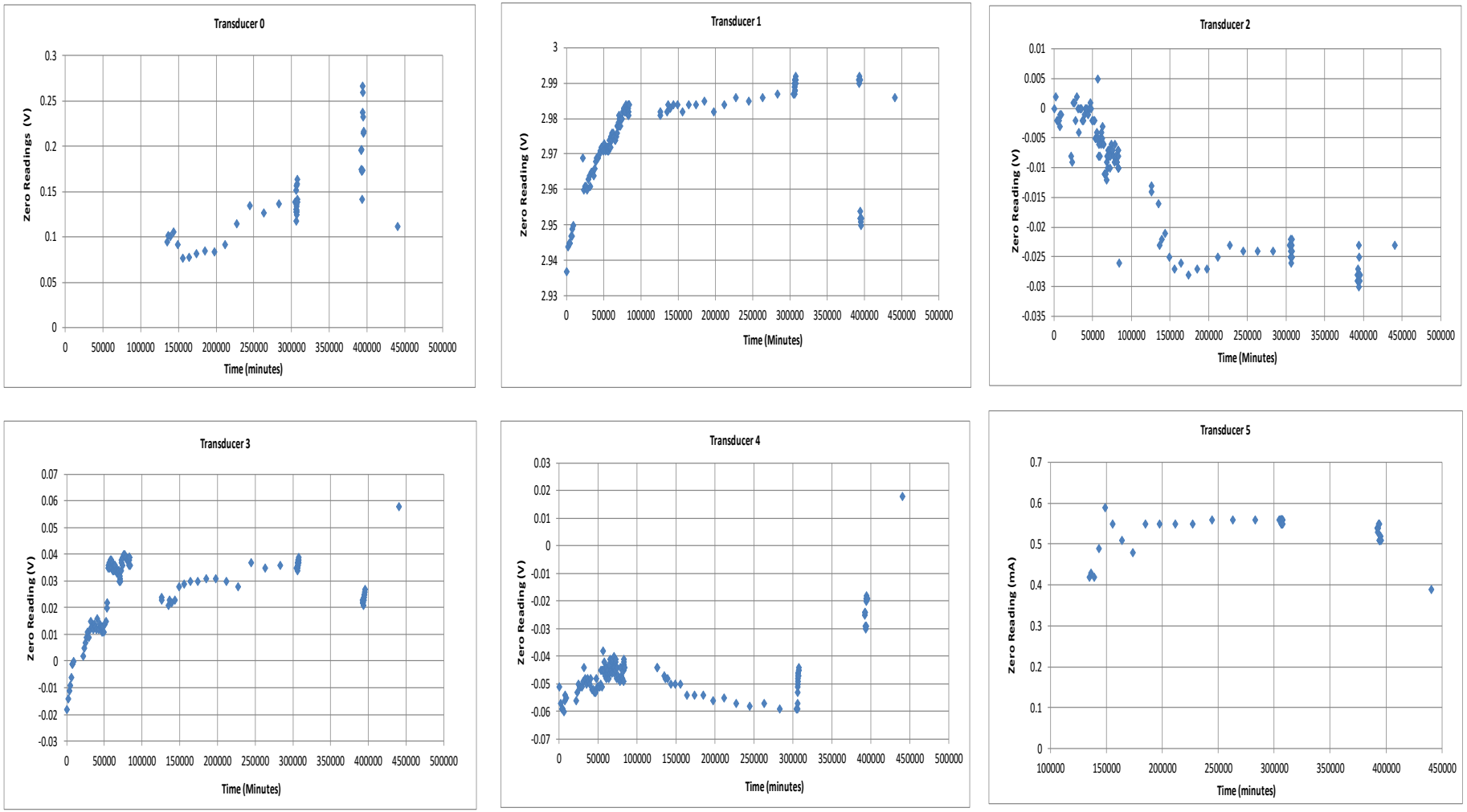

Figure B15: Change of transducer zero reading over time

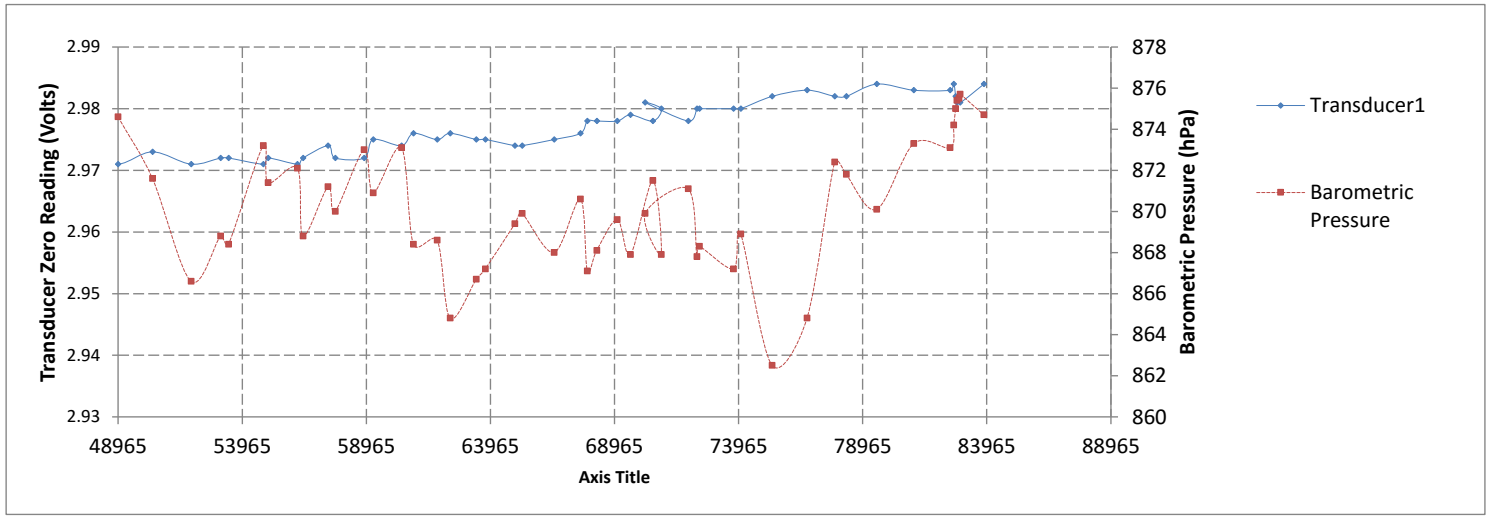

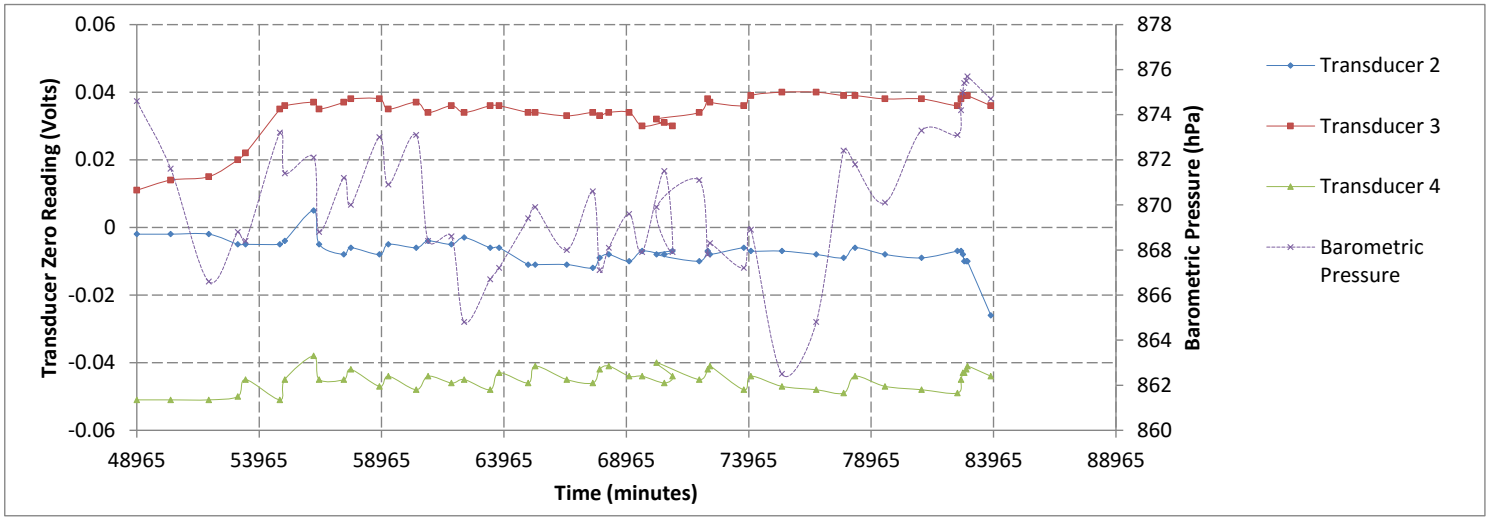

Figure B16: Variation of transducer zero reading with barometric pressure over time

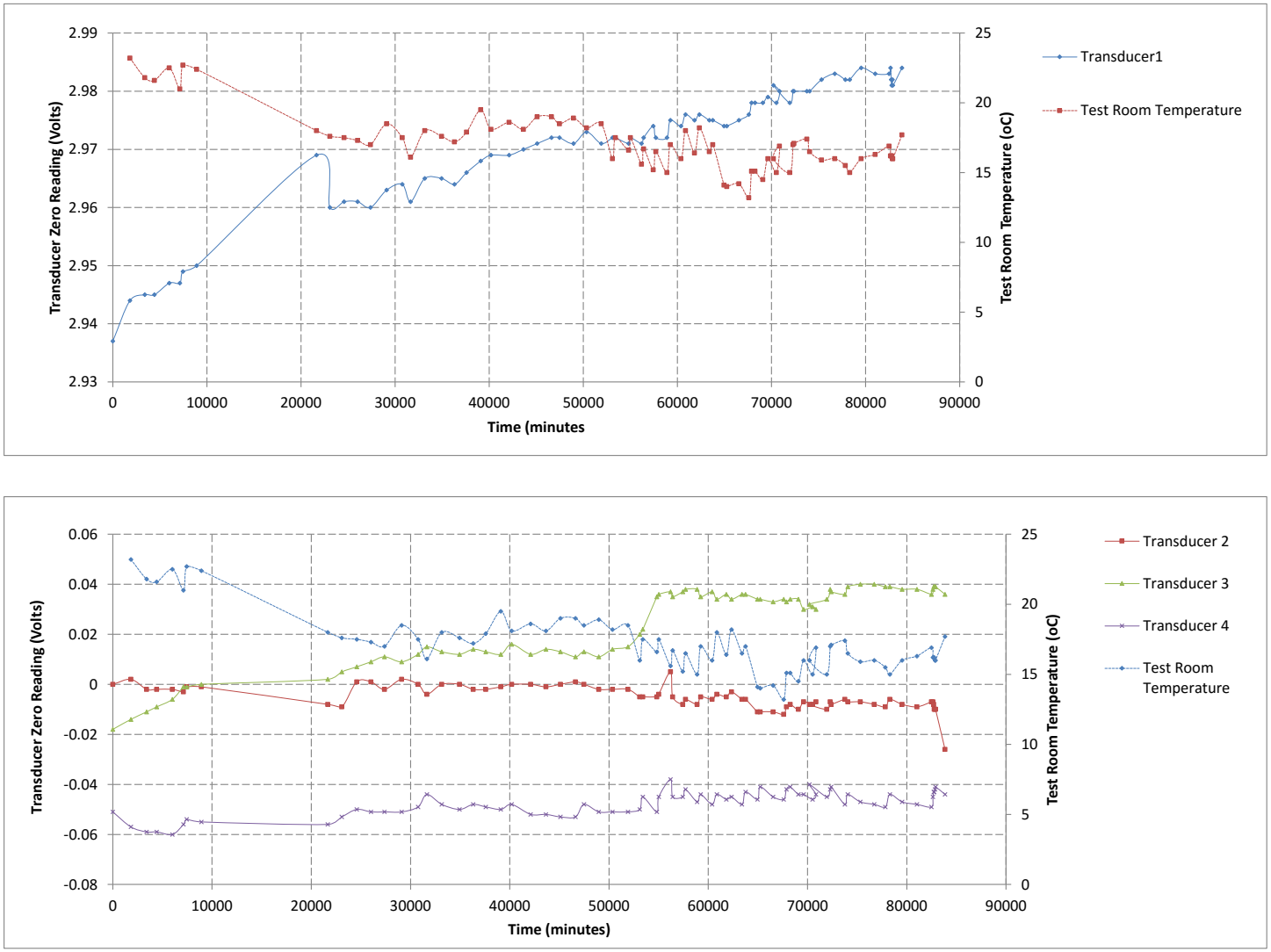

Figure B17: Variation of transducer zero reading with temperature over time

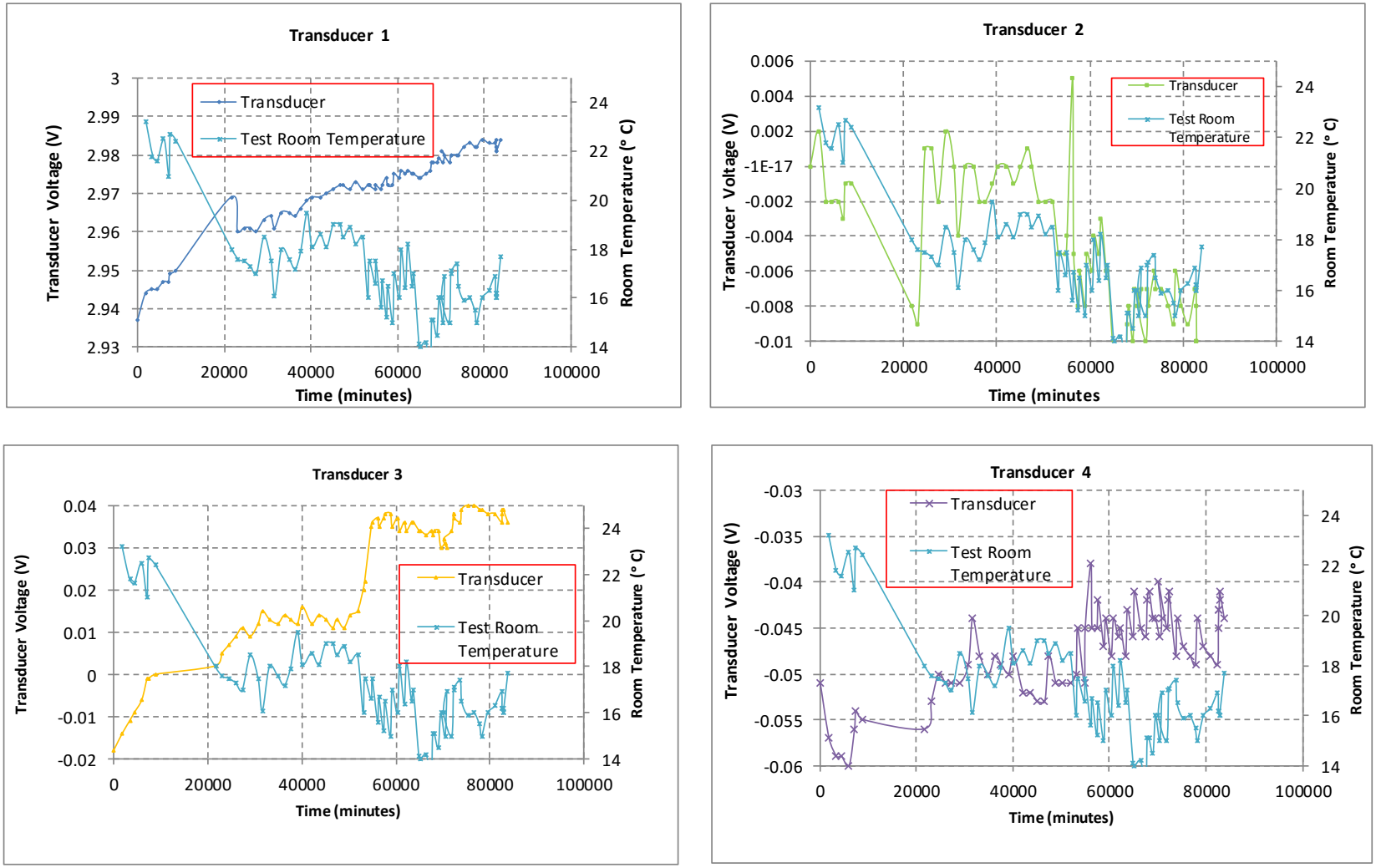

Figure B18: Variation of transducer zero reading with temperature over time

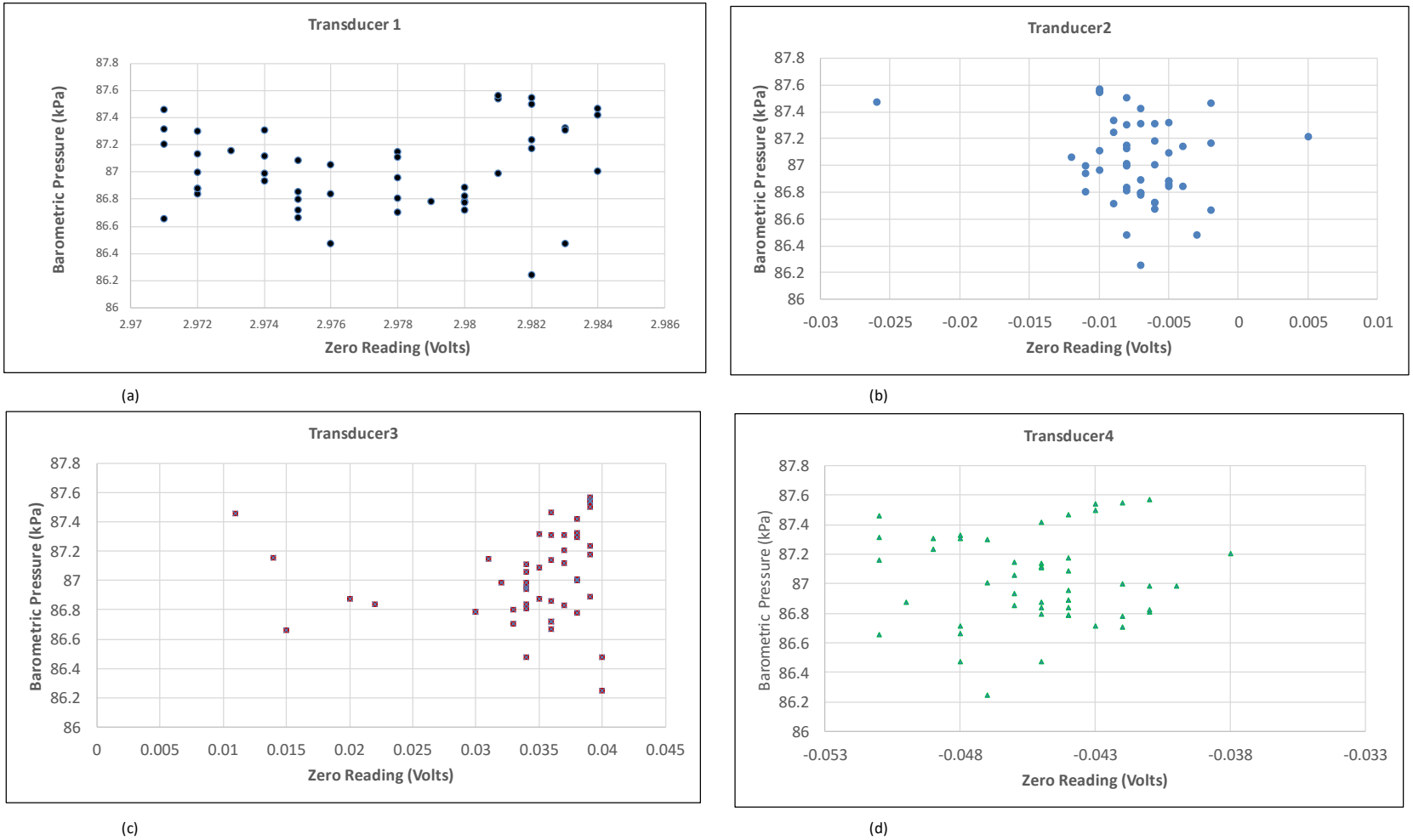

Figure B19: Variation of transducer reading with barometric pressure over time

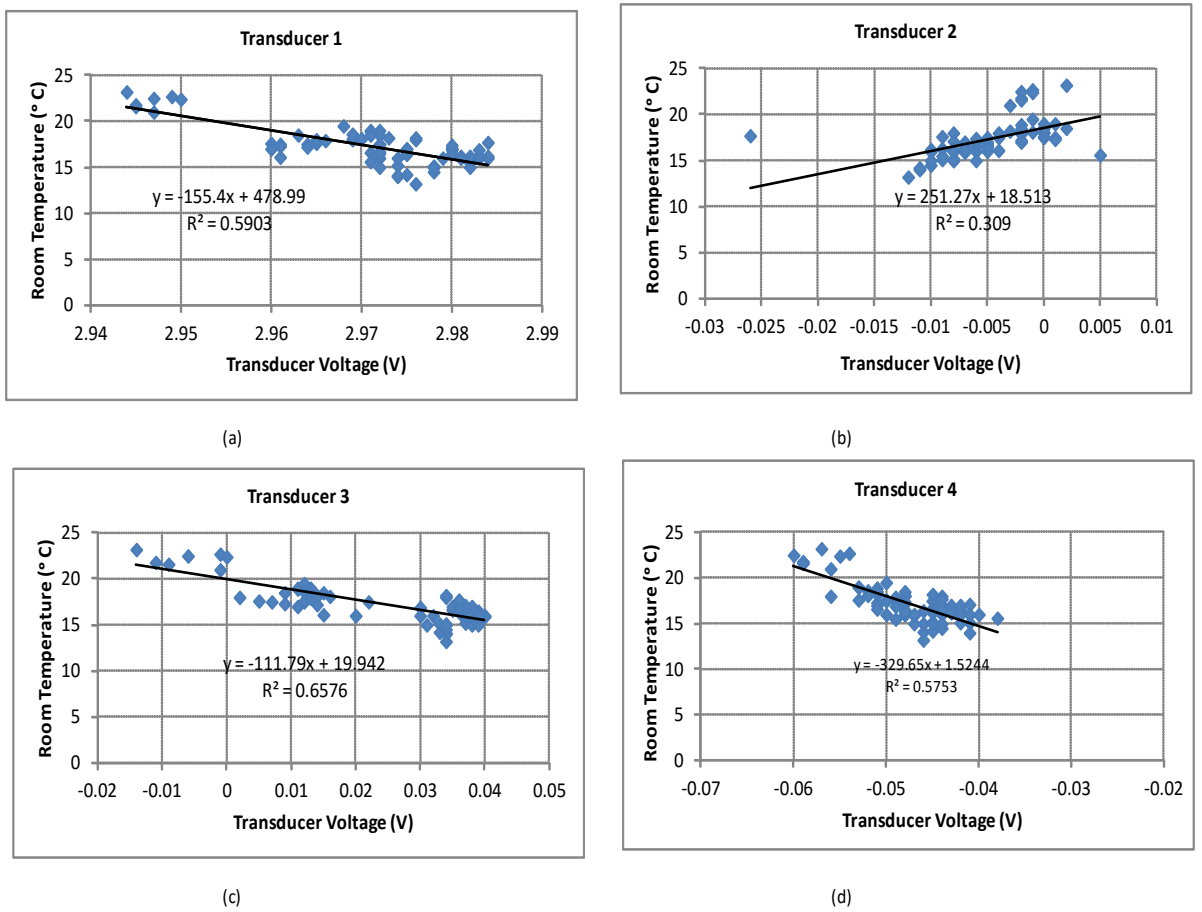

Figure B20: Variation of transducer reading with temperature over time

B8 Experiment FDB Calibrations

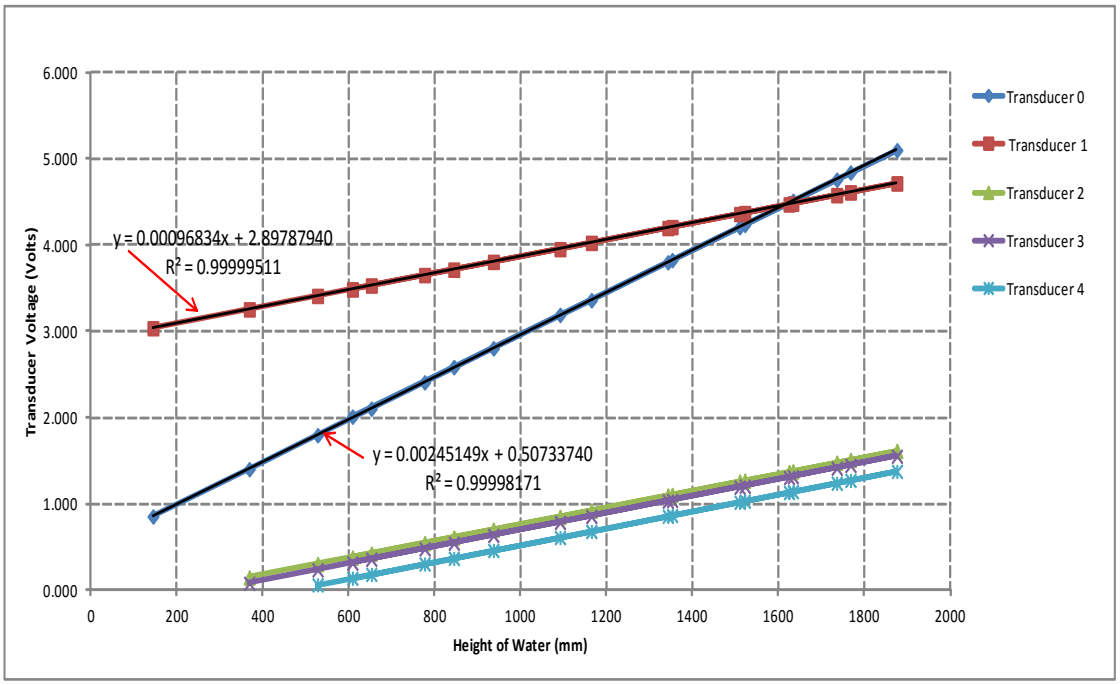

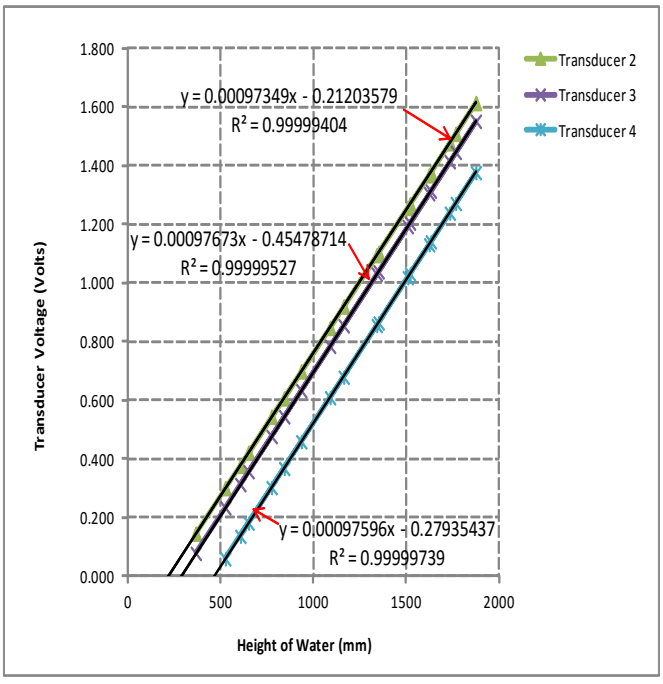

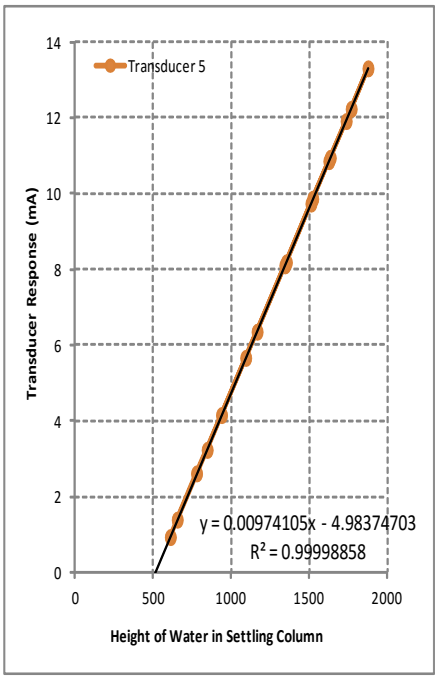

Figure B21: Experiment FDB calibrations

APPENDIX C

List of Samples for Specific Gravity of Solids, XRF and XRD Analysis

Table C1: List of Samples for Specific Gravity of Solids, XRF and XRD Analysis

Sample No.	Description		Colour			Feel	
	Source	Appearance	Eye Estimate dry	Colour Chart dry	Colour Chart wet	Dry	Wet
1	Sieved - 63µm material	Fine powder	Portland cement grey	Light olive	Dark olive	Smooth with gritty	Soapy
2	Sieved - 150µm+63µm material	Small parlicles	Mix white/dark particles	Light olive	Dark olive	Very gritty	Gritty
3	Sieved - 212µm+150µm material	Small parlicles	Mix white/dark particles	Light olive	Dark olive	Very gritty	Gritty
4	Sieved - 300µm+212µm material	Small parlicles	Mix white/dark particles	Light olive	Dark olive	Very gritty	Gritty
5	Crushed Flocculated pieces	Fine powder	Yellowish	Light yellowish orange	Dark reddish brown	Very smooth	Soapy
6	Sediment 15mm - 50mm	Coarse tailings	Dark Grey	Light olive	Dark olive	Gritty more dominant	Gritty
7	Sediment 50mm -85mm	Coarse tailings	Dark Grey	Light olive	Dark olive	Gritty more dominant	Gritty
8	Sediment 85mm -115mm	Coarse tailings	Light Grey	Light olive	Dark olive	Gritty more dominant	Gritty
9	Sediment 115mm - 145mm	Coarse with lumps	Light Grey	Light olive	Dark olive	Gritty more dominant	Gritty
10	Sediment 145mm - 170mm	Coarse with lumps	Light Grey	Light olive	Dark olive	Gritty more dominant	Gritty
11	Sediment 170mm - 205mm	More firm lumps	Light Grey	Light olive	Dark olive	Gritty more dominant	Gritty
12	Sediment 205mm - 230mm	Firmer lumps	Light Grey	Light olive	Dark olive	Gritty more dominant	Gritty Bit soapy
13	Sediment 230mm -265mm	Firmer lumps	Light Grey	Light olive	Dark olive	Smoothness with gritty	Gritty Bit soapy
14	Sediment 265mm - 300mm	Firmer lumps	Light Grey	Light olive	Dark olive	Smoothness with gritty	Gritty Bit soapy
15	Sediment 300mm - 340mm	Firmer lumps	Lighter Grey	Light olive	Dark olive	Smoothness with gritty	Gritty Bit soapy
16	Sediment 340mm -370mm	Firmer lumps	Lighter Grey	Light olive	Dark olive	Smoothness with gritty	Gritty Bit soapy
17	Sediment 370mm -415mm	Firmer lumps	Lighter Grey	Light olive	Dark olive	Smoothness with gritty	Gritty Bit soapy
18	Sediment 415mm -450mm	Big firm lumps	Lighter Grey	Light olive	Dark olive	Smoothness with gritty	Bit more soapy
19	Sediment 450mm -480mm	Lumps are harder	Lighter Grey	Light olive	Dark olive	Smooth soapy feel	Bit more soapy
20	Sediment 480mm - 510mm	Lumps are harder	Lighter Grey	Light olive	Dark olive	Smooth soapy feel	More soapy
21	Sediment 510mm - 540mm	Lumps are harder	Lighter Grey	Light olive	Dark olive/Dark yellow	Smooth soapy feel	Soapy
22	Sediment 540mm - 570mm	Large brick-like firm lumps	Lighter Grey	Light olive	Dark olive/Dark yellow	Smooth soapy feel	Soapy
23	Sediment 570mm - 600mm	Large brick-like firm lumps	Lighter Grey	Light olive	Dark olive/Dark yellow	Smooth soapy feel	Soapy
24	Sediment 600mm - 640mm	Large brick-like firm lumps	Lighter Grey	Light olive	Dark yellow/Dark olive	Smooth soapy feel	Soapy
25	Sediment 640mm - 670mm	Large brick-like firm lumps	Lighter Grey	Light olive	Dark yellow	Smooth soapy feel	Soapy
26	Sediment 670mm - 700mm	Large brick-like firm lumps	Lighter Grey	Light olive	Dark yellow	Smooth soapy feel	Soapy
27	Sediment 700mm - 724mm	Hard lumps crush with effort	Lighter Grey	Light olive	Dark yellow	Smooth soapy feel	Soapy
28	Underflow 2010 Sample	Fine powder	Yellowish	Light Reddish brown	Light reddish orange	Gritty	Gritty
29	Catwalk fines	Fine powder	Light coloured	Light olive	Dark Olive	Soapy with grit	Soapy with grit
30	Underflow 2011 Sample	Small coarse particles	Light coloured	Light grey	Dark Olive	Gritty	Gritty

APPENDIX D

Settlement (SWI) Time Plots

This appendix summarises and compares soil water interface (SWI) change with time for all the experiments as well as relates SWI with both time and logarithm of time for Experiment FDB.

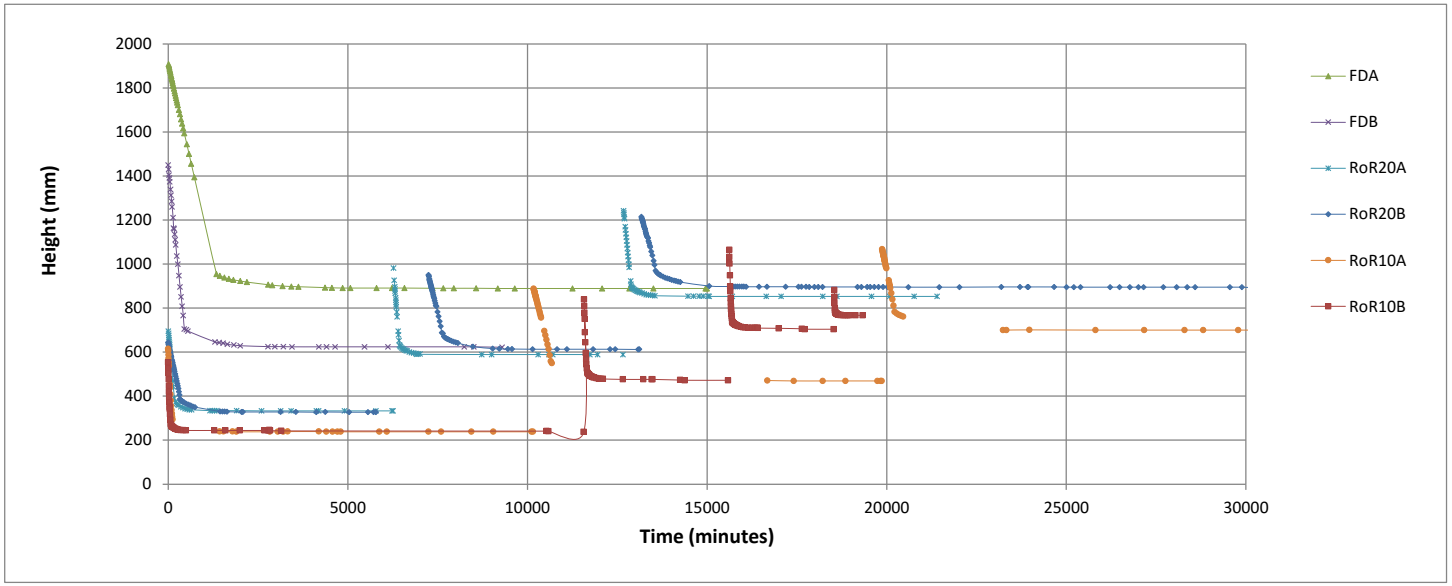

Figure D1: Soil interface height (SWI) versus time plots all experiments

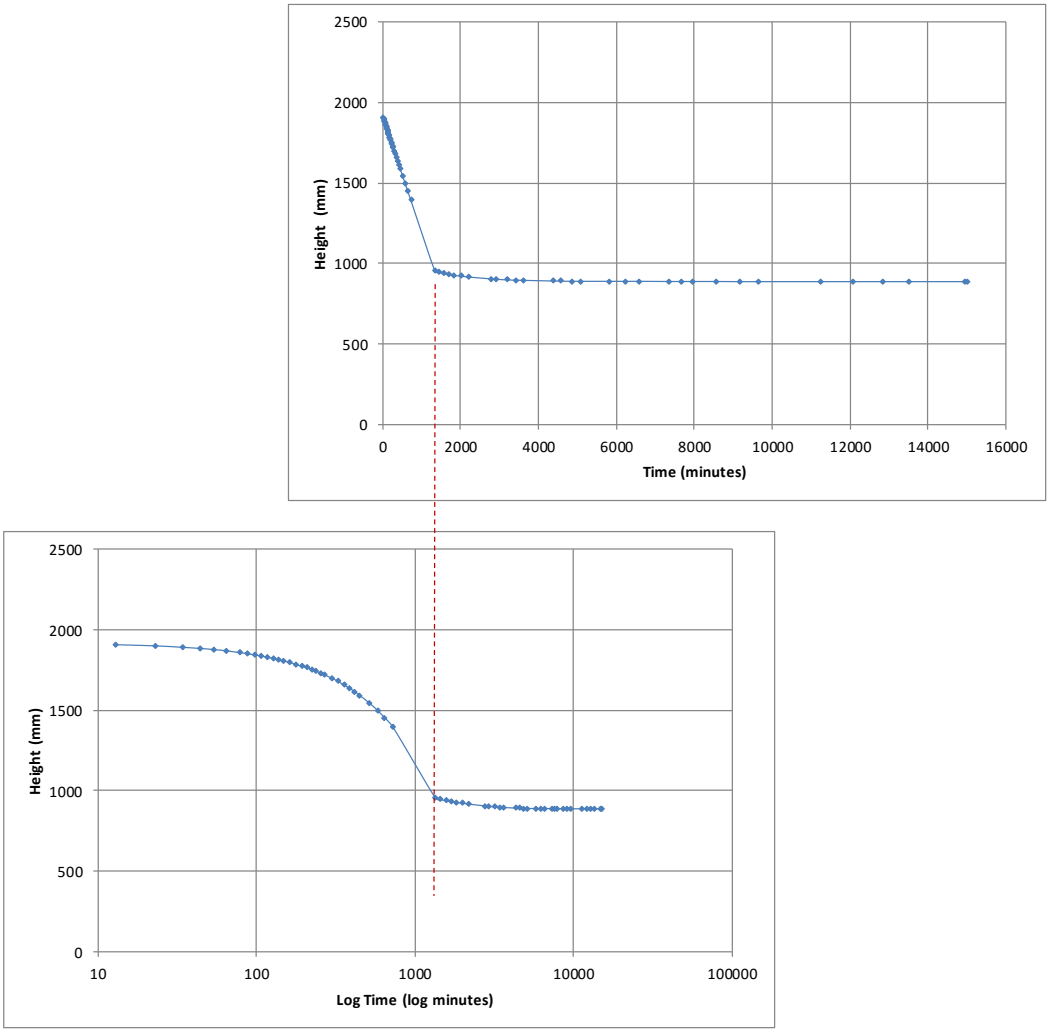

Figure D2: Tailings interface height (SWI) *vs* time and log time plots Experiment FDB

APPENDIX E

Standpipe and Transducer Excess Pore Water Pressures

The appendix contains calculated excess pore water pressure values based on manually collected standpipe and transducer data (Appendix E1 and E2). A comparison of both sets of data is given with transducer data corrected for fluctuations observed in the data (Appendix E3). Graphtec logger transducer data is reported as well as comparisons of excess pore water pressure at Transducers 2 and 3 for all the experiments. The data is reported as listed below.

E1 Manually Collected Standpipe Data

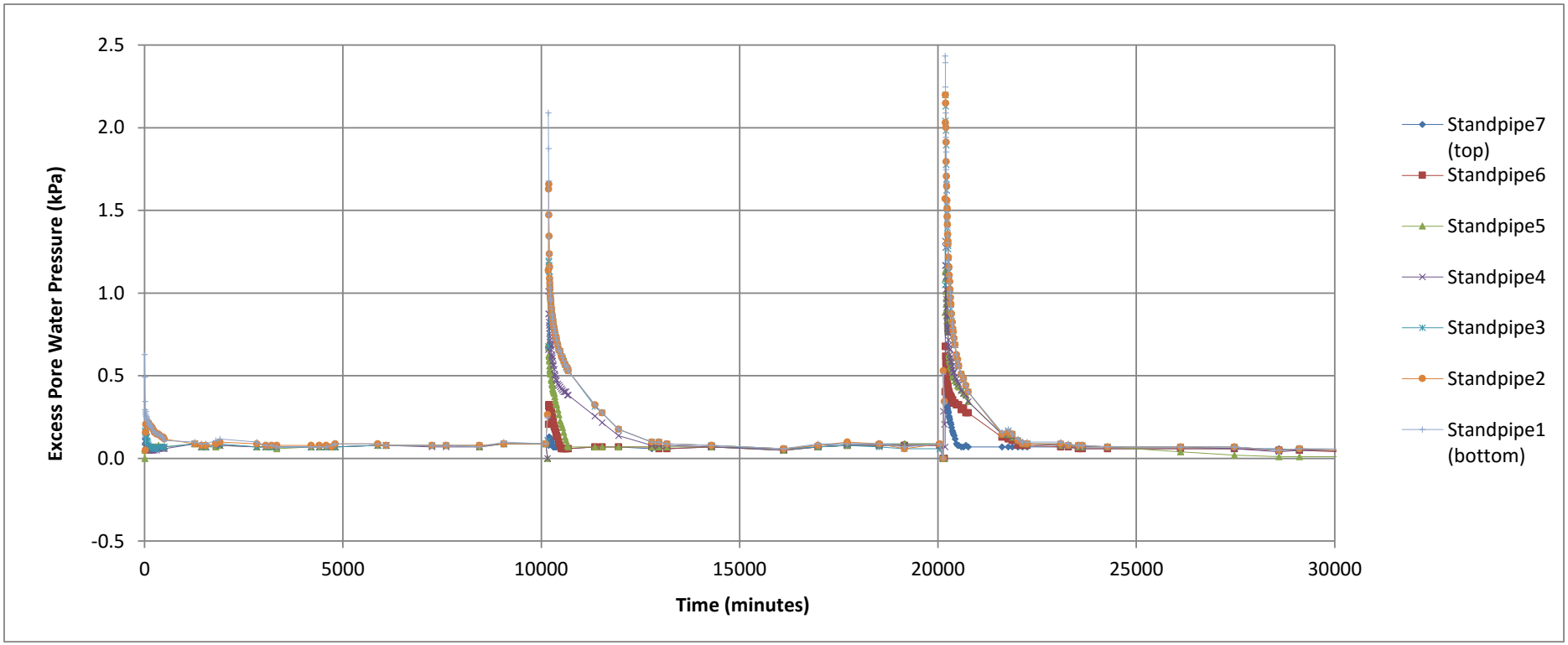

Figure E1: Excess pore water pressure Experiment RoR10A standpipe data

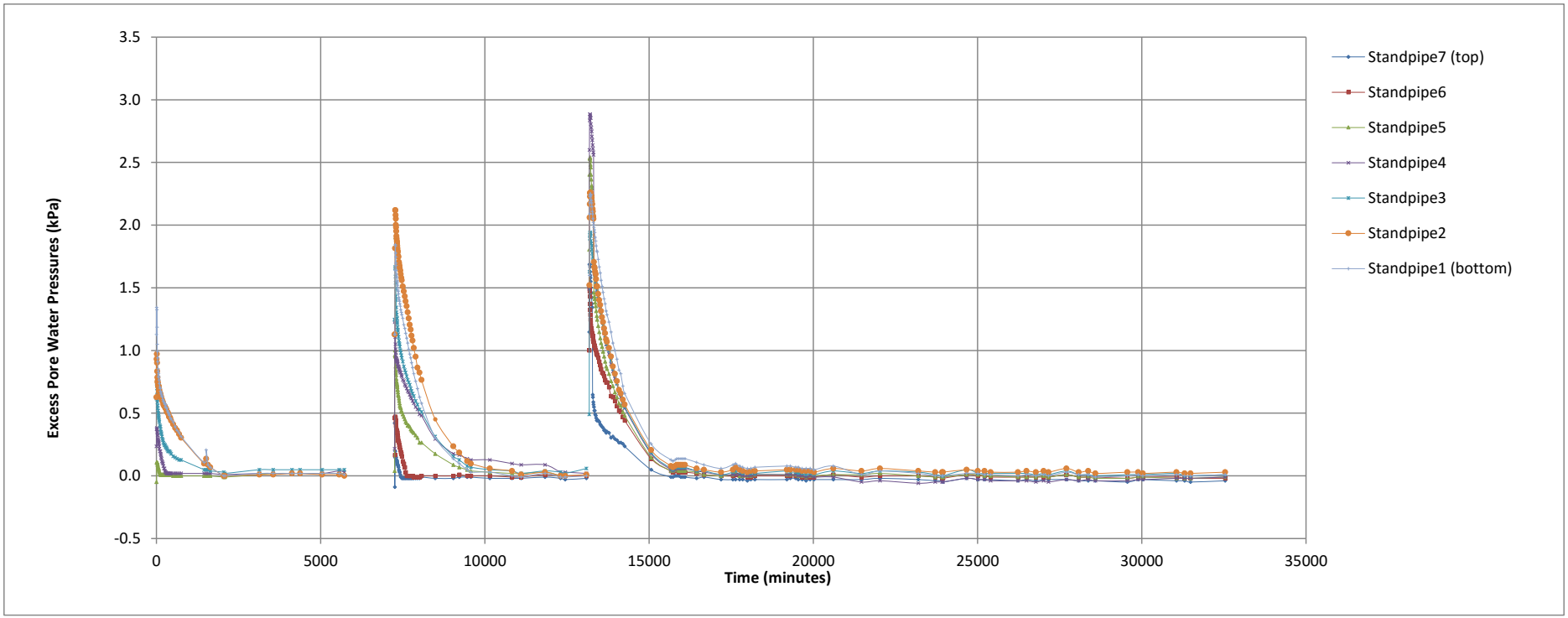

Figure E2: Excess pore water pressure Experiment RoR20B standpipe data

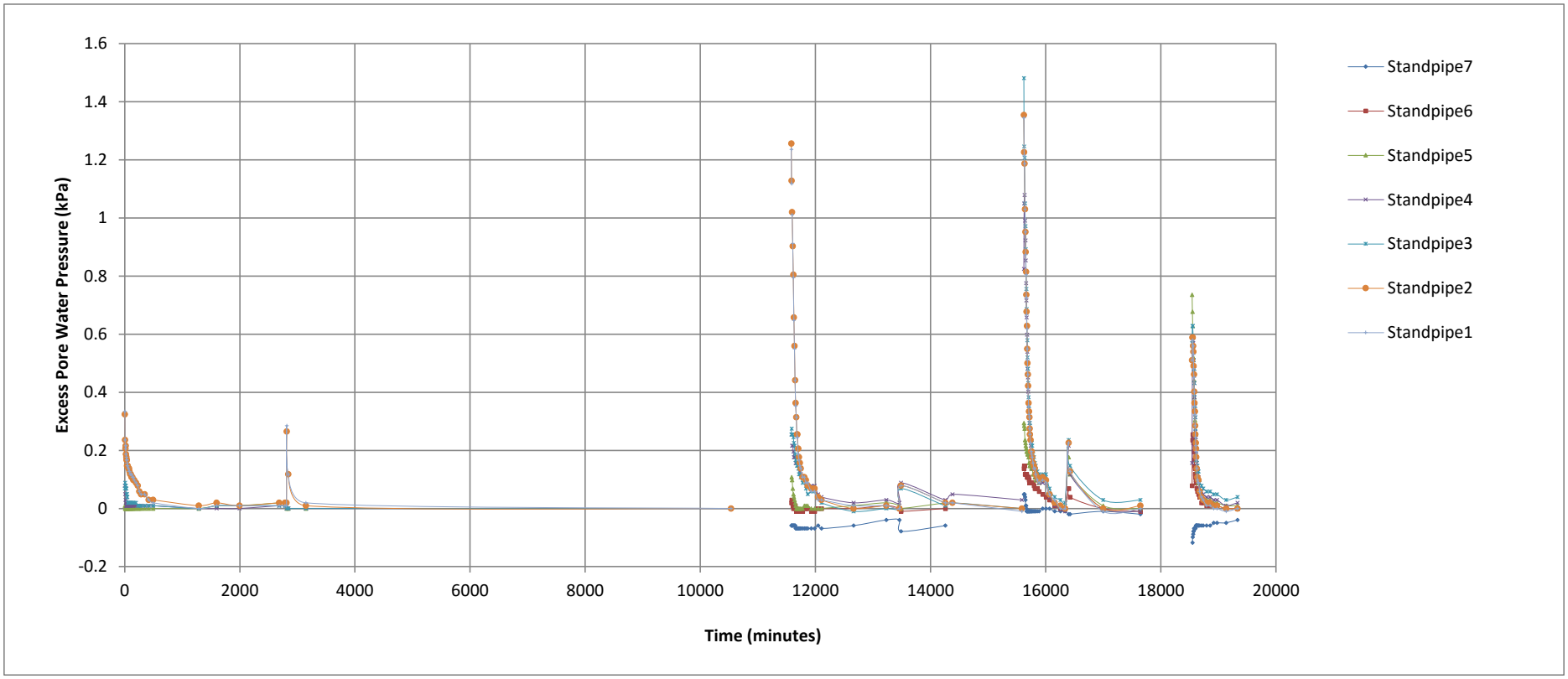

Figure E3: Excess pore water pressure Experiment RoR10B standpipe data

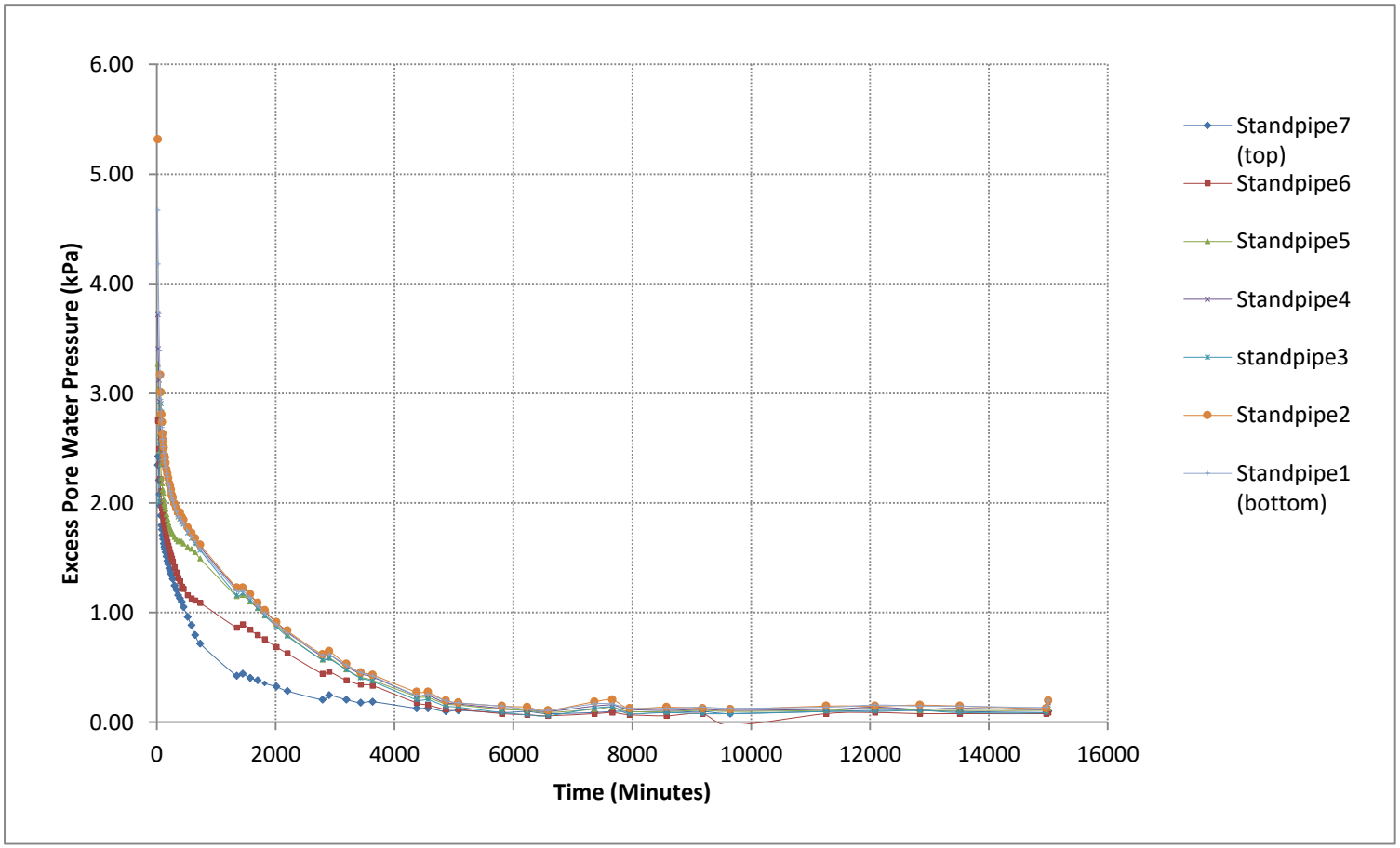

Figure E4: Excess pore water pressure Experiment FDB standpipe data

E2 Manually Collected Transducer Data

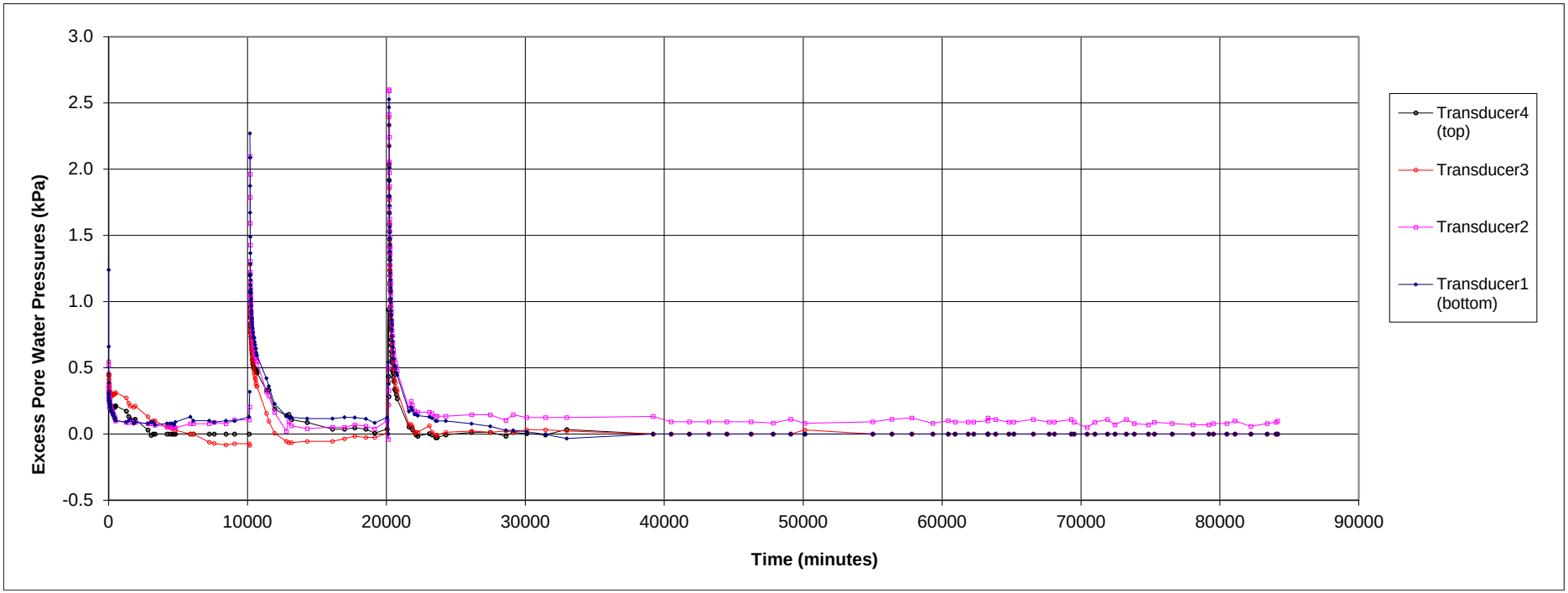

Figure E5: Settlement time plots Experiment RoR10A transducer data

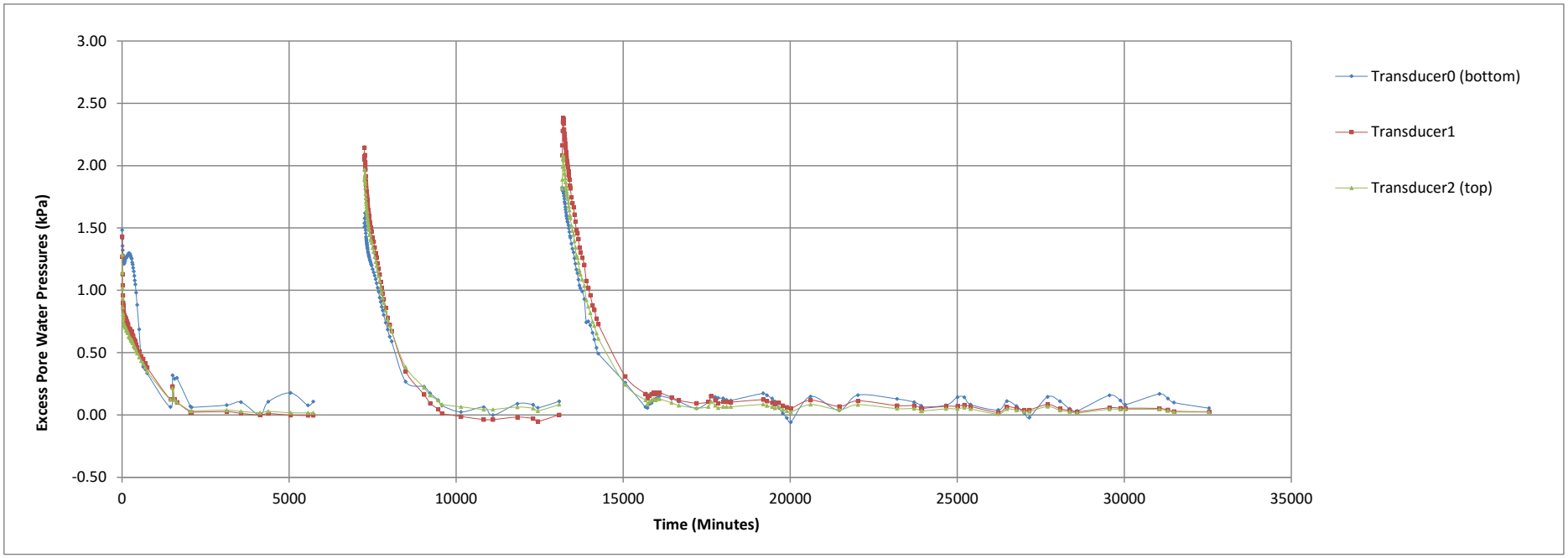

Figure E6: Excess pore water pressure Experiment RoR20B transducer data

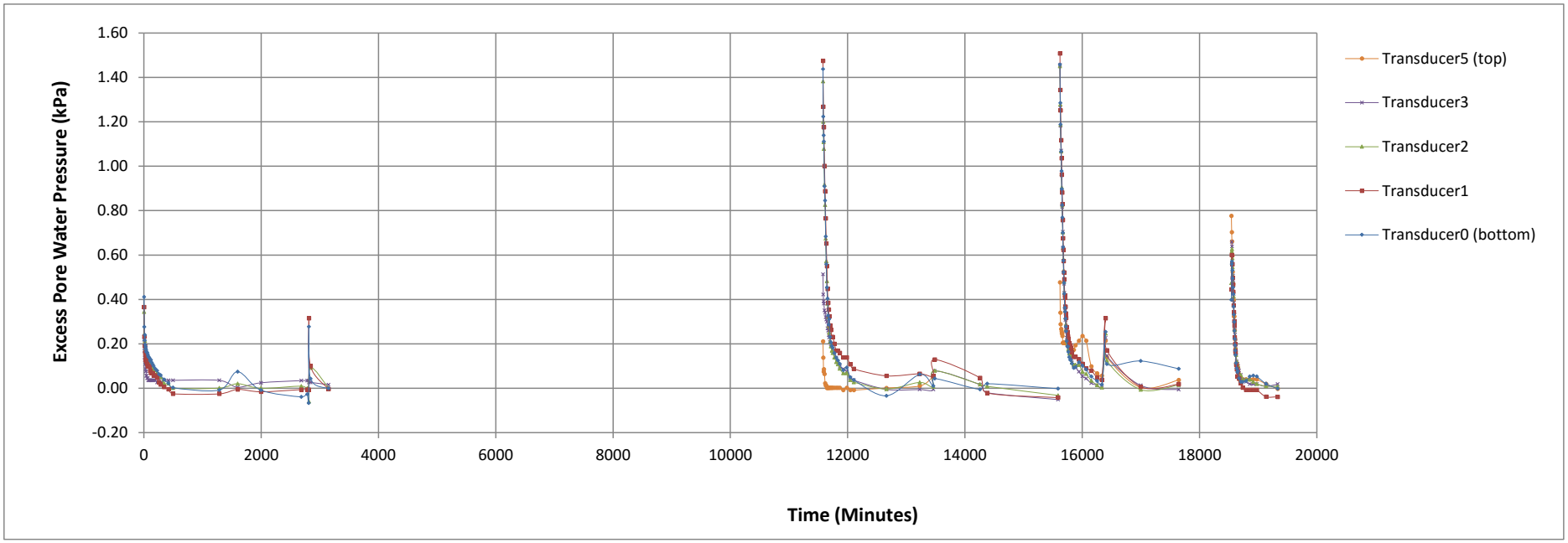

Figure E7: Excess pore water pressure Experiment RoR10B transducer data

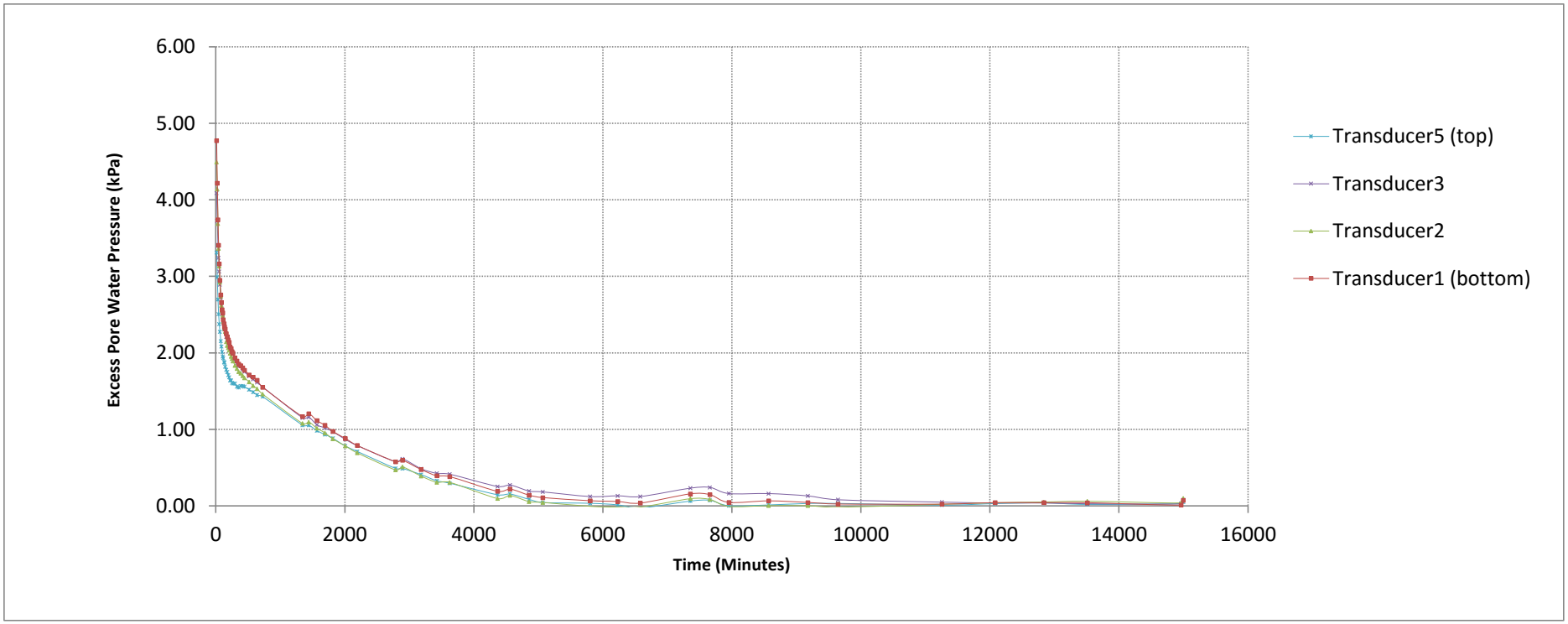

Figure E8: Excess pore water pressure Experiment FDB transducer data

E3 Standpipe and Transducer Paired Data

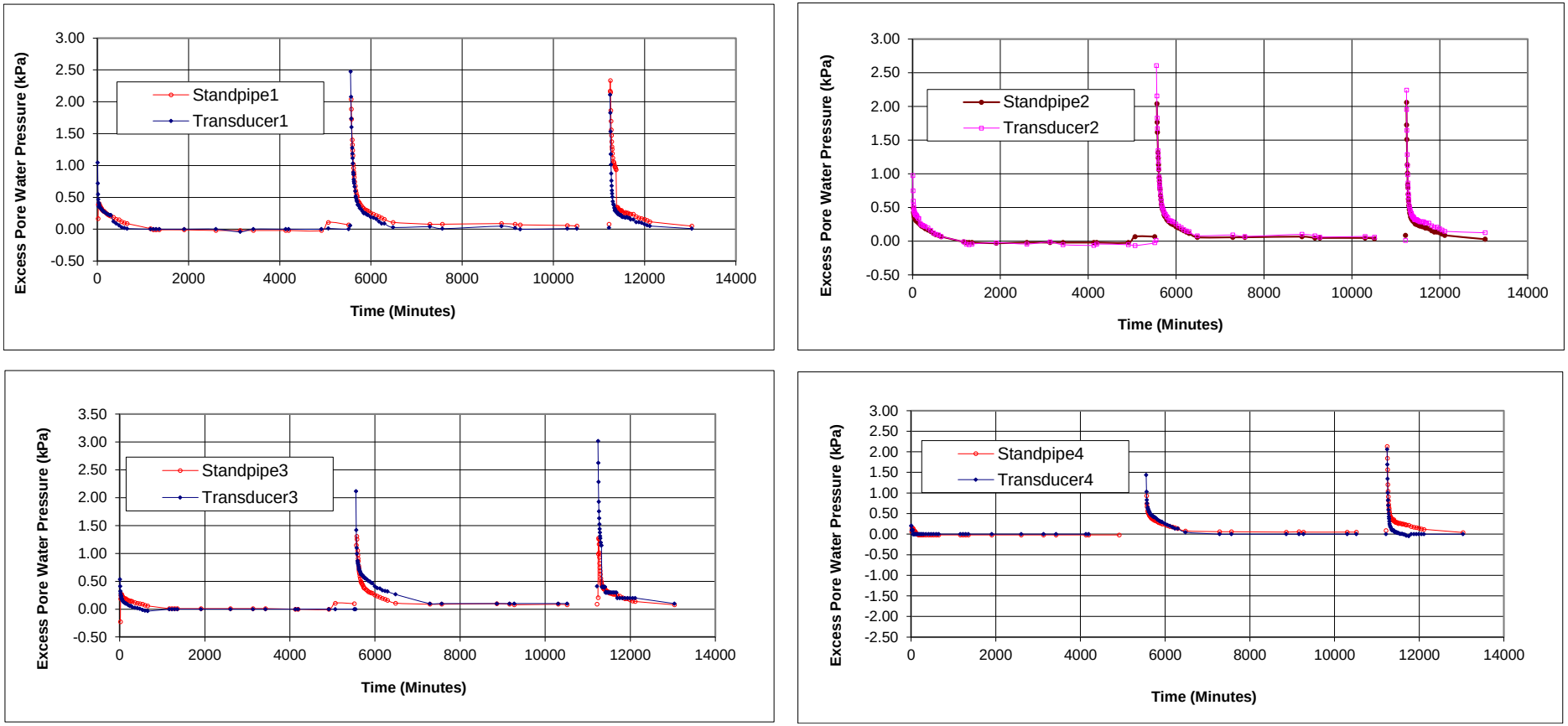

Figure E9: Standpipe and transducer pair excess pore pressure comparisons Experiment RoR20A

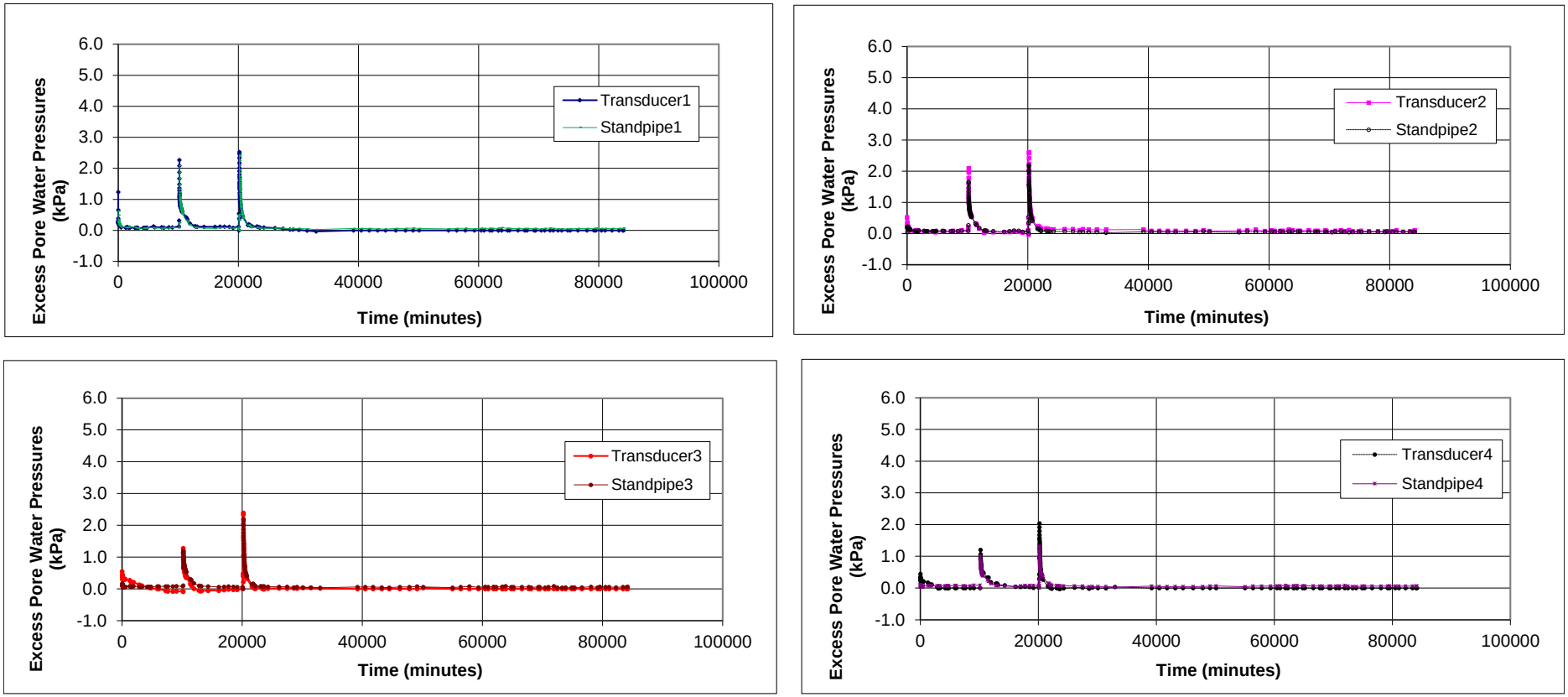

Figure E10: Standpipe and transducer pair excess pore pressure comparisons Experiment RoR10A

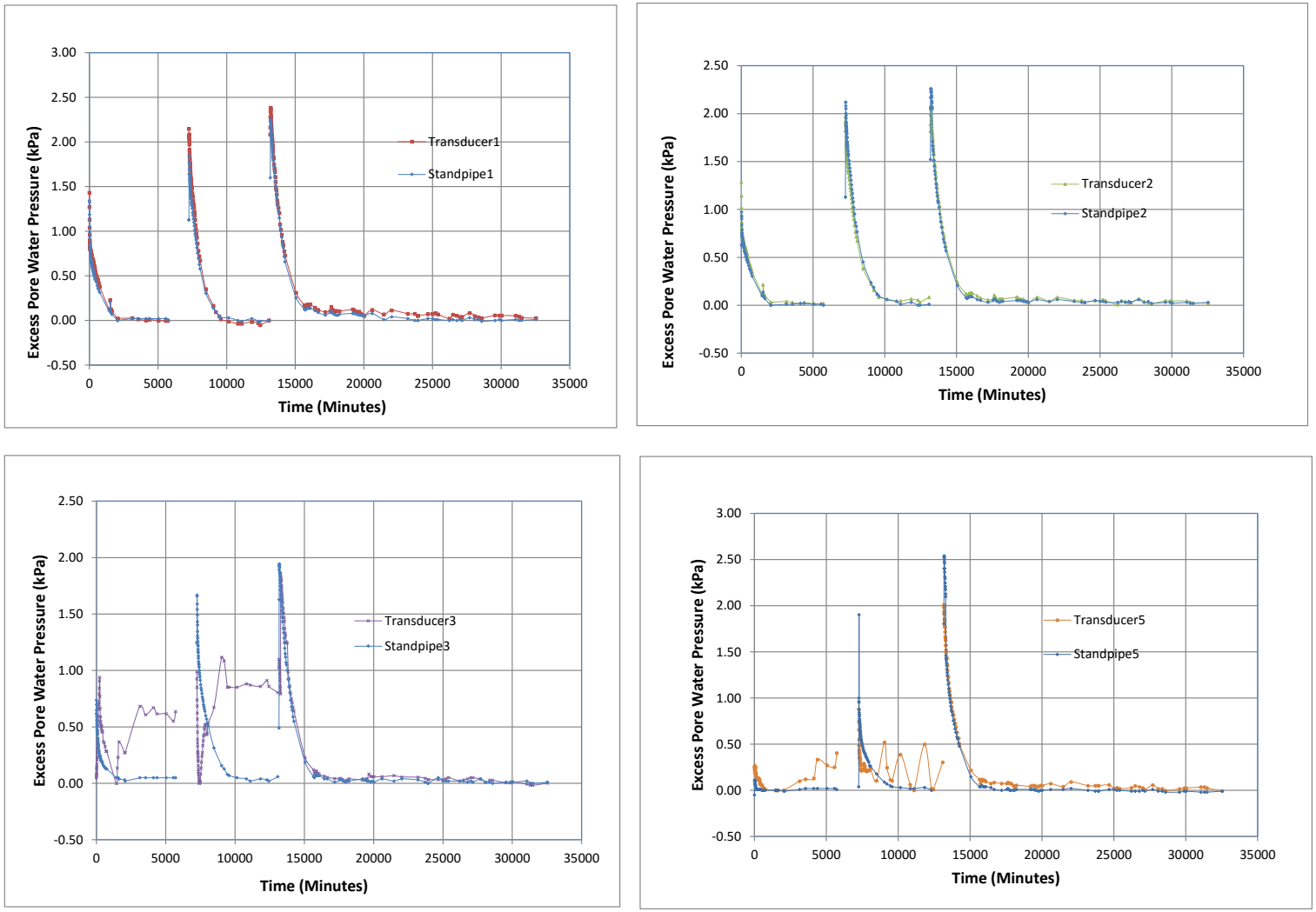

Figure E11: Standpipe and transducer pair excess pore pressure comparisons Experiment RoR20B

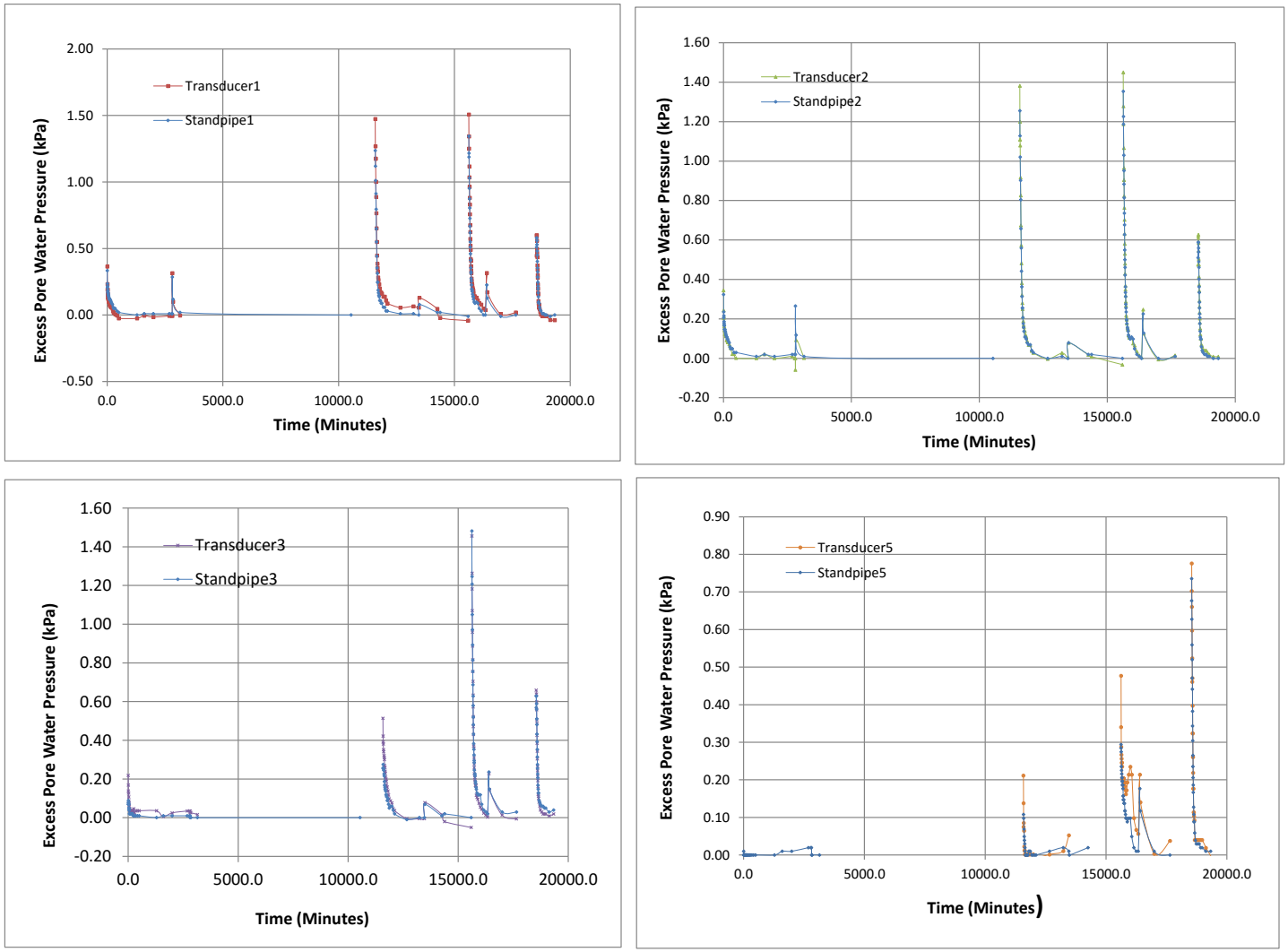

Figure E12: Standpipe and transducer pair excess pore pressure comparisons Experiment RoR10B

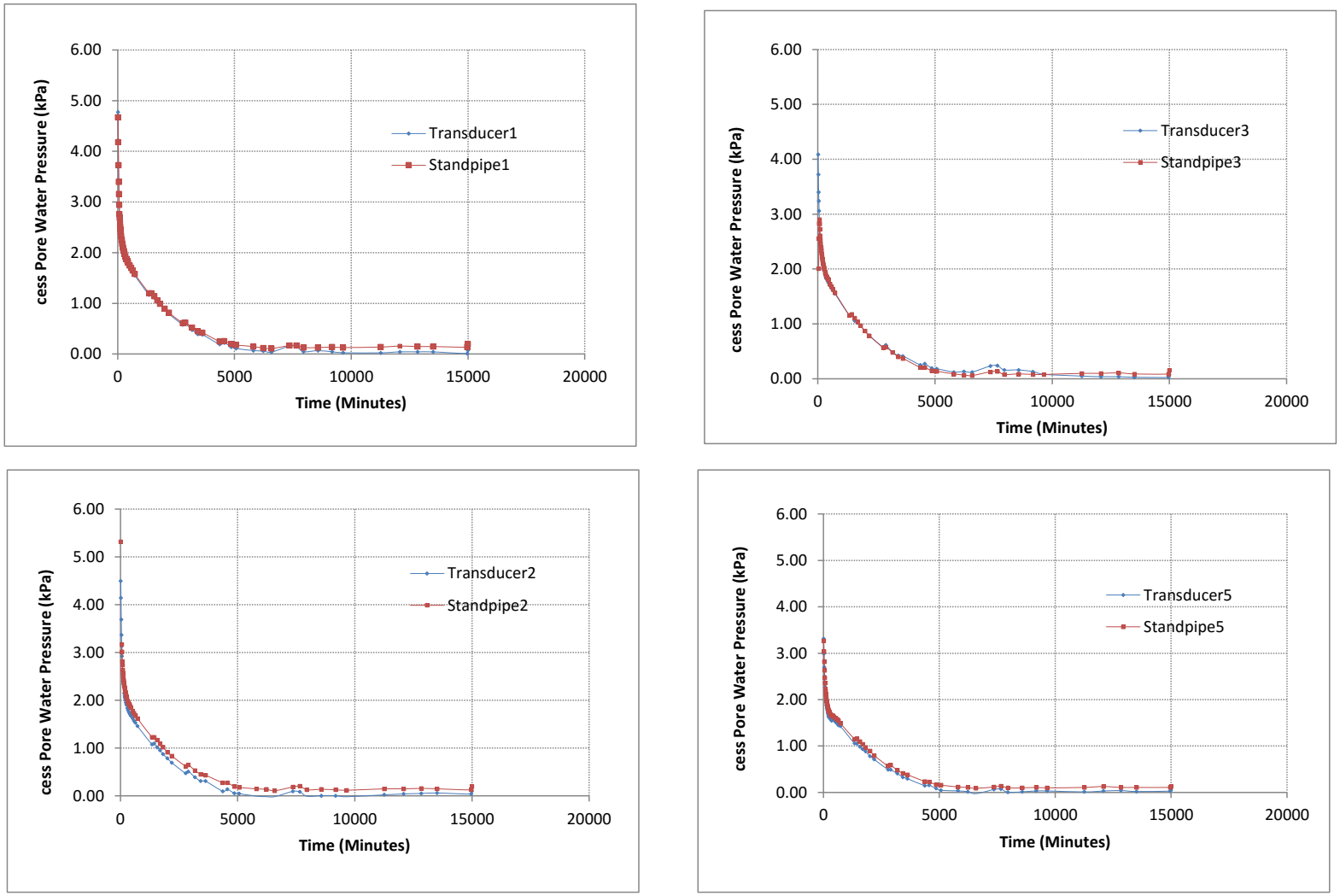

Figure E13: Standpipe and transducer pair excess pore pressure comparisons Experiment FDB

E4 Data Logged Transducer Data

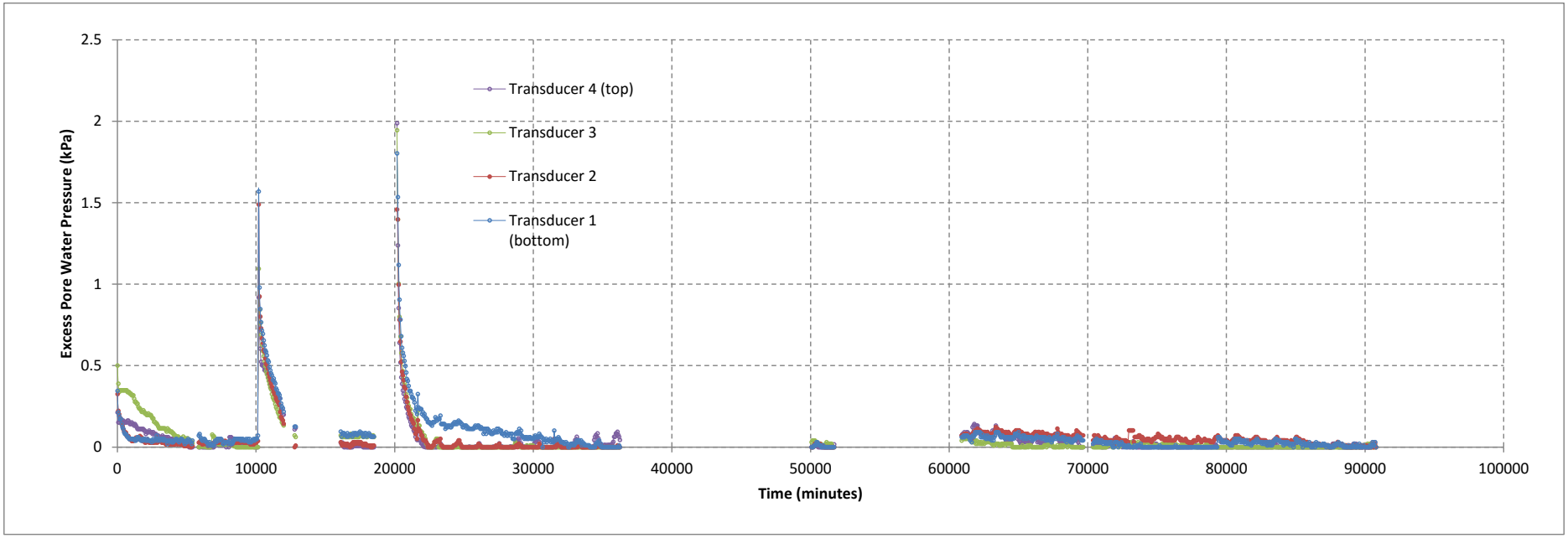

Figure E14(a): Data logger excess pore water pressure trend Experiment RoR10A

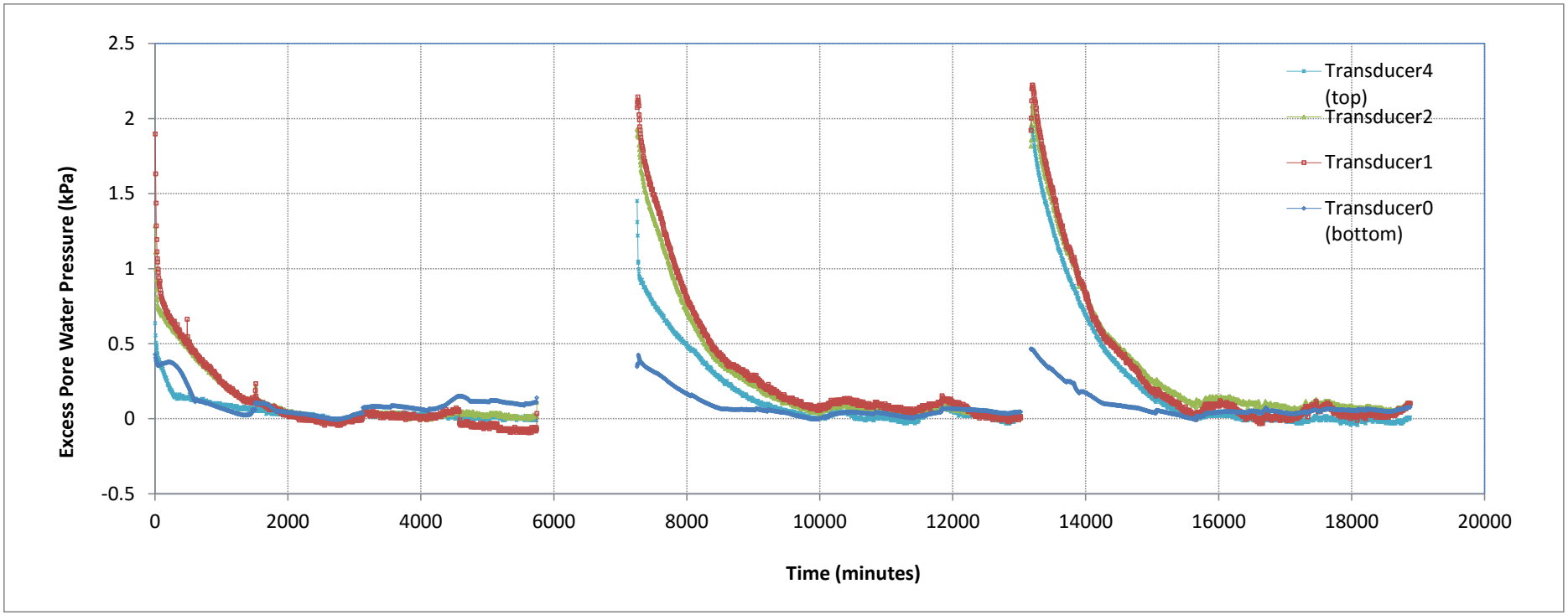

Figure E15 (a): Data logger excess pore water pressure trend Experiment RoR20B

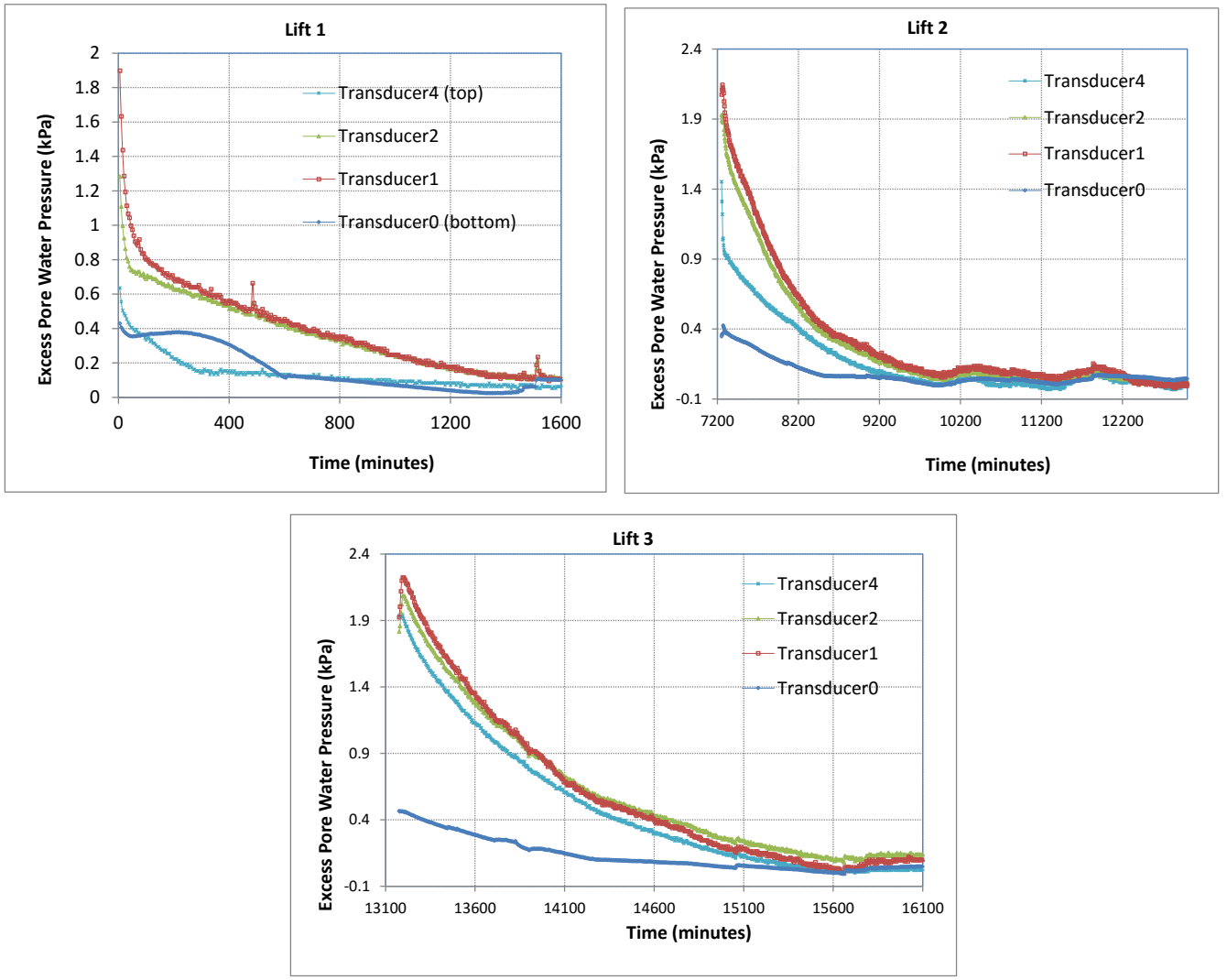

Figure E15 (b): Data logger Experiment RoR20B tailings early pore pressure lift trend

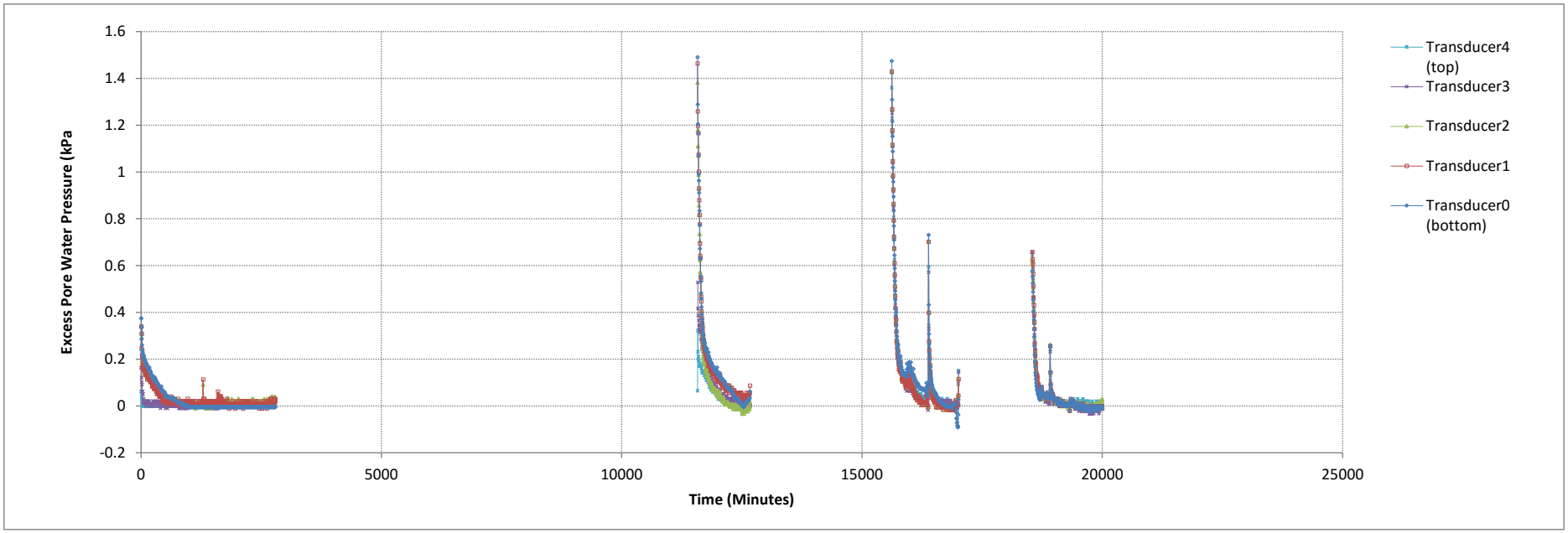

Figure E16 (a): Data logger excess pore water pressure trend Experiment RoR10B

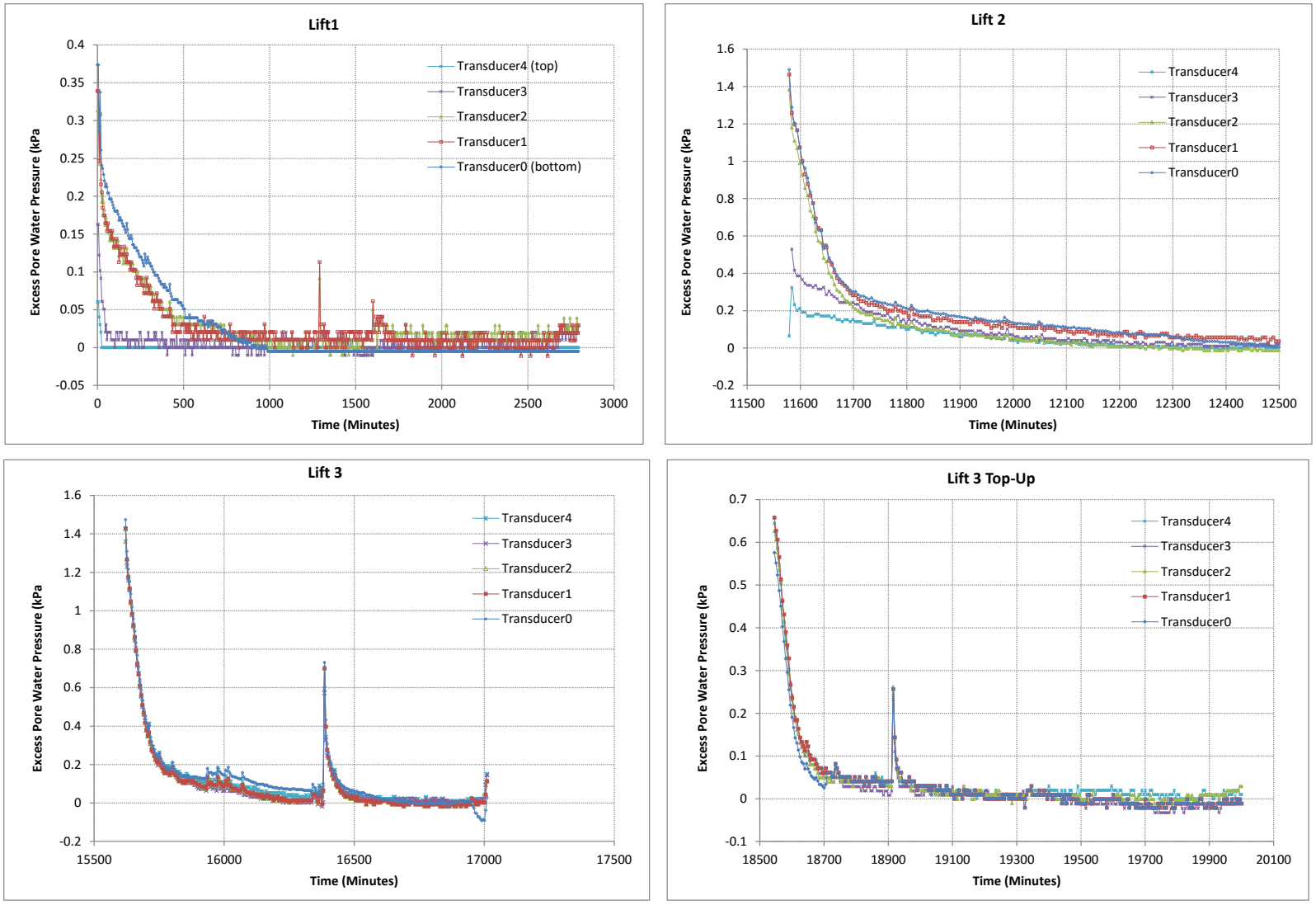

Figure E16 (b): Data logger Experiment RoR10B early pore pressure lift trend

E5 Excess Pore Water Pressure Comparisons

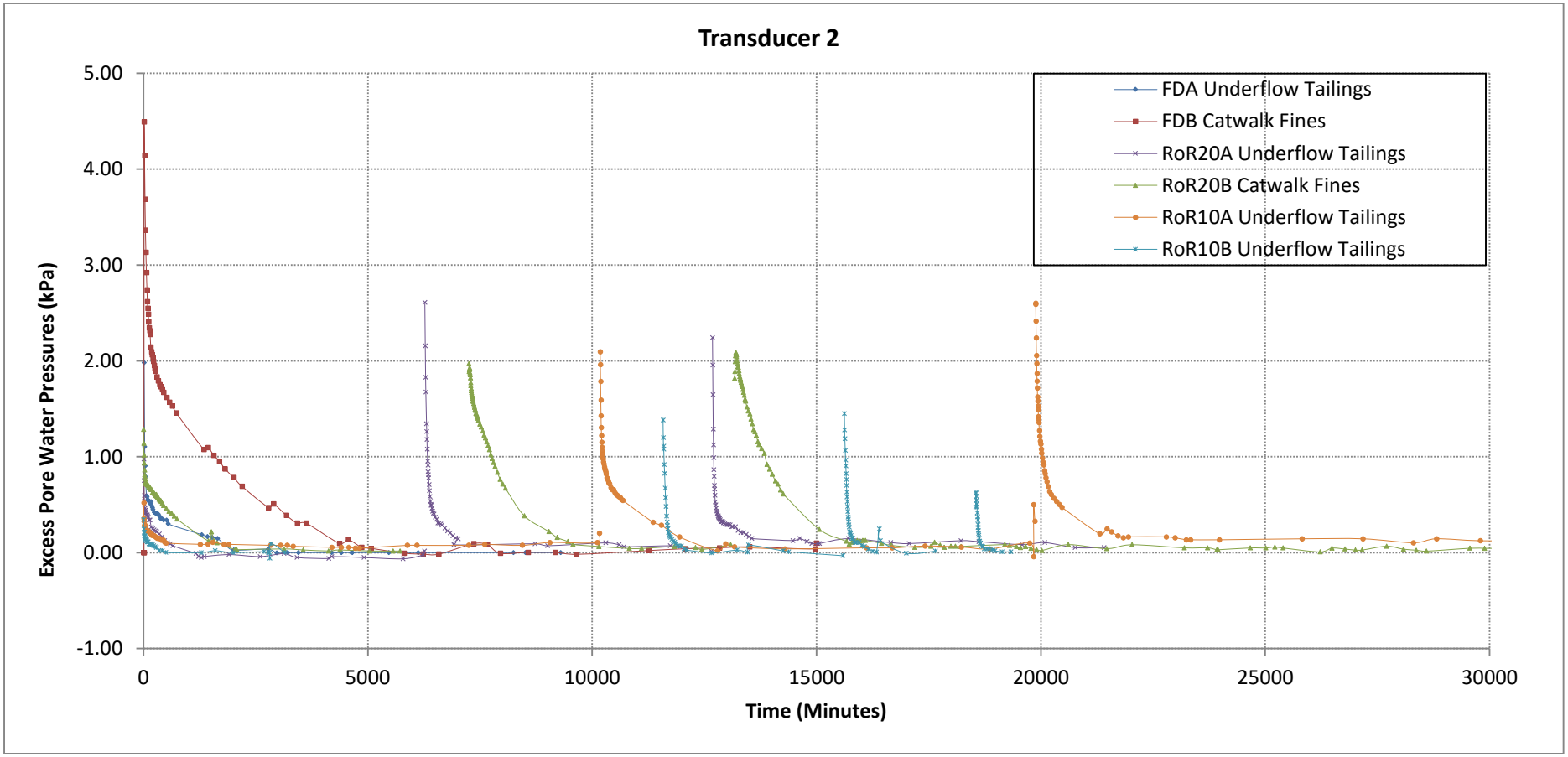

Figure E17 (a): Rate of rise vs excess pore pressures dissipations all experiments – Transducer 2

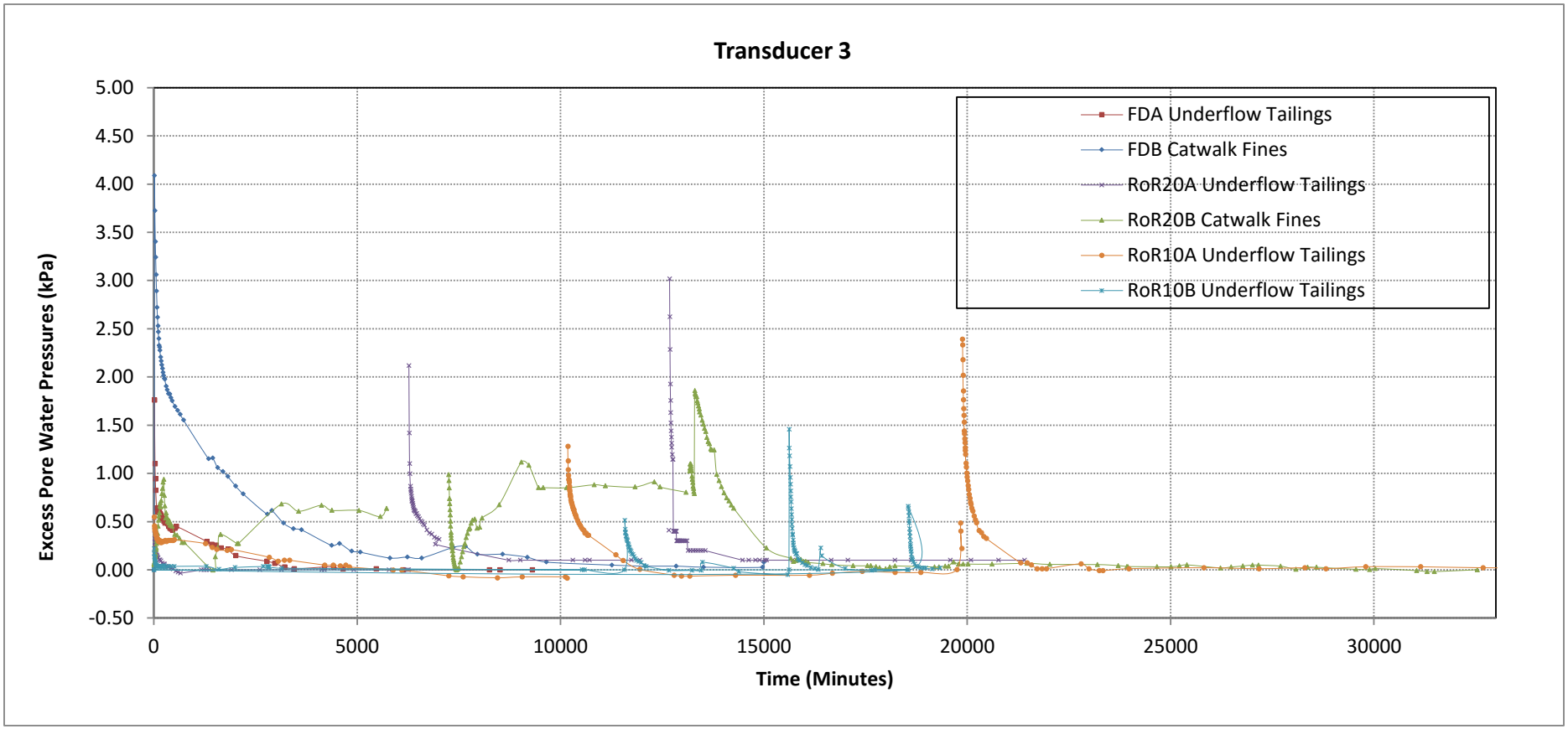

Figure E17 (b): Rate of rise vs excess pore pressures dissipations all experiments – Transducer 3

APPENDIX F

Pore Water Pressure Results

The appendix presents the results of the variation of total heads with time during the sedimentation and consolidation stages of the slurry and deposited tailings for Experiments FDA, FDB, RoR20A, RoR20B, RoR10A and RoR10B.

Experiment FDA and FDB results are depicted on Figures F1 and F2 respectively.

Figures F3 to F6 present the total head change with time for Experiments RoR20A and RoR20B. The results show total heads trends for the different deposition lifts individually and the combined trends showing the three deposition lifts together.

Figures F7 to F10 show the total head change with time for the three deposition lifts under Experiment RoR10B together in one plot in order to compare the deposition lifts as well as the individual deposition lifts shown separately to bring out the trend details in each deposition cycle.

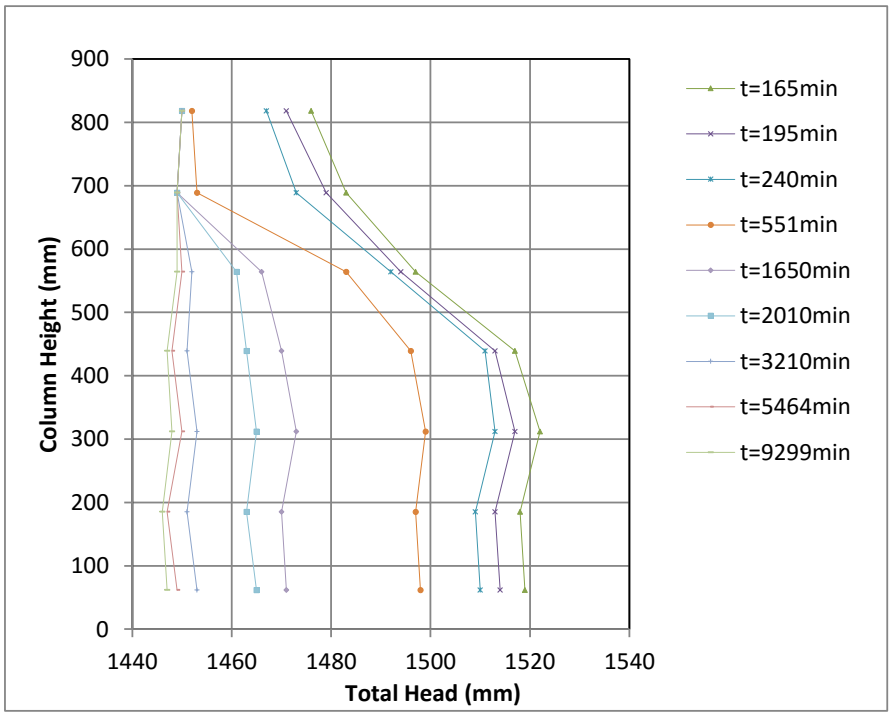

Figure F1: Sedimentation consolidation total heads change with depth Experiment FDA

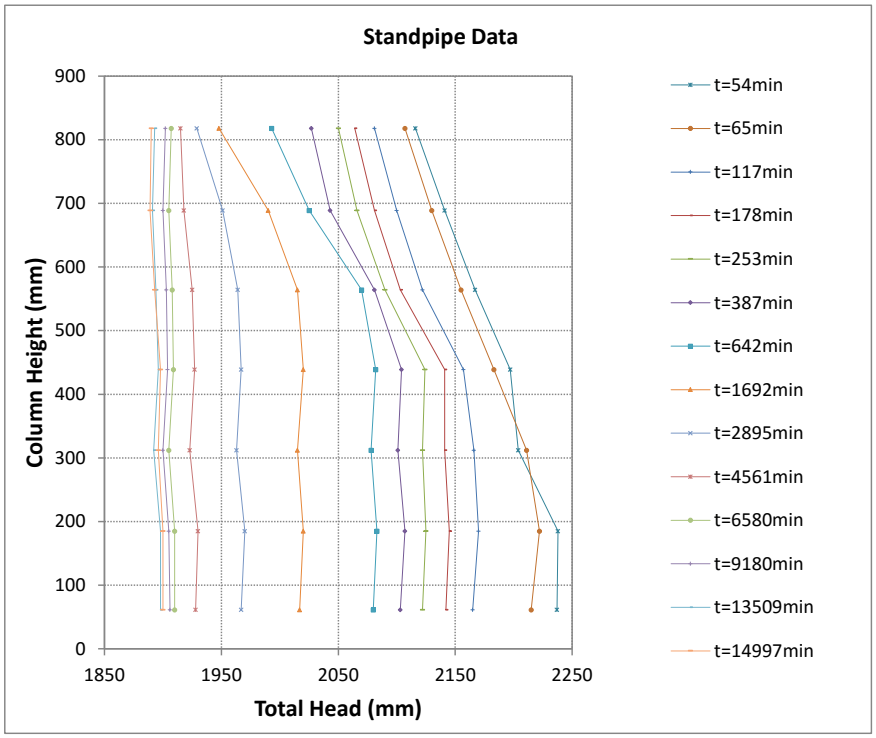

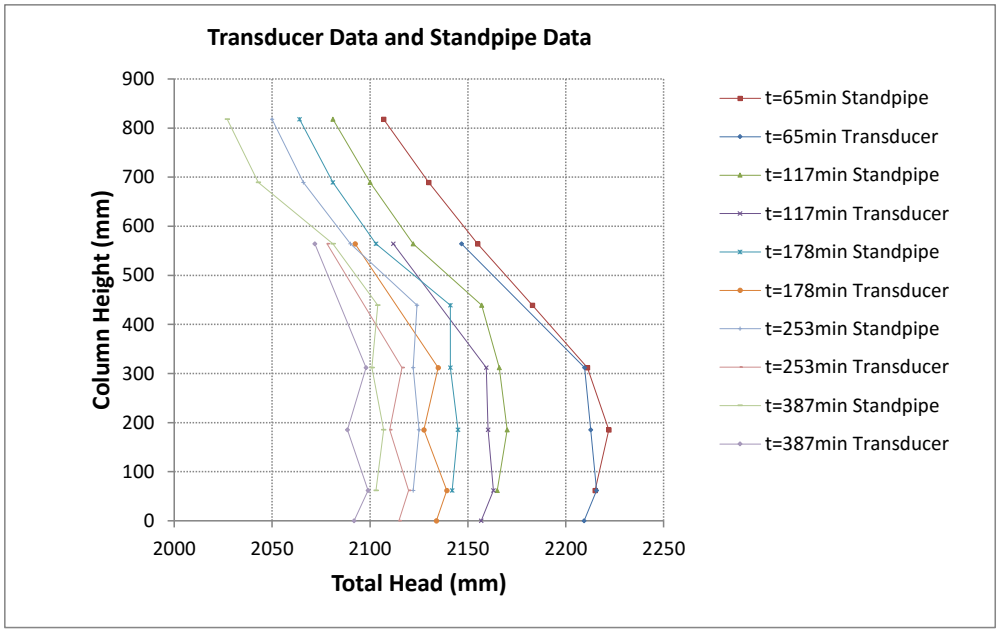

Figure F2: Sedimentation consolidation total heads change with depth Experiment FDB

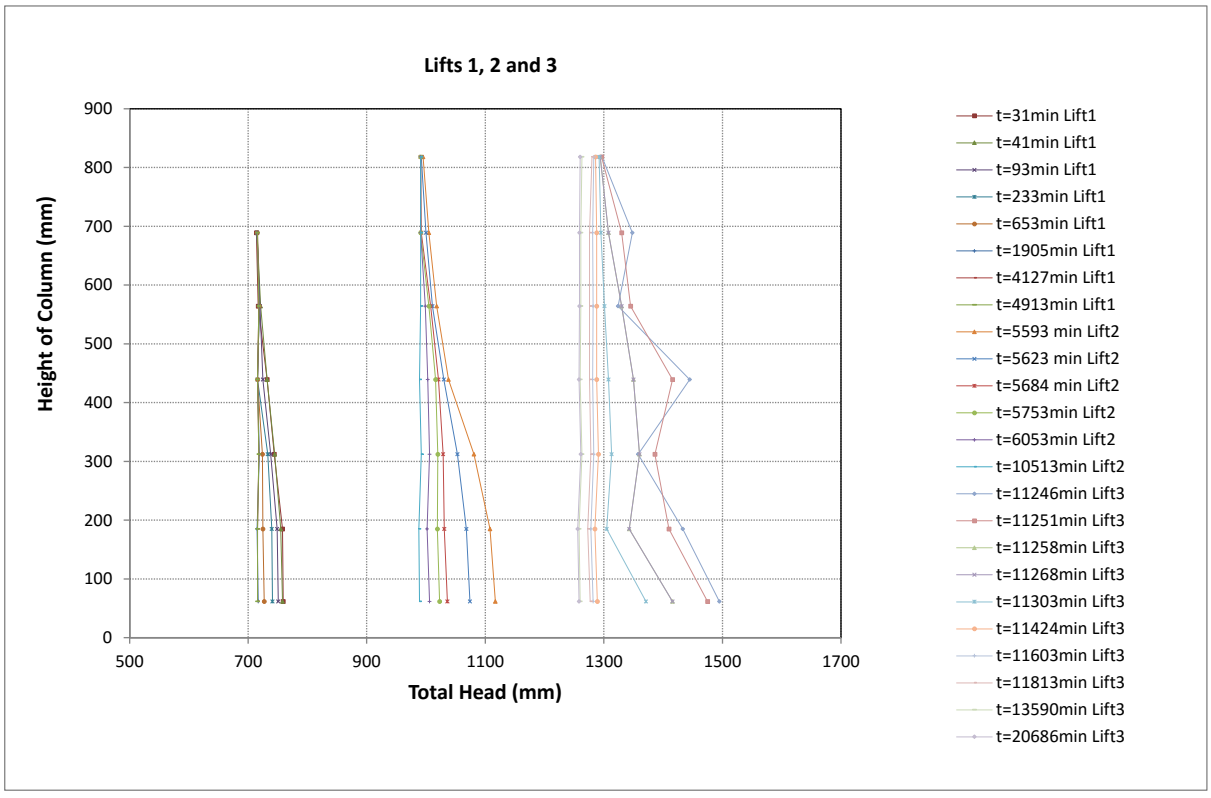

Figure F3: Sedimentation consolidation total heads change with depth Experiment RoR20A

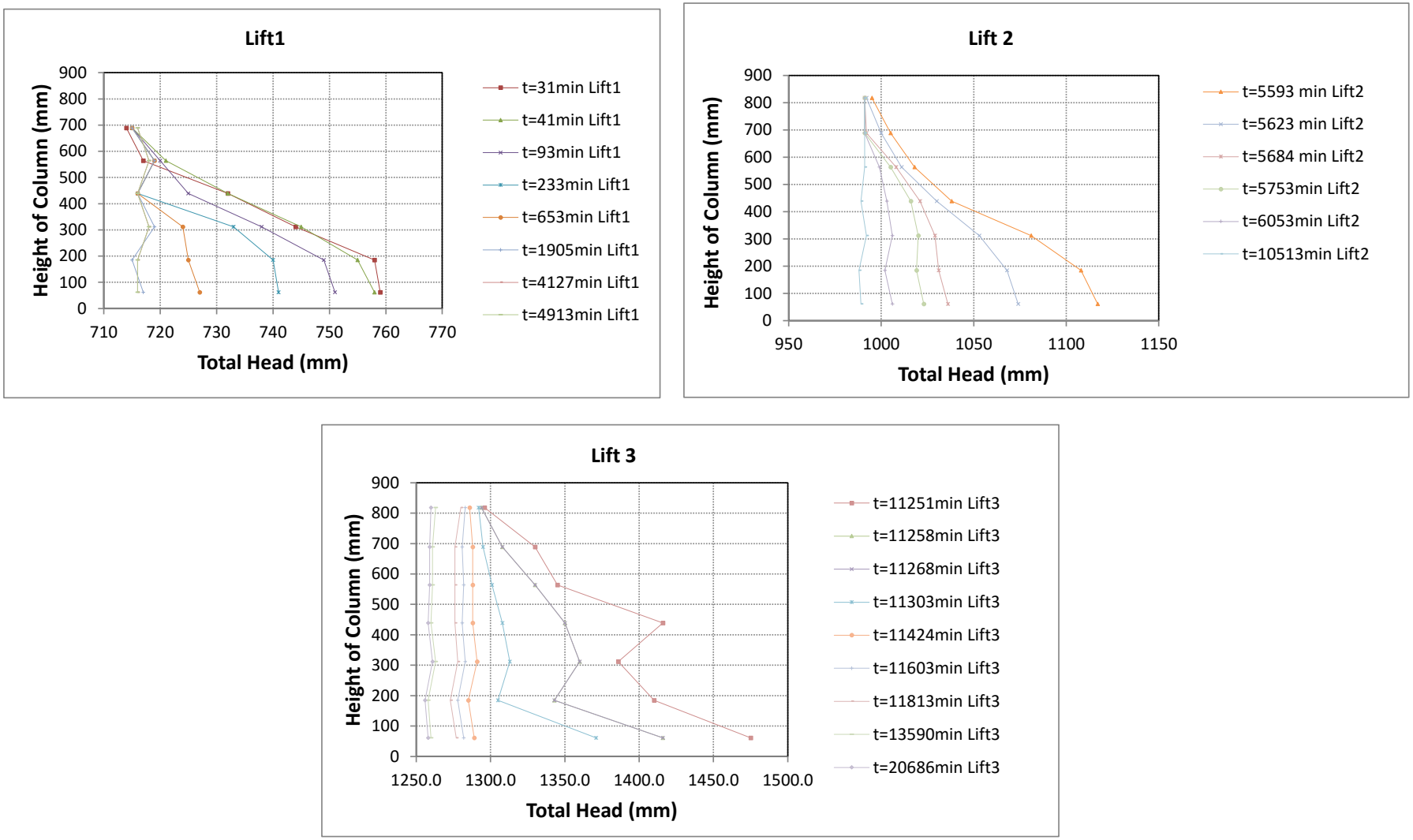

Figure F4: Sedimentation consolidation total heads change with depth Experiment RoR20A

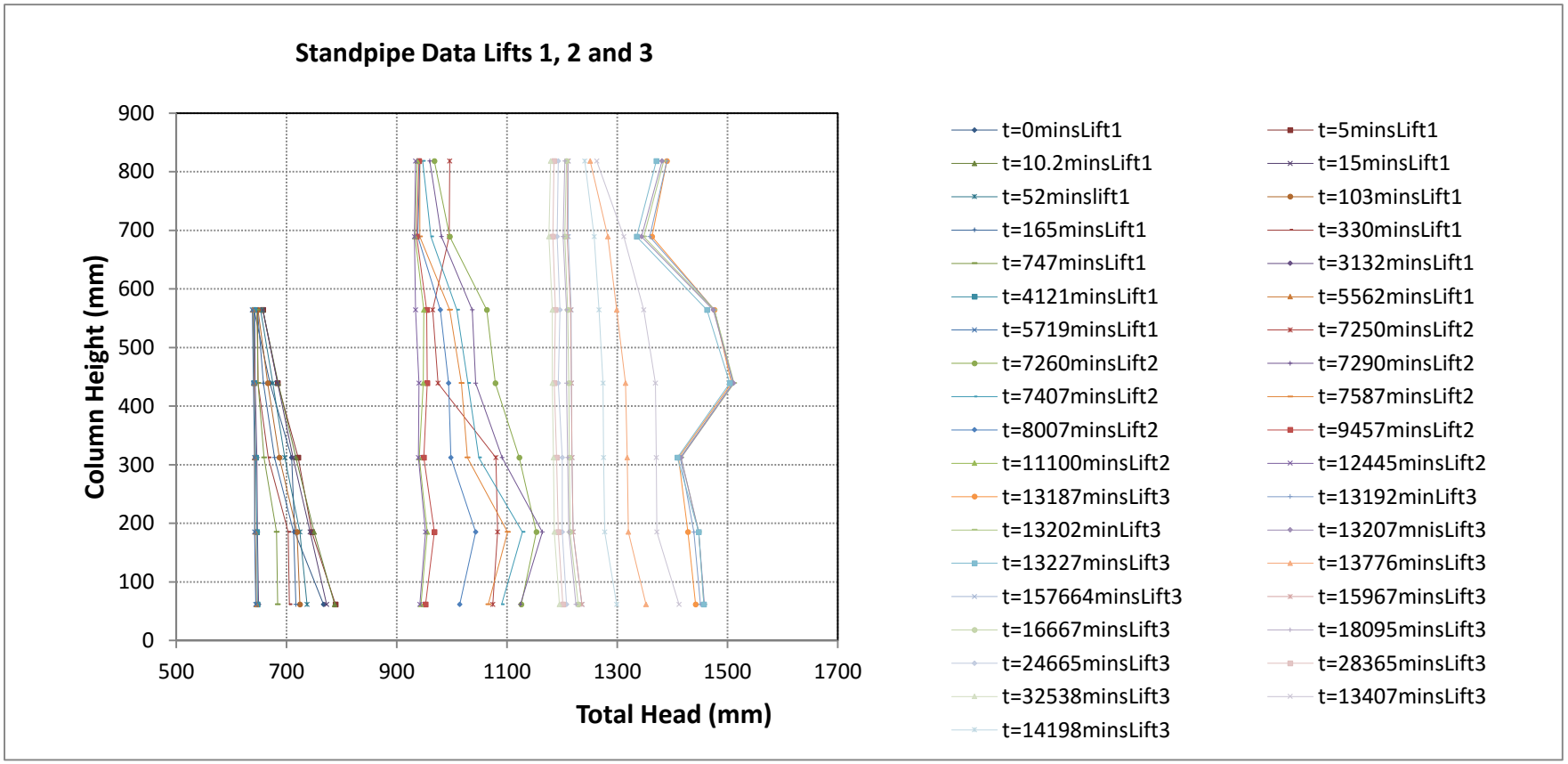

Figure F5: Sedimentation consolidation total heads change with depth Experiment RoR20B

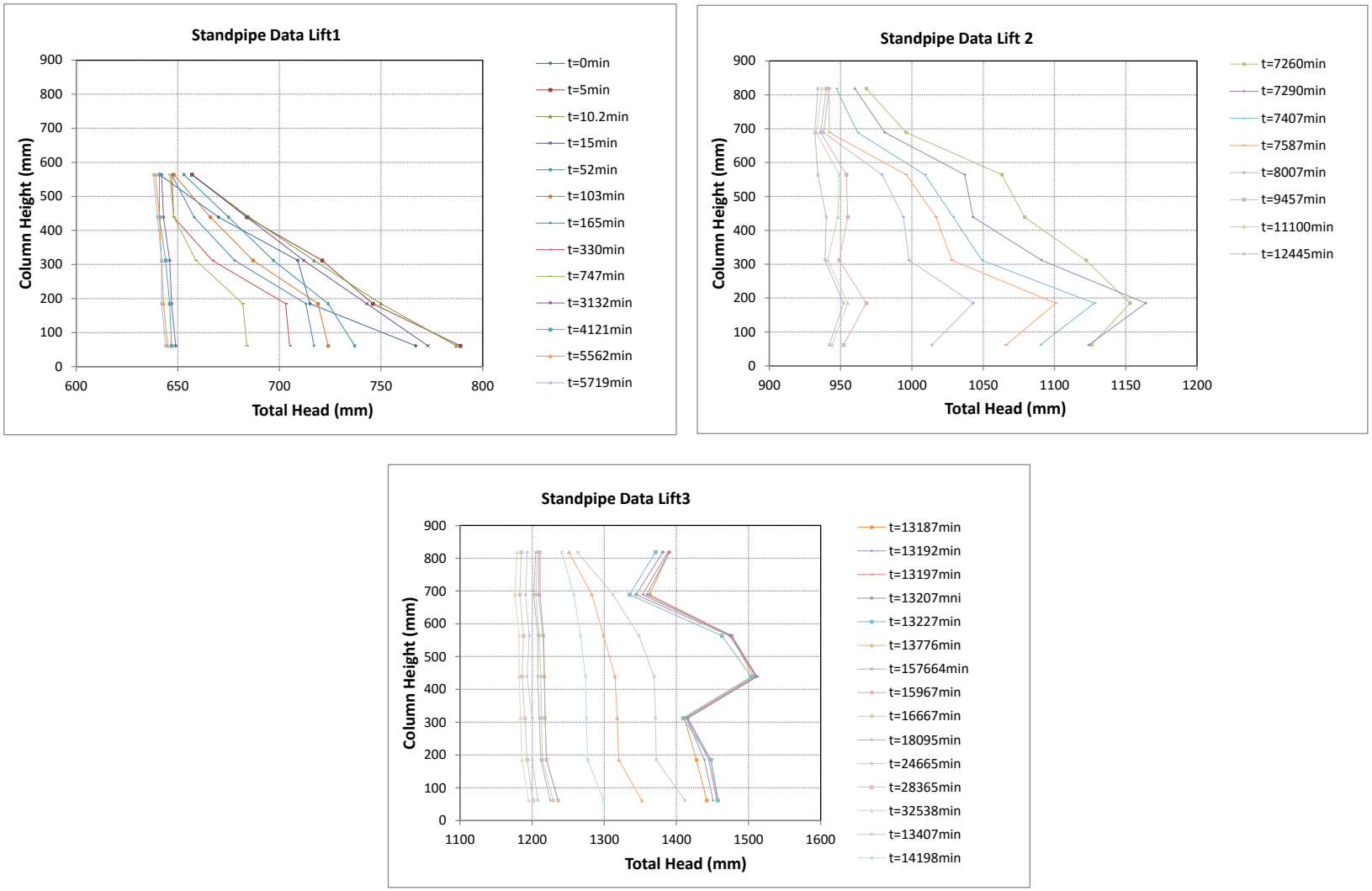

Figure F6: Sedimentation consolidation total heads change with depth Experiment RoR20B

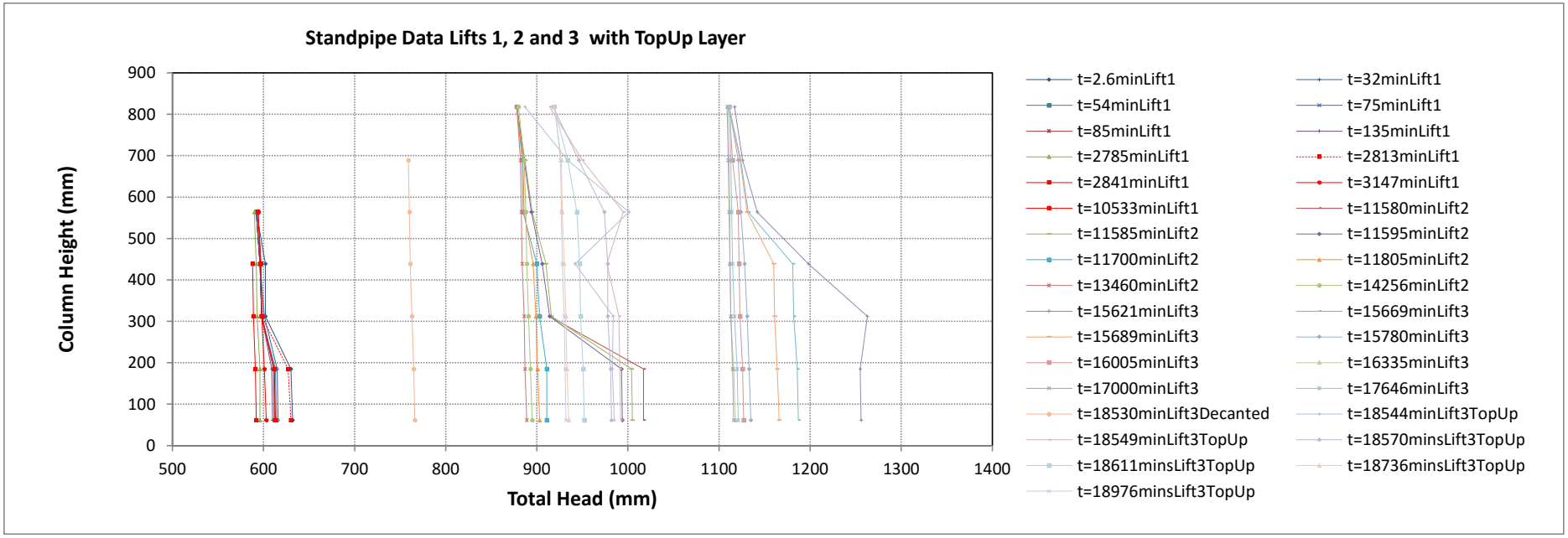

Figure F7: Sedimentation consolidation total heads change with depth Experiment RoR10B

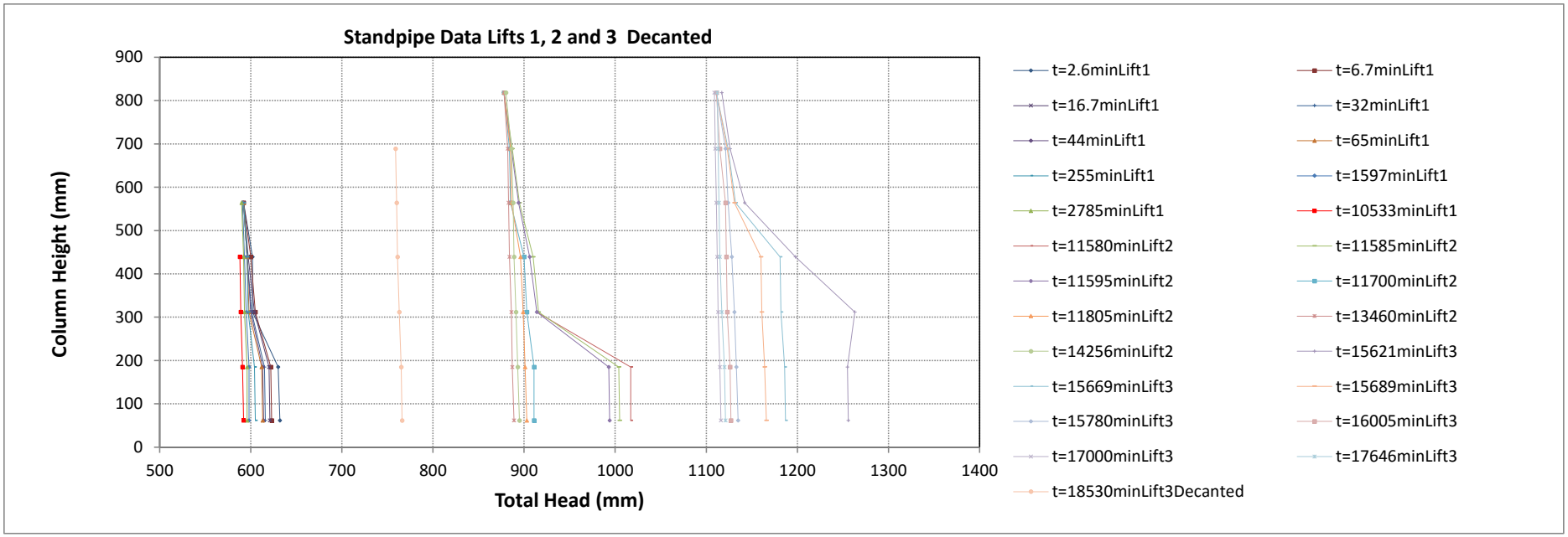

Figure F8: Sedimentation consolidation total heads change with depth Experiment RoR10B

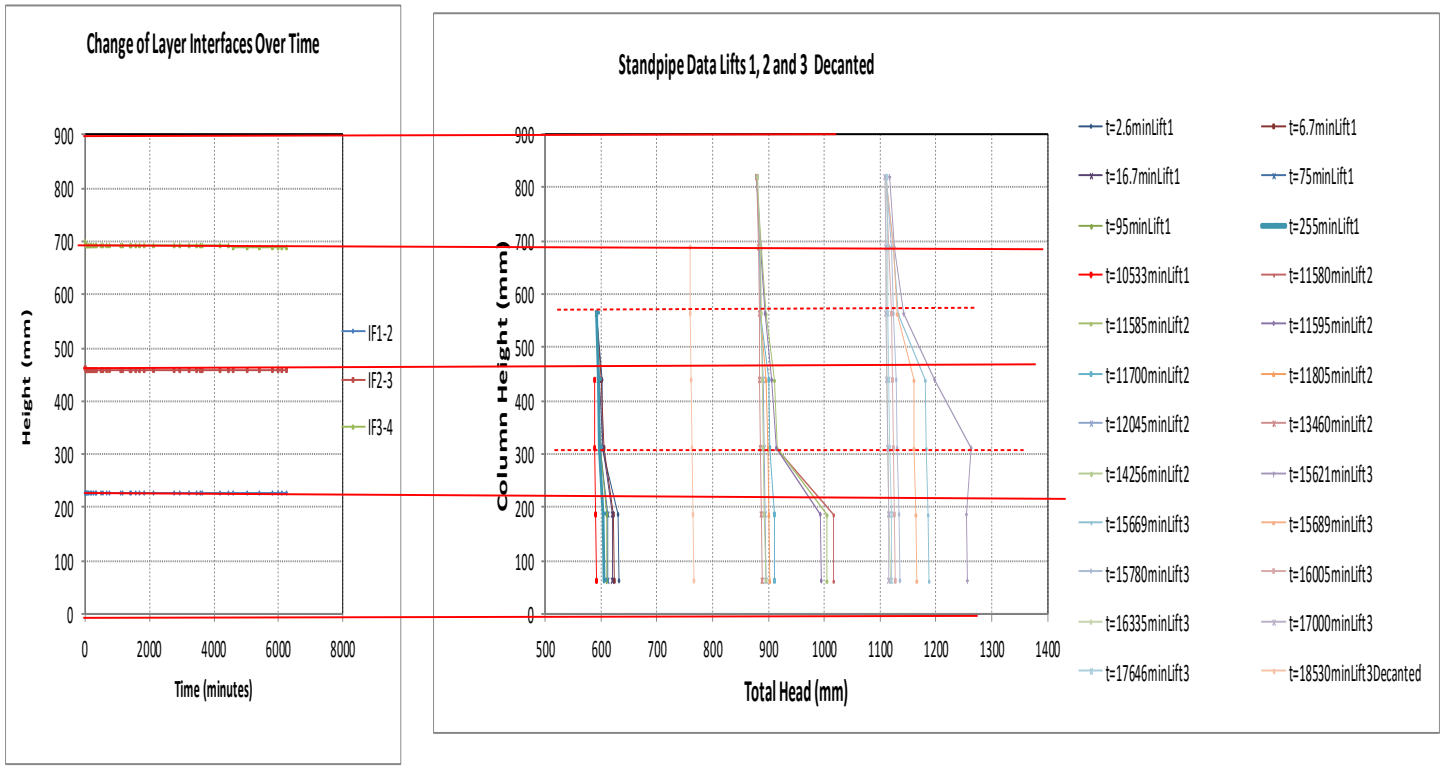

Figure F9: Sedimentation consolidation total heads change with depth Experiment RoR10B

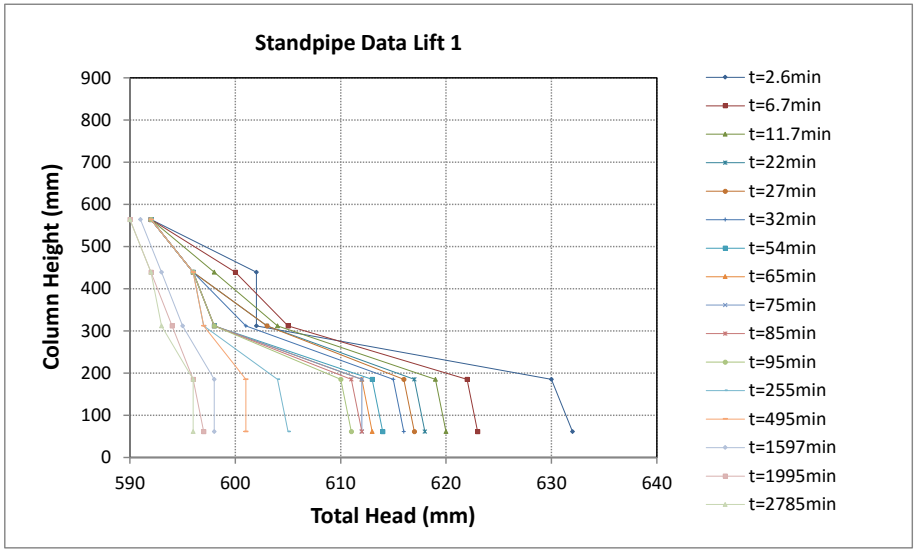

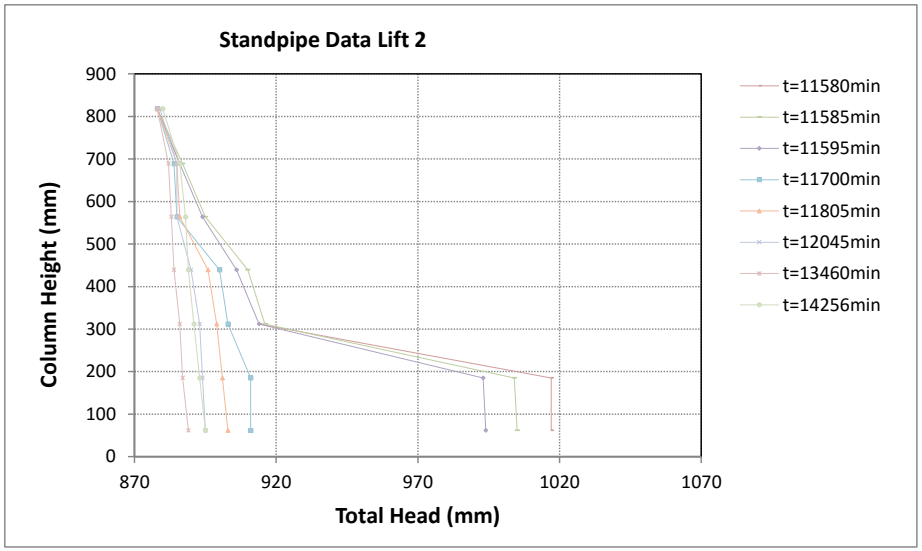

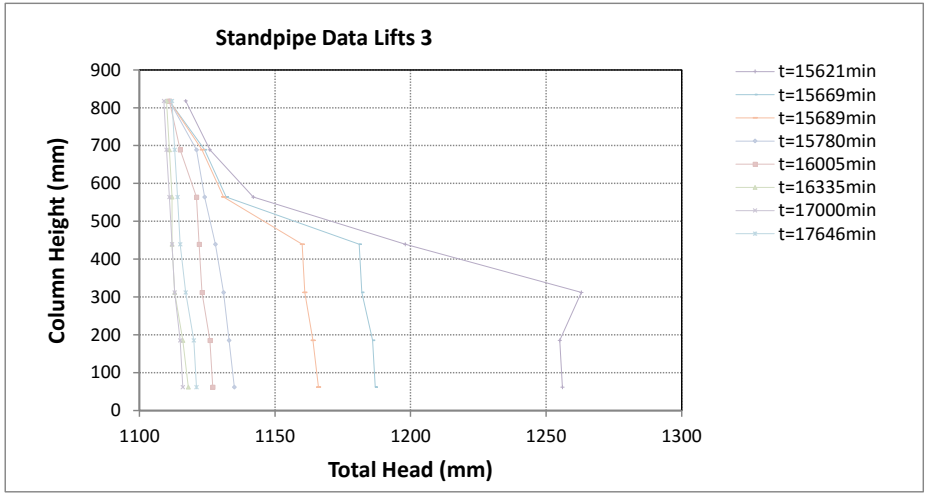

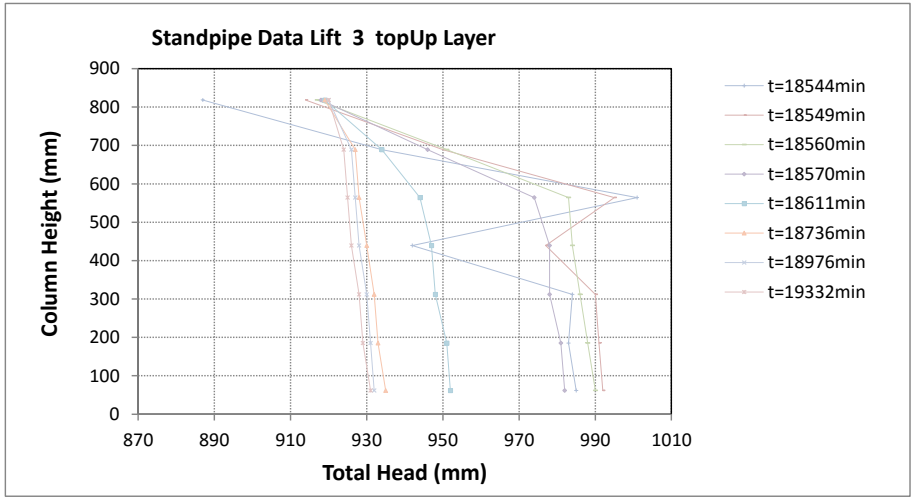

Figure F10: Sedimentation consolidation total heads change with Depth Experiment RoR10B

APPENDIX G

Permeability Test Results

The appendix presents the change of total heads over time during the constant head permeability tests (Experiments RoR20A, RoR20B and RoR10A) and the falling head permeability test (Experiment FDA). The appendix also reports the change in saturated vertical permeability values over time during the various experiments. The variation of vertical permeability with settling column height is also given (Figure G9). The results are presented under the headings listed below.

G1 Permeability Test Total Heads

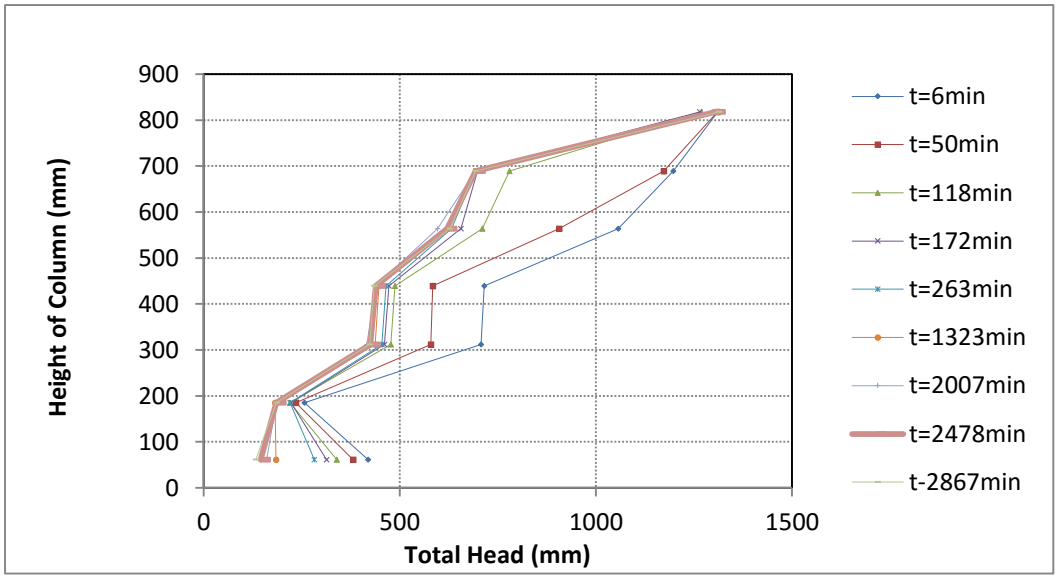

Figure G1: Constant head permeability test change of total head with depth Experiment RoR20A

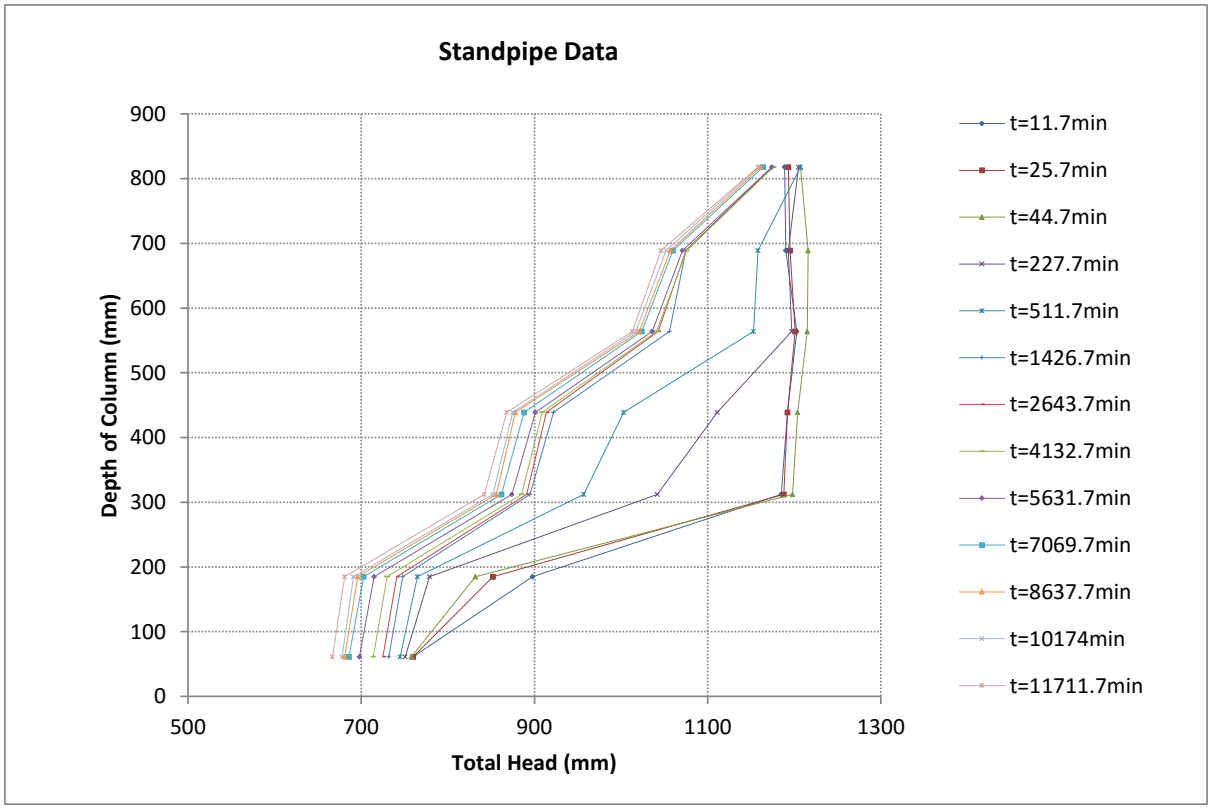

Figure G2: Constant head permeability test change of total head with depth Experiment RoR20B

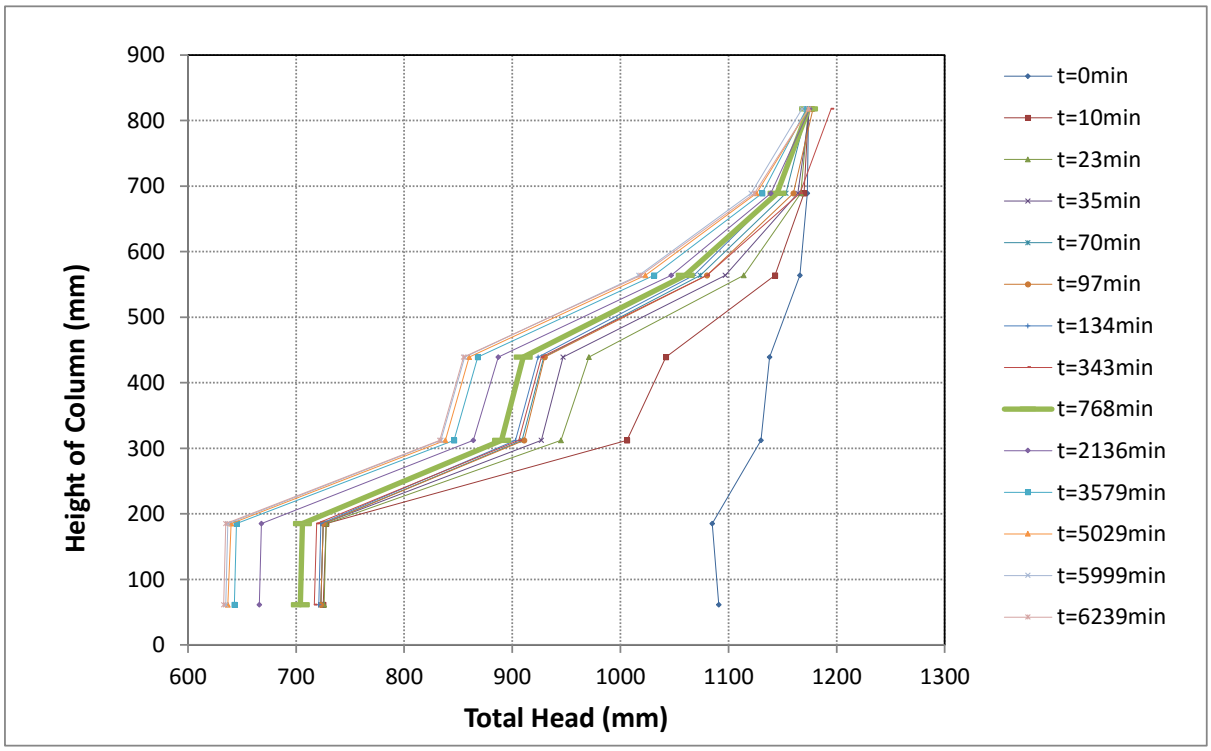

Figure G3 (a): Constant head permeability test change of total head with depth Experiment RoR10B

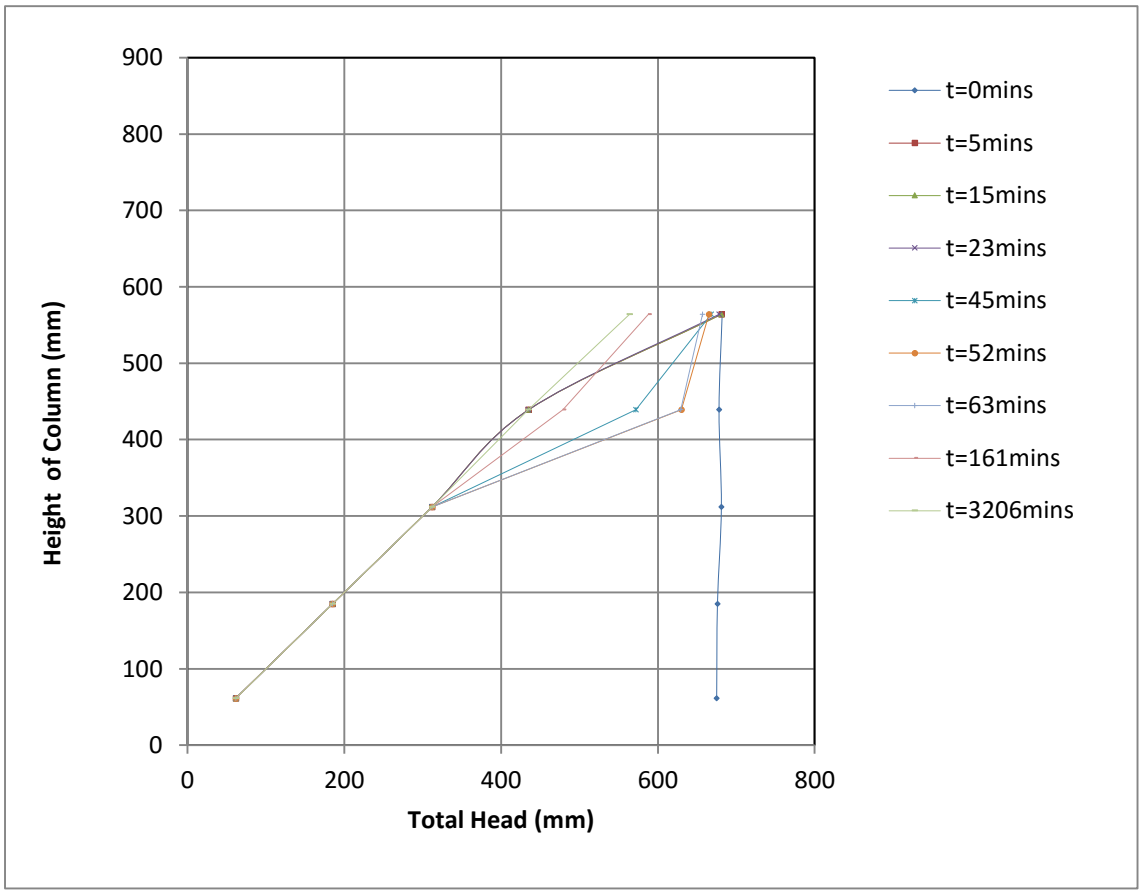

Figure G3 (b): Falling head permeability test change of total head with depth Experiment FDA

G2 Change of Permeability Values with Depth

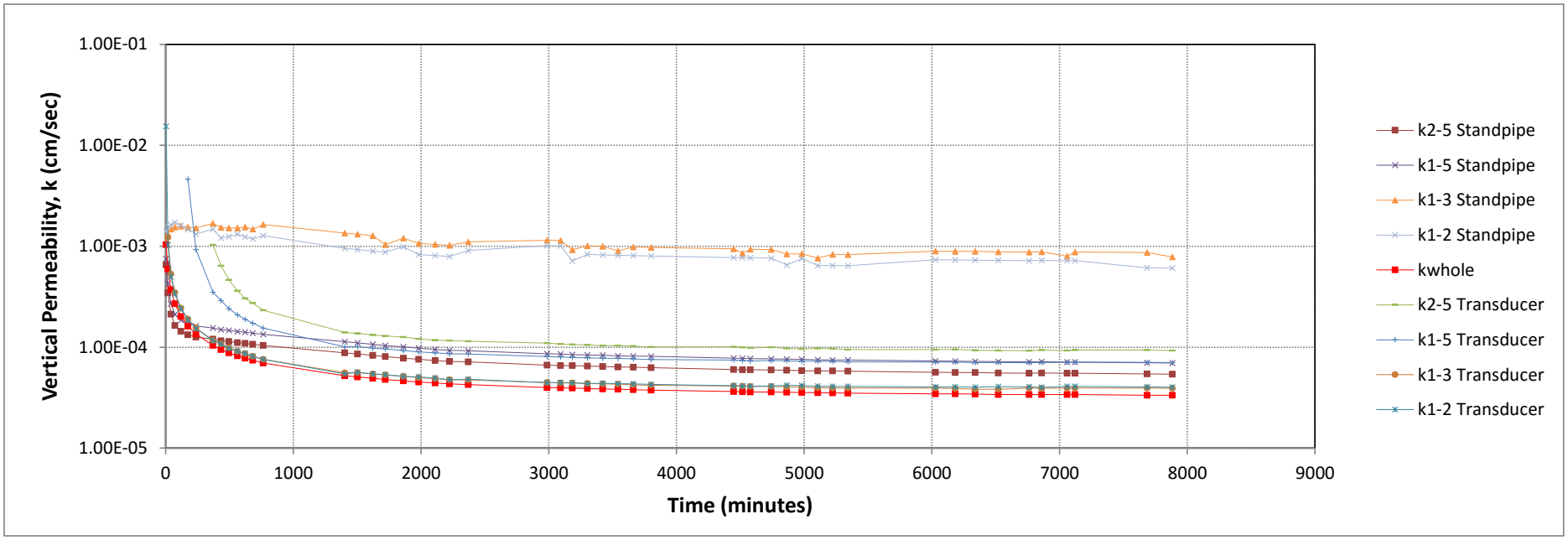

Figure G5: Change of permeability with depth over time Experiment FDB

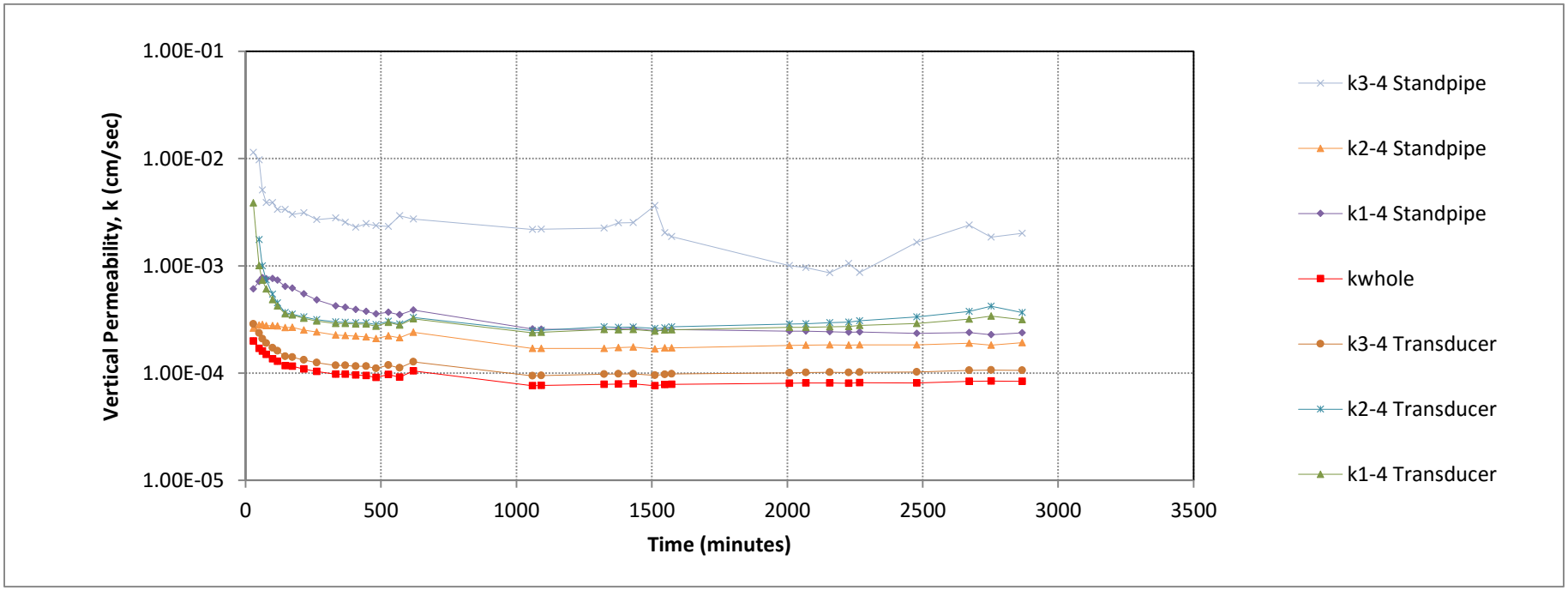

Figure G6 (a): Change of permeability with depth over time Experiment RoR20A

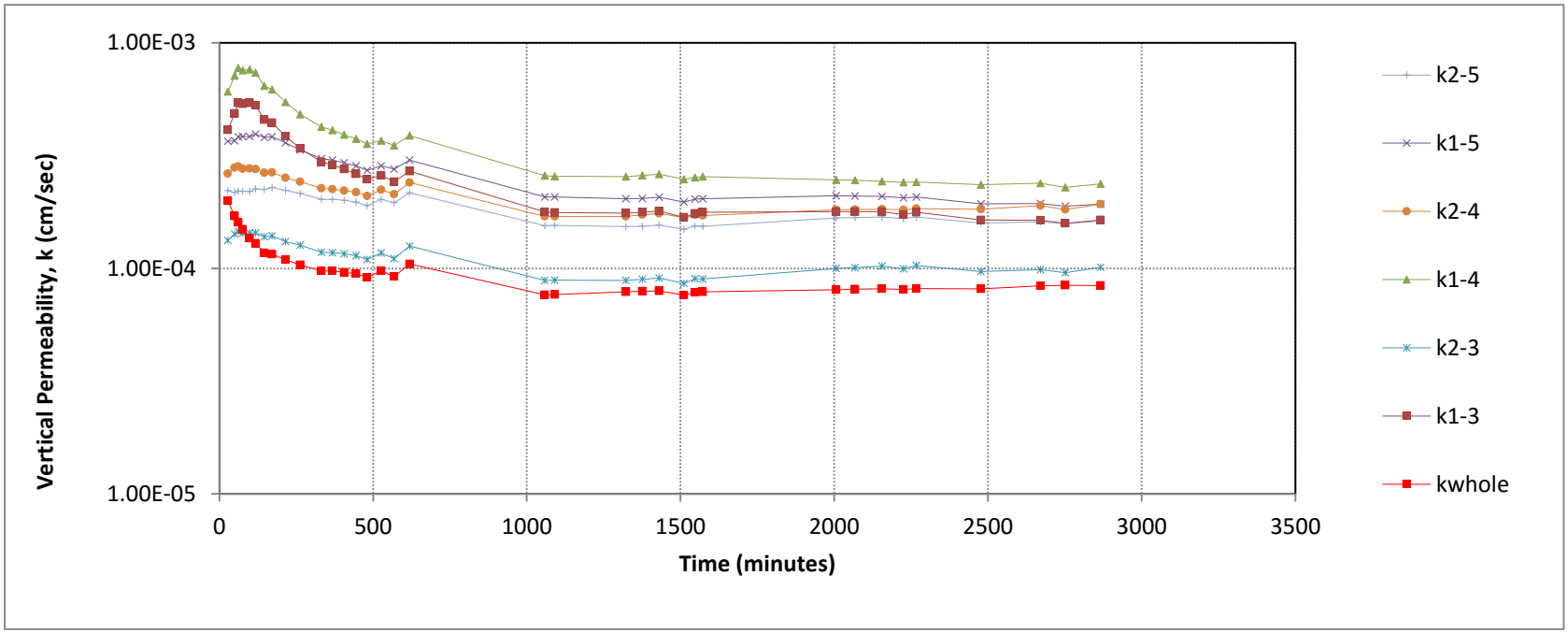

Figure G6 (b): Change of permeability with depth over time Experiment RoR20A: standpipe Data

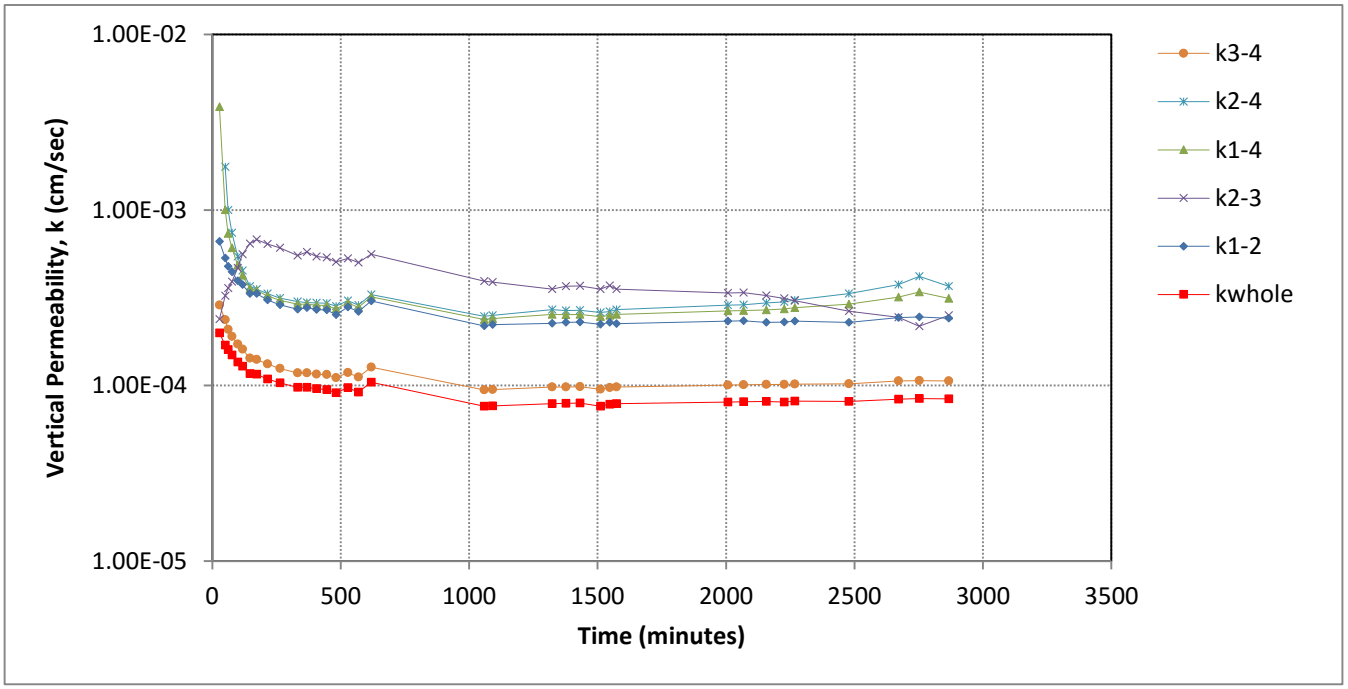

Figure G6 (c): Change of permeability with depth over time Experiment RoR20A: transducer Data

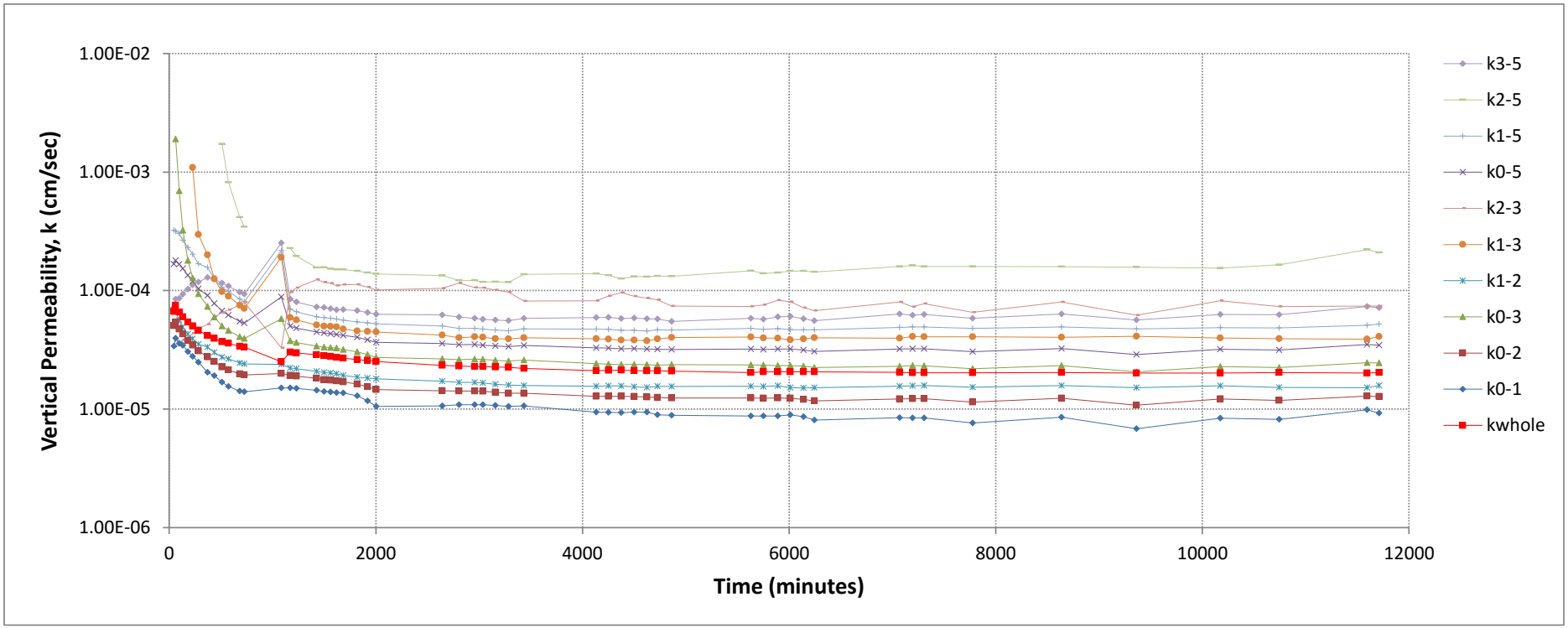

Figure G7 (a): Change of permeability with depth over time Experiment RoR20B: transducer data

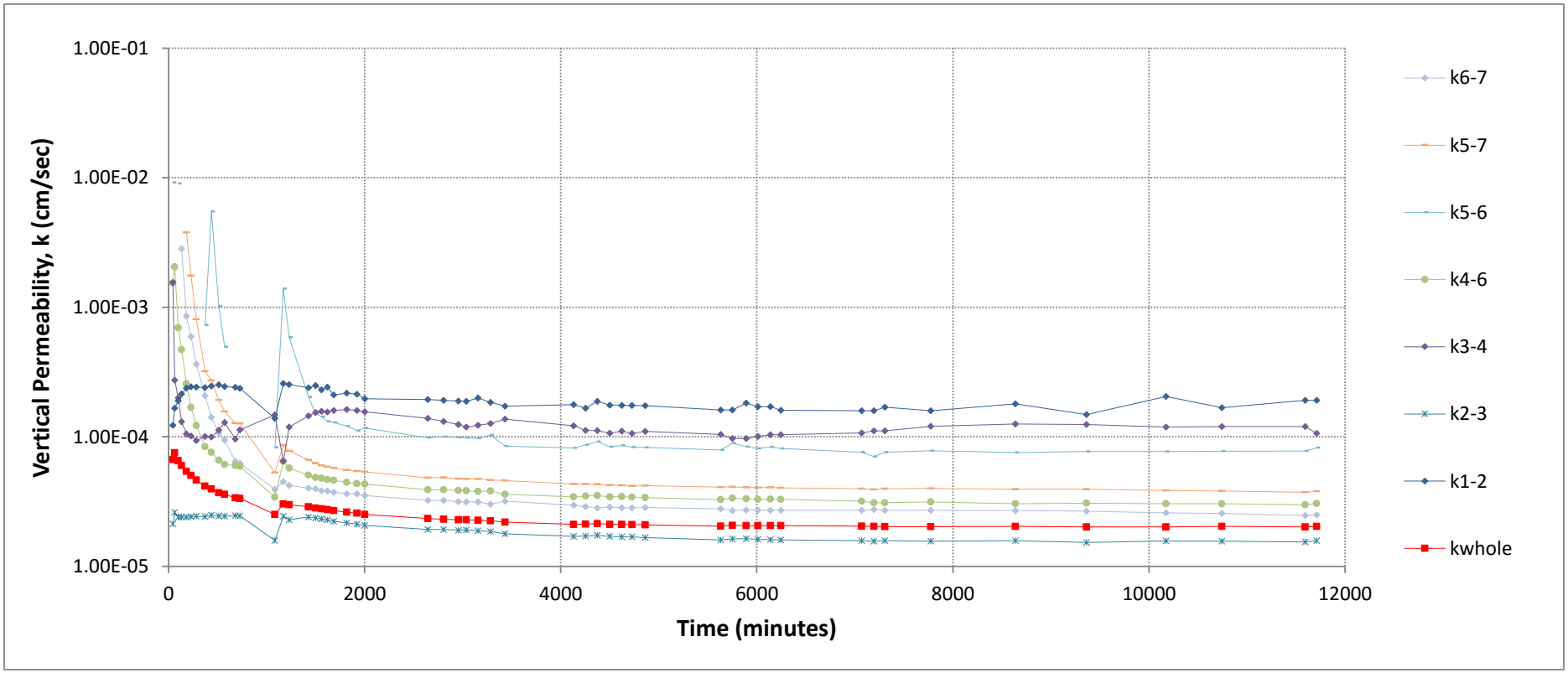

Figure G7 (b): Change of permeability with depth over time Experiment RoR20B: standpipe data

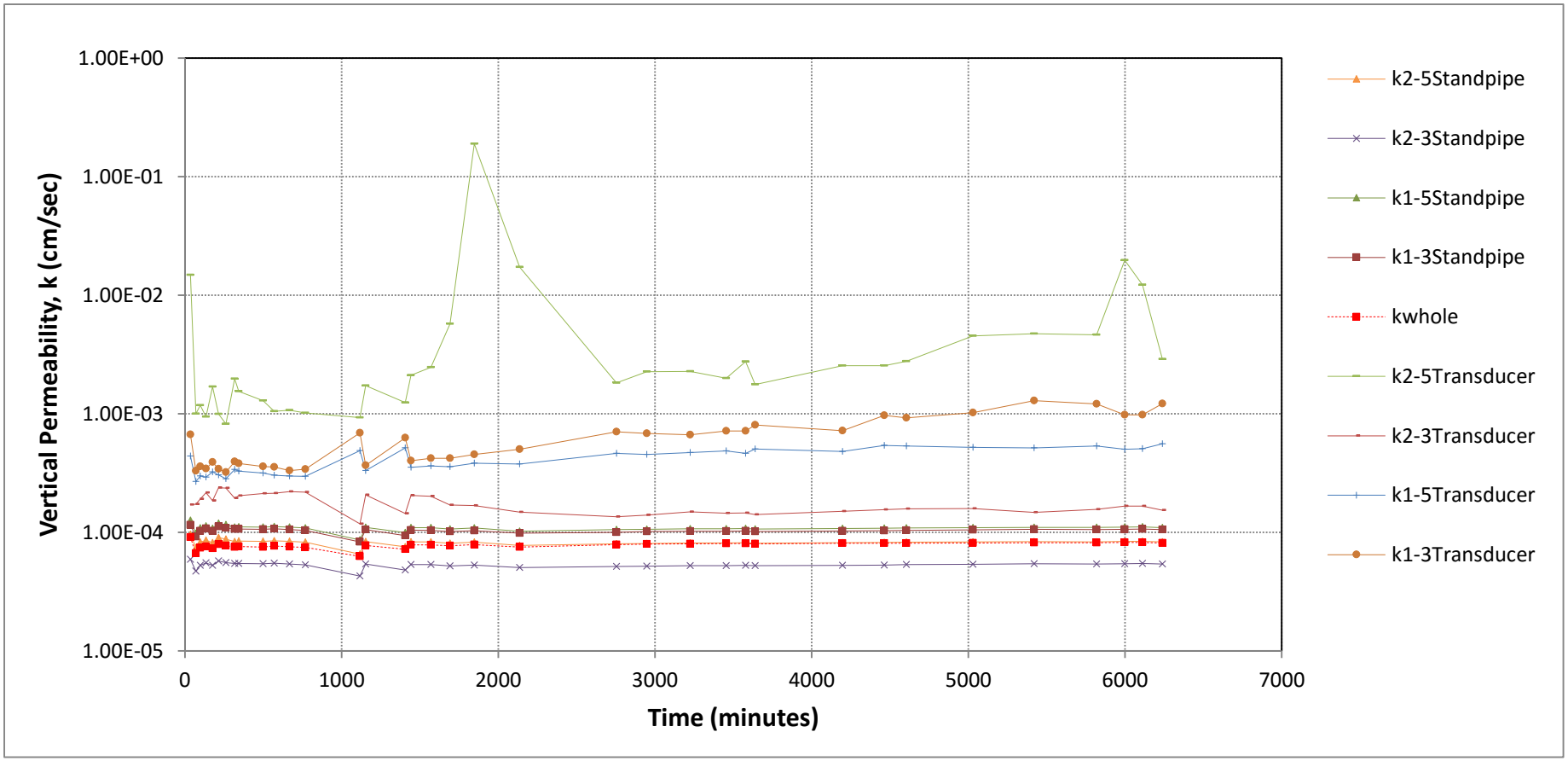

Figure G8 (a): Change of permeability with depth over time Experiment RoR10B: standpipe and transducer Data

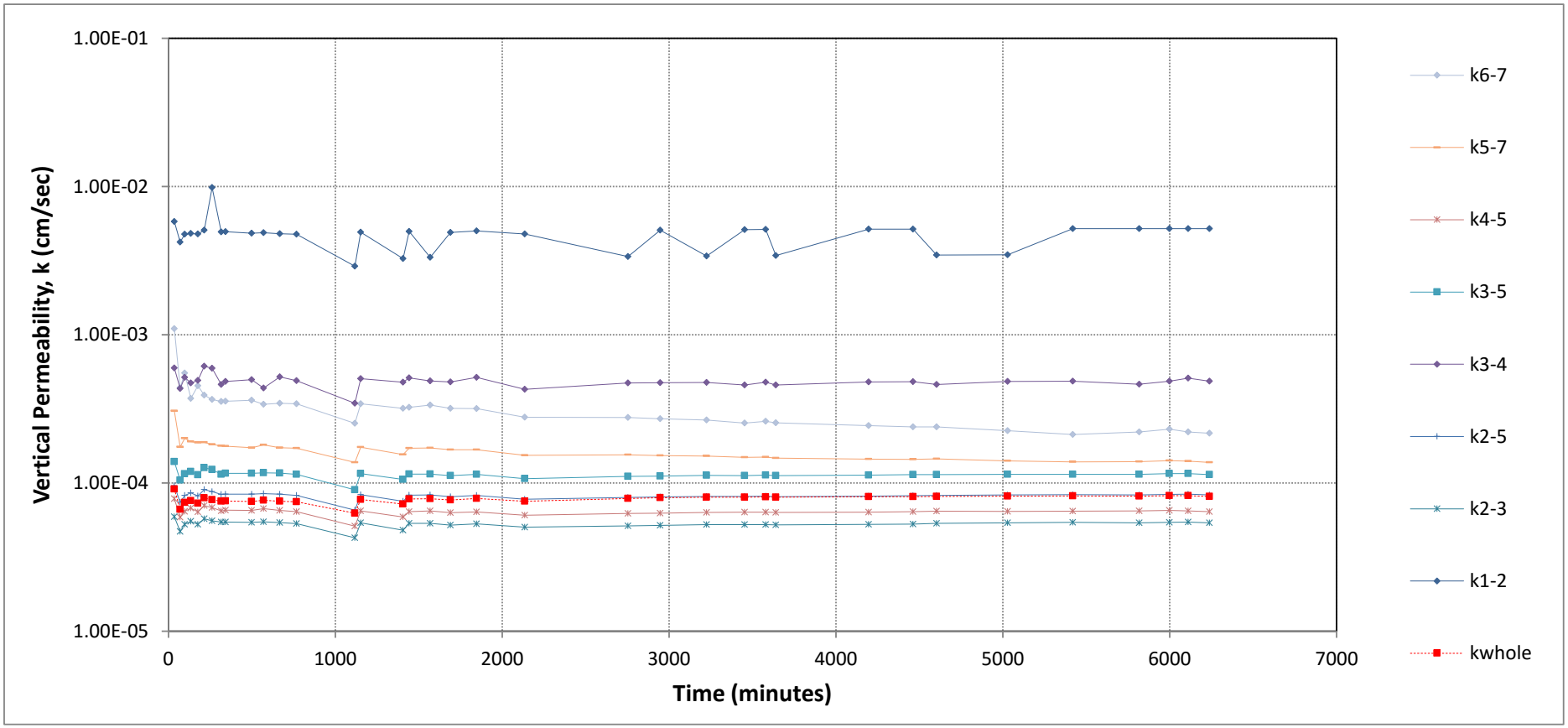

Figure G8 (b): Change of permeability with depth over time Experiment RoR10B: standpipe data

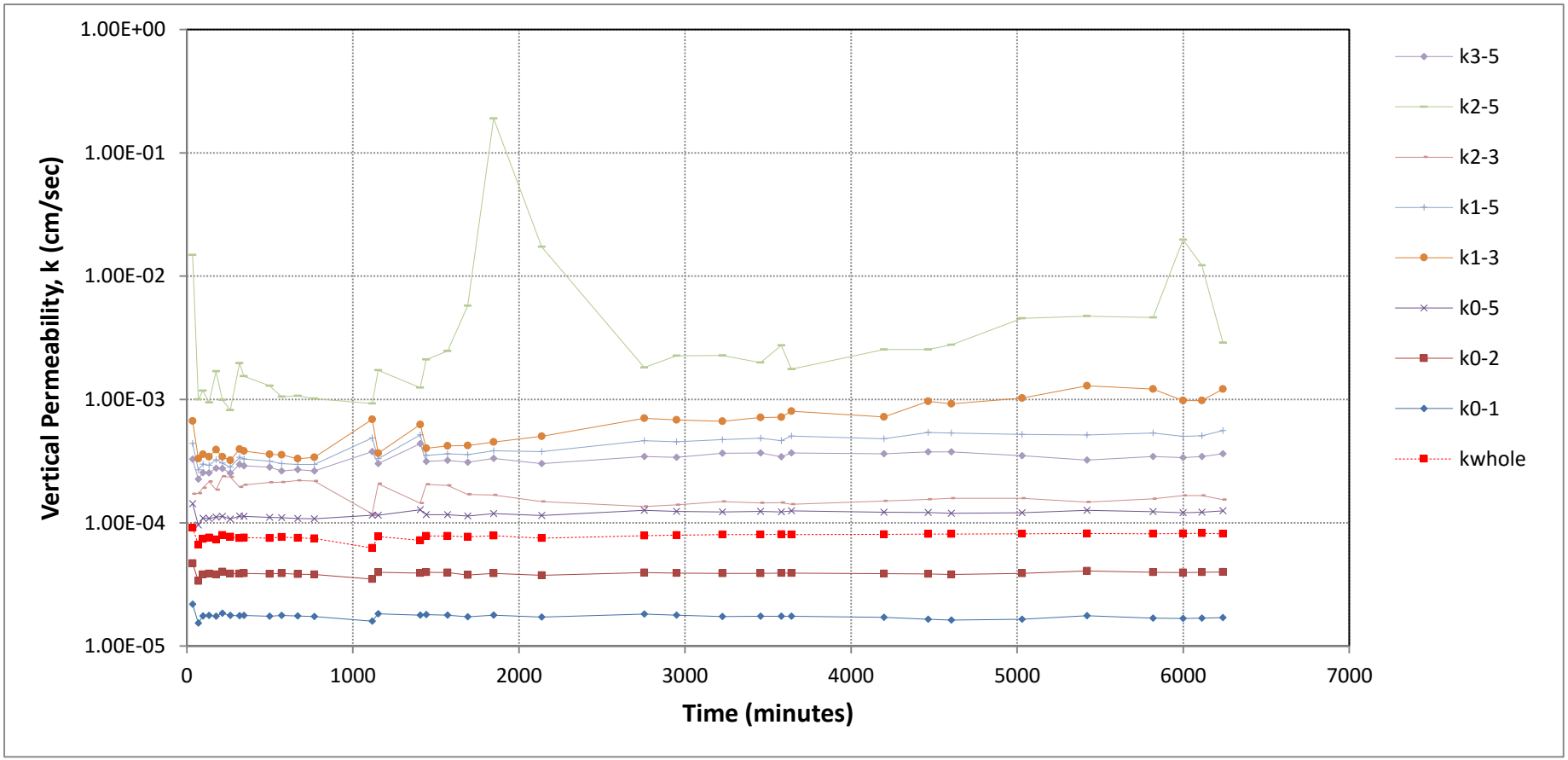

Figure G8 (c): Change of permeability with depth over time Experiment RoR10B: transducer data

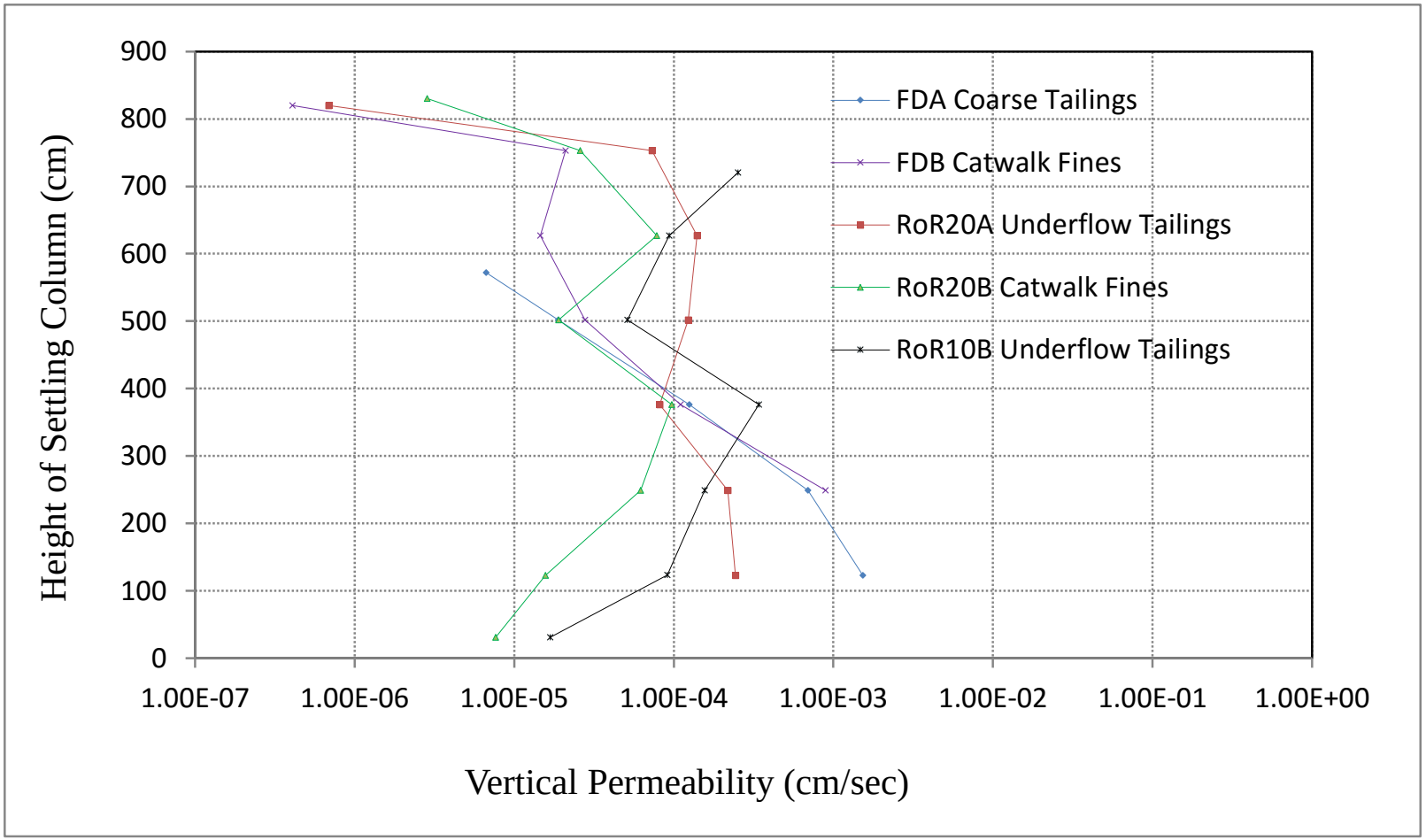

Figure G9: Variation of tailings permeability with depth - Experiments FDA, FDB, RoR20A, RoR20B and RoR10B

APPENDIX H

Particle Size Distribution

Particle size distribution curves are listed for Experiments FDB, RoR20A, RoR10A, RoR10B and RoR 10m/yr without permeability test. Grading curves are shown for both large (100mm) and small interval (30mm) specimen sampling. Comparisons between sieve/hydrometer and Mastersizer particle size grading curves are provided for Experiment FDB.

Particle size grading parameters including hydrometer sample concentration, size percentiles, grading coefficients and grading modulus are listed for experiment samples, complementary samples and recovered column samples from Experiments FDB, RoR20B and RoR10B. The results presentation order is listed below.

H1 Grading Curves

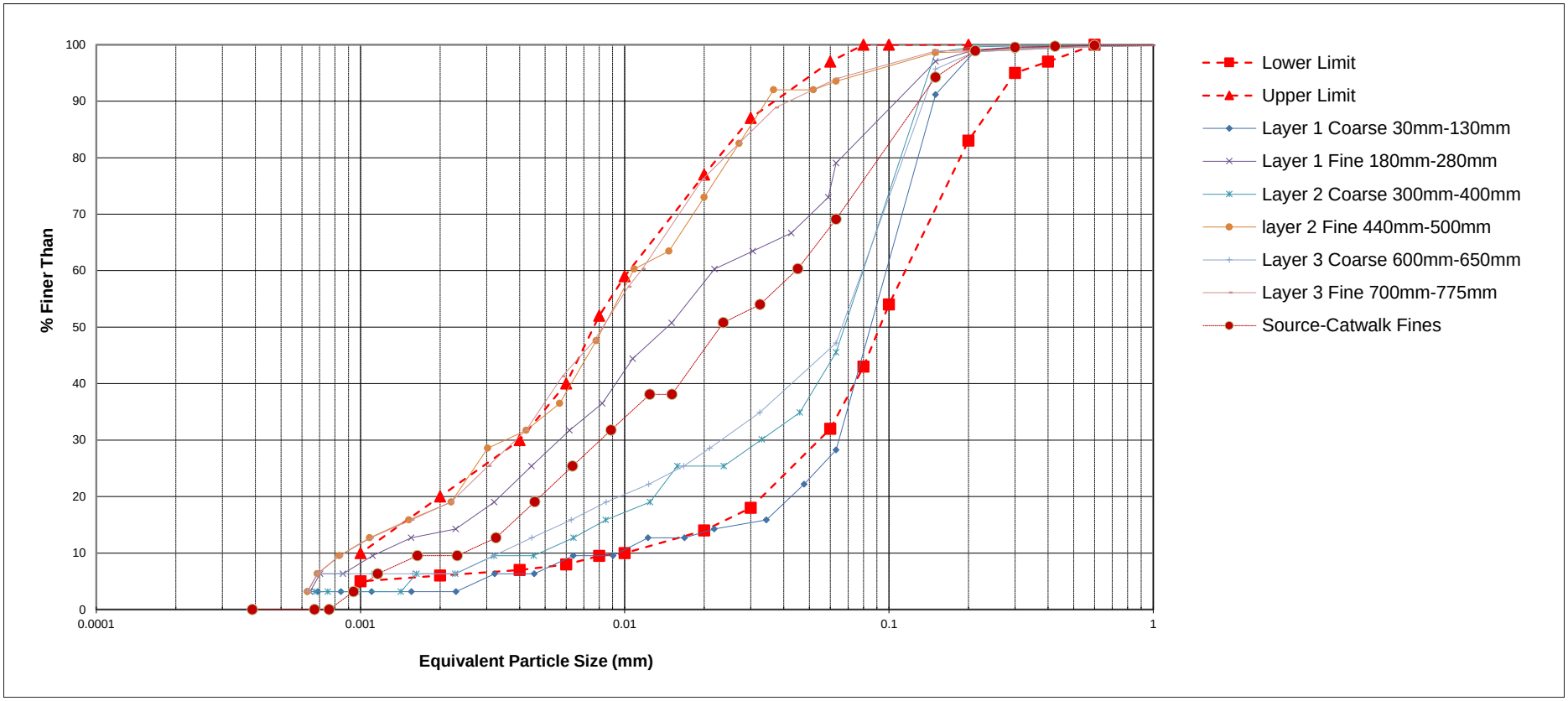

Figure H4: Gradations of recovered Experiment RoR20A sample large interval (100mm) specimen spacing

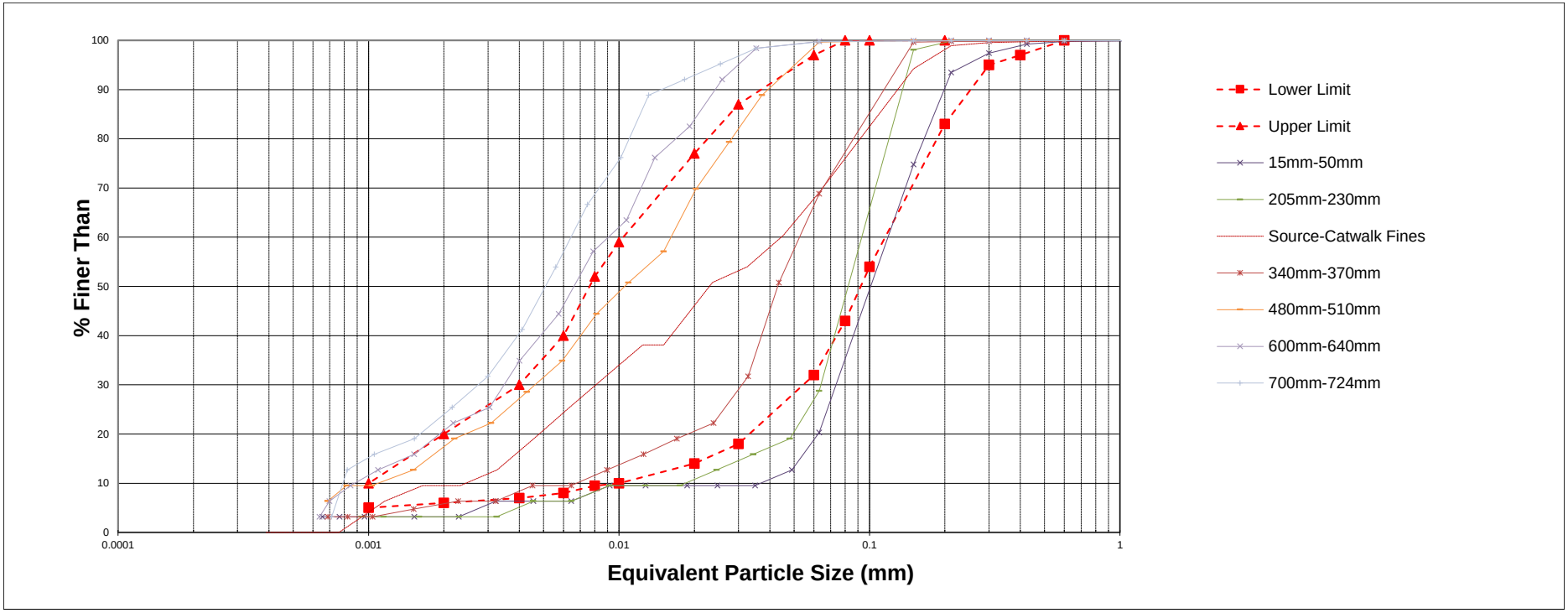

Figure H5: Gradations of recovered Experiment FDB sample large interval (100mm) specimen spacing

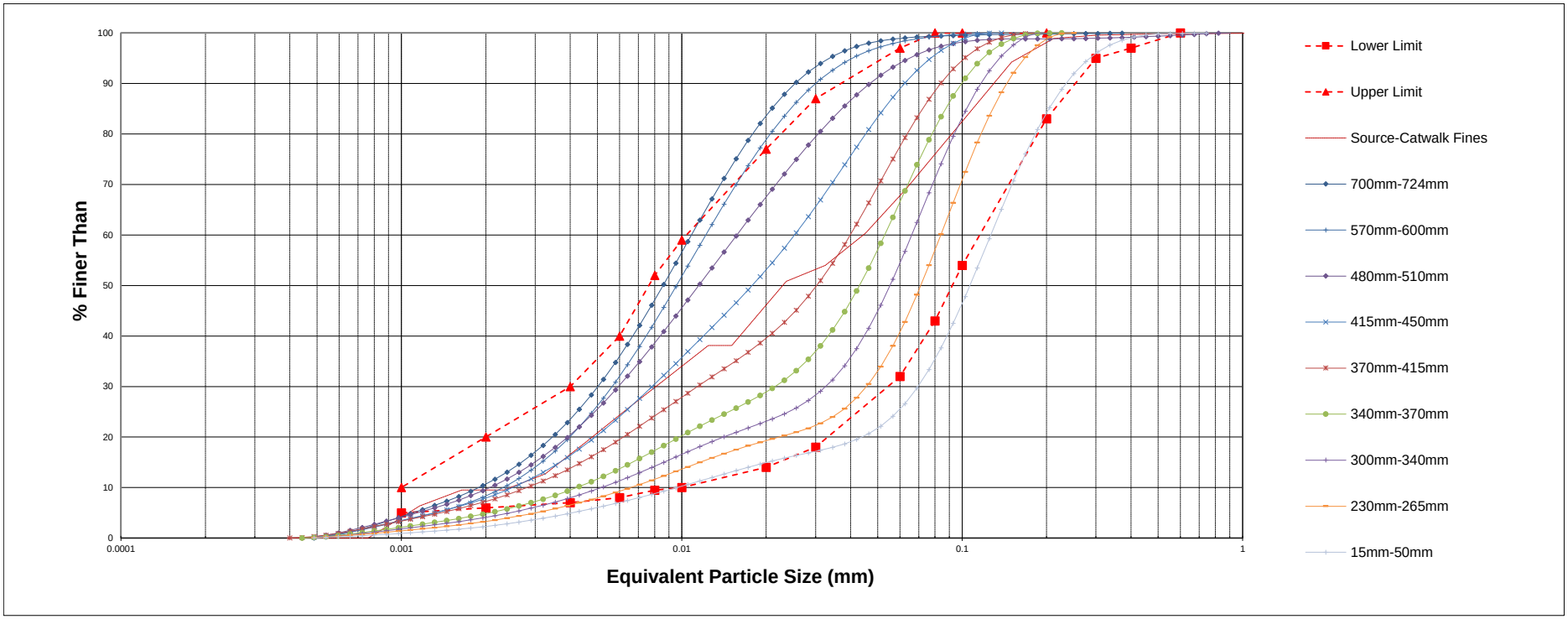

Figure H6: Mastersizer diffraction analysis gradations of recovered Experiment FDB sample small interval (30mm) specimen spacing

(a)

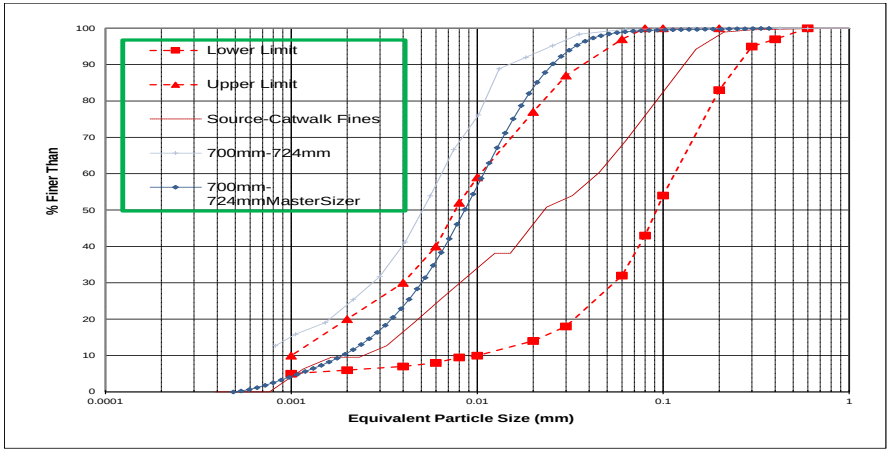

(b)

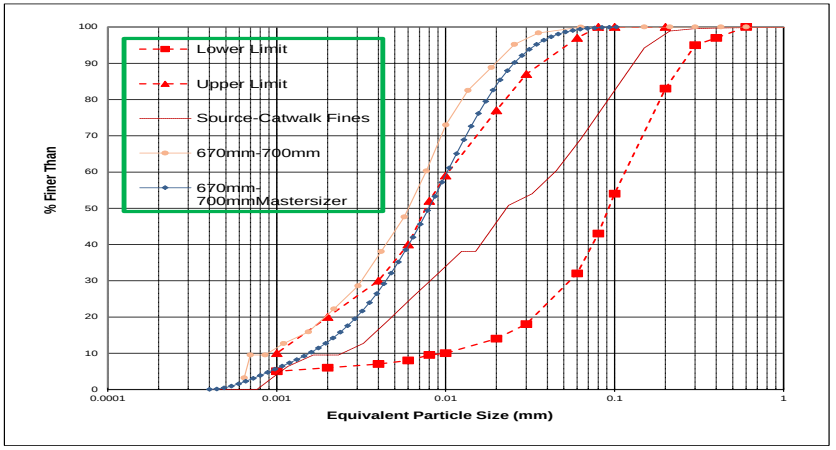

(c)

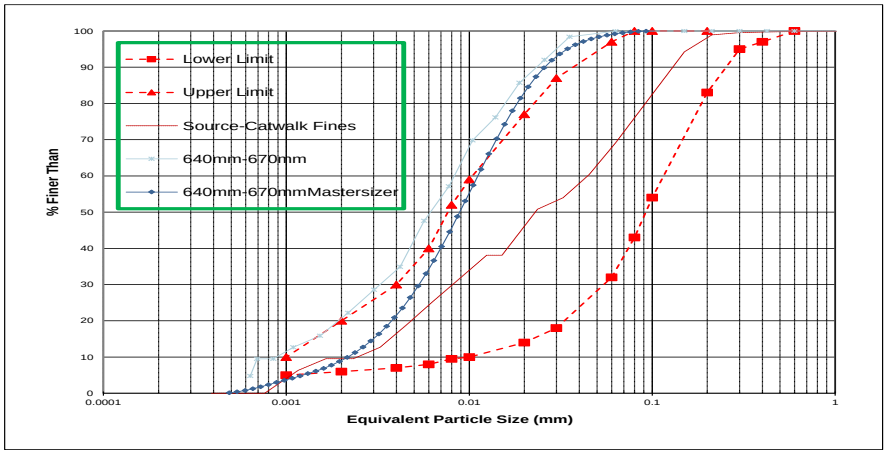

(d)

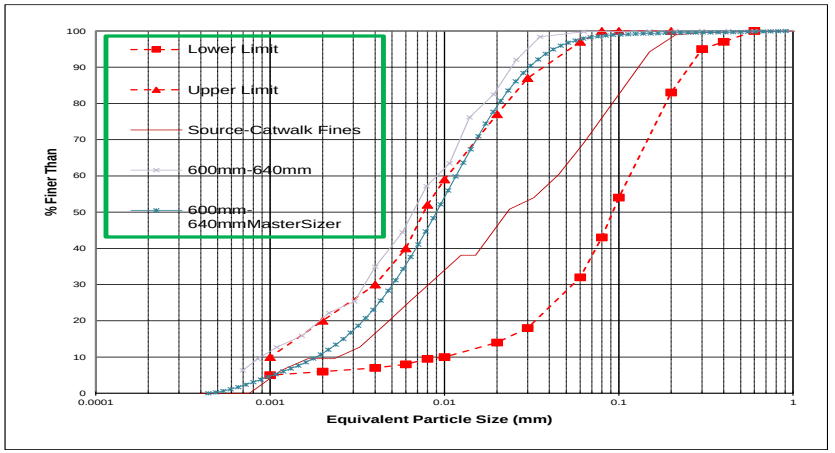

(e)

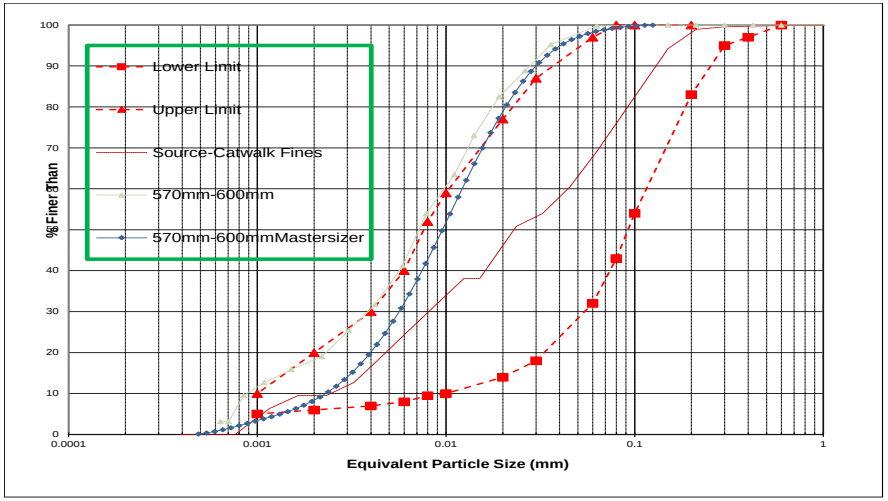

(f)

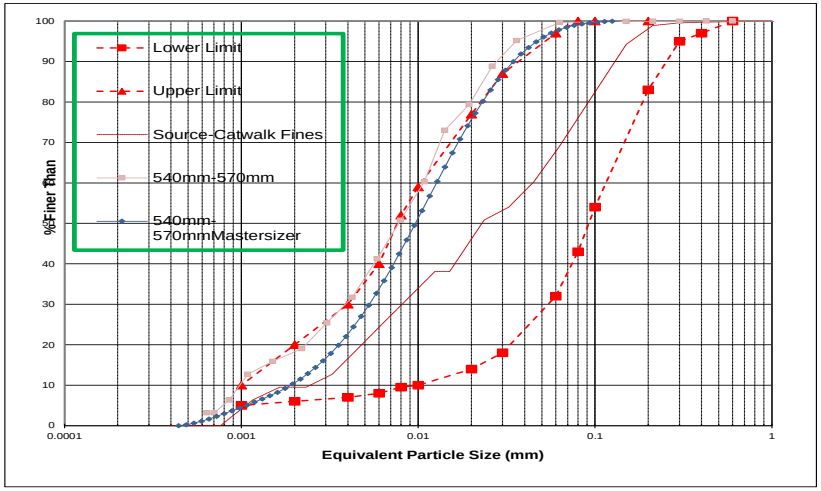

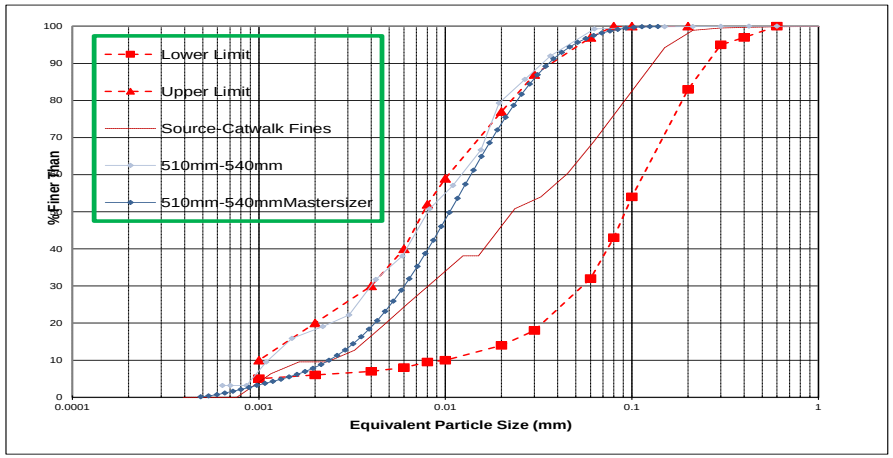

(g)

(h)

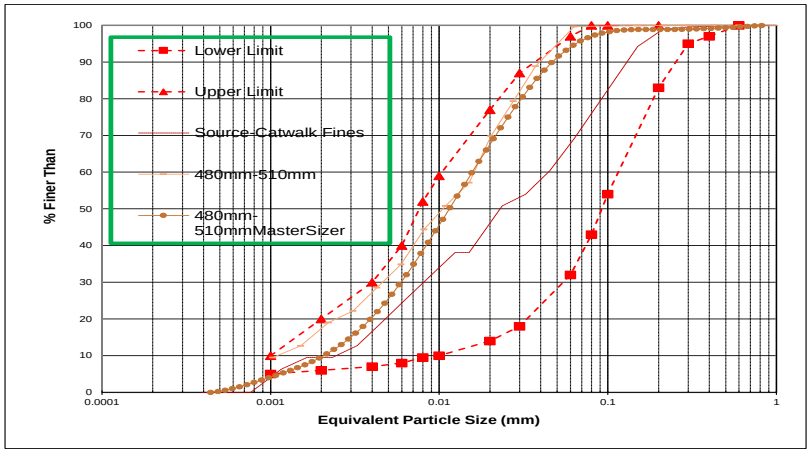

(i)

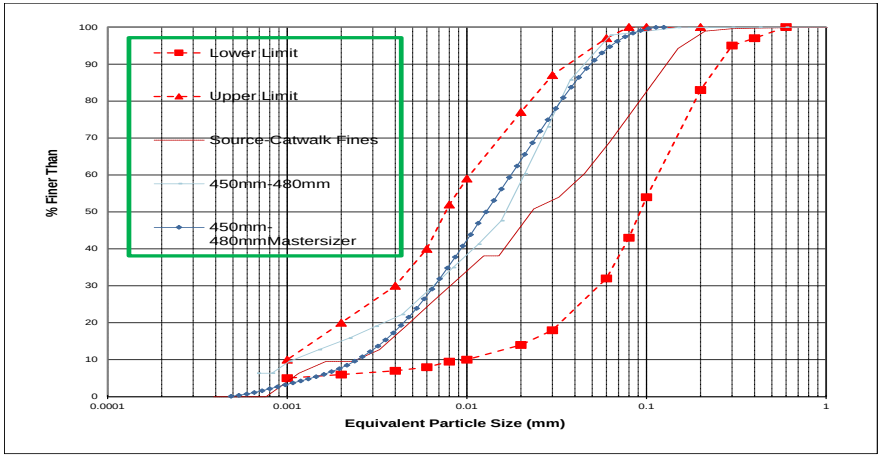

(j)

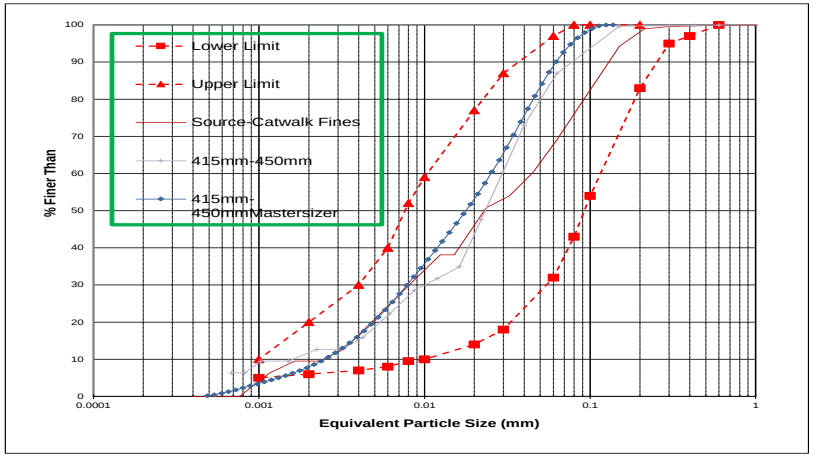

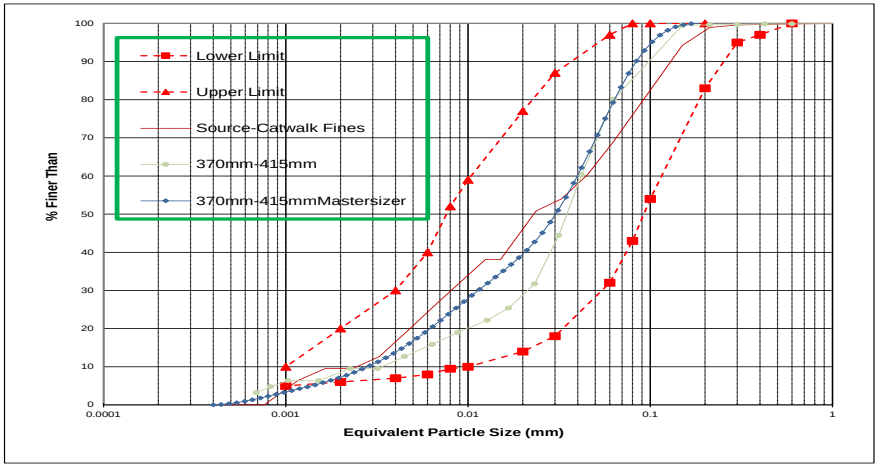

(k)

(l)

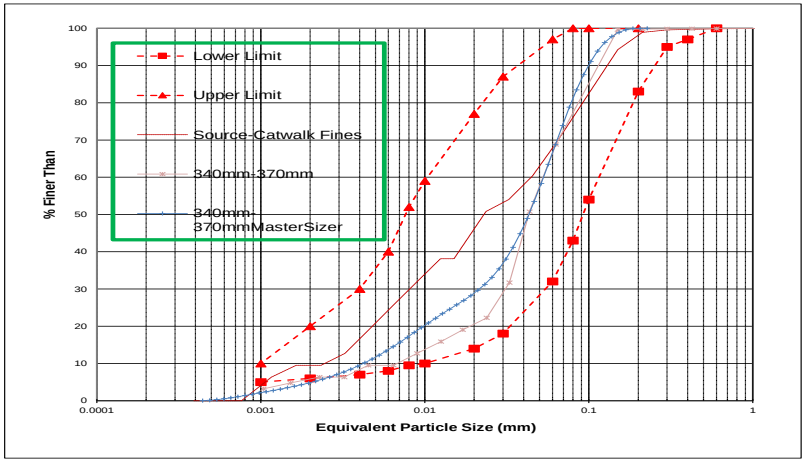

(m)

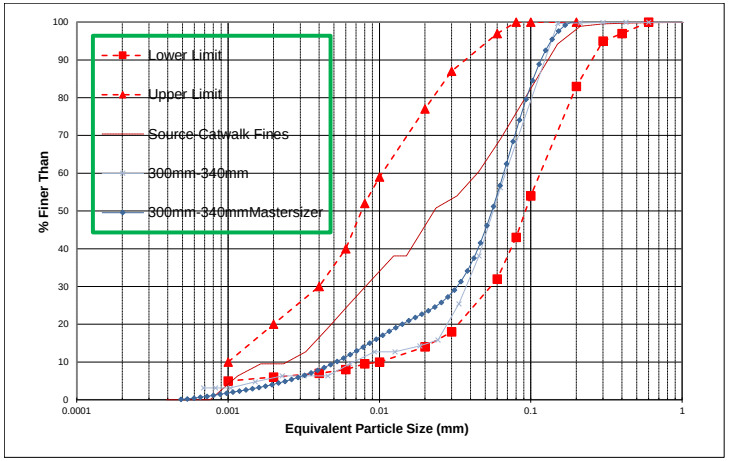

(n)

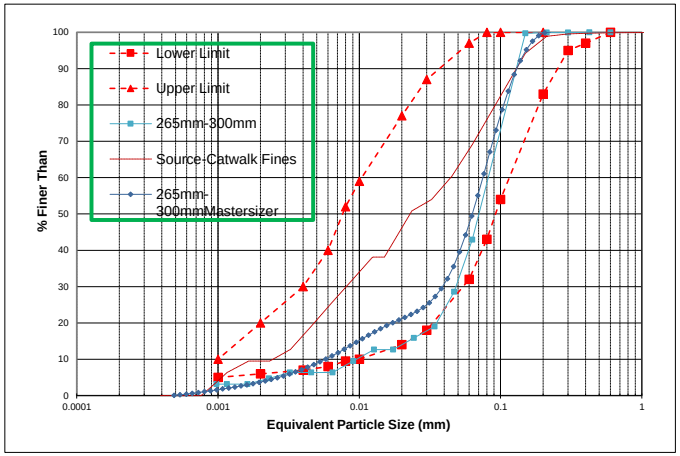

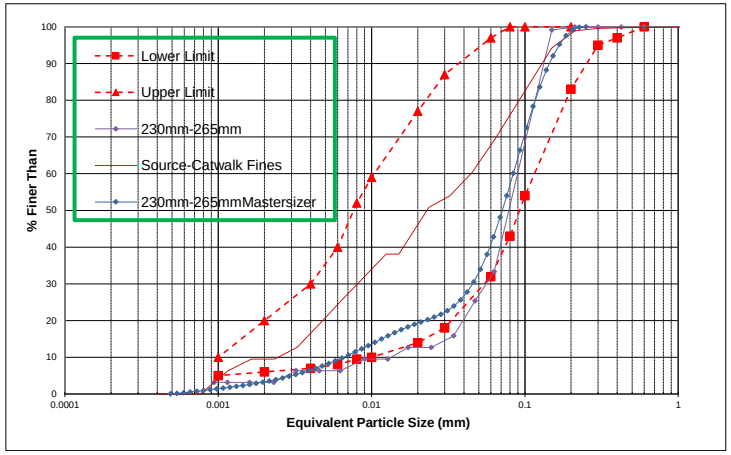

(o)

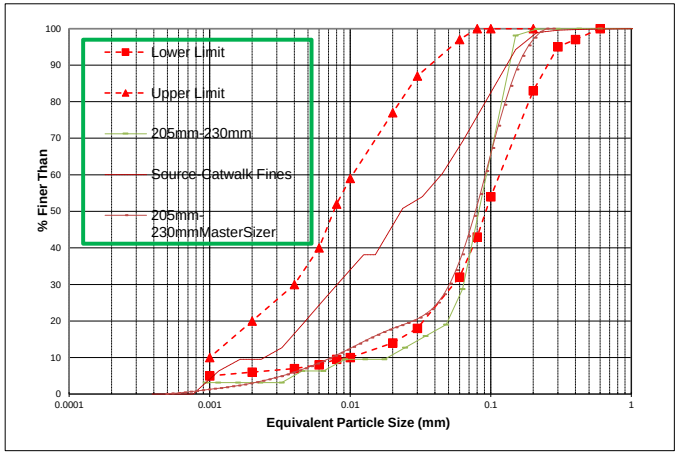

(p)

(q)

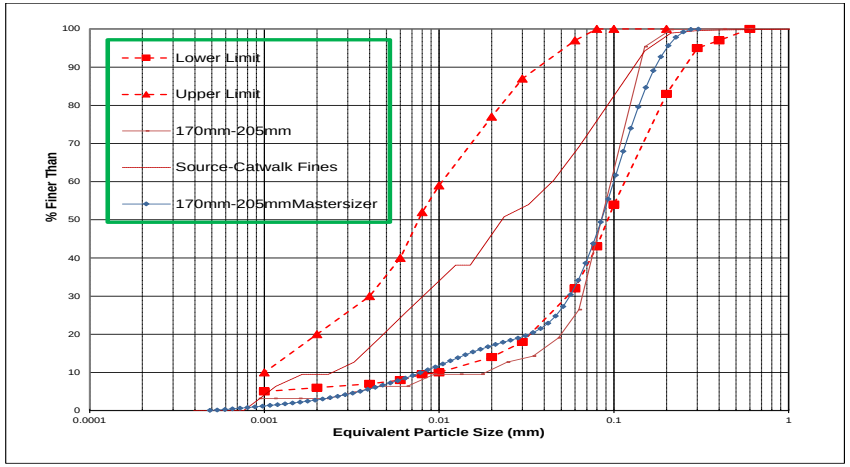

(r)

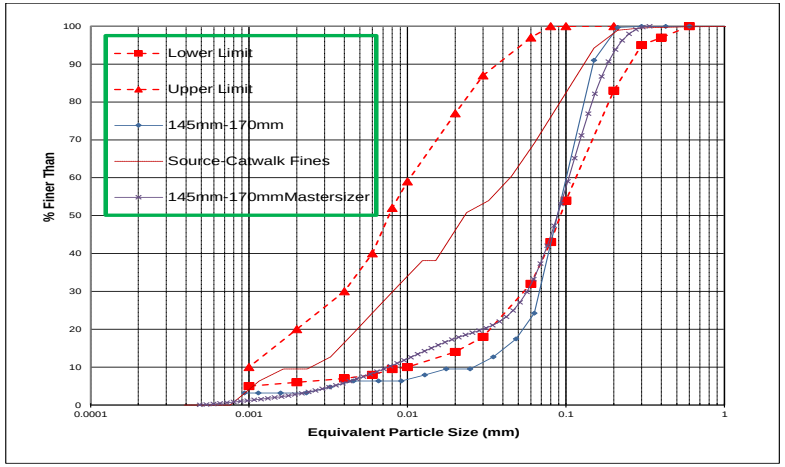

(s)

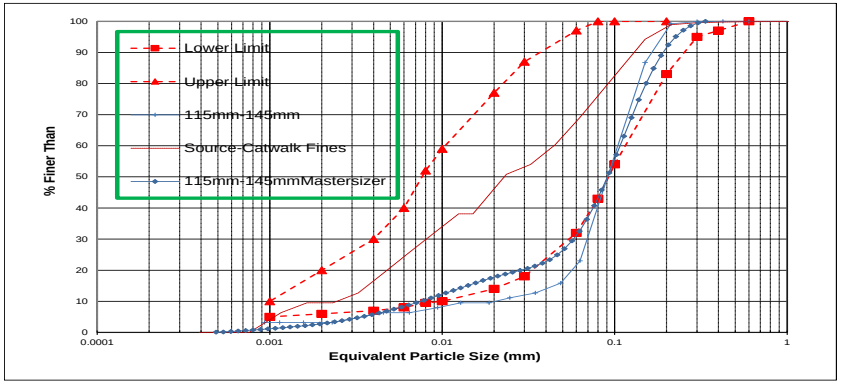

(t)

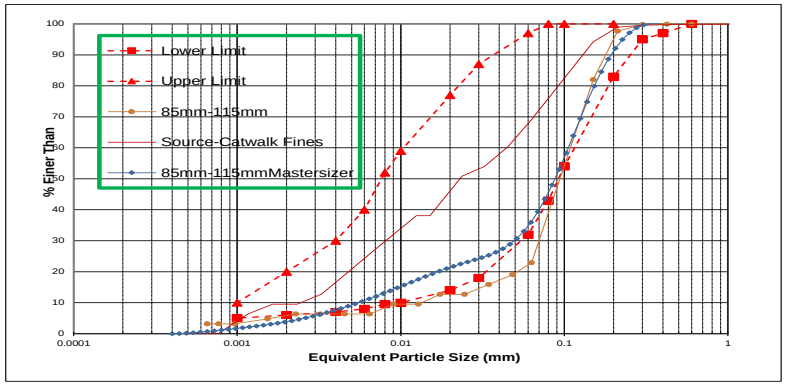

Figure H8: Comparisons: Sieve and Hydrometer & Mastersizer Diffraction Analysis Gradations of Recovered Full Depth Deposition Experiment 6 Catwalk Fines Tailings samples

u)

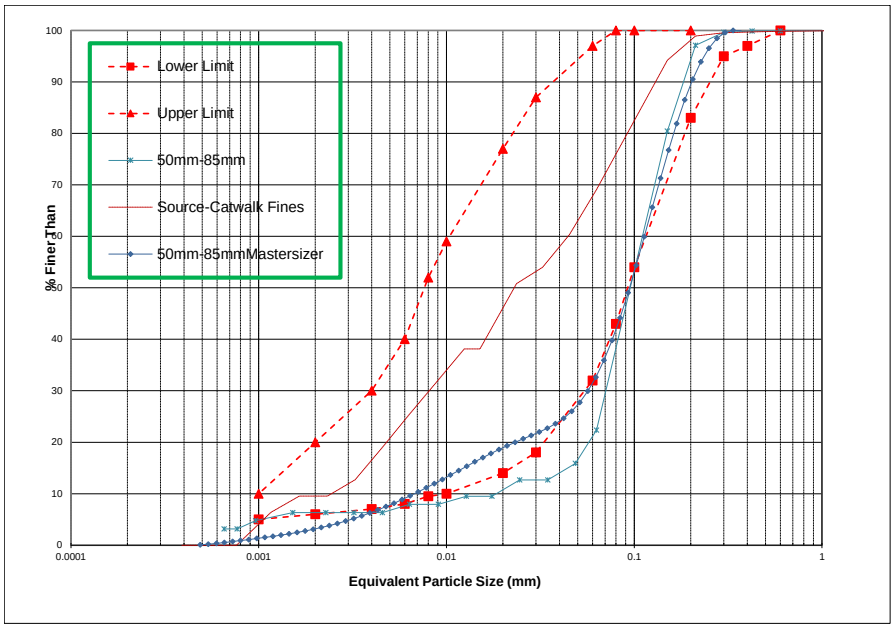

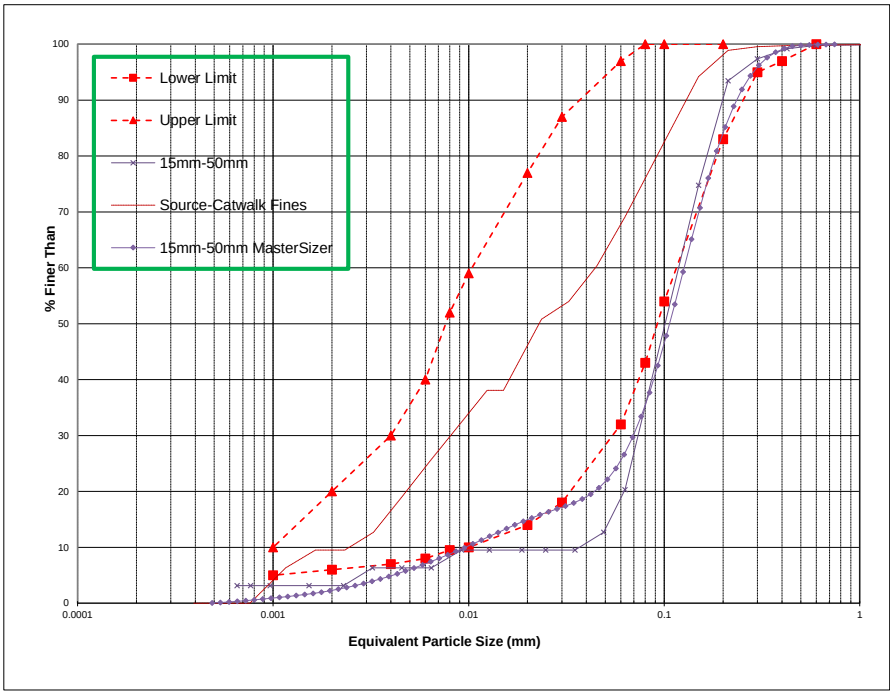

(v) (b)

Figure H8: Comparisons: sieve and hydrometer & Mastersizer diffraction analysis gradations of recovered Experiment FDB samples

H2 Grading Parameters

Table H1: Particle size grading parameter summary table

Test No.	Date	Material Description	63um Wash Material	Pan Material	Total -63um material	Hydrometer Sample Concentration	Gradation Parameters (Percentiles)					Finer Than 0.425mm	Finer Than 0.075mm	Cu d_{60}/d_{10}	Cc $d^2_{30}/d_{60}d_{10}$	Grading Modulus (GM) (P2mm+P425µm+P75µm)
							D_{10}	D_{30}	D_{50}	D_{60}	D_{90}					
			(g)	(g)	(g)	(g/L)	(mm)	(mm)	(mm)	(mm)	(mm)					
1	17/12/2011	Expt Samples - Underflow 2011	30.86	3.17	34.03	34.03	0.02	0.051	0.06	0.06	0.14	100	70	3.00	2.17	0.30
2	17/12/2011	Expt Samples - Underflow 2010	27.18	7.07	34.25	34.25	0.0045	0.035	0.065	0.065	0.15	95	73	14.44	4.19	0.32
3	17/12/2011	Expt Samples -Catwalk Fines	30.95	7.65	38.60	38.60	0.0031	0.02	0.048	0.051	0.14	100	83	16.45	2.53	0.17
4	30/03/2012	Expt Samples - Underflow 2011- Repeat	11.58	1.99	13.57	13.57	0.009	0.065	0.1	0.14	0.2	100	35	15.56	3.35	0.65
5	30/03/2012	Expt Samples - Underflow 2010 - Repeat	17.36	4.53	21.89	21.89	0.009	0.05	0.072	0.094	0.18	97	50	10.44	2.96	0.53
6	30/03/2012	Expt Samples -Catwalk Fines -Repeat	32.79	1.70	34.49	34.49	0.0022	0.011	0.033	0.06	0.13	100	72	27.27	0.92	0.28
7	17/12/2011	Tailings Dam Contol Samples -Underflow	8.94	3.31	12.25	12.25	0.009	0.07	0.11	0.14	0.23	97	32	15.56	3.89	0.71
8	17/12/2011	Tailings Dam Contol Samples -Whole	26.60	5.39	31.99	31.99	0.0015	0.01	0.062	0.062	0.14	100	70	41.33	1.08	0.30
9	17/12/2011	Tailings Dam Contol Samples -Overflow	32.38	3.53	35.91	35.91	0.016	0.05	0.052	0.06	0.13	100	72	3.75	2.60	0.28
10	24/02/2012	Contractor Samples- Penstock	4.87	22.78	27.65	27.65	0.007	0.034	0.061	0.07	0.13	100	62	10.00	2.36	0.38
11	24/02/2012	Contractor Samples- Overflow	17.25	20.07	37.32	37.32	0.003	0.008	0.021	0.05	0.11	100	78	16.67	0.43	0.22
12	24/02/2012	Contractor Samples- Underflow	9.48	6.79	16.27	16.27	0.017	0.06	0.083	0.1	0.17	100	40	5.88	2.12	0.60
13	03/03/2012	RoR 20m/yr-30mm-130mm Layer 1 Coarse	7.82	6.34	14.16	14.16	0.0065	0.065	0.083	0.095	0.15	100	42	14.62	6.84	0.58
14	03/03/2012	RoR 20m/yr-300mm-400mm Layer 2 Coarse	4.61	18.39	23.00	23.00	0.0031	0.031	0.067	0.08	0.13	100	58	25.81	3.88	0.42
15	03/03/2012	RoR 20m/yr-600mm-650mm Layer 3 Coarse	16.32	7.24	23.56	23.56	0.0031	0.022	0.064	0.08	0.14	100	58	25.81	1.95	0.42
16	03/03/2012	RoR 20m/yr-180mm-280mm Layer 1 Fine	33.95	5.55	39.50	39.50	0.0011	0.0054	0.014	0.021	0.1	100	82	19.09	1.26	0.18
17	03/03/2012	RoR 20m/yr-440mm-500mm Layer 2 Fine	40.93	5.89	46.82	46.82	0.00075	0.003	0.008	0.011	0.033	100	95	14.67	1.09	0.05
18	03/03/2012	RoR 20m/yr-700mm-775mm Layer 3 Fine	41.57	5.22	46.79	46.79	0.00075	0.004	0.0081	0.013	0.04	100	94	17.33	1.64	0.06
19	10/03/2012	RoR 20m/yr-30mm-60mm Layer 1 Coarse	5.20	4.62	9.82	9.82	0.011	0.072	0.011	0.13	0.2	100	30	11.82	3.63	0.70
20	10/03/2012	RoR 20m/yr-60mm-90mm Layer 1 Coarse	4.80	5.63	10.43	10.43	0.011	0.071	0.09	0.1	0.17	100	33	9.09	4.58	0.67
21	10/03/2012	RoR 20m/yr-90mm-120mm Layer 1 Coarse	6.00	5.70	11.70	11.70	0.011	0.07	0.09	0.1	0.18	100	38	9.09	4.45	0.62
22	10/03/2012	RoR 20m/yr-120mm-150mm Layer 1 Coarse	0.57	21.72	22.29	22.29	0.0064	0.043	0.07	0.08	0.2	100	46	12.50	3.61	0.54
23	10/03/2012	RoR 20m/yr-150mm-180mm Layer 1 Coarse	9.04	22.59	31.63	31.63	0.0032	0.019	0.045	0.06	0.13	100	70	18.75	1.88	0.30
24	10/03/2012	RoR 20m/yr-180mm-205mm Layer 1 Coarse	22.81	22.37	45.18	45.18	0.0015	0.0041	0.015	0.022	0.07	100	91	14.67	0.51	0.09
25	17/03/2012	RoR 20m/yr-205mm-220mm Layer 1 Fine	28.34	19.85	48.19	48.19	0.0005	0.004	0.008	0.011	0.031	100	96	22.00	2.91	0.04
26	17/03/2012	RoR 20m/yr-220mm-240mm Layer 1 Fine	44.30	5.23	49.53	49.53		0.003	0.006	0.01	0.023	100	98			0.02
27	17/03/2012	RoR 20m/yr-240mm-260mm Layer 1 Fine	46.55	2.39	48.94	48.94	0.0005	0.0028	0.006	0.0076	0.02	100	98	15.20	2.06	0.02
28	17/03/2012	RoR 20m/yr-260mm-280mm Layer 1/2 Mix	13.69	4.93	18.62	18.62	0.0045	0.04	0.085	0.1	0.02	100	48	22.22	3.56	0.52
29	17/03/2012	RoR 20m/yr-280mm-340mm Layer 2 Coarse	8.05	4.08	12.13	12.13	0.012	0.07	0.09	0.1	0.17	100	35	8.33	4.08	0.65
30	17/03/2012	RoR 20m/yr-340mm-360mm Layer 2 Coarse	8.54	7.73	16.27	16.27	0.013	0.06	0.08	0.095	0.16	100	46	7.31	2.91	0.54
31	23/04/2012	RoR 20m/yr-360mm-380mm Layer 2 Coarse	12.06	8.35	20.41	20.41	0.0031	0.037	0.07	0.081	0.14	100	55	26.13	5.45	0.45
32	23/04/2012	RoR 20m/yr-380mm-410mm Layer 2 Coarse	13.83	19.83	33.66	33.66	0.0021	0.02	0.038	0.045	0.12	100	73	21.43	4.23	0.27
33	23/04/2012	RoR 20m/yr-410mm-430mm Layer 2 Fine	34.37	7.35	41.72	41.72	0.001	0.008	0.02	0.03	0.09	100	87	30.00	2.13	0.13
34	23/04/2012	RoR 20m/yr-430mm-450mm Layer 2 Fine	42.32	1.61	43.93	43.93	0.001	0.0051	0.014	0.019	0.07	100	91	19.00	1.37	0.09
35	23/04/2012	RoR 20m/yr-450mm-470mm Layer 2 Fine	46.62	1.07	47.69	47.69	0.00095	0.004	0.0086	0.014	0.031	100	96	14.74	1.20	0.04
36	23/04/2012	RoR 20m/yr-470mm-490mm Layer 2 Fine	48.27	0.35	48.62	48.62	0.0008	0.0033	0.007	0.0095	0.027	100	97	11.88	1.43	0.03
37	31/03/2012	RoR 20m/yr-490mm-510mm Layer 2 Fine	44.58	0.23	44.81	44.81	0.00095	0.0041	0.008	0.011	0.07	100	91	11.58	1.61	0.09
38	31/03/2012	RoR 20m/yr-510mm-530mm Layer 2 Fine	16.27	1.50	17.77	17.77	0.0021	0.04	0.09	0.11	0.2	100	48	52.38	6.93	0.52

Test No.	Date	Material Description	63um Wash Material	Pan Material	Total -63um material	Hydrometer Sample	Gradation Parameters (Percentiles)					Finer Than	Finer Than	Cu	Cc	Grading Modulus (GM)
						Concentration	D_{10}	D_{30}	D_{50}	D_{60}	D_{90}	0.425mm	0.075mm	d_{60}/d_{10}	$d^2_{30}/d_{60}d_{10}$	(P2mm+P425μm+P75μm)
			(g)	(g)	(g)	(g/L)	(mm)	(mm)	(mm)	(mm)	(mm)					
39	31/03/2012	RoR 10m/yr-30mm-50mm Layer 1 Coarse	4.48	16.67	21.15	21.15	0.06	0.09	0.13	0.14	0.21	100	23	2.33	0.96	0.77
40	14/04/2012	RoR 10m/yr-50mm-80mm Layer 1 Coarse	0.23	2.77	3.00	3.00	0.065	0.09	0.11	0.12	0.2	100	20	1.85	1.04	0.80
41	14/04/2012	RoR 10m/yr-80mm-110mm Layer 1 Coarse	5.10	1.08	6.18	6.18	0.009	0.07	0.11	0.12	0.2	100	36	13.33	4.54	0.64
42	14/04/2012	RoR 10m/yr-110mm-165mm Layer 1 Coarse	5.46	2.70	8.16	8.16	0.023	0.075	0.1	0.11	0.17	100	30	4.78	2.22	0.70
43	14/04/2012	RoR 10m/yr-165mm-190mm Layer 1 Fine	48.67	0.04	48.71	48.71	0.0007	0.004	0.0085	0.0105	0.024	100	97	15.00	2.18	0.03
44	14/04/2012	RoR 10m/yr-190mm-220mm Layer 2 Coarse	3.53	1.11	4.64	4.64	0.065	0.09	0.12	0.14	0.2	100	20	2.15	0.89	0.80
45	14/04/2012	RoR 10m/yr-220mm-250mm Layer 2 Coarse	3.84	1.21	5.05	5.05	0.06	0.085	0.11	0.13	0.2	100	25	2.17	0.93	0.75
46	19/04/2012	RoR 10m/yr-250mm-280mm Layer 2 Coarse	3.07	1.61	4.68	4.68	0.06	0.09	0.11	0.12	0.2	100	17	2.00	1.13	0.83
47	19/04/2012	RoR 10m/yr-280mm-300mm Layer 2 Coarse	3.92	2.17	6.09	6.09	0.06	0.08	0.1	0.11	0.18	100	23	1.83	0.97	0.77
48	19/04/2012	RoR 10m/yr-300mm-320mm Layer 2 Fine	48.30	0.37	48.67	48.67	0.001	0.0044	0.009	0.013	0.03	100	97	13.00	1.49	0.03
49	19/04/2012	Full Depth Deposition 15mm-50mm	7.65	2.50	10.15	10.15	0.01	0.072	0.1	0.12	0.2	99	31	12.00	4.32	0.70
50	19/04/2012	Full Depth Deposition 50mm-85mm	8.34	2.82	11.16	11.16	0.018	0.07	0.09	0.105	0.17	100	35	5.83	2.59	0.65
51	19/04/2012	Full Depth Deposition 85mm-115mm	8.35	3.11	11.46	11.46	0.012	0.07	0.094	0.11	0.17	100	35	9.17	3.71	0.65
52	24/04/2012	Full Depth Deposition 115mm-145mm	6.58	3.65	10.23	10.23	0.015	0.07	0.09	0.09	0.16	100	35	6.00	3.63	0.65
53	24/04/2012	Full Depth Deposition 145mm-170mm	7.03	4.29	11.32	11.32	0.023	0.07	0.09	0.1	0.15	100	37	4.35	2.13	0.63
54	24/04/2012	Full Depth Deposition 170mm-205mm	8.91	4.54	13.45	13.45	0.01	0.065	0.085	0.092	0.14	100	42	9.20	4.59	0.58
55	24/04/2012	Full Depth Deposition205mm-230mm	8.03	6.16	14.19	14.19	0.013	0.065	0.083	0.092	0.14	100	42	7.08	3.53	0.58
56	24/04/2012	Full Depth Deposition230mm-265mm	9.98	6.51	16.49	16.49	0.013	0.055	0.08	0.09	0.14	100	48	6.92	2.59	0.52
57	24/04/2012	Full Depth Deposition 265mm-300mm	13.03	8.23	21.26	21.26	0.009	0.05	0.07	0.08	0.15	100	55	8.89	3.47	0.45
58	27/04/2012	Full Depth Deposition 300mm-340mm	13.62	14.47	28.09	28.09	0.0061	0.037	0.055	0.07	0.13	100	66	11.48	3.21	0.34
59	27/04/2012	Full Depth Deposition 340mm-370mm	17.82	16.54	34.36	34.36	0.0046	0.03	0.041	0.051	0.12	100	75	11.09	3.84	0.25
60	27/04/2012	Full Depth Deposition 370mm-415mm	23.48	16.71	40.19	40.19	0.0022	0.021	0.032	0.04	0.1	100	84	18.18	5.01	0.16
61	27/04/2012	Full Depth Deposition415mm-450mm	24.94	18.45	43.39	43.39	0.0011	0.01	0.023	0.03	0.075	100	90	27.27	3.03	0.10
62	27/04/2012	Full Depth Deposition450mm-480mm	42.02	6.72	48.74	48.74	0.001	0.0062	0.015	0.021	0.042	100	97	21.00	1.83	0.03
63	27/04/2012	Full Depth Deposition 480mm-510mm	45.44	4.34	49.78	49.78	0.0011	0.0046	0.011	0.016	0.04	100	99	14.55	1.20	0.01
64	27/04/2012	Full Depth Deposition 510mm-540mm	48.31	1.27	49.58	49.58	0.0011	0.004	0.008	0.012	0.034	100	99	10.91	1.21	0.01
65	27/04/2012	Full Depth Deposition540mm-570mm	49.38	0.41	49.79	49.79	0.001	0.004	0.008	0.011	0.025	100	99	11.00	1.45	0.01
66	27/04/2012	Full Depth Deposition 570mm-600mm	49.65	0.18	49.83	49.83	0.00085	0.004	0.0071	0.01	0.028	100	99	11.76	1.88	0.01
67	27/04/2012	Full Depth Deposition600mm-640mm	49.64	0.17	49.81	49.81	0.0009	0.0035	0.0061	0.009	0.028	100	100	10.00	1.51	0.00
68	27/04/2012	Full Depth Deposition640mm670mm	49.87	0.01	49.88	49.88	0.0009	0.0031	0.006	0.008	0.023	100	99	8.89	1.33	0.01
69	27/04/2012	Full Depth Deposition 670mm-700mm	49.84	0.03	49.87	49.87	0.0007	0.0031	0.006	0.008	0.02	100	100	11.43	1.72	0.00
70	07/05/2012	Full Depth Deposition 700mm-724mm	49.52	0.02	49.54	49.54	0.0008	0.0027	0.005	0.0061	0.014	100	99	7.63	1.49	0.01
71	07/05/2012	Black Cotton Soil for comparison purposes	38.46	0.52	38.98	38.98			0.00095	0.005	0.14	94	85			0.21
72	07/05/2012	Ina Mari Sample Coarse 0mm-155mm	4.59	4.09	8.68	8.68	0.0015	0.0065	0.015	0.02	0.051	100	95	13.33	1.41	0.05
73	07/05/2012	Ina Mari Sample fine/Coarse Mix 155mm-233mm	13.47	6.38	19.85	19.85	0.005	0.03	0.05	0.065	0.12	99	51	13.00	2.77	0.50
74	07/05/2012	Ina Mari Sample fine/Coarse Mix 466mm-620mm	21.25	7.89	29.14	29.14	0.0068	0.047	0.075	0.086	0.13	98	50	12.65	3.78	0.52
75	07/05/2012	Ina Mari Sample Fine 620mm-698mm	43.85	2.78	46.63	46.63	0.041	0.075	0.09	0.105	0.16	98	30	2.56	1.31	0.72
76	11/05/2012	Settling Column Control Sample 0mm-100mm	6.72	3.37	10.09	10.09	0.035	0.07	0.09	0.1	0.15	99	35	2.86	1.40	0.66
77	11/05/2012	Settling Column Control Sample 100mm-150mm	6.35	4.77	11.12	11.12	0.025	0.07	0.09	0.1	0.15	99	35	4.00	1.96	0.66
78	11/05/2012	Settling Column Control Sample 200mm-250mm	8.68	6.04	14.72	14.72	0.013	0.06	0.08	0.09	0.12	100	46	6.92	3.08	0.54
79	11/05/2012	Settling Column Control Sample 250mm-300mm	8.26	12.19	20.45	20.45	0.025	0.052	0.07	0.08	0.13	100	55	3.20	1.35	0.45
80	11/05/2012	Settling Column Control Sample 300mm-350mm	27.72	13.62	41.34	41.34	0.005	0.021	0.031	0.04	0.09	100	87	8.00	2.21	0.13
81	11/05/2012	Settling Column Control Sample 350mm-400mm	44.88	3.28	48.16	48.16	0.0012	0.005	0.011	0.017	0.05	100	97	14.17	1.23	0.03
82	14/05/2012	No Dispersant-Black Cotton Soil	35.82	0.68	36.50	36.50		0.004	0.012	0.022	0.2	95	81			0.24
83	14/05/2012	No Dispersant-Full Depth 700mm-724mm	49.34	0.03	49.37	49.37	0.0095	0.01	0.011	0.012	0.017	100	100	1.26	0.88	0.00
84	14/05/2012	No Dispersant-Full Depth 50mm-85mm	7.68	2.85	10.53	10.53	0.026	0.07	0.095	0.11	0.18	100	32	4.23	1.71	0.68
85	14/05/2012	No Dispersant-ina Mari Sample	17.31	6.03	23.34	23.34	0.0065	0.033	0.065	0.08	0.15	96	55	12.31	2.09	0.49
86	14/05/2012	No Dispersant-Cyclone Underflow	10.86	3.33	14.19	14.19	0.015	0.05	0.055	0.06	0.11	100	76	4.00	2.78	0.24
87	14/05/2012	No Dispersant-Catwalk Fines	31.47	3.32	34.79	34.79	0.0012	0.005	0.011	0.016	0.05	100	96	13.33	1.30	0.04
88	11/05/2009	Crown Penstock Tailings	97.97	0.64	98.61	98.61	0.0015	0.004	0.008	0.0095	0.029	100	100	6.33	1.12	0.00

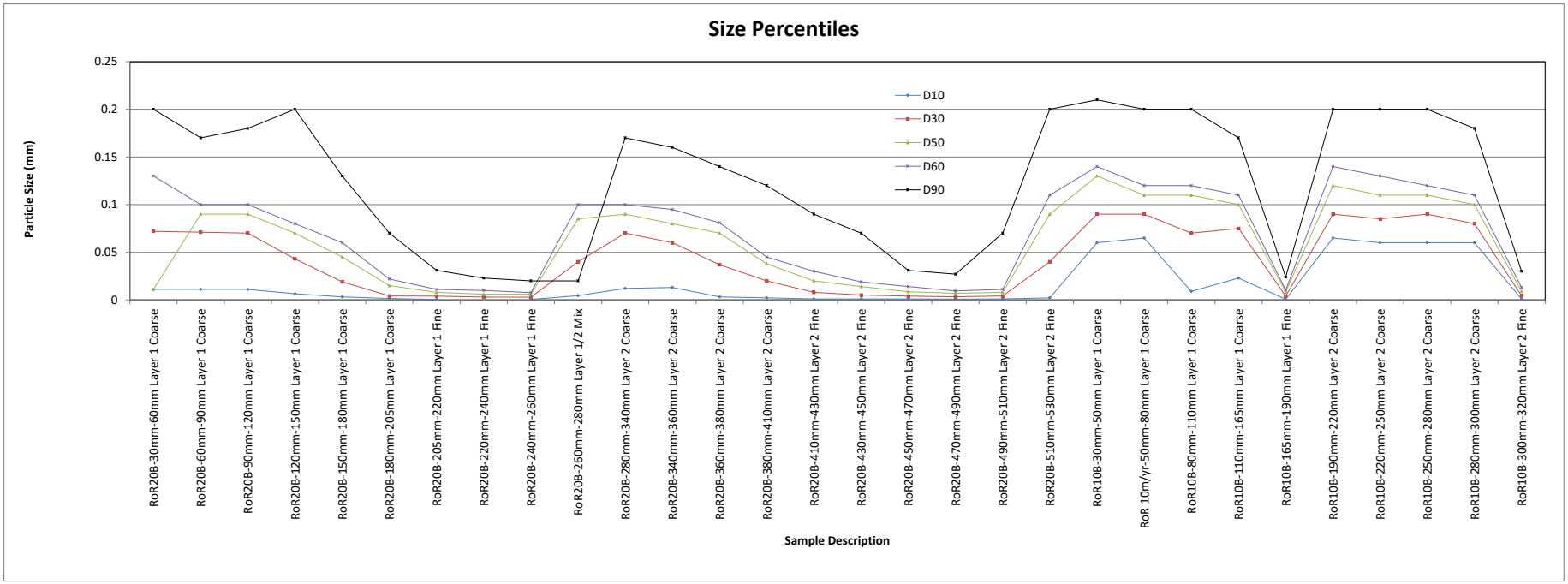

Figure H9: Size percentiles comparisons: source samples, complementary samples and Experiments FDB, RoR20B, RoR10B and RoR 10m/yr without permeability test samples.

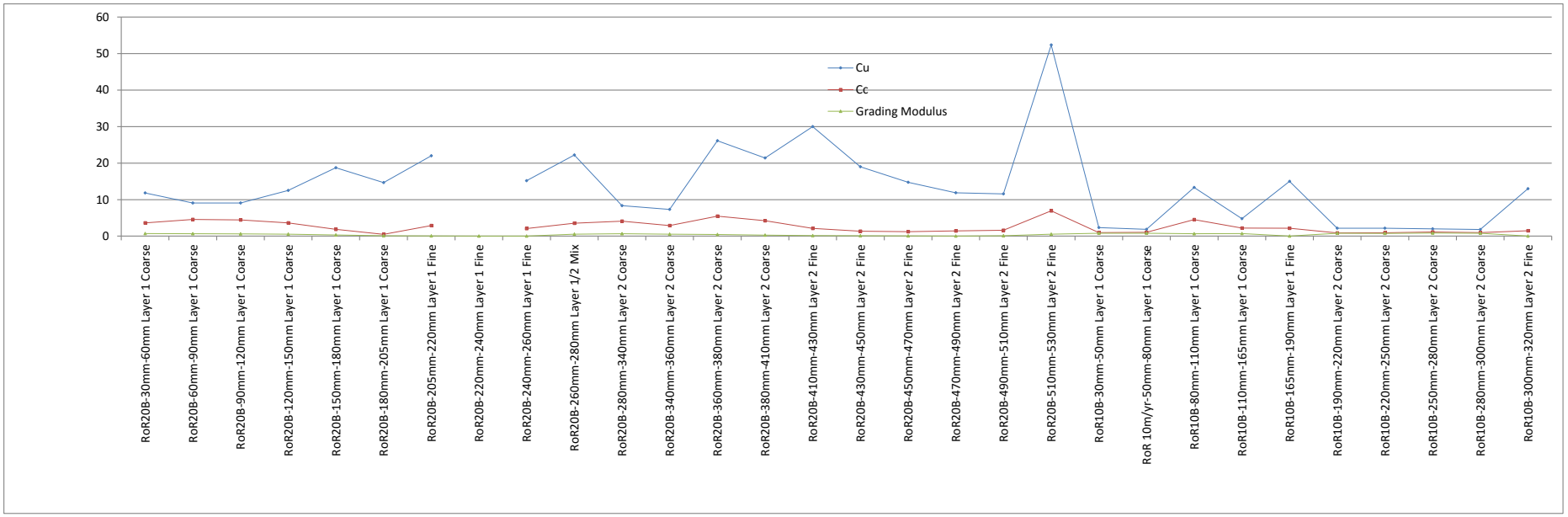

Figure H10: Coefficient of uniformity (C_u), coefficient of gradation (C_z) and grading modulus (GM) comparisons: source samples, complementary samples and Experiments FDB, RoR20B, RoR10B and RoR 10m/yr without permeability test samples.

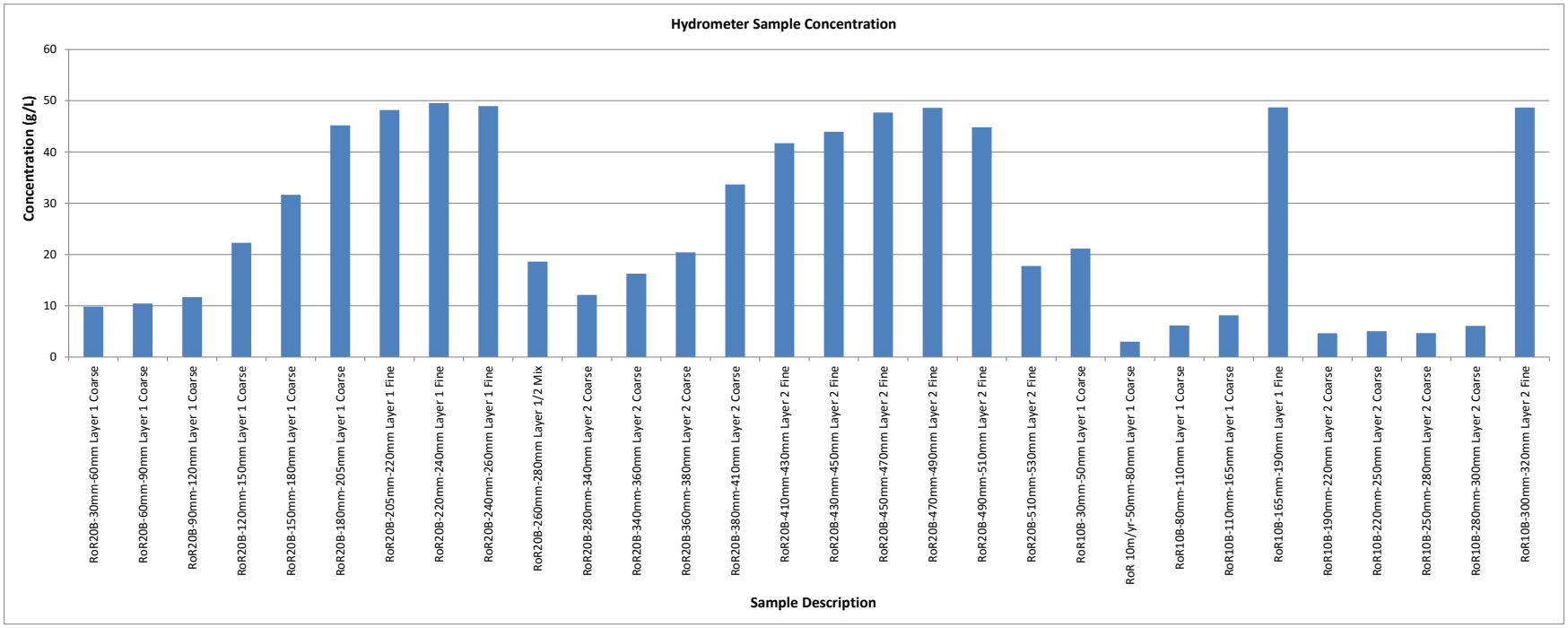

Figure H11: Hydrometer sample concentration comparisons

APPENDIX I

Specific Gravity of Solids and Mineralogy

The appendix reports values of specific gravity of the solids for experiment samples (including sieved and dispersant treated size fractions) and Experiment FDB recovered samples. The variation of specific gravity with column height as well as comparison of values obtained from different methods (density bottle, AccPyc gas displacement pycnometer and XRD data estimates) are also listed.

XRD and XRF based mineralogy and their variation with column height are shown. The order of presentation is listed below.

I1 Specific Gravity of Solids

Table I1: Gold tailings specific gravity of solids results.

Sample Description	Method of Particle Density Determination, ρs ((Mg/m3)		
	Density Bottle Method	AccuPyc 1340 II Gas Pycnometer	XRD Data Estimate
Chemwes Dam 5 Catwalk fines	2.7135	2.7301	2.711391
Chemwes Dam 5 Underflow 2010 Sample	2.6705		2.690915
Chemwes Dam 5 Underflow 2011 Sample	2.6660		2.659354
Chemwes Dam 5 Penstock Tailings	2.7632		
Chemwes Dam 5 Overflow	2.7303		
Chemwes Dam 5 Whole Tailings	2.7087		
Crown Penstock Tailings	2.7463		
Full Depth 700-724mm	2.7936	2.7674	2.716161
Sediment 670mm - 700mm		2.7598	
Sediment 640mm - 670mm		2.7485	
Full Depth 600mm-640mm		2.7749	2.733668
Full Depth 570mm-600mm	2.7109	2.7515	
Sediment 540mm - 570mm		2.7368	
Sediment 510mm - 540mm		2.7337	
Full Depth 480mm-510mm	2.7157	2.7568	2.717999
Sediment 450mm -480mm		2.7153	
Sediment 415mm -450mm		2.728	
Sediment 370mm -415mm		2.7282	
Full Depth 340mm-370mm	2.7128	2.7315	2.694872
Full Depth 300mm-340mm	2.6807	2.7123	
Sediment 265mm - 300mm		2.7072	
Sediment 230mm -265mm		2.7081	
Full Depth 205mm-230mm		2.7299	2.696029
Full Depth 170mm-205mm	2.6462	2.709	
Sediment 145mm - 170mm		2.7099	
Sediment 115mm - 145mm		2.7043	
Full Depth 85mm-115mm	2.6889	2.7139	2.691126
Full Depth 50mm-85mm	2.7020	2.7102	2.688065
Full Depth 15mm-50mm		2.7036	2.682097
Black Cotton Soil	2.6292		
Chemwes Dam 5 Catwalk fines	2.7135	2.7301	2.711391
Full Depth 700-724mm	2.7936	2.7674	2.716161
Full Depth 480mm-510mm	2.7157	2.7568	2.717999
Full Depth 340mm-370mm	2.7128	2.7315	2.694872
Full Depth 85mm-115mm	2.6889	2.7139	2.691126
Full Depth 50mm-85mm	2.7020	2.7102	2.688065

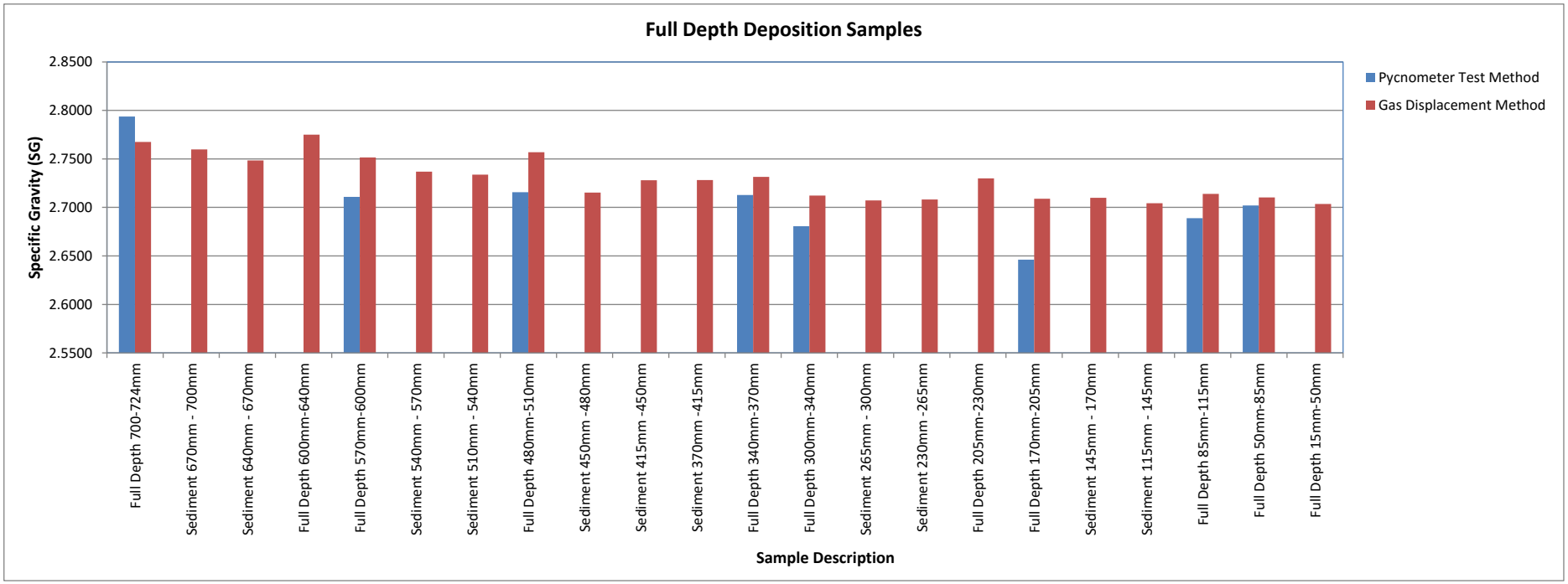

Figure I4: Experiment FDB comparisons of specific gravity of solids determined by different methods: density bottle, and AccuPyc 1340 II gas displacement method

I2 XRD and XRF Derived Mineralogy

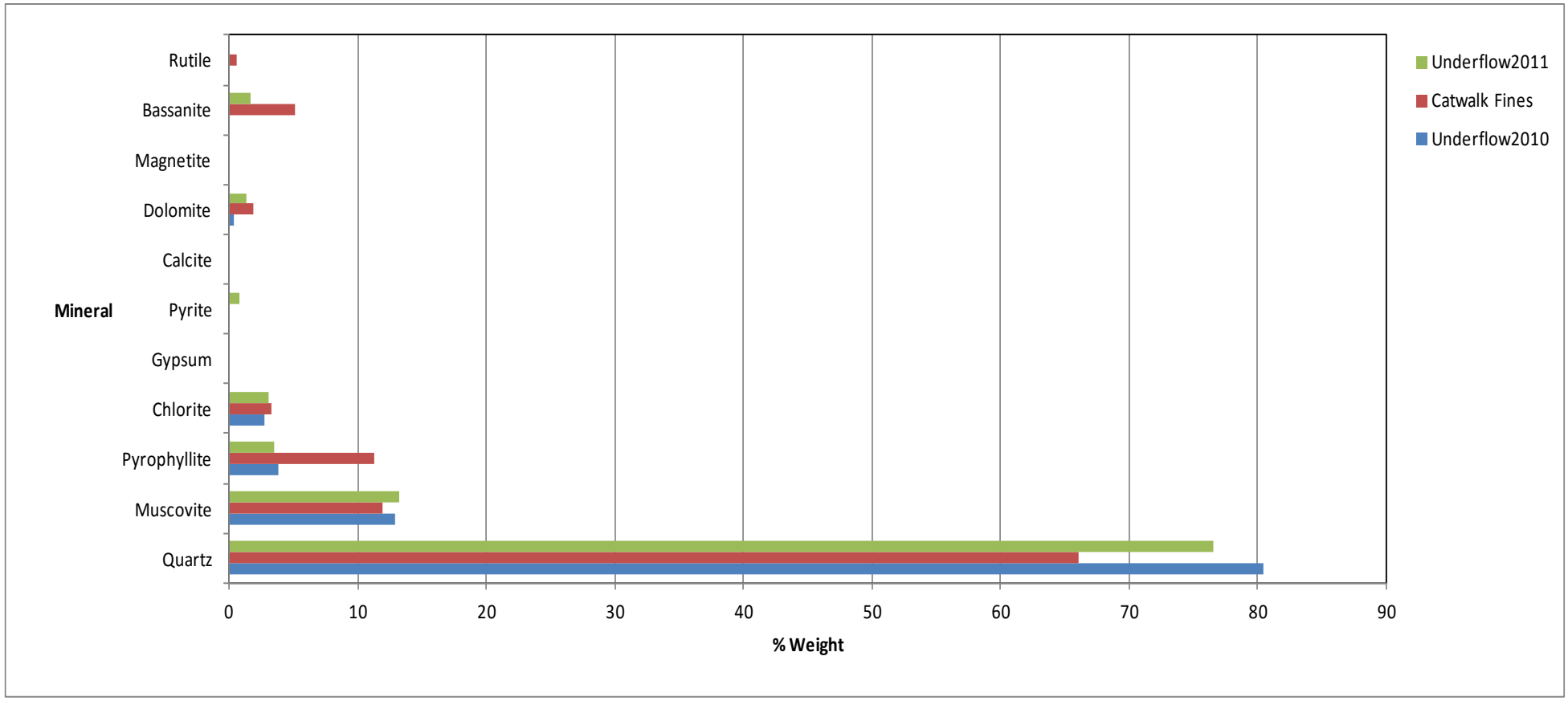

Figure I5: Tailings dam experiment samples XRD derived minerals comparisons

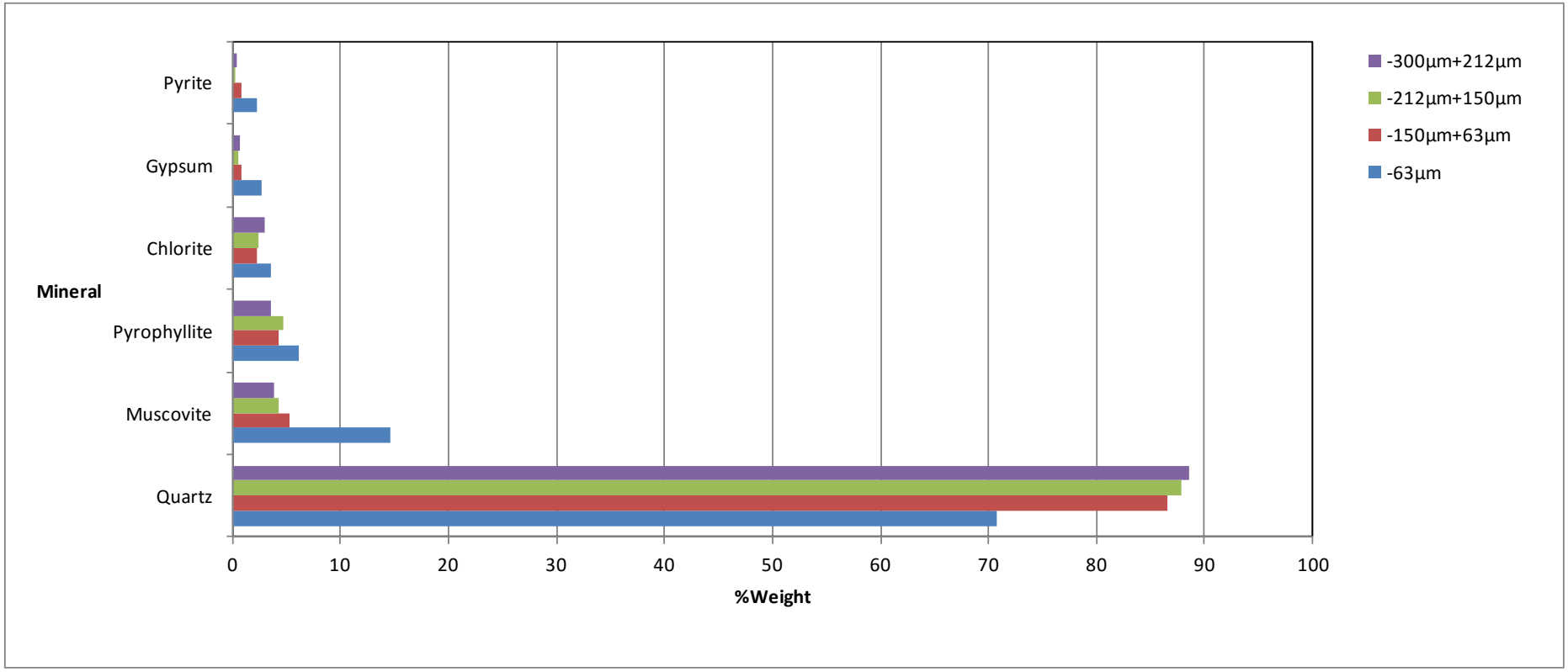

Figure I6: Tailings dam experiment samples XRD derived minerals comparisons of sieved and dispersant treated sample specimen

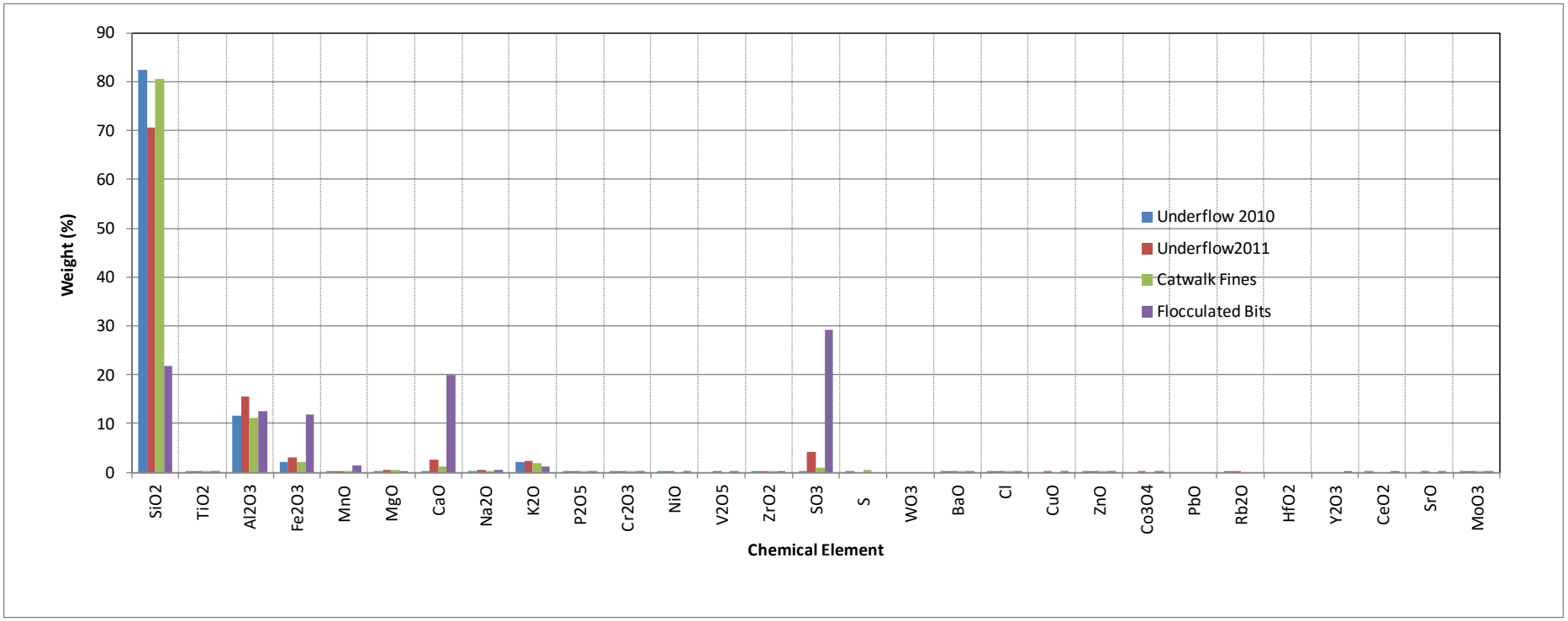

Figure I7: Tailings dam experiment samples XRF derived oxides of minerals comparisons

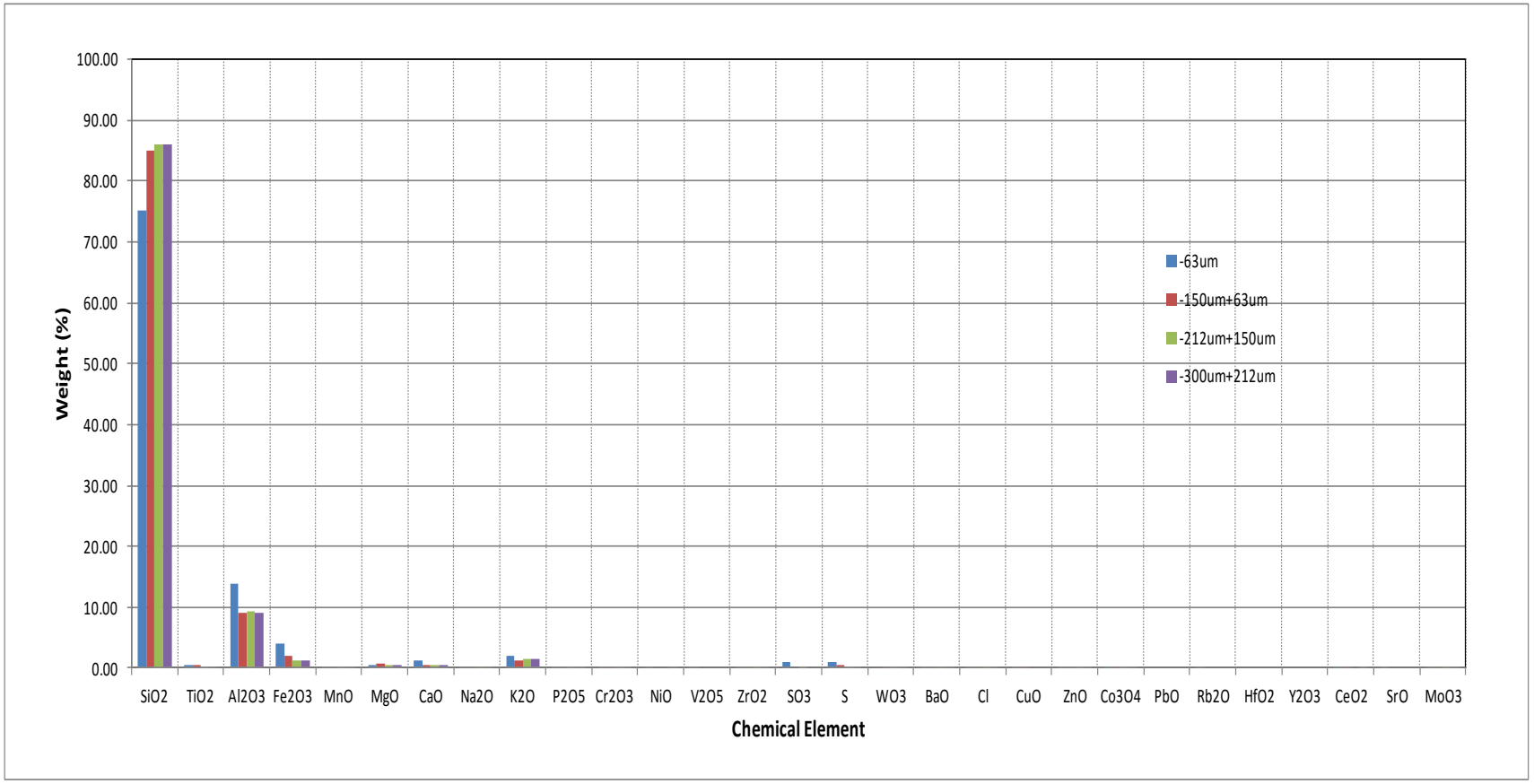

Figure I8: Tailings dam experiment samples XRF derived oxides of minerals comparisons of sieved and dispersant treated sample specimen

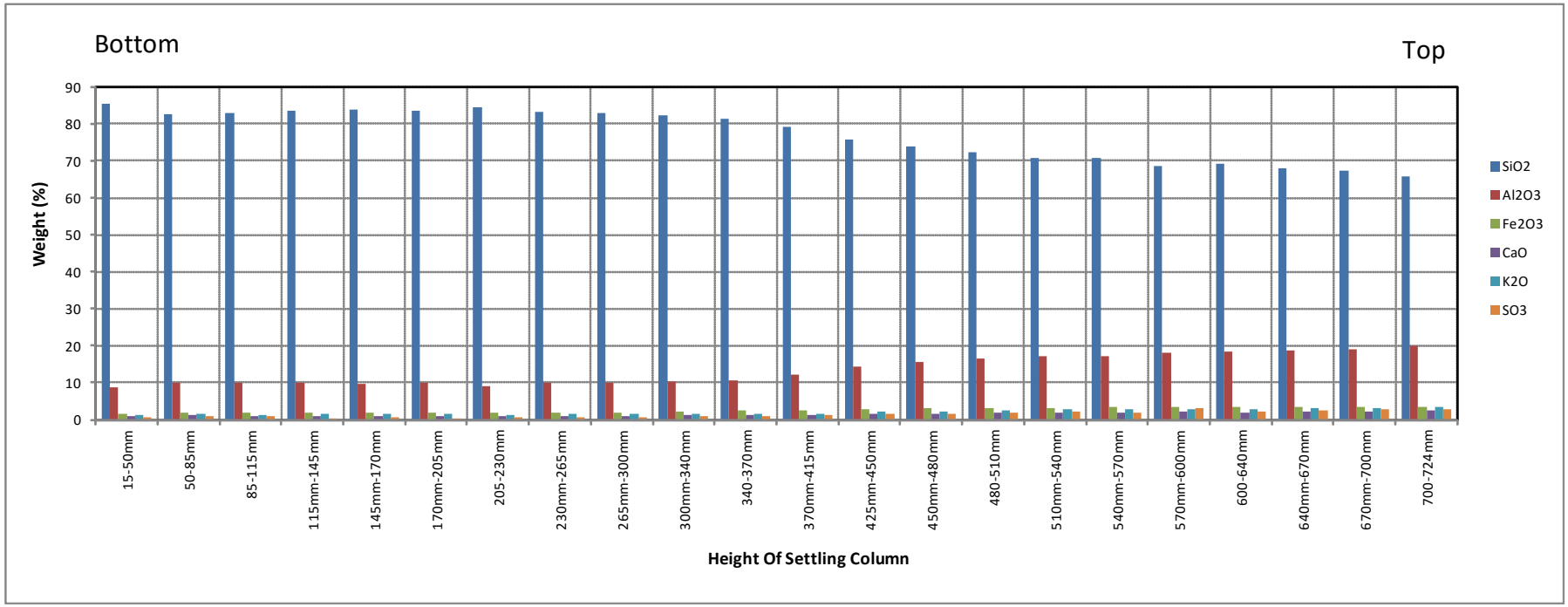

Figure I11: Experiment FDB depth profile samples XRF derived oxides of minerals comparisons

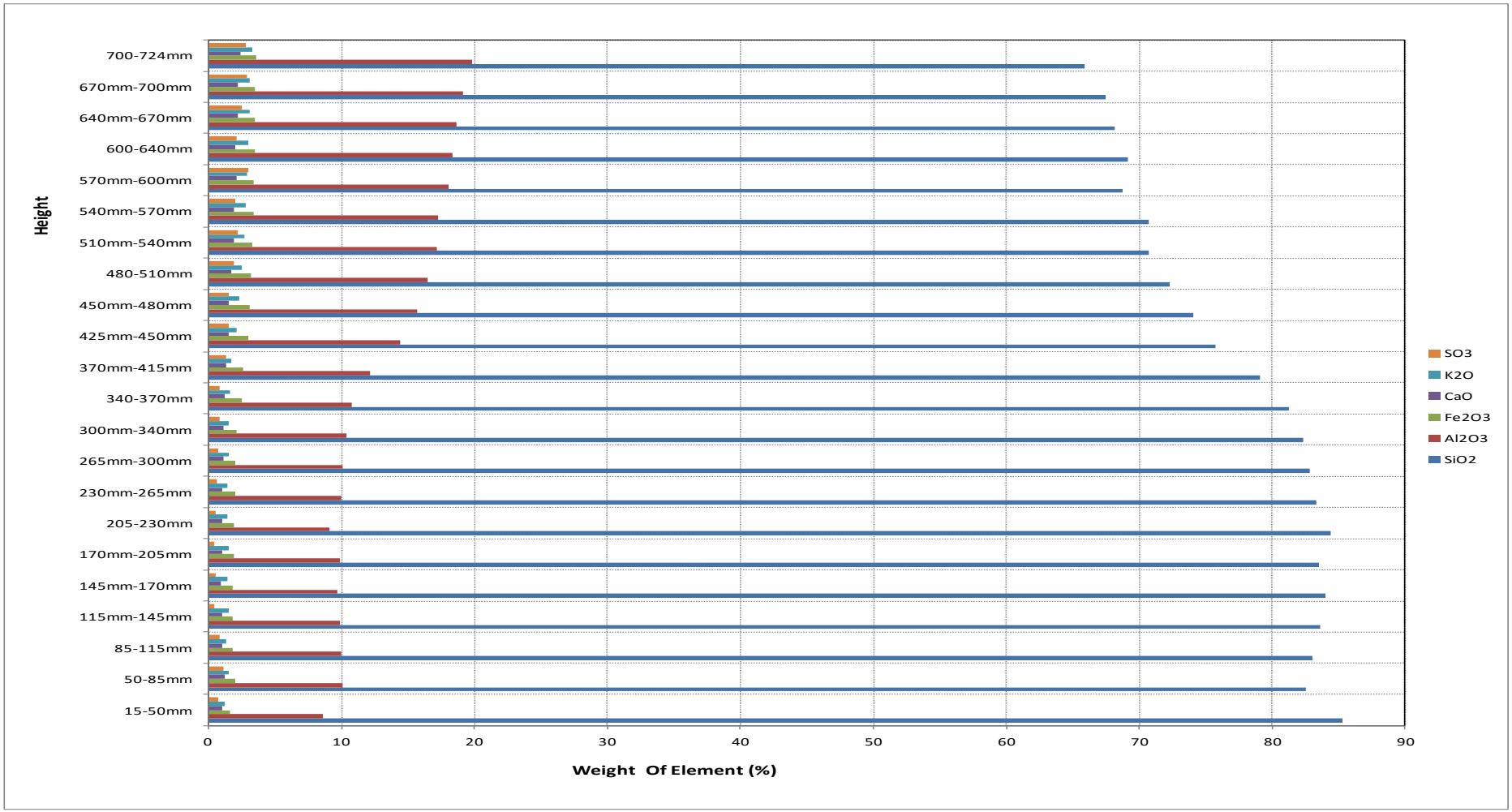

Figure I12: Experiment FDB depth profile samples XRF derived oxides of minerals comparisons

APPENDIX J

SEM Micrographs

The appendix provides a summary of SEM micrographs recovered from Experiments FDB, RoR20B, RoR10B and RoR 10m/yr without permeability test. The appendix presents horizontal and vertical prints side by side for purposes of comparing the different fabric shown in the micrographs.

The appendix contains the following SEM micrographs:

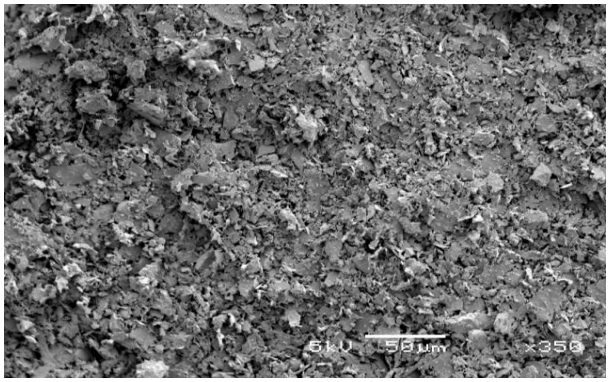

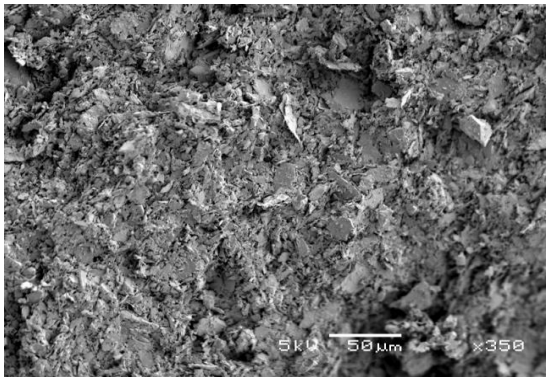

Height 700mm-724mm

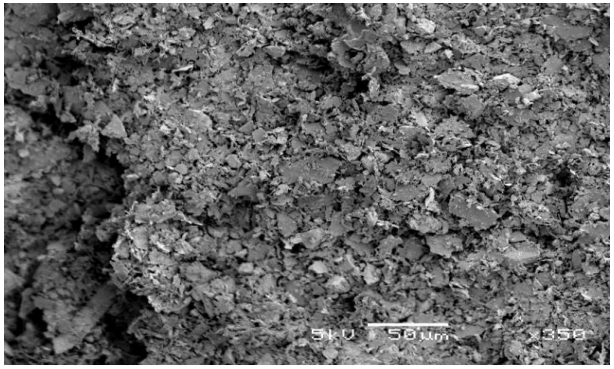

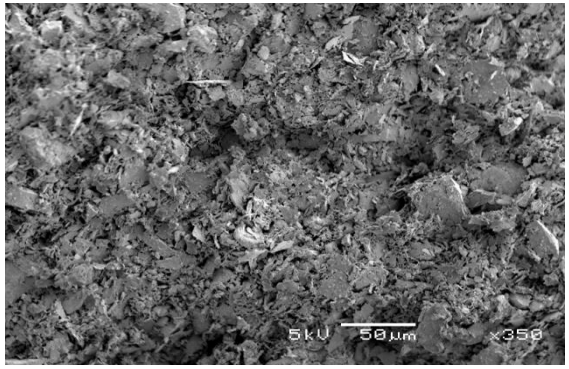

Height 670mm-700mm

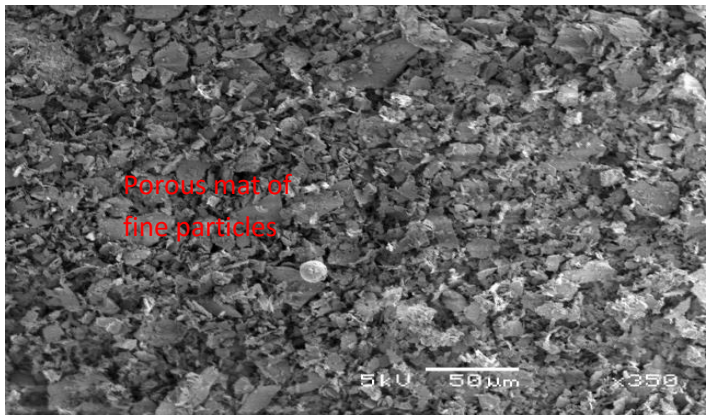

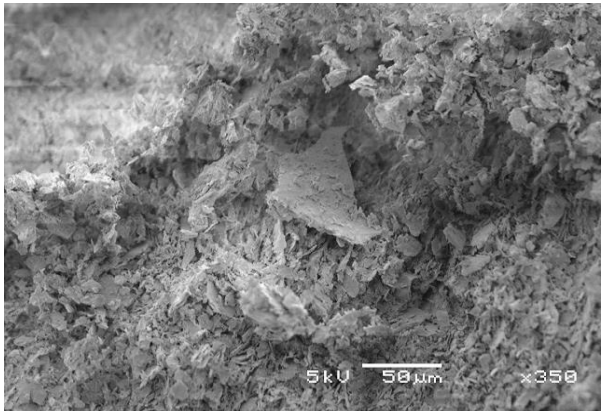

Height 640mm-670mm

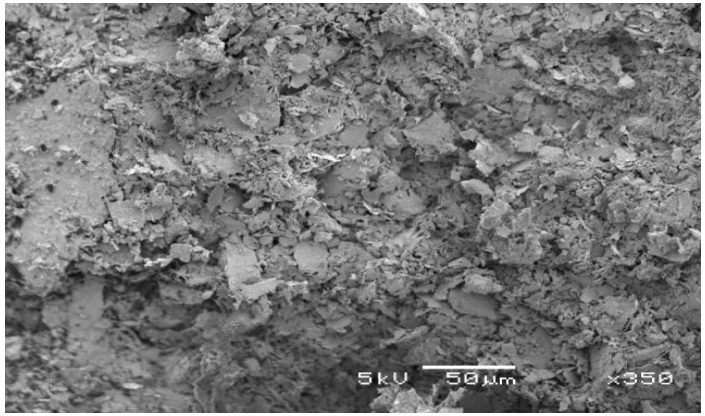

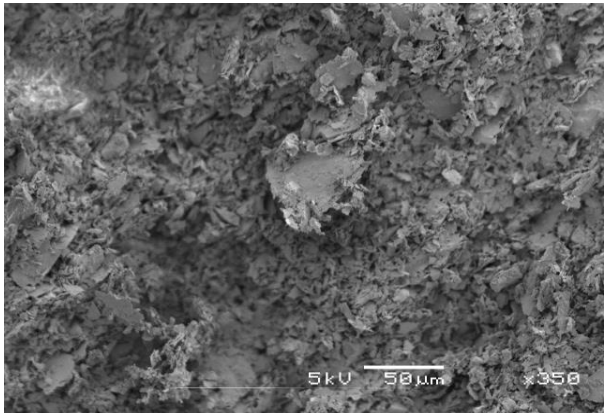

Height 600mm-640mm

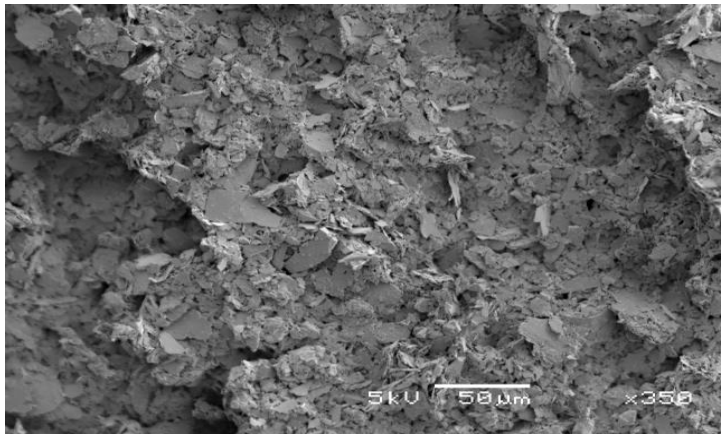

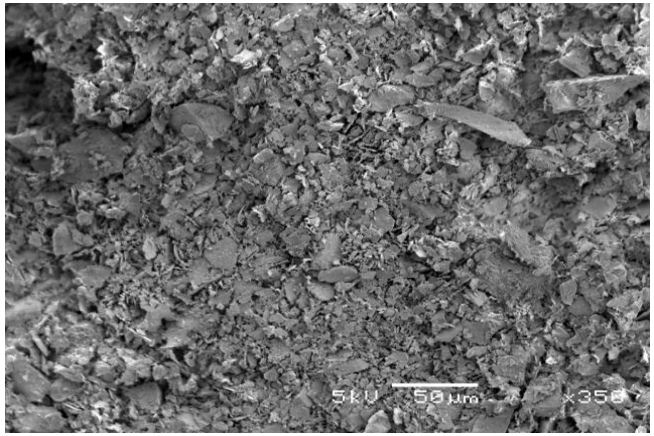

Height 570mm-600mm

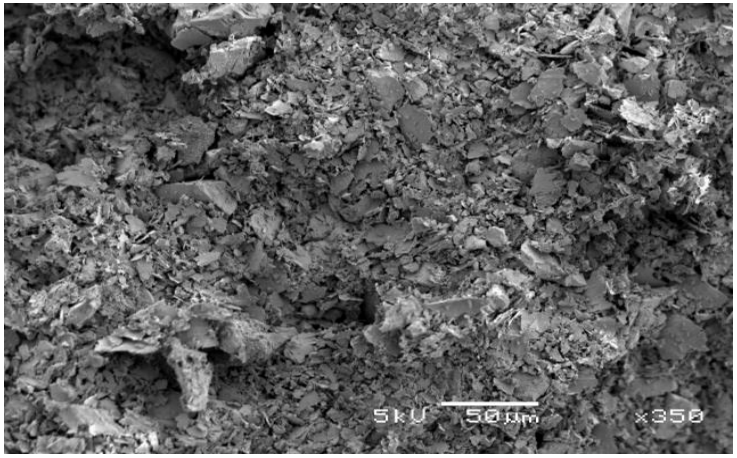

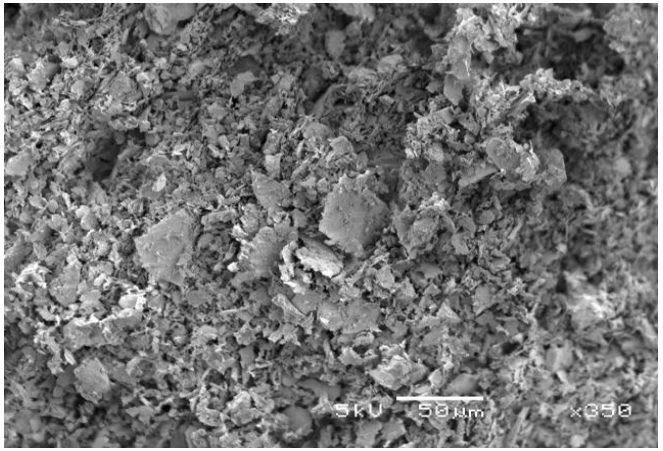

Height 540mm-570mm

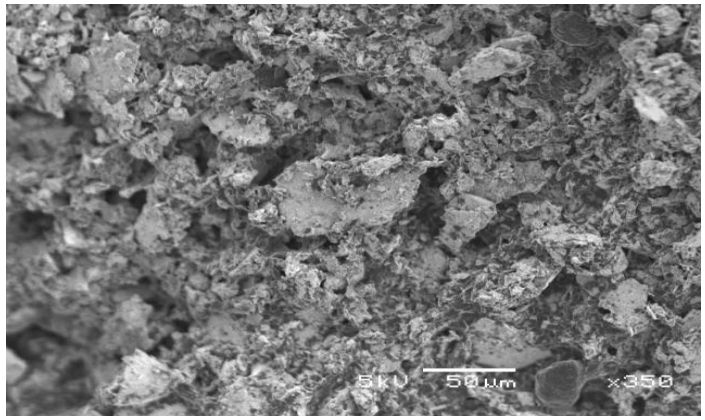

Height 510mm-540mm

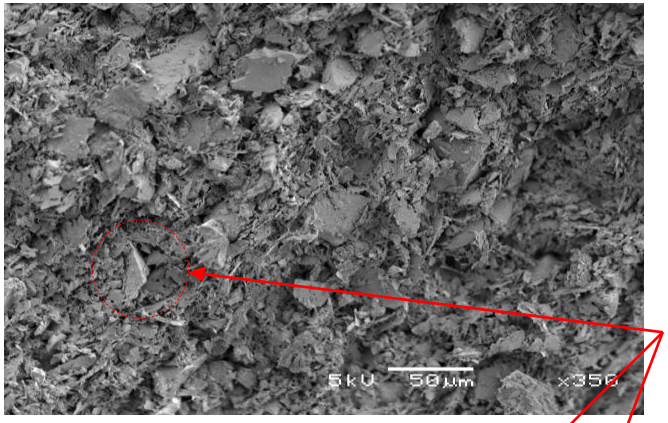

Isolated vertically aligned elongated particles

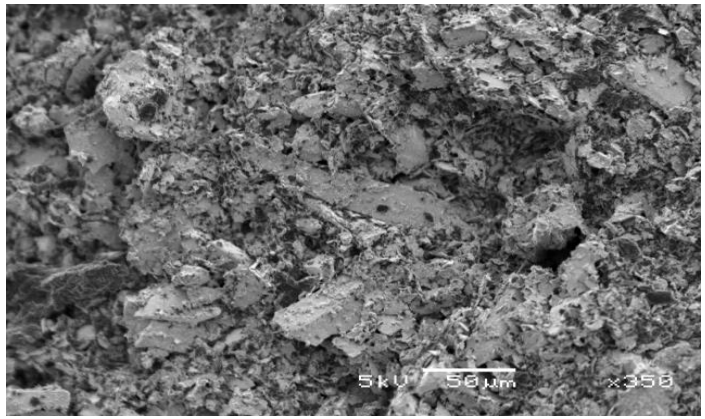

Height 480mm-510mm

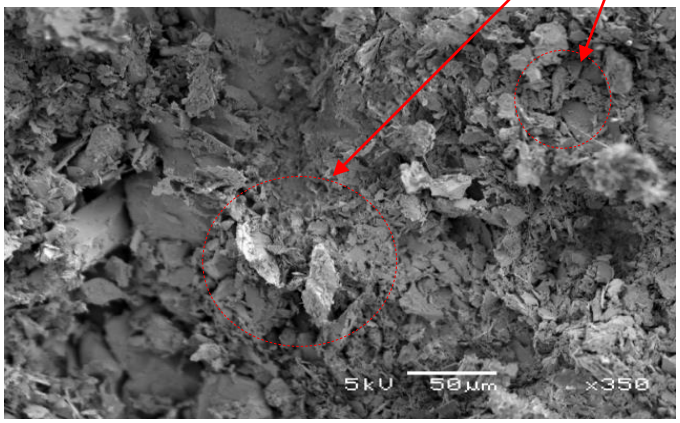

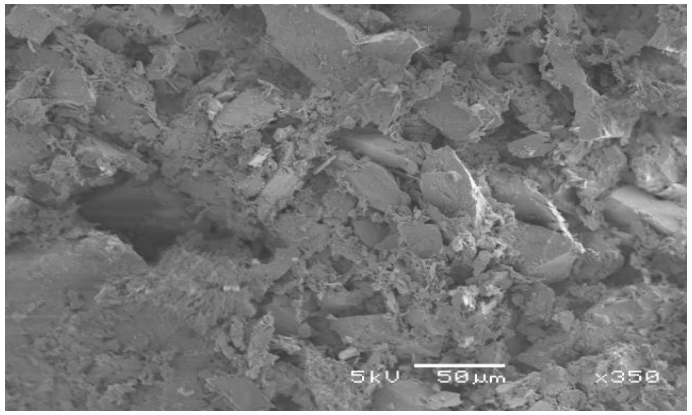

Height 450mm-480mm

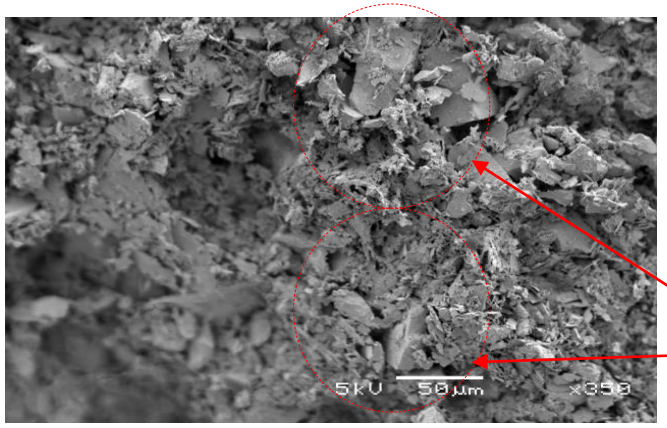

Vertically aligned elongated particles

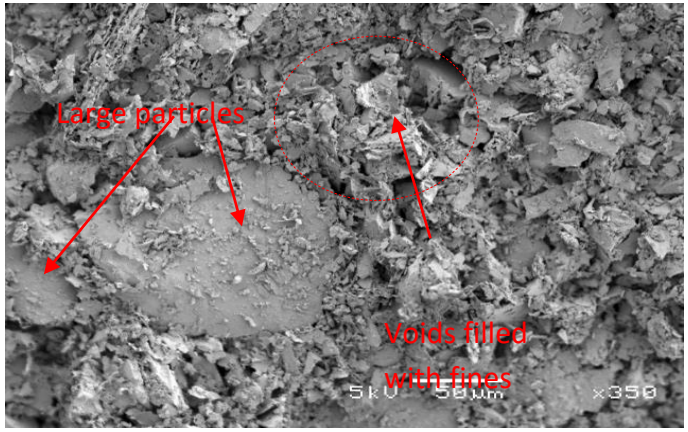

Height 415mm-450mm

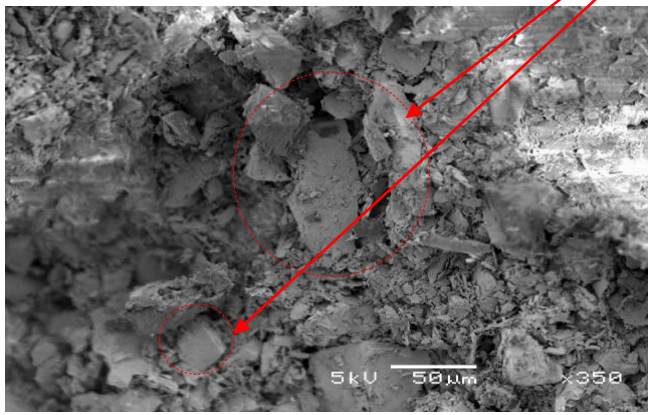

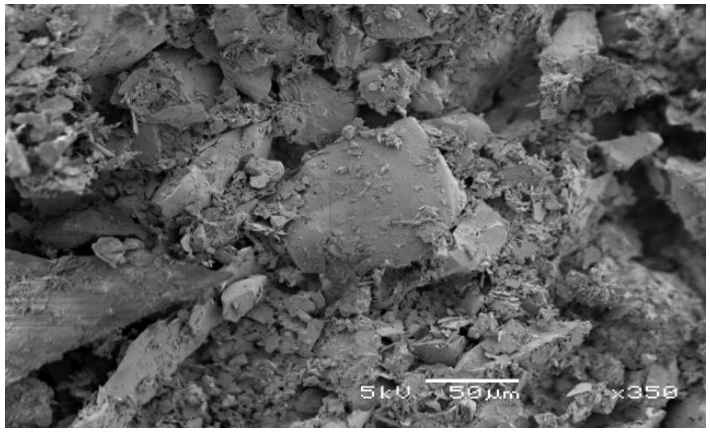

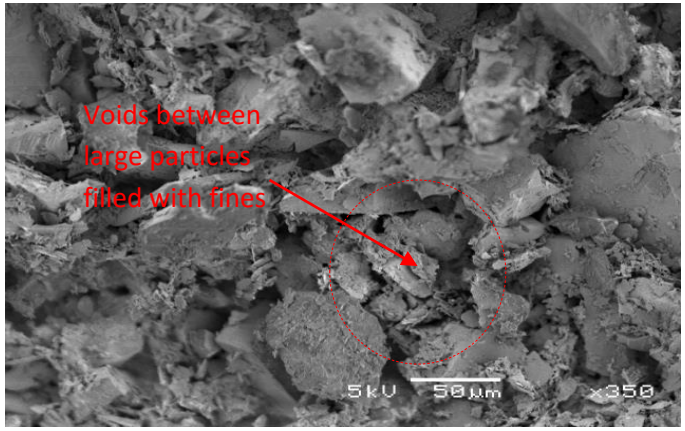

Height 370mm-415mm

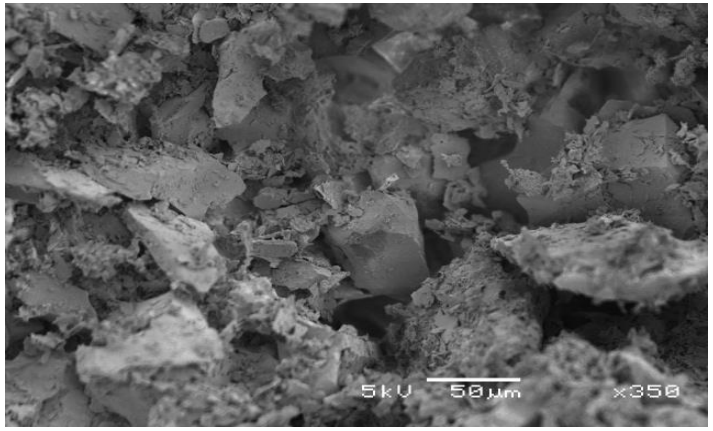

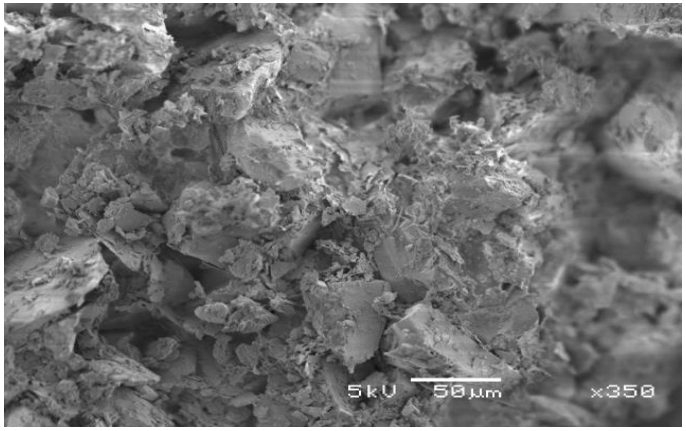

Height 340mm-370mm

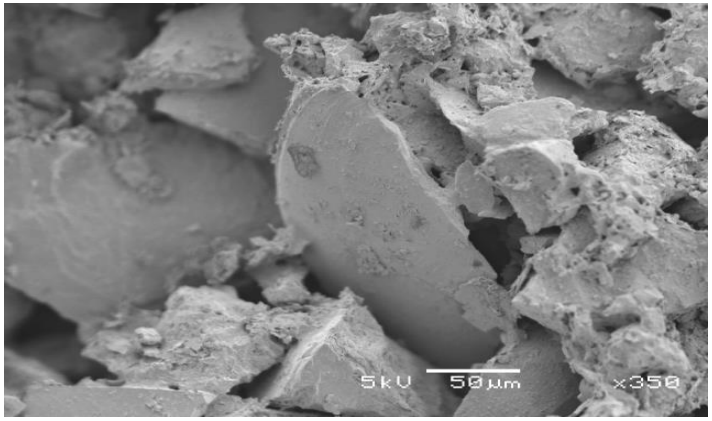

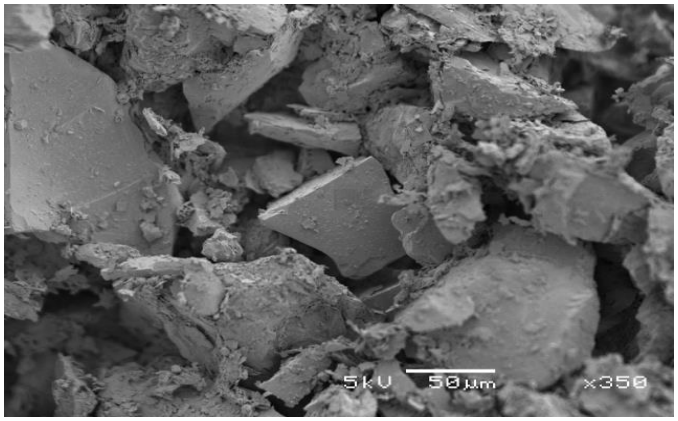

Height 230mm-265mm

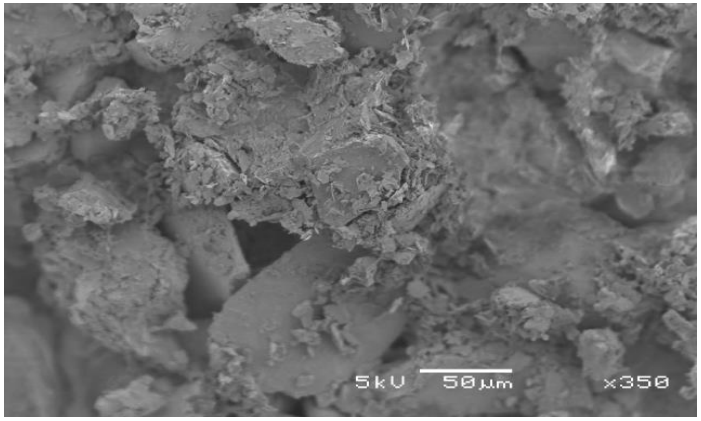

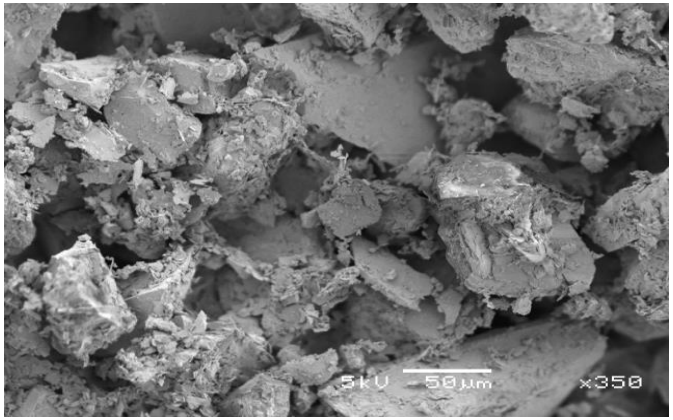

Height 205mm-230mm

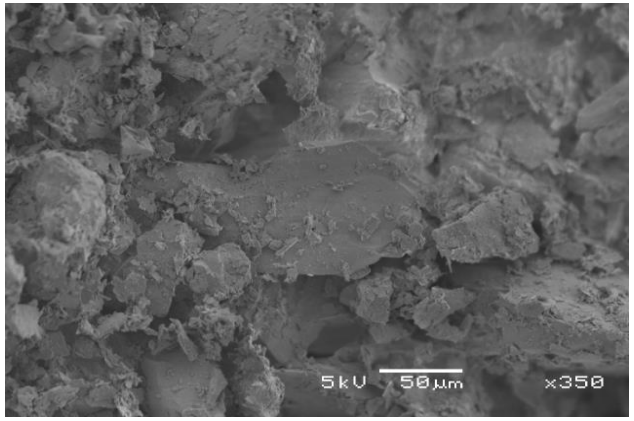

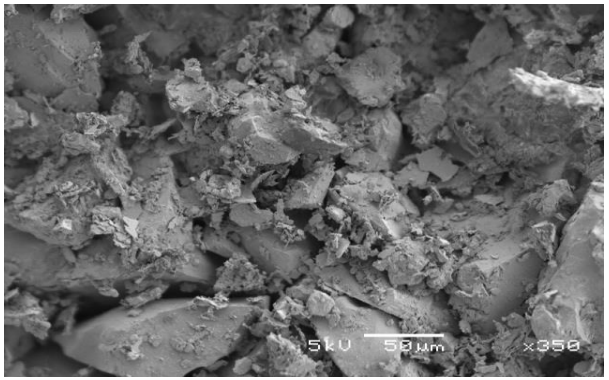

Height 170mm-205mm

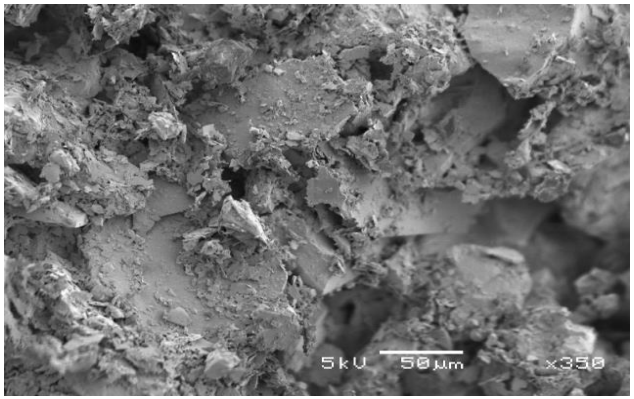

Height 145mm-170mm

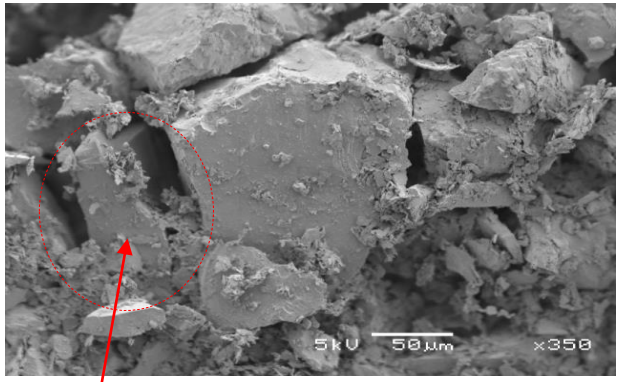

Vertically aligned
elongated particle

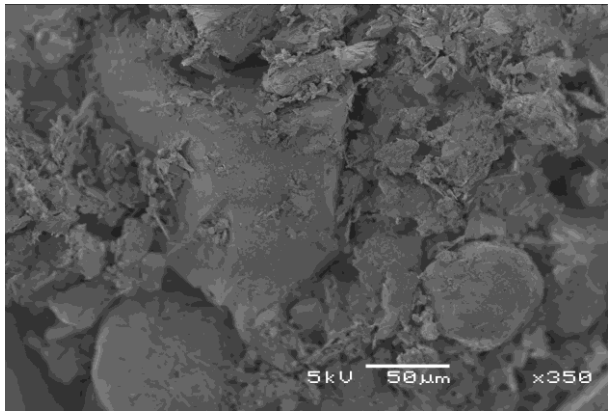

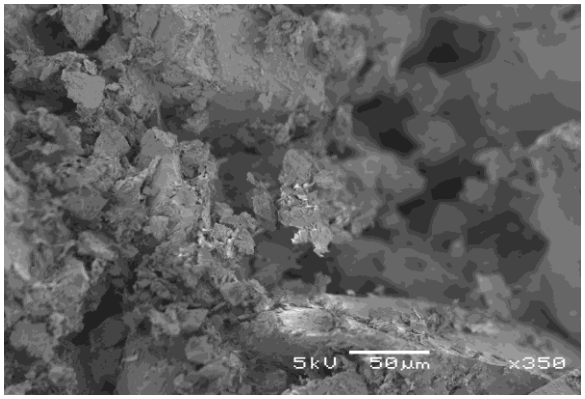

Height 115mm-145mm

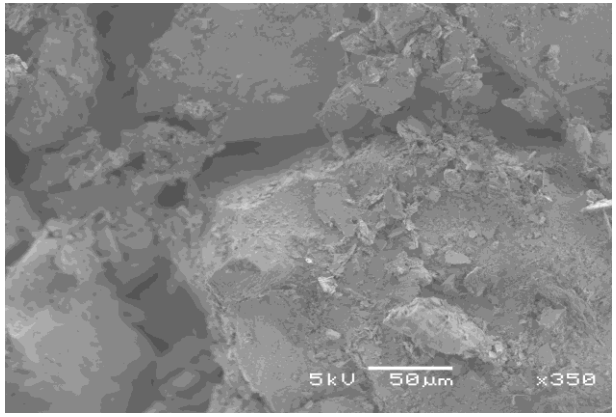

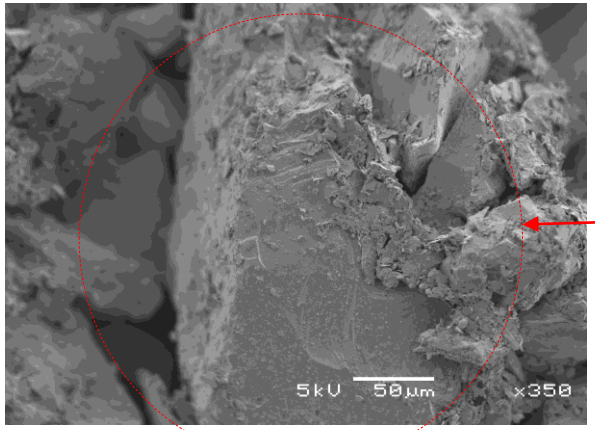

Vertically aligned elongated particle

Height 85mm-115mm

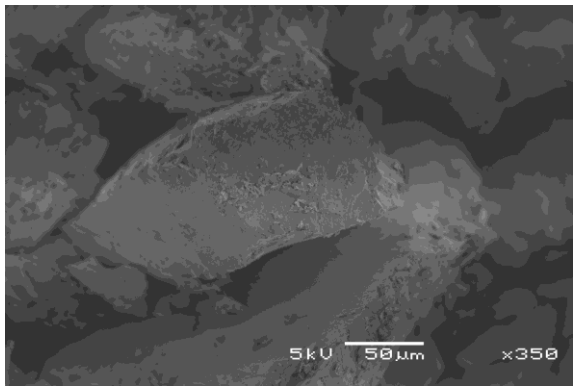

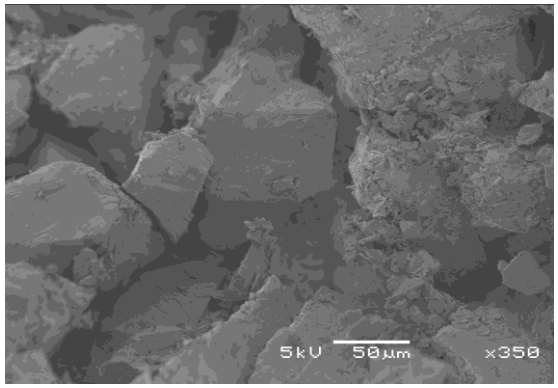

Height 50mm-85mm

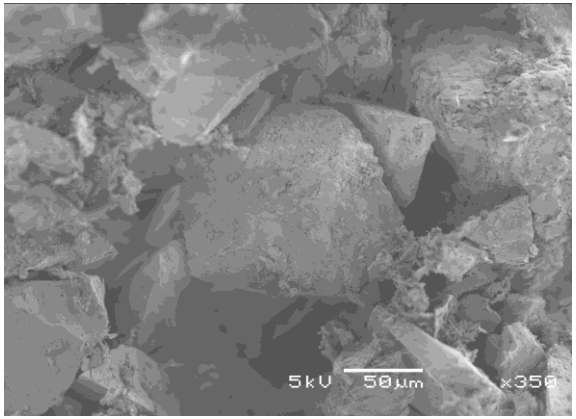

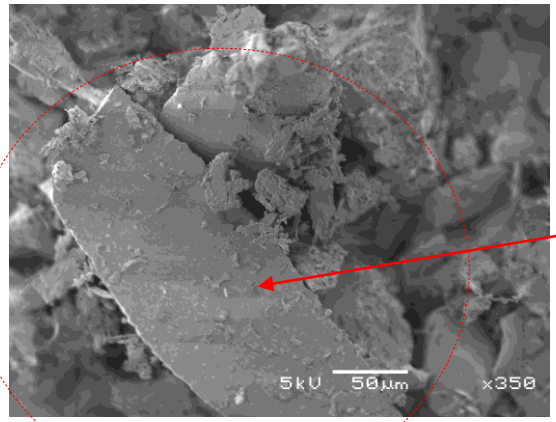

Vertically aligned
elongated particle

Height 15mm-50mm

Figure J1: Experiment FDB SEM micrographs (CG) -horizontal (left) and vertical (right) prints

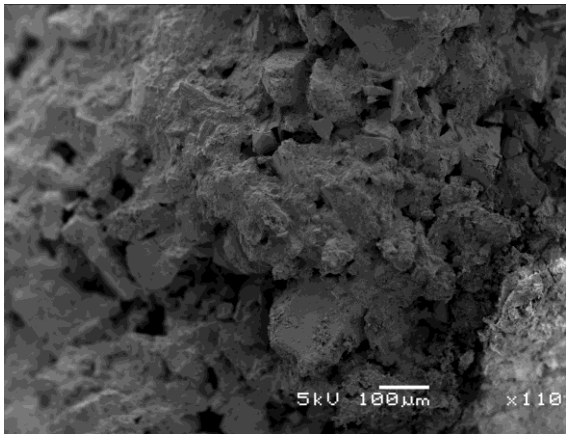

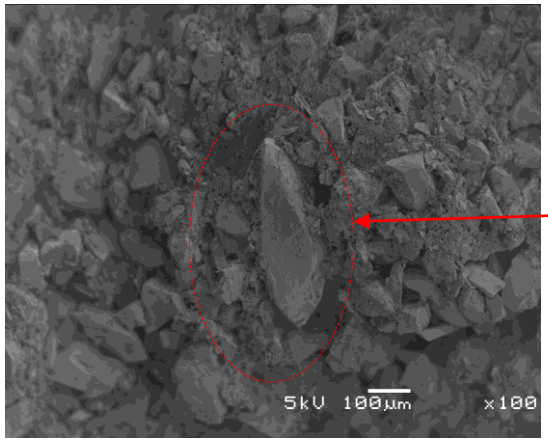

Vertically aligned
elongated particle

RoR20B 600-650mm

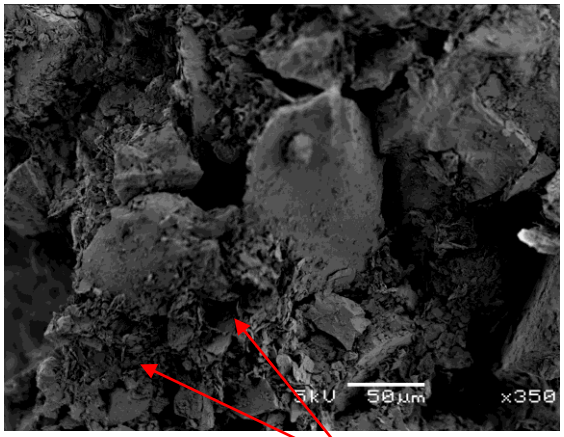

RoR20B 500mm

Fines in voids

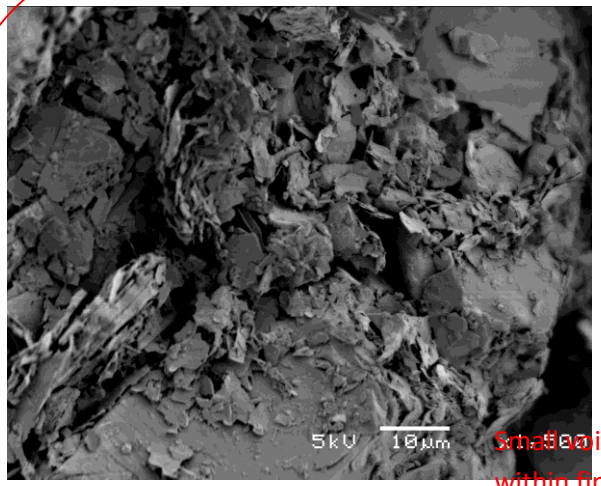

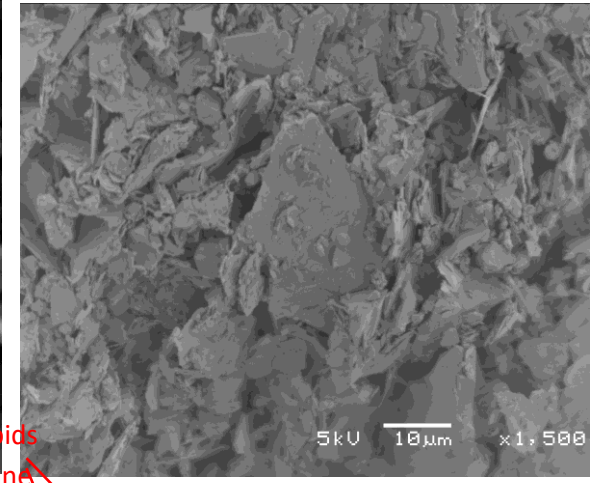

RoR20B 500mm

Small voids within fine particles

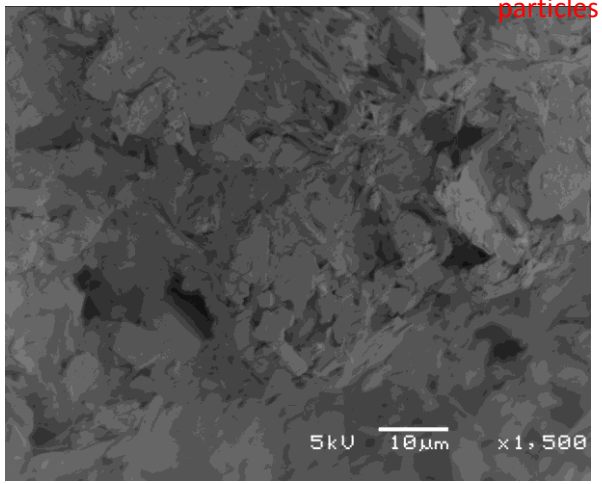

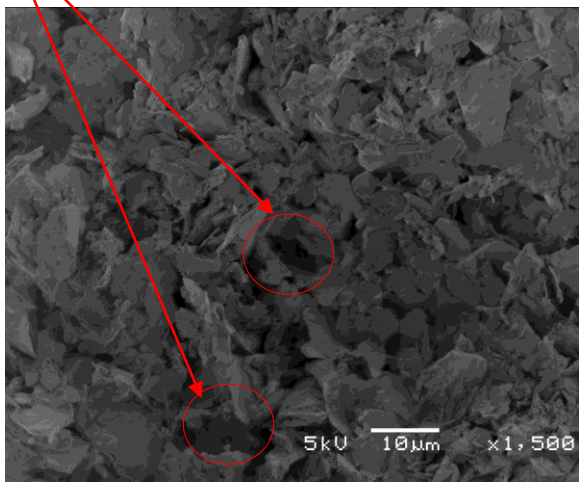

RoR20B 200mm

Porous mat of fine particles

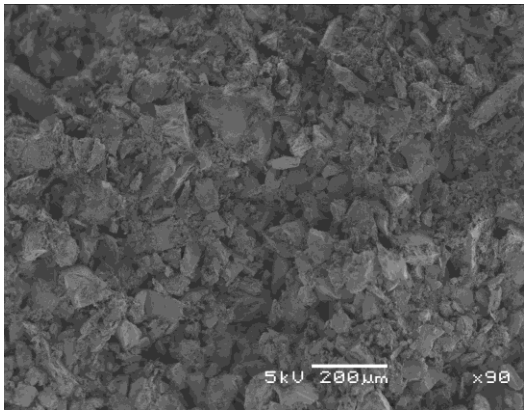

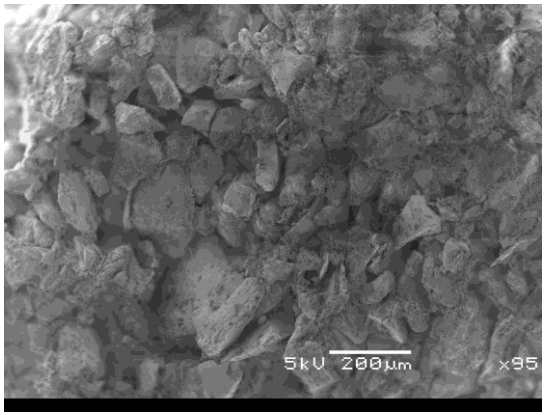

RoR20B 140mm

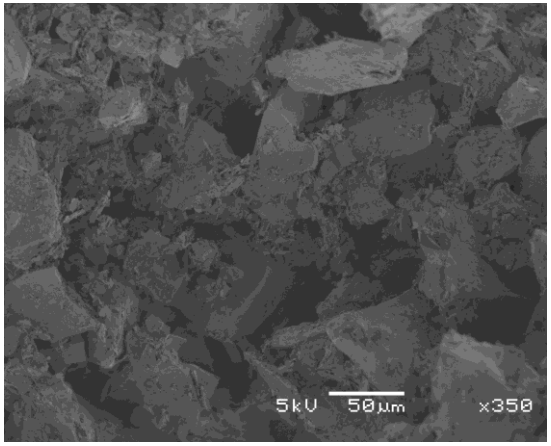

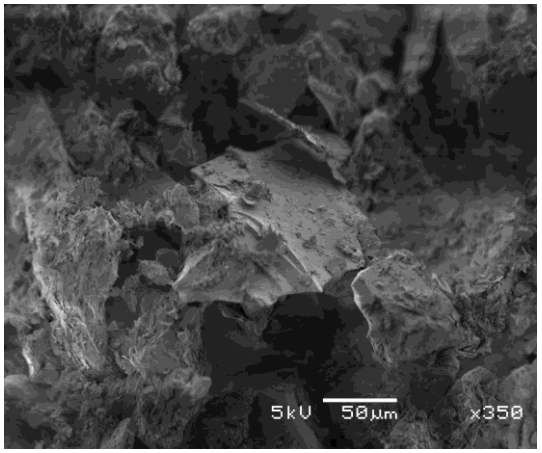

RoR20B 140mm

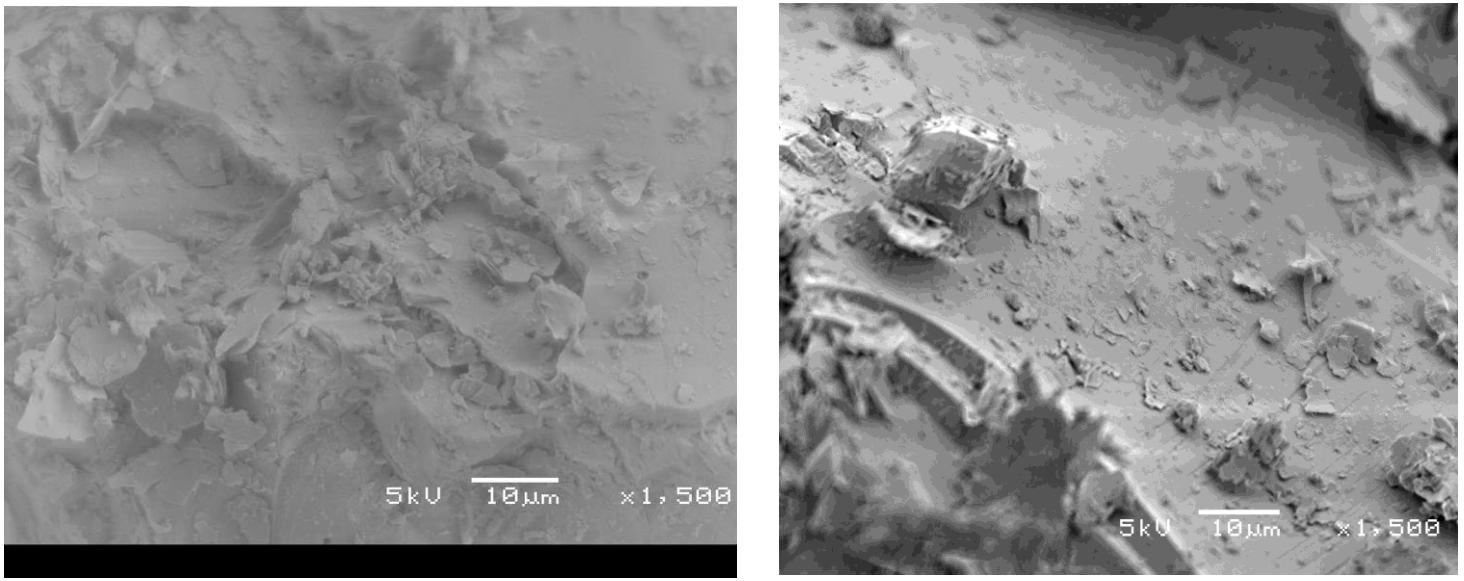

RoR20B 140mm

Figure J2: Experiment RoR20B SEM micrographs (CG) -horizontal (left) and vertical (right) prints

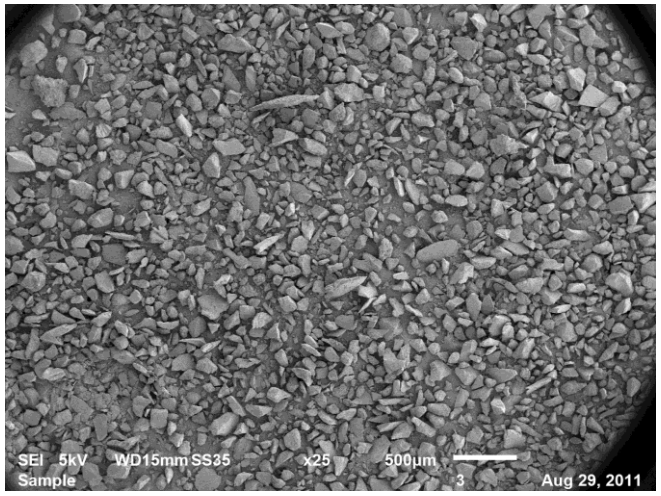

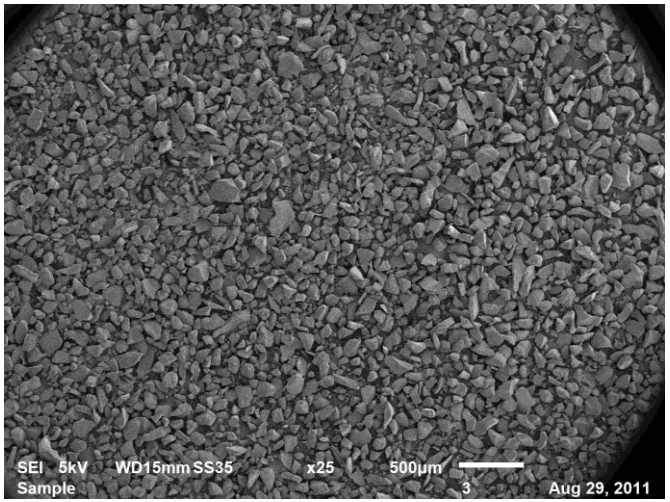

RoR10A 125mm-150mm

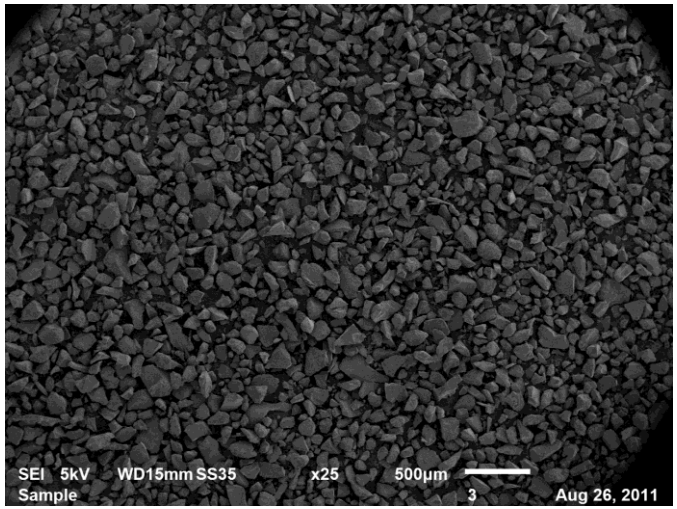

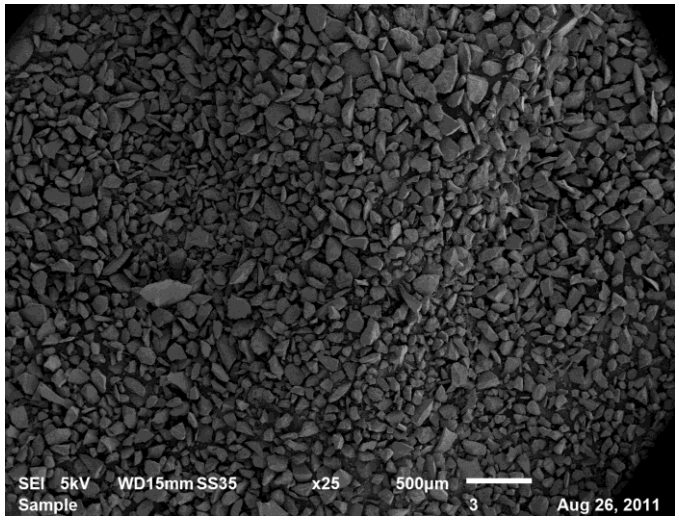

RoR10A 0mm-50mm

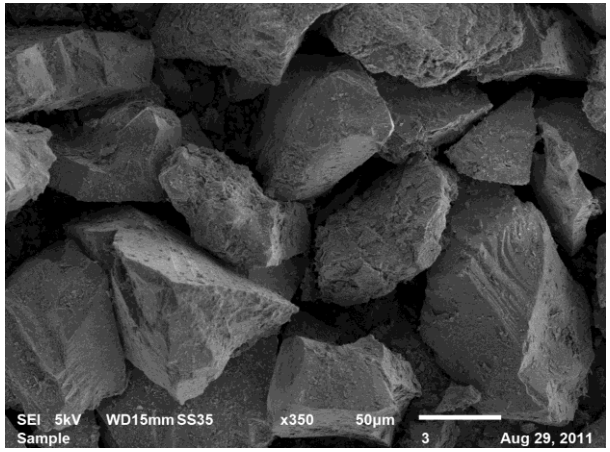

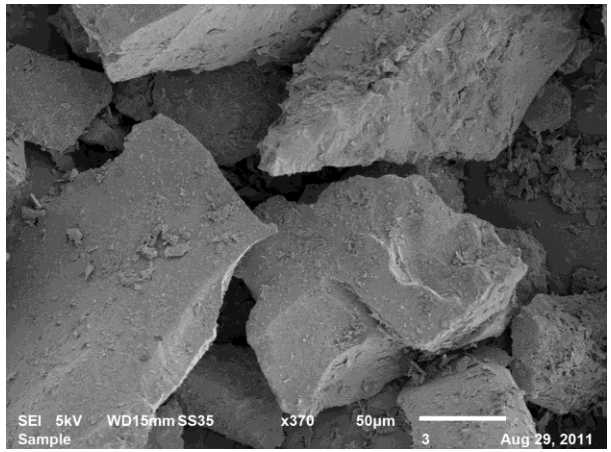

RoR10A 125mm-150mm

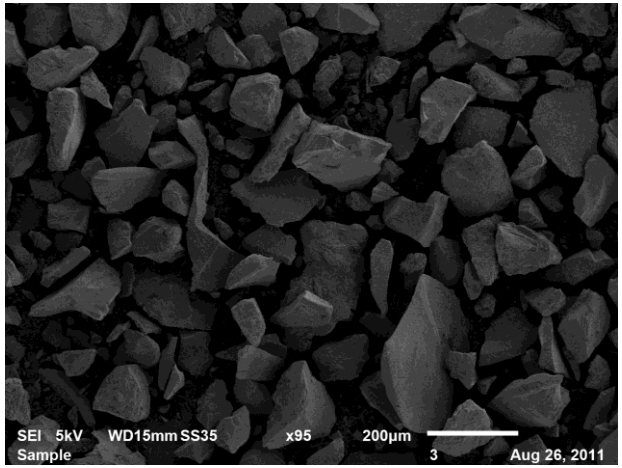

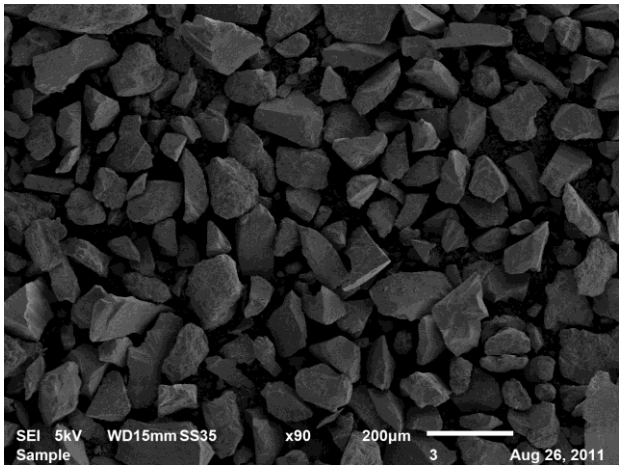

RoR10A 0mm-50mm

Figure J3: Experiment ROR10A (without permeability test) SEM micrographs (CT) -horizontal prints

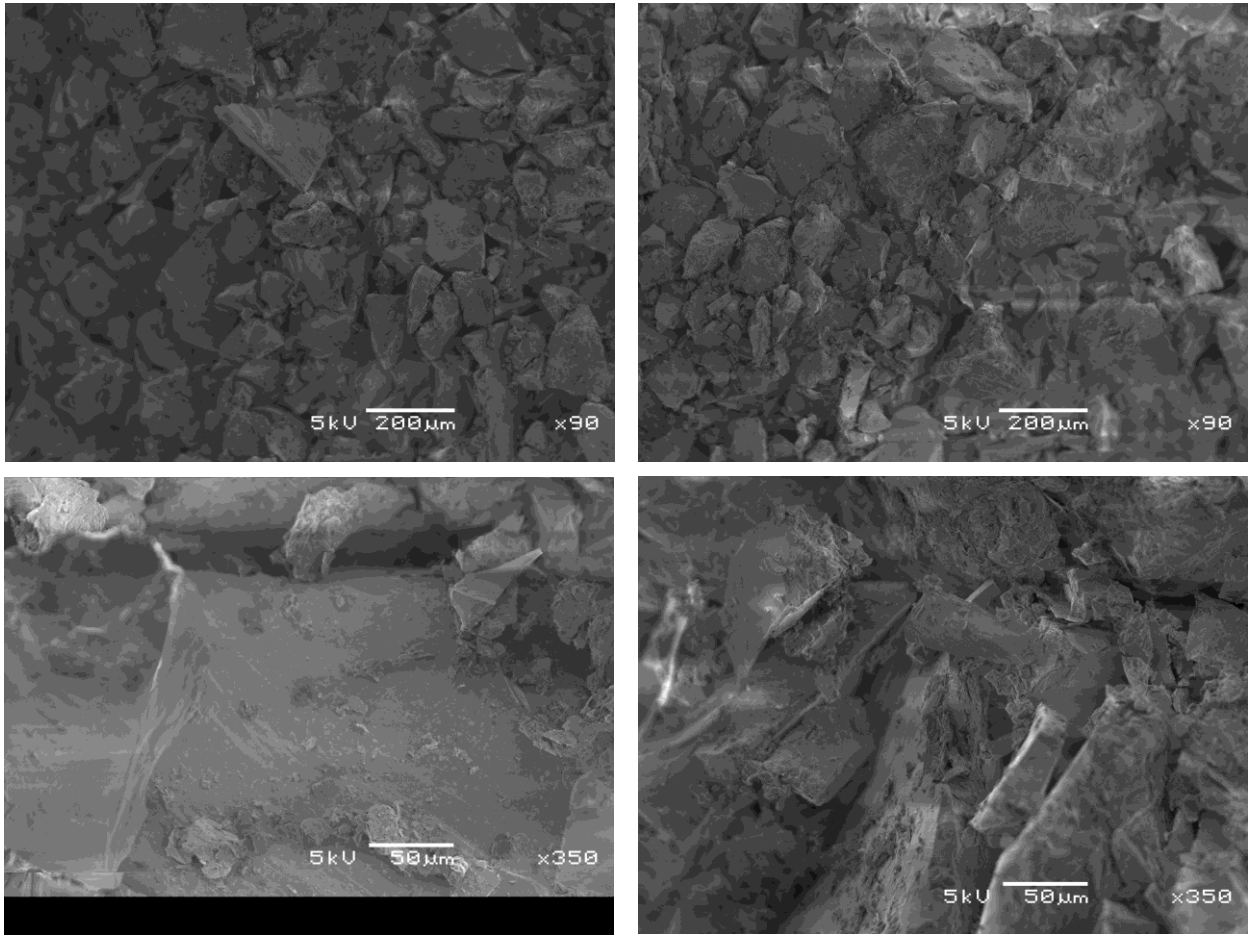

RoR10B 250mm-280mm

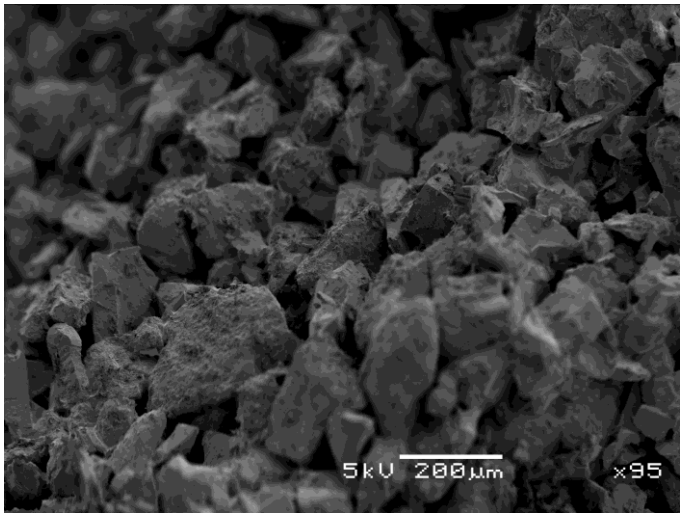

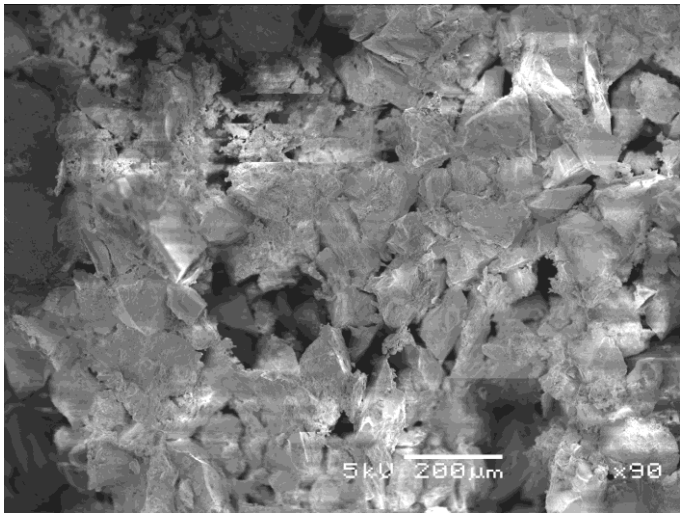

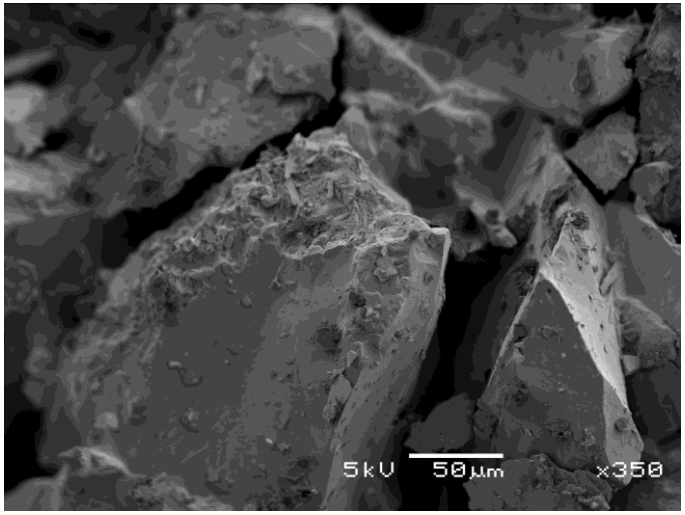

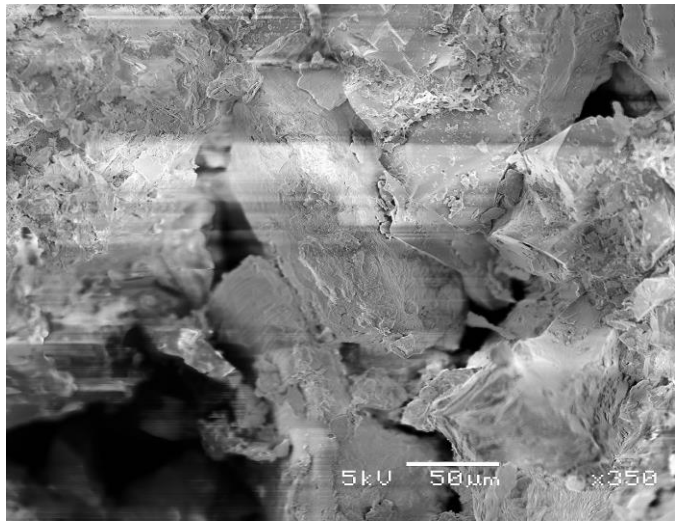

RoR10B 210mm-220mm

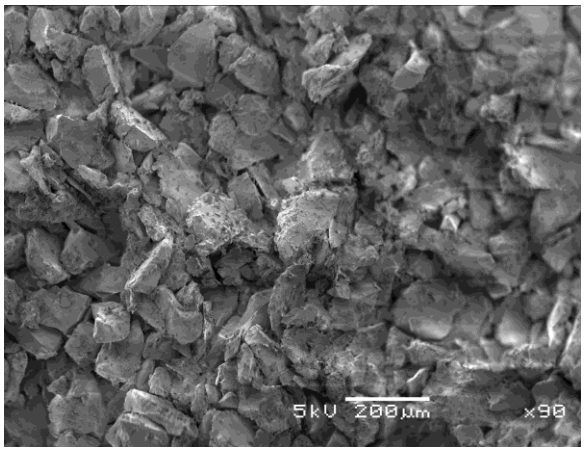

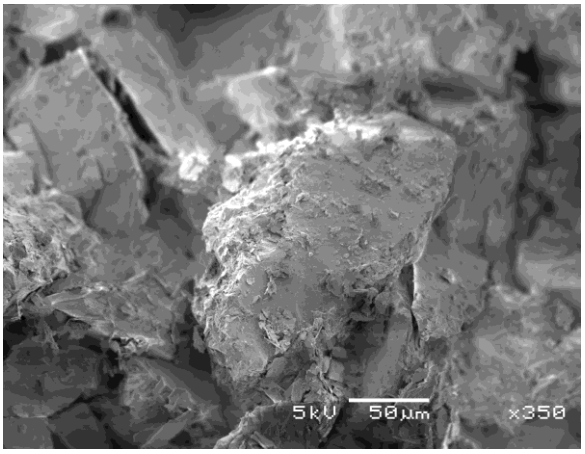

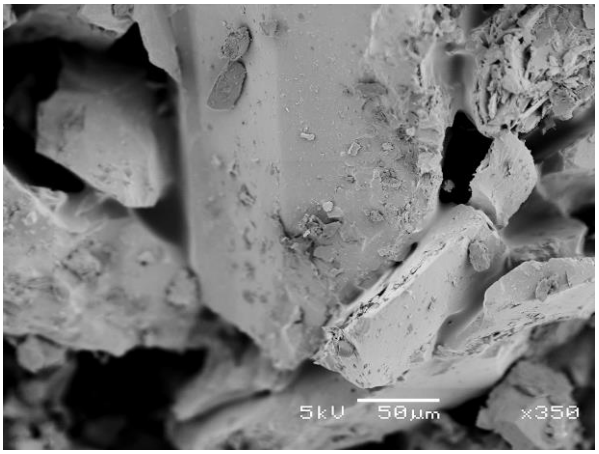

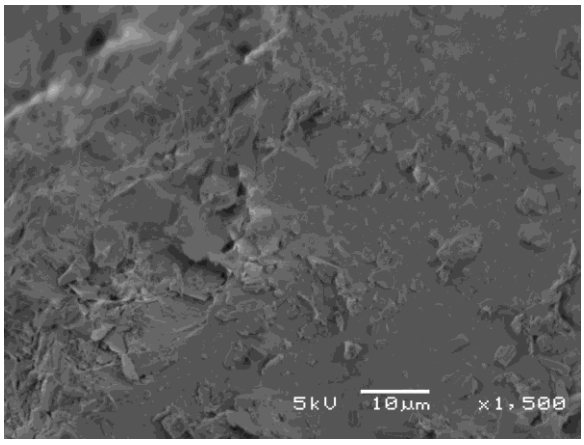

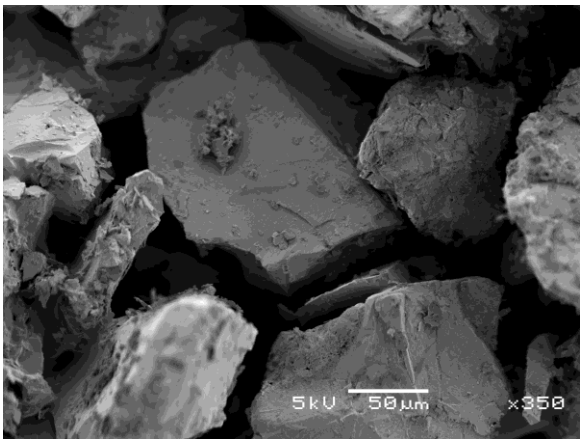

RoR10B 110mm-130mm

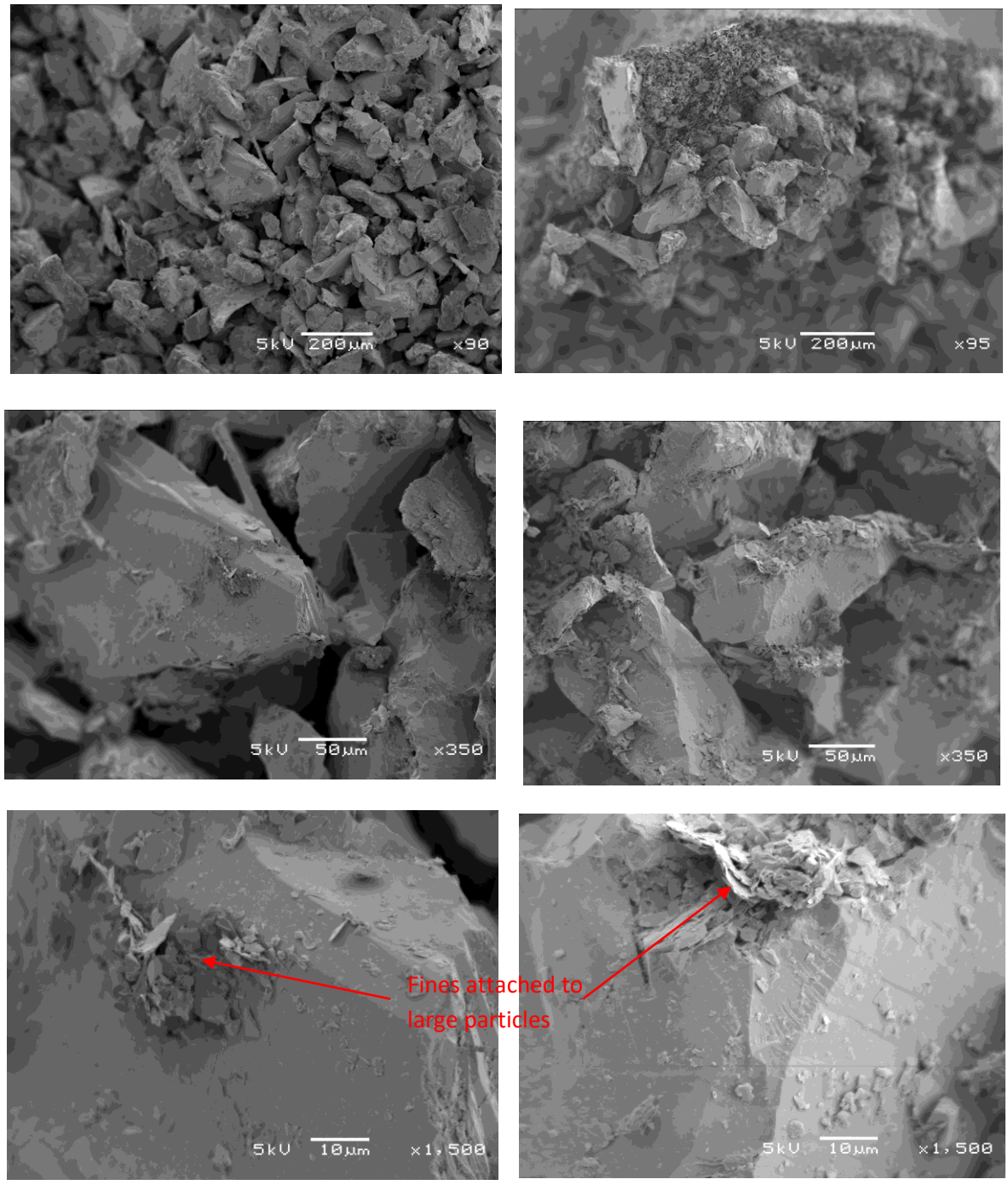

RoR10B 50mm-80mm

Figure J4: Experiment RoR10B SEM micrographs (CG) -horizontal (left) and vertical (right) prints

APPENDIX K

Soil water interface and excess pore pressure change over time

The appendix compares the soil water interface (SWI) and excess pore water pressure changes over time for Experiments FDB (Figure K1), RoR20A Lift 1 (Figure K2), RoR10A Lifts 1 to 3 (Figure K3) and RoR10B Lifts 1 to 3 (Figure K4).

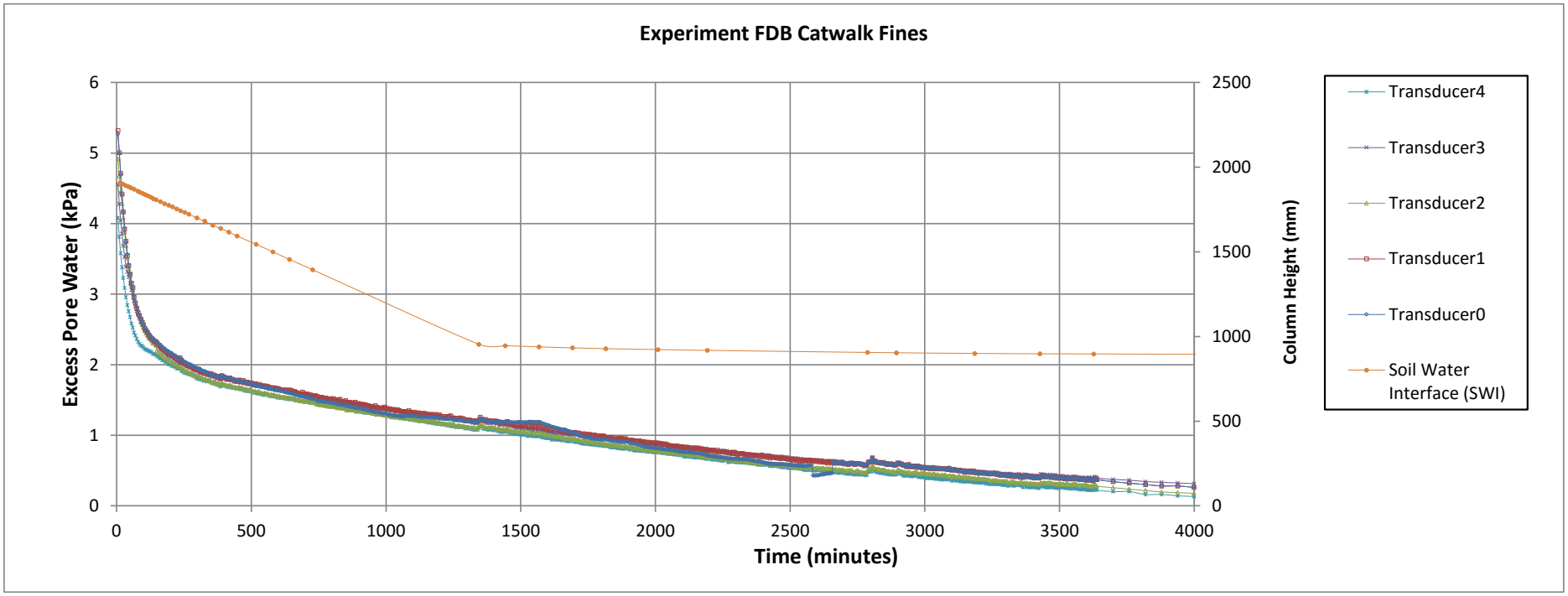

Figure K1: Soil water interface and excess pore pressure change over time - Experiment FDB

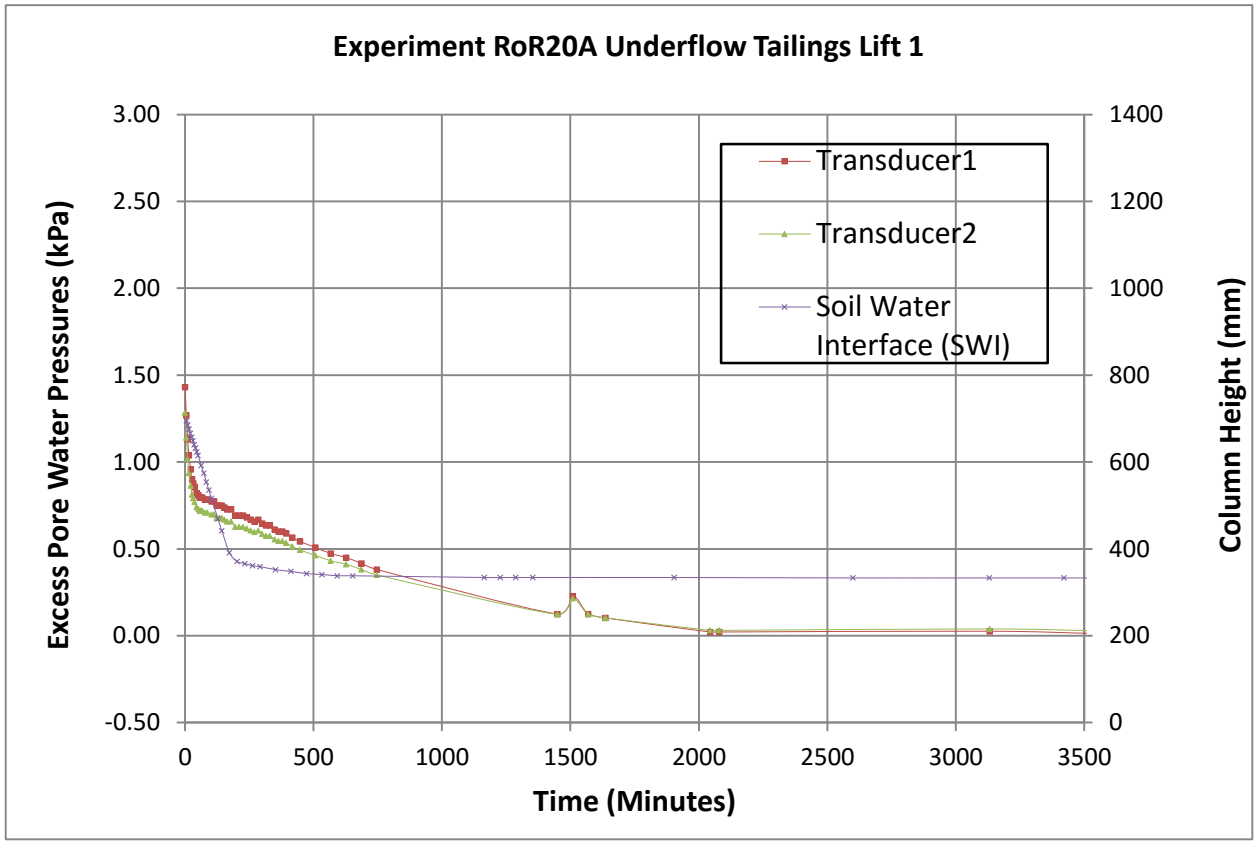

Figure K2: Soil water interface and excess pore pressure change over time - Experiment RoR20A

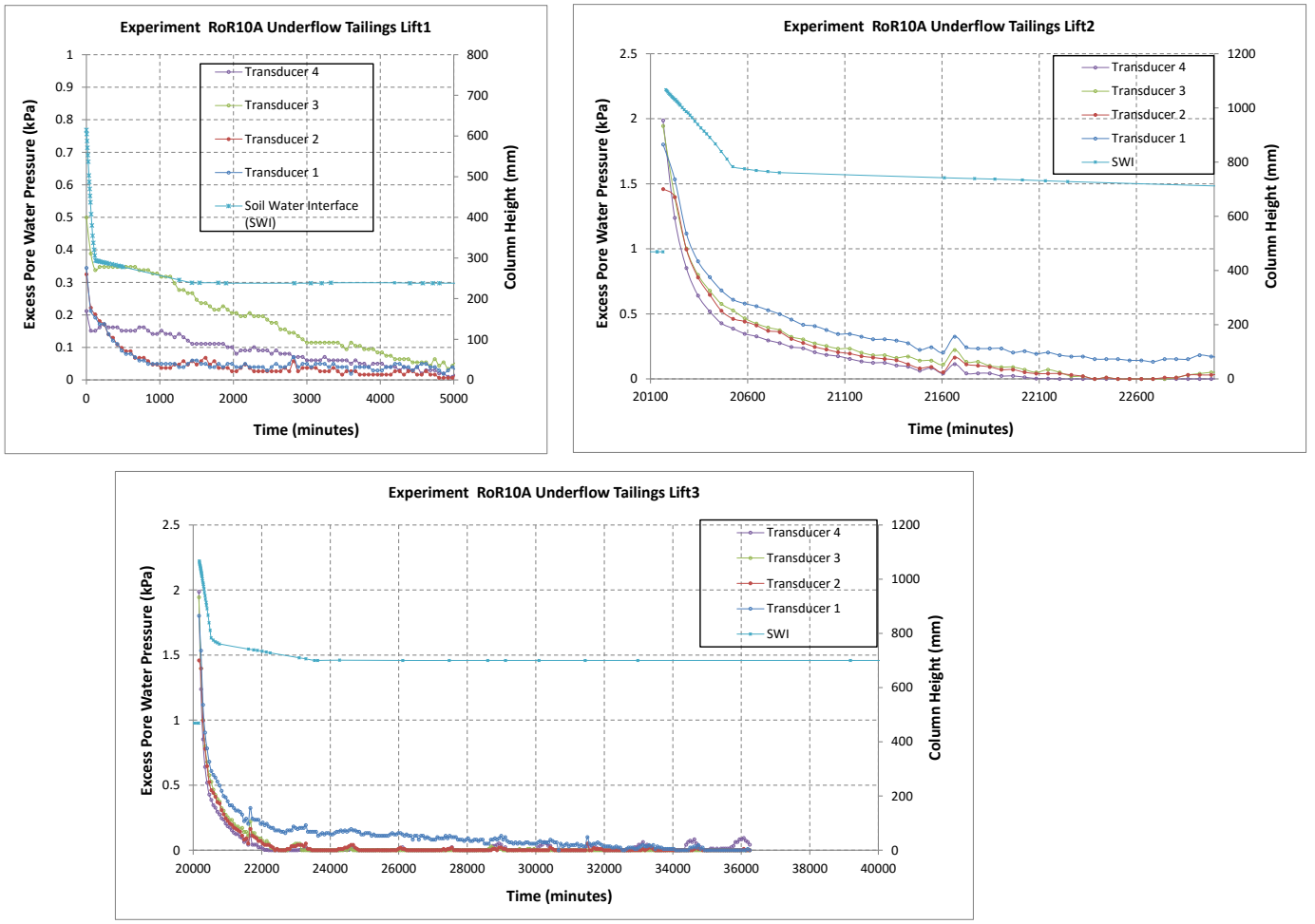

Figure K3: Soil water interface and excess pore pressure change over time - Experiment RoR10A

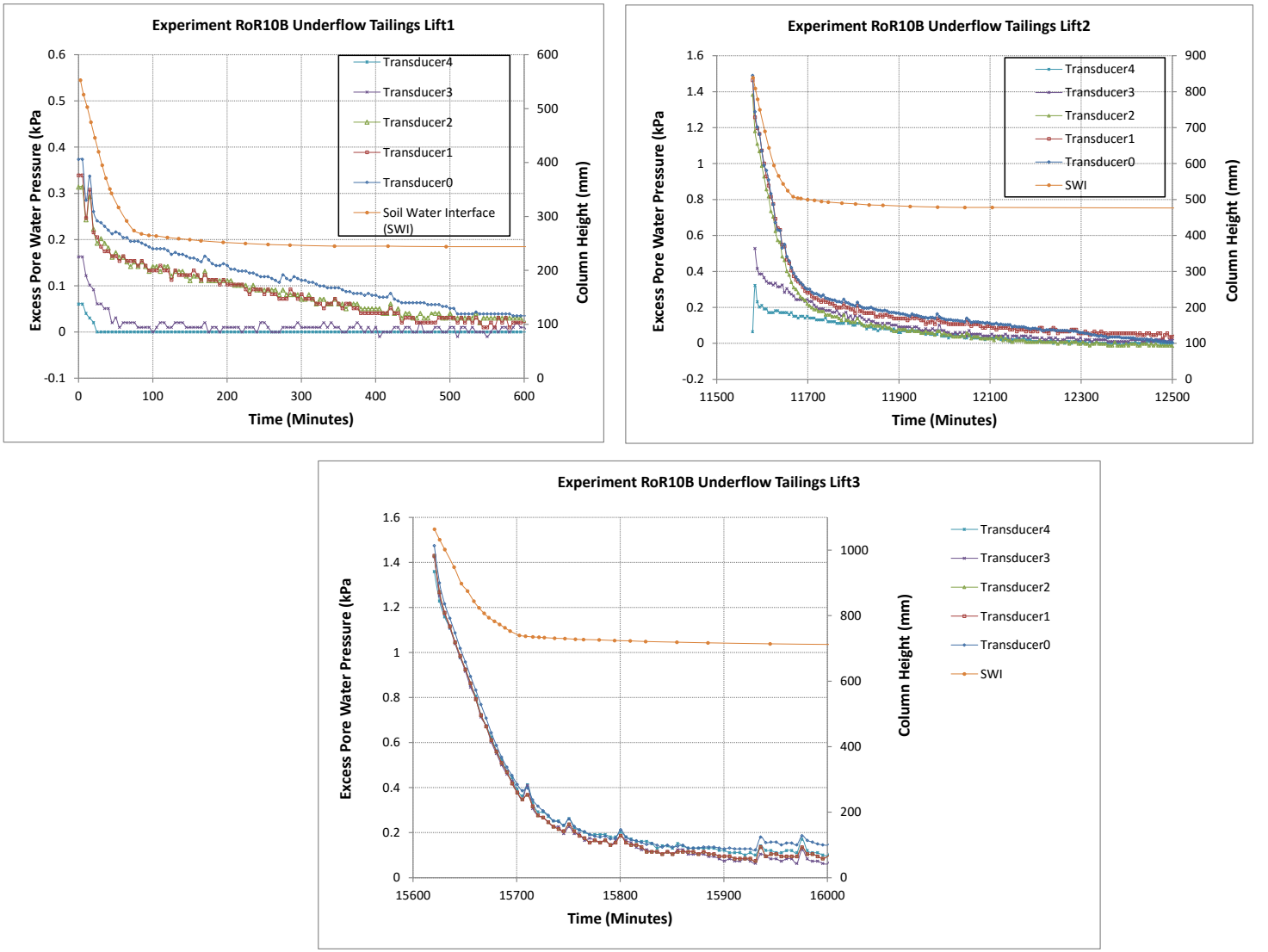

Figure K4: Soil water interface and excess pore pressure change over time - Experiment RoR10B